International Conference of Environmental Remote Sensing and GIS

Zagreb, 2024

Impressum

Scientific committee:

Assoc. Prof. Mateo Gašparović (president), University of Zagreb – Faculty of Geodesy, Croatia

Prof. Geoffrey Henebry, Michigan State University, Department of Geography, Environment, and Spatial Sciences & the Center for Global Change & Earth Observations, USA

Assoc. Prof. Vincenzo Ferrara, University of Rome La Sapienza, Department of Information Engineering, Electronics and Telecommunications, Italy

Assoc. Prof. Sudhir Kumar Singh, University of Allahabad, Nehru Science Centre, IIDS, K. Banerjee Centre of Atmospheric & Ocean, India

Assoc. Prof. Gordana Kaplan, Institute of Earth and Space Sciences, Eskisehir Technical University, Eskisehir, Turkey

Assoc. Prof. Federico Martinelli, University of Florence, Department of Biology, Italy

Sergej Baričević, PhD, University of Zagreb – Faculty of Geodesy, Croatia

Dino Dobrinić, PhD, University of Zagreb – Faculty of Geodesy, Croatia

Iva Gašparović, PhD, State Geodetic Administration, Croatia

Valentas Gružauskas, PhD, Vilnius University, Institute of Computer Science, Lithuania

Txomin Hermosilla, PhD, Natural Resources Canada, Canadian Forest Service, Canada

Damir Klobučar, PhD, Croatian Forests Ltd., Croatia

Andrea Pietrelli, PhD, University de Lyon, Université Claude Bernard Lyon 1, Ecole Centrale de Lyon, INSA Lyon, CNRS, Ampère, France

Ivan Pilaš, PhD, Croatian Forest Research Institute, Croatia

Ronald Pöppl, PhD, University of Vienna, Department of Geography and Regional Research, Austria

Dorijan Radočaj, PhD, Josip Juraj Strossmayer University of Osijek, Faculty of Agrobiotechnical Sciences Osijek, Croatia

Imelda Somodi, PhD, Centre for Ecological Research, Institute of Ecology and Botany, Hungary

Yongze Song, PhD, Curtin University, School of Design and the Built Environment, Australia

Antonio Tupek, PhD, University of Zagreb – Faculty of Geodesy, Croatia

Organizing committee:

Assoc. Prof. Mateo Gašparović (president), University of Zagreb – Faculty of Geodesy, Croatia

Prof. Mladen Zrinjski, University of Zagreb – Faculty of Geodesy, Croatia

Prof. Robert Župan, University of Zagreb – Faculty of Geodesy, Croatia

Sergej Baričević, PhD, University of Zagreb – Faculty of Geodesy, Croatia

Dino Dobrinić, PhD, University of Zagreb – Faculty of Geodesy, Croatia

Dorijan Radočaj, PhD, Josip Juraj Strossmayer University of Osijek, Faculty of Agrobiotechnical Sciences Osijek, Croatia

Antonio Tupek, PhD, University of Zagreb – Faculty of Geodesy, Croatia

Filip Radić, MSc, University of Zagreb – Faculty of Geodesy, Croatia

Marijo Seničić, MSc, University of Zagreb – Faculty of Geodesy, Croatia

Assoc. Prof. Mateo
Gašparović, editor

Foreword

Dear readers,

The University of Zagreb – Faculty of Geodesy is organizing for the first time the International Conference of Environmental Remote Sensing and GIS (ICERS) with the aim of spreading awareness of the application of remote sensing and GIS for the purpose of monitoring changes and environmental protection. The conference was organized within the project „Assessment of the Long-term Climatic and Anthropogenic Effects on the Spatio-temporal Vegetated Land Surface Dynamics in Croatia using Earth Observation Data (ALCAR)" co-financed by the Croatian Science Foundation.

The aim and scope of the ICERS conference is to gather experts and researchers from all over the world in one place and share the latest achievements in the field of remote sensing and GIS, while offering new perspectives for solving problems related to environmental change. Special attention will therefore be given to the application of remote sensing for environmental monitoring, disaster management and response, conservation and biodiversity, innovations in spatial data-acquiring technologies and numerous other topics in the field of remote sensing and GIS.

The Proceedings of the International Conference of Environmental Remote Sensing and GIS are the result of numerous research and scientific projects dealing with the application of remote sensing and GIS. In papers presented, authors show how to utilize new technologies and apply the possibilities of remote sensing in the determination and monitoring of climate change, sustainable development and resource management. The conference is divided into seven sections, which are presented in seven chapters in these proceedings: Remote Sensing for Environmental Monitoring, Disaster Management and Response, GIS for Sustainable Development, Innovations in Spatial Data-Acquiring Technologies, Conservation and Biodiversity, Artificial Intelligence and Big Data and Climate Change Mitigation Politics. The 1st ICERS proceedings encompasses 49 papers written by over 179 authors from over 26 countries from 4 continents.

On behalf of the University of Zagreb – Faculty of Geodesy, as well as on my own behalf, I would like to thank the Conference Scientific and Organizing Committee, keynote speakers, authors of papers, reviewers of articles, sponsors and participants for their contribution to the organization of the 1st International Conference of Environmental Remote Sensing and GIS.

As editor, I hope that this conference proceedings will encourage the academic, public and private sectors to continue their work, research and projects, to network and cooperate to promote new ideas and technologies in remote sensing and GIS for environmental protection. I look forward to continued collaboration, future conferences and new challenges!

My special thanks go to my wife Iva and my daughter Lucija.

Assoc. Prof. Mateo Gašparović

Contents

GIS FOR SUSTAINABLE DEVELOPMENT

INNOVATIONS IN SPATIAL DATA-ACQUIRING TECHNOLOGIES

CONSERVATION AND BIODIVERSITY

ARTIFICIAL INTELLIGENCE AND BIG DATA

CLIMATE CHANGE MITIGATION POLITICS

Remote Sensing for Environmental Monitoring

ADVANCING REMOTE SENSING FOR CONTINUOUS MONITORING AND DETECTION OF WATER POLLUTION INCIDENTS
Gordana Kaplan, Fatma Yalcinkaya, Argyro Tsipa, Andrea Pietrell, Mieyeville Fabien, Vincenzo Ferrara, Ioannis Ieropoulos

MONITORING CHANGES IN CHANNEL MORPHOLOGY ON THE ORLJAVA RIVER BASED ON UAV AND GNSS SURVEYS (POŽEGA-SLAVONIA COUNTY, CROATIA)
Katarina Pavlek, Marin Mićunović, Ivan Čanjevac

UTILIZATION OF USGS SPECTRAL SIGNATURE PROCESSING IN CROATIAN GYPSUM EXPLORATION
Nikola Gizdavec, Erli Kovačević Galović, Marko Copić, Nikolina Ilijanić, Slobodan Miko

DEVELOPMENT OF CROATIAN LAND INFORMATION SYSTEM
Vladimir Jelavić, Delfa Radoš, Marina Kukavica

PLANETSCOPE IMAGERY-BASED MONITORING OF ANNUAL AND SEASONAL DYNAMICS OF LAKES IN TBILISI, GEORGIA
Mariam Tsitsagi, Zaza Gulashvili, Ana Palavandishvili

MONITORING OF HELHEIM GLACIER DYNAMICS USING THE OPEN-SOURCE HIGH-RESOLUTION SATELLITE IMAGERY
Katarina Kolar, Fran Domazetović, Lovre Panđa, Rina Milošević

THE RELATIONSHIP BETWEEN AIR POLLUTION AND SEA SURFACE TEMPERATURE ANOMALIES IN THE NORTHERN ADRIATIC SEA
Luka Mamić, Matea Tomić

VALIDATION OF NEAR-SURFACE WIND SPEED MONTHLY AVERAGES FROM CHELSA CLIMATE DATA IN CROATIA
Dorijan Radočaj, Mateo Gašparović, Mladen Jurišić

UAV-BASED TECHNOLOGIES FOR REMOTE SENSING IN ENVIRONMENTAL MONITORING AND PHYSICAL RESILIENCE ASSESSMENT
Veaceslav Sprincean, Marianna Savva, Ana Birsan, Ion Ganea, Alexei Leu, Marian Jalencu, Mihail Caraman, Alexandr A. Barsuk, Arcadi Chirita, Florentin Paladi

Advancing Remote Sensing for Continuous Monitoring and Detection of Water Pollution Incidents

Gordana Kaplan[1], *, Fatma Yalcinkaya[2], Argyro Tsipa[3,4], Andrea Pietrell[5], Mieyeville Fabien[5], Vincenzo Ferrara[6], Ioannis Ieropoulos[7]

[1] Institute of Earth and Space Sciences, Eskisehir Technical University, Eskisehir, Turkey, kaplangorde@gmail.com

[2] Institute for Nanomaterials, Advanced Technologies, and Innovation, Technical University of Liberec, Liberec, Czech Republic, fatma.yalcinkaya@tul.cz

[3] Department of Civil and Environmental Engineering, University of Cyprus, 75 Kallipoleos, Nicosia 1678, Cyprus, tsipa.argyro@ucy.ac.cy

[4] Nireas International Water Research Centre, University of Cyprus, Nicosia 1678, Cyprus

[5] University de Lyon, Université Claude Bernard Lyon 1, Ecole Centrale de Lyon, INSA Lyon, CNRS, Ampère, F-69621 Villeurbanne, France, andrea.pietrelli7@gmail.com, fabien.mieyeville@univ-lyon1.fr

[6] Department of Information Engineering, Electronics and Telecommunications, University of Rome La Sapienza, Rome, Italy, vincenzo.ferrara@uniroma1.it

[7] Civil, Maritime and Environmental Engineering Department, University of Southampton, Southampton, UK, i.ieropoulos@soton.ac.uk

* corresponding author

Abstract: In the face of increasing industrial pollution, there is an urgent need to enhance water quality monitoring around industrial zones. This research explores the development of an advanced remote sensing system designed to continuously monitor water quality and provide early (timely) warning on changes that could signify environmental risks. With increasing incidences of water pollution due to industrial activities, there is a critical need for more dynamic and proactive monitoring approaches. This study investigates the feasibility of integrating remote sensing imagery to establish a comprehensive monitoring system that measures a spectrum of water quality indicators. At the core of the system lies near real-time data acquisition and processing capabilities, enabling the notification about significant changes in water quality. By leveraging remote sensing imagery, this system aims to provide detailed spatial and temporal analyses of water contaminants. This study could revolutionize the way water quality is monitored in sensitive and critical areas, offering a scalable solution to water management challenges and significantly enhancing environmental protection efforts. The results can contribute to the sustainable management of water resources, ensuring compliance with environmental regulations and safeguarding public health and ecosystems.

Keywords: remote sensing; water pollution; monitoring; Google Earth Engine.

1 Introduction

Rapid industrialization across the globe has been instrumental in driving economic growth and shaping modern societies. However, this development comes with a significant environmental cost, primarily due to the emission of pollutants like hazardous chemicals and microorganisms, which degrade the quality of air, soil, and crucially, water. This pollution not only threatens biodiversity but also poses serious public health risks (Adejumoke et al. 2018, Boyd 2020, Ingrao et al. 2023).

Remote sensing technology has emerged as a key tool in addressing these environmental challenges. It offers unprecedented capabilities for the continuous, detailed observation and analysis of water quality, proving essential for the effective management and preservation of water resources. Studies such as those by Karan and Samadder (2016) and Crioni et al. (2023) have demonstrated the utility of remote sensing in evaluating the impacts of industrial activities like coal mining and tailing dam failures on water quality.

Moreover, the advent of platforms like Google Earth Engine (GEE) has significantly enhanced the potential for long-term environmental monitoring. GEE allows researchers to access a vast archive of historical data, enabling them to conduct detailed longitudinal studies that provide deeper insights into trends and changes in water quality over extended periods (Khan et al. 2023).

Building on these foundational studies, this research investigates the possibility of a remote sensing system explicitly tailored for monitoring water pollution resulting from industrial incidents. The primary goal is to enhance the capability of remote sensing data to detect and monitor such events continuously, thereby ensuring more effective management of water resources in the face of ongoing industrial pollution. This approach should facilitate immediate response and help with long-term environmental planning and mitigation strategies.

2 Materials and methods

This research builds on previous work (Ruppen et al. 2023) examining the impacts of tailings spills on water quality, focusing on a case study involving the Catoca diamond mine incident in Angola. This spill significantly impacted the Tshikapa and Kasaï Rivers, extending into the Democratic Republic of the Congo, affecting both human populations and ecological systems over a course of more than 1,400 kilometers until reaching the Congo River. Using Sentinel-2 satellite imagery, the study evaluates the spatial

and temporal extent of pollution in the rivers following a significant spill in July 2021.

The objective is to investigate a continuous monitoring using remote sensing data, particularly within the GEE platform that will be used to monitor critical junctures where water bodies intersect—areas particularly vulnerable to pollution. The aim is to provide early warnings for water quality deterioration and continuous monitoring, which could be pivotal for proactive environmental management and public health safety.

Consistent with previous research, this study employs high-resolution Sentinel-2 imagery processed on the GEE platform. This approach ensures accessibility to updated and historical data for comprehensive temporal analysis. Special attention is given to the critical area, the flow point of Lova river, where the spillover from the dam is discharged, into the Tshikapa river. This strategic point is often susceptible to rapid changes in water quality due to accumulated runoff from upstream sources.

Table 1. Indices used in this study.

#	Index	Formula	Reference
1	NDTI	$\dfrac{NIR - G}{NIR + G}$	Garg et al. (2017)
2	TI	$\dfrac{R}{G}$	Dasi et al. (2023)
3	NDWI	$\dfrac{G - NIR}{G + NIR}$	Singh et al. (2015)
4	MNDWI	$\dfrac{G - SWIR}{G + SWIR}$	Singh et al. (2015)
5	Ch_a	$\dfrac{RE - R}{RE + R}$	Dasi et al. (2023)
6	FAI	$\dfrac{R - (B + (NIR - B) * (R - B))}{NIR + G}$	Santecchia et al. (2023)
7	HMRI	$\dfrac{SWIR - SWIR\,II}{SWIR + SWIR\,II}$	Santecchia et al. (2023)
8	MPI	NDTI + TI + HMRI	Santecchia et al. (2023)

The utilization of spectral indices in remote sensing is a powerful tool for assessing environmental characteristics, particularly water quality. In the analysis of Sentinel-2 imagery within the GEE platform, several indices are computed to monitor and evaluate the status of water bodies effectively (Table 1). The Normalized Difference Turbidity Index (NDTI) and Turbidity Index (TI), detect and quantify suspended particles in water, providing insights into water clarity and potential contamination (Garg et al. 2017, Dasi et al. 2023). The NDWI and Modified NDWI (MNDWI) highlight water features by suppressing vegetation and enhancing water bodies, crucial for delineating and monitoring aquatic environments (Singh et al. 2015). can affect water quality (Dasi et al. 2023). The floating algae index (FAI) is derived to The Chlorophyll-a Index (Ch_a) helps identify the concentration of chlorophyll, a key indicator of algal blooms that assess water moisture content and floating algae concentration, providing additional details on environmental conditions

that affect water quality (Xue and Su 2017). Lastly, the Heavy Metal Reflectance Index (HMRI) and a composite Metal Pollution Index (MPI), are designed to detect and monitor heavy metals and overall metal pollution within water bodies (Santecchia et al. 2023).

The outcomes of the spectral indices are then cross compared to investigate whether satellite data could be used to detect water pollution immediately following an incident. Specifically, we analyzed the Sentinel-2 data spanning a full year, from January to December 2021, focusing on capturing the environmental conditions before and after the pollution event at the Catoca diamond mine. Due to cloud cover, images exist from April to November. By comparing the calculated indices for this period with the known timing and impact of the spill, we aimed to determine the effectiveness of remote sensing as a tool for early detection of such events, and continuous monitoring afterwards. This approach allowed us to assess the responsiveness of our indices in real-time scenarios and their potential to inform timely environmental management decisions.

3 Results

In the analysis of the Catoca diamond mine incident using various spectral indices derived from Sentinel-2 imagery, distinct patterns were observed in the response of each index to the pollution event (Figure 1).

NDWI and MNDWI, indices, typically used to assess water content, did not show any significant variation around the date of the incident. This was expected, as these indices are not specifically tailored to detect the type of pollutants released during the tailings dam spill.

The NDTI, TI and MPI, showed elevated values on the date of the incident (end of July, 2021), suggesting an increase in water turbidity, which is consistent with the spill investigated in this study. Interestingly, these indices again showed high values in October, indicating another possible event or residual effects from the initial spill. Ch_a, which
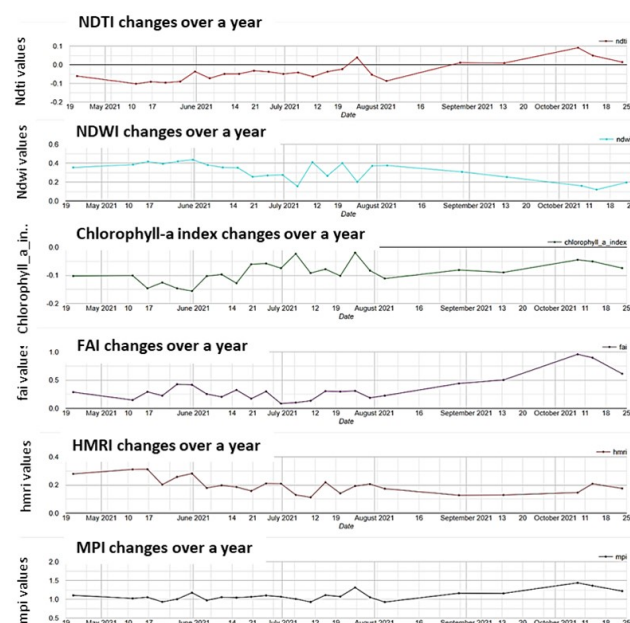
Figure 1. Results of the spectral indices.

is often used to detect algal growth that is potentially indicative of nutrient-rich pollution, registered high values on the incident date. However, similar peaks were observed on other dates, complicating the use of this index alone to pinpoint the specific pollution event.
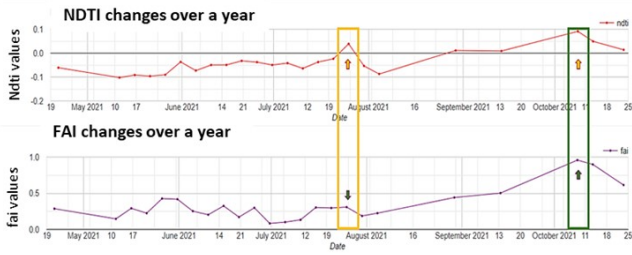
Figure 2. NDTI and FAI emphasizing the incident date and algal blooms.

The FAI did not show elevated values on the day of the incident but did register high readings post-October. This suggests that the index may be more responsive to changes in algal blooms, which could occur as a secondary effect of nutrient influx following the spill.

4   Discussion and Conclusions

The results underscore the complexities of using remote sensing data for environmental monitoring. While certain indices like NDTI and TI can be directly indicative of an incident like a tailings dam spill, others like the Ch_a or FAI may capture broader ecological shifts that require careful interpretation.

The analysis of spectral indices NDTI, TI, and MPI around the incident at the Catoca diamond mine and subsequent months, reveals important insights into the dynamics of water pollution and its detection using remote sensing data.

In October, the situation appeared to evolve. While NDTI and TI remained high, indicating continued elevated turbidity, the FAI also showed exceptionally high values. High FAI is indicative of algal blooms, which often result from nutrient-rich environments that can follow the initial deposit of pollutants such as phosphates or nitrates that fertilize the water (Figure 2).

The differentiation between the sources of turbidity based on the relationship between NDTI, TI, and FAI can be crucial for effective monitoring and remediation efforts. When turbidity indices are high, but FAI is low, this suggests that the water turbidity is likely due to inorganic or non-biological factors such as silt, clay, or heavy metals. This condition would align with incidents like tailings spills.

Conversely, when both turbidity indices and FAI are high, this points towards biological factors compounding the turbidity, particularly algal blooms. In these cases, while initial pollutants may still be present, the ecological response to the nutrient influx is now a significant factor in the water quality issues. Critical environmental data such as the indices reported in this study, can be significantly enhanced with the use of real-time, "living" sensors, such as those based on Bioelectrochemical Systems (BES). BES use live microbial communities to convert biochemical energy locked in organic matter, directly into electricity,

and they have a remarkable ability to respond to environmental perturbations with high sensitivity. This renders BES devices excellent biosensors for environmental events, since these can nicely complement observed index measurements from satellites such as Sentinel-2.

This study builds on the work of Ruppen et al. (2023), enhancing their framework by incorporating advanced indices and proposing new tools for continuously monitoring and detecting water pollution incidents. For future work, it is essential to validate these findings across more diverse case studies and integrate them with living biosensor technologies, such as those based on BES, for a more robust, real-time analysis.

5   References

Adejumoke, I., Adebesin, B. O., Oluyori, A., Adelani-Akande, T., Dada, A. O., Toyin, O. A., 2018. Water pollution: effects, prevention, and climatic impact. In: Glavan, M. (Ed.), Water challenges of an urbanizing world, Intech Open, pp. 33-47.

Boyd, C. E., 2020. Water Quality: An Introduction, third ed. Springer, Cham.

Crioni, P. L. B, Teramoto, E. H., Chang, H. K., 2023. Monitoring river turbidity after a mine tailing dam failure using an empirical model derived from Sentinel-2 imagery. Anais da Academia Brasileira de Ciências 95 (1).

Dasi, A., Vani, K. S., Reddybathina, V., Charpe, A., Tadikonda, U. K., 2023. Estimation of Water Quality Parameters Using Water Indices and GEE. 2023 IEEE International Conference on Contemporary Computing and Communications (InC4), Bangalore, India, 21-22 April, pp. 1-6.

Garg, V, Kumar, A. S., Aggarwal, S.P., Kumar, V., Dhote, P. R., Thakur, P. K., Nikam, B. R., Sambare, R. S., Siddiqui, A., Muduli, P. R., Rastogi, G., 2017. Spectral similarity approach for mapping turbidity of an inland waterbody. Journal of Hydrology 550, 527-537.

Ingrao, C., Strippoli, R., Giovanni, L., Huisingh, D., 2023. Water scarcity in agriculture: An overview of causes, impacts and approaches for reducing the risks. Heliyon, 9 (8).

Karan, S. K., Samadder, S. R., 2016. Reduction of spatial distribution of risk factors for transportation of contaminants released by coal mining activities. Journal of Environmental Management 180, 280-290.

Khan, R. M., Salehi, B., Mahdianpari, M., Mohammadimanesh, F., 2021. Water quality monitoring over finger lakes region using sentinel-2 imagery on google earth engine cloud computing platform. ISPRS Annals of the Photogrammetry, Remote Sensing and Spatial Information Sciences 3, 279-283.

Ruppen, D., Runnalls, J., Tshimanga, R. M., Wehrli, b., Odermatt, D., 2023. Optical remote sensing of large-scale water pollution in Angola and DR Congo caused by the Catoca mine tailings spill. International Journal of Applied Earth Observation and Geoinformation 118.

Santecchia, G.S., Revollo Sarmiento, G.N., Genchi, S.A., Vitale, A.J., Delrieux, C.A., 2023. Assessment of Landsat-8 and Sentinel-2 Water Indices: A Case Study in the Southwest of the Buenos Aires Province (Argentina). Journal of Imaging 9 (9).

Singh, K. V., Setia, R., Sahoo, S., Prasad, A., Pateriya, B., 2014. Evaluation of NDWI and MNDWI for assessment of waterlogging by integrating digital elevation model and groundwater level. Geocarto International 30 (6), 650-661.

Monitoring Changes in Channel Morphology on the Orljava River Based on UAV and GNSS Surveys (Požega-Slavonia County, Croatia)

Katarina Pavlek[1],*, Marin Mićunović[1], Ivan Čanjevac[1]

[1] Department of Geography, University of Zagreb Faculty of Science, Zagreb, Croatia, katarina.pavlek95@gmail.com, mmicunov@geog.pmf.hr, canjevac@geog.pmf.hr
* corresponding author

Abstract: This study investigates morphological changes of distinct meander locations along the Orljava River, using multi-temporal imagery acquired by an unmanned aerial vehicle (UAV) and GNSS surveys since March 2022. The selected sites in the river's middle and lower course without bank protections show high channel dynamics. High-resolution digital surface models (DSMs) with a pixel size of 5 cm and orthomosaics with a pixel size of 1 cm were generated using Agisoft Metashape software. Ground control points and channel cross-section measurements were obtained using real-time kinematic (RTK)-GNSS. Various morphological features were analysed, including bank retreat, channel migration, fluvial sediment bars, and changes in bed level. Automated extraction of riverbank lines covered by low, sparse vegetation was performed using DSMs and convolution functions in ArcGIS Pro, while riverbanks covered by trees were assessed based on orthomosaics and digitised manually. The results showed that the most significant channel changes occurred following a flood event in December 2022. On certain meanders with riverbanks covered by sparse vegetation, the annual bank retreat rate amounted to 10–20 m. In addition, cross-sectional comparisons with data from 2012 revealed an increase in depth of approximately 1 m in the location upstream of the breached mill weir, indicating local bed incision. Although lateral channel migration presents a natural behaviour of actively meandering rivers, recently increased bank erosion is a pressing issue for local farmers due to the proximity of agricultural lands to the riverbanks.

Keywords: channel changes; river meandering; riverbank retreat; remote sensing.

1 Introduction

Rivers are dynamic natural systems that continuously shape the landscape through processes of erosion, sediment transport, and deposition. Actively meandering rivers are particularly dynamic, marked by lateral erosion and migration of meanders across the floodplain. Frequent changes in fluvial landforms contribute to the development of diverse riparian and aquatic habitats (Garófano-Gómez et al. 2017). However, bank erosion and channel migration can present challenges to human settlements and activities, especially in areas where they are closely situated to riverbanks (Bertalan et al. 2018).

Understanding the morphological changes of meandering rivers is essential for effective river management and mitigation of bank erosion and flood risks. Recent developments in remote sensing technologies have facilitated comprehensive and frequent monitoring of river channels and floodplains. Unmanned Aerial Vehicles (UAVs) equipped with high-resolution sensors are especially important for analysing geomorphic units and processes at smaller scales (Hemmelder et al. 2018, Rusnák et al. 2019).

This study investigates distinct meander bend sites on the Orljava River, which is characterised by significant channel dynamics in parts of its middle and lower course where bank protections are absent. By analysing multi-temporal UAV imagery and GNSS-derived topographic data, this research aims to quantify various morphological features and processes, including bank retreat, channel migration, fluvial sediment bars, and changes in bed level. Measured channel changes are compared with available hydrological records and hydromorphological characteristics of the river corridor, including riverbank vegetation, to examine potential controls on river processes. The results of this study are expected to offer valuable insights into the dynamic behaviour of the Orljava River, providing information for nature-based river management.

2 Materials and methods

2.1 Study area

The Orljava River, situated in Croatia's Požega-Slavonia County (Figure 1), is a 93.4 km long tributary of the Sava River (Čanjevac et al. 2022). Due to the round shape of its basin (1600 km^2), the river's hydrology is marked by frequent flash floods, threatening local communities and
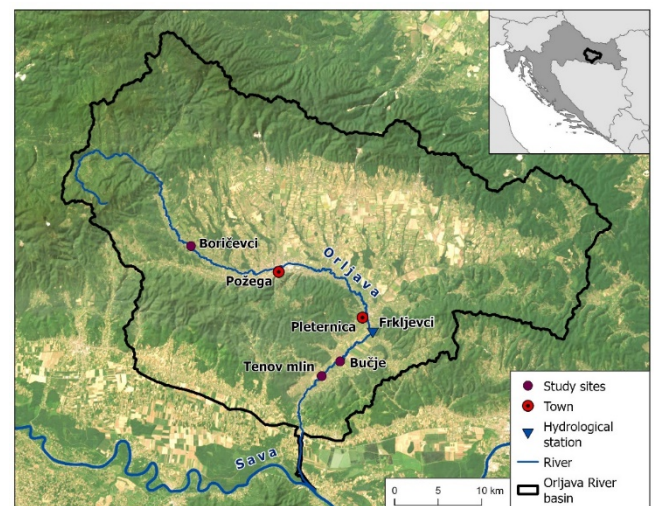
Figure 1. Location of the studied sites in the Orljava River basin.

agriculture in the river valley. The mean flows at the Frkljevci hydrological station are around 7 m³/s, but peak flows can reach more than 200 m³/s (DHMZ n.d.). In its middle and lower course, the Orljava is typified by gravel-bed conditions and active meandering. While the river is not extensively channelized (except in urban areas), various engineering works have been implemented to ensure river stabilization, including bank protections, weirs, artificial levees, and meander cut-offs. Additionally, riparian vegetation is occasionally removed to increase channel capacity.

The most upstream studied site is located near the settlement of Boričevci. Two consecutive meander bends were examined: the first with eroding bank adjacent to grasslands and the other with banks covered by woody vegetation. Channel morphology is characterized by large coarse gravel bars. Under mean flow conditions, the width of the wetted channel is around 10 m. At the downstream studied sites, Bučje and Tenov mlin, the channel bed predominantly consists of fine gravel. The width of the wetted channel during mean flows is approximately 15 m, with the active channel width (including sediment bars) amounting to 40 m. At the site Bučje, two meanders with grassland-covered banks were studied, both upstream and downstream the breached mill weir. At the Tenov mlin site, two consecutive meander bends with and without woody riverbanks were examined. All studied eroding banks are relatively equal in length (100 ± 10 m).

2.2 Field surveys and data processing

Aerial imagery was collected during four fieldwork campaigns conducted in March 2022, March 2023, October 2023, and May 2024. In the first campaign, imagery was captured using a DJI Phantom 4 Pro, while in subsequent campaigns, a DJI Phantom RTK was used. Ground control points and channel cross-section measurements were obtained using RTK-GNSS (Trimble Catalyst DA2). Cross-section measurements were specifically conducted during two campaigns, in October 2022 and October 2023. The surveys were carried out during periods of low-flow conditions to capture the morphological characteristics of the river channel, primarily occurring in early spring or autumn, both preceding and following the peak vegetation period. The UAV imagery was captured from an altitude of 50 m, with the collection of 10 control and 10 check points at each site. Cross-section measurements were conducted at the locations recorded in the 2012 topographic survey by the water management authority.

The UAV imagery was processed in Agisoft Metashape software to generate DSMs (digital surface models) with a pixel size of 5 cm and orthomosaics with a pixel size of 1 cm. Ground control points were used to refine the alignment and scale of the point cloud, enhancing the georeferencing accuracy of the final products.

2.3 Changes in river morphology

Changes in river morphology were analysed using ArcGIS Pro. Lines of eroding riverbanks, covered by sparse, low vegetation, were automatically extracted using an edge detection Laplacian filter applied to DSMs. The Laplacian filter calculates brightness changes to identify edges, enhancing their visibility and setting a threshold to finalize edge detection. A workflow, involving raster reclassification and thinning, was then established to automate the further process. However, analysing riverbanks covered by woody vegetation proved more challenging. The lines of these riverbanks were assessed using both orthomosaics and DSMs, and digitised manually.

The eroded floodplain area between two fieldwork campaigns was measured as the polygon area between two consecutive riverbank lines, while the maximum bank retreat distance was calculated using orthogonal transects from the starting riverbank line. Additional digitised morphological features include the wetted channel and unvegetated bars.

3 Results

According to ground check points, the horizontal error of produced models was estimated to 5 cm and vertical error to 10 cm. The most significant bank retreat, and consequently the largest area of erosion, occurred between the first two surveys (March 2022 – March 2023). Particularly considerable values were observed at the Boričevci left bank (LB), where the river eroded a total of 682 m² of adjacent grassland (Figure 2). The riverbank retreated by an average of 7.3 meters, with a maximum of 20.3 meters. The notable changes in channel morphology include meander rotation towards the east, channel widening and subsequent shifts in the distribution of fluvial bars. At the upstream part of the bend, a mid-
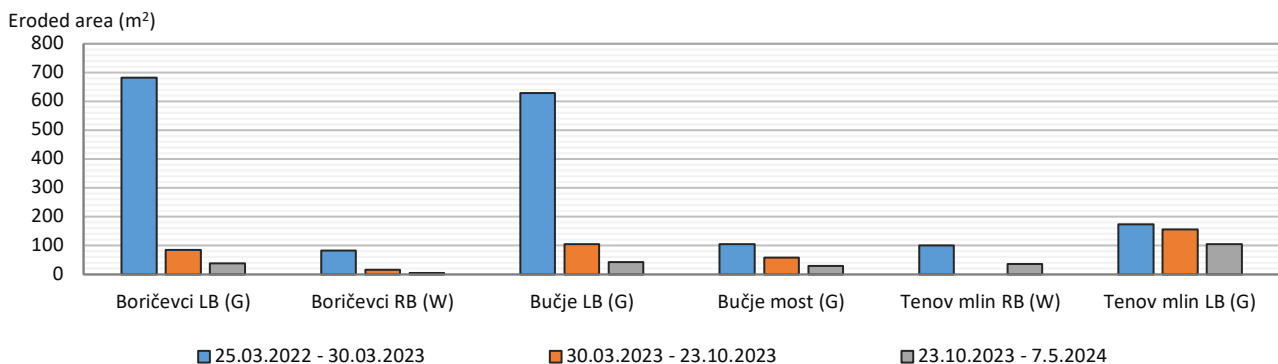
Figure 2. Total eroded floodplain area (m²) between field surveys at the studied meander sites (G - grassland riverbanks, W - woody riverbanks).
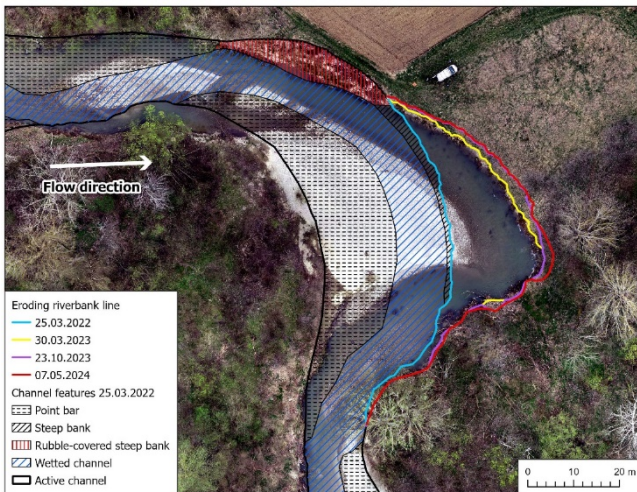
Figure 3. Study site Boričevci left bank, UAV imagery from 30 March 2023.

channel bar was formed in 2023 in the location of a previous side bar (Figure 3).

At the Bučje left bank (LB) site, located upstream of the breached weir, the total eroded area during the first period amounted to 630 m² of agricultural land, with the maximum bank retreat of 10.2 m. In the following two periods, the erosion rates at these two sites were significantly lower. At the site Bučje most (downstream of the breached weir) erosion affected the floodplain to a lesser extent, with erosion rates remaining relatively consistent between the first (8.7 m² per month) and second periods (8.4 m² per month), considering the duration of each period. Similarly, at the site Tenov mlin left bank (LB), total eroded floodplain areas varied less (ranging from 106 to 176 m²) throughout the studied periods.

Generally, the lowest rates of floodplain erosion were measured at meander bends with riverbanks covered by woody vegetation. At the Boričevci site, over the entire study period (March 2022 – May 2024) the meander with woody banks eroded a total of 105.5 m², notably less than the upstream meander with grassland banks, which eroded 803.7 m². Similarly, at the Tenov mlin site, the eroding right bank, covered by woody vegetation, experienced less erosion (138 m²) compared to the downstream meander adjacent to agricultural land, which eroded 435.1 m².

Cross-sectional measurements revealed a dynamic pattern in the changing riverbed level, closely linked to meander migration. However, in the laterally stable part of the channel at the Bučje site, located just upstream of the weir breached in 2016, an increase in depth of approximately 1 m was recorded compared to the 2012 survey data.

4 Discussion

The magnitude, duration, and frequency of high flows play crucial roles in shaping river channel morphology: during floods riverbanks erode widening the channel and fluvial bars are formed (Schumm 1977). In the studied meanders, the highest rates of floodplain erosion and bank retreat were recorded from March 2022 to March 2023, which includes the flood from December 2022, when the peak

flow at the Frkljevci station reached 158 m³/s (DHMZ n.d.). During 2023, no such flood was recorded, which is probably why bank retreat declined.

However, significant differences in eroded area and bank retreat were recorded in studied meanders during the same periods. Local differences in bank erosion rates can be influenced by the type of bank material, variations in channel morphology which affect flow velocity and turbulence, riverbank vegetation cover, and human activities like bank protection measures (Kiss et al. 2019). For the studied sites, precise data on bank material is not available, but it can be considered negligible since the meanders are consecutive and all riverbanks are mainly sandy.

On the other hand, the clear role of vegetation cover has been noted, since meanders with woody riverbanks experienced less erosion. Many studies have shown that vegetation, especially woody vegetation, increases bank strength through deep and strong root systems, reducing erosion (Gurnell 2014, Krzeminska et al. 2019).

At the Boričevci site, effects of channel morphology and human activities are notable. The site is downstream from a straight, narrow section, increasing flow velocity and stream power. The rubble placed by locals under the riverbank to protect adjacent agricultural land, combined with woody vegetation downstream, likely confined erosion to the grassland floodplain toward the east (Figure 3). On the other hand, at the Bučje site, a considerable bank retreat might be related to the breached weir downstream, which increased the local channel slope, therefore enhancing stream power and bank erosion.

5 Conclusions

This study examined morphological changes in three meander bend locations along the Orljava River, Croatia, using UAV imagery and RTK-GNSS channel bed-level measurements. The most significant rates of floodplain erosion occurred between March 2022 and March 2023, coinciding with a significant flood in December 2022. Vegetation cover showed to be an important factor of bank retreat, with meanders covered by woody vegetation experiencing less erosion compared to those adjacent to grasslands. Morphological variations among meanders, such as sinuosity and width, also apparently influenced local hydraulic conditions and bank retreat rates. Human impacts, particularly regarding bank protections and weirs, were also observed.

The removal of riparian vegetation by water managers as part of flood protection measures most certainly increases riverbank erosion, posing challenges for local farmers since agricultural areas are often adjacent to riverbanks. Future strategies should prioritize widening the riparian zone to allow more space for natural river processes in line with nature-based river management principles.

6 References

Bertalan, L., Novák, T., Németh, Z., Rodrigo-Comino, J., Kertész, Á., Szabó, S., 2018. Issues of Meander

Development: Land Degradation or Ecological Value? The Example of the Sajó River, Hungary. Water 10 (11), 1613.

Croatian Meteorological and Hydrological Service (DHMZ). Hydrology department webpages, https://hidro.dhz.hr/ (Accessed 15 May, 2023)

Čanjevac, I., Pavlek, K., Orešić, D., 2022. River lengths in Croatia determined from a topographic map at a scale of 1:25,000. Hrvatski Geografski Glasnik 84 (1), 5-30.

Garófano-Gómez, V., Metz, M., Egger, G., Díaz-Redondo, M., Hortobágyi, B., … Steiger, J., 2017. Vegetation succession processes and fluvial dynamics of a mobile temperate riparian ecosystem: the lower Allier River (France). Géomorphologie: relief, processus, environnement 23 (3), 187-202.

Gurnell, A., 2014. Plants as river system engineers. Earth Surface Processes and Landforms 39 (1), 4-25.

Hemmelder, S., Marra, W., Markies, H., De Jong, S. M., 2018. Monitoring river morphology and bank erosion using UAV imagery – A case study of the river Buëch, Hautes-Alpes, France. International Journal of Applied Earth Observation and Geoinformation 73, 428-437.

Kiss, T., Amissah, G. J., Fiala, K., 2019. Bank processes and revetment erosion of a large lowland river: Case study of the lower Tisza River, Hungary. Water 11 (6), 1313.

Krzeminska, D., Kerkhof, T., Skaalsveen, K., Stolte, J., 2019. Effect of riparian vegetation on stream bank stability in small agricultural catchments. Catena 172, 87-96.

Rusnák, M., Sládek, J., Pacina, J., Kidová, A., 2019. Monitoring of avulsion channel evolution and river morphology changes using UAV photogrammetry: Case study of the gravel bed Ondava River in Outer Western Carpathians. Area 51 (3), 549-560.

Schumm, S.A., 1977. The Fluvial System. John Wiley and Sons, New York.

Utilization of USGS Spectral Signature Processing in Croatian Gypsum Exploration

Nikola Gizdavec[1],*, Erli Kovačević Galović[1], Marko Copić[1], Nikolina Ilijanić[1], Slobodan Miko[1]

[1] Department for Mineral Resources and Marine Geology, Croatian Geological Survey, Zagreb, Croatia, ngizdavec@hgi-cgs.hr, ekovacevic@hgi-cgs.hr, mcopic@hgi-cgs.hr, nilijanic@hgi-cgs.hr, smiko@hgi-cgs.hr

* corresponding author

Abstract: A detailed previous study of the potentiality of mineral raw materials in the Vrlika karst polje showed a high geological gypsum potential that was not precisely determined on existing geological maps. This serves as the primary scientific reason for selecting this study area. The second reason arises from market demands for an increased supply of gypsum, recognized as an environmentally friendly mineral raw material by the Eurogypsum Association. To rapidly assess the 25 km^2 area, remote sensing methods were employed. Data collected from the USGS (the United States Geological Survey) was used, with their scientists having created a database of spectral signatures. By using spectroscopy to study materials, measurements can be compared to the spectral records of sensors located on different platforms, in this case, the ESA´s (the European Space Agency) MSI-Sentinel-2A. The K-means algorithm and NDVI based on WV3 sensor were also used. Comparative analysis of the obtained data with field data led to the conclusion that spectral signatures of gypsum from USGS samples align closely with those from Croatia due to their very similar chemical composition, taking into account the spatial resolution of MSI-Sentinel-2A.

Keywords: USGS Spectral Library data; gypsum; MSI-Sentinel 2-A; WV3; K-means.

1 Introduction

Gypsum is a mineral composed of calcium sulfate dihydrate ($CaSO_4 \cdot 2H_2O$). According to Wilson et al. (2014) the structure of gypsum is formed from layers of CaO 8 polyhedra consisting of "zig-zag" chains bound by similar "zig-zag chains" of SO_4^{2-} units. These double-sheet polyhedral layers are linked by an O(1)–H(2) hydrogen bond. Gypsum forms in sedimentary environments through the evaporation of seawater or saline lakes. When water containing dissolved calcium sulfate evaporates, gypsum precipitates out of solution and accumulates as layers or beds within sedimentary basins. It can be found in various sedimentary settings, including marine basins, evaporite deposits, and continental rifts. Gypsum deposits are economically significant as they are a major source of calcium sulfate, which is used in various industries such as construction, agriculture, and chemical manufacturing. Understanding the geological processes involved in gypsum formation and its occurrence within sedimentary basins is crucial for exploration and exploitation purposes (Warren 2016). According to Shuai et al. (2022), the basis for remote sensing of gypsum lies in the spectral characteristics of calcium sulfate, which exhibit distinctive properties in the VNIR, SWIR, and TIR regions. Gypsum, as

a hydrated calcium sulfate, shows characteristic absorption features in the VNIR and SWIR regions. Specifically, it is characterized by a "triplet" at wavelengths of 1446 nm, 1490 nm, and 1538 nm, as well as at 1750 nm, 1900 nm, and a triplet at 2178 nm, 2217 nm, and 2268 nm (Figure 1). The reason for this lies in the vibrations of hydrogen bonds in the molecular structure of water (Crowley 1991). Due to this reason, these properties are not characteristic for "anhydrous" calcium sulfate types such as anhydrite, nor other evaporites (halite, thenardite, etc., Bishop et al. 2014, Figure 1).
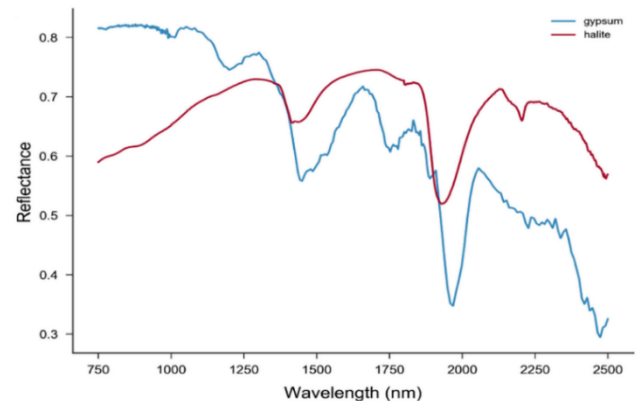
Figure 1. Comparison gypsum and halite spectral signatures (according to Howari et al. 2018).

2 Materials and methods

2.1 Study area and geological settings

Geological exploration of gypsum was conducted in the territory of the Republic of Croatia, Split-Dalmatia County (Figure 2 Left), the area of the Town of Vrlika, south of Vrlika karst polje, within the previous gypsum exploration field "Vranjkovići", and in the area of the former gypsum exploitation field "Vranjkovići" with its immediate vicinity (Figure 2 Right).

According to Dedić (2018), referencing OGK SFRJ sheet Drniš (Ivanović et al. 1977, Ivanović et al. 1978), the geological structure of the Vrlika area highlights two types of sedimentary deposition. One is predominantly carbonate, represented by limestone, dolomite, and Jurassic-Cretaceous breccias, while the other is characterized by a Permian evaporite complex. Permian deposits are characterized by the distinctive development of an evaporite complex: anhydrite, gypsum, fine-grained clastics, carbonates, as well as occasional occurrences of eruptive formations (Figure 2. Right). However, due to the scale of the map and the size of gypsum outcrops, they are not specifically marked on the OGK SFRJ. Therefore, the
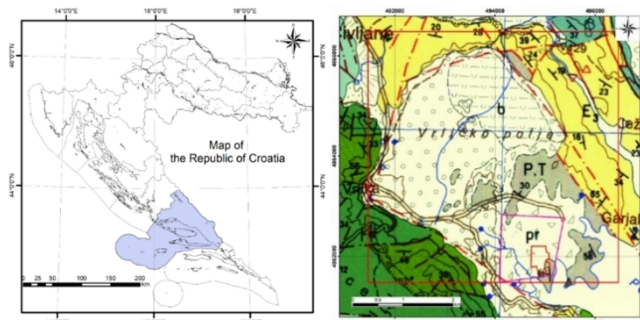
Figure 2. Left: Map of the Republic of Croatia. Split – Dalmatia County is highlighted in blue. Right: Geological Map of Yugoslavia at a scale of 1:100,000 (OGK SFRJ), sheet Drniš clip. Red rectangle represents study area; magenta polygon is a former exploration field "Vranjkovići", red polygon is a former exploitation field "Vranjkovići".

idea is to attempt to identify them through remote sensing methods.

Gypsum deposits are studied on a number of locations, and they are partly exploited. The thickness of gypsum layers is approximately 30 m and they gradually transition into anhydrite which is always located in their base. Dedić (2018) wrote on geochemical and mineralogical characteristics of Upper Permian evaporite sediments from central Dalmatia. Gypsum is made up of 93-96% $CaSO_4 \cdot 2H_2O$.

2.2   Geological mapping

A 38 ha area underwent geological mapping using hand-held GPS devices. The data, initially recorded in the WGS84 system, was subsequently converted to the HTRS96TM system using GIS, ensuring compatibility with digital dataset. The mapping primarily focused on the former exploitation and exploration fields of "Vranjkovići" and their vicinity (Figure 3).
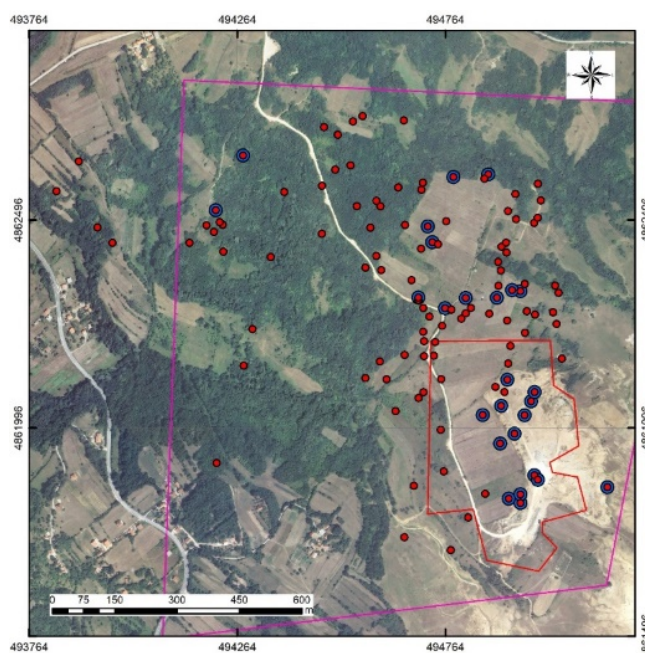
Figure 3. Geological mapping field points. Red dots are all observed points. Blue – red dots are gypsum occurrences.

2.3   Datasets and imagery processing

Publicly available images from the European Space Agency's Copernicus program, specifically the MSI-Sentinel 2A sensor (MSI-S2A), and a commercial image from the WorldView 3 sensor (WV3) sponsored by ESA, were employed in this study. The MSI-S2A sensor offers 13 spectral bands of wavelengths spanning from 443 to 2190 nm, with spatial resolutions of 10 m for four bands, 20 m for six bands, and 60 m for three bands. Conversely, the commercial WV3 image sponsored by ESA encompasses only 5 bands: blue (478 nm), green (546 nm), red (659 nm), NIR1 (831 nm), and Pan (625 nm), with spatial resolutions ranging from 0,31 m to 1,24 m. In this context, the WV3 image was exclusively utilized for more precise discrimination between vegetation and rocks (geological formations) using NDVI (Rouse et al. 1973). After NDVI analysis, 6 raster datasets on USGS Spectral signatures on gypsum were used (Kokaly et al. 2017) which were classified by Kmeans algorithm.

3   Results

The final outcome of geological mapping along with the processing of existing archival data, undoubtedly contributes to a better understanding of results obtained through remote sensing methods. Therefore, an attempt was made to work with this data. The application of NDVI on the MSI-S2A image is shown in Figure 4. In this case only 5 WV3 bands were available, so the NDVI that can distinguish rocks and vegetation was calculated. K-means algorithm (Hartigan 1975, Hartigan and Wang 1979) was used on USGS gypsum raster data fusion (20 classes, 60 iterations, 60,000 random seed). All classes were analyzed in GIS by comparing them to ground truth data and NDVI, and one class was selected that could correspond to gypsum (Figure 4). All obtained results are shown in Figure 4. In the background is the NDVI analysis based on the WV3 sensor. The red areas represent rocks, in this case field terrain marked gypsum. Green indicates vegetation. Blue polygons represent gypsum obtained through analysis of USGS data and the K-means algorithm. White dots are gypsum occurrences (ground truth data). Attached aerial photographs were obtained by an unmanned aerial vehicle (UAV), and gypsum occurrences are clearly visible as white outcrops.

4   Discussion

According to the OGK SFRJ, it is evident that gypsum is not particularly isolated, but it is found within the evaporite complex together with other types of rocks. There are two reasons for that. The first reason is the scale of the map (1:100,000), and the second is the submeter size of gypsum outcrops (Figure 4). Therefore, data digitization and machine learning were approached. Regarding purity, it has been investigated that outcrop in the Republic of Croatia contain 93–96% gypsum (Dedić 2018), while the USGS worked on samples containing 100% gypsum (Kokaly et al. 2017). Therefore, certain deviations are possible in the index processing, and for this reason the K-means algorithm was applied to further narrow down the
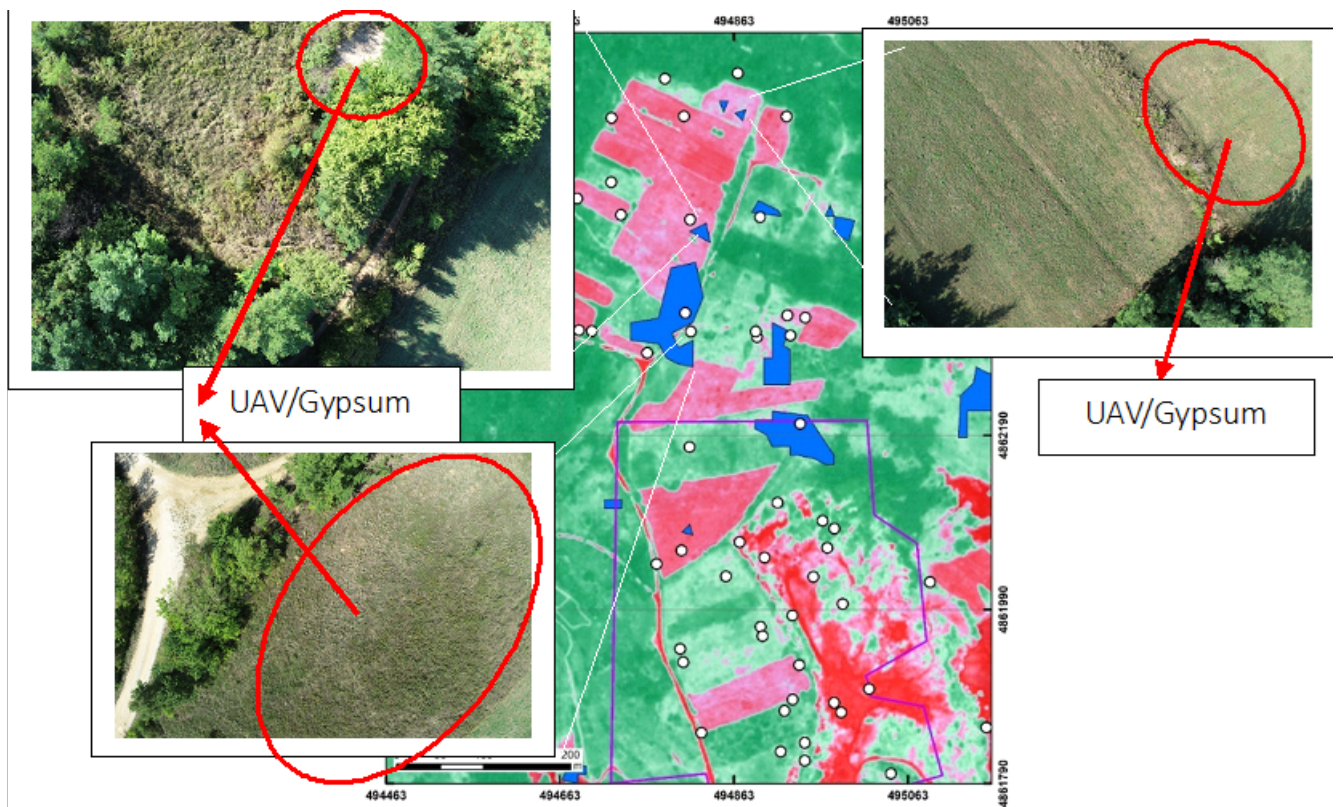
Figure 4. All obtained results; WV3-NDVI; MSI-S2A/USGS/K-means, GT, UAV/gypsum.

possible error. Among other authors who have conducted research on gypsum deposits in the territory of the Republic of Croatia are Šćavničar (1973), Šušnjara (1991), Tišljar (1992), Lukšić and Gabrić (1997), Gabrić et al. (2002), Lukšić and Pencinger (2004), and Dedić (2018). However, the potential of gypsum has not been fully defined regarding its spatial distribution. Therefore, remote sensing techniques were applied to attempt to define its surface potential, with the Vrlika karst polje area being taken as an example. Van der Meer et al. (2014) wrote about the potential of the Sentinel-2A sensor in geological research. They concluded that the results of processing these images support the geological model depicted on the geological map. On the other hand, Kruse and Perry (2013) wrote about the capabilities of the WV3 sensor in mineral mapping. The spectral bands of WV3 should enable the identification and mapping of essential minerals, while the enhanced spatial resolution will enhance the discrimination of intricate alteration mineral patterns. The promising results from WV3 suggest that this sensor will serve as a valuable tool for geological remote sensing.

5   Conclusions

Modern studies on gypsum deposition and sedimentary basins often involve a combination of field mapping, geochemical analysis, remote sensing, and geophysical methods. From the previous chapters, it is evident that research on gypsum in the Republic of Croatia has been continuous for the past 50 years. The obtained results certainly point to the continuation of research using the most modern methods of remote sensing and machine learning which have not been implemented so far. These results will be part of the methodological solutions that

integrate remote sensing with field and laboratory verification, improving the accuracy of assessing the geological potential of mineral raw materials in karst Dinarides, and carbonate terrains overall.

6   References

Bishop, J.L., Lane, M.D., Dyar, M.D., King, S.J., Brown, A.J., Swayze, G.A., 2014. What lurks in the Martian rocks and soil? Investigations of sulfates, phosphates, and perchlorates. Spectral properties of Ca-sulfates: gypsum, bassanite, and anhydrite. American Mineralogist 99 (10), 2105-2115.

Crowley, J.K., 1991. Visible and near-infrared (0.4–2.5 μm) reflectance spectra of playa evaporite minerals. Journal of Geophysical Research: Solid Earth 96 (B10), 16231-16240.

Dedić, Ž., 2018. Geokemijske i mineraloške karakteristike gornjopermskih evaporitnih sedimenata središnjeg dijela Dalmacije, PhD thesis, Faculty of Science, Zagreb.

Gabrić, A., Šinkovec, B., Sakač, K., Kuljak, G., 2002. Ležišta gipsa u Republici Hrvatskoj. Rudarsko -geološko -naftni zbornik 14, 21-36.

Hartigan, J.A., 1975. Clustering Algorithms, John Wiley & Sons Inc., New York.

Hartigan, J.A., Wong, M.A., 1979. Algorithm AS 136: A k-means clustering algorithm. Journal of the royal statistical society. series c (applied statistics) 28 (1), 100-108.

Howari, F.M., Acbas, G., Nazzal, Y., AlAydaroos, F., 2018. Hapke-based computational method to enable unmixing of

hyperspectral data of common salts. Chemistry Central Journal 12, 1-15.

Ivanović, A., Sikirica, V., Marković, S., Sakač, K., 1977. Osnovna geološka karta SFRJ. List Drniš, K 33-9, M 1:100.000. Institut za geološka istraživanja Zagreb. Izd. Savezni geološki zavod, Beograd.

Ivanović, A., Sikirica, V., Sakač, K., 1978. Tumač Osnovne geološke karte SFRJ za List Drniš, M 1:100.000. Institut za geološka istraživanja Zagreb. Izd. Savezni geološki zavod, Beograd.

Kokaly, R.F., Clark, R.N., Swayze, G.A., Livo, K.E., Hoefen, T.M., Pearson, N.C., Wise, R.A., Benzel, W.M., Lowers, H.A., Driscoll, R.L., ... 2017. USGS Spectral Library Version 7. US Geological Survey Data Series 1035, 61.

Kruse, F. A., Perry, S. L., 2013. Mineral mapping using simulated Worldview-3 short-wave-infrared imagery. Remote Sensing 5 (6), 2688-2703.

Lukšić, B., Gabrić, A., 1997. Studija potencijalnosti mineralnih sirovina šireg područja Vrlike. Fond struč. dok. IGI, Zagreb.

Lukšić, B., Pencinger, V., 2004. Geološka prospekcija gipsnih naslaga okolice Srba, Petrova polja i područja Vrlike. Fond struč. dok. IGI, Zagreb.

Rouse, J.W., Haas, R.H., Schell, J.A., Deering, D.W., 1974. Monitoring vegetation systems in the Great Plains with ERTS. NASA Spec. Publ 351 (1), 309.

Shuai, S., Zhang, Z., Lv, X., Hao, L., 2022. Assessment of new spectral indices and multi-seasonal ASTER data for gypsum mapping. Carbonates and Evaporites 7(2), 34.

Šćavničar, B., 1973. Kalupi kristala kamene soli (halita) u klastitima na području Vrlike i Knina (Dalmacija). Geološki vjesnik 16, 155-158.

Šušnjara, A., 1991. Geološka istraživanja evaporita i pratećih naslaga Dalmacije, Like i jugozapadne Bosne i Hercegovine. Fond struč. dok. IGI, Zagreb.

Tišljar, J., 1992. Origin and depositional enviroments of evaporitic and carbonate complex (upper permian) from the central part of the Dinarides (southern Croatia and western Bosnia). Geologia Croatica 45, 115-126.

Van der Meer, F. D., Van der Werff, H. M. A., Van Ruitenbeek, F. J. A., 2014. Potential of ESA's Sentinel-2 for geological applications. Remote sensing of environment 148, 124-133.

Warren, J. K., 2016. Evaporites: A geological compendium. Springer.

Wilson, C. C., Henry, P. F., Schmidtmann, M., Ting, V. P., Williams, E., Weller, M. T., 2014. Neutron powder diffraction–new opportunities in hydrogen location in molecular and materials structure. Crystallography reviews 20 (3), 162-206.

Development of Croatian Land Information System

Vladimir Jelavić[1], Delfa Radoš[1], Marina Kukavica[1,]*

[1] Ekonerg, Zagreb, Croatia, vjelavic@ekonerg.hr, drados@ekonerg.hr, mkukavica@ekonerg.hr
* corresponding author

Abstract: One of the main goals of the LIFE CROatian Land Information System (CROLIS) project is development of a harmonized land monitoring data model that enables integration and processing of Land Cover (LC), Land Use (LU) and land management data from different data sources (national spatial data and publicly available spatial data within the Copernicus mission and services) and its use for a variety of purposes such as Land Use, Land-Use Change and Forestry (LULUCF) reporting and accounting purposes in line with the requirements of international (United Nations Framework Convention on Climate Change, UNFCCC and Paris Agreement, PA) and EU legislation, robust basis for planning and implementation of Greenhouse Gas (GHG) mitigation actions in the land use sector, etc.

Within the project the LU conceptual model was created by the recommendations of European Environment Agency (EEA) when creating CLC+ layers while the LC conceptual model includes (in this early stage of development) a minimum of 6 LC categories identified using newly Object Based Image Analysis (OBIA) approach methodology. The newly developed methodology is applicable throughout the Republic of Croatia, where Accuracy Assessment is correlated with input vector data.

Keywords: Life CROLIS; LULUCF; LC; LU; OBIA.

1   Introduction

To meet the EU's goals of at least a 55% reduction in greenhouse gas emissions by 2030 and creating conditions for climate neutrality by 2050 and fulfilment of the LULUCF reporting requirements under the UNFCCC and PA (Penman et al. 2003), member countries need to establish a comprehensive national geographically explicit system for land monitoring by 2030. In response to the obligations, Croatia in close partnership with the Croatian land monitoring community that includes all authorities and major stakeholders concerned by the monitoring of Land Cover and Land Use changes launched the CROLIS project. One of the main achievements of the CROLIS project is development of a harmonized land monitoring data model which follows EAGLE concept (the goal of EAGLE is to provide tools for resolving ambiguities within nomenclature, and for comparisons and translations between different nomenclatures) that enables integration and processing of Land Cover (LC), Land Use (LU) and land management data from different data sources and its use for a variety of purposes. This new model will be designed by integrating the existing LC and LU information systems and data in Croatia in combination with freely available products (SPOT, Landsat, Aster and Sentinel-2 satellite imageries) and upcoming multi-temporal observations in order to be able to trace back and identify LC and LU changes. Layers for historical years will also be created within the project.

2   CROLIS Land Use Layer

CROLIS Land Use layer was created according to the principles of creating Corine Land Cover + (CLC+) layer. CLC+ layer is the next generation product within the CORINE (Coordination of Information on the Environment) Land Cover (CLC) product. CLC is a comprehensive, detailed, and harmonized dataset on the land cover and land use of the European continent created within COPERNICUS in 1980. CLC product offers a pan-European land cover and land use inventory with 44 thematic classes with new status and change layers updates for every six years (Büttner et al. 2021). In order to improve spatial resolution and separation of land cover from the land use, the EEA made recommendations for the creation of the CLC+ layer.

The CLC+ layer should represent the land use map of each country within the EU Copernicus Land Monitoring Service (CLMS). The basis for creating the CLC+ layer is the spatial data of the relevant national institutions which are categorized by EAGLE (Arnold et al. 2023) translation table. Spatial data are mapped in a raster format according to a hierarchical table of categories.

The CROLIS Land Use layer for the Republic of Croatia (Figure 1) was created based on the spatial data of Croatian Forests, the Paying Agency for Agriculture, Fisheries and
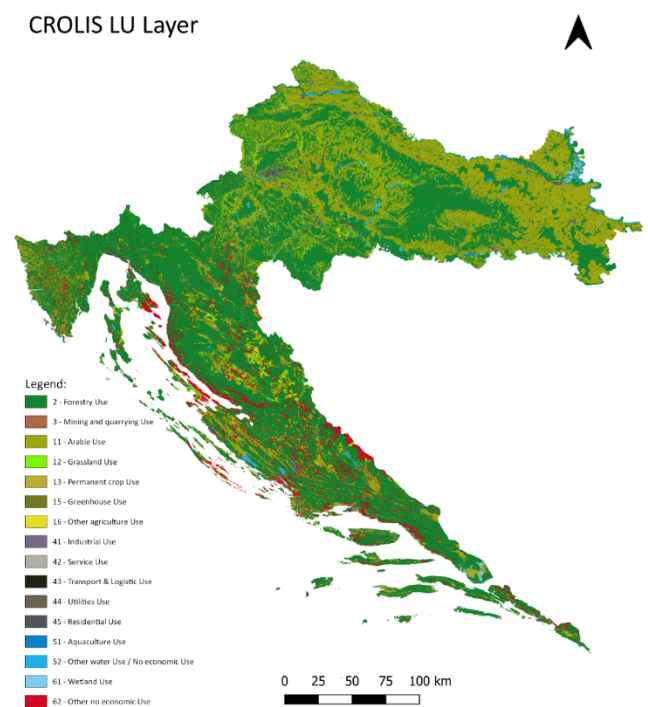
Figure 1. CROLIS LU Layer.

Rural Development, Croatian Roads, Croatian Waters, Croatian Railways, Croatian Highways, the State Geodetic Administration, the Ministry of Economy. The CROLIS LU layer consists of 6 Level-1 categories and 16 Level-2 categories. The hierarchical table proposed by the EEA was used to create the wall to wall CROLIS LU layer, and the spatial resolution of the final raster layer is 5m.

3 CROLIS Land Cover Layer

One of the main components of the CROLIS land information system is the Land Cover status layer, as well as a land cover layers for the historical period. Historical land cover layers will be created as a sample grid system.

At this stage of CROLIS development, the Land Cover status layer includes 6 LC categories: Woody surfaces, Crops surfaces divided into Annual Crops Surfaces and Perennial Crops Surfaces, Grassland Surfaces, Water Surfaces, Artificial Surfaces and Bare land Surfaces. Figure 2 shows the present state of the Land Cover Conceptual model. The final number of LC classes will be defined in cooperation with all project partners upon the implementation of all necessary activities (development of the layer for 2020 and implementation of sampling for the historical period) in the test areas.

Land cover status layer has been crated based on Object Based Image Analysis (OBIA). Object-based image analysis is a method for classifying satellite imagery by segmenting neighboring pixels into shapes with a meaningful representation of the objects. OBIA is usually performed in two steps: (1) image segmentation, and (2) classification. Image segmentation is defined as a method of dividing an image into homogeneous regions. Classification is the process of adding predefined categories to segments. Classification can be done based on threshold; it can be supervised (machine learning) as well as unsupervised (Blaschke 2010, Blaschke et al. 2014).

Input raster data for creating the LC status layer are:

- The digital state orthophoto map (DOF) in RGB and CIR production, official state map with the spatial resolution 0.5 m

- LIDAR nDSM. Normalized Digital Surface Model (nDSM) represents the relative height of natural (vegetation) and constructed (buildings, bridges, etc.) objects located on the Earth's surface in relation to the Earth's surface itself. nDSM is obtained as difference between Digital Surface Model (DSM) and Digital Terrain Model (DTM). NDSM created for the needs of the CROLIS project has spatial resolution 1 meter.
- Sentinel-2 satellite imageries with 13 bands in the visible, near infrared, and short-wave infrared part of the spectrum, spatial resolution of 10 m, 20m and 60m with revisit time 5 days.

In addition to raster data, national vector data from reference national institutions are also used to create the LC status layer.

Within preprocessing, from the raster bands DOF5 and Sentinel-2, corresponding radiometric spectral indices NDVI, NDWI, NDSI, NDBI, SAVI and EVI were made.

Normalized difference vegetation index (NDVI) is sensitive to vegetation greenness and is useful in understanding vegetation density and assessing changes in plant health. NDVI is calculated according to the formula (Gandhi et al. 2015):

$$NDVI = \frac{(NIR - R)}{(NIR + R)} \qquad (1)$$

Normalized Difference Water Index (NDWI) is sensitive to liquid water. NDWI is calculated according to the formula (Picoli et al. 2019):

$$NDWI = \frac{(G - NIR)}{(G + NIR)} \qquad (2)$$

Normalized Difference Soil Index (NDSI) is sensitive to soil moisture, organic matter content, and texture. NDSI is calculated according to the formula (Deng et al. 2015):

$$NDSI = \frac{(R - B)}{(R + B)} \qquad (3)$$

Normalized Difference Built-up Index (NDBI) is sensitive to artificial objects. NDBI is calculated according to the formula (Bhatti and Tripathi 2014):
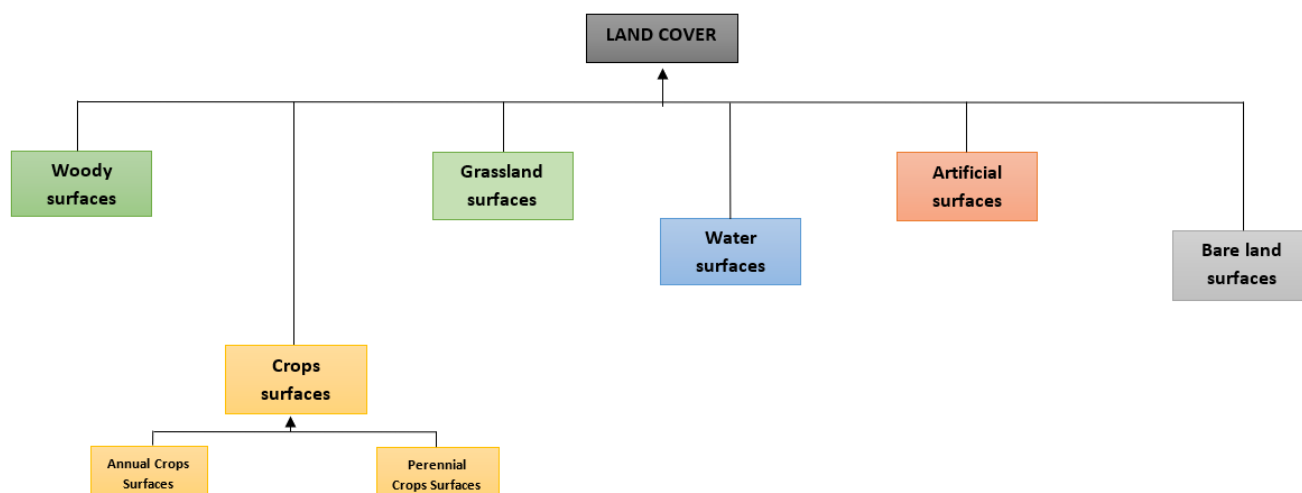
Figure 2. Land Cover Conceptual model.

$$NDBI = \frac{(SWIR - NIR)}{(SWIR + NIR)} \qquad (4)$$

The Soil-Adjusted Vegetation Index (SAVI) method is sensitive to vegetation. SAVI minimize soil brightness influences using a soil-brightness correction factor. SAVI is calculated according to the formula (Jiang et al. 2008):

$$SAVI = \frac{(NIR - R)}{(NIR + R + L)} * (1+L) \qquad (5)$$

Enhanced Vegetation Index (EVI) is sensitive to vegetation, especially in areas with dense vegetation. EVI is calculated according to the formula (Jiang et al. 2008):

$$EVI = 2.5 * \frac{(NIR - R)}{(NIR + 6R - 7.5B + 1)} \qquad (6)$$

In order to separate all the mentioned LC categories, a newly developed methodology has been implemented in the eCognition software. Firstly, the segmentation is performed in 2 steps with a smaller and larger scale parameter in order to separate all the segments well. Categories are assigned to segments based on threshold values and conditions of input data. After this step, there are still uncategorized segments. The categories of uncategorized segments will be assigned in the next step using machine learning classification. All categorized segments are then converted into training samples for machine learning models. Machine learning is performed

Vector Machine (SVM) algorithm with Radial basis function kernel (rbf) has been used to train the model. SVM is based on the linear classifier with the optimal margin in the feature space and thus the learning strategy is to maximize the margin, which can be transformed into a convex quadratic programming problem (Wang 2022). The result of the land cover classification in the test area Osijek is shown in Figure 3.

After the classification, the accuracy assessment was carried out on two test fields, the Istra test field and the Osijek test field. On the Istra test field, the kappa coefficient is 0.89, and the overall accuracy is 0.92, while on the Osijek test field, the kappa coefficient is 0.94, and the overall accuracy is 0.96. One of the main reasons for the difference in kappa coefficients is that the input ARKOD layer containing information of the categories Crops surfaces and Grassland surfaces is better defined for the test area Osijek.

4   Conclusions

The establishment of such a complex land system requires the involvement and participation of all national institutions. The CROLIS project is the first project of its kind that will include the EAGLE system and will be built in accordance with all recommendations for the creation of CLMS layers so that its final products can contribute to

Land cover categories:
- Crops Surfaces
- Artificial Surfaces
- Woody Surfaces
- Grassland Surfaces
- Water Surfaces
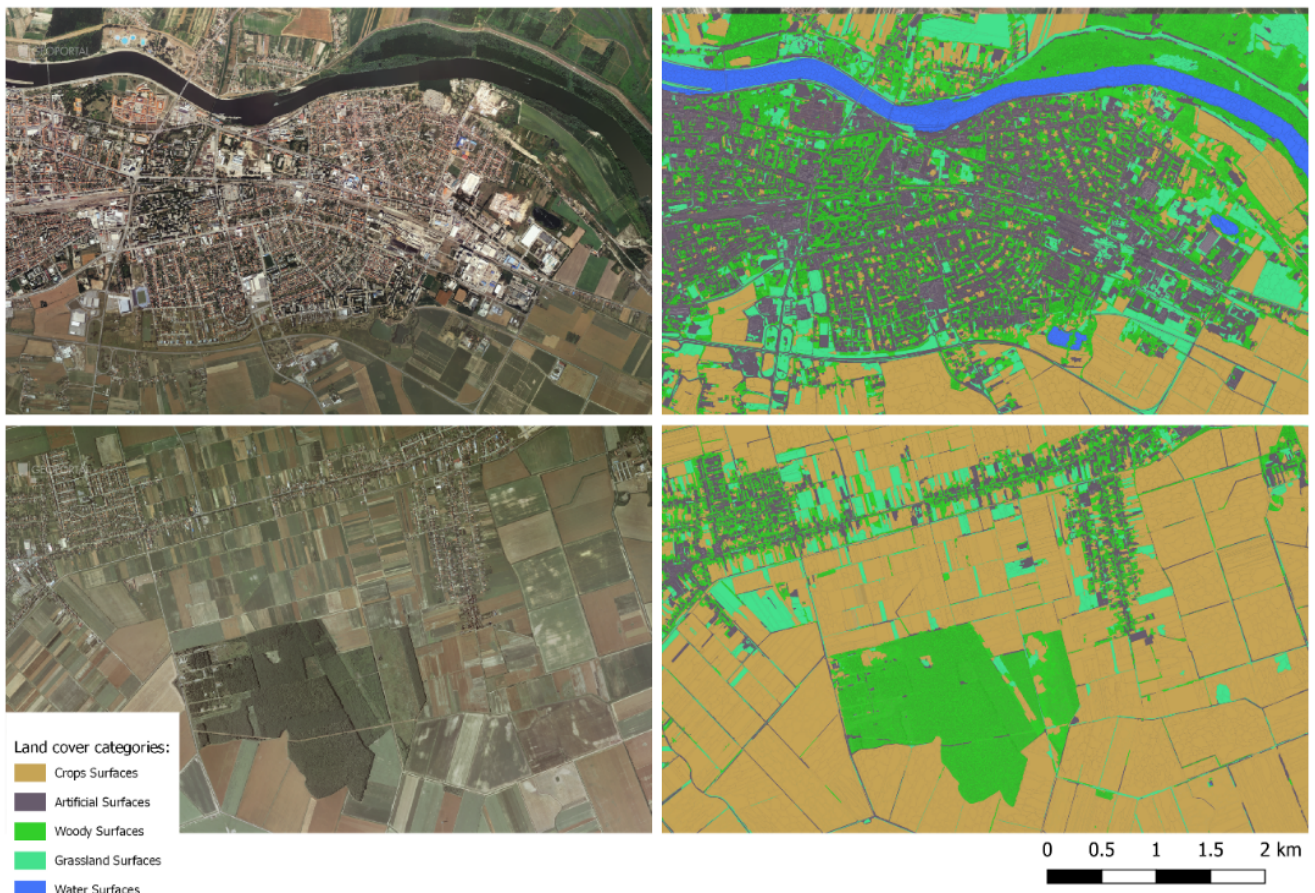
Figure 3. The result of the classification in the test area Osijek.

based on raster input data and its statistics, radiometric spectral indices, and geometric characterization of segments, such as relates to other segments. The Support

numerous fields. The newly developed land cover classification methodology is based on national raster and vector data, and for the first time, nDSM from Lidar

measurements for the whole of the Republic of Croatia has been used for land cover detection. Within the CROLIS project, the creation of an improved ARKOD+ layer is planned. Therefore, this is only the first version of the developed methodology for land cover detection and will be upgraded according to new input data and future needs that the system should meet.

5 References

Arnold, S., Kosztra, B., Banko, G., Milenov, P., Smith, G., Hazeu, G., Bock, M., Caetano, M., Perger, C., 2023. Explanatory Documentation of the EAGLE Concept, Eionet, EEA, Copenhagen.

Bhatti, S.S., Tripathi, N.K., 2014. Built-up area extraction using Landsat 8 OLI imagery, GIScience and remote sensing 51(4), 445-467.

Blaschke, T., Hay, G.J., Kelly, M., Lang, S., Hofmann, P., Addink, E., Tiede, D., 2014. Geographic object-based image analysis–towards a new paradigm, ISPRS journal of photogrammetry and remote sensing 87, 180-191.

Blaschke, T., 2010. Object based image analysis for remote sensing, ISPRS journal of photogrammetry and remote sensing 65 (1), 2-16.

Büttner, G., Kosztra, B., Maucha, G., Pataki, R., Kleeschulte, S., Hazeu, G., Vittek, M., Schröder, C., Littkopf, A., 2021. CORINE Land Cover Product User Manual, Copernicus Land Monitoring Service, CORINE Land Cover, EEA, Copenhagen.

Gandhi, G.M., Parthiban, S., Thummalu, N., Christy, A., 2015. NDVI: Vegetation change detection using remote sensing and GIS – A case study of Vellore District, Procedia computer science 57, 1199-1210.

Jiang, Z., Huete, A.R., Didan, K., Miura, T., 2008. Development of a two-band enhanced vegetation index without a blue band, Remote sensing of Environment 112 (10), 3833-3845.

Penman, J., Gytarsky, M., Hiraishi, T., Krug, T., Kruger, D., Pipatti, R., Wagner, F., 2003. Good practice guidance for land use, land-use change and forestry, IPCC National Greenhouse Gas Inventories Programme, Institute for Global Environmental Strategies, 2108-11, Kamiyamaguchi, Hayama, Kanagawa 240-0115, Japan.

Picoli, M., Machado, P., Duft, D., Scarpare, F., Corrêa, S., Hernandes, T., Rocha, J.V., 2019. Sugarcane drought detection through spectral indices derived modeling by remote-sensing techniques, Modeling Earth Systems and Environment 5 (4), 1679-1688.

Wang, Q., 2022. Support vector machine algorithm in machine learning, In 2022 IEEE International Conference on Artificial Intelligence and Computer Applications (ICAICA), 750-756.

PlanetScope Imagery-based Monitoring of Annual and Seasonal Dynamics of Lakes in Tbilisi, Georgia

*Mariam Tsitsagi[1, *], Zaza Gulashvili[1], Ana Palavandishvili[1]*

[1] Department of Physical Geography, TSU, Vakhushti Bagrationi Institute of Geography, Tbilisi, Georgia, mariam.tsitsagi@tsu.ge, zaza.gulashvili@tsu.ge, ana.palavandishvili@tsu.ge
* corresponding author

Abstract: Lakes have special aesthetic and recreational value in Tbilisi, especially in recent years, as the demand for residential areas near water bodies and the load on the surrounding landscapes have increased. Monitoring small-area water bodies requires high spatial and temporal resolution images. For more precise research, the PlanetScope imagery (3 m) provides excellent data. We recorded the annual and seasonal dynamics of the lake area extent of four lakes in Tbilisi using PlanetScope optical satellite images. The changes observed in the NDVI and NDWI based on the four-season images in ArcMap 10.8.2 for the period of 2017–2023 revealed an interesting trend. Despite the increasing severity of droughts in Tbilisi over the last 30 years, Turtle Lake, which is located hypsometrically high and surrounded by forest landscapes, is the most resistant to annual and seasonal changes. Didi and Patara Lakes, located in steppe landscapes, were particularly vulnerable to changes. Lisi Lake exhibited a similar trend. Changes in lakes located in steppe landscapes have a special seasonal character, and therefore, a noticeable decrease in water level coincides with the summer dry season (August-September). In addition to natural conditions, land use changes are also important. Active development is underway near these lakes. The alarming dynamics of the lake area extent of these lakes confirm that research is important in future conservation decisions for these lakes and their ecosystems.

Keywords: lakes; monitoring; RS; PlanetScope; Tbilisi

1 Introduction

Inland lakes are important sources of fresh water resources. In addition, urban lakes are given recreational value, and in addition to their aesthetic value for the city's population, they often perform alternative health functions. Urban lakes are affected by many factors. Along with climate change, stress is increased by industry and domestic consumption linked to the growth of the city's population and related urban processes.

Urban lakes are usually small in size and relatively vulnerable to lake area changes and eutrophication processes. In parallel with the development of remote sensing, many opportunities have appeared for monitoring lake ecosystems (Niroumand-Jadidi and Bovolo 2021) and the biophysical processes occurring within them (Worqlul et al. 2020, Pham-Duc 2024). For countries such as Georgia, the use of open access data has additional importance. For example, with the spatial expansion of Tbilisi, the capital of Georgia, the demand for new residential areas increased, and Tbilisi actively began to develop around the lakes in

the city (Tsitsagi et al. 2022). Unfortunately, data on the conditions of the lakes in Tbilisi is scarce and less accessible. Several aerial photographs were taken in Tbilisi in the past, but unfortunately, they were either panchromatic or in the visible spectrum. However, in parallel with the expansion and development of the city, we have significant statistical data that we will use in future urban planning.

The aim of this study was to determine the seasonal and annual changes in the extent of the lake area in Tbilisi using PlanetScope images.

2 Materials and methods

Tbilisi is located in eastern Georgia and is distinguished by its varied terrain, climate and landscapes. There are several natural and artificial lakes within Tbilisi. In a specific study, the following natural lakes in Tbilisi were considered: Didi Lake (Figure 1A), Patara Lake (Figure 1A), Lisi Lake (Figure 1B) and Turtle Lake (Figure 1C).
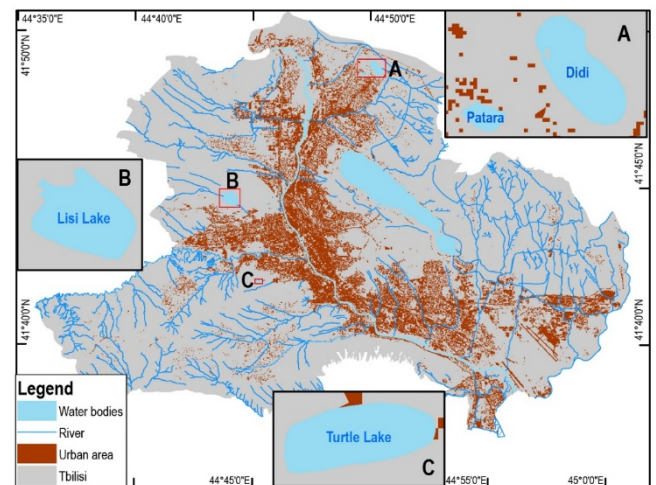
Figure 1. Study area, Tbilisi, Georgia.

Didi Lake (another name Gldani Lake) is located in the north of the city at 546 meters above sea level. The lake is mainly fed by rain and snowmelt water. The level of eutrophication in this region is quite high. There is also Patara lake nearby. Lisi Lake is located in the western part of the city 624 meters above sea level. Lisi Lake is fed by rain, snowmelt and underground water. The area around the lake is a popular place for city residents. Turtle Lake is located in the southern part of the city 686 meters above sea level. Turtle Lake is of landslide origin and is a favorite vacation spot for the population.

To estimate the seasonal and annual changes in the lake area extent, we used PlanetScope images orthoscenes that are geometrically corrected and scaled to surface-

reflectance radiance from the period 2017-2023. PlanetScope imagery has a spatial resolution of 3.7–4.1 m and is recorded in four bands (eight bands since March 2021) in VIS and NIR spectra (Qayyum et al. 2020). Figure 2 details the methodology used in the study. For the study, we selected cloudless images that included only one scene. To avoid bias, we created a mosaic of average monthly values from images of the appropriate detection quality for each month. PlanetScope has several limitations in addition to its high resolution, including limited access, image quality, short record, and lack of SWIR and TIR bands (Abderhalden et al. 2024).

Using selected scenes in ArcMap 10.8, we identified water based on the normalized difference vegetation index (NDVI) (equation 1), normalized difference water index (NDWI) (equation 2, which is one of the most widely used indices to classify water in satellite imagery (Huang et al. 2018)) and visual interpretation of each month's mosaic. The seasonal and annual changes in the lakes were determined using the obtained data. For the NDVI, the following thresholds were used: –1–0.25–water and >0.25–nonwater. For the NDWI, the following thresholds were used: < 0.3 - nonwater and >= 0.3 - water.

$$NDVI = \frac{B_4 - B_3}{B_4 + B_3} \qquad (1)$$

$$NDWI = \frac{B_2 - B_4}{B_2 + B_4} \qquad (2)$$

Where B4 is NIR, B3–red, B2–green bands of PlanetScope imagery.
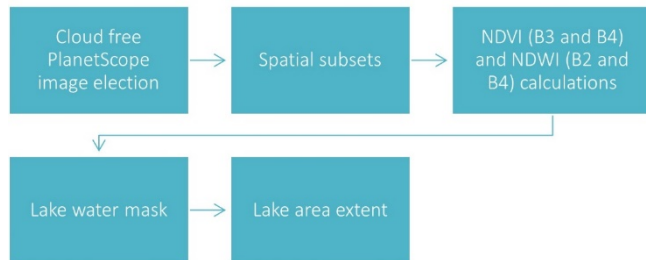
Figure 2. The methodology proposed in this study.

3 Results

According to the obtained results, the extent of lake area in Tbilisi changes according to season and year. Figure 3 shows that the average area of Big Lake was 31 ha in 2017, the average area of Small Lake was 2.8 ha, the average area of Lisi Lake was 42.6 ha, and the total area of Turtle Lake was 4 ha.

Figure 3 shows that these lakes are characterized by seasonal fluctuations. In the case of all four lakes, the low-water season coincided with late summer and early autumn (August–September), and the maximum area of the lakes occurred in late spring (May). It should be noted here that the seasonal fluctuations are most noticeable in the case of Great Lake and Lisi Lake, while in the case of the rest of the lakes, the seasonal changes are less noticeable.

Table 1 shows that the lake area changed during 2017–2023. Similar to the seasonal changes, the annual changes are more noticeable in the case of Didi Lake and Patara

Lake. The area of Didi Lake decreased from 31.03 ha (2017) to 27.3 ha (2023). The area of Lisi Lake also experienced significant changes, from 42.6 ha (2017) to 38.6 ha in 2023.
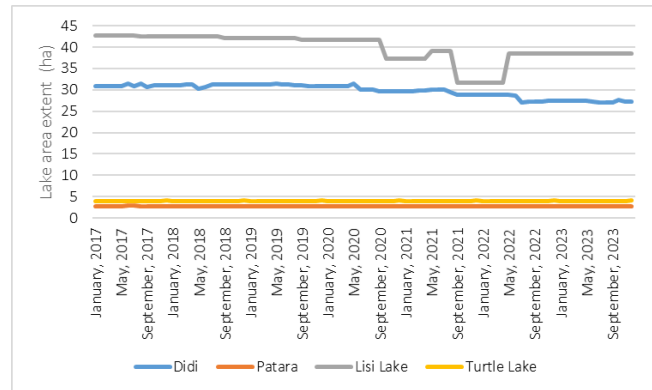
Figure 3. Lake area extent dynamic in 2017–2023 in Tbilisi.

In 2021, it even decreased to 36 ha. For Patara Lake and Turtle Lake, the lake area extent did not actually change during the research period.

Table 1. Lake area extent changes during 2017–2023.

Lake	Lake area extent (ha)						
	2017	2018	2019	2020	2021	2022	2023
Didi	31.04	31.09	31.11	30.27	29.50	28.01	27.27
Patara	2.8	2.69	2.68	2.70	2.71	2.72	2.72
Lisi	42.63	42.37	41.94	40.65	36.06	36.30	38.60
Turtle	4.02	4.18	4.02	4.02	4.02	4.02	4.02

4 Discussion

The purpose of this study was to analyze the seasonal and annual changes in the areas of natural lakes in Tbilisi. As the results showed, Didi Lake and Lisi Lake are the most vulnerable to environmental factors. In their case, we are dealing with the results of the combined effects of natural and anthropogenic factors. Both of them are located in the steppe landscape, and their surrounding areas are devoid of trees and mainly contain grass cover. Therefore, evaporation is high, which leads to the drying of shallow coastal areas. According to studies, the mentioned landscape is one of the most transformed within Tbilisi (Kharebava et al. 2024). Studies confirm that the temperature has increased in the last decade in Eastern Georgia (Elizbarashvili et al. 2017), and the intensity of drought is also increasing (Tatishvili et al. 2023), which in turn affects the loss of water in lakes.

The case of Lisi Lake is interesting. The results show that its area decreased sharply in 2021 (from 40.6 ha (2020) to 36 ha (2021)), and in 2023, its area slightly increased again to 38.6 ha. This is because the area around Lisi Lake is one of the fastest developing areas in Tbilisi, and the high demand for residential areas is caused by the presence of the lake; accordingly, lake restoration measures were planned. Given the lake's previously unsatisfactory water quality (Grim et al. 2010, Jaiani et al. 2013), it is imperative to begin restoration efforts.

An interesting precedent is Patara lake, which is located in the vicinity of Didi lake, but unlike it does not show sharp annual fluctuations. The reason is that it is relatively deep

with a weakly separated coastline. As for Turtle Lake, it is located hypsometrically higher and is surrounded by forest, which reduces evaporation and water loss.

5   Conclusions

Although PlanetScope has a limited number of spectral bands, using the combination of NDVI and NDWI is an effective method for detecting variations in the extent of lake areas. The analysis of seasonal and annual changes in the area of lakes in Tbilisi confirmed that along with the impact of natural factors, anthropogenic intervention is also important, both in a positive and negative context. For example, the decrease in the area of Lisi Lake by 6.5 ha was caused by active construction processes in addition to natural factors. After the restoration measures were implemented, the area of the lake increased by 2.3 ha. The use of open access PlanetScope data for monitoring urban lakes is an alternative for Georgia at this stage, as there is no access to higher resolution data, despite the limitations involved. For example, due to the high level of eutrophication in the Didi Lake, automatic water masking was difficult, and manual delineation was necessary in certain areas. Similar and more detailed studies will play an important role in monitoring urban lakes in Tbilisi and making recommendations for restoration works.

6   References

Abderhalden, J.M., Bly, K.K., Lappe, R., Andreassen, L.M., Rogozhina, I., 2024. Tracking rapid and slow ice-dammed lake changes through optical satellites and local knowledge – a case study of Tystigbreen in Norway. Journal of Glaciology.

Elizbarashvili, M., Elizbarashvili, E., Tatishvili, M., Elizbarashvili, S., Meskhia, R., Kutaladze, N., King, L., Keggenhoff, I., Khardziani, T., 2017. Georgian climate change under global warming conditions. Annals of Agrarian Science 15 (1), 17-25.

Grim, C. J., Jaiani, E., Whitehouse, C. A., Janelidze, N., Kokashvili, T., Tediashvili, M., Colwell, R. R., Huq, A., 2010. Detection of toxigenic Vibrio cholerae O1 in freshwater lakes of the former Soviet Republic of Georgia. Environmental Microbiology Reports 2 (1), 2-6.

Huang, C., Chen, Y., Zhang, S., Wu, J., 2018. Detecting, Extracting, and Monitoring Surface Water from Space Using Optical Sensors: A Review. Reviews of Geophysics 56.

Jaiani, E., Kokashvili, T., Mitaishvili, N., Elbakidze, T., Janelidze, N., Lashkhi, N., Kalandadze, R., Mikashavidze, E., Natroshvili, G., Whitehouse, C. A., Huq, A., Tediashvili, M., 2013. Microbial water quality of recreational lakes near Tbilisi, Georgia. Journal of Water and Health 11 (2), 333-345.

Kharebava, N., Nikolaishvili, D., Tsitsagi, M., 2024. Satellite-Based Analysis of Landscapes Transformation in Tbilisi, Georgia. Bulletin of the Georgian National Academy of Sciences 18 (1), 99-104

Niroumand-Jadidi, M., Bovolo, F., 2021. Water Quality Retrieval and Algal Bloom Detection Using High-Resolution Cubesat Imagery, in: ISPRS Annals of the Photogrammetry, Remote Sensing and Spatial Information Sciences.

Pham-Duc, B., 2024. comparison of multi-source satellite remote sensing observations for monitoring the variations of small lakes: a case study of Dai Lai Lake (Vietnam). Journal of Water and Climate Change 15.

Qayyum, N., Ghuffar, S., Ahmad, H.M., Yousaf, A., Shahid, I., 2020. Glacial lakes mapping using multi satellite PlanetScope imagery and deep learning. ISPRS International Journal of Geo-Information 9 (10).

Tatishvili, M., Palavandishvili, A., Tsitsagi, M., Suknidze, N., 2023. The Big Data for Drought Monitoring in Georgia, in: Springer Proceedings in Business and Economics.

Tsitsagi, M., Kharebava, N., Nikolaishvili, D., Kupatadze, I., Gadrani, L., 2022. Tbilisi Through Time. Georgian Geographical Journal 1 (1).

Worqlul, A.W., Ayana, E.K., Dile, Y.T., Moges, M.A., Dersseh, M.G., Tegegne, G., Kibret, S., 2020. Spatiotemporal Dynamics and Environmental Controlling Factors of the Lake Tana Water Hyacinth in Ethiopia. Remote Sensing 12 (17).

Monitoring of Helheim Glacier Dynamics Using the Open-Source High-Resolution Satellite Imagery

*Katarina Kolar[1], Fran Domazetović[2, *], Lovre Panđa[2], Rina Milošević[3]*

[1] Independent researcher; kata.kolar10@gmail.com

[2] University of Zadar, Center for geospatial technologies, Department of Geography, Trg kneza Višeslava 9, Zadar, Croatia; fdomazeto@unizd.hr, lpanda@unizd.hr

[3] University of Zadar, Center for geospatial technologies, Department of Ecology, Agronomy and Aquaculture, Trg kneza Višeslava 9, Zadar, Croatia; rmilosevi@unizd.hr

* corresponding author

Abstract: In recent years, climate change-driven pressures have been causing accelerated ice loss on the Greenland Ice Sheet, leading to the gradual seal level rise. Monitoring of spatio-temporal changes (STCs) created by ice melt and calving is essential for comprehending present glacial dynamics, as well as for the forecasting of future trends. In this study, we investigate the suitability of open-source high-resolution (HR) satellite imagery from various satellite constellations for monitoring and quantifying of multi-year glacial dynamics. Monitoring of glacial dynamics was applied for a multi-year period (2010–2023) over the Helheim Glacier, one of the largest outlet glaciers of the Greenland Ice Sheet. Multi-year STCs at the Helheim Glacier were determined using the open-source satellite imagery provided by Google Earth Engine (2010–2016) and the Planet constellation (2016–2023). To determine multi-year glacier dynamics, the terminus of the Helheim Glacier was extracted from available satellite imagery. Intensity of linear and areal STCs was calculated for each extracted glacier terminus using the Digital shoreline analysis system (DSAS) extension for ArcGIS 10.1. Available HR open-source satellite imagery has provided insights into the multi-year glacial dynamics of the Helheim Glacier. Although determined multi-year glacier dynamics are highly variable, prominent trend of accelerated retreat at Helheim Glacier was observed for analysed timeframe.

Keywords: glacial dynamics; Helheim; remote sensing; climate change; PlanetScope.

1 Introduction

The Greenland Ice Sheet is experiencing accelerated ice melting and calving due to intensified climate change and gradual sea level rise (Jiang et al. 2020, Box et al. 2022). Monitoring of spatio-temporal changes (STCs) related to the ice melt and calving is crucial for understanding present glacial dynamics and forecasting future trends (Evans et al. 2022). Satellite imagery is emerging as practical and accurate method for monitoring glacial dynamics over large and remote areas (Otosaka et al. 2023). Despite the widespread utilization of open-source imagery with medium spatial resolution (e.g. Landsat or Sentinel), application of high-resolution (HR) satellite imagery remains limited (MacGregor et al. 2020). Therefore, in this study we investigate the suitability of open-source HR satellite imagery from various satellite constellations for monitoring and quantifying of multi-year glacial dynamics.

2 Materials and methods

Monitoring of glacial dynamics was applied for a multi-year period (2010–2023) over the Helheim Glacier (Figure 1B), one of the largest outlet glaciers of the Greenland Ice Sheet (Figure 1A). Several earlier studies have reported intensive retreat of Helheim Glacier (Holland et al. 2016, Stevens et al. 2022).
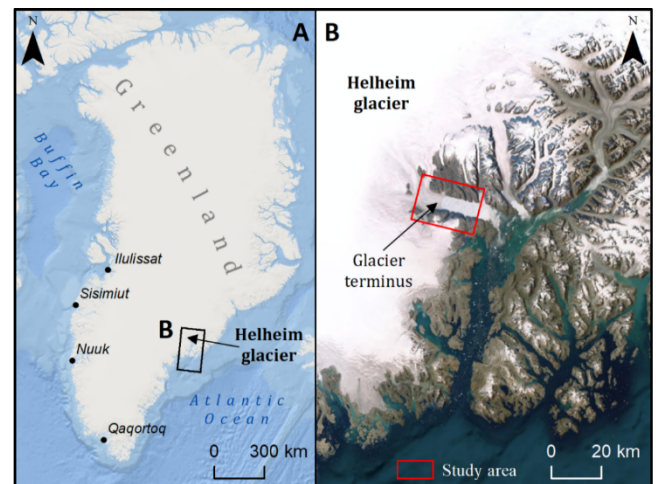
Figure 1. Study area covering Helheim Glacier (Greenland).

Open-source satellite imagery was obtained from two sources, Google Earth Engine (2010–2016) and PlanetScope (2016–2023) (Figure 2).

Satellite imagery covering the Helheim Glacier, acquired through Google Earth Engine, represents HR imagery collected by commercial satellites on various dates, spanning from May 2010 to August 2016. These RGB satellite images were georeferenced (Affine transformation), utilizing multiple tie points situated on hard rock surfaces located outside the dynamic areas of the glacier. Since 2016, multispectral HR imagery collected by the PlanetScope constellation has been available for the Helheim Glacier, with data available for nearly every day.
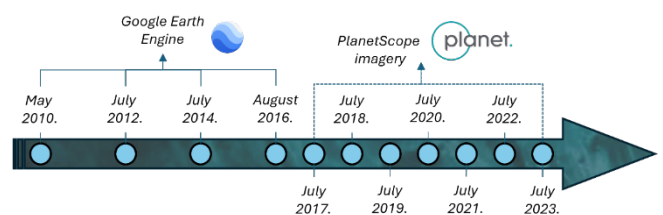
Figure 2. Open-source high-resolution satellite imagery used for analysis of multi-year glacier dynamics (2010–2023).

Thus, HR PlanetScope images with no cloud cover were acquired for each year in the period between 2016 and 2023.

The glacier terminus was manually vectorized at a scale of 1:3000 from each acquired HR satellite image, spanning from 2010. to 2023. To aid manual vectorization, the Normalized Difference Glacier Index (NDGI) was calculated based on each multispectral PlanetScope image using the following equation (1).

$$NDGI = \frac{B_{Green} - B_{NIR}}{B_{Green} + B_{NIR}} \qquad (1)$$

The displacement of the glacier terminus, i.e., glacier advance or retreat, was analyzed using the Digital Shoreline Analysis System (DSAS) extension for ArcGIS 10.1. DSAS allows comparison of line features and calculation of several metrics related to linear STCs (Peppa et al. 2020). Spacing length of transects within DSAS was set to 50 meters, thus enabling the measurement of linear displacement at each 50-meter interval along the entire length of the terminus. In total around 110 transects were used to calculate linear STCs within each mapped terminus. Along with linear STCs, detection of multi-year areal STCs was also performed.

3   Results

The intensity of the detected multi-year linear movement of the glacier terminus is characterized by very high interannual variability and interchange of retreat and advancement phases (Figure 3, Figure 4).

Several phases of intensive glacier retreat can be identified from the detected linear STCs, with average linear retreat ranging from 0.85 km (2010–2012) up to 1.95 km (2019–2020). Maximum retreat of glacier terminus was detected in period between 2018 and 2019, with linear retreat of over 3.5 km. Intensive glacier retreat was in general followed by advancement of terminus in next analyzed period (e.g. 2012–2014, 2017–2018, 2019–2020, 2020–2021, 2022–2023). However, in general the intensity of this advancement was lower than the preceding retreat, ranging from 0.21 km up to 0.82 km. The only exception is the last analyzed period (2022–2023), when a very strong progression was detected, with an average linear
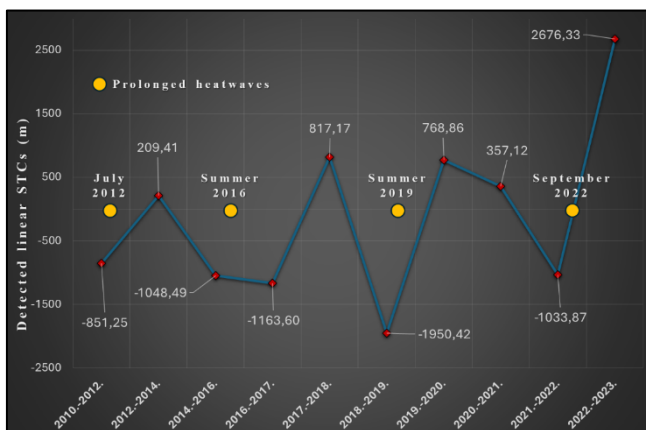
Figure 3. Comparison between intensity of average linear multi-year STCs and occurrence of prolonged heatwaves.

advancement of 2.68 km. Occurrence of such rapid advancement could potentially lead to the very intensive calving and glacier retreat in the following few years.

It should be noted that glacier retreat is more dominant, as within the whole studied period (2010–2023) glacier terminus has retreated for 1.22 km.
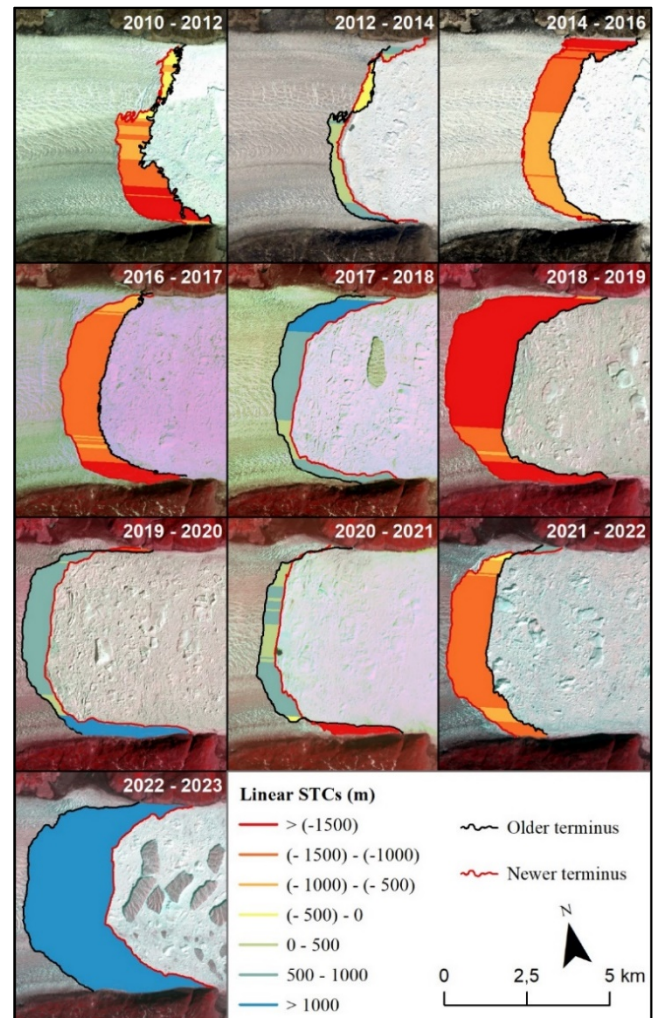
Figure 4. Detected multi-year linear movement of the glacier terminus.

Detected multi-year areal STCs further corroborate the gradual predominant retreat of Helheim Glacier (Figure 5). In overall, Helheim Glacier has retreated for about 6.25 km² within the studied period, thus confirming the predominant ice melt and ice loss. Besides detection of multi-temporal areal STCs, analyzed satellite imagery has allowed detection of large icebergs, formed by gradual calving from glacier terminus (Figure 5).

4   Discussion

Open-source satellite imagery proved to be a good basis for detailed detection of complex glacial dynamics, both in terms of linear and areal STCs. Multispectral HR imagery from PlanetScope constellation has especially great potential for monitoring of glacial dynamics, as it features (1) spectral bands required for easier detection of ice, (2) high spatial resolution required for detection of STCs and (3) daily temporal resolution. The daily temporal resolution

enables the detection of multi-year STCs within such remote areas with frequent cloud and snow cover.
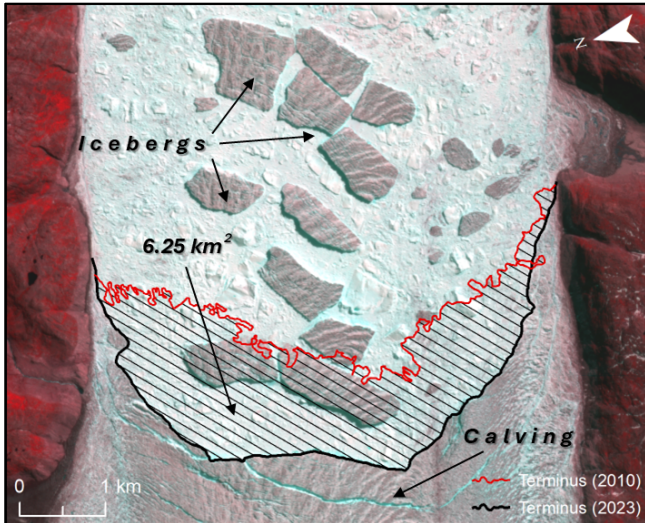
Figure 5. Aerial STCs detected at Helheim Glacier within the whole analyzed time-frame (2010–2023).

Multi-year glacial dynamics detected from open-source satellite imagery corresponds to the results of earlier research (Holland et al. 2016, Stevens et al. 2022). The detected variability in multi-year glacial dynamics can be attributed to the occurrence of prolonged heatwaves, which have been identified as the main cause of ice cover reduction (Neff et al. 2014, Bonne et al. 2015, Tedesco and Fettweis 2020, Jiang et al. 2020). Furthermore, previous research has shown that beside multi-year variability, glacial dynamics at Helheim glacier are also characterized by intensive seasonal variability (Kehrl et al. 2017). Therefore, in future research, we plan to investigate the link between heatwaves and seasonal glacial dynamics in more detail.

5   Conclusions

Carried research has demonstrated that open-source HR satellite imagery has great potential for monitoring of complex glacial dynamics over large and remote areas. Due to the combination of high spectral, temporal and spatial resolution, imagery from PlanetScope constellation has proven particularly effective for detection and quantification of glacial dynamics. Therefore, such open-source HR satellite imagery could be used for monitoring of multi-year and seasonal glacial dynamics over other glaciers of the Greenland Ice Sheet and other parts of the World.

6   References

Bonne, J. L., Steen-Larsen, H. C., Risi, C., Werner, M., Sodemann, H., Lacour, J. L., ... Masson-Delmotte, V., 2015. The summer 2012 Greenland heat wave: In situ and remote sensing observations of water vapor isotopic composition during an atmospheric river event. Journal of Geophysical Research: Atmospheres 120 (7), 2970-2989.

Box, J. E., Hubbard, A., Bahr, D. B., Colgan, W. T., Fettweis, X., Mankoff, K. D., ... Fausto, R. S., 2022. Greenland ice sheet climate disequilibrium and committed sea-level rise. Nature Climate Change 12 (9), 808-813.

Evans, E., Fraser, A. D., Cook, S., Coleman, R., Joughin, I., 2022. An observation-based approach to calculating ice-shelf calving mass flux. Remote Sensing of Environment 272, 112918.

Holland, D. M., Voytenko, D., Christianson, K., Dixon, T. H., Mei, M. J., Parizek, B. R., ... Holland, D., 2016. An intensive observation of calving at Helheim Glacier, East Greenland. Oceanography (Washington, DC) 29 (4), 46.

Jiang, S., Ye, A., Xiao, C., 2020. The temperature increase in Greenland has accelerated in the past five years. Global and planetary change 194, 103297.

Kehrl, L. M., Joughin, I., Shean, D. E., Floricioiu, D., Krieger, L., 2017. Seasonal and interannual variabilities in terminus position, glacier velocity, and surface elevation at Helheim and Kangerlussuaq Glaciers from 2008 to 2016. Journal of Geophysical Research: Earth Surface 122 (9), 1635-1652.

MacGregor, J. A., Fahnestock, M. A., Colgan, W. T., Larsen, N. K., Kjeldsen, K. K., Welker, J. M., 2020. The age of surface-exposed ice along the northern margin of the Greenland Ice Sheet. Journal of Glaciology 66 (258), 667-684.

Neff, W., Compo, G. P., Martin Ralph, F., Shupe, M. D., 2014. Continental heat anomalies and the extreme melting of the Greenland ice surface in 2012 and 1889. Journal of Geophysical Research: Atmospheres 119 (11), 6520-6536.

Otosaka, I. N., Horwath, M., Mottram, R., Nowicki, S., 2023. Mass balances of the Antarctic and Greenland ice sheets monitored from space. Surveys in Geophysics 44 (5), 1615-1652.

Peppa, M. V., Maharjan, S. B., Joshi, S. P., Xiao, W., Mills, J. P., 2020. Glacial Lake evolution based on remote sensing time series: A case study of Tsho Rolpa in Nepal. ISPRS Annals of the Photogrammetry, Remote Sensing and Spatial Information Sciences 3, 633-639.

Stevens, L. A., Nettles, M., Davis, J. L., Creyts, T. T., Kingslake, J., Ahlstrøm, A. P., Larsen, T. B., 2022. Helheim Glacier diurnal velocity fluctuations driven by surface melt forcing. Journal of Glaciology 68 (267), 77-89.

Tedesco, M., Fettweis, X., 2020. Unprecedented atmospheric conditions (1948–2019) drive the 2019 exceptional melting season over the Greenland ice sheet. The Cryosphere 14 (4), 1209-1223.

The Relationship between Air Pollution and Sea Surface Temperature Anomalies in the Northern Adriatic Sea

Luka Mamić[1,3,]*, Matea Tomić[2]

[1] Department of Civil, Building and Environmental Engineering, Sapienza University of Rome, Rome, Italy, luka.mamic@uniroma1.it

[2] Department of Geomatics, Faculty of Science and Technology (RealTek), Norwegian University of Life Sciences (NMBU), N-1432 Ås, Norway, matea.tomic@nmbu.no

[3] Interdepartmental Research Center of Geomatics (CIRGEO), University of Padua, Padua, Italy

* corresponding author

Abstract: Air pollution emissions are recognised as a significant climate driver contributing to global warming and its multiple impacts. A key consequence is sea-level rise, which is largely driven by increased air and sea temperatures. This study examines trends and spatial correlations of sea surface temperature (SST) and air pollutants in the Northern Adriatic Sea from 2019 to 2022 using publicly available multi-satellite data. The Advanced Very-High-Resolution Radiometer (AVHRR) data were used to calculate SST anomalies, while TROPOspheric Monitoring Instrument (TROPOMI) and the Copernicus Atmospheric Monitoring Service (CAMS) data provided insights into air pollution. Trend analysis revealed a significant increase in SST of about 0.6 °C/yr. Spatial correlation analysis revealed strong positive correlations between SST anomalies and air pollutants in the Rijeka Bay. These results highlight the intertwined nature of air pollution and SST anomalies influenced by climate change and anthropogenic activities.

Keywords: sea surface temperature; Adriatic Sea; air pollution; climate change.

1   Introduction

In the recent years, the natural balance of the Earth's climate system has mainly been disrupted by the excessive accumulation of human-induced greenhouse gases, contributing to the increased mean temperature of the Earth. Covering about three quarters of the Earth's surface, the world's oceans are storing an estimated 91 percent of the excess heat energy trapped in the Earth's climate system by greenhouse gases (NOAA 2024). Accumulation of the heat, which is going faster in the upper layers of the ocean than in the bottom layers, is causing the thermal expansion of the ocean, which is, together with ice-mass loss, one of the main contributors of the sea level rise (Cazenave and Cozannet 2014). Therefore, Global Climate Observing System (GCOS) defines SST as one of the essential climate variables (ECV), since sea surface is a boundary between the ocean and the atmosphere. Thus, SST plays a key role in regulating climate, responds to its natural variability and human-driven climate changes (Pisano et al. 2020).

Human-driven climate change, which has been mostly caused by the excessive burning of fossil fuels over the past 150 years, has drastically changed the air quality. Key air pollutants with large impacts on public health (Lave and Seskin 2013) and the environment (Saurabh Sonwani and Vandana Maurya 2019) are, among others, surface ozone (O_3), nitrogen dioxide (NO_2), carbon monoxide (CO), and particulate matter (PM). Increase in temperature can lead to degraded air quality and extreme pollution events (Fiore et al. 2015).

To date, several studies have assessed the SST variations in the Adriatic Sea (Pisano et al. 2020, Bonacci et al. 2021, García-Monteiro et al. 2022) to investigate long-term and seasonal variability, as well as the impact of the air pollutants from nearby ports in the Adriatic Sea on the air quality (Vilke et al. 2022, Mei et al. 2023), but none of them has addressed dependence of air pollution on SST.

Thus, this is the first study to undertake the investigation of the connection between the air pollution variability and the SST in the Northern Adriatic Sea which is chosen as the area of interest because it is directly connected to a European hotspot for air pollution, the Po Valley (Lonati and Riva 2021). In addition, the largest ports of the Adriatic Sea are in its northern part: Trieste (Italy), Venice (Italy), Koper (Slovenia) and Rijeka (Croatia). This also contributes to the increased levels of air pollution, since the port transport sector increases pollutant emissions (Vilke et al. 2022, Owusu-Mfum et al. 2023). Therefore, the main objective of this study is to perform the long-term analysis of SST, SST anomalies and different air pollutants (CO, NO_2, surface O_3, PM_{10} and dust), as well as their spatial and temporal variability to determine the possible dependency between the two variables.

2   Materials and methods

2.1   Study area

The Northern Adriatic Sea includes the coastal regions of north-eastern Italy, western Slovenia, and western Croatia. Italy's longest river, the Po, flows into the Adriatic Sea near Venice. Its valley, surrounded by the Alps to the north and the Apennines to the south, acts as a natural basin, creating a microclimate that often traps pollutants. This, in combination with the high density of people, agriculture, traffic and industry often result in high levels of air pollutants (Lonati and Riva 2021).

2.2   Used datasets

The National Oceanic and Atmospheric Administration's (NOAA) AVHRR instrument provides SST data with high spatial (4 km) and temporal (twice a day) resolution. Sentinel-5P is the first Copernicus mission with the primary objective of monitoring the Earth's atmosphere. It is

equipped with the TROPOMI spectrometer providing atmospheric measurements related to air quality daily. CAMS is dedicated to providing numerous global and regional information on air quality. SST and TROPOMI data were collected by the Google Earth Engine (GEE), while CAMS data was downloaded from CAMS Atmosphere Data Store. A short description of each analyzed pollutant is given in Table 1.

2.3 Methodology

The best quality daily SST data were downloaded for the period 1982-2022. Data from 1982-2015 were used to calculate mean monthly SST reference values. SST values from 2019 to 2022 are then subtracted from the reference SST to obtain SST anomalies. Used TROPOMI data are L3 offline data from GEE already pre-processed for quality, covering the period from 2019 to 2022. AVHRR and TROPOMI data have been resampled to match the spatial resolution of CAMS data by averaging within pixels. CAMS data are derived from European air quality forecasts, validated against in situ observations, and cover the period from the end of June 2020 to 2022. All values in the dataset outside the three medians of the mean absolute deviation (MAD) were defined as outliers and removed. Monthly mean values were calculated to plot time-series graphs, providing insights into long-term trends and seasonal patterns. The Pearson correlation coefficient of each pollutant with SST anomalies was calculated with a significance level of $p < 0.05$ for all 10 km pixels in the study area. In addition, the Inverse Distance Weighting (IDW) spatial interpolation was used to fill-in the missing values and obtain a continuous correlation maps.

Figure 1. Average SST anomalies (2019-2022) over the study area. Blue dots represent cities with largest ports in the study area.

3.1 Time-series plots

Time-series graphs of monthly SST, SST anomalies and selected air pollutants are shown in Figure 2, together with their trend lines.
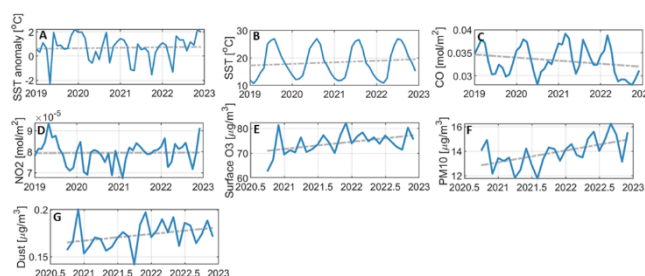
Figure 2. Time series of: a) SST anomaly, b) SST, c) CO, d) NO2, e) surface O3, f) PM10, g) dust in the study area.

Table 1. Air pollutants analyzed in this study.

N.	Pollutant	Description	Source	Temporal resolution	Spatial resolution	Units
1	CO	Total vertical column of CO	TROPOMI	daily	1.132 km	mol/m^2
2	NO$_2$	Total vertical column of NO$_2$	TROPOMI	daily	1.132 km	mol/m^2
3	Dust	Fraction in PM$_{10}$	CAMS	hourly	10 km	µg/m^3
4	Surface O$_3$	O$_3$ concentration at ground level	CAMS	hourly	10 km	µg/m^3
5	PM$_{10}$	Concentration of PM smaller than 10 micrometres in diameter	CAMS	hourly	10 km	µg/m^3

3 Results

Mean SST anomalies over the observed period are shown in Figure 1.

3.2 Spatial correlation plots

The relationship between air pollutants and SST anomalies is shown in Figure 3 expressed as the Pearson correlation coefficient for each pixel in the study area.
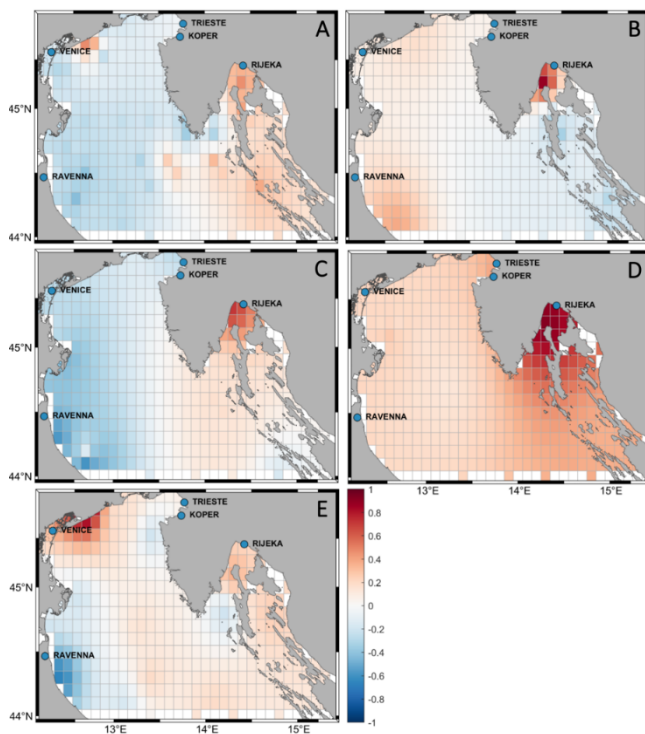
Figure 3. Pearson correlation coefficients (p < 0.05) with SST anomalies of: a) CO, b) NO_2, c) surface O_3, d) PM_{10} and e) dust over the study area.

4 Discussion and summary

4.1 Trend analysis

Time-series graphs from 2019 to 2022 for SST and TROPOMI variables, and from June 2020 to 2022 for CAMS variables, shown in Figure 2, provide insight into their trends and seasonal patterns. The SST in the study area has a strong regular seasonal pattern with an increasing trend of about 0.6 °C/yr, while García-Monteiro et al. (2022) estimated the average annual increase of SST in the entire Adriatic Sea from 2003 to 2019 to be about 0.1 °C/yr. The observed SST anomalies in our study also have a specific seasonality, where negative anomalies are observed in spring or autumn months, while the strongest positive anomalies are observed in winter and summer months. On the other hand, TROPOMI gives us an insight into the CO and NO_2 trends in our study area, and while CO has a strong negative trend in the observed period, the NO_2 trend remains the same over the years. There is a significant decrease in NO_2 levels in 2020, which may be related to the COVID-19 lockdown at that time, as reported in other studies (Tonion and Pirotti 2022). CAMS data for surface O_3, PM_{10} and dust show strong positive trends for all three pollutants, indicating that air pollution is a growing challenge in the Northern Adriatic Sea.

4.2 Spatial correlation analysis

Correlation maps between air pollutants and SST anomalies in the study area (Figure 3) provide information about their change on a spatial scale. CO shows medium positive correlations around the urban areas of Venice and Rijeka, and low positive correlations along the east coast and islands. On the other hand, NO_2 shows strong positive

correlations in the Rijeka Bay. Marine traffic, including shipping and cruise ships, is reported as a source of NO_2 in port cities and coastal areas (Owusu-Mfum et al. 2023). Ground level O_3 is also an increasing pollutant in coastal urban areas (Pan et al. 2017), and increased concentration of O_3 is strongly connected with increase in SST in the Rijeka Bay, while negative correlations are distributed along the west coast. Another important pollutant in coastal areas, as reported by Owusu-Mfum et al. (2023), is PM_{10}, which has only positive correlations with SST anomalies in the study area. Again, the strongest correlations are observed in the Rijeka Bay. Although dust pollution is related to PM_{10}, it has a different relationship with SST anomalies in our study area, where the highest positive correlations are found around Venice, while stronger negative correlations are found in the urban area south of Ravenna, like O_3. Strong connection between increased levels of air pollutants and increase in SST can be explained by the fact that the Rijeka Bay is a semi-enclosed coastal area, where sea currents are west-northwest (WNW) directed (Domian et al. 2005).

This study set out to examine trends and spatial relationships between the change in SST and levels of different air pollutants in the North Adriatic Sea. Based on the presented results, it is found that the strongest correlation between SST anomalies and air pollution is found in the Rijeka Bay, because of its specific location. However, future studies should investigate non-linear correlations between SST anomalies and air pollution, and put a greater focus on other influencing variables which can have impact on observed parameters in this study (e.g. sea currents or wind patterns). Policy makers should use these findings to develop strategies to reduce air pollution and address climate change impacts in the region.

5 References

Barale, V., Schiller, C., Villacastin, C., Tacchi, R., 2004. The Adriatic Sea surface temperature historical record from advanced very High Resolution Radiometer data (1981–1999). International Journal of Remote Sensing 25 (7-8), 1363-1370.

Bonacci, O., Bonacci, D., Patekar, M., Pola, M., 2021. Increasing Trends in Air and Sea Surface Temperature in the Central Adriatic Sea (Croatia). Journal of Marine Science and Engineering 9 (4), 358.

Cazenave, A., Cozannet, G.L., 2014. Sea level rise and its coastal impacts. Earth's Future 2, 15-34.

Domijan, N., Mihanović, H., Leder, N., Gržetić, Z., 2005. Harmonička i spektralna analiza morskih struja u sjevernom dijelu Riječkog zaljeva. Pomorski zbornik 43 (1), 193-205.

Fiore, A. M., Naik, V., Leibensperger, E. M., 2015. Air Quality and Climate Connections. Journal of the Air & Waste Management Association 65 (6), 645-685.

García-Monteiro, S., Sobrino, J. A., Julien, Y., Sòria, G., Skokovic, D., 2022. Surface Temperature trends in the

Mediterranean Sea from MODIS data during years 2003–2019. Regional Studies in Marine Science 49, 102086.

Lave, L. B., Seskin, E. P., 2013. Air pollution and human health. RFF press.

Lonati, G., Riva, F., 2021. Regional Scale Impact of the COVID-19 Lockdown on Air Quality: Gaseous Pollutants in the Po Valley, Northern Italy. Atmosphere 12 (2), 264.

Mei, F., Renzi, M., Bonifazi, M., … 2023. Long-term effects of air pollutants on respiratory and cardiovascular mortality in a port city along the Adriatic sea. BMC Pulm Med 23, 395.

NOAA, 2024. Climate change: Ocean heat content, https://www.climate.gov/news-features/understanding-climate/climate-change-ocean-heat-content (Accessed 18 May, 2024)

Owusu-Mfum, S., Hudson, M. D., Osborne, P. E., Roberts, T. J., Zapata-Restrepo, L. M., Williams, I. D., 2023. Atmospheric pollution in port cities. Atmosphere 14 (7), 1135.

Pan, S., Choi, Y., Jeon, W., Roy, A., Westenbarger, D. A., Kim, H. C., 2017. Impact of high-resolution sea surface temperature, emission spikes and wind on simulated surface ozone in Houston, Texas during a high ozone episode. Atmospheric environment 152, 362-376.

Pisano, A., Marullo, S., Artale, V., Falcini, F., Yang, C., Leonelli, F. E., Santoleri, R., Buongiorno Nardelli, B., 2020. New Evidence of Mediterranean Climate Change and Variability from Sea Surface Temperature Observations. Remote Sensing 12 (1), 132.

Saurabh Sonwani, S. S., Vandana Maurya, V. M., 2019. Impact of air pollution on the environment and economy. In: Air pollution: Sources, impacts and controls. Wallingford UK: CAB International, pp. 113-134.

Tonion, F., Pirotti, F., 2022. SENTINEL-5P NO2 data: Cross-validation and comparison with ground measurements. In: The International Archives of the Photogrammetry, Remote Sensing and Spatial Information Sciences. pp. 749-756.

Vilke, S., Tadić, F., Ćelić, J., Debelić, B., 2022. The impact of northern Adriatic ports container throughput on air quality environmental parameters. Zeszyty Naukowe Akademii Morskiej w Szczecinie.

Validation of Near-surface Wind Speed Monthly Averages from CHELSA Climate Data in Croatia

Dorijan Radočaj[1],*, Mateo Gašparović[2], Mladen Jurišić[1]

[1] Department of Agricultural Engineering and Renewable Energy Sources, Faculty of Agrobiotechnical Sciences Osijek, Osijek, Croatia, dradocaj@fazos.hr, mjurisic@fazos.hr

[2] Chair of Photogrammetry and Remote Sensing, Department of Cartography and Photogrammetry, University of Zagreb – Faculty of Geodesy, Zagreb, Croatia, mateo.gasparovic@geof.unizg.hr

* corresponding author

Abstract: This study validated monthly averages of near-surface wind speed (NSW) from the 1km Climatologies at high resolution for the earth's land surface areas (CHELSA) climate data using long-term ground truth data from 22 climate stations operated by the Croatian Meteorological and Hydrological Service (DHMZ). The CHELSA NSW monthly averages resulted in the coefficient of determination (R^2) from 0.390 to 0.691 and the normalized root mean square error in range of 0.409–0.635. A significant difference in validation results was observed between the October-April and March-September periods, with mean R^2 values of 0.655 and 0.442, respectively. There is a slight temporal discrepancy between CHELSA v2.1 (1981–2010) and the latest official DHMZ climate data (1971–2000), which may affect the accuracy of CHELSA data in Croatia. However, it could also indicate the effects of climate change on NSW, which produced higher residuals from DHMZ ground truth data in warmer May–September period and in coastal DHMZ climate stations. To complement on the current study, future research should resolve the temporal delay with the eventual publication of more recent ground truth data from DHMZ. Additionally, similar open climate datasets should be included to determine the most suitable 1 km resolution climate data source in Croatia.

Keywords: Croatian Meteorological and Hydrological Service (DHMZ); accuracy assessment; open climate data; climate change.

1 Introduction

Remote sensing technologies have become essential for producing precise and high-resolution climate datasets (Yang et al. 2013). Among them, the Climatologies at high resolution for the earth's land surface areas (CHELSA) provide rasterized climatic variables at 1 km spatial resolution, allowing for detailed analysis and modelling at regional to global scales (Karger et al. 2020). The relationship of high-resolution raster climate data based on ground truth observations determines the reliability of predictive mapping used in the creation of such datasets. Ground truth climate data, which are direct measurements of key climatic variables like temperature, precipitation, and humidity at specific locations and time intervals, are usually provided by climate and meteorological stations under governmental agencies (Colston et al. 2018). Uncertainties persist due to the intrinsic unpredictability of climatic events, sensor limits, and computational complexity, even with breakthroughs in remote sensing

technology (Xu et al. 2021). Validation ensures that raster datasets accurately reflect local variations and temporal trends by closely examining the alignment between remote sensing estimates and ground-based observations across various landscapes and climatic regimes. This procedure confirms the accuracy of data obtained by remote sensing and identifies any biases or inaccuracies caused by sensor peculiarities, algorithmic errors, or environmental factors.

Enabling cross-comparison and data fusion is crucial to fully utilize a range of similar climatic datasets, such as WorldClim (Fick and Hijmans 2017). The unique advantages of each dataset can be utilized by combining them, such as the temporal continuity of ground-based observations and the geographical scope of remote sensing data. Verifying raster climate databases against ground truth observations can additionally identify discrepancies and biases in the long-term monthly climate averages, facilitating the harmonization of different datasets (Katrandzhiev et al. 2022). The integration and cross-comparison of datasets was made possible by such harmonization, leading to a more comprehensive understanding of climate dynamics and trends in previous studies. This integrated approach enhances the ability to monitor changes in the environment, assess the impacts of climate change, and develop effective plans for adaptation and mitigation in response to global warming (Abbass et al. 2022).

The aim of this study was to evaluate the accuracy of near-surface wind speed (NSW) CHELSA monthly averages according to ground truth Croatian Meteorological and Hydrological Service (DHMZ) climate stations in Croatia. As Croatian area consists of three distinct biogeoregions (Continental, Alpine and Mediterranean), the results of this study are expected to provide observations on the effects of environmental conditions to climate data accuracy, providing guidance for future studies.

2 Materials and methods

The input data for the validation of near-surface wind speed monthly averages consisted of two main data sources: 1) ground truth monthly averages from DHMZ climate stations from 1971–2000 period, and 2) CHELSA v2.1 monthly averages according to 1981–2010 period (Karger et al. 2020). Both data sources represent the most recent official datasets from their respective sources, which ultimately produced a slight temporal discrepancy due to the lack of availability of more recent DHMZ data.

The geospatial analysis and validation were performed using R v4.0.3 with "terra" package. CHELSA rasters were reprojected to the Croatian Terrestrial Reference System (HTRS96/TM) using the bilinear interpolation.

The ground truth data consisted of only 22 DHMZ climate stations due to restrictions on their availability imposed by responsible DHMZ personnel for the purpose of this study. Their geospatial distribution across the study area, covering the entire land area of Croatia, is displayed in Figure 1.
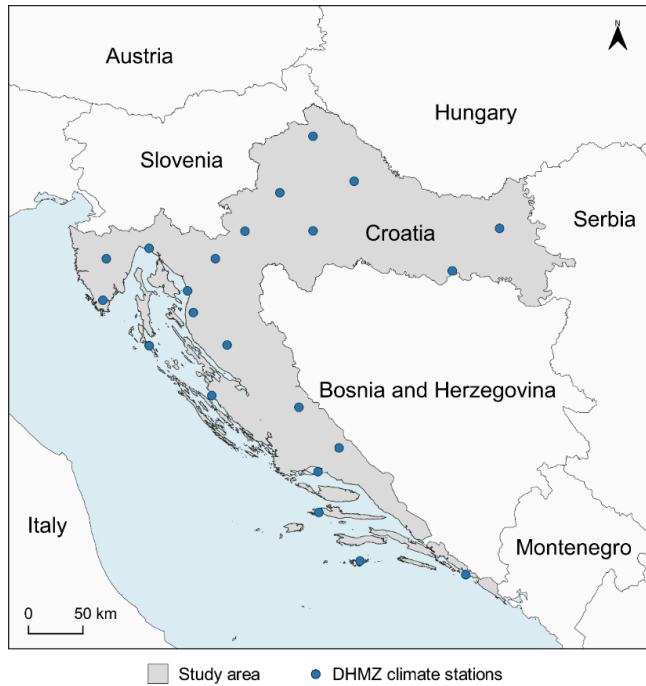
Figure 1. The geospatial distribution of ground truth climate DHMZ stations.

The CHELSA v2.1 near-surface wind speed monthly average rasters were acquired using CHELSA file browser from the Cyberduck client. The rasters were clipped to the study area and reprojected to HTRS96/TM in 1 km spatial resolution. The average monthly near-surface wind speed
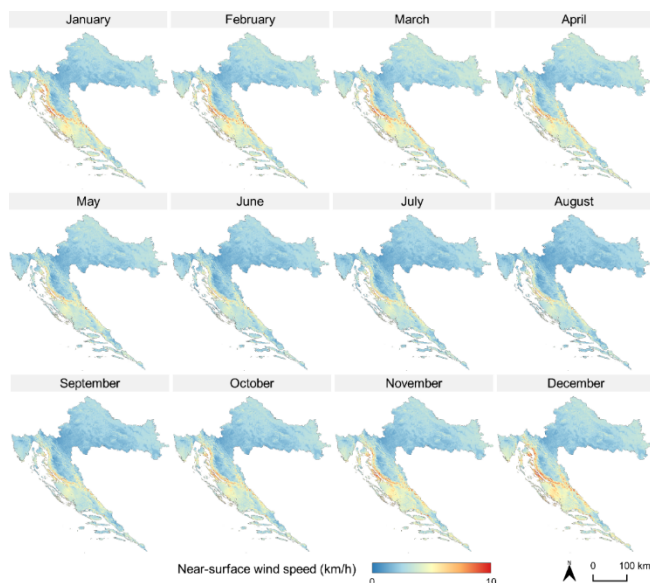
Figure 2. The display of average monthly NSW rasters in Croatia.

rasters in Croatia are displayed in Figure 2. The validation of CHELSA near-surface wind speed monthly averages according to the ground truth DHMZ climate station data was performed according to three statistical metrics: coefficient of determination (R^2), root mean square error (RMSE) and normalized RMSE (NRMSE). These metrics provide complementary information on relative (R^2) and absolute (RMSE and NRMSE) accuracy of evaluated CHELSA rasters. Moreover, R^2 and NRMSE have normalized value ranges from 0 to 1, enabling accuracy comparison between months regardless of the residuals and average near-surface wind speed values. The higher R^2 and lower RMSE and NRMSE indicated higher accuracy of CHELSA near-surface wind speed monthly averages according to the ground truth DHMZ climate stations.

3   Results and Discussion

The highest accuracy of CHELSA near-surface wind speed monthly averages in terms of overall fit was observed in January, February, and December, as indicated by the high R^2 (Table 1). However, December exhibited a higher error rate, indicating a complex relationship between fit represented by R^2 and error magnitude from RMSE and NRMSE, which requires further research. The disagreement in CHELSA near-surface wind speed monthly averages, as represented by either high or low both R^2 and RMSE, could indicate a consistent bias of near-surface wind speed in CHELSA dataset, as well as the limited variability in its values (Chicco et al. 2021). Despite the presence of three distinct biogeoregions in Croatia (Continental, Alpine and Mediterranean) (Pilotto et al. 2020), the yearly averages of available DHMZ climate stations had a value range of 1.3–3.3 km/h, which may also distort validation results due to few stations with noticeably higher yearly average.

Table 1. The properties of available ground truth climate DHMZ stations used in the study.

Month	R^2	RMSE	NRMSE
January	0.689	1.16	0.578
February	0.687	1.06	0.499
March	0.620	1.08	0.488
April	0.565	0.95	0.433
May	0.451	0.87	0.438
June	0.396	0.77	0.409
July	0.390	0.80	0.437
August	0.476	0.78	0.450
September	0.496	0.97	0.541
October	0.648	1.02	0.518
November	0.687	1.15	0.559
December	0.691	1.30	0.635

A clear seasonal variability pattern was observed, with poorer performance during the summer months (June to September) in terms of both fit and error measures. This fluctuation suggests that the accuracy of CHELSA monthly average rasters may be impacted by the exclusion of important seasonal elements or other time-variant predictors from its framework. Its accuracy could be

enhanced by retraining it to consider the discovered time-variant or seasonal impacts, either by incorporating new variables or by utilizing more a suitable modeling approach for different seasons of the year.

Figure 3 represents the monthly residuals magnitude of CHELSA near-surface wind speed according to the ground truth DHMZ climate stations. There is a notable distinction between residuals in northern (primarily Continental region) and southern (primarily Mediterranean region) parts of Croatia, with the largest residuals across all months concentrated in the southern coastal part of Croatia. It could also indicate the effects of climate change on more recent near-surface wind speed monthly averages, which produced higher residuals in warmer May–September period and in coastal DHMZ climate stations. There were also less available ground truth DHMZ climate stations in the eastern part of Croatia, which likely impacted CHELSA validation procedure as incomplete coverage with ground truth data produced similar results in a previous study (Radočaj et al. 2023). For smaller study areas, this issue could be resolved by establishing a local network of meteorological stations and interpolating their

data, which is usually viable for valuable agricultural areas (Ramirez-Villegas and Challinor, 2012).

Therefore, future studies should be based on denser ground truth climate station data and temporal discrepancy between CHELSA or similar dataset with the ground truth data should be resolved, if possible due to DHMZ data availability. Additionally, the inclusion of other climate parameters and similar datasets in the validation approach, such as WorldClim (Fick and Hijmans, 2017), could provide a more complete assessment of the reliability of open data climate rasters in 1 km spatial resolution.

4 Conclusions

This study proved an overall moderate accuracy of near-surface wind speed monthly averages from CHELSA according to available ground truth DHMZ climate stations, with high variability of accuracy metrics across the year. There was a slight disagreement in terms of accuracy from a relative (quantified by R^2) and absolute standpoint (quantified by RMSE and NRMSE), likely indicating a consistent bias of near-surface wind speed in CHELSA
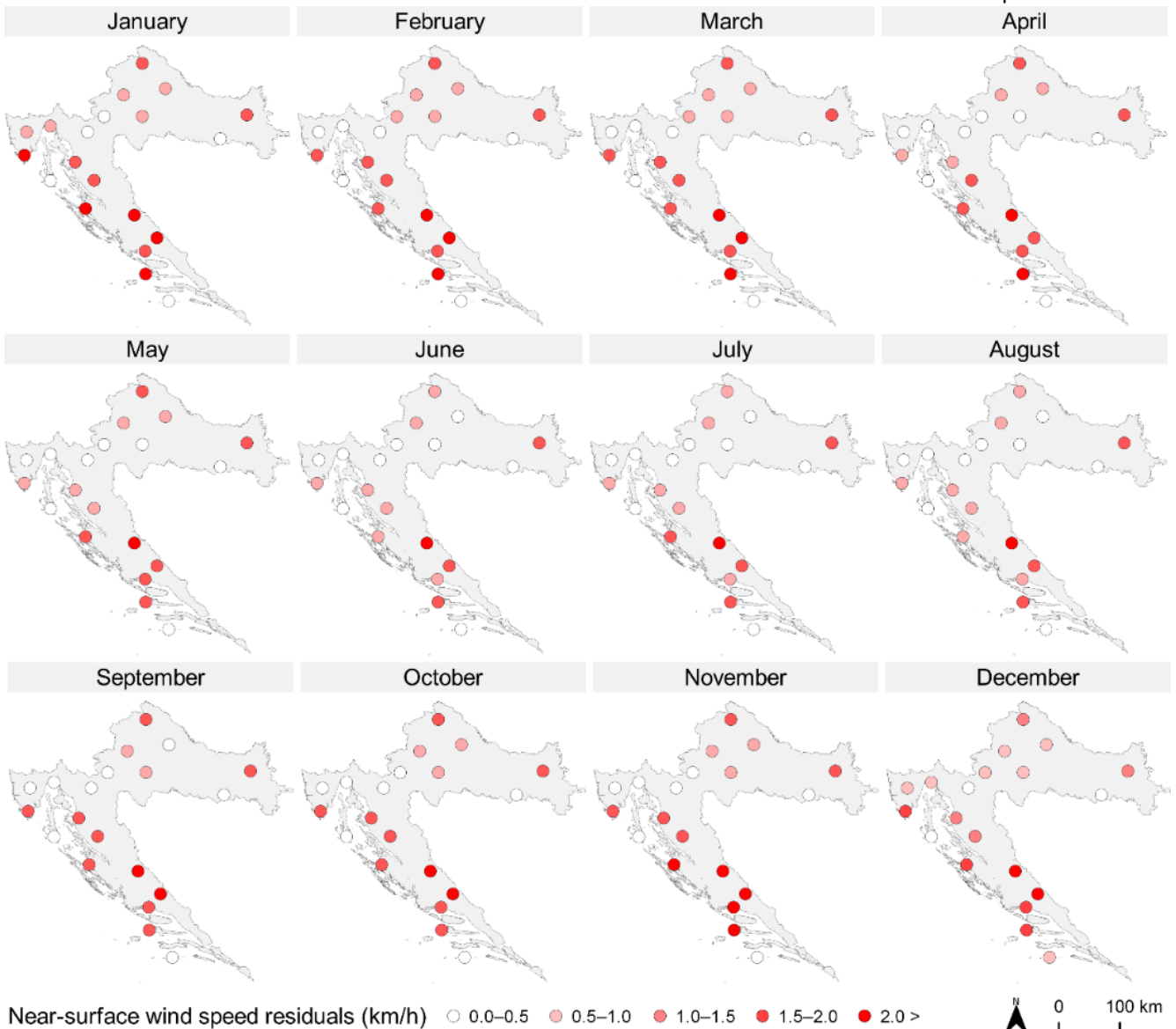
Figure 3. The display of NSW residuals of CHELSA monthly averages according to the ground truth DHMZ climate stations.

dataset. Despite the presence of three distinct biogeoregions in Croatia, the yearly averages of available DHMZ climate stations had a relatively limited variability in its values. A notable distinction between residuals in northern continental region and southern Mediterranean region of Croatia was observed, with the largest residuals concentrated in the southern coastal part of Croatia. It could also indicate the effects of climate change on more recent near-surface wind speed monthly averages, which produced higher residuals in warmer May–September period and in coastal DHMZ climate stations. To improve the study, future research should resolve the temporal discrepancy with the eventual publication of more recent ground truth data from DHMZ. Additionally, similar open climate datasets should be included to determine the most suitable 1 km resolution climate data source in Croatia.

5   References

Abbass, K., Qasim, M. Z., Song, H., Murshed, M., Mahmood, H., Younis, I., 2022. A review of the global climate change impacts, adaptation, and sustainable mitigation measures. Environmental Science and Pollution Research, 29 (28), 42539-42559.

Chicco, D., Warrens, M. J., Jurman, G., 2021. The coefficient of determination R-squared is more informative than SMAPE, MAE, MAPE, MSE and RMSE in regression analysis evaluation. Peerj computer science, 7, e623.

Colston, J. M., Ahmed, T., Mahopo, C., Kang, G., Kosek, M., de Sousa Junior, F., … The, M. E., 2018. Evaluating meteorological data from weather stations, and from satellites and global models for a multi-site epidemiological study. Environmental research, 165, 91-109.

Fick, S. E., Hijmans, R. J., 2017. WorldClim 2: new 1-km spatial resolution climate surfaces for global land areas. International journal of climatology, 37 (12), 4302-4315.

Karger, D. N., Schmatz, D. R., Dettling, G., Zimmermann, N. E., 2020. High-resolution monthly precipitation and temperature time series from 2006 to 2100. Scientific data, 7 (1), 248.

Katrandzhiev, K., Gocheva, K., Bratanova-Doncheva, S., 2022. Whole System Data Integration for Condition Assessments of Climate Change Impacts: An Example in High-Mountain Ecosystems in Rila (Bulgaria). Diversity, 14 (4), 240.

Pilotto, F., Kühn, I., Adrian, R., Alber, R., Alignier, A., Andrews, C., … Haase, P., 2020. Meta-analysis of multidecadal biodiversity trends in Europe. Nature communications, 11 (1), 3486.

Radočaj, D., Jurišić, M., Rapčan, I., Domazetović, F., Milošević, R., Plaščak, I., 2023. An Independent Validation of SoilGrids Accuracy for Soil Texture Components in Croatia. Land, 12 (5), 1034.

Ramirez-Villegas, J., Challinor, A., 2012. Assessing relevant climate data for agricultural applications. Agricultural and forest meteorology, 161, 26-45.

Xu, L., Chen, N., Chen, Z., Zhang, C., Yu, H., 2021. Spatiotemporal forecasting in earth system science: Methods, uncertainties, predictability and future directions. Earth-Science Reviews, 222, 103828.

Yang, J., Gong, P., Fu, R., Zhang, M., Chen, J., Liang, S., Xu, B., Shi, J., Dickinson, R., 2013. The role of satellite remote sensing in climate change studies. Nature climate change, 3 (10), 875-883.

UAV-based Technologies for Remote Sensing in Environmental Monitoring and Physical Resilience Assessment

*Veaceslav Sprincean[1, *], Marianna Savva[1], Ana Birsan[1], Ion Ganea[1], Alexei Leu[2], Marian Jalencu[1], Mihail Caraman[1], Alexandr A. Barsuk[1], Arcadi Chirita[1], Florentin Paladi[1]*

[1] Research Laboratory Environmental Physics and Modeling Complex Systems (ePhysMCS Lab), Moldova State University, Chisinau, Moldova, veaceslav.sprincean@usm.md

[2] PRIDE SYSTEM, Chisinau, Moldova, alexei@leu.md

* corresponding author

Abstract: Multispectral sensors have been shown to be effective in the identification of different components of the environment, showcasing opportunities for their use in the maintenance and improvement of the ecosystem services' quality and the sustainable use of natural resources. Moreover, main current outcomes include: 1) Integration of the *eALERT* platform for real-time environmental monitoring and instant warning, and LiDAR technology into a complex, advanced monitoring and surveillance platform; 2) Development of physical technologies with the unmanned aerial vehicles (UAV) application in monitoring and precise quantitative analysis of critical infrastructures. Software application is used in connection with the UAV-based measuring station for computational modeling of environmental factors, which facilitates the analysis and interpretation of the monitoring results.

Keywords: UAV; natural and artificial ecosystems; critical infrastructure; fluorescence analysis; sensors.

1   Introduction

Currently, modern technologies witness a vertiginous expansion, being widely used in various human activities by providing a solid support in decision-making for monitoring and evaluating the state of natural and artificial ecosystems (Sandbrook 2015, Yang et al. 2017). In this context, our systemic approach is inspired by the interdisciplinary applications, computational modeling of environmental factors, UAV-based 3D mapping through Pix4Dmapper photogrammetry, etc. The application of modern intelligent technologies allows for the first time the implementation of a national complex system of exact monitoring of environmental factors with the application of UAVs through modern optical methods and different types of real-time sensors. The obtained results facilitate formulation of scientifically based recommendations regarding the adjustment of technological processes with the aim of reducing the effects of atmospheric pollution, soil surface degradation and the instability of urban and natural ecosystems (Sprincean et al. 2023). Also, the monitoring of some natural and artificial ecosystems in the Orheiul Vechi Natural-Cutural Reserve protected area aims at providing data for the analysis of biological variables with a decisive role in ensuring the sustainability of ecosystems (Birsan et al. 2023).

2   Materials and methods

An integrated UAV-based system composed of a drone, measuring station and a dedicated software application was developed and used for exact monitoring and computational modeling of environmental factors, such as PM-pollution, organic compounds, formaldehyde, hydrogen chloride, hydrogen cyanide etc. DYS D800 X-8 professional multi-rotor aerial photography and heavy lift platform comes prebuilt from high quality metal and carbon fiber components simply (Figure 1). Flight controller and cameras package are added to make up professional standard aerial monitoring platform. As shown in Figure 1, HD camera (1) to control the flight and visualization of the objects under study, the Survey3 multispectral camera (2) and laser emitter (3) are installed on the DYS D800 X-8 drone platform. The drone

Figure 1. Drone-based technique used to record the fluorescence of plants under the remote laser excitation.

flies above the crowns of trees and with the help of camera (1) the object is selected for research, after which the

multispectral camera (2) is switched on and the beam of laser (3) is pointed in direction of the object under study.

Also, the additional system functionality consists of air quality monitoring with dust and gas sensors, measurement of environmental conditions, real-time data recording in the cloud and measuring station, data recording in the form of HD movie with measurement parameters streamed online, measurement data streamed to a computer by using remote multi-channel communication Wi-Fi or GSM, and data from any period with measured parameters saved on the station and cloud service. The choice of vegetation index for plant monitoring depends on the biological peculiarities of the species, as well as on the developmental stage of the plants. Software application for computational modeling of environmental factors in connection with this measuring station, which facilitates the analysis and interpretation of the monitoring results, has been developed as an integrated mobile system for exact monitoring and computational modeling of environmental factors. Figure 2 shows an example of the performed 3D mapping and the monitoring data processing.
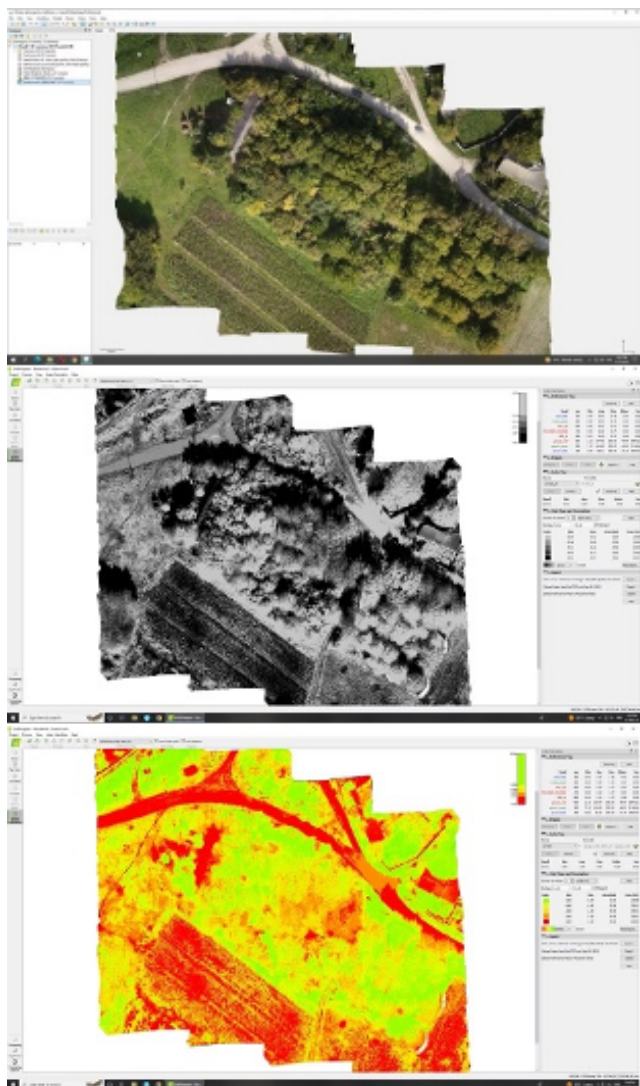
Figure 2. Digital 3D mapping and data processing.

Monitoring of the cultural-natural heritage is the basic condition for the conservation of the Orheiul Vechi reserve ecosystem. For this reason, the identification of ways to monitor the protected area with the help of advanced technologies, based on UAV, represents another innovative approach. Multispectral indices to monitor vegetation, such as Normalized Difference Vegetation Index (NDVI), are applied. The research regarding the analysis of the spectral features of the vegetation in the Orheiul Vechi protected area was carried out at the stage of senescence. So, the phenology of plants varies significantly due to the coloring of foliage, the differences being more pronounced, which allows the differentiation of plant categories and their health.

3 Results

The drone-based technique was used to record the fluorescence of plants under remote laser excitation (Figure 3). The study of fluorescence spectra of plants makes it possible to assess their condition based on the chlorophyll content in plant tissues (Wang et al. 2017). Laser radiation sources with wavelengths of 405 nm and 450 nm are applied. Changing the spectral dependence of fluorescence makes it possible to detect plant diseases at early stages. Photoluminescence spectra for the leaf samples of peach, apple, plum and grapevine have also been excited with ultraviolet (UV) radiation of wavelength 337.4 nm and violet radiation of wavelength λ=405 nm. The edge of the absorption band is approximated with the limiting wavelength of the diffuse reflection coefficient $R_d(\lambda)$ from which R_d reaches the saturation threshold. Photoluminescence spectra were recorded with spectrophotometric equipment with a high optical power monochromator of type MOR-2. Also, diffuse reflection and photoluminescence spectra are investigated for soil and leaf samples collected at different stages of development.

Figure 3. Laser radiation images with wavelengths of 405 nm (left) and 450 nm (right).

Apart from highlighting the presence and state of vegetation, the multispectral data obtained in the near infrared region provided the possibility of identifying the main elements of the studied area: roads, houses etc., and allowed their classification into four main classes of land use/coverage: 1) land covered with spontaneous vegetation (grasses, shrubs, and trees); 2) cultivated agricultural land; 3) land devoid of vegetation; 4) land with constructions. The remote sensing method allowed for the highlighting of the areas covered with vegetation not only in the populated area, but also in the areas covered by spontaneous vegetation, as well as on agricultural land.

Biophysical, biological and structural parameters of the vegetation can be extracted from the remote sensing data. Thus, based on the degree of reflection of the electromagnetic radiation, the comparison of images shown in Figure 4 denotes the presence of plants with different degrees of vitality. The shades of light gray to white, in the right image, attest the existence of plant species with a well-developed crown, an abundant biomass and increased chlorophyll content. We would also like to mention that the information obtained with the help of remote sensing regarding the floristic structure and composition is extremely valuable for the inventory of protected areas, the interaction of biotic and abiotic components largely resulting in many other characteristics of ecosystems.

Figure 4. The health status of plants is assessed using the multispectral device. Images are taken with the RGB and NIR camera, respectively.

4 Discussion

The proposed technique is combined with the *eALERT* platform for real-time environmental monitoring (https://ealert.md) and the UAV-based collection of airborne pollutants followed by their fluorescence spectral measurements. This has been proved to be useful in studying air pollution due to the small size and weight of our pollutants collection device. The use of drones allows particle collection at various altitudes and over extended areas, which may be difficult when applying other methods (Shi et al. 2015). Collection time is subject to the drone flight time and does not depend on the air flow rates. Automated flight paths combined with LiDAR and other sensors provide a faster, safer, more accurate, and cost-effective solution. Moreover, the remote sensing technique can be extended to the physical security and critical infrastructure protection, in particular to the protection of critical infrastructure elements with a focus on energy, transport and ICT. Moreover, the security threats can be mitigated by applying an integrated approach including organizational aspects, training, technologies for monitoring, modeling, and UAV-based surveillance to enhance the capacity for physical resilience in critical entities (Zhang and Zhu 2023).

UAVs have already become an affordable and cost-efficient tool to quickly map a targeted area for many emerging applications in the arena of ecological monitoring, biodiversity conservation, and agriculture (Díaz-Delgado and Mücher 2019, Victor et al. 2024). The development of the UAV-based methods used for vegetation monitoring is fascinating (Wallace et al. 2012, Yang et al. 2020, Hassan et al. 2021). The vegetation stage of the leaves and their type can be determined both by the edge of the diffuse reflection band and the numerical value of the diffuse reflection coefficient in the slope region of the dependence $R_d(\lambda)$. When the leaves are excited with the UV radiation, the samples emit photoluminescence bands with intensity maxima at certain wavelengths characteristic of their vegetation type and stage. One can also mention that some indices, being used independently, provide sufficient information for plant monitoring during most of the growing season. However, since the life cycle of plants includes several distinct stages, to be more informative, the indices used in monitoring plants at different stages of development require adjustments or can be used in combination with other variables. From the multitude of biological variables, the chlorophyll content represents the most important parameter in the evaluation of the physiological states of plants. Assessment of plant photosynthetic performance based on the reflectance measurements with high spectral resolution has shown a strong ability to detect fine variations in spectral absorption features related to the chlorophyll changes.

5 Conclusions

The advanced technologies of remote sensing, together with the traditional methods and procedures of data collection evaluated by direct observation and analysis, are of real help for solving the problems of natural and artificial ecosystems related to the environmental protection and biodiversity conservation. The use of drones in ecosystem monitoring offers numerous benefits, contributing to the efficient management of ecosystem resources, the timely identification and management of environmental problems, the sustainable agricultural development as a result of monitoring plant health etc.

6   References

Birsan, A., Sprincean, V., Ganea, I., 2023. Opportunities for the practical use of intelligent technologies in the evaluation of some biological variables. Studia Universitatis Moldaviae 1 (171), 53-64.

Díaz-Delgado, R., Mücher, S., 2019. Editorial of Special Issue Drones for biodiversity conservation and ecological monitoring. Drones 3, 47, 1-4.

Hassan, M.A., Yang, M., Rasheed, A., Tian, X., Reynolds, M., Xia, X., Xiao, Y., He, Z., 2021. Quantifying senescence in bread wheat using multispectral imaging from an unmanned aerial vehicle and QTL mapping. Plant Physiology 187(4), 2623-2636.

Sandbrook, C., 2015. The social implications of using drones for biodiversity conservation. Ambio 44, 636-647.

Shi, Y., Ji, Y., Sun, H., Hui, F., Hu, J., Wu, Y., Fang, J., Lin, H., Wang, J., Duan, H., Lanza, M., 2015. Nanoscale characterization of $PM_{2.5}$ airborne pollutants reveals high adhesiveness and aggregation capability of soot particles. Scientific Reports 5, 11232, 1-10.

Sprincean, V., Chirita, A., Leontie, L., Astilean, S., Focsan, M., Craciun, A.-M., Paladi, A., Andruh, V., Paladi, F., 2023. Advanced physical technologies with the UVS application in environmental security. In: Daponte, P., Paladi, F. (Eds.), Monitoring and protection of critical infrastructure by unmanned systems. NATO Science for Peace and Security Series, D: Information and Communication Security 63, Amsterdam: IOS Press, pp. 101-113.

Victor, N., Maddikunta, P.K.R., Mary, D.R.K., Murugan, R., Chengoden, R., Gadekallu, T.R., Rakesh, N., Zhu, Y., Paek, J., 2024. Remote Sensing for agriculture in the era of Industry 5.0 - A survey. IEEE Journal of Selected Topics in Applied Earth Observations and Remote Sensing 17, 5920-5945.

Wallace, L., Lucieer, A., Watson, C., Turner, D., 2012. Development of a UAV-LiDAR system with application to forest inventory. Remote Sensing 4 (6), 1519-1543.

Wang, H., Qian, X., Zhang, L., Xu, S., Li, H., Xia, X., Dai, L., Xu, L., Yu, J., Liu, X., 2017. Detecting crop population growth using chlorophyll fluorescence imaging. Applied Optics 56 (35), 9762-9769.

Yang, M., Hassan, M.A., Xu, K., Zheng, C., Rasheed, A., Zhang, Y., Jin, X., Xia, X., Xiao, Y., He, Z., 2020. Assessment of water and nitrogen use efficiencies through UAV-based multispectral phenotyping in winter wheat. Frontiers in Plant Science 11, 927, 1-16.

Yang, G., Liu, J., Zhao, C., Li, Z., Huang, Y., Yu, H., Xu, B., Yang, X., Zhu, D., Zhang, X., Zhang, R., Feng, H., Zhao, X., Li, Z., Li, H., Yang, H., 2017. Unmanned aerial vehicle remote sensing for field-based crop phenotyping: Current status and perspectives. Frontiers in Plant Science 8, 1111, 1-26.

Zhang, Z., Zhu, L., 2023. A review on unmanned aerial vehicle remote sensing: Platforms, sensors, data processing methods, and applications. Drones 7 (6), 398, 1-42.

Disaster Management and Response

PROCESSING LIDAR DATA FOR GEOMORPHOLOGICAL MAPPING OF ACTIVE FAULTS: A CASE STUDY OF SVETA NEDELJA FAULT (ŽUMBERAK MT.)
Josipa Maslač, Branko Kordić, Petra Jamšek Rupnik, Bojan Matoš

PLUVIAL FLOOD HAZARD ANALYSIS IN THE SUB-CATCHMENT OF THE METKOVIĆ CITY
Lovre Panđa, Nino Krvavica, Ante Šiljeg, Fran Domazetović, Ivan Marić, Silvija Šiljeg, Rina Milošević

STRATEGIES FOR CIVIL-MILITARY GEOGRAPHICAL SUPPORT TO DEFENCE AND SECURITY OPERATIONS
Mladen Viher

EFFECTIVE SPATIAL PLANNING OF WATCHTOWERS FOR THE DETECTION OF WILDFIRE HOTSPOTS IN THASOS ISLAND, GREECE
Stavros Sakellariou, Christos Christakis, Stergios Tampekis, Olga Christopoulou, Athanasios Sfougaris

FORECASTING ATMOSPHERIC AIR POLLUTION IN TEHRAN USING RANDOM FOREST MODEL
Nilufar Makky, Zahra Eghrari

Processing Lidar Data for Geomorphological Mapping of Active Faults: A Case Study of Sveta Nedelja Fault (Žumberak Mt.)

Josipa Maslač[1,], Branko Kordić[1], Petra Jamšek Rupnik[2], Bojan Matoš[3]*

[1] Department of Geology, Croatian Geological Survey (HGI-CGS), Zagreb, Croatia, jmaslac@hgi-cgs.hr, bkordic@hgi-cgs.hr

[2] Geological Survey of Slovenia (GeoZS), Ljubljana, Slovenia, petra.jamsek-rupnik@geo-zs.si

[3] Department of Geology and Geological Engineering, Faculty of Mining, Geology and Petroleum Engineering, University of Zagreb, Zagreb, Hrvatska, bmatos@rgn.hr

* corresponding author

Abstract: The development of environmental remote sensing technology (ERS) plays a crucial role in modern tectonic geomorphological analyses and consequently in the mapping of active faults. High-resolution terrain imaging provides a deeper insight into landscape evolution and the differentiation of geomorphic forms associated with various geological structures. For this study, utilizing reclassified airborne point cloud dataset, we generated several digital elevation models (DEMs) with a resolution of 0.5 and 1 m, optimised for remote geomorphological analysis, empowering the identification of structural discontinuities that have been active in the most recent geological period, i.e. active fault traces visible in the landscape. GIS processing of the DEMs resulted in multiple raster layers that were used to generate digital drainage networks and various terrain features such as slope, aspect, multidirectional hillshade, openness, etc., leveraging remote sensing data. The processing procedure of combined ERS and GIS technologies previously applied in the Hrastovica area for the mapping of the Petrinja-Pokupsko Fault, the main source of the Petrinja 2020 Earthquake (Mw 6.4), is now applied to the Sveta Nedelja Fault in Žumberak Mountain. The integration includes morphometric analysis of elevation differences, detection of tectonic deformation over time and identification of characteristic geomorphic forms associated with active faults. The results derived from the analysis of raster dataset in combination with geological data are initial step towards detailed mapping of the Sveta Nedelja Fault. Further studies based on these fundamental datasets are essential for a better understanding of tectonic processes and their environmental impacts, particularly for the assessment of natural hazards and risks.

Keywords: tectonic geomorphology; processing lidar; active faults; geohazard.

1 Introduction

The earthquakes that struck Croatia in 2020 raised awareness among the public about the unpredictable hazards and risks presented by active faults. To reduce earthquake damage in the future and enhance disaster risk management, an essential requirement is the development of a database and map of active faults as a fundamental prerequisite for seismic hazard assessment (SHA) (Coburn and Spence 2002). Over the past two decades, laser technology has emerged as the most significant method for spatial data acquisition. In Croatia,

over the past few years, the main sources of DEM data have primarily been Copernicus 25 m DEM and ESRI Terrain 5 m DTM. However, ALS (Airborne laser scanning) data opens new possibilities for geomorphological studies. Its development has made it possible to generate lidar-derived high-resolution DEMs even in areas with dense vegetation (Figure 1), previously a limitation of the aero photogrammetric method.
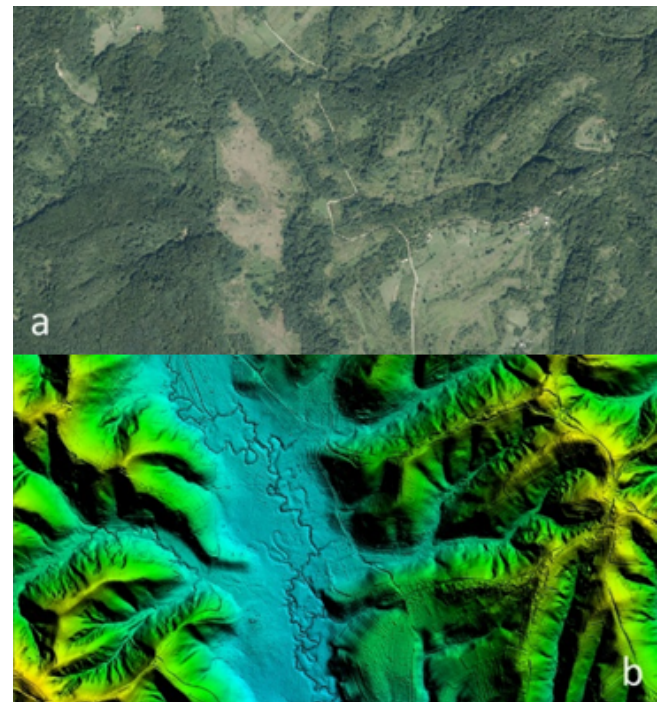
Figure 1. Comparison of forest-covered area in orthophoto imagery (a) and LiDAR-generated DEM (b).

Modern application of tectonic geomorphology considers a high-resolution DEM (≤1 m) as essential input data for any analysis contributing to topographic accuracy and providing new insights into landscape-shaping processes (Burbank and Anderson 2011). The initial utilization of these data to identify active faults occurred following the Petrinja 2020 Earthquake when the Croatian Geological Institute acquired ALS data for Hrastovica Mt. These data were the fundamental data in detecting both short-term activities, evidenced by geomorphological mapping of earthquake-induced changes on the field (Baize et al. 2022), and long-term activity, assessed through detailed geomorphological analyses (Henriquet et al. in prep). This study aims to showcase the efficacy of lidar data processing procedure that is applicable to remote

geomorphological mapping of tectonic activity indicators within the Sveta Nedelja Fault area (Žumberak Mt.).

2 Materials and methods

We have obtained point cloud data from the State Geodetic Administration (DGU) for research purposes. This data is provided in LAZ (Lidar area) format files, each covering an area of 1 km^2. Depending on whether the area is open, covered with dense vegetation, or saturated, the point cloud resolution on the ground ranges from 4 to 6 points per m^2. The point cloud is classified into 10 classes and provided in the HTRS96/TM reference coordinate system and the HVRS71 reference height coordinate system (URL 1).

The point cloud with classified data has been filtered for the ground-related class. There are no points in water-covered areas due to the limitations of lidar technology in collecting spatial data on non-reflective surfaces. Bilinear interpolation fill method was utilized within a GIS environment to address areas lacking elevation data points.

2.1 DEM processing

A DEM with a 1 m resolution was created for preliminary geomorphological investigation of a wider research area encompassing Žumberak and Vukomerić Hills. It was utilized for visualizing of various raster datasets employed in the initial qualitative analysis of active faults: i) Sveta Nedelja Fault, located in the southern part of Žumberak, and ii) extension of the Petrinja-Pokupsko Fault System in the Vukomerić area. Afterwards, DEM with a resolution of 0.5 m were derived for more precise analyses, detailed geomorphological mapping, and on-site verification of results. Additionally, to enhance the smoothness and continuity of DEM, bilinear interpolation techniques were implemented.

2.2 Raster visualization

For both datasets, identical cartographic techniques were used for advanced data visualization using the QGIS software package. Layer overlay with transparency enhances the visualization method through blending mode and allows us to produce new visualizations with a 3D impression of terrain without graphic design software. This includes Relief Visualization Toolbox (Kokalj and Hesse 2017) designed specifically for visualizing local scale raster data, derived from ALS missions. Specifically, we generated Slope Degree, Slope Aspect, Contours (1 m equidistance), Hillshade, Multidirectional Hillshade, Positive and Negative Openness and Sky View Factor (SVF) raster as initial dataset for tectonic analyses.

Relief shading, also known as hillshading, is a cartographic technique used in GIS and remote sensing to visually represent terrain by generating a shaded relief from a DEM. Among various techniques, Yoëli's method (Zakšek et al. 2011) has become standard in GIS software due to its straightforward computation and interpretation. It assumes the terrain is a Lambertian surface illuminated by direct light from a fictive light source at an infinite distance. Where areas perpendicular to the light beam are the most illuminated, and those with an incidence angle of 90° or more are in shadow.

A single light beam may not reveal linear structures that lie parallel to it, making some small or elongated landforms less visible or even invisible. This limitation of one-directional hillshading arises from anisotropy (directional dependence). Another possibility is to use isotropy-based visualisation with multidirectional lighting, which can create a 3D impression of relief independent of light direction. In this study, we have used *Red Relief Image Map* (RRIM) (Chiba et al. 2008) which extends the *Openness* parameter (Yokoyama et al. 2002) and slope gradient information. Openness visualization is more suitable for automatic detection of linear structures because it exposes numerous edges, while *SVF-based* visualization is better for distinguishing slopes (Zakšek et al. 2011). To enhance the 3D effect, multiple visualization techniques were used, combining contour lines with slope degree and slope aspect raster to display the steepness and direction of the slopes.

2.3 Drainage network processing

The drainage network for an entire area was modelled by the Hydrology Toolbox (ESRI). The initial data preparation involved filtering and correcting DEM for anomalies and artefacts that could affect natural flow patterns. Data accuracy depends on the resolution, distance between sampling cells, and the type and method of data sampling. Calculation of a flow direction raster (Jenson and Dominique 1988) assumes that flow is determined by the direction of the steepest change from each cell of the previously smoothed elevation raster. Identifying streams and catchments required processing the flow accumulation raster, which shows the amount of water passing through each cell. Following the delineation of watersheds and streams, the accuracy of modelled network was verified through comparison with actual drainage network from Topographic Maps, Basic Maps of Croatia and INSPIRE hydrographic database (URL 2). If changes were necessary, the drainage network was calibrated by adjusting parameters and algorithms to match real data better.

3 Results

Hillshading of high-resolution DEMs (DGU, 1 m and 0.5 m) has significantly enhanced the visualization of landforms (Figure 2) in comparison with previously used hillshades of 25 m (Copernicus) and 5 m (ESRI Terrain), which often mask linear changes in ridges, valleys, and terraces – key geomorphological markers of active tectonics.

The shading effect with varied colouring has improved the identification of landforms by employing multiple light sources from different directions. The limitation of one-directional hillshading has been effectively overcome, thus emphasizing relief features with diverse orientations. This model serves as a basemap for subsequent 2D and 3D visualizations (Figure 3), acting as the initial step for tectonic geomorphology research, such as digital geomorphological mapping and topographic analysis,

including *SWATH profile* assessments (Pérez-Peña et al. 2017).
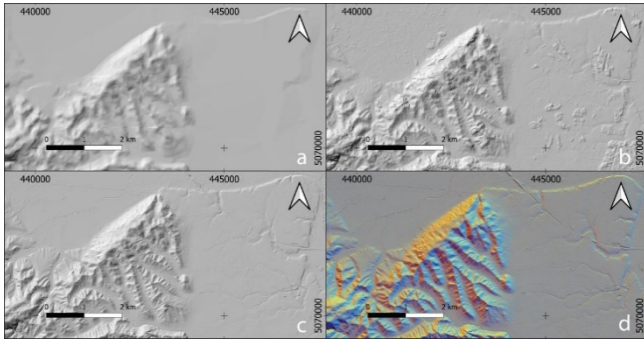
Figure 2. Generated hillshading of Svetonedeljski Breg area from various sources used for interpretation: Copernicus DEM 25m (a), ESRI Terrain DTM 5m (b), DGU DEM 1m (c) and 0.5m (d). The last one is a multidirectional colored hillshade.

The generated drainage network provides precise stream paths that are pivotal for hydrogeological and geomorphological analysis. These are instrumental in identifying changes in drainage patterns, deviations, and stream capturing along the fault zones, which are evident as knick-points in morphometric studies (Figure 3). Additionally, the precise drainage network crossing over an active fault can also be utilized to define horizontal displacements and estimate activity rates.

4   Discussion

Based on the existing data, the processed point cloud data provided by DGU has resulted in a high-resolution elevation model. This model provides a deeper understanding of landscape evolution and the differentiation of geomorphic forms associated with various geological structures, by implementing the methods and principles of tectonic geomorphology (Burbank and Anderson 2011). Optimized for remote geomorphological analysis, the 1 m and 0.5 m DEMs facilitate the identification of structural discontinuities that have been active in the most recent geological period (2.58 million years ago). These high-resolution datasets enable the accurate detection of active fault traces in the landscape. Additionally, tectonic activity manifests in the evolution of the drainage network, whose representation is significantly improved through this methodology. In comparison to the previously utilized INSPIRE database, the newly generated drainage network enhances spatial accuracy and rectifies deficiencies in the depiction of drainage patterns. The main findings obtained by remote survey of the Sveta Nedelja Fault in the Žumberak Mountain need further verification in the field. The integration of GIS database within platforms allows efficient fieldwork, crucial in confirming shallow subsurface tectonic deformations to validate the reliability of digital relief interpretation.

5   Conclusions

Processed rasters have become fundamental datasets essential for a better understanding of tectonic processes and their environmental impacts, particularly for the assessment of natural hazards and risks. Applying combined ERS and GIS technologies to the morphotectonic analysis of the Sveta Nedelja Fault in the Žumberak
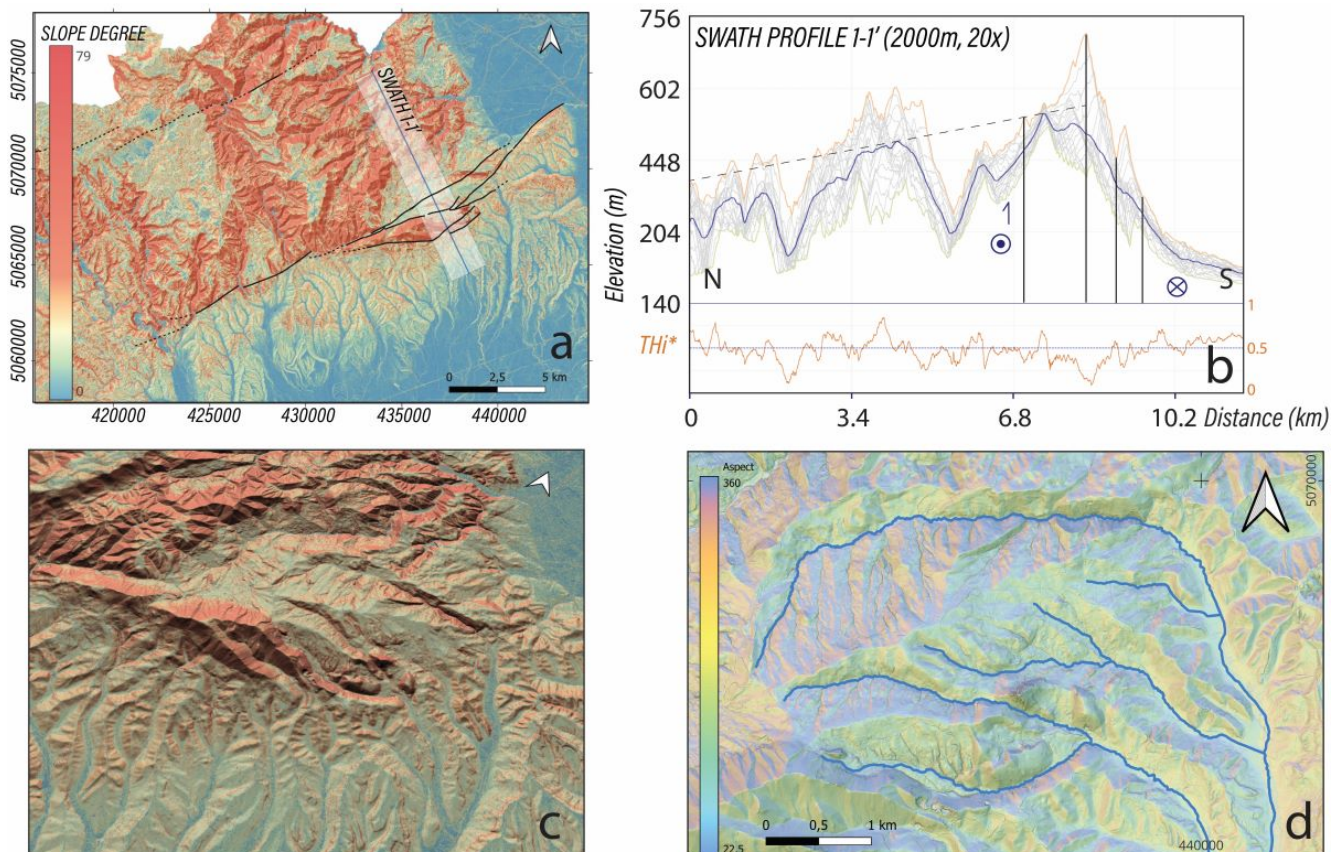
Figure 3. Example of applying visualizations for topographic analysis of Sveta Nedelja Fault: slope degree map (a), SWATH profile (b), 3D view of slope degree map overlaid on DEM (c), and Konšćica stream basin on SVF and Slope Aspect basemap (d).

Mountain has proven successful, representing a new approach in the study of active faults in Croatia. This integration includes morphometric analysis of elevation differences, detection of tectonic deformation over time and identification of characteristic geomorphic forms associated with surface active fault trace. The results derived from the analysis of raster dataset in combination with geological data are initial step towards detailed tectono-geomorphic mapping of the Sveta Nedelja Fault.

6   References

Baize, S., Amoroso, S., Belić, N., Benedetti, L., Boncio, P., Budić, M., … Ricci, T., 2022. Environmental effects and seismogenic source characterization of the December 2020 earthquake sequence near Petrinja, Croatia. Geophysical Journal International 230 (2), 1394-1418.

Burbank, D.W and Anderson, R.S., 2011. Tectonic Geomorphology. 2nd ed., John Wiley & Sons Ltd.

Chiba, T., Kaneta, S., Suzuki, Y., 2008. Red relief image map: New visualization method for three dimensional data. The International Archives of the Photogrammetry, Remote Sensing and Spatial Information Sciences 37, 1071-1076.

Coburn, A. Spence, R., 2002. Earthquake Protection. 2nd ed., John Wiley & Sons Ltd., Chichester, England.

Jenson, S. Domingue, J., 1988. Extracting Topographic Structure from Digital Elevation Data for Geographic Information System Analysis. Photogrammetric Engineering and Remote Sensing 54, 1593-1600.

Kokalj, Ž. Hesse, R., 2017. Airborne laser scanning raster data visualization: A Guide to Good Practice. Ljubljana: Založba ZRC.

Pérez-Peña, J. V., Al-Awabdeh, M., Azañón, J.M., Galve, J.P., Booth-Rea, G., Notti, D., 2017. SwathProfiler and NProfiler: Two new ArcGIS Add-ins for the automatic extraction of swath and normalized river profiles. Computers & Geosciences 104, 135-150.

Yokoyama, R. Pike, R.J., 2002. Visualising Topohraphy by Openness: A New Application of Image Processing to Digital Elevation Models. Photogrammetric Engineering and Remote Sensing 6 (3), 3.

Zakšek, K., Oštir, K., Kokalj, Ž., 2011. Sky-View Factor as a Relief Visualization Technique. Remote Sensing 3 (2), 398-415.

URL 1: LiDAR aerial survey product specifications, https://dgu.gov.hr/multisenzor sko-zracno-snimanje-republike-hrvatske/5700. (Accessed 10 May, 2024)

URL 2: Using TK, HOK and INSPIRE basemaps, https://geoportal.dgu.hr/. (Accessed 17 May 2024)

Pluvial Flood Hazard Analysis in the Sub-catchment of the Metković City

Lovre Panđa[1],*, Nino Krvavica[2], Ante Šiljeg[1], Fran Domazetović[1], Ivan Marić[1], Silvija Šiljeg[1], Rina Milošević[3]

[1] University of Zadar, Department of Geography, Center for Geospatial Technologies, Zadar, Croatia, lpanda@unizd.hr; asiljeg@unizd.hr; fdomazeto@unizd.hr; imaric1@unizd.hr; ssiljeg@unizd.hr

[2] University of Rijeka, Faculty of Civil Engineering, Rijeka, Croatia, nino.krvavica@uniri.hr

[3] University of Zadar, Department of Ecology, Agronomy and Aquaculture, Center for Geospatial Technologies, Zadar, Croatia, rmilosevi@unizd.hr

* corresponding author

Abstract: Urban pluvial floods are a significant natural threat worldwide. In recent decades, their frequency and impact have been increasing primarily due to the combined effects of climate change, urbanization, and inadequate infrastructure. These floods result from intense rainfall overwhelming drainage systems. The research focuses on a specific 1.64 km² sub-catchment in Metković, chosen for its unique geographical, climatological, and ecological characteristics. Meteorological data spanning 1961-2020 from the Ploče station were utilized to analyse rainfall, producing hyetographs defining synthetic rainfall for various return periods. High-resolution spatial data, gathered using aeroLiDAR technology, facilitated the creation of digital surface (DSM) and terrain models (DTM). Additional data collection involved unmanned aerial vehicle (UAV) systems and a multispectral camera to generate a model with ten spectral bands. A hybrid approach combining Geographic Object-Based Image Analysis (GEOBIA) and manual correction was employed to develop a land cover and land use (LULC) model. This model, alongside infiltration, roughness, and imperviousness models derived from it, served as input data for pluvial flood hazard analyses. These analyses, conducted according to the methodology proposed within the Interreg STREAM project, involved hydrological-hydraulic simulations using HEC-RAS software. The outcomes comprise maps depicting water depth, velocity, and hazard levels corresponding to different probabilities. The research contributes to understanding and mitigating the risks associated with urban pluvial floods.

Keywords: urban pluvial floods; flood hazard; very-high resolution models.

1 Introduction

Floods are considered one of the greatest threats to humanity, leading to loss of life, damage to infrastructure, and significant economic losses (Singh et al. 2018). Climate change, intensive exploitation of natural resources, and improper land use have altered the hydrological response of catchments. These factors increase the frequency and severity of flood events. Furthermore, the combination of exposed, vulnerable, and inadequately prepared populations can exacerbate such situations and even generate additional risks. Insufficient capacities of authorities and public rescue services in these situations further increase the risk posed by major flood events (UNDRR 2010, Chaumillon et al. 2017). The rapid population growth in urban areas increases exposure to floods, and the risk is compounded by uneven social vulnerability, inadequate infiltration, and increased surface water runoff (Ochoa Rodriguez et al. 2012, de Moel et al. 2015). Therefore, flood prevention and mitigation in urban areas are recognized as international priorities that include flood hazard and risk assessments and the preparation of effective flood mitigation measures (WMO 2010). Although historically, fluvial floods have been the most documented, pluvial floods in urban areas have had the highest frequency share since 2000 compared to other types of floods in the same period (WGF 2016). Modeling flood hazards is a crucial part of flood risk assessment, risk management planning, and flood protection measures. Therefore, the main objective of this study is to conduct an analysis of pluvial flood hazards based on very high-resolution (VHR) spatial data collected using modern geospatial technologies.

2 Materials and methods

The research focuses on a specific 1.64 km² sub-catchment in Metković, chosen for its unique geographical, climatological, and ecological characteristics (Figure 1). Pluvial flood hazard analyses in the Metković sub-catchment were carried out following the methodology proposed and elaborated within the Study of flood hazard and risk assessment due to heavy rainfall and sea action in pilot areas in Croatia (Interreg STREAM 2023).

The methodological framework can be divided into several steps: 1) collection and processing of meteorological data; 2) collection and processing of aeroLiDAR data; 3) collection and processing of multispectral data; 4) Creation of VHR LULC and derivation of infiltration, roughness, and imperviousness models; 5) pluvial flood hazard analysis.
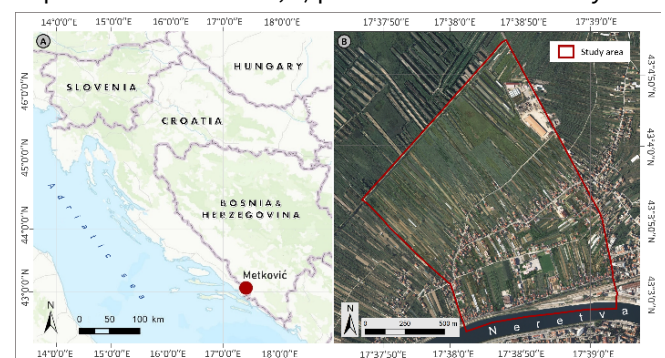
Figure 1. Geographical position of the study area: (A) In Croatia; (B) In Metković.

2.1 Collection and processing of meteorological data

The methodology for generating the design storm in Croatia has been presented in previous studies and scientific papers (Krvavica et al. 2018, Krvavica and Rubinić 2020), and further elaborated and improved within the framework of the Interreg project STREAM. Meteorological data spanning 1961-2020 from the Ploče station were utilized to analyse rainfall, producing hyetographs defining synthetic rainfall for various return periods. The generation of the design storm was carried out in three steps. Firstly, the identification and extraction of relevant storms from a series of measured pluviograph data were performed. Next, a dimensionless form of the design storm was defined for various durations. Finally, the design storm was generated for different durations and probabilities of occurrence.

2.2 Collection and processing of aeroLiDAR data

The aeroLiDAR survey utilized the UAV DJI Matrice M300 RTK along with the DJI Zenmuse L1 LiDAR payload. The survey mission was scheduled for 68 minutes, with a ground-sampling distance (GSD) of 2.73 cm/pix and a point-cloud density of 141 pts/m^2. The flight altitude was set at 100 m with a speed of 10 m/s, and the sensor's side overlap was set to 20%. Direct georeferencing was employed during data collection, with pre-flight calibration of devices to ensure accuracy. The LiDAR model's accuracy was evaluated using 229 checkpoints (CPs) collected by the RTK GNSS Trimble R12i. The reference points were compared with the collected point cloud and the RMSE was calculated. The acquired point cloud was processed using DJI Terra and Spatix softwares, with output in *.las* format. Data processing involved the exclusion of anthropogenic objects and vegetation, followed by five steps of data harmonization, including grouping point clouds based on recorded profiles, reducing inconsistencies across profiles, removal of intersecting points, smoothing, and thinning or removing inactive points. The resulting model was DTM, a basic spatial layer in hydrological-hydraulic simulations.

2.3 Collection and processing of multispectral data

A UAV Trinity F90+ equipped with a dual multispectral camera system (MicaSense RedEdge-MX Dual MS) was deployed for the multispectral survey. Data collection utilized the direct georeferencing method, incorporating global navigation satellite system (GNSS) and inertial measurement unit (IMU) data to accurately position the sensor platform during data acquisition. A total of nine CPs were acquired using the RTK GNSS Trimble R12i to assess the accuracy of the georeferencing system, as well as a base point (BP) for the UAV's iBase base station. UAV missions were planned with QBase 3D software, considering terrain morphology, desired detail levels, and flight duration. For multispectral imaging, front and side overlaps of 75% and 70% were selected, respectively, with a flight altitude of 120 m resulting in a GSD of 8.33 cm/px. Pre-flight calibration included the UAV's IMU and compass, along with radiometric calibration of the multispectral sensor using a reference panel, CRP2. The aerial photogrammetry process commenced post-calibration, accounting for atmospheric variations by repeating radiometric calibration after each mission. Geocoding of images primarily relied on UAV's flylog records and base station data, followed by processing using Agisoft Metashape software. This software facilitated the generation of a VHR 3D model through well-defined settings and steps, including photo orientation, dense point cloud derivation, deep filtering, and sensor location optimization. The resulting model was exported as UAV$_{MS}$.

2.4 Creation of VHR LULC and derivation of infiltration, roughness, and imperviousness models

The first step in the process of the pluvial flood hazard analysis was the derivation of VHR models (infiltration, roughness, and imperviousness) which are very important spatial layers for the accurate hydrological-hydraulic simulations in HEC-RAS software. To derive these three models, a VHR Land Use/Land Cover (LULC) model must be created. The development of the LULC model employed a hybrid method that combined GEOBIA (Blaschke 2010) with manual refinement techniques (MacFaden et al. 2012). This methodology encompassed several steps. Initially, UAV$_{MS}$ image segmentation was conducted, where optimal parameter values for spectral and spatial details, as well as minimum segment size, were selected through an iterative process (n=25). Subsequently, in the second step, training samples were added using a probabilistic method of systematic sampling. The third step involved image classification using both Maximum Likelihood Classifier (MLC) and Support Vector Machine (SVM) algorithms. In the fourth step, accuracy assessment was performed using metrics such as Overall Accuracy (OA) and the Kappa Coefficient (KC) to determine the more accurate model between MLC and SVM. The fifth step entailed enhancing the quality of the LULC through manual interventions. The sixth step involved the derivation of infiltration, roughness, and imperviousness models by assigning specific values to LULC classes. For the infiltration model, a Curve Number (CN) was assigned to each LULC class based on the hydrological soil group according to the NRCS methodology (Hoeft 2020). For the roughness model, Manning's roughness coefficient (n) was added to the classes (Alizadeh and Berton 2023), while for the imperviousness model, LULC was reclassified into impermeable surfaces (such as buildings, greenhouses, asphalt, and water bodies) and permeable surfaces (various classes of vegetation etc.) (Šiljeg et al. 2023).

2.5 Pluvial flood hazard analysis

The flood hazard analysis was conducted for floods of small, medium, and large probabilities, with these probabilities being associated with the return period (5, 25, 100 years). The flood hazard analysis is based on hydrological-hydraulic simulations of surface runoff from heavy rainfall in HEC-RAS 6.0 software (Brunner 2021). The mathematical model of surface runoff from heavy rainfall consists of the following steps: 1) Defining the DTM; 2) Defining spatial parameters of infiltration processes; 3) Defining spatial density of built-up areas (impermeability);

4) Defining spatial distribution of roughness; 5) Defining spatial domain of the model and generating computational network; 6) Defining boundary conditions; 7) Defining numerical calculation parameters; 8) Defining scenarios. All spatial layers, including DTM, infiltration, roughness, and imperviousness models, are directly implemented into the HEC-RAS. The spatial model domain corresponds to the catchment area. The computational network is defined within the model domain, using a structured hexagonal grid with a width of 5.0 m. Three boundary conditions are defined in the model, two at the domain boundaries (line boundary conditions) and one across the entire domain surface (surface boundary condition): 1) At the land boundary of the domain, a condition of normal flow with average terrain slope is specified; 2) At the "river" boundary of the domain, a high sea level is specified (+0.5 m above mean sea level); 3) Across the domain surface, a spatially homogeneous but time-variable rainfall is defined in the form of a hyetograph (design storm). For numerical analysis of water flow, an unsteady 2D calculation was used along with the Diffusion Wave method with a time-variable time step. For the implicit calculation, the parameter $\theta = 1.0$ was used, and the PARDISO algorithm was used to solve matrices (Brunner 2021). The time step is dynamically calculated based on the CFL number ranging from 0.8 to 4.0. An analysis of three scenarios (5, 25, and 100 years) was conducted, and for each scenario, five calculations were performed for rainfall durations of 1, 3, 6, 12, 24 hours.

3   Results

The result of the rainfall analysis yielded synthetic rainfall durations for three probabilities (return periods of 5, 25, and 100 years), represented by rainfall intensity profiles known as rainfall hyetographs.

These hyetographs were generated to represent different durations and probabilities of occurrence, as illustrated in Figure 2A. After processing LiDAR data in DJI Terra, a DSM was generated (Figure 2B). Subsequently, a VHR DTM was created (Figure 2E) using Spatix software. The LiDAR model's accuracy resulted in an RMSE value of 0.0387 m, indicating a high level of accuracy. Despite the potential for higher spatial resolution in the DTM, the processing complexity necessitated exporting the model at a spatial resolution of 0.5 m. This DTM served as the basic spatial layer for the hydrological-hydraulic analyses. The UAV$_{MS}$ model, with a spatial resolution of 0.08 m, comprised 10 spectral bands (Figure 2C). The UAV$_{MS}$ model's accuracy was assessed using nine collected CPs, resulting in an RMSE of 0.0336 m. The UAV$_{MS}$ model was used to generate the VHR LULC model. Through visual interpretation, specific parameters for the GEOBIA segmentation process were selected (spectral detail (20), spatial detail (19) and minimum segment size (15)), resulting in SVM and MLC classification models. A total of 6489 samples were added across 19 classes. The SVM algorithm demonstrated higher accuracy in classification and was improved by manual corrections (Figure 2D). By reclassifying the SVM LULC model and assigning values for CN, n, and 0 or 1, infiltration (Figure 2F), roughness (Figure 2G), and imperviousness (Figure 2H) models were generated. The simulation results presented the temporal dynamics of surface runoff, depicted as maximum recorded water depths and velocities. Finally, the outcome was depicted as models illustrating the maximum values of all parameters for each scenario. Figure 3 shows the depth (A) and velocity (B) of water, as well as the overall flood hazard level (C) for low-probability floods (100 years).

The subject sub-catchment has very low elevation differences and is predominantly flat, with a slight slope from the Neretva River embankment to the Jerkovac embankment, which defines the main direction of surface runoff. The greatest water depths occur in undeveloped areas between roads. Water velocities are very low due to gentle terrain slopes, with the highest levels of danger occurring in areas with the greatest water depths.
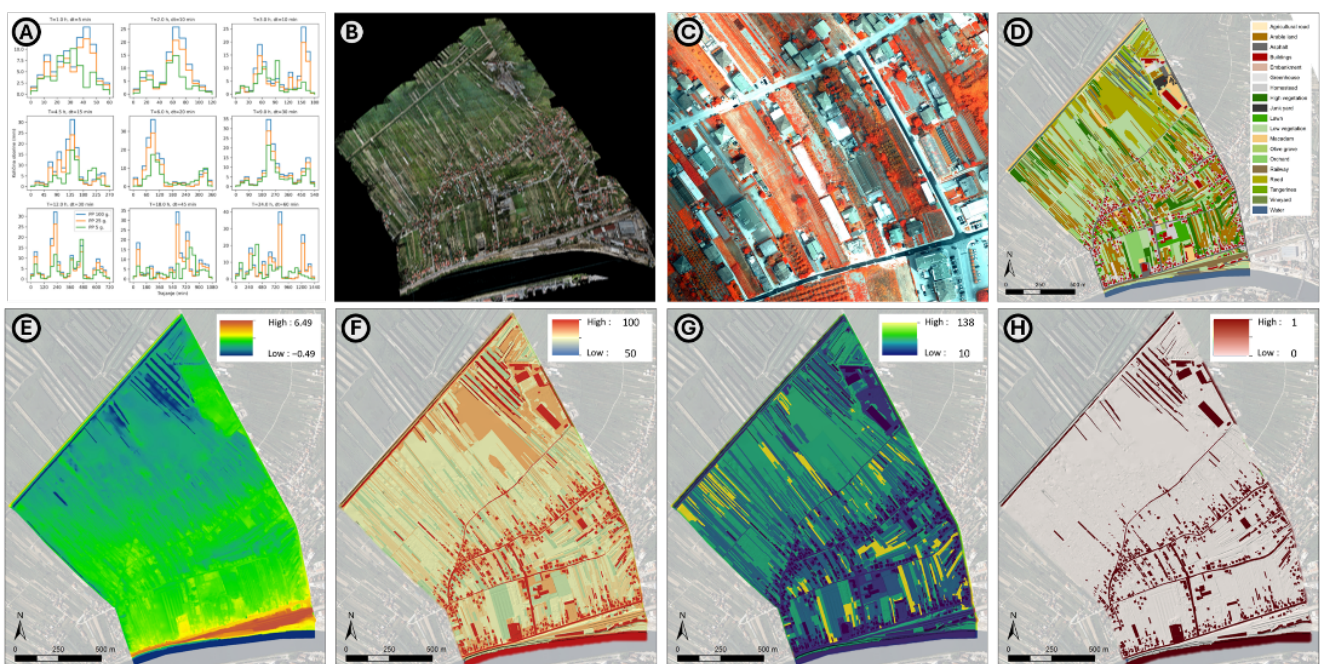
Figure 2. (A) Rainfall hyetographs; (B) DSM; (C) UAVMS; (D) LULC; (E) DTM; (F) Infiltration; (G) Roughness; (H) Imperviousness.

4   Discussion

Numerous user-defined parameters in the processes of data collection (UAV and multispectral camera calibration, flight altitude, flight speed, flight mission type, front and side overlap, etc.), processing (software, filtering data process, classification algorithms, number of LULC classes, number of samples, etc.), and analysis (size and type of computational network, boundary conditions, numerical calculation parameters, calculation method, etc.) can

automatic rain gauges uniformly distributed throughout the watershed is recommended to obtain a more accurate picture of the rainfall regime. Additionally, monitoring water levels in main channels would greatly facilitate future flood analyses and ensure more reliable flood mitigation measures. Flood hazard analyses in urban areas can be further enhanced by integrating wastewater drainage systems into a coupled 1D/2D hydraulic model to simulate combined surface flow and pipe flow. To
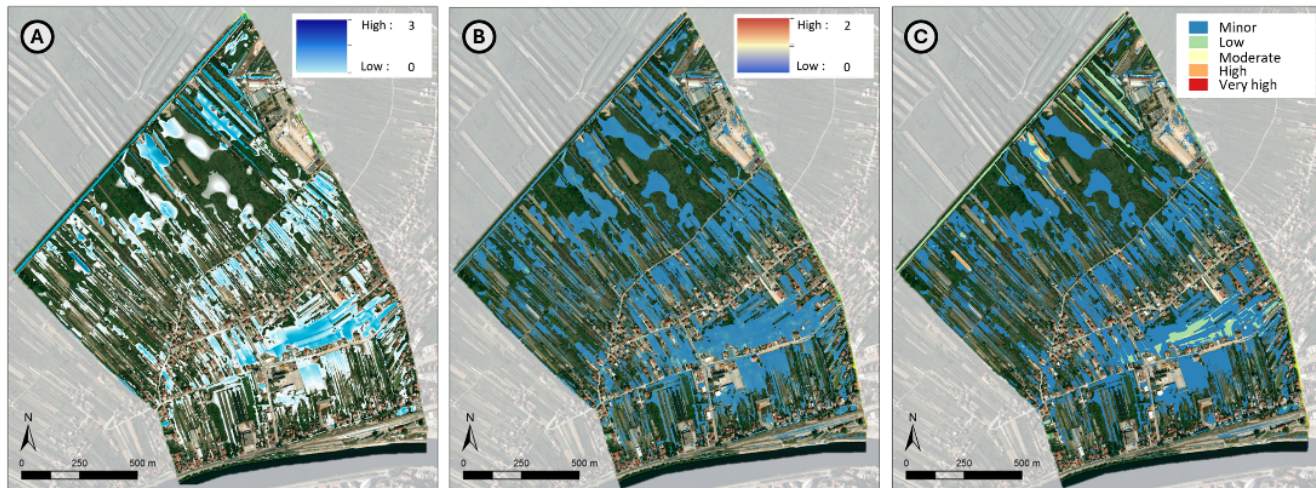
Figure 3. (A) Water depth; (B) Water velocity; (C) Flood hazard level.

influence the output results. Therefore, it is crucial to approach the research process carefully and thoroughly. The VHR LULC model serves as an extremely important input data for hydrological-hydraulic analyses.

The process of UAV$_{MS}$ segmentation and selection of a suitable classification algorithm presents a challenge. Parameters such as spectral and spatial detail and minimum segment size align with previous research utilizing GEOBIA (Šiljeg et al. 2023). Extremely low accuracy assessment results of the LULC model are attributed to the large number of classes with similar spectral characteristics (Dihkan et al. 2013). To obtain a more accurate model, it is necessary to manually correct misclassified segments of UAV$_{MS}$ (Qu et al. 2021). Such a corrected model can provide reliable information on land cover and land use, which can assist decision-makers and emergency services in flood situations. Hydrological-hydraulic analyses based on accurate DTM, and models of infiltration, roughness, and imperviousness derived from LULC can accurately depict water depths and velocities, thus indicating the level of risk from pluvial floods in different scenarios (Interreg STREAM 2023).

5   Conclusions

The occurrence of pluvial floods in the research area is significantly influenced by the terrain topography and hydrological conditions, as well as by the built drainage and flood defence system (channels and embankments). Urban flood analysis using higher resolution and more detailed data has resulted in significantly more precise and reliable flood hazard maps compared to previous analyses. For more accurate and reliable modelling of pluvial floods, the installation of several meteorological stations with

accomplish this, a survey of the entire drainage system, including manholes and pipelines, is necessary.

6   References

Alizadeh, B., Rouzbeh B., 2023. CN-N: A Python-Based ArcGIS Tool for Generating SCS Curve Number and Manning's Roughness. Water 15 (20), 3581.

Blaschke, T., 2010. Object Based Image Analysis for Remote Sensing. ISPRS Journal of Photogrammetry and Remote Sensing 65 (1), 2-16.

Brunner, G.W., 2021. HEC-RAS 6.0 2D User's Manual.

Chaumillon, E., Bertin X., Fortunato, A.B., Bajo, M., Schneider, J.L., Dezileau, L., Walsh, J.P, Michelot, A., Chauveau, E., Créach, A., Hénaff, A., Sauzeau, T., Waeles, B., Gervais, B., Gwenaële J., Baumann, J., Breilh, J.F., Pedreros, R., 2017. Storm-Induced Marine Flooding: Lessons from a Multidisciplinary Approach. Earth-Science Reviews 165, 151-84.

De Moel, H., Jongman, B., Kreibich, H., Merz, B., Penning-Rowsell, E. Ward, P. J., 2015. Flood Risk Assessments at Different Spatial Scales. Mitigation and Adaptation Strategies for Global Change 20 (6), 865-890.

Dihkan, M., Guneroglu, N., Fevzi K., Guneroglu, A., 2013. Remote Sensing of Tea Plantations Using an SVM Classifier and Pattern-Based Accuracy Assessment Technique. International Journal of Remote Sensing 34 (23), 8549-8565.

Hoeft, C.C., 2020. Incorporating Updated Runoff Curve Number Technology into NRCS Directives. 78-87.

Interreg STREAM., 2023. Docs&Tools - STREAM - Italia-Croatia, https://programming14-20.italy-croatia.eu/web/stream/docs-and-tools. (Accessed 23 October, 2023)

Krvavica, N., Jaredić, K., Rubinić, J., 2018. Metodologija Definiranja Mjerodavne Oborine Za Dimenzioniranje Infiltracijskih Sustava. Građevinar 8.

Krvavica, N., Rubinić, J., 2020. Evaluation of Design Storms and Critical Rainfall Durations for Flood Prediction in Partially Urbanized Catchments. Water 12 (7).

MacFaden, S.W., O'Neil-Dunne, J.P.M., Royar, A.R., Lu, J.W.T., Rundle, A.G., 2012. High-Resolution Tree Canopy Mapping for New York City Using LIDAR and Object-Based Image Analysis. Journal of Applied Remote Sensing 6 (1), 063567.

Ochoa Rodriguez, S., ten Veldhuis, M.C., Maksimović, Č., Schertzer, D., Willems, P., 2012. Scientific Challenges for Enhancing Urban Pluvial Flood Resilience. in Geophysical Research Abstracts. Vol. 14. Copernicus GmbH.

Qu, L., Chen, Z., Li, M., Zhi, J., Wang, H., 2021. Accuracy Improvements to Pixel-Based and Object-Based Lulc Classification with Auxiliary Datasets from Google Earth Engine. Remote Sensing 13 (3), 453.

Singh, P., Sinha, V.S.P., Vijhani, A. Pahuja, N., 2018. Vulnerability Assessment of Urban Road Network from Urban Flood. International Journal of Disaster Risk Reduction 28, 237-250.

Šiljeg, A., Marinović, R., Domazetović, F., Jurišić, M., Marić, I., Panđa, L., Radočaj, D., Milošević, R., 2023. GEOBIA and Vegetation Indices in Extracting Olive Tree Canopies Based on Very High-Resolution UAV Multispectral Imagery. Applied Sciences 13 (2), 739.

Šiljeg, A., Panđa, L., Marinović, R., Krvavica, N., Domazetović, F., Jurišić, M., Radočaj, D., 2023. Infiltration Efficiency Index for GIS Analysis Using Very-High-Spatial-Resolution Data. Sustainability 15 (21), 15563.

UNDRR., 2010. Emerging Challenges for Early Warning Systems in Context of Climate Change and Urbanization, http://www.undrr.org/publication/emerging-challenges-early-warning-systems-context-climate-change-and-urbanization. (Accessed 10 April, 2024)

WGF., 2016. Pluvial Flooding: An EU Overview; European Commission and Water Group Floods (WGF), https://environment.ec.europa.eu/topics/water/floods_en. (Accessed 11 April, 2024)

WMO., 2010. PWS – 21: Guidelines on Early Warning Systems and Application of Nowcasting and Warning Operations (WMO/TD-No. 1559). https://library.wmo.int. (Accessed 11 April, 2024)

Strategies for Civil-Military Geographical Support to Defence and Security Operations

Mladen Viher[1], *

[1] Department for military studies, Croatian Defence Academy "Dr. Franjo Tuđman", Zagreb, Croatia,
   mviher.academia@gmail.com

* corresponding author

Abstract: The possibilities offered by modern GIS and remote sensing technologies provide great opportunities for their dual purpose. The availability of applications, materials as well as appropriate training and literature makes them relevant in geographic intelligence support to military operations (GEOINT). Even usage of the open sources, such as Copernicus and USGS, enable limited operationalization in area survey and detection of changes with significant potential for education and training of the expert staff. In order to make the best use of this potential, a significantly improved civil-military cooperation is needed, whereby defence and security organizations are given the opportunity to acquire professional knowledge from the relevant scientific fields, and academic and private partners are enabled to acquire knowledge and practical experience in the skills and organization of military operations. This work, using the method of multi-criteria analysis, an objective comparison of available strategies are made. The result of the applied multi-criteria analysis favours a permanent, integrated civil-military organization with a high degree of coordination and interoperability based on the existing organization of state ministries, without the need to establish new specialized institutions.

Keywords: GEOINT; dual-use; remote sensing; multi criteria analysis.

1   Introduction

The modern geospatial environment is characterized by complexity that requires mastering of significant IT capabilities. It is a favourable circumstance that modern technologies for the analysis of geospatial information in support of military operations (GEOINT) are at a high level of development and are widely available. GEOINT was created for military needs, through the process of intelligence preparation of the battlefield, and the developed methods and procedures found great use in civilian applications. Civilian and military experts jointly participated in their development, so GEOINT is one of the best examples of their synergy and dual use.

Continuous training of GEOINT specialists is enabled through NATO and the EU, and available open sources, although they provide limited operational GEOINT capabilities, it still has great opportunities for research and development of new methods to support GEOINT training at the national level. Currently, significant national capabilities for GEOINT are scattered across segments and levels of society, there are no national strategic and doctrinal documents for the development of this capability, nor integrated training programs at the

necessary levels of expertise (Viher 2021). Situations of natural and technical disasters encourage us to improvise and ad-hoc solutions whose positive experiences are forever lost in the absence of a system of lessons learned for GEOINT. The main objective of the text is a suggestion of integrating existing national capabilities in the way of the most effective strategy. An example of a dual-use GEOINT product is shown on the Figure 1.

Figure 1. An example of dual-use GEOINT product; change detection of the Sentinel-1 satellite Synthetic Aperture Radar (SAR) imagery after demolition of the Novaja Kahovka dam on June 6, 2023, scattering coefficient difference shows flooded areas (red), two SAR-s were compared (Google Maps as the base layer).

2   Materials and methods

Using the BOCR (Benefits-Opportunities-Costs-Risks) framework for the analytical network process, the gains, opportunities, costs and risks of five alternatives were analysed, all were ranked by success in the BOCR synthesis, and their success rates were also quantitatively compared. A hybrid network and hierarchical structure runs through the entire model; in the BOCR framework, the criteria are connected in a network, while the alternatives under them are in a hierarchical relationship (Figures 2 to 5).

Benefits (Figure 2) are the basic functions and purpose of GEOINT; support for operations carried out by military and security organizations and institutions, concept development and experimentation (CD&E) for the future development of capabilities as new technologies and doctrines are introduced, international activities (bilateral and multilateral; NATO and EU) and participation in higher education in order to maintain capabilities through the expert education of one's own staff.
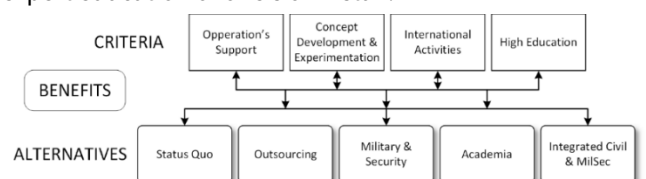
Figure 2. Benefits have four criteria among five alternatives.

Alternatives differed most across opportunities (Figure 3, Table 2). Opportunities represent the possible organizational and personnel superstructure of GEOINT. Initiating and participating in scientific research projects is an easily achievable upgrade. Advisory and consultation at the strategic level contributes to decision-making at the highest level as well as to the long-term national development of GEOINT as a dual-purpose discipline. Attracting experts and the possibility of establishing centres of excellence contribute significantly to the personnel quality and sustainability of the GEOINT system. A significant opportunity for personal development is the possibility of attracting and developing reserve officers - Subject Matter Experts (SME) for GEOINT, who will undergo parts of military training for: intelligence tasks, work in headquarters and knowledge of the processes of military decision-making, although they do not have the authority to command. The most important opportunity is the creation of interministerial cooperation through the systematic and solid connection of the responsible ministries: defence and security, internal affairs, science, economy and EU funds.
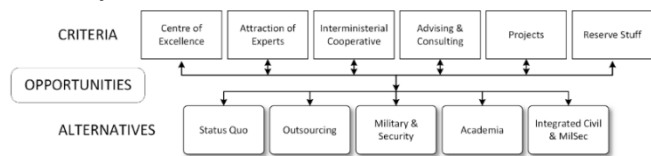
Figure 3. Opportunities have six criteria among five alternatives.

Costs are tracked through necessary investments in equipment, data, projects and personnel (Figure 4). In this paper, the costs are compared qualitatively, but they can also be expressed quantitatively in future detail assessments.
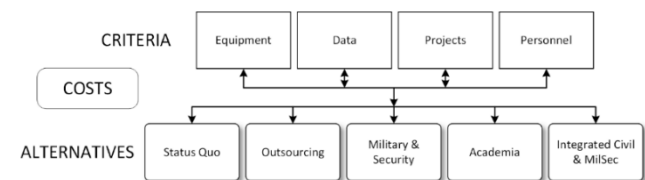
Figure 4. Costs are considering four generic criteria based on qualitative scales.

Among the five alternatives, the risks can be divided into: impossibility and inadequate equipping of the GEOINT system, failure of attracting and retaining personnel, impossibility of realizing projects due to material or organizational deficiencies, and security risks from foreign intelligence activities (Figure 5).
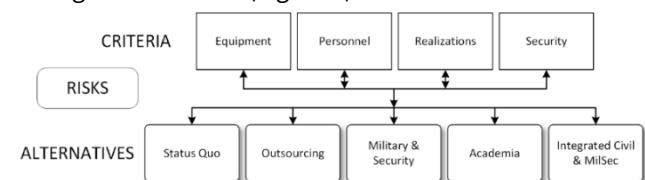
Figure 5. Risks are considered over four generic criteria.

In the search for an optimal strategy of GEOINT support for military operations, the former positive experience of cooperation with civilian factors (academia, public institutions and the enterprises) was included, as well as the complementary of existing capabilities. Five

strategies for GEOINT support to military operations are assumed in the paper. At one extreme, they extend from the maintenance of the existing state (Status Quo) in which GEOINT is at the stage of rudimentary development, dependent on enthusiasm and the ability to improvise, but almost completely outside the existing NATO strategies, doctrines, standards and standard operating procedures. The next strategy is outsourcing, where there are no development and organization costs, but product prices are extremely high, there is no accumulation of knowledge in the system, and the security risks are the greatest in that case. The strategy of leaving GEOINT to the academic community opens up access to new methods and technologies, as well as an out-of-the-box way of thinking. At the same time, the social networks of experts are expanding significantly, attracting young people interested in GEOINT, which is a prerequisite for the future establishment of reserve officers' corps. The negative side of this strategy is that a wide and heterogeneous mass of experts represents a security challenge. Assigning the GEOINT development strategy to the Ministry of Defence and the Ministry of the Interior, with the professional support of the relevant departments of science and economy, has its advantages in better defining the needs of the Armed Forces, the highest level of military-security expertise and the best security of processes, personnel and infrastructure.

3   Results

Already developed ANP-BOCR methods were used in the work, we refer the reader to the original works of the founder of this method (Saaty and Vargas 2013) Tables 1 to 4 compare the criteria (ANP) and then the alternatives according to the layer of criteria (AHP). Saaty's importance ratings were used; 1 = equal, 2 = weak, 3 = moderate, 4 = moderate plus, 5 = strong, 6 = strong plus, 7 = very strong, demonstrated, 8 = very, very strong and 9 = dominating and their reciprocal values. In all cases inconsistency must be lower than 0.1.

The best alternatives in benefits and opportunities carry with them the highest estimated costs (Table 3). The ANP-BOCR method enables a good balancing of gains and investments although it is not a method for planning and optimizing GEOINT capability budgets.

Similar to the COSTS criteria the RISKS criteria (Table 4) have the same assessments between the alternatives and the criteria so both Tables 3 and 4 are quite simple.

The outcome of the BOCR model (B*O) / (C * R) (Saaty, 2013) finds the integrated civil-military coordination among responsible ministries and well-connected institutions and organizations – tied to mutual, preferably international, projects and activities. The second ranked alternative; GEOINT under full responsibility to national defence and security have just 41% of success of the best ranked alternative. The worst alternative of the Status Quo maintaining clearly shows that in the case of integrated civil-military cooperation in the GEOINT we will have the progress of two orders of magnitude.

Table 1. Relative importance of the criteria and alternatives in benefits.

Benefits - Inconsistency 0.016290	**High education**	**International activities**	**Operational support**	
CD&E	1	5	1/3	
High education		5	1/3	
International activities			1/5	
wrt CD&E - Inconsistency 0.08553	**Integrated**	**MIL&SEC**	**Outsourcing**	**Status quo**
Academia	1/7	1/3	1	5
Integrated		5	7	9
MIL&SEC			5	7
Outsourcing				4
wrt High education - Inconsistency 0.08465	**Integrated**	**MIL&SEC**	**Outsourcing**	**Status quo**
Academia	1/5	2	5	7
Integrated		5	7	9
MIL&SEC			4	7
Outsourcing				3
wrt International act. - Inconsistency	**Integrated**	**MIL&SEC**	**Outsourcing**	**Status quo**
Academia	1/5	1/3	1	6
Integrated		5	6	9
MIL&SEC			4	7
Outsourcing				3
wrt Operat. support - Inconsistency	**Integrated**	**MIL&SEC**	**Outsourcing**	**Status quo**
Academia	1/7	1/6	1/2	1/3
Integrated		3	7	9
MIL&SEC			5	5
Outsourcing				2

Table 2. Relative importance of the criteria and alternatives in opportunities.

Opportunities - Inconsistency 0.07731	**Attract. of experts**	**Centre of excel.**	**Interminist. cooperat.**	**Projects**	**Reserve stuff**
Advising & consulting	1/4	1	3	3	2
Attraction of experts		1	3	3	2
Centre of excellence			5	4	5
Interminist. cooperative				1/3	1/2
Projects					2
wrt Advising and Consult. - Inconsistency	**Integrated**	**MIL&SEC**	**Outsourcing**	**Status quo**	
Academia	1/5	1/3	1	5	
Integrated		4	6	9	
MIL&SEC			4	7	
Outsourcing				4	
wrt Attraction of exper. - Inconsistency 0.05874	**Integrated**	**MIL&SEC**	**Outsourcing**	**Status quo**	
Academia	1/4	3	1	5	
Integrated		5	5	9	
MIL&SEC			1	5	
Outsourcing				6	
wrt Center of excellence - Inconsistency 0.06968	**Integrated**	**MIL&SEC**	**Outsourcing**	**Status quo**	
Academia	1/5	2	2	6	
Integrated		5	5	9	
MIL&SEC			3	5	
Outsourcing				4	
wrt Interministerial co. - Inconsistency 0.06814	**Integrated**	**MIL&SEC**	**Outsourcing**	**Status quo**	
Academia	1/5	1	4	5	
Integrated		6	7	9	
MIL&SEC			5	7	
Outsourcing				2	
wrt Projects - Inconsistency 0.07067	**Integrated**	**MIL&SEC**	**Outsourcing**	**Status quo**	
Academia	1/5	3	1	6	
Integrated		5	6	9	
MIL&SEC			1/3	4	
Outsourcing				5	
wrt Reserve stuff - Inconsistency 0.06743	**Integrated**	**MIL&SEC**	**Outsourcing**	**Status quo**	
Academia	1/7	1/5	1	3	
Integrated		5	6	9	
MIL&SEC			5	7	
Outsourcing				2	

Table 3. Relative importance of the criteria and alternatives in costs.

Costs - Inconsistency 0.05770	Equipment	Projects	Stuff	
Data	2	3	1/3	
Equipment		4	1/2	
Projects			1/6	
wrt Costs criteria - Inconsistency 0.085530	Integrated	MIL&SEC	Outsourcing	Status quo
Academia	1/3	3	3	7
Integrated		5	4	9
MIL&SEC			1	7
Outsourcing				5

Table 4. Relative importance of the criteria and alternatives in risks.

Risks - Inconsistency 0.05810	Realization	Security	Stuff	
Equipment	1/2	1/5	1/4	
Realization		1/3	1/2	
Security			1	
wrt Risks criteria	Integrated	MIL&SEC	Outsourcing	Status quo
Academia	3	3	1/3	1/7
Integrated		1	1/6	1/9
MIL&SEC			1/6	1/7
Outsourcing				1/3

Table 5. The outcome of the BOCR model highly favourites the integrated strategy.

	Raw	Normalized	Ideal	RANK
Integrated	13.9949	0.6740	1.0000	1st
MIL&SEC	5.7507	0.2769	0.4109	2nd
Academia	0.6713	0.0323	0.0480	3rd
Outsourcing	0.2678	0.0129	0.0191	4th
Status quo	0.0805	0.0039	0.0057	5th

4 Discussion and conclusions

The most developed strategy is represented by an integrated model of military-civilian cooperation that fully utilizes existing national resources and does not require the opening of new organizations and institutions. In that strategy, the emphasis is on developed and sustainable interdepartmental cooperation and on a joint national strategy for GEOINT.

In addition to active participation and promotion of an integrated model of national GEOINT on conferences such as ICERS, it is necessary to take practical steps to identify and connect future stakeholders in the activities. In this sense, it is necessary for the Republic of Croatia to join the international activities offered by the initiatives of the EU (European Defence Agency, Sat Centre, Horizon Europe, etc.) and NATO (Science and Technology Organization, Science for Peace, ACT-CD&E, etc.). One of the first steps should be the signing of the Charter on Space and Disasters by the responsible Ministry of Internal Affairs, this step will significantly speed up the processes of civil-military integration.

5 References

Saaty, T., L., Vargas, L., G., 2013. Decision Making with the Analytic Network Process (Second Edition), International Series in Operations Research and Management Science, Springer New York.

Viher, M., Žiža, I., Radun, B., Tomljenović, I., Čvrljak, M., Kušan, V., Vuković, J., Knežević, L., 2021. GEOINT in natural and technical disasters, Proceedings of the 1st Croatian Conference on Earthquake Engineering (1CroCEE), 22-24 March 2021, Zagreb, Croatia, 397-403.

Effective Spatial Planning of Watchtowers for the Detection of Wildfire Hotspots in Thasos Island, Greece

Stavros Sakellariou[1,2], Christos Christakis[2,], Stergios Tampekis[3], Olga Christopoulou[1], Athanasios Sfougaris[4]*

[1] Department of Planning and Regional Development, University of Thessaly, 38334, Volos, Greece

[2] Department of Environmental Sciences, University of Thessaly, 41500 Larisa, Greece, cchristakis@uth.gr

[3] Department of Forestry and Natural Environment Management, Agricultural University of Athens, 3 Dimokratias St., 36100 Karpenisi, Greece

[4] Department of Agriculture Crop Production and Rural Environment, University of Thessaly, 38446 Volos, Greece

* corresponding author

Abstract: Forest fires, beyond the obvious ecological role that plays in forest ecosystems, can be a detrimental factor to natural and human ecosystems downgrading the quality of life of local population. The paper aims to enhance forest fire prevention through the prompt detection of fire events, a fact that would immediately alarm the firefighting forces to contain and mitigate the severity of this phenomenon. To this end, viewshed analysis has been implemented taking into consideration multiple factors: the overlapping effect minimization; the visibility maximization with a certain number of observatories; the sufficient visibility of certain land cover types. The results indicate the selection of four groups of observatories (each group covered a sufficient percentage of visibility) covering almost 70% of the entire island which is considered a satisfying figure given the rough topography of the study area. After these first 20 positions, the incorporation of extra locations would provide marginal profit in visibility terms. Therefore, the selection of the number of groups of observatories is mainly a political decision weighting the interaction of environmental protection and financial restrictions.

Keywords: fire hotspots; visibility analysis; GIS; Thasos island; Greece.

1   Introduction

Forest fires, beyond the obvious ecological role that plays in forest ecosystems, can be a detrimental factor to natural and human ecosystems downgrading the quality of life of local population. Due to specific peculiarities of some geographic regions, many countries in the Mediterranean Sea are at high risk for high severity forest fires as statistics indicates (Sakellariou et al. 2017). These peculiarities are related to specific climatic conditions, topography, and the high degree of interaction of forest with urban areas. Thus, fire prevention constitutes the most significant strategy to tackle high severity forest fires with unpredictable consequences in natural environment and social web. In addition, the restoration cost could reach massive amount of funding. To this end, several models have been developed aiming to detect any forest fire event as quickly as possible. Many researchers have focused on different aspects of fire prevention. In this project, we concentrate our attention to the detection of fire hotspots through a certain number of locations that maximize both the visibility and financial effectiveness. To this end, aim of the project is to find the best positions for the establishment of observatories based on visibility efficacy (both in absolute and relative terms: positions that guarantee large areas of visibility, covering the most susceptible and critical land covers simultaneously). Even though numerous applications on viewshed analysis for certain socioeconomic activities have been implemented (Mouflis et al. 2008, Zhou et al. 2011) there is a shortage of research focusing on forest fires phenomenon (Temiz and Tecim 2009, Pompa-García et al. 2010, Pompa-García et al. 2012, Kang et al. 2013, Sivrikaya et al. 2013). Hence, here we would like to emphasize the added value of visibility analysis on forest fires events. The results indicated that not only the highest locations were effective, but other positions with lower altitudes proved to be very efficient in terms of visibility.

2   Materials and methods

Thasos constitutes a small island which is located in the north-eastern region of Greece. Figure 1 depicts the geographical characteristics of the study area, namely, the exact geographic position of the island in a national and global perspective; the elevation variation across the study domain as well as some cartographic characteristics (projection system, coordinates, scale of map). Thasos island is characterized by significant parts of mountainous areas. The elevation levels fluctuate from 0 (coastal areas) to 1,204 meters. The higher altitudes can be found in the interior of the island, especially in the central and north-eastern region. The dominant land cover type consists of forested areas (63%), followed by agricultural fields (21%), shrubs (13%) and 1% of livestock area, arid land and residential area respectively (Sakellariou 2016).
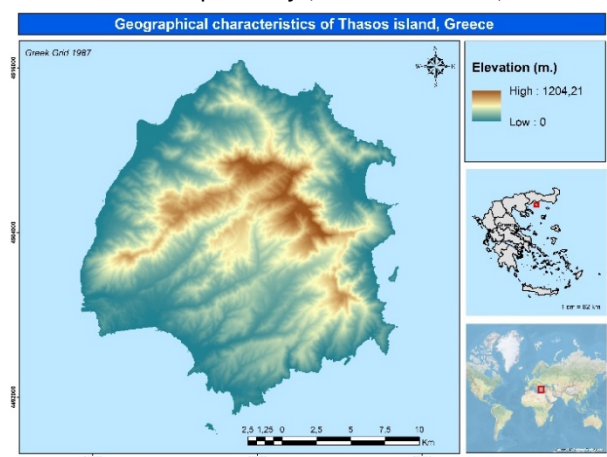
Figure 1. Geographical position and elevation levels of the study area.
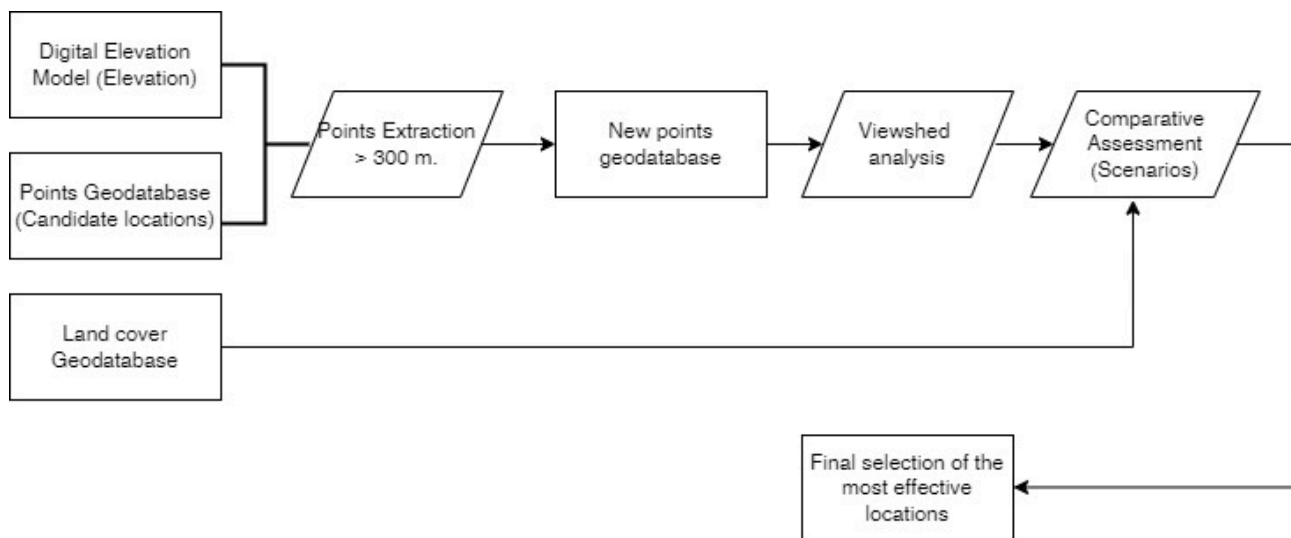
Figure 2. Flowchart of viewshed analysis.

The primary data that was used for this project was the digital elevation model (DEM) of Thasos island and a point geodatabase that reflected the points features across the ridge of mountains (HMGS 2012). In addition, a layer of land cover was used so that we can determine the overlay of visible area and the corresponding land cover type. The cornerstone of this project is relied on viewshed analysis which is integrated in the Geographical Information Systems. We removed all potential locations that lied below 300 meters due to the fact that and fire event could be relatively easily detected by the moving vehicles as well as by the boats approaching the island. However, it should be highlighted the fact that many potential locations above 300 meters are characterized by visibility which approaches the coastline. This happens due to the size and topography of the island. After we have extracted the final potential locations for the observatories, we conducted a viewshed analysis for each location recording the individual capacity of visibility. Next, we proceeded to a comparative assessment of all positions with the corresponding visibility potential and the spatial configuration of the visible area. Locations with high degree of overlapping visibility were removed. Finally, the most efficient locations which met specific criteria (low degree of overlapping visibility; type and significance of land cover type) were chosen trying to minimize the number of potential observatories with the maximum visible area. In the same context, the interrelation of visible area and the corresponding land cover type was calculated, so that we are able to protect the most vulnerable regions.

One more parameter which was defined is related with the suggested elevation of potential watchtower. This factor plays a crucial role, since the higher the observatory the higher visibility is expected. So, taking into account the normal circumstances in Greece, the suggested elevation was defined to 3 meters above the ground. The following chart (Figure 2) summarizes the inputs, methods and the corresponding outputs of this project.

3   Results and discussion

Initially, the geodatabase consisted of 100 candidate locations which are located on the top of ridges. We consequently removed all positions that lied under the elevation level of 300 meters. After this procedure, we implemented the viewshed analysis for each point and calculated the final visibility potential in terms of visible hectares. Figure 3 shows the visibility potential of all 55 remaining locations.
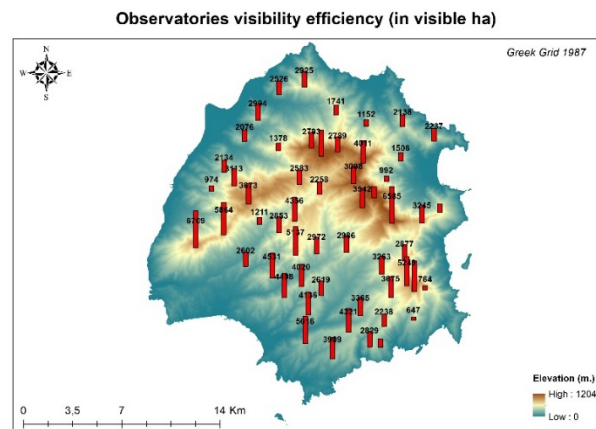
Figure 3. Visibility potential for each candidate location.

As we may see from Figure 3, there is a great variability in visibility capability of each position which is based both on altitude level and the underlying topography of the island. Thus, we had to proceed to a comparative analysis of all these locations, taking into account the overlapping effect as well as the extent and the visibility magnitude of each land cover type.

To this end, we decided to recommend 20 potential locations for the establishment of observatories for two main reasons. Firstly, the suggested 20 positions reduce the overlapping effect (covering adjacent regions) and cover a significant area of critical land cover types. Secondly, we adopted a theoretical scenario of employing all the 55 locations and the gained area (in terms of visibility) was quite marginal. Hence, after the finally selected 20 best positions, the visible added value can be characterized quite marginal. Figure 4 presents the final

selected locations and the respective visible area per group of observatories (each group consists of 5 potential observatories meeting a crucial threshold of visibility effect). As we may notice from Figure 4, the majority of the study area is adequately covered by selecting 20 potential locations. After this number, the added value of extra observatories offer quite limited value. From statistical point of view, the first 5 selected locations (First Group) covered 40.4% of the whole study area; the second group covered 15.8%; the third group covered 8.8%, while the last one covered 4.2%. In total, almost 70% (69.2%) of the entire island is covered by the establishment of the suggested 20 observers. If we adopted the unrealistic scenario (establishment of another 35 observers), the total visibility percentage would approach 80%. So, the proposal of establishment of another 35 observers would just add 10% of visibility in total, which is not feasible in financial terms.
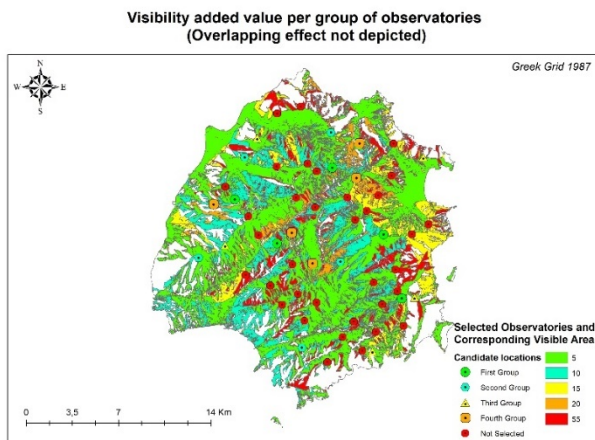
Figure 4. Final selected locations and their respective visible area.

Figure 5 summarizes the viewshed analysis with land cover types. First of all, it should be highlighted that 82% of total forests in the island is now visible from the proposed scenario (20 observers). 73% of agricultural and residential areas respectively are covered by this scheme. 83% of livestock is visible, but this was expected, due to the small area of this specific land cover type. Finally, 53% of shrubs is only visible from this scenario.
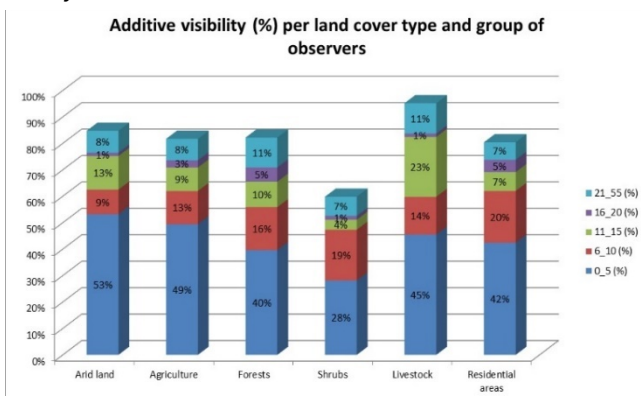
Figure 5. Additive visibility per land cover type.

Here, it should be mentioned that, except the first group of observatories, the visibility potential for the other groups only refer to the additive visibility (having removed any overlapping effect). That is why, the first group seem to have the greatest visibility potential. Another reason is that

we sought to find the best locations for the other groups which met the criteria of overlapping minimization, taking into account the types of land cover. As we may notice from the Figure 6, almost all the groups offered substantial additive visibility. The last group was included because it covers added regions of forests, agriculture and residential areas which are all considered very important aspects. The inclusion of extra groups of watchtowers would almost fall in the same curve as the last one (fourth group). Hence, the selection of maximum 20 locations is considered the best solution given the specific characteristics of the island.
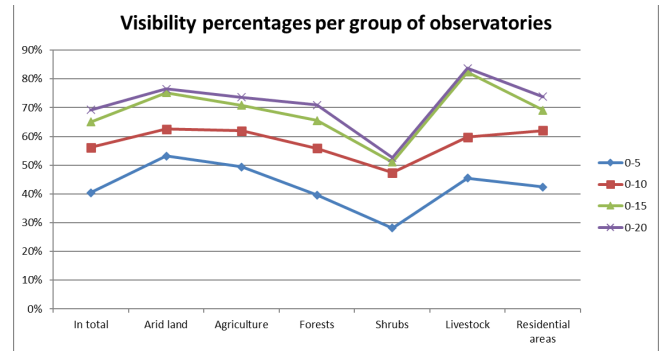
Figure 6. Cumulative visibility potential per group of observatories and land cover types.

4 Conclusions

The paper aims to enhance forest fire prevention through the prompt detection of fire events, a fact that would immediately alarm the firefighting forces to contain and mitigate the severity of this phenomenon. To this end, viewshed analysis has been implemented taking into consideration multiple factors.

First, we needed to choose only candidate locations that are above 300 meters and secondly, a thorough comparative assessment and analysis was followed in order to select the best locations for the establishment of observatories. The primary factors that were involved in the analysis were: the overlapping effect minimization; the visibility maximization with a certain number of observatories; the sufficient visibility of certain land cover types.

The results indicate the selection of four groups of observatories (each group covered a sufficient percentage of visibility) covering almost 70% of the entire island which is considered a satisfying number given the rough topography of the study area. After these first 20 positions, the incorporation of extra locations would provide marginal profit in visibility terms. Therefore, the selection of the number of groups of observatories is mainly a political decision weighting the interaction of environmental protection and financial restrictions. The nature of land cover types may contribute to this final selection given the priorities of any society.

5 References

HMGS, 2012. Hellenic Military Geographic Service.

Kang, S. C., Lee, S.Y., Lee, B., 2013. The Study on the viewshed analysis and the estimation of proper number of forest fire surveillance cameras (Focusing on Samcheok-Si).

Journal of Korean Society of Hazard Mitigation, 13(3), 131-137.

Mouflis, G. D., Gitas, I.Z., Iliadou, S., Mitri, G.H., 2008. Assessment of the visual impact of marble quarry expansion (1984–2000) on the landscape of Thasos island, NE Greece. Landscape and Urban Planning, 86(1), 92-102.

Pompa-García, M., Solís-Moreno, R., Rodríguez-Téllez, E., Pinedo-Álvarez, A., Avila-Flores, D., Hernández-Díaz, C., Velasco-Bautista, E., 2010. Viewshed Analysis for Improving the Effectiveness of Watchtowers, in the North of Mexico. The Open Forest Science Journal, 3(1), 17-22.

Pompa-García, M., Zapata-Molina, M., Hernández-Díaz, C., Rodríguez-Téllez, E., 2012. Geospatial Model as Strategy to Prevent Forest Fires: A Case Study. Journal of Environmental Protection, 3(09), 1034-1038.

Sakellariou, S., 2016. Design and development of a Spatial Decision Support System (SDSS) for the prevention and confrontation of natural disasters: the case of forest fires in Thasos island. PhD Dissertation (In Greek). Department of Planning and Regional Development. School of Engineering. University of Thessaly.

Sakellariou, S., Tampekis, S., Samara, F., Sfougaris, A., Christopoulou, O., 2017. Review of state-of-the-art decision support systems (DSSs) for prevention and suppression of forest fires. Journal of Forestry Research, 28(6), 1107-1117.

Sivrikaya, F., Saglam, B., Akay, A.E., Bozali, N., 2013. Evaluation of forest fire risk with GIS. Polish Journal of Environmental Studies, 23(1), 187-194.

Temiz, N., Tecim, V., 2009. Geographical information systems as a decision support system in forest management. SDU Journal of Science, 4(2), 213-223.

Zhou, D., Wang, B.J., Shi, B., 2011. GIS viewshed analysis of visual pollution assessment for mine environment. Guilin Gongxueyuan Xuebao/Journal of Guilin University of Technology, 31(2), 207-212.

Forecasting Atmospheric Air Pollution in Tehran Using Random Forest Model

Nilufar Makky[1,], Zahra Eghrari[2]*

[1] RSGIS Department., University of Tabriz, Tabriz, Iran, rsgis.nilufarmakki73@gmail.com
[2] GIS Department, College of Eng, University of Tehran, Tehran, Iran, zahraeqrari@ut.ac.ir
* corresponding author

Abstract: Air pollution poses a significant threat to human health, particularly for those with respiratory issues. Since 2018, the Sentinel-5 TROPOMI has been identified as the most effective tool for monitoring air pollution. We conducted an assessment of environmental factors such as precipitation, NDBI (Normalized Difference Built-up Index), temperature, and population to understand the impact of air pollution in megacities, especially in Tehran, from 2020 to 2024. Our study focused on atmospheric pollutants including CO, O_3, Aerosol, NO_2, and SO_2. Using the Random Forest model, we predicted pollutant concentrations and achieved an R2 value exceeding 0.90 for all parameters. Recognizing and understanding these environmental factors is crucial for effective government crisis management.

Keywords: Sentinel-5; air pollution; precipitation; temperature; NDBI; population growth; random forest model.

1 Introduction

Urban populations surged from 751 million in 1950 to 4.2 billion in 2018, dramatically altering city landscapes and exacerbating atmospheric air pollution (Jonson et al. 2020, Glencross et al. 2020). Air pollution's detrimental effects on human health and the environment highlight the urgency of addressing this issue (Glencross et al. 2020, Tainio et al. 2021). Major contributors include emissions from automobiles, aviation, industrial activities, mining, fossil fuel use, and agriculture (Colvile et al. 2001, Ciais et al. 2020). Urban expansion, land use changes, increased traffic, and industrial emissions significantly impact air quality (Kastratović 2019). Air pollution causes millions of premature deaths annually, underscoring the need for effective management strategies (Giles-Corti et al. 2016). Rising temperatures and natural disasters further emphasize the importance of addressing climate challenges (Boer and Hendrix 2000, Kaufmann et al. 2011, Eghrari et al. 2023, Kamran et al. 2023, Makky et al. 2023, Anggraini et al. 2024). Nitrogen dioxide (NO_2) is a critical pollutant causing significant health and ecological damage (Damtoft et al. 2008). Satellite observations, such as TROPOMI, provide essential insights into NO_2 levels and highlight the pandemic's effects on air quality (Duprè et al. 2010). Fossil fuel emissions and pollutants like ozone and aerosols exacerbate urban air pollution and climate change (Li et al. 2021). Cities face significant challenges related to energy consumption and air pollution, with transportation being a major factor. Measures like low emission zones have had mixed results in reducing NO_2 levels (Mojtehedzadeh 2019, Eghrari et al. 2023). In Tehran, addressing transportation and industrial impacts on air pollution is crucial, with research focusing on alternative transportation modes and satellite data to predict pollutant patterns (Fernandez-Moran et al. 2021). In this study, we aim to predict the concentrations of five air pollution parameters to identify the regions where each type of pollution poses the greatest risk to human health.

2 Materials and methods

Using the Google Earth Engine cloud-based platform streamlines the analysis of the intricate interplay between environmental factors and the Earth's surface. This study delves into the dynamic relationship between key environmental factors precipitation, temperature, population growth, and Normalized difference built-up index, additionally pollutants such as CO, NO_2, SO_2, Aerosol, and O_3 within Tehran city. The European Space Agency's Sentinel-5 Precursor (Sentinel-5P) is a crucial Earth Observation satellite equipped with the innovative TROPOMI sensor, designed to bridge the gap between the Envisat mission and the upcoming launch of Sentinel-5 (UN). The TROPOMI sensor, a nadir-viewing imaging spectrometer, plays a vital role in monitoring air pollution by measuring electromagnetic

spectral wavelengths from UV to SWIR spectrum. With a
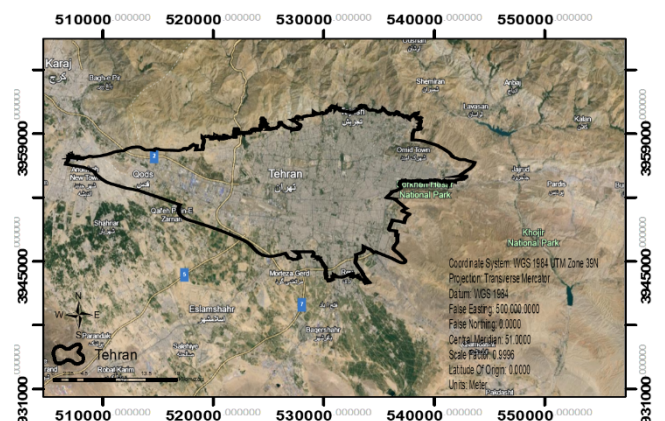
Figure 1. Overview of the study area.

push-broom configuration and a wide swath of 2600 km on the ground, the sensor ensures thorough coverage, albeit with varying pixel dimensions for different spectral bands. The sensor's Level-1B and Level-2 data products have been widely acclaimed for their utility in atmospheric pollution mapping and monitoring (Tabunschik et al. 2023). In our study, we used 60 images per month from 2020 to 2024 for each air pollution parameter. In addition, we obtained 48 images for each environmental factor. We then averaged these images to create one composite image per year for

each environmental factor. Utilizing a robust Random Forest model, we precisely determined the concentrations of Atmospheric Pollutant Parameters (APP) in Tehran. This city Located at coordinates 51°19' E, 35°41' N, Tehran, the capital of Iran, boasts a unique geographical setting. Nestled amidst the Alborz Mountains in the north and bordered by a central desert in the south, the city exhibits distinct elevation and climate differences between its northern and southern regions (Zargari et al. 2024). Figure 1 and Figure 2 indicates the study area and methodology.

This approach allowed for the collection of diverse and accurate data to understand the complex relationship between environmental factors and pollution dynamics. Sentinel-5 data was beneficial for assessing pollutants and predicting air pollution in high-risk areas, such as those with vulnerable populations (Trenchev et al. 2023). Air and environmental pollution, resulting from natural and human activities, are impacted by seasonal variations affecting pollutant levels (Bekkar et al. 2021).
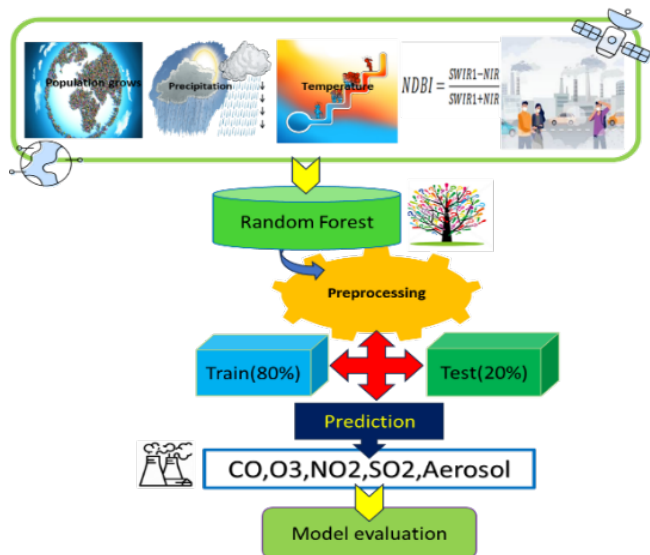
Figure 2. Data processing methodology.

3   Results

Environmental factors such as Precipitation, NDBI, Temperature, and population were presented in Figures 3–6. Furthermore, the Figures 7–11 indicate the most significant parts of the city facing various pollution parameters. Additionally, Figure 12 illustrates the correlation coefficient between pollution parameters and environmental factors.
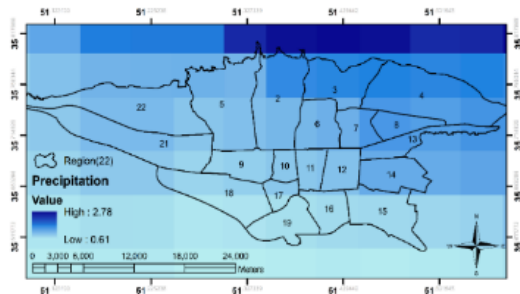
Figure 3. Precipitation values.
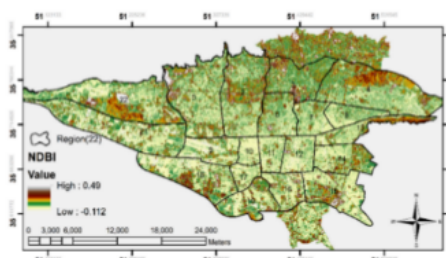
Figure 4. NDBI values.
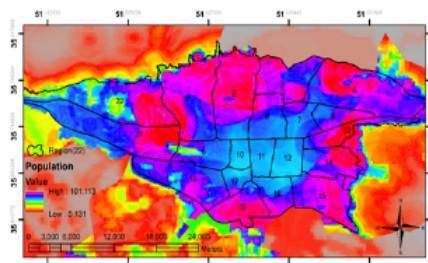
Figure 5. Population values.
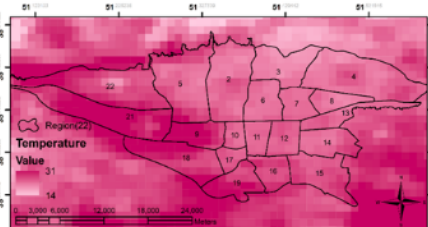
Figure 6. Temperature values.
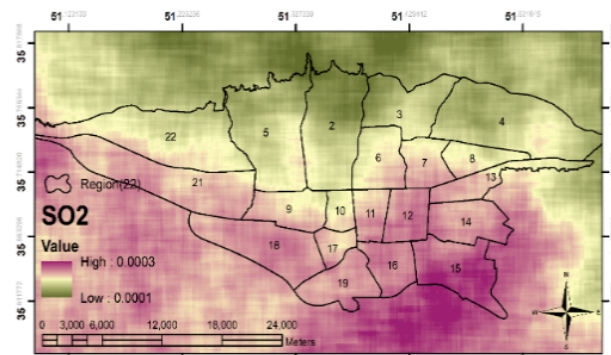
Figure 7. Illustrating predicted concentration of SO_2 in Tehran based on RF.
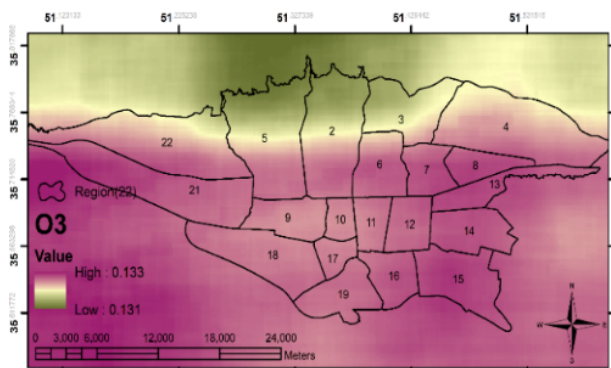
Figure 8. Illustrating predicted concentration of O_3 in Tehran based on RF.
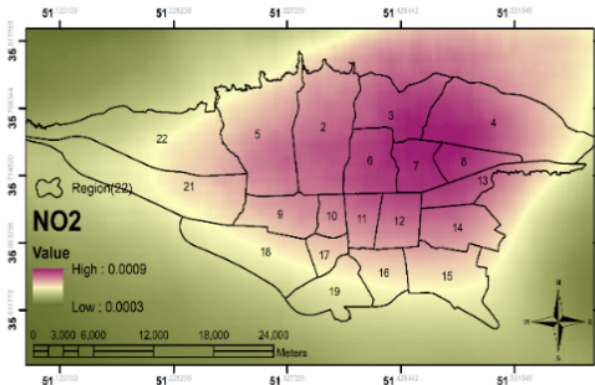
Figure 9. Illustrating predicted concentration of NO₂ in Tehran based on RF.

The Random Forest model (Khajavi and Rastgoo 2023) is applied to predict the Atmospheric Pollutant Parameters in Tehran (Table 1), all accuracy assessments are indicated.
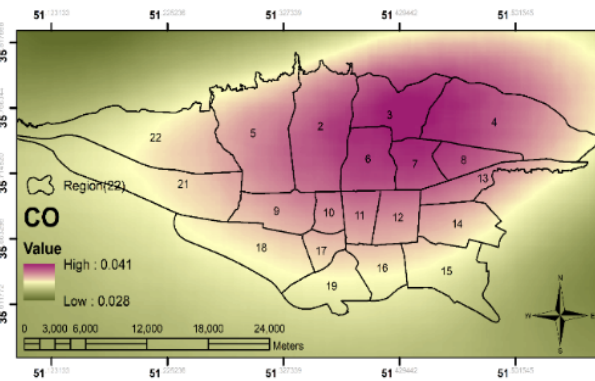
Figure 10. Illustrating predicted concentration of CO in Tehran based on RF.
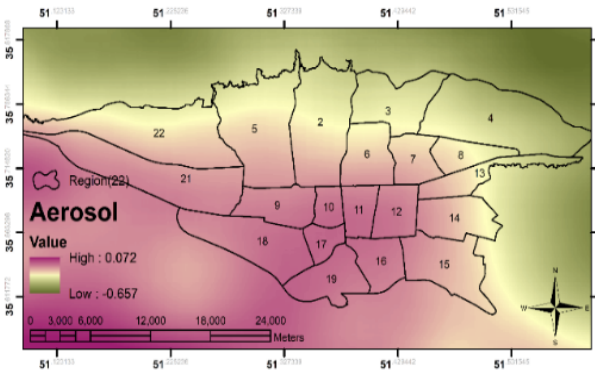
Figure 11. Illustrating predicted concentration of Aerosol in Tehran based on RF.
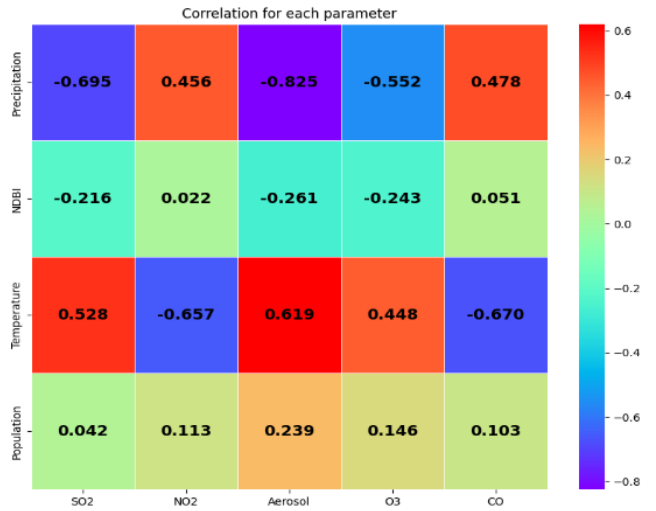
Figure 12. Cross-correlation between environmental factors and Atmospheric Pollutant Parameters.

4   Discussion

This study showed that the Random Forest model accurately predicts atmospheric pollutant concentrations in Tehran and revealed complex relationships between pollutants and environmental factors. Interestingly, precipitation was negatively correlated with aerosol and O_3 levels, indicating a cleansing effect. Positive correlations were found between temperature and pollutants, as well as population and pollutants, highlighting the impact of these factors on air quality.

5   Conclusions

The RF model was highly accurate in predicting APP concentrations in Tehran city using environmental factors and time series pollutant data from 2020 to 2024, with an R^2 value exceeding 0.90 for All, Train, and Test data. Correlation analysis revealed relationships between atmospheric pollutants (SO_2, O_3, NO_2, CO, aerosol) and environmental factors (Precipitation, NDBI, Temperature, Population). Precipitation showed a strong negative correlation with aerosol (–0.8253) and O_3 (–0.5524), suggesting a mitigating effect on these pollutants. Temperature had positive correlations with SO_2 (0.5282) and aerosol (0.6194), and negative correlations with NO_2 (–0.6567) and CO (–0.6698). Population positively correlated with all pollutants, indicating a link to urbanization and emissions. These findings enhance understanding of pollutant-environment relationships and emphasize the importance of considering multiple factors in air quality management.

Table 1. Random Forest (RF) Model Performance Metrics for Air Quality Predictions.

Parameter	All (R²)	Train (R²)	Test (R²)	All (NRMSE)	Train (NRMSE)	Test (NRMSE)
CO	0.9569	0.9428	0.9276	0.0485	0.0685	0.0673
NO₂	0.9515	0.9510	0.9422	0.0245	0.0340	0.0662
SO₂	0.9330	0.9194	0.9177	0.0605	0.0886	0.0832
O₃	0.9648	0.9573	0.9443	0.0522	0.0851	0.0819
Aerosol	0.9033	0.9094	0.9059	0.0811	0.0999	0.1196

6   References

Anggraini, T.S., Irie, H., Sakti, A.D., Wikantika, K., 2024. Machine learning-based global air quality index development using remote sensing and ground-based stations. Environmental Advances 15, 100456.

Boer, E.P.J., Hendrix, E.M., 2000. Global optimization problems in optimal design of experiments in regression models. Journal of Global Optimization 18 (4), 385-398.

Ciais, P., Wang, Y., Andrew, R., Bréon, F.-M., Chevallier, F., Broquet, G., Nabuurs, G.-J., Peters, G., McGrath, M., Meng, W., ... 2020. Biofuel burning and human respiration bias on satellite estimates of fossil fuel CO_2 emissions. Environmental Research Letters 15, 074036.

Colvile, R.N., Hutchinson, E.J., Mindell, J.S., Warren, R.F., 2001. The transport sector as a source of air pollution. Atmospheric environment 35, 1537-1565.

Damtoft, J.S., Lukasik, J., Herfort, D., Sorrentino, D., Gartner, E.M., 2008. Sustainable development and climate change initiatives. Cement and Concrete Research 38 (2), 115-127.

Duprè, C., Stevens, C.J., Ranke, T., Bleeker, A., Peppler-Lisbach, C.O.R.D., Gowing, D.J., Dise, N.D., Dorland, E., Bobbkink, R., Diekmann, M., 2010. Changes in species richness and composition in European acidic grasslands over the past 70 years: The contribution of cumulative atmospheric nitrogen deposition. Global Change Biology 16, 344-357.

Eghrari, Z., Delavar, M.R., Zare, M., Beitollahi, A., Nazari, B., 2023. Land subsidence susceptibility mapping using machine learning algorithms. ISPRS Annals of the Photogrammetry, Remote Sensing and Spatial Information Sciences X-4/W1-2022, 129-136.

Eghrari, Z., Delavar, M.R., Zare, M., Mousavi, M., Nazari, B. and Ghaffarian, S., 2023. Groundwater level prediction using deep recurrent neural networks and uncertainty assessment. ISPRS Annals of the Photogrammetry, Remote Sensing and Spatial Information Sciences. X-1/W1-2023. 493-500.

Fernandez-Moran, R., Gómez-Chova, L., Alonso, L., Mateo-García, G., López-Puigdollers, D., 2021. Towards a novel approach for Sentinel-3 synergistic OLCI/SLSTR cloud and cloud shadow detection based on stereo cloud-top height estimation. ISPRS Journal of Photogrammetry and Remote Sensing 181, 238-253.

Giles-Corti, B., Vernez-Moudon, A., Reis, R., Turrell, G., Dannenberg, A.L., Badland, H., Foster, S., Lowe, M., Sallis, J.F., Stevenson, M., Owen, N., 2016. City planning and population health: a global challenge. The Lancet 388 (10062), 2912-2924.

Glencross, D.A., Ho, T.R., Camina, N., Hawrylowicz, C.M., Pfeffer, P.E., 2020. Air pollution and its effects on the immune system. Free Radical Biology and Medicine 151, 56-68.

Jonson, J.E., Gauss, M., Schulz, M., Jalkanen, J.-P., Fagerli, H., 2020. Effects of global ship emissions on European air pollution levels. Atmospheric Chemistry and Physics 20, 11399-11422.

Kamran, K.V., Makky, N., Charandabi, N.K., 2023. Investigating the flooded area of Bangladesh by Sentinel_1 and CHIRPS images in the GEE system. Intercontinental Geoinformation Days (IGD) 6, 83-88, Baku, Azerbaijan.

Kastratović, R., 2019. Impact of foreign direct investment on greenhouse gas emissions in agriculture of developing countries. Australian Journal of Agricultural and Resource Economics 63, 620-642.

Kaufmann, R.K., Kauppi, H., Mann, M.L., Stock, J.H., 2011. Reconciling anthropogenic climate change with observed temperature 1998–2008. Proceedings of the National Academy of Sciences 108 (29), 11790-11793.

Li, M., Liu, W., Bi, M., Cui, Z., 2021. Dynamic substance flow analysis of lead in the fossil fuel system of China from 1980 to 2018. Journal of Cleaner Production 313, 127918.

Makky, N., Valizadeh Kamran, K., Karimzadeh, S., 2023. Impact of Global Warming on water height using machine learning algorithms. Proceedings of the 5th International Electronic Conference on Remote Sensing, 7-21 November 2023, MDPI: Basel. Switzerland.

Mojtehedzadeh, M., 2019. Assessment of Urban Transport System in Tehran. Suti Report; United Nations Economic and Social Commission for Asia and Pacific (ESCAP): Bangkok, Thailand. Available online: https://www.unescap.org/ sites/default/files/Tehran.pdf (Accessed on 17 July 2019).

Tainio, M., Andersen, Z.J., Nieuwenhuijsen, M.J., Hu, L., de Nazelle, A., An, R., Garcia, L.M., Goenka, S., Zapata-Diomedi, B., Bull, F., ... 2021. Air pollution, physical activity and health: A mapping review of the evidence. Environment international 147, 105954.

Zargari, M., Mofidi, A., Entezari, A., Baaghideh, M., 2024. Climatic comparison of surface urban heat island using satellite remote sensing in Tehran and suburbs. Scientific Reports 14 (1), 643.

GIS for Sustainable Development

COMPARISON OF TWO SOLAR POTENTIAL METHODS ON ROOFTOPS USING LIDAR DATA
Katarina Barnjak, Mario Miler, Luka Rumora, Damir Medak

ADVANCING LAND-COVER CLASSIFICATION IN CROATIA: IMPLEMENTATION OF A PILOT PROJECT FOR ARKOD+ AND CROLIS LU INITIAL LAYER CREATION
Matjaž Štanfel, Dragan Vitas, Mladen Majcen, Dario Perešin

SPATIAL ANALYSIS OF INFRASTRUCTURE TYPES IN KIZILDAĞ NATIONAL PARK USING REMOTE SENSING AND GIS
E. Seda Arslan, Ömer K. Örücü

UTILIZING REMOTE SENSING DATA FOR SPECIES DISTRIBUTION MODELLING OF BIRDS IN CROATIA
Andreja Radović, Sven Kapelj, Louie Thomas Taylor

SIMULATION OF LAND USE AND LAND COVER CHANGE AND URBAN SPRAWL PREDICTION IN LUCKNOW METROPOLITAN AREA USING MARKOV CHAIN MODEL
Vijay Kumar Singh Rathore, Sudhir Kumar Singh, Anjani Kumar Singh

RS-GIS MONITORING OF AFGHANISTAN-KAZAKHSTAN-PAKISTAN CITIES UNSUSTAINABLE DEVELOPMENT
Gaukhar Meldebekova, Sholpan Kulbekova, Noor Nabi Dahar, Chakalov Andrey, Muhammad Ilyas, Syed Imran Moazzam Shah, Janay Sagin

CHARACTERIZATION OF VALLEYS AND GULLIES OF THE NORTH AND CENTRAL VELEBIT COASTAL SLOPE
Klara Grošanić, Marin Mićunović, Sanja Faivre

RS AND GIS APPLICATION FOR THE ALTERNATIVE SCENARIOS AND REGIONS FOR HYDROGEN EXPLORATION
Janay Sagin, Dani Sarsekova, Raushan Amanzholova, Rebecca King, Kairat Amanzholov, Baktybek Duisebek, Muhammad Ilyas, Noor Nabi Dahar, Syed Imran Moazzam Shah

Comparison of Two Solar Potential Methods on Rooftops Using LIDAR Data

*Katarina Barnjak[1], Mario Miler[2], Luka Rumora[2,] *, Damir Medak[2]*

[1] University of Zagreb – Faculty of Geodesy, Zagreb, kbarnjak@geof.hr

[2] Chair of Geoinformatics, Department of Geomatics, University of Zagreb – Faculty of Geodesy, Zagreb, mario.miler@geof.unizg.hr, luka.rumora@geof.unizg.hr, damir.medak@geof.unizg.hr

* corresponding author

Abstract: This paper presents a comprehensive assessment of rooftop solar potential in the urban environment of Karlovac, Croatia, using LIDAR (Light Detection and Ranging) data. In the midst of increasing demand for sustainable energy solutions, rooftop photovoltaic systems offer a promising opportunity for decentralized energy generation. However, their efficient use requires precise estimation of solar potential at high spatial resolution. This study uses LIDAR data together with Geographic Information System (GIS) techniques to assess the viability of rooftop photovoltaic systems. The methodology involves processing data from LIDAR-derived digital surface models (DSMs) with various software tools to derive key roof characteristics such as slope and orientation. Solar radiation data is then integrated to estimate the solar energy potential of each roof. A GIS analysis is then carried out to visualize and interpret the spatial distribution of solar potential in the study area. Preliminary results show that the solar potential on the individual roofs varies considerably due to differences in orientation and inclination. In addition, the study highlights the impact of urban morphology on the accessibility of solar installations. The results provide valuable insights for urban planners, policy makers and energy stakeholders interested in promoting the use of renewable energy and optimizing urban energy infrastructure. In summary, this study underlines the usefulness of LIDAR data in combination with GIS analysis for the assessment of rooftop solar potential and thus provides an important guidance for sustainable urban energy planning in Karlovac, Croatia, and similar areas worldwide.

Keywords: rooftop solar potential; LIDAR; GIS; DSM.

1 Introduction

Solar energy is a clean and renewable resource that is becoming an increasingly important source of energy due to its availability and long-term viability. Cities will soon be forced to look for new energy sources based on electricity and other renewable energy sources. The use of solar energy is important for energy planning, environmental protection and sustainable development. For this reason, a methodology for estimating solar potential is needed. More accurate methods for estimating solar potential are needed as more and more households and businesses consider the possibility of small photovoltaic (PV) systems. Rooftop systems are practical because they do not take up additional space, but utilize the available space.

Many researchers have studied the solar potential in different areas using several different software. Mujić and Karabegović (2023) used SAGA GIS, GRASS GIS and PVGIS to calculate the solar potential. Dodig and Djapić (2024) used ArcGIS to calculate the solar potential of rooftops in the city of Belgrade. Gulben et al. (2019) used SAGA GIS to create solar energy potential maps, while Bajat et al. (2020) used it to calculate grids for potential solar radiation.

This paper focuses on the analysis and visualization of rooftop solar potential using DSMs (digital surface models) obtained from LiDAR (Light Detection and Ranging) data. LiDAR technology provides high-resolution data that is well suited for the creation of high-precision 3D geometry. A comparison of two methods for calculating the solar potential of roofs was carried out and the results were analysed on a daily and seasonal basis. This work is the first case study in Croatia on solar potential using LIDAR data.

2 Materials and methods

In this study, the calculations of the solar potential of roofs were carried out using the GRASS GIS and SAGA GIS plugins in QGIS. The area of Karlovac and its immediate surroundings were analyzed. Karlovac is a city in central Croatia, located at the interface between the lowlands and the mountainous regions of Croatia.

LiDAR data was collected for this area and used to create a DSM and DTM (Digital Terrain Model). The data was provided by the "DGU" (Croatian State Geodetic Administration). First, the DSM was used to calculate the slope and aspect. Next, GRASS GIS and its function r.sun.insoltime enable the calculation of the total solar potential for a given day of the year. The DTM and the previously determined values for slope and aspect were used as mandatory input parameters together with the number of the day of the year. The daily solar potentials were calculated for four days in 2023 within different seasons, namely: February 15, May 15, August 15 and November 15. The results obtained represent the total daily solar potential of the input grid, expressed in Wh/m², which was divided by 1000 using the QGIS Raster Calculator function to obtain the total daily solar potential in kWh/m². To visualize the solar potential of the roofs, only the roofs from the obtained raster were extracted and displayed.

The second solar potential was also calculated with SAGA GIS for the same data. The Potential Incoming Solar Radiation function was used to calculate the solar potential. One of the mandatory input data is the Sky View Factor, which indicates the proportion of visible sky above

a given observation point and is determined using the Sky View Factor command in SAGA GIS. The input data used are the DSM, the sky view factor raster, the average value for the water vapor pressure in the air, the height of the atmosphere and the solar radiation constant. We used the same parameters as in Gorički et al. (2017), including solar radiation constant 1367 W/ m2, atmospheric height 12 000 m and water vapor pressure in the air 10 mbar. In this case, a raster was created showing the daily solar potential expressed in kWh/m². The roofs for the obtained raster were extracted from the rest, as in the previous case, and this representation is further analyzed. The rasters created using different methods were compared visually and using statistical values. The QGIS function "Clip raster by mask layer" was used to extract three roofs from the difference raster, which are analyzed in more detail. The "Zonal statistics" function" was used to calculate the minimum, maximum, arithmetic mean, median and standard deviation for each side of the roof. The R program was used to create a boxplot display for the four analyzed data for both methods. Unlike GRASS GIS, SAGA GIS can select a longer time period in addition to a day. Using the Potential Incoming Solar Radiation function of SAGA GIS and the same input parameters as for the daily solar potential, the solar potentials were calculated for four periods of the year. The first period includes the total solar potential of January, February and March, the second April, May and June, the third July, August and September and the fourth October, November and December. Microsoft Excel was used to create a bar chart showing the mean values of the solar potential for four periods.

3   Results

First, the solar potential was calculated for four days in 2023. The data was analyzed for each day. The daily solar potential values were calculated using the GRASS GIS and SAGA GIS programs (Figure 1).

To observe the influence of orientation on the different methods of determining solar potential, the raster difference was examined for three roofs. As shown in Figure 2, one roof is oriented north-south (Figure 2a), another is oriented east-west (Figure 2b) and the third is a flat roof (Figure 2c). We have divided the first roof into two levels, one facing north and the other facing south. The second roof has one plane facing east and the other facing west. The third roof is a flat roof. In this way, we examine 5 cases: a roof facing north, south, east and west and a flat roof. Depending on this, the difference between the two methods also changes. Table 1 shows the statistical values for each case. To analyze the statistics for each date and method, the statistical values for four dates and both methods are graphically displayed in a boxplot (Figure 3).

In the further analysis, the SAGA GIS was used to calculate the solar potential for four periods of the year. Statistical data were also calculated in order to recognize the dependence of the solar potential on the season. Figure 4
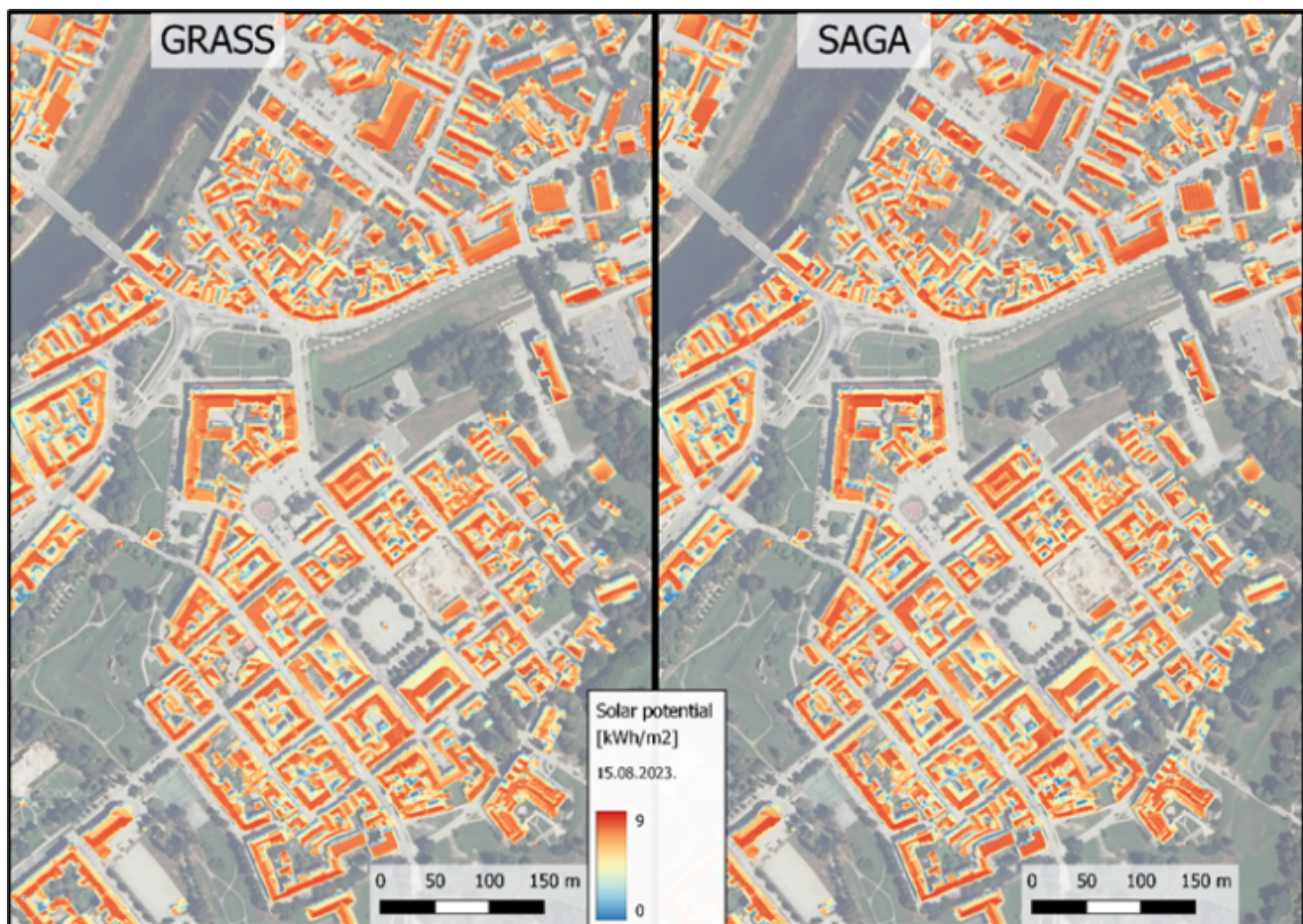
Figure 1. Solar potential values obtained using GRASS GIS and SAGA GIS for August 15, 2023.

shows the mean value of the solar potential as a function of the season.
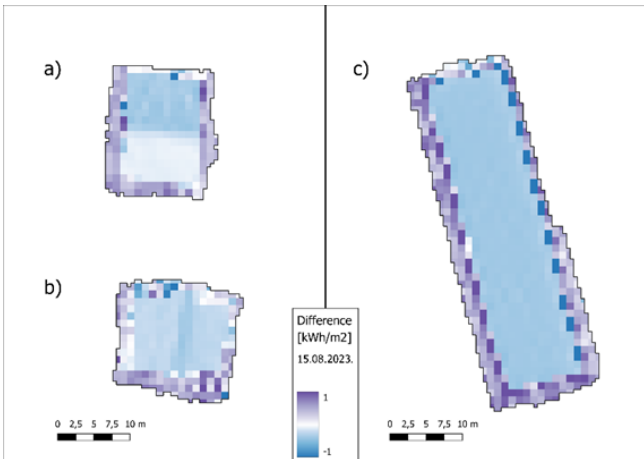
Figure 2. Values of the solar potential difference between the GRASS and SAGA calculation methods for August 15, 2023.

Table 1. Statistical values for roofs in difference raster.

DIFFERENCE	MIN	MAX	MEAN	MEDIAN	ST. DEV.
North roof	-1,31	1,34	-0,11	-0,34	0,43
South roof	-0,42	0,90	0,11	-0,07	0,33
West roof	-1,47	1,07	-0,02	-0,21	0,39
East roof	-1,54	1,38	-0,01	-0,23	0,42
Flat roof	-2,12	1,38	-0,11	-0,37	0,56

The processing time was also examined. The processing time for the daily calculation of the solar potential with GRASS GIS was about two hours and with SAGA GIS about 20 minutes. In addition, the processing of SAGA GIS took three days for each of the four time periods.
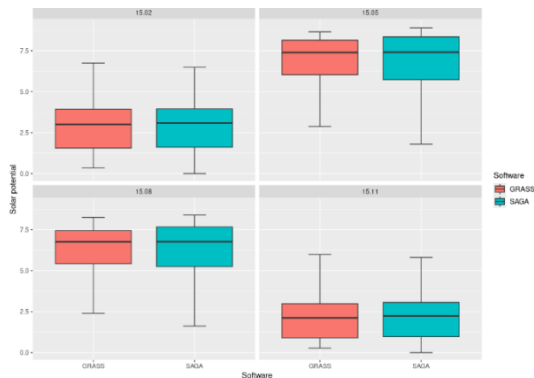
Figure 3. Statistics for each day and method.

Figure 4. Mean value of solar potential for four periods of the year.

4 Discussion

Figure 1 shows that the representation obtained by SAGA is slightly, but not significantly, darker than that obtained by GRASS. It is therefore to be expected that the solar potential values of SAGA are higher than those of GRASS. However, the relationships between the solar potentials of the roofs within the same grid look the same for both results. Their relationship can be determined more precisely using the GRASS and SAGA difference grid. The negative result is where SAGA has higher values than GRASS, and it is obvious that they predominate at all roof levels. There is a positive result where GRASS values are higher, and we can see this on the edges of the roofs. The predominance of the blue color confirms to us that the result obtained by SAGA indicates slightly higher values for solar potential. We looked at the three roofs in detail and examined the difference in raster values, especially in their case. On each roof we can see that the edge values are positive and mostly between 0 and 1. The interior of the roofs is mostly between 0 and −1. It is visually apparent that the north side has a darker shade of blue than the south side. The solar potential difference values are closer to zero on the south side. In this case, it is best represented by the median, which is −0.34 for the north side and −0.07 for the south side. Therefore, the two methods for calculating the potential differ only slightly when representing the south side of the roof and more when representing the north side. The east and west sides of the roof are obviously the same. The shade of blue is darker than that on the south side, but lighter than that on the north side. This is also confirmed by their median, which is −0.21 for the western and −0.23 for the eastern part of the roof. It can also be seen that the differences between the eastern and western orientations are equally large. The differences are greatest at the edges of the roofs, regardless of the orientation. The greatest difference can be seen on a flat roof. This is best confirmed by the greater intensity of blue and the median, which deviates the most from zero and is −0.37. It is therefore noticeable that GRASS and SAGA differ the most on the flat roof and the least on the south side of the gable roof. The daily values of the solar potential were calculated for a further three days in different seasons. We compared the differences in the results using the statistical values shown in the graph (Figure 3). For each day and method, there is a boxplot showing the median, quartiles and range of values covered by the data; outliers are not shown. We can see that the medians for both methods are remarkably close to each other and almost the same. The minimum and maximum differ slightly, as do the quartiles. However, the differences are not very pronounced. From Figure 4, we can conclude that GRASS GIS and SAGA GIS provide very similar results, which is in line with Mujić and Karabegović (2023), who concluded that the results between GRASS and SAGA GIS have maximum deviations of up to 0.96%. From all this, we can conclude that the charts are not very different and we can consider them both credible. However, one notable difference is the time it takes to calculate the results, with SAGA proving to be faster, confirming the statement by Gulben et al. (2019) that SAGA GIS is much faster than GRASS GIS.

Figure 5 also shows that the highest value of solar potential is reached in the summer months, especially from April to June. It is similar to the boxplot, where all values are highest on May 15. August 15 shows slightly lower values, which also applies to the period from July to September. The lowest values for solar potential are in the period from October to December, which is also confirmed by the statistical values for November 15. This is consistent with the findings of Gorički et al. (2017), who concluded that solar radiation is highest in July and lowest in December.

5   Conclusions

Solar energy is a clean and renewable resource that is becoming an increasingly important energy source due to its availability and long-term viability. More accurate methods of estimating solar capacity are needed as more homes and businesses consider the possibility of small photovoltaic (PV) systems. Rooftop systems are practical because they do not require additional space, but utilize existing space. This paper presents a comprehensive assessment of the solar potential of rooftops in the urban environment of Karlovac, Croatia, using LiDAR data. The difference in the rasters between GRASS and SAGA shows that SAGA has higher values on all roof levels, while GRASS has higher values on the roof edges. It is noticeable that GRASS and SAGA differ most on the flat roof and least on the south side of the multi-gable roof. Although there are some differences in the statistical values with an average difference of 0.01 kWh/m², it can be concluded that GRASS GIS and SAGA GIS deliver equivalent results. The solar potential reaches the highest value in the summer months and the lowest in the period from October to December.

6   References

Bajat, B., Antonijević, O., Kilibarda, M., Sekulić, A., Luković, J., Doljak, D., Burić, D., 2020. Space-time high-resolution data of the potential insolation and solar duration for Montenegro. Spatium, 44.

Dodig, A., Djapic, V., 2024. Digital Solution to Estimate Solar Power Potential of Rooftops in City of Belgrade. In Conference on Information Technology and its Applications, Springer, Cham, pp. 362-374.

Giannelli, D., León-Sánchez, C., Agugiaro, G., 2022. Comparison and evaluation of different gis software tools to estimate solar irradiation. ISPRS Annals of the Photogrammetry, Remote Sensing and Spatial Information Sciences, 4, 275-282.

Gorički, M., Poslončec-Petrić, V., Frangeš, S., Bačić, Ž., 2017. Analysis of solar potential of roofs based on digital terrain model. The international archives of the photogrammetry, remote sensing and spatial information sciences, 42, 37-41.

Mujić, N., Karabegović, A., 2023. Calculating and comparing solar radiation results using GIS in the City Sarajevo area. In 2023 18th Conference on Computer Science and Intelligence Systems (FedCSIS) IEEE, pp. 285-290.

Advancing Land-Cover Classification in Croatia: Implementation of a Pilot Project for ARKOD+ and CROLIS LU Initial Layer Creation

Matjaž Štanfel[1],*, Dragan Vitas[1], Mladen Majcen[2], Dario Perešin[2]

[1] Sinergise Solutions d.o.o., Cvetkova 29, 1000 Ljubljana, Slovenia, matjaz.stanfel@planet.com, dragan.vitas@planet.com

[2] Agencija za plaćanja u poljoprivredi, ribarstvu i ruralnom razvoju, Ulica grada Vukovara 269d, 10 000 Zagreb, Croatia, mladen.majcen@apprrr.hr, dario.peresin@apprrr.hr

* corresponding author

Abstract: The pilot study was conducted in collaboration with the Paying Agency for Agriculture, Fisheries and Rural Development (PAAFRD), with implementation led by Sinergise Solutions d.o.o. and KING ICT d.o.o. as executors. This pilot initiative was integral for fulfilling objectives outlined in the LIFE CROLIS project, with PAAFRD as a key partner. The primary aim of the pilot project was to analyse training data and evaluate methodologies for automating land cover classification within the Republic of Croatia using Sentinel-2 satellite imagery. Additionally, the project aimed to generate an initial vectorized spatial dataset of agricultural land parcels (ARKOD+) by application of a delineation algorithm on aerial imagery. Over a period of 10 months, starting on May 23, 2023, the project consisted of multiple phases organized into work packages, including, among others: analysis of input data and spatial frameworks, developing and applying algorithms for land-cover classification and field delineation, evaluating results, preparing future methodology recommendations for field data collection/validation, and creating a GIS viewer. Additionally, a comparison was conducted between the use of PlanetScope Fusion and Sentinel-2 imagery for calculating markers identifying agricultural use in the Koprivničko-križevačka region. This paper presents the framework, methodologies, and outcomes of this pilot project, shedding light on the feasibility and effectiveness of utilizing satellite data for automated land classification, with implications for land management and policy development.

Keywords: CROLIS; ARKOD+; agriculture; land cover classification; automated delineation.

1   Introduction

The LIFE CROLIS project deals with the development of a harmonised data model for land monitoring in the Republic of Croatia with the aim of developing and establishing the first multi-level and multi-purpose land monitoring system. The establishment of the CROLIS system will enable better climate policy planning (mitigation and adaptation) in various sectors at the level of the Republic of Croatia. Additionally, the application of data from CROLIS will enable more precise reporting and calculation of greenhouse gas emissions and sinks from the LULUCF sector (land use, land-use conversion and forestry) and the CROLIS system will provide a stable basis for planning and implementing climate change mitigation activities through reducing emissions and increasing greenhouse gas sinks in the LULUCF sector.

With new EU legislation, including the adopted Regulation (EU) 2023/839 of the European Parliament and of the Council, which simplified the reporting and compliance rules and set out the targets of the Member States for 2030 on improving monitoring, reporting, and tracking of progress, the establishment of the Land Monitoring System in Croatia becomes an obligation.

One of the most important effects of the establishment of CROLIS is the precise reporting of greenhouse gas sinks in the LULUCF sector. According to the CROLIS project, the entire land area of the Republic of Croatia will be included in a harmonised land monitoring information system and, as a result, new information will be obtained about the connection between Croatian land management practices and emission factors. This will help to introduce land management practices with lower greenhouse gas emissions, and ultimately will help achieve reductions in greenhouse gas emissions.

Since the ARKOD (LPIS) system includes only agricultural areas whose owners submit a request for payment of incentives, for now less than 50% of the total agricultural areas in the Republic of Croatia are registered in ARKOD. After the establishment of CROLIS, all agricultural areas will be determined and officially registered, which will enable better planning of climate change mitigation measures.

2   Materials and methods

2.1   Training data

Training data was collected and analysed for 7 Land Use/Land Cover (LU/LC) classes: forest, water, build-up area, permanent grasslands, arable land, permanent crops, and karst pastures. Validation was based on analysis of NDVI (Normalized Difference Vegetation Index) signals for 2020 and 2022 and manual visual control based on aerial imagery. Data was provided by the State Geodetic Administration,

Croatian State Forest Enterprise, and PAAFRD, and was iteratively selected based on iteration results. The initial dataset was filtered by area and shape with the goal of increasing homogeneity in the LU/LC sample. Objects narrower than 10m were excluded from the sample.

Special attention was given to the training data for agricultural parcels, as it was crucial not only for CROLIS, but also for training the model for ARKOD+, where borders of each agricultural parcel had to follow visible parcel borders on aerial imagery. For this case, PAAFRD controls
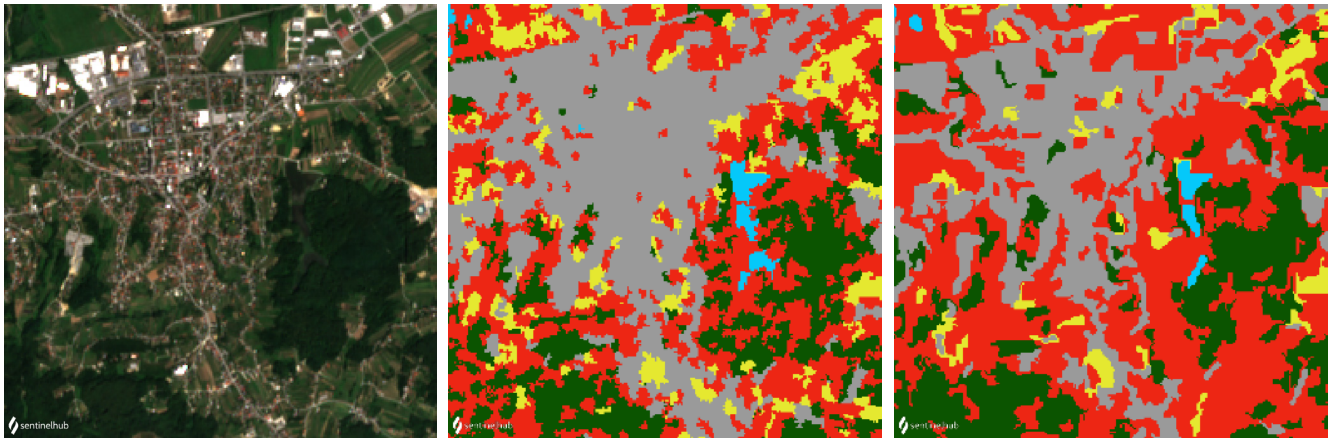
Figure 1. Comparison of true color (left), pixel-based classification (middle) and segmented objects classification (right) around city of Ivanec for 2022.

data was used. Out of 22,410 agricultural parcels, 5,375 (24%) were marked as acceptable. Additionally, 587 parcels were added after editing of quality assurance control made by the executor making a total of 5,962 samples distributed over Croatia. Non-agricultural samples were used as "negative" training data.

For validation purposes, collaboration with the Croatian State Forest Enterprise was established, and with the usage of drones, aerial imagery was created and used to validate land cover changes on a small sample.

2.2 Processing

2.2.1 Land-use / land-cover classification

We compared the machine-learning (pixel-based LightGBM) approach, as showcased in blog-post series (Lubej 2018) with the object-based model.

We first tested LU/LC prediction per pixel, which resulted in substantial salt-and-pepper noise. Sieving was applied to smooth the prediction, but this led to artefacts, primarily seen on linear features. This issue was partly addressed by applying coregistration to the temporal stack of images, but the results still contained patches of obvious misclassifications. As an alternative, an object-based approach was attempted. We applied Felzenszwalb Segmentation (Felzenszwalb and Huttenlocher 2004) to the maxNDVI image for the whole year (separately for 2020 and 2022), segmenting areas into objects. NDVI signals of pixels within objects were averaged, and prediction was run for each object. The results proved more suitable for comparison

between years, and therefore this method was selected for the pilot (Figure 1).

In the next iteration, segmentation into objects was done by considering quarterly values of NDVI, Normalized Difference Water Index and Normalized Difference Built-up Index to reduce influence of changes within objects during the year.

Classification for the whole country was made in 2 iterations. In the first iteration, it was identified that the model could benefit from additional samples from agricultural areas, which were then added in the second iteration. Although we saw significant improvements in the

second iteration when comparing confusion matrices, interpretation should be done with caution, as we observed that the performance on the validation set may not fully reflect the predictive capabilities across the entire dataset. This discrepancy is likely attributable to the high quality ("clean") nature of the reference data, which comprises samples exclusively representing a single land cover type.

It is noteworthy that our analysis is conducted by using Sentinel-2 imagery, where significant signal mixing can occur. Notably, a single 10m x 10m pixel often captures data from multiple land cover types simultaneously, influenced by numerous factors that determine the predominant signal within that pixel.

Land cover changes were detected by intersecting LU/LC classes from 2020 and 2022 and retaining results where predicted classes changed. Changes were retained only if pseudo-probability for the predicted group in each year
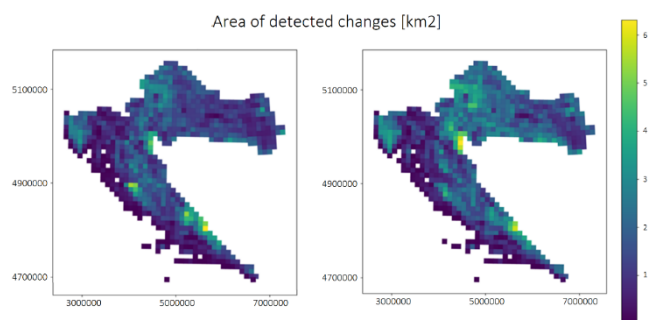
Figure 2. LU/LC changes between 2020 and 2022. First iteration left, second iteration on the right.

was significant (above 0.98), and change was larger than 4 Sentinel-2 pixels (Figure 2).

2.2.2 Field delineation of agricultural parcels

The eo-grow framework (Batič et al. 2023) was used to tackle the issues of processing scalability, by enabling coordination of clusters to run the EO workflows over large areas.

Delineation of agricultural fields was done on normalized aerial imagery with 0.5m resolution made in 2022 and 2021, which included spectral bands for red (R), green (G), blue (B), and near-infrared (NIR). The area of the country

was divided into 230,000 tiles with dimensions 1100x1100 pixels and an overlap of 100 pixels.

We rasterized the positive polygons (training data for agricultural areas) to create extent and boundary masks. As there was more negative reference data (in terms of total area), to avoid overrepresentation of the negative reference pixels, we computed the number of "negative" and "positive" pixels in each of the tiles and then down-sampled the negative pixels in a way that the ratio between the two is roughly equalized.

Different experiments were done: training models with different datasets (changing ratio of negative vs positive samples), changing learning rate (from 0.001 to 0.0001), precision (from 16 to 32), and epochs (from 75 to 150).

The evaluation of the models was done on 1200 locations distributed across the country. The best model achieved IoU 0.82 and accuracy 0.93 on the evaluation dataset (Figure 3).

The model was run on the entirety of Croatia, and results were simplified in postprocessing, where holes and parcels with an area of less than 100m2 removed.

2.2.3 Trend of agricultural activities on delineated parcels

On an area of 24x24km within Koprivničko-križevačka region, Sentinel-2 and PlanetScope Fusion NDVI signals were extracted for time range 2018–2023 for each parcel. Bare-soil and mowing markers were then calculated to monitor agricultural trends. The marker records an observation on the signal, and contains both the nature of the observation and the time it was manifested on the parcel (Devos et al. 2021). Out of 24,145 parcels, 27% (6,491) were monitored only with PlanetScope Fusion due to Sentinel's resolution limitation. 97 parcels were too small to contain even a single PlanetScope Fusion pixel (3x3m), and therefore were not analysed. 17,557 (73%) parcels had signals from both sources. A commercial solution, provided by executor, Sinergise, was used for marker calculation (Sinergise 2024).

Bare-soil marker did not show significant trend changes with around 8,000–11,000 parcels having at least 1 bare-soil observation through the year.

Differences in marker results were noticed between PlanetScope Fusion and Sentinel-2 on parcels with heterogenous crops. The PlanetScope Fusion bare-soil marker was more sensitive to partial changes within parcels.

3 Results

Field delineation resulted in 2,848,790 agricultural parcels with a total area of 1,822,550 ha.

It was noticeable that higher accuracy results were achieved in continental parts of Croatia. In coastal areas and islands, initial results would require manual editing (as expected) to precisely follow borders of agricultural parcels.

Karst pasture borders represent a challenge, as this kind of land use often does not have borders that are clearly visible from aerial imagery. Karst pastures are often declared over forested or bare-soil areas with sparse vegetation, with no clear contrast between two neighbouring fields - making it hard to determine field boundaries from aerial imagery alone.

Preliminary LU/LC classification results proved that cautiously-selected training data can significantly improve results, and with an established framework and methodology, iterations could be calculated, often providing a fast feedback loop important for improvement of ground truth.

Lastly, the monitoring of land-use changes and maintenance of the ARKOD+ layer (delineated parcels) is possible with markers which could be used to prove agricultural use of land, or as a potential change-detector (homogeneity, forest probability etc.). However, the 10m resolution of Sentinel-2 creates an issue for small or narrow parcels which don't contain at least 1 whole Sentinel-2 pixel.

Figure 3. Training the delineation model. From left to right; aerial imagery true color, aerial imagery NIR, predicted parcel extent, predicted parcel boundary.

Marker analysis revealed a negative trend in the number of mowed parcels. On both Sentinel-2 and PlanetScope Fusion, the number of mowed parcels decreased. On average, approximately 8,000 of the 17,557 parcels were mowed in 2018, decreasing to approximately 5,174–7,863 mowed parcels in 2023, depending on the source.

4 Discussion

The area of delineated parcels is smaller than the PAAFRD estimate of 2,695,037 ha (Narodne novine 2013), likely due to results for karst pastures, for which visible boundaries are hard or even impossible to precisely detect with the field delineation model. Results seem to be mainly suitable for arable land, with room for improvement for permanent

crops and grasslands. A larger and more diverse sample of training data is needed to improve the quality, especially over coastal areas. The need for larger and more diverse sample data is also true for LU/LC classification. Although initial results look promising, it seems there is still room for improvement in segregation between arable land and permanent crops in coastal areas where we did not have significant distribution of training data.

As for agricultural monitoring purposes, PlanetScope Fusion showcased as advantageous compared to Sentinel-2 on small and narrow parcels. On larger parcels, lower revisit time did not significantly improve results. As changes are expected to occur on delineated parcels over the years, it seems sensible to monitor parcels homogeneity as an indicator of potential parcel border change.

5 Conclusions

The pilot study resulted in important guidelines for the collection and preparation of training data, which proved highly significant. Preparation of the training data in advance will accelerate the process of carrying out necessary activities to reach the objectives of the CROLIS project. This acceleration may ultimately support the establishment of an information system to realize these goals.

Also, the results that were obtained through the delivery of the pilot project determined the guidelines surrounding the methodology that will be applied during the establishment of the future information system. The initial results of ARKOD + parcels through the automatic classification method confirm significant progress in the creation of LU agricultural land, and for the purposes of achieving the goals derived from the CROLIS project.

6 References

Batič, M., Lukšič, Ž., Milčinski, G., 2023. eo-grow-Earth Observation framework for scaled-up processing in Python. In EGU General Assembly Conference Abstracts (pp. EGU-16802).

Devos, W., Sima, A. and Milenov, P., 2021. Conceptual basis of checks by monitoring. JRC127678

Felzenszwalb, P. F., Huttenlocher, D. P., 2004. Efficient graph-based image segmentation. International journal of computer vision 59, 167-181.

Lubej, M., 2018. Land Cover Classification with eo-learn: Part 1, https://medium .com/sentinel-hub/land-cover-classification-with-eo-learn-part-1-2471e8098195. (Accessed 30 April, 2024)

Narodne novine, 2013. Strategija upravljanja i raspolaganja imovinom u vlasništvu Republike Hrvatske za razdoblje od 2013. do 2017. Godine, https://narodne-novine.nn.hr/clanci/sluzbeni/2013_06_76_1532.html. (Accessed 30 April, 2024)

Sinergise, 2024. Area monitoring - markers, https://area-monitoring.sinergise.com /docs/markers. (Accessed 30 April, 2024)

Spatial Analysis of Infrastructure Types in Kızıldağ National Park Using Remote Sensing and GIS

E. Seda Arslan[1,]*, Ömer K. Örücü[1]

[1] Department of Landscape Architecture, Suleyman Demirel University, Isparta, Türkiye, sedaarslan@sdu.edu.tr, omerorucu@sdu.edu.tr

* corresponding author

Abstract: Protected areas are pivotal in sustaining life and enhancing human well-being. A comprehensive comprehension of such areas' ecological and natural attributes is imperative for delineating infrastructure modalities aimed at fostering sustainability. In this vein, an analytical methodology was employed to scrutinize land utilization patterns, topographical features, slope gradients, and aspects within the confines of Kızıldağ National Park (KNP). Given the presence of rural settlements surrounding KNP, a spatial analysis of land use and land cover, within the framework of an infrastructure-centric approach, emerges as a viable avenue for discerning prospective challenges and conflicts. The study delineates infrastructure types into four categories – namely green, blue, gray, and yellow –illustrated spatially within the study area. Remote sensing techniques utilizing Sentinel-2A satellite imagery were deployed for data acquisition. Indices such as NDVI, NDWI, and SAVI were scrutinized to identify infrastructure systems and quantified in hectares. The findings reveal that green infrastructure predominates over other infrastructure types within the study area.

Keywords: infrastructure; Sentinel-2A; remote sensing; Kızıldağ National Park; GIS.

1 Introduction

Understanding land use and land cover plays a pivotal role in ecological planning research (Musetsho et al. 2021, Wang et al. 2021). The preferred method in scientific research for comprehending natural resource distributions and their utilization patterns is through the spatial representation of current land cover (Luo et al. 2008, Vizzari 2011, Song et al. 2018, Kiliç and Arslan 2022). Considering the holistic perspective with which landscapes are currently comprehended, owing to the intersection of their numerous dimensions, a thorough assessment of infrastructure types necessitates a more expansive analysis of the structure and interrelations among various landscape components (Degerickx et al. 2020, Arslan et al. 2021).

The utilization of land cover data is frequently observed in determining the relationship between landscape due to its close association with the ecosystem it represents (Burkhard et al. 2012, Koschke et al. 2012, Kandziora et al. 2013). This study aims to identify different land cover types based on the assumption of their potential in landscape. In this study, green infrastructure represents a strategically planned network consisting of natural and semi-natural areas (European Union 2013). Blue infrastructure encompasses all water elements such as rivers, channels,

lakes, and wetlands (Bioveins 2017). Yellow infrastructure comprises cultivable areas, pastures, and mixed agricultural lands (Arslan et al. 2021). Grey infrastructure represents all structures, roads, and other urban constructions (Bioveins 2017).

In this context, an analytical methodology was employed to examine land utilization patterns, topographic features, slope gradients, and aspects within the confines of Kızıldağ National Park (KNP). Considering the presence of rural settlements surrounding KNP, a spatial analysis of land use and land cover, within an infrastructure-centric framework, emerges as a promising approach for identifying potential challenges and conflicts. The research categorizes infrastructure types into four groups—green, blue, gray, and yellow—illustrated spatially within the study area. Remote sensing techniques utilizing Sentinel-2A satellite imagery were used for data acquisition. Indices such as Normalized Difference Vegetation Index (NDVI), Normalized Difference Water Index (NDWI), and Soil Adjusted Vegetation Index (SAVI) were analyzed to identify infrastructure systems and quantified in hectares.

Accordingly, the research questions addressed in the study are as follows:

1. What is the relationship between the identified infrastructure systems in the study area and the slope, aspect, elevation, and climatic characteristics?
2. What is the potential of NDVI, NDWI, and SAVI indices obtained from satellite images in detecting infrastructure systems?
3. Which infrastructure type (blue, green, yellow, gray) dominates in terms of area size in the study area?

2 Materials and methods

2.1 Study area

Kızıldağ National Park established on May 19, 1969, is a national park in southern Türkiye. It is in the Yenişarbademli-Şarkikaraağaç-Aksu districts of Isparta Province. Situated in the southwestern region of Turkey amid the lakes district, Kızıldağ National Park (KNP) ranks among the largest national parks in the country covering 80,427.48 hectares. Esteemed for its natural splendor, it serves as a prominent destination for outdoor recreation and nature-based tourism (Figure 1).

2.2 Data preparation and analysis

Sentinel 2A satellite images were used to identify infrastructure types in the study area. The Multi-Spectral Imager (MSI) of Sentinel 2A encompasses a spectral range spanning 443 to 2190 nanometres (nm), offering a swath width of 290 kilometers and achieving spatial resolutions
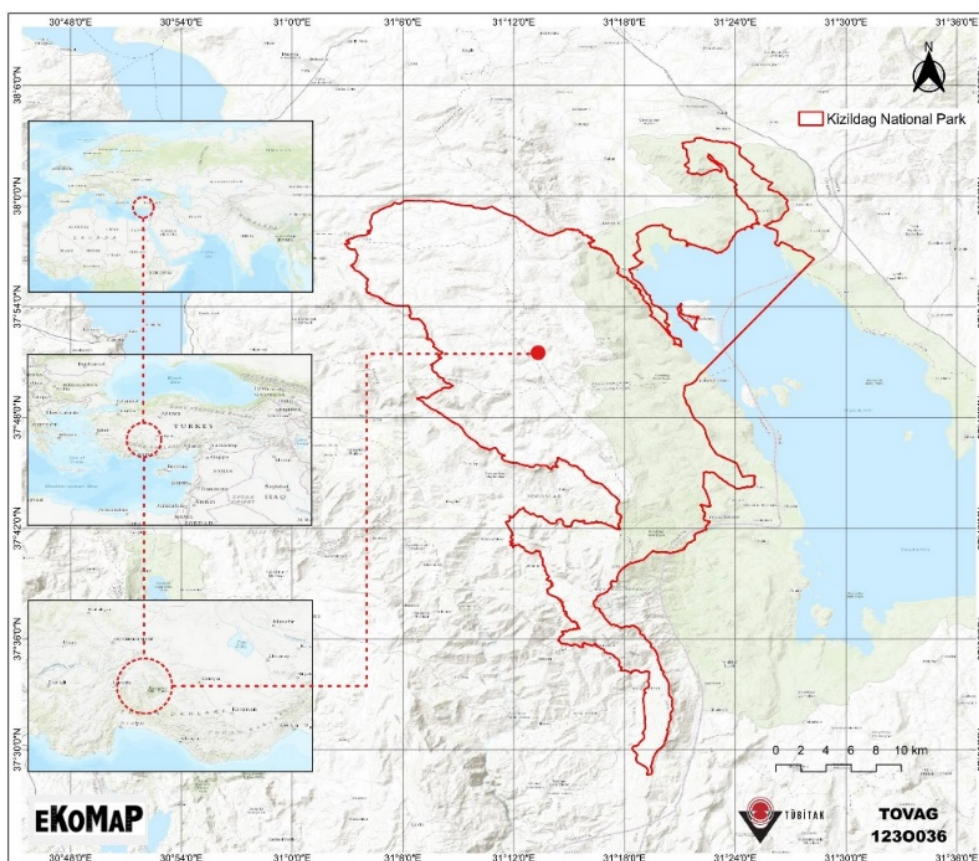
Figure 1. Study area.

of 10 meters for four visible and near-infrared bands, 20 meters for six red edge and shortwave infrared bands, and 60 meters for three atmospheric correction bands. Images dated June 25, 2023, during the most distinct vegetation period, were obtained from https://scihub.copernicus.eu/ and subjected to preprocessing, supervised classification, and validation analyses using QGIS software. Two satellite images have been downloaded. The merging of the bands of the two downloaded satellite images was conducted using the Layer Stack tool under the Raster menu of ERDAS Imagine 2015 software. Radiometric corrections of the satellite images were performed using the semi-automatic classification plugin (SCP) of QGIS 3.34.4 software, and they were saved in the WGS-84-UTM-Zone-36N coordinate system. NDVI, NDWI, EVI (Enhanced Vegetation Index), SAVI, and NDBI (Normalized Difference Built-up Index) indices were generated for the study area. In addition, a Digital Elevation Model (DEM) obtained from the ALOS PALSAR (Advanced Land Observing Satellite) satellite with a resolution of 12.5x12.5 meters was used for surface analysis (slope, aspect, elevation) in the study.

NDVI, SAVI, and EVI indices were utilized to identify green and yellow infrastructures, NDBI index for identifying gray, and NDWI index for identifying blue infrastructures.

NDWI is used for the detection and analysis of water bodies. This Index was used to determine blue infrastructure in the study area. NDVI represents the difference in spectral values reflected by plants depending on the presence of chlorophyll, and it is used to determine the vitality and health status of plants. This Index was used to determine green infrastructure in the study area. NDBI (Normalized Difference Built-up Index) is used to detect built-up areas and is typically employed to identify urban development. This Index was used to determine gray infrastructure in the study area. Another index used in the study is SAVI (Soil Adjusted Vegetation Index). This Index was used to determine yellow infrastructure in the study area.

In the study, a pixel-based supervised classification method was used on the 8-4-2 band combination. Sample areas (training pixels) were selected in locations characterizing four types of infrastructure. These include blue infrastructure (water surfaces), green infrastructure (forest areas and plant communities), yellow infrastructure (agricultural areas and cultivated fields), and grey infrastructure (settlement areas, roads, bare rocky areas, etc.). This technique classifies each pixel in the image based on its spectral value and the groups of example pixels provided during the training phase, thereby assigning the pixels in the image to the defined sub-classes. Subsequently, the Accuracy Assessment command in the ERDAS IMAGINE 15 software was employed to determine the accuracy of the obtained classification data. For the classification accuracy analysis, 135 randomly selected ground control points were used. The ground control data were obtained from field studies and CORINE 2018 Land cover data.

3 Results

The mean elevation within the research domain is recorded at 1347 meters. Elevation demonstrates a declining gradient from west to east. Dedegöl Mountain, situated south of the KMP border, marks the apex in elevation, while
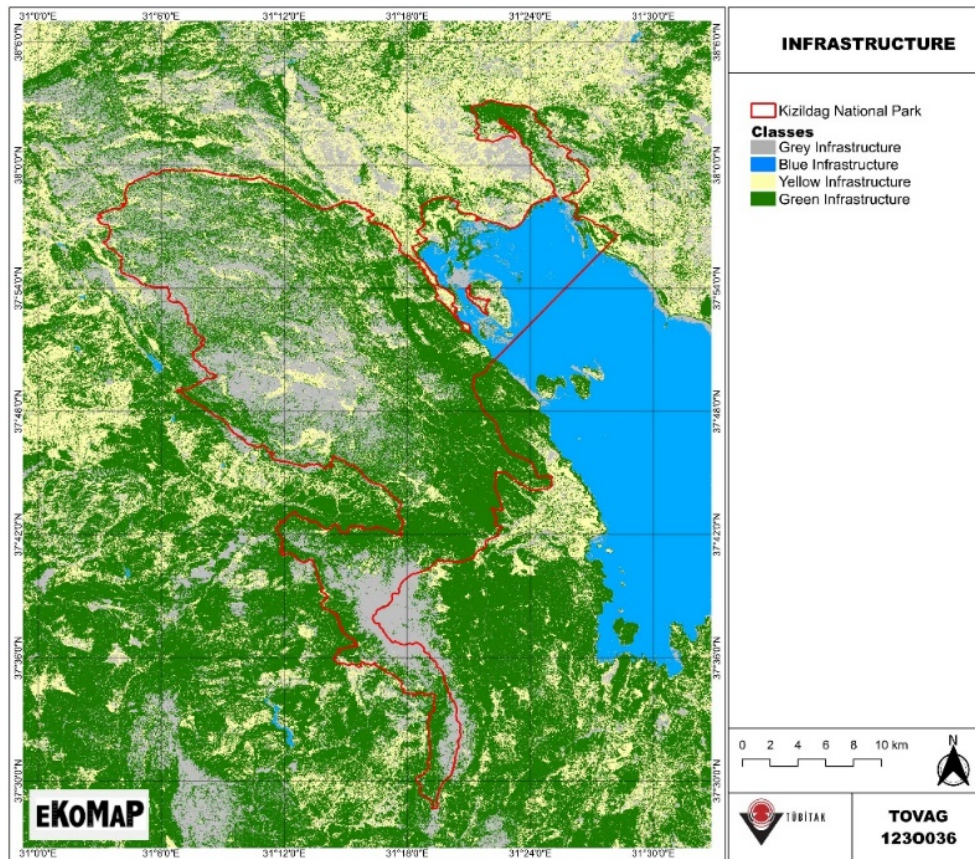
Figure 2. Infrastructure types in the study area.

Beyşehir Lake represents the lowest region. The slope gradients within the study area have been examined across 7 classes. Flat areas and those with slopes close to flat (0–2%) constitute 2.2% of the area. Approximately 55% of the area falls within the 6–24° slope range. The average slope is at approximately 11°. The prevailing aspect in the region is northeast-southwest.

Utilizing data from Sentinel 2A satellite imagery, maps have been generated for normalized vegetation index, normalized water index, soil-adjusted vegetation index, and enhanced vegetation index. The analysis of NDVI indicates that values between –1 and –0.1, corresponding to water-covered areas, account for 6591.74 hectares. Conversely, regions with NDVI values greater than the 0.2 threshold, indicating vegetative cover are represented at 50,880.18 hectares. Similarly, NDWI analysis shows that values within the 0–1 range represent water surfaces, which have been recalculated to cover 8,140.27 hectares following reclassification.

The map illustrating landscape infrastructure types within the study area is presented in Figure 2. Based on Figure 2, it has been calculated that 48% of the study area consists of green infrastructure, 8% comprises blue infrastructure, 30% is composed of grey infrastructure, and 14% is attributed to yellow infrastructure.

'Overall classification accuracy' was calculated as 85.19% and 'overall Kappa statistics' = 0.7782 according to the result of the accuracy assessment.

4 Conclusions

In this study, infrastructure systems are evaluated based on the area they cover and the topographical characteristics of these areas. The potential of determining the infrastructures of the indices used in the study is associated with it. When infrastructures are correlated with the topography of the area, it is determined that the dominant infrastructure type in the area is green infrastructure. The green infrastructure approach has gained visibility for planning landscapes and understanding the features of the land in recent years. It is expected that the results of this study will contribute to the development of methods for the spatial analysis of infrastructure systems and assist in the development of strategies for the sustainability and management of these systems. Consequently, an ecological point of view can contribute to the technology to provide a comprehensive planning approach.

5 References

Arslan, E. S., Nordström, P., Ijäs, A., Hietala, R., Fagerholm, N., 2021. Perceptions of Cultural Ecosystem Services: Spatial differences in urban and rural areas of Kokemäenjoki, Finland. Landscape Research 46 (6), 828-844.

Bioveins, 2017. Bioveins Project. http://bioveins.eu/. (Accessed 23 February 2022)

Burkhard, B., Kroll, F., Nedkov, S., Müller, F., 2012. Mapping ecosystem service supply, demand and budgets. Ecological Indicators 21, 17-29.

Degerickx, J., Hermy, M., Somers, B., 2020. Mapping functional urban green types using high resolution remote sensing data. Sustainability 12 (5), 2144.

European Union, 2013. "Building a green infrastructure for Europe. European Commission" Directorate General for the Environment. https://data.europa.eu/doi/10.2779/54125 (Accessed 24 February 2022).

Kandziora, M., Burkhard, B., Müller, F., 2013. Mapping provisioning ecosystem services at the local scale using data of varying spatial and temporal resolution. Ecosystem Services 4, 47-59.

Kiliç, E., Arslan, E. S., 2022. Spatial analysis of infrastructure systems with remote sensing techniques: The case of Burdur Basin. Turkish Journal of Forestry | Türkiye Ormancılık Dergisi 23 (2), 146-155.

Koschke, L., Fürst, C., Frank, S., Makeschin, F., 2012. A multi-criteria approach for an integrated land-cover-based assessment of ecosystem services provision to support landscape planning. Ecological Indicators 21, 54-66.

Luo, J., Yu, D., Xin, M., 2008. Modeling urban growth using GIS and remote sensing. GIScience and Remote Sensing, 45 (4), 426-442.

Musetsho, K. D., Chitakira, M., Nel, W., 2021. Mapping land-use/land-cover change in a critical biodiversity area of south Africa. International Journal of Environmental Research and Public Health 18 (19), 10164.

Song, Y., Wright, G., Wu, P., Thatcher, D., McHugh, T., Li, Q., Li, S. J., Wang, X., 2018. Segment-based spatial analysis for assessing road infrastructure performance using monitoring observations and remote sensing data. Remote Sensing 10 (11), 1696.

Vizzari, M., 2011. Spatial modelling of potential landscape quality. Applied Geography 31 (1), 108-118.

Wang, Z., Xu, M., Lin, H., Qureshi, S., Cao, A., Ma, Y., 2021. Understanding the dynamics and factors affecting cultural ecosystem services during urbanization through spatial pattern analysis and a mixed-methods approach. Journal of Cleaner Production, 279.

Utilizing Remote Sensing Data for Species Distribution Modelling of Birds in Croatia

Andreja Radović[1,], Sven Kapelj[2], Louie Thomas Taylor[2]*

[1] Ruđer Bošković Institute, Department for Marine and Environmental Research, Laboratory for informatics and environmental modelling, Zagreb, Croatia, andreja.radovic@irb.hr

[2] BIOM, BirdLife Croatia, Zagreb, Croatia

* corresponding author

Abstract: This study focuses on modelling the distribution of bird species in Croatia using spatial variables derived from remote sensing satellite systems. The project involved data preparation, spatial analysis, and model creation to assess the entire territory of Croatia. Environmental variables were categorized into morphometric, habitat, bioclimatological, and landscape heterogeneity variables, all of which influence bird population distribution. The study utilized data from the European Space Agency (ESA) and NASA, including optical and radar sensors, to create a coverage map at a 10 m resolution. The study aslo employed the algorithm described for calculating habitat heterogeneity variables, including connectivity, diversity, and number of categories, crucial in spatial modelling of bird populations. Additionally, WorldClim bioclimatic variables were used, derived from temperature and precipitation data, reflecting the connection between bioclimatic conditions and vegetation types, and hence, bird populations. Modelling was conducted using the Maxent algorithm for habitat suitability assessment and a Random Forest algorithm (RF) for variable selection. All data preparation, manipulation, and model creation were performed in the R environment, utilizing various packages such as openxlsx, sf, terra RandomForest, and others. This interdisciplinary approach provides insights into the spatial distribution of bird populations in Croatia and demonstrates the utility of remote sensing data in species distribution modelling and habitat suitability assessments.

Keywords: bird; spatial modelling; Random Forest; Maxent; valorisation.

1   Introduction

The purpose of this research was to review the conservation objectives and measures for selected bird species (Table 1) in designated areas of the Ecological network of Croatia (Figure 1), based on species distribution modelling using all available data on birds in Croatia. Spatial valorisation of areas for bird species using species distribution modelling (SDM) is crucial for identifying critical habitats, assessing biodiversity, and planning effective conservation strategies, aligning with the objectives of the EU Birds Directive. By predicting species distributions and anticipating environmental changes, SDM informs targeted conservation efforts and sustainable land use planning, ensuring compliance with the Directive's goal of protecting all wild bird species naturally occurring in the European Union.

Table 1. Ecological groups on which habitat suitability spatial models were created

Ecological Group	Number
Woodpeckers	9
Birds of Prey	15
Rock Partridge	1
Nightjar	1
Hazel Grouse	1
Wetland Birds of Prey	3
Herons, Gulls, Spoonbills, Sacred Ibis,	15
Shoreline Nesters	2
Waterfowl, Grebes, Plovers, Coots, and	26
Songbirds	11
Waders and Cranes	16
Bitterns, Moorhens, Crakes, and Little	6
Mountain Owls	2
Western Capercaillie	1
Olive-tree Warbler	1

All analyses were based on data collected from all available sources of data on birds in Croatia available to authors and had a goal to assess, beside suitability of Croatian territory for the breeding, wintering and flyway populations of birds also the quality of data by producing spatial distribution models and evaluate it in help of expert-based system. We need the element of expert-based valorisation due to
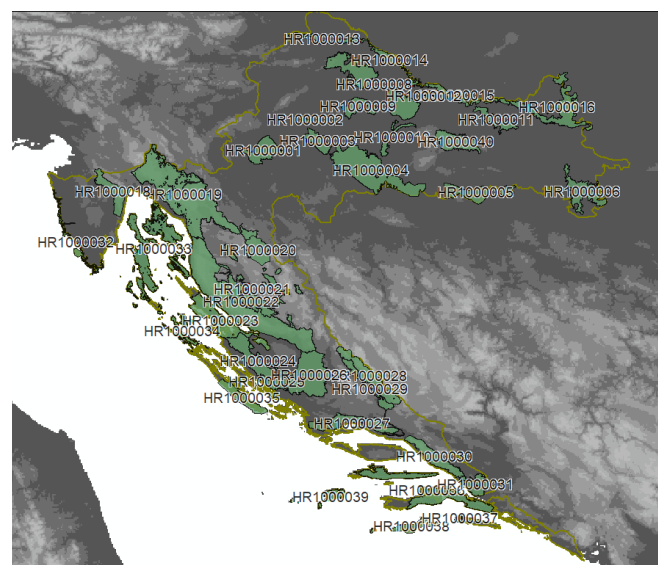
Figure 1. Position of Ecological network sites in Croatia where beside complete state territory, evaluation for each site is given, not presented in paper, available on request.

author's persuasion that for some species models cannot be used at all due to problems in the way data on birds are collected in time.

2 Materials and methods

The project combines spatial modeling with expert knowledge systems, utilizing spatial models with independent datasets on species presence within and beyond Croatia's borders. Observational data for all seasons were collected from the a) Global Biodiversity Information Facility (GBIF) (GBIF.org 09 July 2023; bird dataset 1) and b) from national sources BirdLife Croatia and Ministry of Economy and Sustainable Development and are data from numerous projects and research (bird dataset 2).

Only environmentally available variables, accessible to all for basic insights into Croatian bird populations' climatic conditions, were collected, aiding expert decision-making decisions based on modelling results. Modelling on national data are performed with breeding, wintering and flyover populations of 111 bird species. Results of Maxent model results base od GBIF datasets are available upon request and not presented in details in the paper.

Second part was the modelling bird populations from nationally collected data on birds. We prepared numerous environmental variables in order to detect, by using advanced machine learning methods, the most important set influencing detected population patterns. Data from satellite systems were obtained from EU Copernicus, NASA and JRC web services. The final goal was to prepare base for estimation population sizes as providing input for adequately defining conservation objectives and measures for insufficiently known bird species. Spatial datasets characterizing environmental conditions were methodically prepared at diverse spatial resolutions and harmoniously aggregated to meet specific requirements. All datasets and spatial models adhered to the projection system outlined by the EU Environment Agency EEA (EPSG: 3035) and only final results transformed to Croatia's official two-dimensional projection (EPSG: 3765). Prior to generating any spatial datasets, reference grids were established for the territory of Croatia. Reference raster grids of various spatial resolutions (10 m, 100 m, 500 m, 1,000 m, 10,000 m) were crafted to facilitate the creation of appropriate spatial datasets. Environmental variables selected for spatial model development can be classified into four categories: morphometric, habitat, bioclimatic, and area heterogeneity variables, all pivotal in understanding the spatial distribution of bird populations. These categories were informed by extensive scientific literature (Riitters et al. 2002, Fahrig 2003, Elith et al. 2006, Abatzoglou et al. 2018). Given the complexity of modeling numerous species and populations, a comprehensive suite of spatial datasets was prepared. Morphometric variables, including digital elevation models (EU-DEM (raster) version 1.1, Apr. 2016). and derivatives like the wetness index (WI) and slope were prepared. Habitat datasets largely relied on existing habitat maps of Croatia (Bardi et al. 2016). Two types of datasets were formulated: 1) indicating habitat

presence or absence in reference grid units and 2) the surface area of each habitat type in reference grids. For model development, all nationally available data were utilized, encompassing data from projects such as the EU Natura 2000 Integration Project (NIP) (Mikulić et al. 2016) and CroFauna, alongside data collected during the SMART (Kapelj et al. 2024) project. Integrating these datasets required substantial data manipulation due to variations in data structures. Bioclimatic variables (Hijjmans et al. 2023) are utilized to generate biologically significant variables, crucial for modeling species distribution due to documented associations with vegetation types and bird populations.

Assessment of Croatia's territory for each species/population combination is obtained with both algorithms: 1) Maxent giving information of habitat suitability for the species in range 1–100; later reclassified bases on descriptive statistics onto 4 classes) and 2) classification type Random Forest (RF) for providing classification of Croatia's territory into two categories suitable (1) and unsuitable (0) with environmental variables that are the most important for obtained classification. For the purpose of the modelling procedure we defined, for all bird species and territory of Croatia seasons in the way: 1) breeding (April – August); 2) migration/flyway (September – December) and 3) wintering (January – March). This, not optimal way was the only possible for modelling such a big number of species and populations. The Maxent algorithm was implemented in two ways: using open species occurrence data from the GBIF database for all species in the project, 5000 observations were selected with a unique seed, covering all seasons (breeding, wintering, migration). Observations were divided by seasons. Background pseudo-absence points were generated in the same spatial extent, such as areas covering breeding points for each species. Environmental variables were probed at species occurrence and background points. The algorithm, through mathematical methods, attempts to recognize maximum entropy, pinpointing locations where environmental differences between presence and absence points are greatest. This model ultimately supported the expert-based component of defining species abundance concerning Croatia's position in the species' global range. Additionally, previously described variables specific to Croatia, describing habitats at the national classification level, were utilized. The result is a habitat suitability index for species/populations on a scale of 1–100, categorized into habitat quality classes. Models with an AUC statistic below 70% were not used in further analyses. The RF algorithm was used to classify Croatian territories into two classes: areas where breeding/wintering/migratory bird populations are likely to exist and areas where such populations are unlikely to be found. Confusion matrix statistics were used for model evaluation, focusing on the correct prediction of Class 1 (presence of species). The model was built on a random forest of 1,000 classification trees. As the algorithm builds classification trees by selecting a smaller subset of variables, the absolute importance of variables in describing the detected species

distribution is determined. With 1000 trees, adequate replication was ensured, enabling the calculation of relevant statistics for model evaluation. The traditional 70% data training and 30% testing split, common in statistical model development, was not feasible due to very small data sets, and it was unnecessary given the large number of classification trees for error calculation, so we used only 15% of data for model evaluation.

3   Results

Results are presented for only one species, one population – breeding population of *Microcarbo pygmaeus*, as example. The species is one whose distribution is mainly defined by climatological (bioclimatological) variables with 10 most important variables identified by the RF classification algorithm model as decisive for classifying a pixel at 1 km spatial resolution as suitable habitat (1) or unsuitable habitat (0) are as follows: 1) elevation; 2) bio5; 3) area under habitat class A4 national classification - Reeds, cattails, tall sedges, and tall rushes; 4) bio9; 5) bio18; 6) bio11; 7) bio11; 8) bio3; 9) bio10 and 10) area under habitat class A1 national classification - Temporary standing water bodies (description of bioclim variables at: https://www.worldclim.org/data/bioclim.html) (Figures 2, 3). The modeling results from a) the Maxent algorithm (HIS values) and b) the RF classification algorithm (0,1). Maxent values are then reclassified into 4 classes of suitability over Croatian territory and overall statistics given for complete territory and separately for each Ecological network site for further comparison.

4   Discussion

Developing spatial models for individual populations in this project presented several challenges or factors to consider when interpreting modeling results. Bird data were not collected over time systematically (covering complete set of environmental gradients) or completely randomly, inherently carrying errors in models violating the assumptions the data for the model should meet. There is an error in data collected for territorial birds distributed across complete territory with evident lack of data on areas
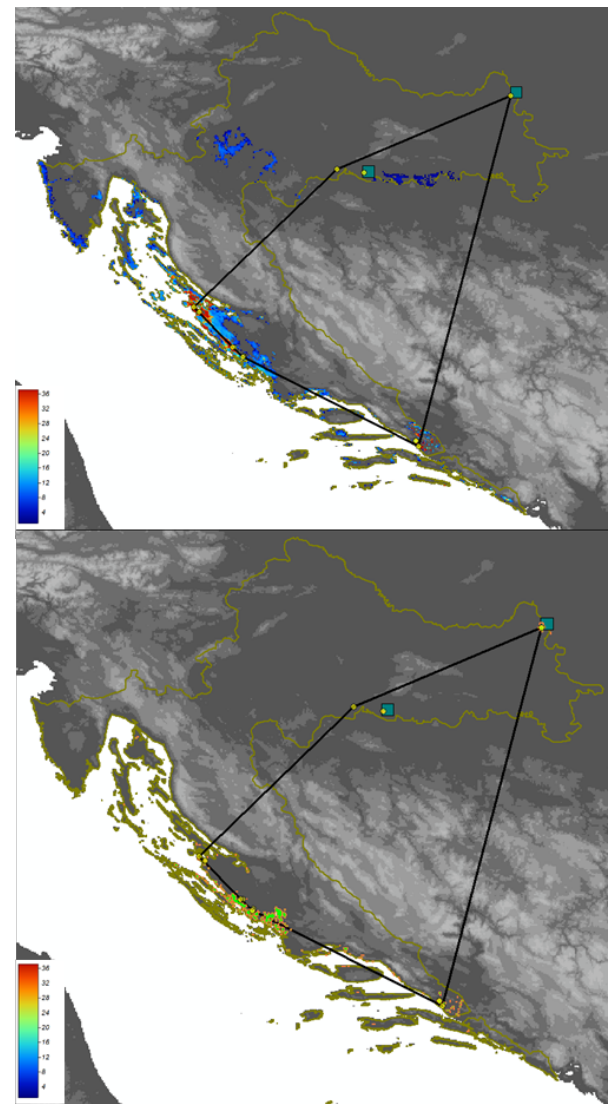
Figure 2. Breeding population habitat suitability for species Microcarbo pygmaeus base map – DEM, top) Maxent algorithm and bottom) classification RF (green), national data not older than 25 years (yellow circles) with convex hull around (black polygon); data from last 5 years (green squares); Maxent valorization of Croatian territory with legend
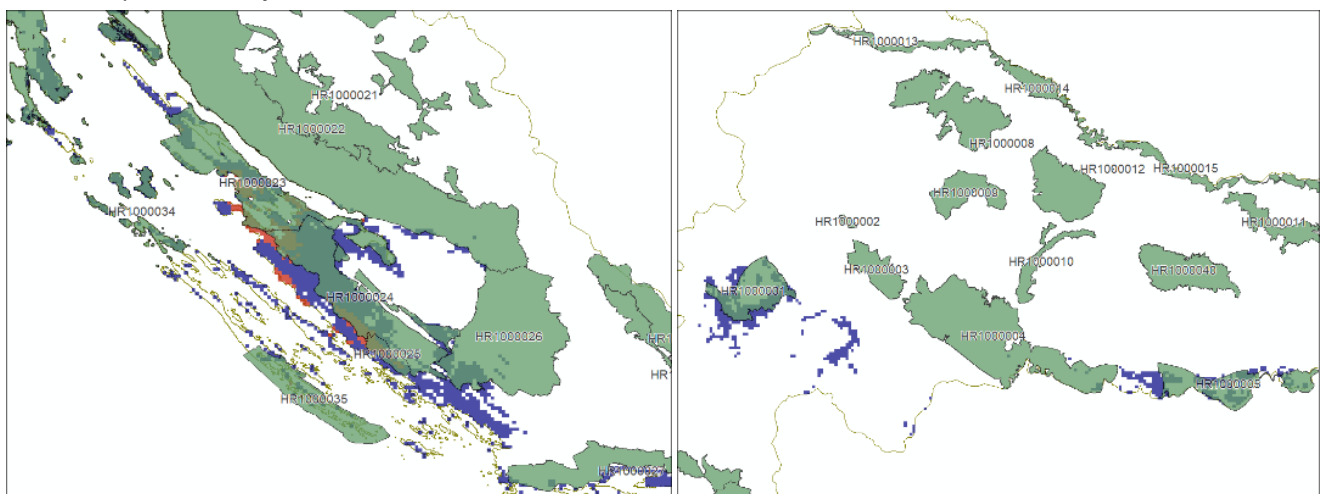
Figure 3. Final statistics of Maxent algorithm habitat suitability valorization at national scale for breeding population of Microcarbo pygmaeus zoom at 1) North Dalmatia (left) and 2) central Croatia (right).

that are less interesting to researchers. On the modeling resolution (1 km), the rarefaction curve (results not presented here) did not reach an asymptote on a five-year scale for most of the species/habitat at 5 km scale, indicating insufficient investigation of habitat types. The inconsistent collection of data on species absence requires careful scrutiny of resulting findings. Data are gathered only in environmental conditions deemed suitable for the species, lacking representation across the entire feature space. Uneven sampling efforts, correlated with environmental gradients, contribute to the heterogeneity of recorded species. Furthermore, modeling a large set of populations in the same environment presents challenges, requiring unique parameters for each species across different seasons and geographic locations. Despite data limitations, models were developed using presence-only data. Given these constraints, reliance on fauna and flora databases in Croatia is essential for interpreting analyses and results. Addressing these concerns, we advocate for improved data collection practices within the Croatian scientific community and encourage alignment with established procedures to enhance the reliability of mathematical modeling, particularly in mitigating sampling bias, crucial for algorithms like Maxent and Random Forest.

5   References

Abatzoglou, J.T., Dobrowski, S.Z., Parks, S.A., Hegewisch, K.C., 2018. TerraClimate, a high-resolution global dataset of monthly climate and climatic water balance from 1958-2015. Scientific Data 5, 170191.

Bardi, A., Papini, P., Quaglino, E., Biondi, E., Topić, J., Milović, M., Pandža, M., Kaligarič, M., Oriolo, G., Roland, V., Batina, A., Kirin, T., 2016. Karta prirodnih i poluprirodnih ne-šumskih kopnenih i slatkovodnih staništa Republike Hrvatske. AGRISTUDIO s.r.l., TEMI S.r.l., TIMESIS S.r.l., HAOP.

Elith, J., Graham, C.H., Anderson, R.P., Dudík, M., Ferrier, S., Guisan, A., Hijmans, R.J., Huettmann, F., Leathwick, J.R., Lehmann, A., Li, J., Lohmann, L.G., Loiselle, B.A., Manion, G., Moritz, C., Nakamura, M., Nakazawa, Y., Overton, J.M., Peterson, A.T., Phillips, S.J., Richardson, K., Scachetti-Pereira, R., 2006. Novel methods improve prediction of species' distributions from occurrence data. Ecography 29 (2), 129-151.

Elith, J., Graham, C.H., ... 2006. Novel methods improve prediction of species' distributions from occurrence data. Ecography 29 (2), 129-151.

Fahrig, L., 2003. Effects of habitat fragmentation on biodiversity. Annual Review of Ecology, Evolution, and Systematics 34 (1), 487-515.

Hijmans, R.J., Barbosa, M., Ghosh, A., Mandel, A., 2023. geodata: Download.

Kass, J.M., Muscarella, R., Galante, P.J., Bohl, C.L., Pinilla-Buitrago, G.E., Boria, R.A., Kapelj, S., Radović, A., Zec ... 2023. Završno izvješće Usluge definiranja SMART ciljeva očuvanja i osnovnih mjera očuvanja ciljnih vrsta i stanišnih tipova - Grupa 5: Definiranje ciljeva i mjera očuvanja za nedovoljno poznate vrste ptica, Udruga BIOM, Geonatura, DOPPS, Zagreb, 36.

Mikulić, K., Kapelj, S., Zec, ... 2016. Završno izvješće za skupinu Aves. In: Mrakovčić, M., Mustafić, P., Jelić, D., Mikulić, K., Mazija, M., Maguire, I., Šašić Kljajo, M., Kotarac, M., Popijač, A., Kučinić, M., Mesić, Z. (Eds.), Projekt integracije u EU Natura 2000 - Terensko istraživanje i laboratorijska analiza novoprikupljenih inventarizacijskih podataka za taksonomske skupine: Actinopterygii i Cephalaspidomorphi, Amphibia i Reptilia, Aves, Chiroptera, Decapoda, Lepidoptera, Odonata, Plecoptera, Trichoptera. OIKON-HID-HYLA-NATURA-BIOM-CKFF-GEONATURA-HPM-TRAGUS, Zagreb, pp. 1-49.

Riitters, K.H., Wickham, J.D., O'Neill, R.V., Jones, K.B., Smith, E.R., Coulston, J.W., Wade, T.G., Smith, J.H., 2002. Fragmentation of continental United States forests. Ecosystems 5, 815-822.

Simulation of Land Use and Land Cover Change and Urban Sprawl Prediction in Lucknow Metropolitan Area Using Markov Chain Model

Vijay Kumar Singh Rathore[1,], Sudhir Kumar Singh[2], Anjani Kumar Singh[1]*

[1] Department of Geography, K.S. Saket P.G. College, Ayodhya, Uttar Pradesh. India, vksrathore707@gmail.com, anjanikumarsingh358@gmail.com

[2] K. Banerjee Centre of Atmospheric and Ocean Studies, IIDS, Nehru Science Centre, University of Allahabad, Prayagraj, Uttar Pradesh, India, sudhirinjnu@gmail.com

* corresponding author

Abstract: This study aims to simulate LULC and predict urban sprawl. Predictive modeling was conducted using the Land Change Modeler (LCM) from Clark Labs, employing advanced algorithms like Multi-Layer Perceptron-Neural Network (MLP-NN) and Markov Chain (MC). LCM was trained with 12 variables including elevation and distances from roads, rails, water bodies, forests, built-up areas, etc. The model prediction accuracy has been accessed by evaluating Receiver Operating Characteristic (ROC) values. The ROC/AUC values for agricultural land, vegetative cover, built-up, waterbody, scrub land and sodic land has been recorded as 0.62, 0.65, 0.91, 0.71, 0.79 and 0.81, respectively. The findings highlight a significant increase in built-up areas, indicative of urban sprawl, alongside decreases in agricultural land, wasteland, and tree cover from 2020 to 2030.

Keywords: land change modeller (LCM); multi-layer perceptron-neural network (MLP-NN); Markov chain (MC); Urban sprawl; physical drivers.

1   Introduction

In recent years, academic interest in local and regional Land Use and Land Cover change (LULCC) processes has surged. Assessing LULCC is crucial for addressing environmental issues like unplanned development, loss of arable land, and habitat destruction. The escalating population in major metropolitan cities of the world causes urban area expansion, altering Land Use and Land Cover (LULC) and inducing urban sprawl. Predicting LULCC and urban sprawl aids in planning for future infrastructure, healthcare, education, and service needs, essential for resource management. The LULCC research community has developed numerous spatially explicit models integrating geospatial data, aiding in better management of land resources and providing precise assessments,

evaluations, and future scenario projections. (Sohl et al. 2016). LULC models are employed to analyse and forecast land use dynamics, offering insights into the socio-economic and environmental ramifications. These models, utilizing techniques like Markov chain, Artificial Neural Network, Cellular Automata, and Logistic Regression.

The Land Cover Change Model (LCM) of TerrSet is an advanced framework merging GIS and remote-sensing technologies to analyse and predict LULCC, employing intricate algorithms like Multi-Layer Perceptron-Neural Network (MLP-NN) and Markov Chain (MC). MLP-NN, a machine learning method, discerns complex data relationships, identifying drivers like land-use policies, economic dynamics, and population growth (Onate-Valdivieso and Sendra 2010).

The present study aims to simulate the LULCC in the study area and to know the future urban sprawl. The outcomes of the study will provide an insight for the planners to achieve the goals of sustainable development and for the management of natural resources effectively.

2   Materials and methods

Area under Master plan boundary – 2031 of Lucknow Municipal Corporation has been selected for this study (Figure 1).

The research utilized LANDSAT satellite data sourced from the United States Geological Survey (USGS) website. Decade- spanning satellite imagery from 2000, 2010, and 2020 was employed. All three satellite images were corrected radiometrically and atmospherically for classification process which performed using the pixel-based maximum likelihood supervised classification technique. In the present study, images were classified into 6 LULC such as Agricultural Land (AL), Vegetative Cover (VC), Built-up (BU), Waterbody (WB), Scrub Land (SCL) and
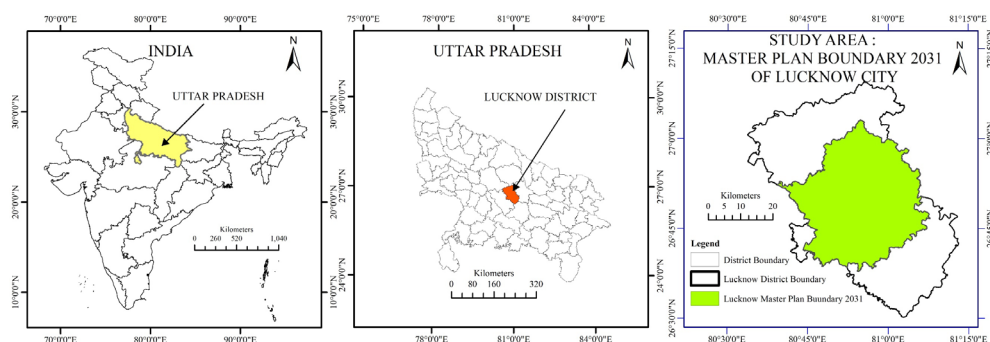
Figure 1. Study Area.

Table 1. Variable and their sources used in the study.

Sr. No.	Variables	Types of Variables	Source
1	Elevation	Static	SRTM DEM 30 M
2	Distance from Roads	Dynamic	Digitized from Google Earth
3	Distance from Railway Lines	Dynamic	Digitized from Google Earth
4	Distance from Waterbody	Dynamic	Digitized from Google Earth
5	Distance from Forest	Dynamic	Digitized from Google Earth
6	Distance from Built-up	Dynamic	Built-up layer is obtained from LULC classified map of 2010
7	Distance from Airport	Static	Digitized from Google Earth
8	Distance from Railway Stations	Static	Digitized from Google Earth
9	Distance from Bus Stands	Static	Digitized from Google Earth
10	Distance from Metro Stations	Static	Digitized from Google Earth
11	Distance from Hospitals	Static	Digitized from Google Earth
12	Population Density	Static	Population Density data of all the wards of Lucknow Municipal Corporation and villages were obtained from Census 2011.

Sodic Land (SOD). For accuracy assessment of classified images high resolution Google earth image is used as referenced data. Error matrix or confusion matrix were prepared for each classified images using these sample pints and referenced data. Kappa coefficient was calculated from confusion matrices. The majority analysis has been conducted on the classified images for better predictive results.

For Simulation of LULCC classified LULC data of 2000, 2010 and 2020 have been used. Along with 12 variables were used in the study as shown in Table 1 and Figure 2. Except

elevation euclidian distance rasters were generated to all the variables and these variables were transformed to natural log scale for better prediction accuracy.

After identifying potential driver variables, the LCM multilayer perceptron (MLP) was used to generate transition potential maps. MLP, an artificial neural network capable of handling highly nonlinear variables (Sangermano et al. 2010), groups and models multiple transitions in a single sub-model

(Eastman et al. 2005). It incorporates only those driver variables with strong predictive ability into the
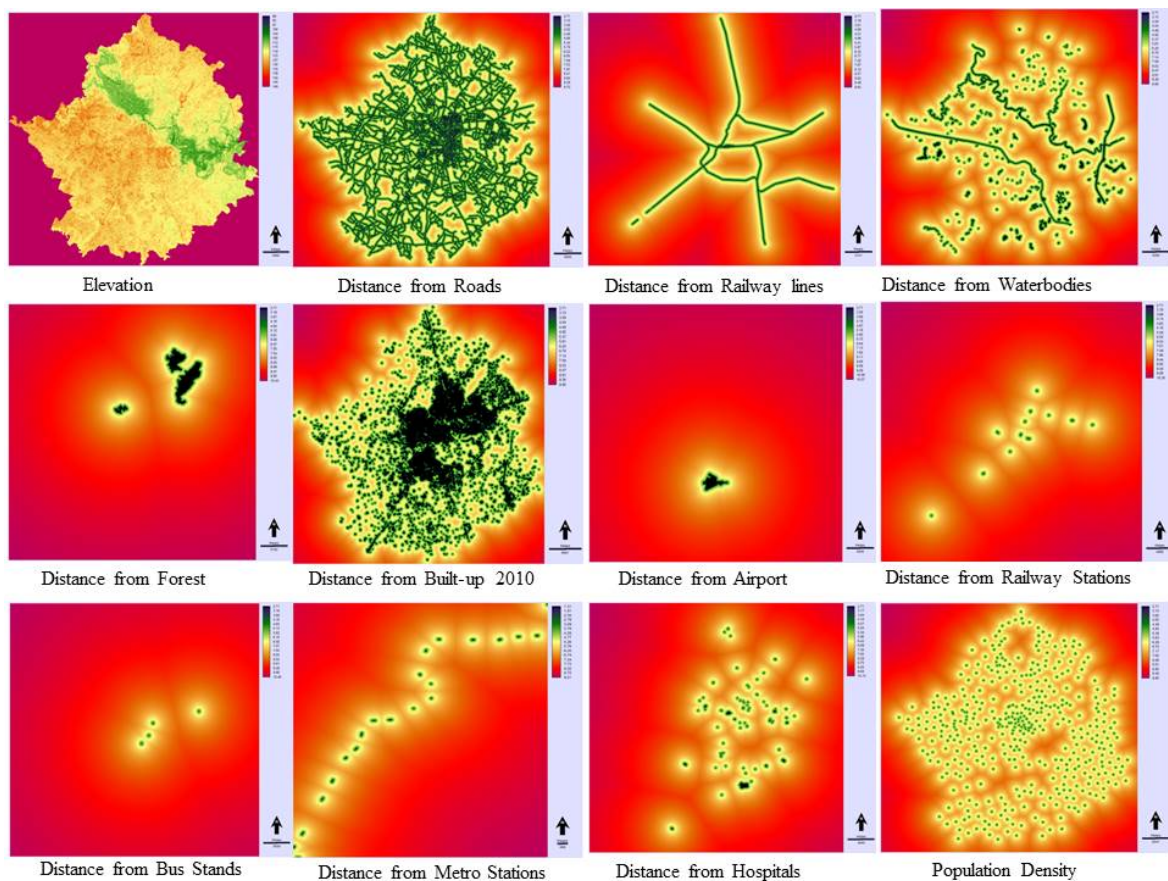
Figure 2. Variables used in the study.

computational process to produce various transition potential maps for each submodel, automatically representing the suitability for changes between LULC classes (Eastman 2012). In this study, the MLP was trained using predefined driver variables and LULC maps from 2000 (start) and 2010 (end) for model development. The Markov Chain model in LCM was applied to estimate future LULC changes based on previous land cover data and conversion probabilities. LCM generates hard and soft predicted maps using Markov Chain analysis, which provides a transition probability matrix quantifying each transition's change (Eastman 2015, Singh 2022). Validation of the prediction/simulation is an important aspect of any modelling as it assesses the model's predictive power and therefore statistical validation procedures has been applied to validate the predicted LULC map of the year 2020. Validation is performed through two ways - Figure of Merit (FOM) method and ROC method (Gidey et al. 2017).

3   Results

The LULC maps for 2000, 2010, and 2020 are given in Figures 3. The Kappa coefficients for 2000, 2010, and 2020 are 0.91, 0.90, and 0.92, respectively, indicating good classification performance with all values above 0.90.

A transition map has been created using LULC maps from 2000 and 2010. Over this period, 29 transitions were identified. All these transitions were used for modelling of transition potentials. To run transition sub models MLP neural network technique was adopted. The transition potential maps for each transition have been produced. For the prediction of future LULC which includes the built-up areas as well, Markov chain method is used. In this method initial LULC layer of 2000 and final LULC layer of 2010 were used to generate the transition probability matrix of each LULC classes from 2000 to 2010. Based on these probabilities a predicted map of LULC of 2020 was generated (Figure 4).
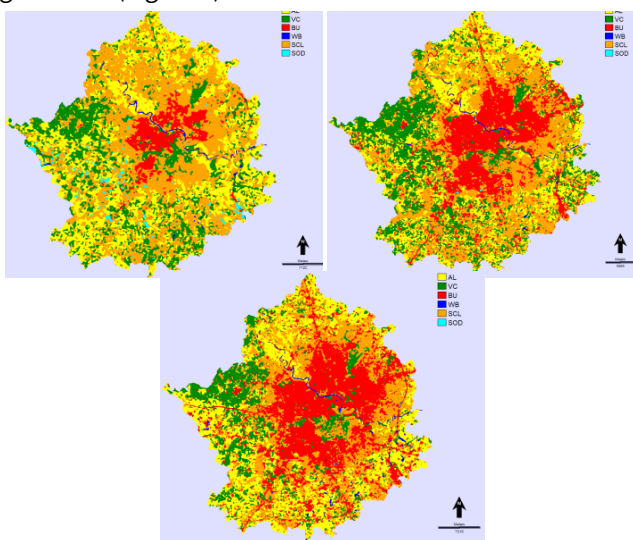
Figure 3. LULC 2000 (top left), 2010 (top right) and 2020 (bottom).

Using this predicted map of 2020 and actual classified map of LULC of 2020 validation process was conducted. In the FOM validation process a map showing hits, misses and false alarms has been generated. Counting each and

applying in the formula of calculating FOM the accuracy of prediction is obtained. Here 4 hits, 10 misses and 40 false alarms are found. Thus, FOM accuracy is 7.4%. The ROC/AUC values recorded for agricultural land, vegetative cover, built-up, waterbody, scrub land, and sodic land are 0.62, 0.65, 0.91, 0.71, 0.79, and 0.81, respectively. The ROC index of 0.91 for built-up indicates that the model has performed very well in predicting this built-up class. Similarly, the ROC index values of 0.81 for sodic land and 0.79 for scrub land indicate good prediction accuracy for these classes. The ROC index values of 0.62 for agricultural land, 0.65 for vegetative cover, and 0.71 for waterbody suggest fair prediction accuracy for these categories. Accuracy of Predicted LULC of 2020 shows that this model can be used for further predictions. So for 2030 transition probability has been generated and a predicted layer of LULC of 2030 (Figure 4) was obtained from model.
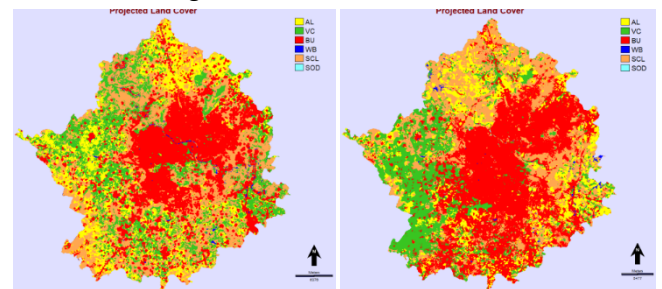
Figure 4. Predicted LULC map of 2020 (left) and 2030 (right).

4   Discussion

Area (hectare) for each LULC class in different years is given in the Table 2. In 2000 the expansion of the built up class was very less as compared to other LULC classes. It was just 5% of the total area. Scrub land was the dominant LULC class in 2000 followed by agricultural land. In 2010 Built-up class experienced a big change in areal extent and jumped to 20.53 % of the total study area. Scrub land remained the dominating class. In 2020 Area of built up again increased to 29.15 % of the total study area. The Agricultural area decreased significantly from 34,931.70 ha in 2000 to 27,128.07 ha in 2010 but then increased to 31,374.36 ha by 2020. This fluctuation might be due to urban expansion and conversion of agricultural lands to other uses, followed by efforts to reclaim or expand agricultural activities. Vegetative Cover category showed an increase from 24,357.60 ha in 2000 to 26,013.96 ha in 2010, likely due to reforestation or conservation initiatives. However, by 2020, it decreased sharply to 17,776.89 ha, possibly due to urbanization. The area under waterbody category slightly decreased from 804.24 ha in 2000 to 652.86 ha in 2010 but increased to 1,224.90 ha by 2020. In Scrub Lad class there was a decrease from 52,566.75 ha in 2000 to 42,848.73 ha in 2010, and further to 35,818.83 ha in 2020. This reduction could be attributed to land conversion for agriculture, urban development, or afforestation efforts replacing scrublands with more productive land uses. The predicted land use/land cover (LULC) map for 2020 within the study area indicates that built-up areas are the predominant category, followed by scrub land, vegetative cover, agricultural land, water bodies, and sodic land. Table 2

Table 2. Table showing area in hectare for LULC classes.

LULC class	2000	2010	2020	Predicted 2020	Predicted 2030
AL	34931.7	27128.07	31374.36	21832.92	18181.8
VC	24357.6	26013.96	17776.89	24578.19	22190.13
BU	7281	24984.81	35496.99	38877.3	50321.07
WB	804.24	652.86	1224.9	550.98	491.04
SCL	52566.75	42848.73	35818.83	35534.88	30174.66
SOD	1582.38	79.02	72.54	30.96	46.53

provides the area of each LULC class in the 2020 predicted LULC map. However, the actual classified LULC map for 2020 presents a different pattern, where scrub land is the dominant category, followed by built-up areas, agricultural land, vegetative cover, water bodies, and sodic land. The specific areas for each LULC class in the actual classified map are also provided in Table 2. Notably, the area under the built-up category differs between the predicted and actual classified maps: the actual classified map shows 35,496.99 ha, while the predicted map shows 38,877.3 ha, a difference of 3,380.31 ha. Despite this discrepancy, the error margin of 2.7% is considered negligible given the study area's total extent of 122,072 ha. Thus, the difference between the predicted and actual classified LULC maps does not significantly affect the overall conclusions of the study.

The LULC classes have been changed significantly in the predicted maps for 2030. In the 2030 predicted map the built-up category has become the dominant LULC class with an area of 50321.07 ha. These tremendous changes in built-up class indicate a significant transformation of the landscape in the study area over the coming years.

It is apparent from the predicted built-up maps of 2020 and 2030 that there is a gradual and continuous increase in the built-up area. This increase in built-up area will expend the areal extent of Lucknow city towards outer sides. The map of 2030 clearly explained the sprawling character built up class.

5   Conclusions

The accuracy of simulation model results depends on many factors. One key factor is the quality of the input data, especially multi-scale data from various satellite images at different resolutions. Using diverse data can introduce errors and uncertainty. Properly preparing this data, including correct classification of satellite images, is challenging but crucial. Mixed pixels can lower classification accuracy, and the choice of a classification algorithm is important. Every simulation model has internal limitations that affect accuracy. For simulating urban growth, all relevant factors (economic, social, ecological, etc.) must be considered.

6   References

Eastman JR. 2012. IDRISI Selva manual. Worcester, Mass: Clark labs-Clark University.

Eastman JR. 2015. TerrSet manual. Accessed in TerrSet version 18, 1-390.

Eastman JR, Van Fossen ME, Solarzano LA., 2005. Transition potential modeling for land cover change. GIS, Spatial Analysis and Modeling 17, 357-386.

Gidey, E., Dikinya, O., Sebego, R., Segosebe, E., Zenebe, A., 2017. Cellular automata and markov chain (CA_Markov) model-based predictions of future land use and land cover scenarios (2015–2033) in Raya, northern Ethiopia. Modeling Earth System Environment 3, 1245-1262.

Onate-Valdivieso F., Sendra J.B., 2010. Application of GIS and remote sensing techniques in generation of land use scenarios for hydrological modeling. Journal of Hydrology 395 (3-4), 256-263.

Sangermano, F., Eastman, J. R., Zhu, H., 2010. Similarity weighted instance-based learning for the generation of transition potentials in land use change modeling. Transactions in GIS 14 (5), 569-580.

Singh, V. G., Singh, S. K., Kumar, N., Singh, R. P., 2022. Simulation of land use/land cover change at a basin scale using satellite data and markov chain model. Geocarto International 37 (26), 11339-11364.

Sohl, T.L., Wimberly, M.C., Radeloff, V.C., Theobald, D.M., Sleeter, B.M., 2016. Divergent projections of future land use in the United States arising from different models and scenarios. Ecological Modelling 337, 281-297.

RS-GIS Monitoring of Afghanistan-Kazakhstan-Pakistan Cities Unsustainable Development

Gaukhar Meldebekova[1], Sholpan Kulbekova[2], Noor Nabi Dahar[1], Chakalov Andrey[1], Muhammad Ilyas[1], Syed Imran Moazzam Shah[1], Janay Sagin[1,] *

[1] Kazakh-British Technical University, Almaty, Kazakhstan, gaukharr@mail.ru, n_dahar@kbtu.kz, a_chakalov@kbtu.kz, m.ilyas@kbtu.kz, s.shah@kbtu.edu, j.sagin@kbtu.kz

[2] National Research Center for Seismological Observations and Research, Almaty, Kazakhstan, kulbekovasholpan@gmail.com

* corresponding author

Abstract: Afghanistan-Kazakhstan-Pakistan cities have similar unsustainable development with intensive urbanization, overexploitation of natural resources, groundwater uncontrolled extractions, intensive construction activities by destroying landscapes. Several cities from these countries are under comparison investigations: currently Kabul from Afghanistan, Almaty from Kazakhstan, and next target to add Pakistan cities. Kabul and Almaty are in the similar locations: valley area, surrounded by the mountains. Both cities have poorly managed housing construction in the very densely populated areas, which are under high risks of the big earthquake activities. Both cities destroy the surrounding mountains slope areas with elimination of the trees? Destroying the natural water movement water, watershed systems with devasting expansion of dangerous building constructions in the very dense overpopulated areas. Soil erosion, landslides in the mountainous areas are getting more intensive in both cities. Rapid cities populations increase water consumption, including groundwater extraction, which induce the ground subsidence. Kabul city was investigated by the spatial-temporal evolution of ground deformation phenomena and its main governing processes by using C-Band Sentinel-1 derived Interferometric Synthetic Aperture Radar (InSAR) time-series from both ascending and descending orbits to extract the two-dimensional (2D) surface displacement field. Four subsidence bowls were distinguished with highly variable spatial extents and deformation magnitudes over four separate aquifer basins, with the maximum value of −5.3 cm/year observed in the Upper Kabul aquifer basin, which potentially caused the land subsidence in Kabul and could be intensified during the earthquakes. The Kabul city research methods are under adaptation for Almaty city ground subsidence investigation. The RS-GIS based FEMA HAZUS tool for earthquake, flood events with financial estimations, construction damage impacts, planning scenarios programs are under our learning activities for adaptation also.

Keywords: geographic information system (GIS); remote sensing (RS).

1 Introduction

The real-time analysis and forecasting of weather, floods, and agricultural crops lost, or damaged owing to floods and rainfall are some typical uses for remote sensing and Geographic Information System (GIS) technology. Remote sensing (RS) and GIS technologies are invaluable for real-time weather forecasting, flood analysis, and assessing the impact on agriculture due to adverse weather events. In countries like Afghanistan, Pakistan, and Kazakhstan (Figures 1–3), which face challenges in sustainable urban development, the integration of remote sensing with GIS (RS-GIS) proves crucial. These rapidly urbanizing nations often witness unsustainable growth patterns, including haphazard urban planning, decaying infrastructure, and worsening environmental degradation (Gauhar et al. 2022) and (Herold et al. 2008).

Figure 1. Almaty (Kazakhstan) city view – Source: Google Images.

RS-GIS facilitates the monitoring of urban expansion, enabling policymakers, urban planners, and researchers to observe and analyze changes in land use, infrastructure, and environmental conditions over time. It combines aerial photos, satellite imagery, and geospatial data to provide vital insights into demographic shifts, urbanization trends, and their ecological impacts. RS-GIS is essential in disaster risk management in these regions, which are prone to earthquakes, landslides, and floods. By analyzing spatial data, identifying at-risk areas, and implementing risk reduction measures, authorities can reduce potential losses and enhance urban resilience.

Figure 2. Hometown a view of Mari Abad, City Quetta – Pakistan; Source: Google Images.

Role of RS-GIS in Monitoring Urban Development, RS, remote sensing involves acquiring data about the Earth's surface through satellite or aerial and environmental conditions (Jensen 2007) and (Li and Weng 2005). High-resolution satellite images and aerial photographs are invaluable for detecting and analysing urban growth patterns, infrastructure development. RS and GIS are pivotal in urban monitoring, providing detailed data about the Earth's surface through satellites and aerial images.

Figure 3. Kabul – Afghanistan city view – Source: Google Images.

Particularly in Afghanistan, Pakistan, and Kazakhstan, RS-GIS technologies are instrumental in tracking rapid urban growth, often marked by unregulated expansion due to socio-economic and political dynamics. These regions, with unique challenges like recovery from conflicts or rapid resource-driven urbanization, benefit significantly Pakistani cities to understand urban dynamics and their unsustainable development patterns. For example, RS and GIS in Pakistani cities, the integration of RS and GIS is critical for assessing urban dynamics and unsustainable development patterns. Also, as populations grow, cities like Kabul, Almaty, and Quetta face increasing demands for groundwater to support domestic, agricultural, and municipal needs. These rapidly expanding urban areas, which are among the most water-stressed in the world, are experiencing significant Drops in water levels due to overexploitation of aquifers. RS-GIS data supports strategic urban planning, helping to reduce ecological impacts and promote sustainable development practices. Such data-driven insights are essential for informed decision-making and effective urban management, their findings indicated a decline in green areas due to construction activities, stressing the importance of sustainable urban development practices. Challenges and Limitations, despite the advantages of RS-GIS technologies, several challenges and limitations need to be addressed (Longley et al. 2015) and (Murzagalieva et al. 2016). Up-to-date satellite imagery and spatial data can be a challenge, particularly in conflict-affected regions like Afghanistan, Pakistan.

2   Research areas

The research paper focuses on the use of RS and GIS to monitor and analyse the unsustainable development patterns in the cities of Afghanistan, Kazakhstan, and Pakistan. These countries, despite their geographical and cultural diversity, share common challenges related to urbanization and environmental sustainability.

2.1   Urban Sprawl and Land Use Changes

The growth of urban areas, alterations in land use patterns, and their effects on natural resources and agricultural land. Urban sprawl transforms green spaces into built environments, impacting ecosystems. By utilizing satellite imagery, the study identifies trends in urban expansion, highlighting critical areas and forecasting future changes. Urban sprawl is a widespread issue, especially prevalent in less developed countries where people increasingly move to mega cities and large urban centres. This trend has drawn the attention of experts in urban geography, environmental studies, and city and regional planning.

2.2   Environmental Degradation

Assessing the extent of environmental degradation due to rapid urbanization, including deforestation, loss of biodiversity, and pollution in targeted cities by integrating RS and GIS data, the study quantifies the environmental impact of urban development and identifies critical areas that require immediate intervention to prevent further degradation.

2.3   Water Resources Management

Analysing the impact of urban development on water resources, including issues related to water scarcity, quality, and distribution (Figure 4).

2.4   Socio-Economic Impacts

The research identifies socio-economic challenges such as housing shortages, infrastructure strain, and displacement of local communities. These issues underscore the importance of inclusive and sustainable urban planning and challenges faced by urban populations, such as increased living costs, inadequate housing, and the pressure on public services and infrastructure.

2.5   Policy and Governance

Effective policies and governance structures are essential for managing urban growth and promoting sustainable development current policies and governance structures are inadequate in addressing the challenges of urbanization.

3   Research methodology

Sentinel-1, a space mission of the European Space Agency (ESA), has resulted in a paradigm shift in the field of InSAR: configurations of the constellation, small perpendicular and temporal baselines, and free data availability allow accumulation of a long-term archive of globally consistent data. A stack of 106 ascending and 101 descending Sentinel-1 Single Look Complex (SLC) products obtained in Interferometric Wide Swath (IWS) mode spanning the period from October 2014 to May 2019 were utilized in this study. SAR data parameters used for this study are described in Table 1, while the spatial and temporal baselines of the generated interferograms are shown in Figure 5 and Figure 6.
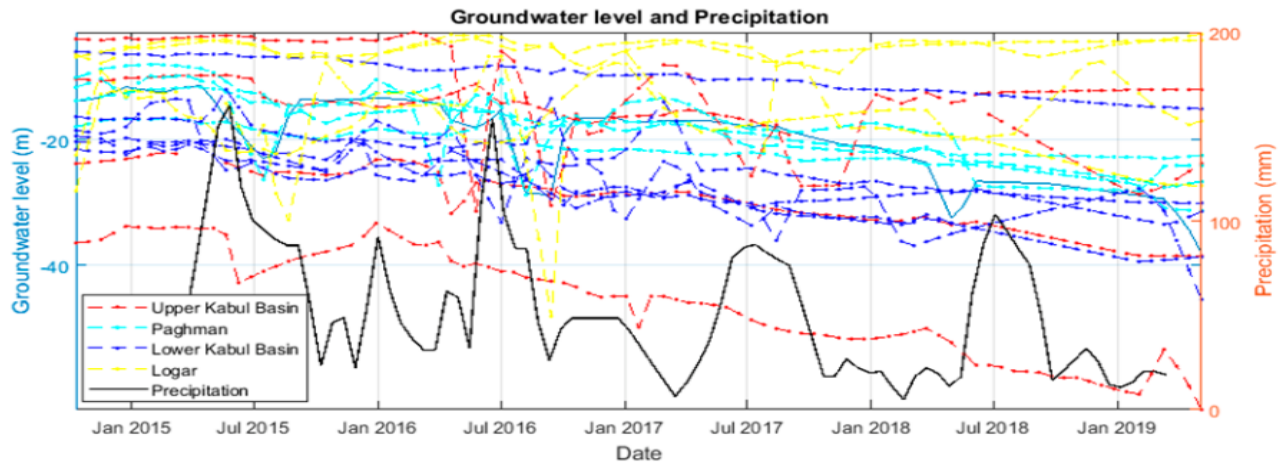
Figure 4. Observed groundwater drawdown in fourteen wells across the network. Precipitation time-series is retrieved from CRU TS 4.03 (Meldebekova et al. 2020).
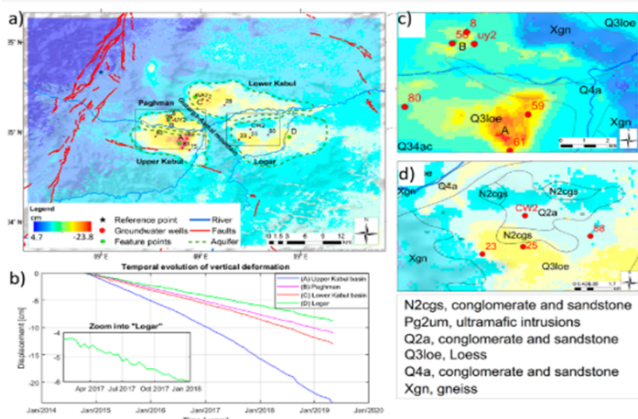
Figure 5. Spatial and temporal characteristics of subsidence: (a) Spatial distribution of subsidence bowls, displayed as cumulative vertical displacement (unit: cm). Red solid lines are mapped faults. (b) Temporal evolution of maximum vertical deformation at each of the four-subsiding bowls. The inset plot illustrates small-scale deformation variations in Logar. (c) Magnified view of the Paghman riverbanks (Meldebekova et al. 2020).
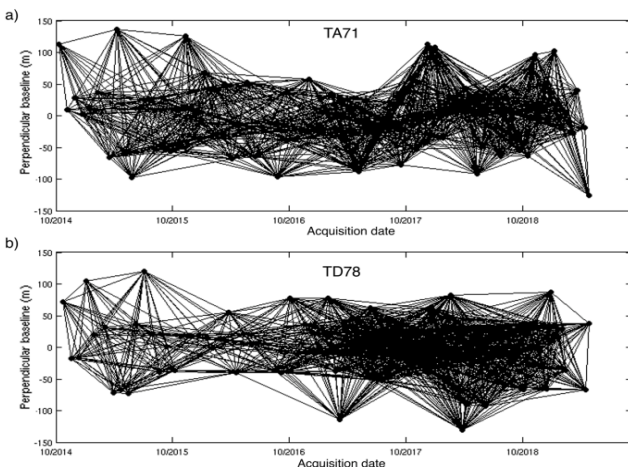
Figure 6. Spatial and temporal baselines of interferograms in (a) ascending TA71 and (b) descending TD78 tracks (Meldebekova et al. 2020).

Table 1. Summary of Synthetic Aperture Radar (SAR) Data used.

Satellite	S-1	S-1
Orbit	Asc	Desc
Path	71	78
Mean Angle of Incidence	39.9040	41.6189
Heading Angle	-13.018	-193.011
Number of Scenes	106	101
Number of Interferograms	1822	1825

Cross-correlation of datasets allows computing the time lag between the cause-effect events using the following equation (1) (Meldebekova et al. 2020):

$$\Delta t = \frac{\Delta\phi * T}{2\pi}. \qquad (1)$$

Data preprocessing includes the following steps: (1) ensuring that irregularly spaced datasets have a uniform time increment by interpolating missing gaps between the consecutive InSAR acquisition dates; (2) interpolating groundwater level time-series to a more temporally dense InSAR time-series; and (3) removing the trend from InSAR-derived results.

4   Discussion and conclusion

The integration of RS and GIS has provided a robust framework to monitor unsustainable urban development and facilitate sustainable growth strategies in cities across Afghanistan, Kazakhstan, and Pakistan. This study utilized multi-geometry Sentinel-1 InSAR data from 2014–2019 to analyse ground subsidence in Kabul caused by groundwater overexploitation, revealing significant vertical displacements and localized horizontal shifts across various aquifer basins. Key findings indicate substantial subsidence, particularly in areas with soft clay sediments, closely correlating with the decreases in groundwater levels. The study underscores the anthropogenic origins of these deformations, highlighting broader urban challenges such as rapid expansion at the cost of natural spaces and agricultural lands, escalating environmental issues, and the intensification of water scarcity. It stresses the urgent need for collaborative efforts among policymakers, urban planners, and stakeholders to embrace comprehensive policy reforms and innovative

governance models. These efforts are critical to mitigate the impacts of urban sprawl, ensure water sustainability, and achieve socio-economic stability, ultimately guiding cities towards resilient and sustainable development.

5 References

Gauhar M., Chen Y., Zhenhong L., Chuang S., 2020, Quantifying Ground Subsidence Associated with Aquifer Overexploitation Using Space-Borne Radar Interferometry in Kabul, Afghanistan. Remote Sensing 12 (15), 2461.

Herold, M., Couclelis, H., Clarke, K.C., 2008. The role of spatial metrics in the analysis and modeling of urban land use change. Computers, Environment and Urban Systems 29 (4), 369-399.

Jensen, J.R., 2007. Remote Sensing of the Environment: An Earth Resource Perspective. Pearson Prentice Hall.

Li, X., Weng, Q., 2005. Using Landsat ETM+ imagery to measure population density in Indianapolis, Indiana, USA. Photogrammetric Engineering & Remote Sensing 71 (8), 947-958.

Longley, P. A., Goodchild, M. F., Maguire, D. J., Rhind, D. W., 2015. Geographic Information Systems and Science. Wiley.

Meldebekova, G., Yu, C., Li, Z., Song, C., 2020. Quantifying ground subsidence associated with aquifer overexploitation using space-borne radar interferometry in Kabul, Afghanistan. Remote Sensing, 12(15), 2461.

Murzagalieva, Z., Shaikenov, Y., Kurmangalieva, S., 2016. Environmental impact assessment of urban growth in Almaty using remote sensing and GIS technologies, Procedia Environmental Sciences, 29, 208-209.

Samimi, C., Qarehghahi, R., 2017. Urban expansion and land use change detection in Kabul city using multi-temporal Landsat imagery, Journal of Urban Planning and Development 143 (4).

Stefanov, W.L., Ramsey, M.S., Christensen, P.R., 2001. Monitoring urban land cover change: An expert system approach to land cover classification of semiarid to arid urban centers, Remote Sensing of Environment 77, 173-185.

Characterization of Valleys and Gullies of the North and Central Velebit Coastal Slope

Klara Grošanić[1,], Marin Mićunović[1], Sanja Faivre[1]*

[1] University of Zagreb, Faculty of Science, Department of Geography, Marulićev trg 19/II, Zagreb, Croatia,
   klara.grosanic@student.geog.pmf.hr, mmicunov@geog.pmf.hr, sfaivre@geog.pmf.hr
   * corresponding author

Abstract: Climate change is an important issue today, affecting many geomorphological processes in different environments. Increased frequency of precipitation extremes results in frequent flooding and gullying. Consequently, short and intense rainfalls cause the activation of torrential flows, activating numerous dry valleys and gullies. The coastal slope of Velebit Mountain hosts deep valleys and gullies of various dimensions from a few meters to thousands of meters in length. In this research, a morphometric analysis of selected valleys and gullies and their drainage basins in the area of North and Central Velebit was conducted in GIS using a digital elevation model, topographic maps and satellite imagery. 114 valleys and gullies and their corresponding drainage basins were identified, with an average length of 1.2 km and average basin area of 2.6 km². Strong correlations were found between the area of drainage basins and 1) the lengths of the gullies and 2) the Strahler stream order of the main channel. Lateral profiles showed possible differences in erosion activity. The obtained results contribute to the existing knowledge about the morphology of valleys and gullies on the Velebit coastal slope, but also encourage further research using GIS and remote sensing.

Keywords: geomorphology, gullies, gully erosion, GIS, Velebit.

1   Introduction

Definitions of gullies are often inconsistent due to the various forms they take worldwide (Thwaites et al. 2021). Generally, gullies are described as elongated landforms formed by intermittent flows activated by intense rainfall, ranging up to several hundred meters in length, tens of meters in width, and depths of 20 to 30 meters, sometimes making them difficult to differentiate from (dry) valleys. Gully depths exceed their width, and their cross-sections take the shape of the letter V (Goudie 2004). It is important to emphasize the hydrological aspect of their formation: by torrential flows due to intense rainfall that rapidly transport eroded material, often causing significant damage to surrounding land and infrastructure (Castillo and Gómez 2016, Jahić 2017). This is why interest in researching gullies and gully erosion has increased since the beginning of the 21st century, especially in the Mediterranean region (Castillo and Gómez 2016, Domazetović et al. 2019).

Velebit Mountain is part of the External Dinarides with a total length of 145 km. According to Bognar's (2001) geomorphological regionalisation of Croatia, Velebit belongs to the meso-geomorphological region 2.1.7. Velebit Mountain ridge-massif. In this analysis, the Northern and Central Velebit coastal slope was assessed. Northern Velebit extends from Oltari to Veliki Alan pass, while Central Velebit continues south to the Oštarije pass. In this study, the eastern boundary of the research area was defined by the boundaries of gully and valley drainage basins (Figure 1). The coastal slope consists predominantly of carbonate deposits from Mesozoic (at higher altitudes) and Cenozoic eras (at lower altitudes) (Mamužić and Milan 1966, Nikler et al. 1967, Mamužić et al. 1969, Sokač et al. 1970, Sokač et al. 1974). Due to the carbonate composition, the coastal slope is characterized by karst relief forms and the absence of permanent surface drainage (Rogić 1958). The area belongs to the humid subtropical climate type Cfa (Filipčić 1998), with an average annual temperature of 15.6 °C and an average annual precipitation of 1285 mm (DHMZ 2023). Most of the precipitation falls during the colder half of the year, however, short and intense rainfall is common during the summer months (Šegota and Filipčić 1996, Perica and Orešić 1999).

The aim of this research is to present the basic morphometric characteristics of gullies, valleys and their
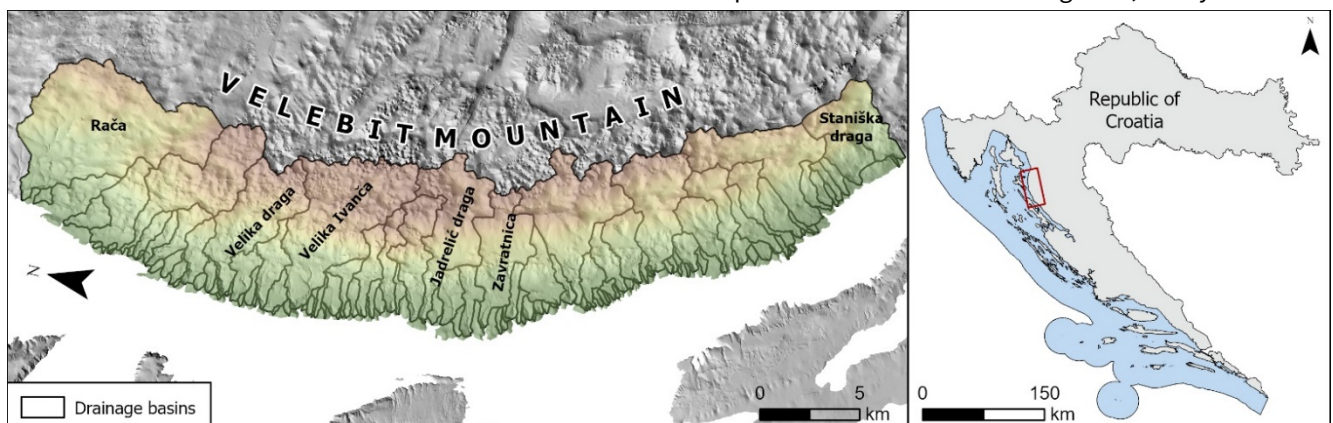
Figure 1. Map of drainage basins on the coastal slope of North and Central Velebit.

drainage basins on the coastal slope of North and Central Velebit with the help of remote sensing and GIS methods. Obtained results will contribute to the existing knowledge about gullies and valleys in this area and serve as a base for further studies on their formation.

2   Materials and methods

Gully, valley and drainage basin data was derived from a digital elevation model (DEM) of the Republic of Croatia with a pixel size of 5x5m (DGU 2019), using the Hydrology toolset in the Spatial Analyst extension of ArcGIS Pro. The morphometric analysis of the drainage basins was conducted using the Slope, Aspect and Focal statistics functions. Gully and valley thalwegs were extracted using the functions Fill, Flow direction and Flow accumulation. The values of the resulting raster were reclassified into two classes using the Set Null function with a threshold value of 1000, thereby isolating pixels indicating relevant flow paths. Gully and valley extents were then mapped by tracing the acquired thalwegs. High-resolution satellite imagery (Maxar technologies, CNES/Airbus), orthophoto provided by State Geodetic Administration (2021) and extents of intermittent streams in the Croatian base map 1:5000 (DGU n.d.) were utilized to verify the results obtained in ArcGIS Pro software. The Stream Order function was used to classify the streams using the Strahler method. Drainage basins were delineated using the Basin function in the Hydrology toolset. The areas of the drainage basins and lengths of mapped gullies and valleys were calculated in ArcGIS Pro. For easier visualization, relief shading was generated using the Hillshade function. Longitudinal and lateral profiles of six selected gullies and valleys were obtained using the Profile function.

3   Results

3.1   Drainage basin properties

The slope values of extracted drainage basins were classified into 6 categories. The most common slope category throughout is 12°–32° (steep terrain), accounting for 67.3% of the area. Additionally, two parallel segments of lower slope values, 0°–12°, can be highlighted at altitudes of 100–300 and 600–900 meters above sea level. Western slope orientation dominates throughout the studied area. The relief energy of the studied area mostly falls into two categories according to Bognar (1992): 100 – 300 m/km^2 (55.9%) and > 300 m/km^2 (36.9%). 114 drainage basins of gullies and valleys were identified, their sizes varying from 0.03 km^2 to 41.76 km^2, while the average basin size is 2.62 km^2. Based on the digital elevation model, thalwegs were derived, and their streams classified using the Strahler stream order. The Pearson's correlation coefficient of 0.69 was calculated between the basin area and the highest Strahler order of their thalwegs, which present a moderately strong correlation (Šošić and Serdar 2002).

3.2   Gully and valley properties

The average length of gullies and valleys is 1200 m, with the shortest gully being 61 m and the largest 17,068 m long.

The Pearson's correlation coefficient between the basin area and the length of the corresponding gullies and valleys equals 0.82, indicating a strong correlation. A total of 96 simple gullies (without tributaries) and 18 complex valleys (with 1 or more tributaries) were identified. Complex valleys coincide with the largest drainage basins extending to the very top of the coastal slope and the main ridge. Simple gullies extend perpendicular to the direction of the slope and are prevalent in Central Velebit, while greater complexity and density of gullies and valleys is visible in Northern Velebit. The 86 % of simple gullies initiate under 300 m above sea level while the heads of the longest ones are generally not found above 1000 m above sea level. A gully density of 0.35 gullies/km^2 was determined in the researched area.

The longitudinal profiles of Rača, Zavratnica, and Staniška Draga gullies are mostly uniform, with no significant changes in slope along the course, while Velika Ivanča clearly exhibits two pronounced segments of lower inclination. Upper reaches are generally characterized by steeper slopes. Lateral profiles of the lower reaches of are mostly symmetrical. Widths of the gullies and valleys range from 150 m to 500 m. The bottoms of gullies Rača, Velika Ivanča, Jadrelić Draga, and Zavratnica are more rounded, and their profiles take on a U shape. A different shape of the lateral profile, transitioning from U to V, is observed in Velika Draga and Staniška Draga. The profiles reveal that the incisions vary from 35 m to 200 m. Lateral profiles of the upper reaches are more uneven compared to the lower reaches where greater differences in shapes can be observed. Here, on the upper reaches gullies and valleys widths range from 55 m (Zavratnica) to 300 m (Rača) and incisions range from 5 m at Staniška Draga to 50 m at Rača. As expected, it is evident that widths and depths of gullies and valleys of the upper reaches are smaller compared to those of the lower reaches.

4   Discussion

Processes that shape gullies are influenced by hydrological and climatic conditions, as well as lithology (Thwaites et al. 2021). Larger forms like valleys are also influenced by structural properties of the area (Ballut and Faivre 2012). Slope is a major factor in activation of gullies and valleys and sediment transport by flash floods, as well as the erosive power of the flow (Faivre et al. 2011, Ružić et al. 2011). Steep slopes increase surface runoff but also reduce infiltration on carbonate substrates enabling incision. Morphometric analysis of the studied area revealed the prevalence of slopes ranging from 12° to 32°, which, according to previous studies, favors the formation of gullies. Consequently, denudation processes become stronger on slopes above 12°, leading to increased intensity of linear erosion (Lončar 2009, Faivre et al. 2011). Two elongated areas of gentler slopes (0°–12°) have been detected in the analysis, which, according to Bognar (1994), correspond to the upper pediment (formed from Eocene to Miocene) and the lower pediment (formed from Pliocene to Pleistocene). Further downstream, and towards the coast, the incisions deepen, forming deep gullies, as revealed by the analysis of selected lateral

profiles. Climate characteristics of a region have a significant impact on erosion intensity (Goudie 2004). In the studied area, the lowest amount of precipitation occurs in summer, while the maximum occurs in autumn, mainly in the form of short and intense showers that trigger flash floods and initiate gully formation (Perica and Orešić 1999) which has also been recorded on the nearby island of Krk (Faivre et al. 2011).

The heads of the identified gullies and valleys are located within the inclination class of 12°–32° and at elevations of up to 1000 meters, where the incision into the substrate begins due to the formation of torrential flows. The longitudinal profiles are characterized by relatively uniform slopes, but some deviations have been identified. Larger, steep declines within certain gullies can be attributed to anthropogenic elements, especially roads, and thus influence erosion intensity and sediment transport. Deviation from the equilibrium state may indicate incision or tectonic activity after the main phase of formation (Benac 1992). More pronounced differences have been observed in the lateral profiles, where the presence of U and gentle V shapes is visible. According to Goudie (2004) and Kirkby and Bracken (2009), after the incision process, slope processes dominate on steep gully sides, causing the filling of the gully bed and consequently smoothing the slopes within, taking on rounded shapes. The cause of differences in the shape of the gully and valley profiles may be also the difference in activity (those with V profiles are still actively incising into the slope, while those with a U shape are dominated by slope processes).

The formation and evolution of gullies and valleys in this area must be contextualized within the Pleistocene glaciation and the Holocene sea-level rise. The existence of glaciers during the Last Glacial Maximum in North and Central Velebit has been proven, parts of which expanded into the area of the coastal slope (Faivre and Bognar 2006). The melting of glaciers formed powerful flows that drained towards the bottom of the then dry Velebit Channel and formed deeply incised gullies and valleys (Faivre et al. 2019). With the rise in sea level in the Holocene (Surić et al. 2009), the bottoms of the formed gullies and valleys were submerged, forming coves (Faivre and Mićunović 2017). Erosional base level changes result in reduction of the intensity of incision, and the gullies are gradually filled with loose material, with the occurrence of repeated flash flood activation during periods of intense rainfall (Benac 1992, Faivre et al. 2011).

5 Conclusions

On the coastal slope of Northern and Central Velebit, an analysis of the digital elevation model, topographic maps and remote sensing data revealed 114 gullies and valleys with an average length of 1.2 km and corresponding drainage basins with an average area of 2.62 km². Strong correlations were found between the area of drainage basins and 1) the lengths of the gullies and 2) the Strahler stream order of the main channel. Additionally, an analysis of longitudinal and lateral profiles of six selected gullies and valleys was conducted.

The formation of gullies and valleys in the studied area is conditioned by geological, geomorphological, hydrological, vegetational and climate characteristics of the region, with the greatest role played by high slope values (12°–32°) and climate with simultaneous occurrences of seasonal intense rainfall. We assume that the main incision phase occurred during the Last Glacial Maximum, enhanced by periodical melting of the Velebit mountain glaciers when water flowed towards the then-existing erosional base level, forming deep gullies and valleys. Subsequent sea level rise in the Holocene submerged the mouths of gullies and valleys, forming deep bays, after which the incision process slowed down. Predominantly U-shaped lateral profiles confirm this thesis, indicating denudation processes on the slopes and the relative age of the analyzed gullies and valleys. However, there are differences in the profile shapes, suggesting differences in their age and activity. The obtained results contribute to the existing knowledge about the morphology of valleys and gullies on the Velebit coastal slope, but also encourage further research with the help of GIS and remote sensing. GIS and remote sensing proved particularly useful in this research as the Velebit coastal slope covers a large, sometimes hardly accessible area. Satellite imagery and topographic maps revealed to be useful in all phases of this research and especially in the verification of the obtained results.

6 Data

Croatian Meteorological and Hydrological Service (DHMZ), 2023: Meteorological data for Senj station.

Državna geodetska uprava (DGU), n.d.: Croatian base map – WMS.

Državna geodetska uprava (DGU), 2021: Digital ortophoto 1:5000 – WMS.

7 References

Ballut, C., Faivre, S., 2012. New data on the dolines of Velebit mountain: An evaluation of their sedimentary archive potential in the reconstruction of landscape evolution. Acta Carsologica 41 (1), 59-74.

Benac, Č., 1992. Recentni geomorfološki procesi i oblici u području Riječkog zaljeva. Geografski glasnik 54, 1-18.

Bognar, A., 1992. Inženjersko geomorfološko kartiranje. Acta Geographica Croatica 27 (1), 173-185.

Bognar, A., 2001. Geomorfološka regionalizacija Hrvatske. Acta Geographica Croatica 34 (1), 7-29.

Castillo, C., Gómez, J. A., 2016. A century of gully erosion research: Urgency, complexity and study approaches. Earth - Science Reviews 160, 300-319.

Domazetović, F., Šiljeg, A., Lončar, N., Marić, I., 2019: Development of automated multicriteria GIS analysis of gully erosion susceptibility, Applied geography 112.

Faivre, S., Bognar, A., 2006. Geomorphological traces of the younger Pleistocene glaciation in the central part of the Velebit Mt. Hrvatski geografski glasnik 68 (2), 19-30.

Faivre, S., Mićunović, M., 2017. Rekonstrukcija recentnih morfoloških promjena žala uz pomoć metode ponovljene fotografije – primjer žala Zogon na otoku Hvaru (Srednji Jadran). Geoadria 22 (2), 165-192.

Faivre, S., Pahernik, M., Maradin, M., 2011. The gully of Potovošća on the Island of Krk – the effects of short-term rainfall event. Geologia Croatica 64 (1), 67-80.

Faivre, S., Galović, L., Sümegi, P., Cvitanović, M., Náfrádi, K., 2019. Palaeoenvironmental reconstruction of the Milna valley on the island of Vis (Central Adriatic) during the late Holocene. Quaternary International 510, 1-17.

Goudie, A. S., 2004. Encyclopedia of Geomorphology, Routledge, London.

Jahić, M., 2017. Bujice i njihova klasifikacija. 11th International Scientific Conference on Production Engineering, Rome, 395-398.

Kirkby, M.J., Bracken, L.J., 2009. Gully processes and gully dynamics. Earth Surface Processes and Landforms 34 (14), 1841-1851.

Lončar, N., 2009. Geomorfološka regionalizacija srednjeg i južnog dijela otoka Paga. Geoadria 14 (2), 5-25.

Mamužić, P., Milan, A., Korolija, B., Borović, I., Majcen, Ž., 1969: Osnovna geološka karta SFRJ 1:100.000, List Rab L33–114. – Institut za geološka istraživanja, Zagreb, (1959–1965); Savezni geološki institut, Beograd.

Mamužić, P., Milan, A., 1966: Tumač za list Rab; Savezni geološki institut, Beograd. pp. 35.

Nikler, L., Galović, I., Mamužić, P., Šušnjara, A., 1976: Tumač za list Gospić; Savezni geološki institut, Beograd. pp. 57.

Perica, D., Orešić, D., 1999. Prilog poznavanju klimatskih obilježja Velebita. Acta Geographica Croatica 32, 45-68.

Rogić, V., 1958. Velebitska primorska padina. Acta Geographica Croatica 2 (1), 8-119.

Ružić, I., Benac, Č., Ilić, S., Sušanj, I., Ljutić, K., 2011. Promjene korištenja zemljišta i regulacija bujičnih vodotoka: Utjecaj na žala Liburnije i otoka Cresa. In: Biondić D. et al. (Eds.), 5. Hrvatska konferencija o vodama: Hrvatske vode pred izazovom klimatskih promjena, Hrvatske vode, Opatija, pp. 771-782.

Sokač, B., Bahun, S., Velić, I., 1970; Tumač za list Otočac; Savezni geološki institut, Beograd. pp. 38.

Sokač, B., Nikler, L., Velić, I., Mamužić, P., 1974: Osnovna geološka karta SFRJ 1:100.000, List Gospić L33–127. – Institut za geološka istraživanja, Zagreb (1963–1967); Savezni geološki institut, Beograd.

Surić, M., 2009. Rekonstruiranje promjena morske razine na istočnoj obali Jadrana (Hrvatska) – pregled. Geoadria 14 (2), 181-199.

Šegota, T., Filipčić, A., 1996. Klimatologija za geografe, Školska knjiga, Zagreb.

Šošić, I., Serdar, V., 2002. Uvod u statistiku, Školska knjiga, Zagreb.

Thwaites, R. N., Brooks, A. P., Pietsch, T. J., Spencer, J. R., 2021: What type of gully is that? The need for a classification of gullies. Earth Surface Processes and Landforms 47, 109-128.

RS and GIS Application for the Alternative Scenarios and Regions for Hydrogen Exploration

Janay Sagin[1], *, Dani Sarsekova[2], Raushan Amanzholova[1], Rebecca King[1], Kairat Amanzholov[1], Baktybek Duisebek[1], Muhammad Ilyas[1], Noor Nabi Dahar[1], Syed Imran Moazzam Shah[1]

[1] School of Information Technology and Engineering, Kazakh-British Technical University, Almaty, Kazakhstan, j.sagin@kbtu.kz, r_amanzholova@kbtu.kz, r.king@kbtu.kz, ka_amanzholov@kbtu.kz, b.duisebek@kbtu.kz, m.ilyas@kbtu.kz, n_dahar@kbtu.kz, s.shah@kbtu.kz

[2] Faculty of Water, Land and Forest Resources, Kazakh National Agrarian University, Almaty, Kazakhstan, sarsekova.dani@kazatu.kz

* corresponding author

Abstract: The Central Asian (CA) region is one of the regions most impacted by climate change and water shortages in the world. Some programs require the proper investigations, before implementation stage. Kazakhstan plans to use water from the Caspian Lake to produce and export hydrogen. As a part of the HYRASIA ONE cooperation program, Kazakhstan plans to construct a major "green" hydrogen production facility. This facility will be one of the largest in the world, and will desalinate water drawn from the Caspian Lake, which is in the Mangistau Region. The Caspian Lake is already shrinking, feeding concerns that it will have the same fate as the Aral Lake. As of now, proper scientific investigation that accounts for alternative scenarios and includes hydrogen producing regions is missing. In the transboundary Moselle-Saar River basin, a former coal mining district, researchers found significant reserves of "white" hydrogen, totalling up to 250 million tons. Like the previously mentioned regions, Central Asia is very rich with mineral resources, including iron-rich, uranium minerals, which produce hydrogen through serpentinization and radiolysis from underground water. Researching water replenishment in Central Asia, including carrying out precipitation analysis and hydrological data collection, is critical to understanding the situation. This paper will address the current effort to apply RS and GIS for alternative scenarios and exploring potentially hydrogen rich regions.

Keywords: geological hydrogen; Kazakhstan; Moselle-Saar; green hydrogen.

1 Introduction

In 2023, Kazakhstan faced severe droughts, which were then followed by devastating floods in 2024. Other impacts of climate change include changes in precipitation patterns, more frequent temperature extremes. These changes have a negative impact on Kazakhstan's agricultural production. This then threatens Kazakhstan's food and environmental security (UNECE 2023). To mitigate climate change and other challenges that impact water resources, many countries invest in foresight adaption programs, sustainable engineering for emergency events, and plans on how to deal with more frequent floods and droughts in advance (Millennium 2023). In the past, man-made intensive agricultural activities diminished the soil sustainability, increasing desertification (Hassani et al. 2021). Foresight research

works are getting important, with some organisations starting to support such efforts. In Kazakhstan, challenges facing the study of water resources include weak scientific support for professional project management of water resources with a scientifically based financial forecast of expenses, and the lack of cooperation among ministries (emergency agencies, water, agriculture, internal affairs) and industry. For example, Kazakhstan is targeted to continue the industrial water extraction from the Caspian Lake to produce hydrogen and export through HYRASIA ONE project, along with continuing current intensive oil and gas extraction from the Caspian Lake area (UN 2023). Namibia has a project like Kazakhstan's Mangistau hydrogen program (DW 2023). It will be reasonable to adapt, review more comparison studies, how similar projects are in development, what issues they may cause. The challenge in executing Kazakhstan's HYRASIA ONE project stems from issues regarding water resource availability and the high electricity costs in the West Kazakhstan. It would be prudent to explore alternative solutions that are cost-effective and environmentally friendly, thus avoiding any adverse impact on nature.

2 Materials and methods

The research group employs a comparative-descriptive methodology to analyse more sustainable regions and alternative technologies for hydrogen exploration. This involves synthesising insights from literature reviews and collaborative brainstorming sessions among research groups. This allows the research group to identify the alternatives solutions for further investigation (Figure 1).

Research questions: 1) Is it sustainable to expand the HYRASIA ONE project in the Caspian Lake area? How can this project disrupt the Caspian Lake?; 2) Are there alternative regions and technologies for hydrogen explorations in Kazakhstan?; 3) What would be reasonable measures to adopt for more sustainable hydrogen exploration programs?

It is important to investigate Kazakhstan's hydrogen production plan for sustainability. This will require proper scientific investigations, surveys taken among the local people, and support from the Mangistau Region's inhabitants. Hydrogen production in the Caspian region will require much effort with approvals. At the same time, it will be reasonable to prepare alternative, more sustainable scenarios, where it will be reasonable to
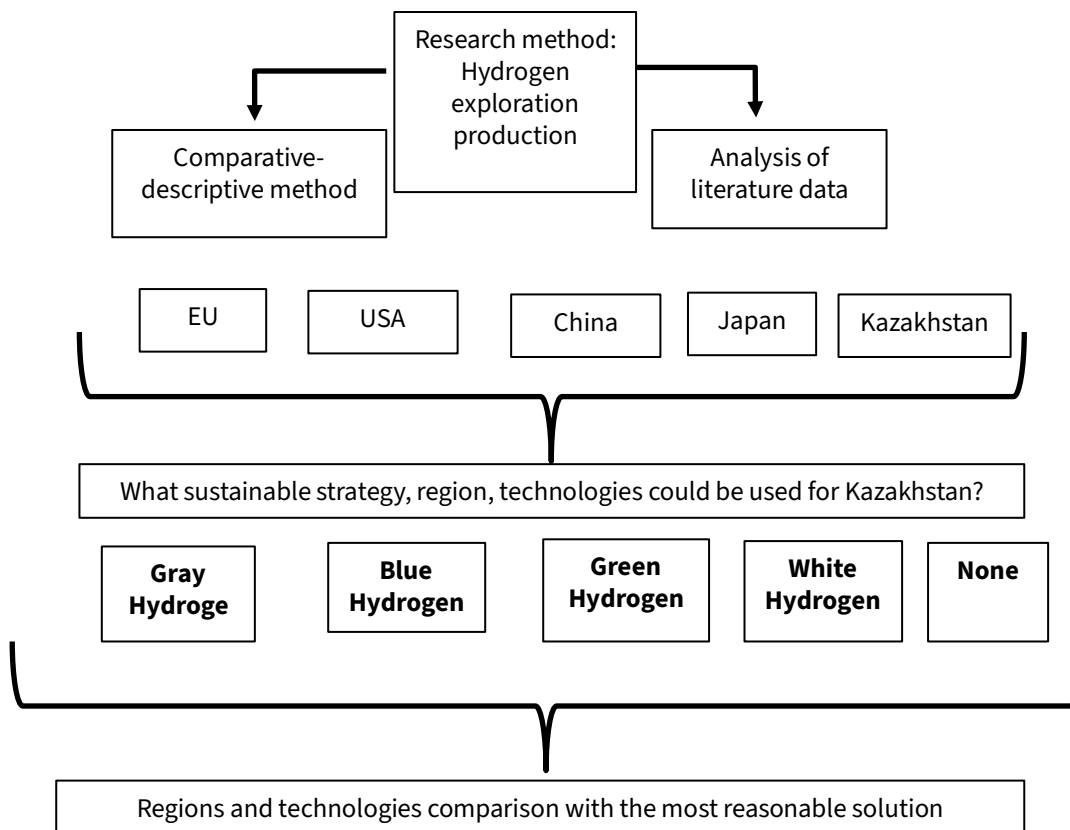
Figure 1. Block diagram of research methods for sustainable hydrogen.

produce hydrogen without harming the environment. Moreover, the HYRASIA ONE project is solely designed to export hydrogen, without developing Kazakhstan's internal usage.

3   Results

Most countries are targeted to set up their own internal hydrogen hubs with intensive investment hydrogen research programs. An extensive examination of patents associated with hydrogen production was conducted spanning the years 2018 to 2023. This analysis utilised the Derwent World Patents Index (DWPI) from Web of Science, Clarivate Analytics (Derwent 2023). An examination of the International Patent Classification (IPC) codes indicates that electrolysis has emerged as the predominant method for hydrogen production, with a total of 611 patents published over the span of 10 years (IPC 2023). This surpasses other methods such as thermal decomposition and photolysis, which collectively garnered 464 patents during the same period. The USA is intensively supporting the scientific work of academic researchers in cooperation with the Hydrogen Hubs Industry, increasing publications and patents on hydrogen. This is to develop their domestic market for the use of hydrogen, including for use by agricultural corporations, in irrigation, and for transport (Gonzalez 2023). China is recognized as the world leader in hydrogen production with a production of 33 million tons of hydrogen per year, which is 1/3 of world production. Production occurs primarily in oil or coal-fired units of oil refineries or chemical plants. It is still cheaper to produce hydrogen using coal than through electrolysis of natural gas or water, costing around 0.7–1.2 Chinese Yuan (CNY)

(US\$0.1–0.19) per cubic metre of hydrogen production. There are plans to increase hydrogen production to 120 million tons by the year 2060 (Gong et al. 2022). The China Hydrogen Alliance anticipates that hydrogen production derived from renewable energy sources could potentially reach 100 million tons by the year 2060.

Instead, the Caspian Lake, a potential alternative region for hydrogen production can be in the north of Kazakhstan, in cooperation with Russia and China. Here, Russia can provide inexpensive water resources, natural gas, and coal to produce hydrogen. Annually, 16.5 cubic kilometres of water from Kazakhstan flow into the Arctic Ocean through Russia (Figure 2). Using this water for hydrogen production could be a viable option. The generated hydrogen could then be used in the southern regions of Kazakhstan for agriculture.

Climate change's rising temperatures are leading to melting glaciers and rising ocean levels. Coastal zones and islands are going under water (Harlan 2023). Desalination and industrial use of water from the landlocked endorheic basins and lakes, such as the Caspian and Aral Lakes, are ultimately unsustainable. These activities are so destructive to the environment, that it would be reasonable to prohibit them. Instead, it is more rational to stimulate the development of technologies for the use of water from the rivers flowing into oceans (Yapiyev et al. 2017). Northern Kazakhstan will be more reasonable to produce electricity, including water and electricity availability at reasonable costs.

As a result, it would be reasonable to investigate the application of Russian and Chinese hydrogen producing technologies in Northern Kazakhstan. This includes

Figure 2. Kazakhstan's transboundary rivers with North region, realising 16.5 km³ into Arctic Ocean through Russia.

technologies that produce hydrogen and ammonia, including from coal (Gray Hydrogen), natural gas (Blue Hydrogen) and water (Green Hydrogen). In Northern Kazakhstan's case, electricity, and resources (water, natural gas, and coal) will be relatively inexpensive and production technologies are more interconnected and efficient for hydrogen-ammonia facilities. Ammonia is widely used in the production of agricultural fertilisers and is currently the best solution for the fertiliser industry (UN 2023).

4   Discussion

Transporting hydrogen from Northern Kazakhstan to regions those facing water resource challenges near the Aral Sea region, would be a viable solution. In this scenario, hydrogen transportation costs would be comparable to those of energy resources like oil, gas, gasoline, and diesel, making it economically feasible. Hydrogen would be classified as an energy resource, which would garner greater respect from local communities compared to the current perception of water resources as inexpensive or free. This perception often complicates the implementation of water-saving and efficiency measures in Kazakhstan (Adenova et al. 2023). Achieving a balanced utilisation of natural resources and adopting sustainable practices for mineral fertilisers necessitates a foundation of comprehensive knowledge and the deployment of advanced irrigation technologies with support from scientific and Technical Vocational Education and Training (TVET). The introduction of the hydrogen market in Kazakhstan has the potential to revolutionise people's perspectives and enhance efficiency in water resource management. The connected opportunities are related to the potential exploration of geological "white" hydrogen (Figure 3).
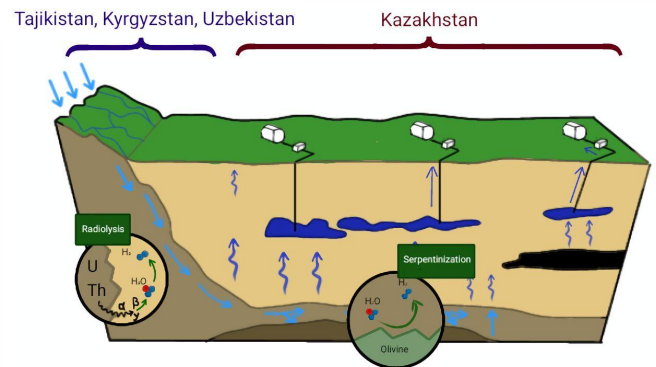
Figure 3. The diagram exhibits a potential of Central Asian countries for cooperation in groundwater resource use to prospect natural geological "white" hydrogen production, modified from Hand (2024).

Numerous countries are currently engaged in "white" hydrogen exploration, which has been compared to a modern-day gold rush. This fervour extends to regions like the German French border, which boasts the world's largest underground reserves of "white" hydrogen. On the territory of the transboundary Moselle-Saar River basin, a former coal mining district, are large volumes of natural geological "white" hydrogen, with an estimated volume of up to 250 million tons (Bettayeb 2023). Kazakhstan does not have "white" hydrogen exploration activities and programs dedicated to identifying underground geological "factories." This program can relate to the NEXUS-water, food, energy activities. RS and GIS technologies combined with geophysical studies would be reasonable to expand in applications for the alternative scenarios and regions for hydrogen exploration.

5   Conclusions

Combining RS and GIS technologies with geophysical studies is a viable approach to investigating alternative scenarios and potential hydrogen-rich regions. Efforts like

these require support for research and the development of TVET programs that include a connected chain of colleges and universities. Improving educational programs is essential for expanding Kazakhstan's hydrogen programs.

6   References

Adenova, D., Tazhiyev, S., Sagin, J., Absametov, M., Murtazin, Y., Trushel, L., Miroshnichenko, O., Zaryab, A., 2023. Groundwater Quality and Potential Health Risk in Zhambyl Region, Kazakhstan. Water 15, 482.

Bettayeb, K., 2023. A gigantic hydrogen deposit in northeast France? CNRS News, 26 July 2023. https://news.cnrs.fr/articles/a-gigantic-hydrogen-deposit-in-north east-france. (Accessed 5 May, 2024)

Derwent Innovations Index on Web of Science, 2023. https://clarivate.com/products/ scientific-and-academic-research/research-discovery-and-workflow-solutions/webofscience-platform/derwent-innovations-index-on-web-of-science/. (Accessed 3 May, 2024)

DW news, 2023. Green hydrogen: Is the Global South paying for Germany's energy transition? https://www.youtube.com/watch?v=75dXFyQ5m9Y. (Accessed 2 May, 2024)

Gong S., Du Z., Mu X., 2022. Research Progress of Ammonia Decomposition Catalysts for Hydrogen Generation. Acta Petrolei Sinica (Petroleum Processing Section) 38 (6) 1506-1519.

Gonzalez C., Hydrogen Nebraska, 2023. Nebraska, two partner states bid to be 'hydrogen hub' that could bring $1 billion in federal funds, https://nebraskaexaminer.com/2023/04/06/nebraska-two-partner-states-bid-to-be-hydrogen-hub-that-could-bring-1-billion-in-federal-funds/. (Accessed 25 April, 2024)

Hand, E., 2024. Hidden Hydrogen: Does Earth hold vast stores of a renewable, carbon-free fuel? Science 379, 6633.

Harlan C., Washington post, 2023. The planet is warming so fast, it could cross a key climate limit in 2024, https://www.washingtonpost.com/climate-envir onment/2023/12/08/climate-change-threshold-cop28-dubai/. (Accessed 15 April, 2024)

International Patent Classification (IPC), 2023, https://www.wipo.int/classifications/ ipc/en/. (Accessed 10 April, 2024)

Millennium Project, 2023. Global challenge 2. How to provide everyone with enough clean water without conflict? https://www.millennium-project.org/challenge-2/. (Accessed 5 April, 2024)

UN, 2023. Department of Economic and Social Affairs, Sustainable Development, Hydrogen and Ammonia fertilizers for Sustainable Agriculture and New Global Framework for Managing Nature programs, https://sdgs.un.org/partnerships/ hydrogen-and-ammonia-fertilizers-sustainable-agriculture-and-new-global-framework. (Accessed 5 April, 2024)

UNECE, GIZ Germany, 2023, Green Central Asia: strengthening regional dialogue on climate, environment, and security https://unece.org/sites/default/files/2023-06/6_1_Milow_RUS.pdf. (Accessed 3 April, 2024)

Yapiyev, V., Sagintayev, J., Inglezakis, V.J.; Samarkhanov, Z., Verhoef, A., 2017. Essentials of endorheic basins and lakes: a review in the context of current and future water resource management and mitigation activities in Central Asia, Water 2017 9(10), 798.

Innovations in Spatial Data-Acquiring Technologies

ENHANCING SATELLITE-DERIVED BATHYMETRY USING THE DIFFERENT SENTINEL-2 SPECTRAL BANDS IN THE MIDDLE ADRIATIC
Ljerka Vrdoljak

GLOBAL OPEN MAPS FOR THE INTEGRATED MONITORING AND ASSESSMENT PROGRAMME OF THE MEDITERRANEAN SEA AND COAST
Martina Baučić, Frane Gilić, Antonio Morić Španić, Daria Povh Škugor

A DEEP LEARNING ALGORITHM FOR WATER BODY MAPPING FROM SENTINEL 2 DATA
Gordana Jakovljević, Miro Govedarica

APPLICATION OF REMOTE SENSING IN COASTAL GEOMORPHOLOGY: A CASE STUDY OF ZORAĆE VELO, HVAR ISLAND, CENTRAL ADRIATIC
Marin Mićunović, Sanja Faivre

COMPARATIVE ANALYSIS OF UNMANNED AERIAL VEHICLE LAND COVER CLASSIFICATION OF TWO STUDY SITES IN SERBIA
Ivana Miličić, Nina Pajević, Bojana Ivošević

TESTING THE PERFORMANCE OF HAND-HELD PERSONAL LASER SCANNING SYSTEMS FOR PRECISION FOREST INVENTORY
Andro Kokeza, Luka Jurjević, Fran Domazetović, Ivan Marić, Ante Šiljeg, Damir Medak, Krunoslav Indir, Danko Kuric, Ivan Balenović

UTILIZATION OF UNDERWATER ROVS FOR THE EVALUATION AND RESEARCH OF THE UNDERWATER ENVIRONMENT -EXAMPLE OF MARINE OUTFALLS SURVEILLANCE IN THE WIDER AQUATORIUM OF THE CITY OF SPLIT
Konrad Kiš, Katja Franc

DECLINING SEA SURFACE HEIGHT IN THE CASPIAN SEA BASED ON SENTINEL-3A DATA
Nilufar Makky, Khalil Valizadeh Kamran

Enhancing Satellite-Derived Bathymetry Using the Different Sentinel-2 Spectral Bands in the Middle Adriatic

Ljerka Vrdoljak[1],*

[1] Hydrographic department, Hydrographic Institute of the Republic of Croatia, Split, Croatia, ljerka.vrdoljak@hhi.hr
* corresponding author

Abstract: Bathymetry, the measurement of seafloor depths, underpins numerous marine research and navigation safety. However, less than 25% of global oceans and seas are mapped at high resolution due to the high-cost of traditional ship or airplane-based survey methods. Satellite Derived Bathymetry (SDB) offers a rapid, cost-effective alternative for shallow marine areas using optical satellite data. This study augments existing SDB algorithms by incorporating the Sentinel-2 Band 1 (Coastal Aerosol) with Band 4 (Red) in the Log-Band Ratio (LBR) algorithm for the Middle Adriatic's shallow waters. Using a one-year dataset of Sentinel-2 imagery for the Šibenik channel, the study evaluates the new spectral combination's effectiveness. Results indicate that the Coastal Aerosol band, despite its lower spatial resolution, improves bathymetric accuracy in shallow waters (0-5 meters) compared to traditional blue/green ratio. The new combination achieved a NMedAE of 0.22, outperforming the green/blue model's 0,79 NMedAE in the same depth range. The switch SDB model, integrating both spectral combinations, provided bathymetric coverage up to 20 meters depth, ensuring improved accuracy in coastal areas.

Keywords: remote sensing; earth observation; seafloor mapping; optical bathymetry; switch model.

1 Introduction

Bathymetry refers to the measurement of depths to model the topography of the seafloor. Bathymetric data provide a framework for almost all marine-related research from geodynamics to the safety of navigation, supporting activities related to blue growth (Wölfl et al. 2019).

Currently, less than 25% of the world's seas and oceans are mapped at high resolution due to high cost and/or duration of traditional survey techniques, which rely on ships (acoustic systems) or airplanes (LiDAR) as survey platforms (Seabed 2030, 2024).

Compared to traditional survey methods, Satellite Derived Bathymetry (SDB) is recognized as a rapid and cost-effective method for estimating bathymetry in shallow parts of the seas using data collected by the optical satellite sensors (IHO 2024). Since the 1970s, SDB methods have significantly evolved in accuracy and popularity, largely due to the availability of extensive multispectral image (MSI) databases from Earth observation missions such as Landsat and Sentinel.

Compared to other two main concepts of SDB—the photogrammetric approach and the 'physics-based' approach, empirical methods known as the 'ratio approach' feature simpler algorithms, though they require a set of known depths for model calibration. The log-band ratio (LBR) algorithm applies the linear regression to model the mathematical relations between the ratio of the green and blue bands (pseudo-depth model pSDB) and prerequisite survey data (Stumpf and Holderied 2003). This method is independent of changes in the seafloor substrate, can be adapted to other combinations of visible light (VIS) bands, and different satellite images.

Previous studies demonstrated the potential of using other combinations of spectral bands, beyond the classical blue and green, to minimize negative effect of higher turbidity, submerged vegetation, or water attenuation on SDB (Dierssen et al. 2003, Poursanidis et al. 2019, Caballero and Stumpf 2020, Vrdoljak and Kilić-Pamuković 2022).

Proximity to the shoreline, where various human activities and wave action occur, often resuspends sediments from the seabed into the water column, contributing to higher turbidity in the shallowest marine areas. In previous research (Vrdoljak and Kilić-Pamuković 2022), a switch algorithm for SDB (Caballero and Stumpf, 2020) was adapted using a combination of spectral Band 2 – Blue (B2), Band 3 – Green (B3), and Band 4 – Red (B4) from Sentinel-2 MSI, which proved effective for the shallowest marine areas in the Middle Adriatic.

The aim of this study is to extend the existing algorithm by combining Band 1 – Coastal aerosol (B1) and B4 of the Sentinel-2 MSI. The focus of the research was on the shallowest parts of the marine areas where traditional methods are less effective. Using the LBR algorithm as the base of the switch algorithm, analysis and comparison of the results were performed to assess the effectiveness of the new spectral combination in the marine areas of the Middle Adriatic.

2 Materials and methods

In this study, a switch SDB algorithm (Caballero and Stumpf 2020), adapted to Middle Adriatic (Vrdoljak and Kilić-Pamuković 2022) was used to predict bathymetry from Sentinel-2 MSI.

Study area was marine area of Šibenik channel located in Middle Adriatic (Figure 1a). Part of the Šibenik channel was surveyed with Kongsberg EM-3002 D multibeam system to assure safety of navigation by Hydrographic Institute of the Republic of Croatia in 2014. Collected data, categorized as Special-Order Survey (IHO, 2022) and referenced to Mean Low Lower Water (MLLW), was used for vertical calibration and validation of SDB (Figure 1b). For the area of Šibenik channel, a one-year period (2017 -2018) of Sentinel-2 MSI was evaluated for estimation of SDB and based on quality statistics an optimal image was depicted. A workflow for SDB estimation (Vrdoljak and Kilić Pamuković 2022) was adapted (Figure 2).
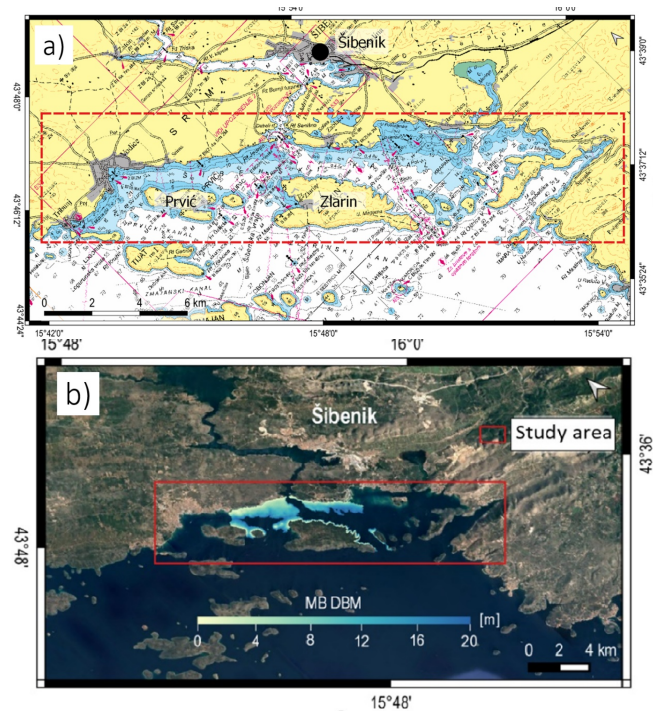
Figure 1. Location of study area in Middle Adriatic. (a) Red line on a nautical chart (GeoAdriatic, 2022) indicates the marine area of interest for SDB estimation. (b) In-situ MB survey data, randomly chosen 25% were control points, the remaining 75% were denoted as check points.

(Vanhellemont and Ruddick 2018). In addition, ACOLITE DSF corrected the MSIs for sun glint and masked the land areas. Median filter was applied to reduce remaining noise in the MSIs. Two spectral combinations were chosen Green (G) combining B2 and B3, and Red (R) combining B1 and B4. Multibeam bathymetry model (MB DBM) and B1 were interpolated using bilinear interpolation to match the 10-meter resolution of B2, B3, and B4. PSDB models were estimated using LBR algorithm (Stumpf and Holderied 2003) in both spectral combinations for all the MSIs. Randomly chosen 25 % of MB DBM were used as control points for the vertical calibration

of pSDB performed by linear regression. Rest of the points were set as check data. Resulting R SDBs and G SDBs were validated against check data. Following statistics were used for quality assessment: Mean absolute error (MAE), Median absolute error (MedAE), and Standard deviation (St.dev.). Upon the results, an optimal MSI for SDB estimation was chosen. G SDB and R SDB of the optimal image were compared using Normalized Median of Absolute Error (NMedAE) to determine coefficients for the switch SDB. Switch SDB was calculated by the weighted mean (Caballero and Stumpf 2020, Vrdoljak and Kilić-Pamuković 2022):

All scenes were processed with ACOLITE Dark Spectrum
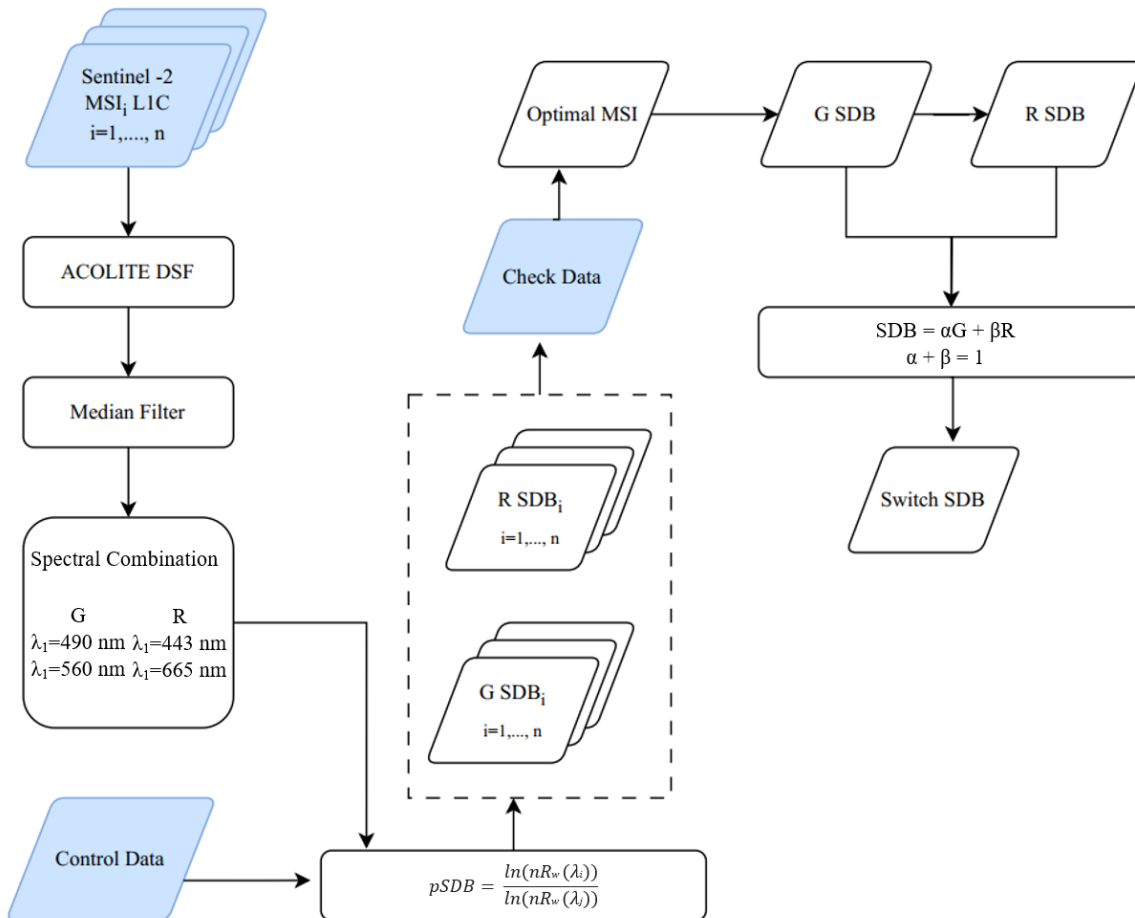
Figure 2. Procedure for the SDB estimation (adapted after Vrdoljak and Kilić-Pamuković, 2022).

Fitting algorithm for atmospheric correction to obtain Bottom of the Atmosphere reflectance (BOA)

$$\text{switch SDB} = \begin{cases} \text{SDB R for SDB R} < 3 \\ \text{SDB G for SDB R} > 3 \text{ AND SDB G} > 5 \\ \alpha \text{SDB G} + \beta \text{SDB R for SDB R} \geq 3 \text{ AND SDB G} \leq 5 \end{cases} \tag{1}$$

while

$$\alpha = \frac{5 - \text{SDB R}}{3}, \beta = 1 - \alpha. \tag{2}$$

3   Results

In this research, the possibility of using the Sentinel-2 B1 for SDB retrieval in shallow coastal parts of marine areas was analyzed.

Based on SDB quality statistics, MSIS2A20170329 was selected as the optimal one. The G SDB model covered marine areas up to 20 meters in depth with a MAE of 1.55 m, a MedAE of 1.14 m, and a standard deviation of 2.13 m. The R SDB model covered areas up to 5 meters in depth with a MAE of 0.44 m, a MedAE of 0.33 m, and a standard deviation of 0.62 m. To evaluate the performance of each spectral combination, comparisons were made within the same depth ranges (Table 1).

The G DBM model showed varying NMedAE with depth, ranging from 79% for depths of 0–3 meters to 10% for 15–20 meters. Conversely, the R DBM model showed lower changes in NMedAE values for the shallow depths of 0–3 meters (22%) and 3–5 meters (10%). In comparison with the G SDB, the R DBM model demonstrated better performance in the shallowest depth range of 0–5 meters in terms of depth quality. The combined SDB model, which integrates G SDB and R SDB, is presented in Figure 3. Compared to G SDB alone, the combined model shows residuals up to twice as small in the shallowest depths.

Specifically, the NMedAE is 39% for the 0 to 3–meter range and 18% for the 3 to 5–meter range. The R SDB model achieved higher accuracy in the shallowest parts (up to 5 meters), while the G SDB model extended coverage and maintained quality to depths of up to 20 meters, ensuring continuous bathymetric estimation throughout the study area.

Table 1. NMedAE (%) of G DBM and R DBM in different depth ranges.

NMedAE (%)					
Spectral Combination	**Depth Range**				
	0–3	3–5	5–10	10–15	15–20
G	79	29	20	12	10
R	22	10	-	-	-

4   Discussion and conclusions

The present study evaluated the potential of downscaled Sentinel-2 B1 for bathymetry estimation in the shallowest marine areas of the Middle Adriatic.

Previous research (Vrdoljak and Kilić-Pamuković 2022) using a switch algorithm (Caballero and Stumpf 2019) adjusted for the Middle Adriatic, combined spectral bands B2, B3, and B4, resulting in a model with lower residuals in the shallowest marine areas (Figure 4).

Compared to other VIS bands of Sentinel-2 MSI, B1 has the lowest spatial resolution and a higher signal-to-noise ratio.

This study demonstrated that despite its limitations B1, when downscaled to a 10-meters resolution, enhanced bathymetric estimation in the shallowest marine areas.
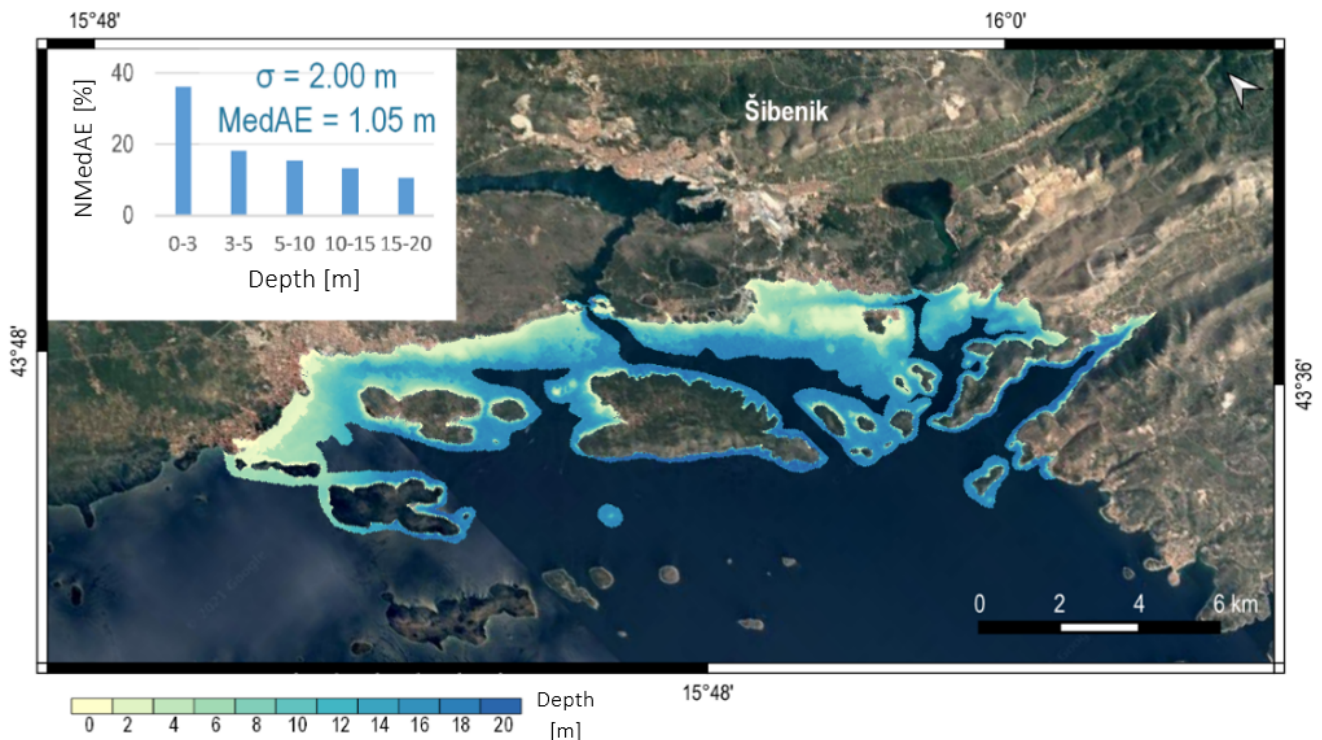
Figure 3. Switch SDB in Šibenik channel.

The LBR algorithm incorporating B1 and B4 improved coastal bathymetry accuracy in the shallowest depth range (0-5 m), with NMedAE of 22% in the 0-3 m depth range and NMedAE of 10% in the 3-5 m depth range. Compared to results from previous research (Figure 4), the spectral combination of B1/B4 showed a negligible but better performance.
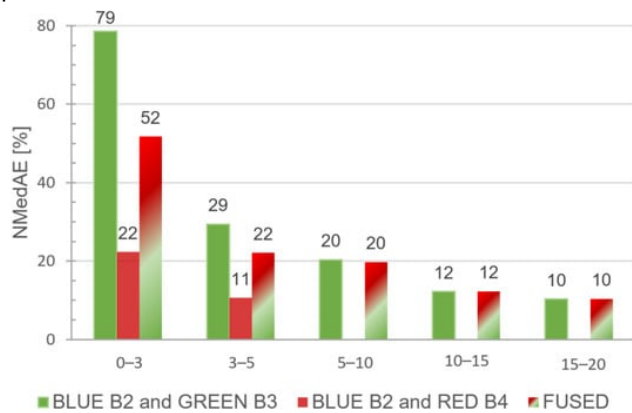
Figure 4. Results of SDB validation from previous research by Vrdoljak and Kilić-Pamuković (2022) show NMedAE values for B2 and B3, B2 and B4, and fused (switch) SDB across different depth ranges.

The model was augmented by the classic B2/B3 ratio with the switch SDB algorithm to ensure continuous SDB estimation up to 20 meters depth in the Šibenik channel. The result was a switch SDB model covering marine areas up to 20 meters with improved quality in coastal parts with depths up to 5 meters.

These improvements underline the importance of selecting the optimal spectral band for bathymetry estimation, which is important for many marine-related research projects needing up-to-date bathymetry.

Acknowledgments: This research was part of Ljerka Vrdoljak's PhD thesis, titled "Modeling of Seafloor Topography Using Satellite Optical Sensor Data, Satellite Altimetry, and In Situ Soundings."

5 References

Caballero, I., Stumpf, R., 2020. Towards Routine Mapping of Shallow Bathymetry in Environments with Variable Turbidity: Contribution of Sentinel-2A/B Satellites Mission. Remote Sensing 12, 451.

Dierssen, H.M., Zimmerman, R.C., Leathers, R.A., Downes, T.V. Davis, C.O., 2003. Ocean color remote sensing of seagrass and bathymetry in the Bahamas Banks by high-resolution airborne imagery. Limnology and Oceanography 48 1(2), 444-455.

GeoAdriatic HHI. Hrvatski portal prostornih podataka o moru. https://geoadriatic.hhi.hr/. (Accessed 15 May 2022).

International Hydrographic Organization IHO, 2024. B-13 Edition 1.0.0. Guidance to Satellite Derived Bathymetry IHO, Monaco. https://iho.int/uploads/user/pubs/bathy/B_13_Ed100_032024.pdf.

International Hydrographic Organization IHO, 2022. S-44 Edition 6.1.0. IHO Standards for Hydrographic Surveys. IHO, Monaco. https://iho.int/uploads/user/pubs/standards/s-44/S-44_Edition_6.0.0_EN.pdf.

Poursanidis, D., Traganos, D., Reinartz, P., Chrysoulakis, N., 2019. On the use of Sentinel-2 for coastal habitat mapping and satellite-derived bathymetry estimation using downscaled coastal aerosol band. International Journal of Applied Earth Observation and Geoinformation 80, 58-70.

Seabed 2030. https://seabed2030.org/our-mission/ (Accessed 15 May, 2024.)

Stumpf, R.P., Holderied, K., 2003. Determination of Water Depth with High-Resolution Satellite Imagery over Variable Bottom Types. Limnology and Oceanography 48 (1), 547-556.

Vanhellemont, Q., Ruddick, K., 2018. Atmospheric correction of metre-scale optical satellite data for inland and coastal water applications. Remote Sensing of Environment 216, 586-597.

Vrdoljak, L., Kilić Pamuković, J., 2022. Assessment of Atmospheric Correction Processors and Spectral Bands for Satellite-Derived Bathymetry Using Sentinel-2 Data in the Middle Adriatic. Hydrology, 9(12), 215.

Wölfl, A.-C., Snaith, H., Amirebrahimi, S., Devey, C.W., Dorschel, B., Ferrini, V., Huvenne, V.A.I., Jakobsson, M., Jencks, J., Johnston, G., Lamarche, G., Mayer, L., Millar, D., Pedersen, T.H., Picard, K., Reitz, A., Schmitt, T., Visbeck, M., Weatherall, P., Wigley, R., 2019. Seafloor Mapping – The Challenge of a Truly Global Ocean Bathymetry. Front. Mar. Sci. 6, 283.

Global Open Maps for the Integrated Monitoring and Assessment Programme of the Mediterranean Sea and Coast

Martina Baučić[1,]*, Frane Gilić[1], Antonio Morić Španić[2], Daria Povh Škugor[3]

[1] Faculty of Civil Engineering, Architecture and Geodesy, University of Split, Split, Croatia, mbaucic@gradst.hr, fgilic@gradst.hr

[2] PINUS NIGRA, Split, Croatia, amoricspanic@gmail.com

[3] Priority Actions Programme/Regional Activity Centre (PAP/RAC), Split, Croatia, daria.povh@paprac.org

* corresponding author

Abstract: The Integrated Monitoring and Assessment Programme (IMAP) aims to quantitatively assess the status of the Mediterranean Sea and coast in an integrated way. There are 27 indicators that are linked to one of 11 Ecological Objectives. Candidate Common Indicator 25 "Land cover change" (CCI25) has focused on urbanisation – a process that highly compromises ecosystem integrity and is irreversible. CCI25 calculates shares of five land cover classes for the coastal zone of 10 km width. Additional parameters calculate areas under protection and areas up to 5 m above sea level. After the initial calculation, the calculation is repeated every 6 years and changes are detected. The CCI25 is demanding in terms of data: it requires homogeneous data of the entire Mediterranean; certain spatial and temporal resolution; and fitting the semantics of the indicator. National data cannot meet these needs, so the use of global open maps has been tested. This paper presents results for key data sets: land cover, elevation and coastline. The coastline from OpenStreetMap fully meets the needs as well as the Copernicus DEM 30 global surface model. Regarding land cover data, the ESA WorldCover Project has been revealed as the most promising one.

Keywords: ecological objectives; IMAP; land cover; land take; Mediterranean.

1   Introduction

The environmental resources on the coastal area of the Mediterranean is continuously under pressure of anthropogenic activities and climate change impacts (EEA 1999, Papamichael et al. 2022). The process of urbanisation, or land take, is particularly important because it can be considered an irreversible process. Monitoring land cover changes is a key segment for spatial planning and making future decisions in accordance with sustainable development.

The Integrated Monitoring and Assessment Programme of the Mediterranean Sea and Coast and Related Assessment Criteria (IMAP) (UNEP/MAP 2017) established 11 ecological objectives (EO) and 27 common indicators of which 4 are candidates. In this paper, focus is given to the EO 8 Coastal Ecosystems and Landscapes and Candidate Common Indicator 25 "Land cover change" (CCI25) aiming to support the balanced allocation of uses, preserving open coastal space, securing setback zones, avoiding urban sprawl and securing ecosystem health. CCI25 provides an analytical base for The Integrated Coastal Zone Management (ICZM) Protocol (UNEP/MAP/PAP 2008). The Priority Actions Programme Regional Activity Centre (PAP/RAC) is assisting the countries in the implementation of the Protocol's provisions. Being a Candidate Common Indicator, the CCI25 is still in a testing phase. With the aim of testing and improving the CCI25, the comprehensive study was conducted. As the result, the Guiding Factsheet was reviewed and updated (Baučić et al. 2022a). The analytical units are upgraded with Low Elevation Coastal Zone (LECZ) - an area prone to coastal flooding, erosion and salinization (Ali et al. 2022); data sources are updated with open-source data; the mapping units are scaled down from 25 ha to 1 ha; and the change detection units are scaled down from 5 ha to 1 ha. The CCI25 is demanding in terms of data: it requires homogeneous data of the entire Mediterranean; certain spatial and temporal resolution; and fitting the semantics of the indicator. National data cannot meet these needs, so the use of global open maps has been tested. This paper presents results for key data sets: land cover, elevation and coastline.

CCI25 parameters are defined for the coastal zone - an area on the land that is within 10 km from the coastline. This area is further subdivided into three coastal strips: from 0 to 300 m; 300 to 1000 m; and from 1 to 10 km from the coastline. Final reporting units for CCI25 parameters are defined by further dividing coastal strips with administrative units. Additionally, CCI25 parameters are calculated for protected areas and Low Elevation Coastal Zone (LECZ) - the zone that is contiguous to the coastline; under 5 m above sea level; and within the coastal zone. CCI25 quantifies land use/land cover changes in coastal zones for the time interval of 6 years. For the first monitoring, there are 13 indicator parameters and for the second and every subsequent one, there are additional six parameters to be calculated. First monitoring parameters include the calculation of areas under five land cover classes (built-up areas, agricultural, forest and semi natural land, wetlands and water); areas under protection and inside LECZ. Second monitoring parameters include the calculation of land cover change and change in protected areas. CCI25 parameters provide data for various analyses (such as land take per coastal strips). Data aggregation on a national level enables comparison among countries. The pressures of urbanisation to coastal ecosystems could be identified and geolocated but responsibility is on local institutions to interpret and understand these processes, and the drivers behind them.

2   Materials and methods

The upgrading the methodology for CCI25 included work from desktop search to testing and validation on the pilot sites. This paper has focused on elaboration of adequacy of open data for CCI25 calculation. First step was to identify candidate data sources based on the requirements given in the CCI25 Guidance Factsheet. Second step was to test candidate data on pilot area, and third step involved validation against aerial images and higher quality data (Baučić et al. 2022b). Pilot site covers the coastal zone of Albania, Montenegro, Bosnia and Herzegovina, and the south part of Croatia, in total covering 6.424 km².

2.1   Land-use / land cover data (LU/LC data)

Three sources for LU/LC data are selected for testing purposes: Copernicus Coastal Zones (CCZ), data sets for year 2012 and 2018 (Copernicus 2024a); ESA WorldCover Project Land cover (ESA WCP), data set for year 2020 (ESA 2024); and Copernicus Global Land Cover and Change (CGLCC), data sets for year 2015 and 2018 (Copernicus 2024b). All three datasets satisfy the requirements of the CCI25 regarding spatial resolution. Copernicus Coastal Zones do not cover the entire coastal area of the Mediterranean but only the northern coasts located in the European Economic Area countries. Classification of the CCZ data best matches the required classification system. Another two data sets are using the UN-LCCS classification system developed by UN FAO (FAO 2024). In the context of land take detection, the most important disparity between UN-LCCS and the CCI25 classification system is in the definition of urban green areas, dump and construction sites. CCI25 classifies them as urban areas because they serve urban functions, while in UN-LCCS urban green areas are considered as a certain type of natural vegetation, while dump and construction sites as bare land. Use of the UN-LCCS classification system could lead to underestimation of built-up areas because certain land cover classes are not recognized as having urban functions.

The CCI25 parameters are calculated for the pilot area by all three data sources and results are compared. CGLCC for 2018 was the only data set available for the same year as CCZ data. Thus, the area-based comparison of these two data sets is elaborated. The areas covered by LU/LC classes in coastal zones (0–10 km) are noticeably different when calculated from these two data sets. The largest absolute and relative difference were expressed in agricultural areas, where 106.2 km² (1.66%) more are recorded by the CGLCC. The second largest difference is reflected in built-up areas, where 88.1 km2 (1.37%) more are recorded by the CCZ data. The next step was visual inspection of data on the eleven locations, significant for the monitoring of land cover change. Aerial photos from the reference year are used as higher quality data. Additionally, selected data sets are compared with each other (Baučić et al. 2022c). Figure 1 illustrates visual inspection for the location of Luštica bay in Montenegro.

| Aerial images (VHR 2012–18, ESRI 2020) | Copernicus Coastal Zones data | Copernicus Global Land Cover | ESA WorldCover Project |
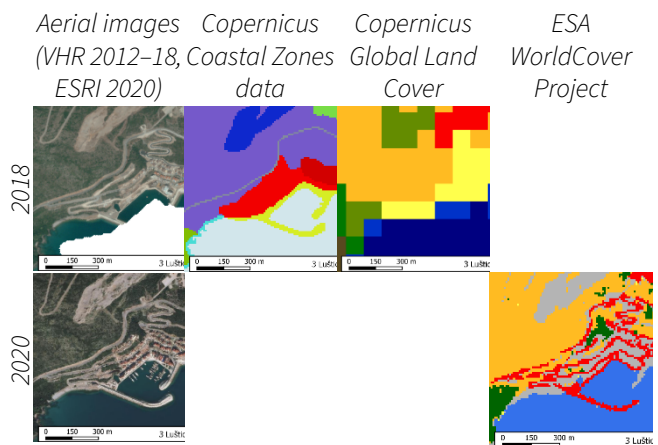
Figure 1. Luštica bay – comparison of various LU/LC data with aerial images.

2.2   Coastline

Five open coastline data sets have been identified as potentially suitable for calculating CCI25: EU-Hydro; EEA coastline for analysis; EMODNet coastline; Global Self-consistent, Hierarchical, High-resolution Geography Database (GSHHG); and OpenStreetMap (OSM) coastline (Figure 2).

Figure 2. Five coastline datasets identified as potentially suitable for calculating CCI 25.

For the pilot site, a visual inspection over aerial images is performed. The OSM coastline was fitting the best and thus it is selected for testing purposes. OSM coastline data is based on crowdsourced volunteered geographic information and metadata only declared date of last update (OSM 2024). The requirements in the CCI25 factsheet define MMU for linear elements of 100 m. The OSM coastline is validated for the pilot area by visual inspection against the aerial images from the same year. Attention was given on determining whether the coastline includes all details such as small bays, rocks, small facilities in ports, docks and similar. Conclusion of the visual inspection is that the OSM coastline satisfies the CCI25 requirements.

2.3   Elevation data

The elevation datasets identified as potentially suitable for calculating parameters for this indicator are the following: Copernicus DEM 30; FABDEM; ALOS World 3D – 30 m; ASTER GDEM; and SRTM DEM. By vertical accuracy, Copernicus DEM 30 (Copernicus 2024c), and FABDEM (Fathom 2024) are the most accurate and thus further used for testing and validation.

changes and their verification. ESA WCP data is the best source due to its superior spatial resolution of 10 m and it is planned to be updated annually. The main disadvantage of the ESA WCP is the fact that different algorithms, training data, and input variables were used to produce data for 2020 and 2021. This makes land cover change analysis problematic because some changes are a direct result of these differences, and do not represent a real change in land cover.

Figure 3. Copernicus DEM (a, c and e) and FABDEM elevation data (b, d and f).

Regarding spatial resolution, as CCI25 requires 1 ha as MMU and 100 m for linear elements, both elevation data sources satisfy the requirements. CCI25 includes Low Coastal Elevation Zone (LECZ) as an additional analytical unit, thus it is necessary to delineate elevation of 5 m above sea level. According to declared vertical accuracies of Copernicus DEM (2 and 4 m), delineation of the lowest zones 0–1 m, 1–2 m, and 2–5 m could be vague (Figure 3, a, c and e). Visual inspection revealed that for the lowest elevation zones Copernicus DEM data are characterised by many small zones (Figure 3, a, c and e), often at the level of individual pixels proving that Copernicus DEM data is loose for the lowest zones. FABDEM data represent the same low-lying terrain with more homogeneous elevation zones.

3   Results and discussion

Based on the testing described above, the most adequate global open maps for the CCI25 calculation are: ESA WCP product for LU/LC data; OpenStreetMap for coastline; and Copernicus DEM 30 global surface model for delineation of LECZ.

Regarding LU/LC data sets, the CCZ data is a superior data source for the CCI25 calculation, but it does not cover the whole Mediterranean region. Common pitfall of CGLCC and ESA WCP data is in the use of the UN-LCCS classification system that could lead to underestimation of built-up areas and agricultural land. CGLCC does not recognize construction sites as land take areas and additional visual inspection of aerial images should be used for detecting

Visual inspection in the pilot area showed that the OSM coastline includes linear details of 100 m minimum size and fits aerial images well. Final recommendation is to check OSM data before use e.g. by visual inspection over aerial images. If necessary, OSM coastline should be manually edited and thus updated.

As FABDEM is freely available only for non-commercial purpose, the Copernicus DEM is suggested as the most suitable for conducting CCI25 calculations, keeping in mind that elevation threshold of 5 m is the lowest one that could be used for construction of Low Elevation Coastal Zone (LECZ).

4   Conclusions

In the context of the development of satellite technologies and the available global open maps, one should reconsider existing spatial planning practice in such a way as to include free satellite data. Such an effort is presented here. The methodology for CCI25 was adapted to satellite data products that brought benefits: spatial and temporal resolution increased; CCI25 can be calculated immediately and without data collection costs. The compromise was in adoption of an UN-LCCS classification system that identifies the land cover class regardless of use, but it will lead to the quantification of urban green areas.

5   References

Ali, E., W. Cramer, J. Carnicer, E. Georgopoulou, N.J.M. Hilmi, G. Le Cozannet, and P. Lionello, 2022. Cross-Chapter Paper 4: Mediterranean Region. In: Climate Change 2022: Impacts, Adaptation and Vulnerability, Cambridge, UK and New York, USA.

Baučić, M., Morić-Španić, A., Gilić, F., 2022a. Upgraded Guidance Factsheet for Candidate Common Indicator 25 "Land cover change" - Rationale and Background, PAP/RAC, Split, Croatia.

Baučić M., Morić Španić A., Gilić F., 2022b. Report and GIS database with calculation of the LCC indicator for the pilot areas. Report; PAP/RAC, Split, Croatia.

Baučić M., Morić Španić A., Gilić F., 2022c. Validation of testing results for upgraded LCC Indicator 25 in pilot areas. Report; PAP/RAC, Split, Croatia.

Copernicus, 2024a. Copernicus Land Monitoring Service, Coastal Zones, https://land.copernicus.eu/en/products/coastal-zones. (Accessed 11 June, 2024)

Copernicus, 2024b. Copernicus Land Monitoring Service, Dynamic Land Cover, https://land.copernicus.eu/en/products/global-dynamic-land-cover. (Accessed 11 June, 2024)

Copernicus, 2024c. Copernicus DEM - Global and European Digital Elevation Model (COP-DEM, https://spacedata.copernicus.eu/collections/copernicus-digital-elevation-model. (Accessed 11 June, 2024)

EEA, 1999. "State and pressures of the marine and coastal Mediterranean environment", Copenhagen, Denmark.

ESA, 2024. Worldwide land cover mapping, https://esa-worldcover.org/en. (Accessed 11 June, 2024)

FAO, 2024. Land Cover Classification System (LCCS), https://www.fao.org/land-water/land/land-governance/land-resources-planning-toolbox/category/det ails/en/c/1036361/. (Accessed 11 June, 2024)

Fathom, 2024. Global Terrain Data – FABDEM+, https://www.fathom.global/prod uct/fabdem/. (Accessed 11 June, 2024)

OSM, 2024. Open Street Map, Coastlines, https://osmdata.openstreetmap.de/ data/coastlines.html. (Accessed 11 June, 2024)

Papamichael, I., Voukkali, I., Zorpas, A.A., 2022. Mediterranean: main environmental issues and concerns. Euro-Mediterranean Journal for Environmental Integration 7(4), 477-481.

UNEP/MAP/PAP, 2008. Protocol on Integrated Coastal Zone Management in The Mediterranean. PAP/RAC, Split, Croatia.

UNEP/MAP, 2017. Integrated Monitoring and Assessment Programme of the Mediterranean Sea and Coast and Related Assessment Criteria.

A Deep Learning Algorithm for Water Body Mapping from Sentinel 2 Data

Gordana Jakovljević[1,], Miro Govedarica[2]*

[1] Faculty of Architecture, Civil Engineering and Geodesy, University of Banja Luka, Bosnia and Herzegovina, gordana.jakovljevic@aggf.unibl.org

[2] Faculty of Technical Science, University of Novi Sad, Serbia, miro@uns.ac.rs

* corresponding author

Abstract: Water is vital for the life on the Earth. Human health, food security, and economic growth are all water dependent. Monitoring of water bodies and their spatial changes is crucial for understanding the impact of human activities and climate changes on aquatic ecosystems. Remote sensing data provides large amounts of data that have been extensively used for monitoring water bodies, geometry, topology, associated attributes, and their changes. However, water body delineation is challenging due to sensor limitations, cloud presence, and atmospheric conditions. This paper presents a novel approach leveraging Convolutional Neural Networks (CNNs) for extracting water bodies from Sentinel-2 imagery. The efficacy of the proposed algorithm is rigorously evaluated across heterogeneous terrains encompassing diverse riverine and lacustrine features. Key metrics such as overall accuracy, F1 score, precision, and recall are employed to quantitatively assess algorithmic performance. Our findings underscore the promising potential of deep learning techniques in accurately delineating water bodies and monitoring their dynamic behaviour within intricate environmental contexts at local, regional, and global scales.

Keywords: inland water body; Sentinel-2; CNN; geometry.

1   Introduction

Water is essential for life, supporting humans, animals, plants, and entire ecosystems. Recently, the effects of global climate change and human activities on the spatial and temporal variations in water quality and quantity have gained increasing attention. These changes in surface water bodies impact agricultural and industrial production, ecological balance, environmental conditions, and food and health safety. Accurate and rapid information about the spatial distribution, persistence, and quality of surface water is crucial for sustainable water usage and protection from feature degradation. Remote sensing covers large geographic areas at various spatial, spectral, and temporal resolutions, and provides extensive data used for analysing surface water bodies and their dynamics. Satellite images are particularly valuable for obtaining information about water bodies in remote, inaccessible, extremely large, or hazardous areas, such as during floods. Over the past three decades, multi-source satellite imagery of different resolutions has been utilized for extracting data on surface water bodies.

Until now, a variety of algorithms have been used for water body delineation from satellite images, ranging from simple spectral indices to deep learning models. Jiang et al. (2021) have been using the Sentinel-2 Water Index and OTSU thresholding for the detection of water bodies. Similarly, Lekhak et al. (2023) combined the spectral indices and slop information with the threshold method to provide more accurate water body mapping. Although threshold-based methods can be used to delineate water pixels, they yield inconsistent results due to high spatial and temporal variation among regions. A wide range of Machine Learning (ML) algorithms, such as Supported Vector Machine (SVM) and Decision Trees (DT) has been used to address that limitation. Acharya et al. (2019) tested the performance of 6 different ML algorithms for surface water extraction in Landsat 8 images. The Random Forest (RF) provided the highest accuracy followed by Gradient Boosted Machines (GBM). Jakovljevic et al. (2018) was adopted the SVM for water body extraction resulting in a kappa coefficient of 0.89 for Sentinel 2 images. Although ML algorithms can provide high accuracy, they are mainly based on spectral information of the training samples, which can lead to the misclassification of surfaces with similar spectral signatures such as dark areas (topographic and cloud shadows), buildings, snow, etc (Kumar et al. 2014). Moreover, the performance of ML algorithms mainly depends on expert-designed features, which limits generalization ability.

In recent years, deep learning algorithms, particularly Convolution Neural Networks (CNN), have been widely used for image classification (Kim et al. 2022), object detection (Galvez et al. 2018), and semantic segmentation (Alam et al. 2021). The deep learning models have been used for the classification and change detection of remote sensing data. Li et al. (2019) adopted the Fully Connected Network (FCN) model to extract water bodies from Very High Resolution (VHR) images and significantly outperform the indices and ML-based methods. Similarly, Erdem et al. (2021) used U-Net architecture for automatic shoreline extraction from Landsat 8 images with high accuracy (F1: 99.79%).

This paper presents an automatic method for the identification of inland water bodies of different sizes and shapes in complex environment conditions based on Sentinel 2 images.

2   Study area

The Republic of Serbia is in Southeast Europe, covering part of the Pannonian Plain and the Central and Western Balkan Peninsula (Figure 1). Serbia covers 88,361 km^2 of which 56.8 % is cropland, and 36.6 % is covered by forest (OECD 2024). The almost entire territory of Serbia belongs

to the Danube (Black Sea) basin. The Danube is the lagers river in Serbia and the second largest river basin in Europe, covering 801,463 km^2 over 19 countries and more than 81 million people (ICPDR 2024). The tributes of the Danube in Serbia are Sava, Tisa, Drina, and Great Morava (Morava) (Figure 1).
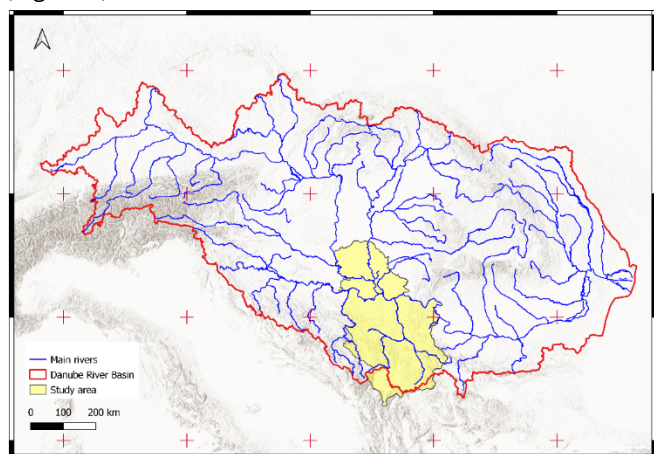
Figure 1. Study area.

3   Materials and methods

Semantic segmentation aims to assign the set of predefined class labels to each pixel in the image (Janai et al. 2020). According to the structure, CNN models for semantic segmentation can be divided into encoder-decoder and spatial pyramid pooling. The encoder-decoder consists of an encoder function that converts the input data into feature maps by using convolution, activation, and pooling layer and a decoder function that up-samples the encoder features maps and converts them to segmentation results. The U-Net architecture (Ronneberger et al. 2015) (Figure 2a) consists of an encoder that captures contextual information and a symmetrical decoder that restores spatial resolution. The encoder followed the typical architecture of CNN (convolution, activation, max pooling), progressively decreasing feature maps resolution, and increasing the number of feature channels per encoder at the same time. The skip connection is used to connect resolution feature maps from the encoder with a corresponding up-sampled output of the decoder, which allows the network to learn back relevant features that are lost after pooling operations and to predict more precise outputs based on that information. In this paper, the ResNet 50 (He et al. 2016) was used as an encoder part of the network. The architecture of ResNet 50 has four stages. The network performs the initial convolution and max pooling using 7x7 and 3x3 kernel sizes, respectively. Afterward, stages 1, 2, 3, and 4 consist of 3, 4, 6, 3 ResNet building blocks (Figure 2b). As the network progress from one stage to another, the feature map resolution is reduced by 2 in terms of height and width while the number of feature channels is doubled. The decoder is fully symmetrical to the encoder, and it is used to restore feature map resolution enabling precise localization. Each step in the decoder consists of 2x2 up sampling that halves the number of feature channels concatenation with the corresponding feature map from the encoder path, followed by two 3x3 convolutions, BN,

and ReLU activation functions. In the final layer, a 1 × 1 convolution with the Sigmoid activation function is used to predict the probability of a pixel being assigned to a water or non-water class.

(a)

(b)
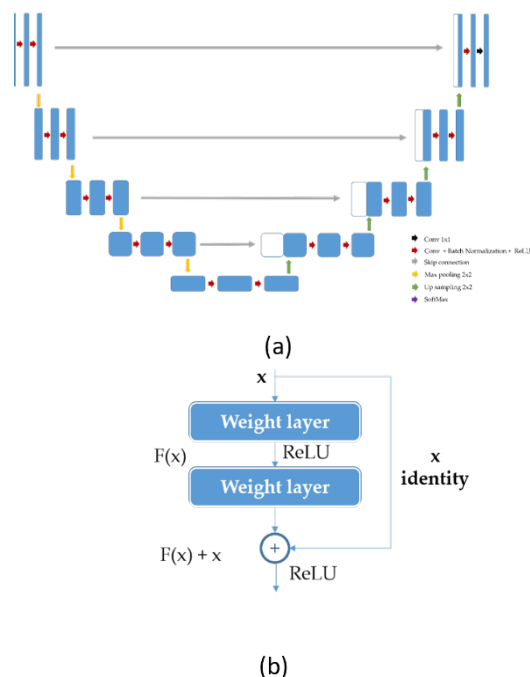
Figure 2. (a) UNet architecture for semantic segmentation, (b) ResNet 50 building block.

The performance of a deep learning network is strongly dependent on a large amount of training data, which is needed to understand hidden patterns of data. Transfer learning has been widely used for solving an insufficient data problem (Castelluccio et al. 2015). Fine-tuning of existing networks that are trained on large datasets such as ImageNet is most used in practice (Penatti et al. 2015). ImageNet is a large and diverse dataset with more than 14 million images labelled into 1000 classes.

In addition to limited size, datasets for the classification of inland water bodies are highly imbalanced since most pixels represent non-water classes. To prevent imbalance learning, enlarge dataset, and reduce over-fitting the data augmentation was used. In this research, clipping, rotating, flipping, and translating were used.

To assess the accuracy of the implemented model the recall, precision, F1-score, and estimate of Kappa coefficient were calculated, as shown in Foody (2008).

Implementation: Dataset was split into 80% for training and 20% for validation. The network is fine-tuned on the dataset created during preprocessing. The cross-entropy and Stochastic Gradient Descent were selected as loss function and optimization algorithm. The GPU limited the batch size, and it was chosen as big as possible for each network. The models were implemented in the Python 3 programming language by using artificial intelligence libraries such as PyTorch, TensorFlow, Keras, and Matplotlib. The training of the networks was done using the publicly available cloud platform Collaboratory (Google Colab).

4   Results

Accuracy assessment of the proposed model for Sentinel 2 is based on 861 and 13600 image patches for validation and test phases. The results of the accuracy assessment are presented in Table 1.

Table 1. Results of accuracy assessment for water body extraction from Sentinel 2.

Phase	Precision	Recall	F1-score	Kappa
Validation	0.90	0.95	0.92	0.92
Test	0.81	0.99	0.89	0.89

The visual inspection shows (Figure 3) that detected wetlands and channels are more completed comparing to masks, which also decrease the precision.

The visual inspection of results (Figure 3) shows that the water bodies extracted from the satellite images followed a similar pattern with true data. As can be seen from the figure, the algorithm can detect lakes, large rivers, and even small ponds or reservoirs with high accuracy (Figure

The difference between F1 score during the validation and test phase was 3% indicating the algorithm's high generalization ability. Therefore, it can be used for automatic water body detection from different areas without manual intervention. These results are also confirmed by Billson et al. (2023). It is observed that during the test phase recall value increases while the precision decreases meaning that on the one hand algorithm is more secure that the pixel labelled as water represents the water body in the real world but on the other hand, it includes more non-water pixels in water class. Although the proposed approach produces stable results on large and medium size water bodies, the extraction of narrow streets and small lakes remains challenging.

6   Conclusions

In this paper, the methodology for automatic inland water body mapping based on UNet architecture and Sentinel 2 images have been proposed. The Kappa coefficient, precision, recall, and F1-score were calculated to evaluate the performance. The high value and visual inspection

Figure 3. Visual comparison of extracted water bodies for different water body types (a), (b) large river (> 400 m width), (c) medium river (width around 100 m), (d), (e), (f) small rivers (width between 10-35 m), (g) lake, (h) wetland, (i) artificial channels (Jakovljevic 2020).

3a, Figure 3b, Figure 3g). As expected, the lowest accuracy is obtained for small and narrow streams. The small water bodies were overestimated (Figure 3d, Figure 3e, Figure 3f) due to mixed pixels producing lower precision.

5   Discussion

Motivated by recent success in deep learning, this research focused on using those methods to improve the water body mapping from satellite images. As presented results indicated, the proposed approach provides water body detection in the complex environment from optical with consistently high F1-score and kappa coefficient despite varying topology, land-use/land cover, and atmospheric conditions. Similarly, Yan et al. (2022) has reported an F1-score of 0.9 for mapping lakes from Sentinel-2 by using the Unet architecture.

show that ResUNet 50 is not sensitive to low albedo surfaces such as built-up areas, roads, or shadows, which is one of the primary sources of errors during water body extraction from remote sensing data. Comparison of validation and test accuracy (F1: 0.89 vs 0.92) indicates great generalization ability and the possibility to apply the algorithm for automatic water body detection over different areas.

7   References

Acharya, T. D., Subedi, A., Ha Lee, D., 2019. Evaluation of Machine Learning Algorithms for Surface Water Extraction in a Landsat 8 Scene of Nepal. Sensors 19 (12), 2769.

Alam, M., Wang, J.-F., Guangpei, C., Yunrong, L., Chen, Y., 2021. Convolutional Neural Network for the Semantic Segmentation of Remote Sensing Images. Mobile Networks and Applications, 200-215.

Billson, J., Islam, M., Sun, X., Cheng, I., 2023. Water Body Extraction from Sentinel-2 Imagery with Deep Convolutional Networks and Pixelwise Category Transplantation. Remote Sensing 15 (5), 1253.

Castelluccio, M., Poggi, G., Sansone, C., Verdoliva, L., 2015. Land Use Classification in Remote Sensing Images by Convolutional Neural Networks.

Erdem, F., Bayram, B., Bakirman, T., Vayrak, O. C., Akpinar, B., 2021. An ensemble deep learning-based shoreline segmentation approach (WaterNet) from Landsat 8 OLI images. Advances in Space Research 67 (3), 964-974.

Foody, G. M., 2008. Harshness in image classification accuracy assessment. International Journal of Remote Sensing 29 (11), 3137-3158.

Galvez, R. L., Bandala, A. A., Dadios, E. P., Vicerra, R., Maningo, J., 2018. Object Detection Using Convolutional Neural Networks. TENCON 2018 - 2018 IEEE Region 10 Conference, 2023-2027, Jeju, Korea.

He, K., Zhang, X., Ren, S., 2016. Deep Residual Learning for Image Recognition. IEEE International Conference on Computer Vision and Pattern Recognition (CVPR).

ICPDR. (2024, 05 10). Countries of the Danube River Basin. Retrieved from ICPDR: https://www.icpdr.org/main/danube-basin/countries-danube-river-basin. (Accessed 13 June 2024)

Jakovljevic, G., 2020. Multidimensional model of use remote sensing data and geospatial services in water management according to INSPIRE and WFD specification, PhD thesis. Novi Sad: Faculty of Technical Science, University of Novi Sad.

Jakovljevic, G., Govedarica, M., Alvarez-Taboada, F., 2018. Waterbody mapping: a comparison of remotely sensed and GIS open data sources. International Journal of Remote Sensing 40 (8), 2936-2964.

Janai, J., Guney, F., Behl, A., Geiger, A., 2020. Computer Vision for Autonomous Vehicles: Problems, Datasets and State of the Art. Foundations and Trends in Computer Graphics and Vision 12 (1-3), 1-308.

Jiang, W., Ni, Y., Pang, Z., Li, X., Ju, H., He, G., Qin, X., 2021. An Effective Water Body Extraction Method with New Water Index for Sentinel-2 Imagery. Water 13 (12), 1647.

Kim, H., Cosa-Linan, A., Santhanam, N., Jannesari, M., Maros, M. E., Ganslandt, T., 2022. Transfer learning for medical image classification: a literature review. BMC Medical Imaging 22 (1), 69.

Kumar, L., Sinha, P., Taylor, S., 2014. Improving image classification in a complex wetland ecosystem through image fusion techniques. Journal of Applied Remote Sensing 8 (1), 083616.

Lekhak, K., Rai, P., Budha, P. B., 2023. Extraction of water bodies from Sentinel-2 imagery in the foothills of Nepal Himalaya. International Journal of Environment and Geoinformatics 10 (2), 70-81.

Li, L., Yan, Z., Shen, Q., Cheng, G., Gao, L., Zhang, B., 2019. Water body extraction from very high spatial resolution remote sensing data based on fully convolutional networks. Remote Sensing 11 (10), 1162.

OECD. (2024, 05 10). Retrieved from Land cover in countries and regions: <https://stats.oecd.org/Index.aspx?DataSetCode=LAND_COVER. (Accessed 13 June 2024)

Penatti, O. A., Nogueira, K., dos Santos, J. A., 2015. Do deep features generalize from everyday objects to remote sensing and aerial scene domains? 2015 IEEE Conference on Computer Vision and Pattern Recognition Workshops (CVPRW). Boston: IEEE.

Ronneberger, O., Fischer, P., Brox, T., 2015. U-Net: Convolutional Networks for Biomedical Image Segmentation. MICCAI 2015.

Yan, K., Li, J., Zhao, H., Wang, C., Hong, D., Du, Y., Wang, S., 2022. Deep Learning-Based Automatic Extraction of Cyanobacterial Blooms from Sentinel-2 MSI Satellite Data. Remote Sensing 14 (19), 4763.

Application of Remote Sensing in Coastal Geomorphology: A Case Study of Zoraće Velo, Hvar Island, Central Adriatic

Marin Mićunović[1],*, Sanja Faivre[1]

[1] University of Zagreb, Faculty of Science, Department of Geography, Zagreb, Croatia
mmicunov@geog.pmf.hr, sfaivre@geog.pmf.hr
* corresponding author

Abstract: In this study we analyse coastal landforms in Velo Zoraće Bay on the island of Hvar, the cliff, the beach and the drainage basin behind the beach. This study examines their evolution over the past 200 years, as well as recent seasonal changes. The oldest period was analysed using the Franciscan Cadastre from 1834, the second using Croatian State Geodetic Administration aerial images from the 1950s, and the most recent period was studied using unmanned aerial vehicle (UAV) and Global navigation satellite system (GNSS) in the field. The collected data was processed using the Agisoft software. High-resolution models (orthomosaic – 1cm, Digital Elevation Model (DEM), and Digital Surface Model (DSM) – 3cm were created, and their horizontal and vertical accuracy was determined using Ground Control Points (GCPs). All analyses were done in ArcGIS Pro software.

Particular attention is paid to the cliff formed in Paleogene flysch. As flysch is a soft rock, it is prone to denudation. According to the obtained data, the cliff has eroded an average of 16 m over the last 200 years, i.e., the annual retreat of the cliff is 9.3 cm, which roughly corresponds to the recent seasonal changes observed in the field from spring 2021 and autumn 2022. Extreme denudation was observed, up to 0.5 m in places, which could be associated with intense rainfall events. These events led to the formation of gullies and to the activation of slope processes on the cliff face. During the same period, the beach shoreline moved landward for 17 m, while the beach area reduced by approximately 30%.

Keywords: beach; cliff; flysch; erosion; UAV.

1 Introduction

Coastal zones are dynamic and complex environments characterized by constant changes. Natural processes, combined with anthropogenic pressures, play crucial roles in the evolution of these areas, influencing particularly coastal geomorphological features such as beaches and cliffs. Coastal erosion, one of the dominant processes, leads to significant land loss and changes in coastal morphology, including cliff retreat and beach reduction in beach surface areas (Davison-Arnott et al. 2019). Although beach erosion is a major issue in coastal zones, erosion also significantly impacts cliffs, deltas, and coastal swamps (Bird 2008). Furthermore, recent climate changes affect coastal areas through sea level rise and intense rainfalls, increasing vulnerability of coastal zones (Brunel and Sabatier 2007, Faivre et al. 2011, Luiendijk et al. 2018). Therefore, the research of coastal zones is becoming more common today, particularly in the framework of coastal management (Alexandrakis and Poulos 2014). Remote

sensing and technological advancements made research in coastal geomorphology easier and precise, utilizing numerous tools (Miccadei et al. 2019, Casella et al. 2020, Mićunović et al. 2021, Marco-Pereto et al. 2024).

This paper focuses on the coastal landforms in Velo Zoraće Bay on the island of Hvar and examines their evolution over the past 200 years. Particular emphasis is placed on the recent seasonal changes observed in the last few years. The study area includes a cliff formed in Paleogene flysch, a type of soft sedimentary rock that is particularly vulnerable to denudation processes, as well as the beach, which is also subject to significant erosion. By employing a combination of archival data, aerial imagery, and modern remote sensing methods, this research aims to provide a comprehensive analysis of the coastal dynamics in Zoraće Velo Bay.

2 Materials and methods

2.1 Study area

Zoraće Velo Bay is located eastern of the town of Hvar (Figure 1), on the southern side of the island. Geologically, the entire bay lies at the contact point between Paleogene flysch and Lower Cretaceous limestones (Figure 1) what allowed the formation of particular geomorphological properties of the bay with a beach and a cliff.
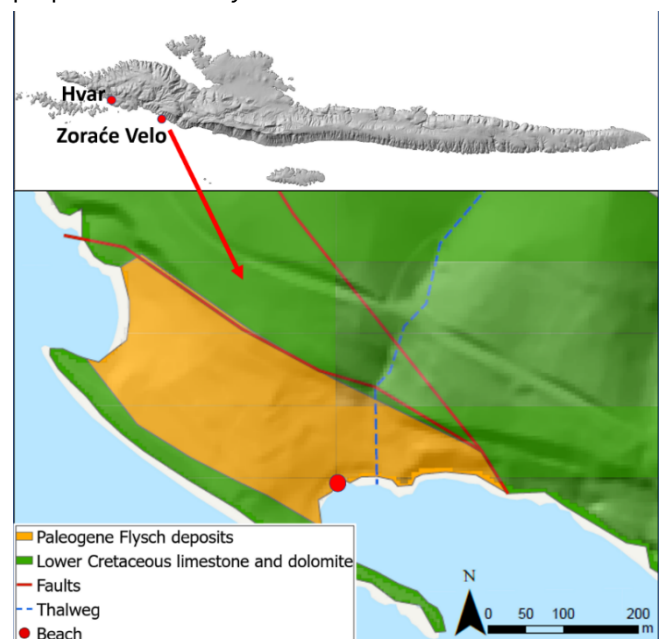

Figure 1. Geological map of Zoraće Velo Bay (Marinčić and Majcen 1976).

The beach is predominantly composed of fine-grained sediment (sand), but it also contains some coarser

sediment (gravel and pebbles), which have been brought in and accumulated from nearby gullies. The island has a Mediterranean climate, with typical maximum rainfall occurring in the winter months. Recently, climate change has manifested through more intense rainfall events, impacting coastal landforms, particularly beaches and cliffs (Faivre et al. 2011, Vlastelica et al. 2017).

2.2   Data acquisition and processing

This research is based on the analysis of beach and cliff evolution over the past 200 years, as well as on the seasonal changes in cliff morphology over the past few years.

The oldest period refers to the 1834 Franciscan Cadastre from the Austro-Hungarian Monarchy, where the beaches were mapped as separate parcels. The cadastral data were georeferenced, digitized, and analyzed using ArcGIS Pro software. The next period refers to the mid-20th century, utilizing black and white aerial images from the Croatian State Geodetic Administration, on which the beach and cliff were also digitized and analyzed. The recent period was analyzed using a UAV and the precise Trimble Catalyst DA2 RTK-GNSS. Field recording and data collection were conducted in March 2021 and November 2022 using a DJI Phantom 4 Pro v2.0 with an FC6310 RGB camera with a resolution of 20 megapixels. The flight was conducted at an altitude of 20–30 meters with 70–80% overlapping images. 10 Ground Control Points (GCPs) and 5 Ground Check Points were collected. The collected data were processed using Agisoft Metashape software. High-resolution models were obtained, including an orthomosaic with 1 cm resolution, and DEM and DSM with 3 cm resolution.

2.3   Geomorphological changes

Geomorphological changes on the beach and the cliff over the past 200 years were analyzed using ArcGIS Pro software. They were assessed by examining beach area changes and changes in beach shoreline positions. Digitized polygons and lines were compared and measured using the Near tool and Summary Statistics. For the recent period, the beach shoreline was automatically generated from the created DEM using raster data management tools, where pixels at 0 m elevation were defined. Changes in the cliff were analyzed by tracking shifts in the position of the cliff edge, focusing on the highest parts of the cliff. The digitized line was also analyzed using the Near tool and Summary Statistics. Recent seasonal changes in the cliff, observed during fieldwork, were analyzed using models generated in ArcGIS Pro software. These changes were examined using topographic profiles at six cross-sections, which revealed variations in material volume and the positions of the lowest and highest parts of the cliff. These profiles were analyzed using the Interpolate Shape and Profile tools according to the height of the generated DSM. Positional and digitizing errors were considered (Mićunović et al. 2021, Mićunović and Faivre 2024).

3   Results

The analysis of the collected data revealed significant changes in Zoraće Velo Bay over the past 200 years, as well

as in the recent period. The largest recorded beach area was in 1834. According to the cadastral surveys the beach area was 1431.6 m^2. By the mid-20th century, the area had decreased to 1160.6 m^2 and today it is 976.4 m^2. These measurements indicate that the beach eroded by 18.9% from 1834 to the mid-20th century and by an additional 15.9% from the mid-20th century to the present day. Over the entire 200-year period, the beach has lost 31.8% of its surface area. A similar trend was observed in the shoreline retreat, which moved inland by 17.3 m over the past 200 years. In the first period, the shoreline retreated by 10.78 m, and in the second, it retreated by 9.61 m (Figure 2).

Significant changes have been also recorded on the cliff (Figure 2). Analysis of the data revealed a cliff retreat averaging 16 m over the past 200 years. In some places, the cliff has eroded by more than 20 m. The annual cliff retreat was calculated to be 9.6 cm/yr in the last ~200 years. There are no particular changes in the rates between the periods analyzed.

Short-term changes on the cliff were analyzed from spring 2021 to autumn 2022 (Figure 2 and Figure 3). Profiles from A to D relates to cliff segments with slope lower of 55°, while profiles E and F to slopes exceeding 55°.

Changes on cliff segments from A to D which have lower slopes, showed cliff retreat of 10-20 cm on average in a year and half. Profile B showed a retreat of over 0.5 m in the same period. During fieldwork, along the same coastal segment (the A-D coastal sector) slope processes were active. Their effects can be seen in the profiles (Figure 3) as eroded material accumulated at the base of the cliff.

Profiles E-F recorded changes in the upper part of the cliff, with a visible retreat of about 10 cm. Profile E, in particular, showed changes at the base of the cliff, where 0.5 meters of sediment had accumulated. Overall, the cliff retreated by an average of 10 cm across all profiles during the studied period.

4   Discussion

The changes on the Zoraće Velo beach are consistent with the erosion trend observed on the island of Hvar. The general reduction in beach area of about 30% is below the island average of 50% (Mićunović and Faivre 2024).

However, the shoreline retreat of ~17 meters is significant and the largest recorded on the island of Hvar (Mićunović and Faivre, 2024). Consequently, this fact points to a backward movement of the beach. This prompted a detailed investigation of the entire Zoraće Velo Bay to identify better geomorphological processes affecting changes of the beach. According to these results, one would expect a much greater reduction in beach area. However, this particular beach is bordered by a cliff formed in flysch. As flysch is an easily erodible sediment, the process of cliff retreat has enabled such significant shoreline shift.

This particular beach is one of the few formed in flysch on the island of Hvar. The unique bay, bordered by carbonate bedrock, allowed the preservation of flysch deposits. Obtained data shows that denudation affected the cliff and
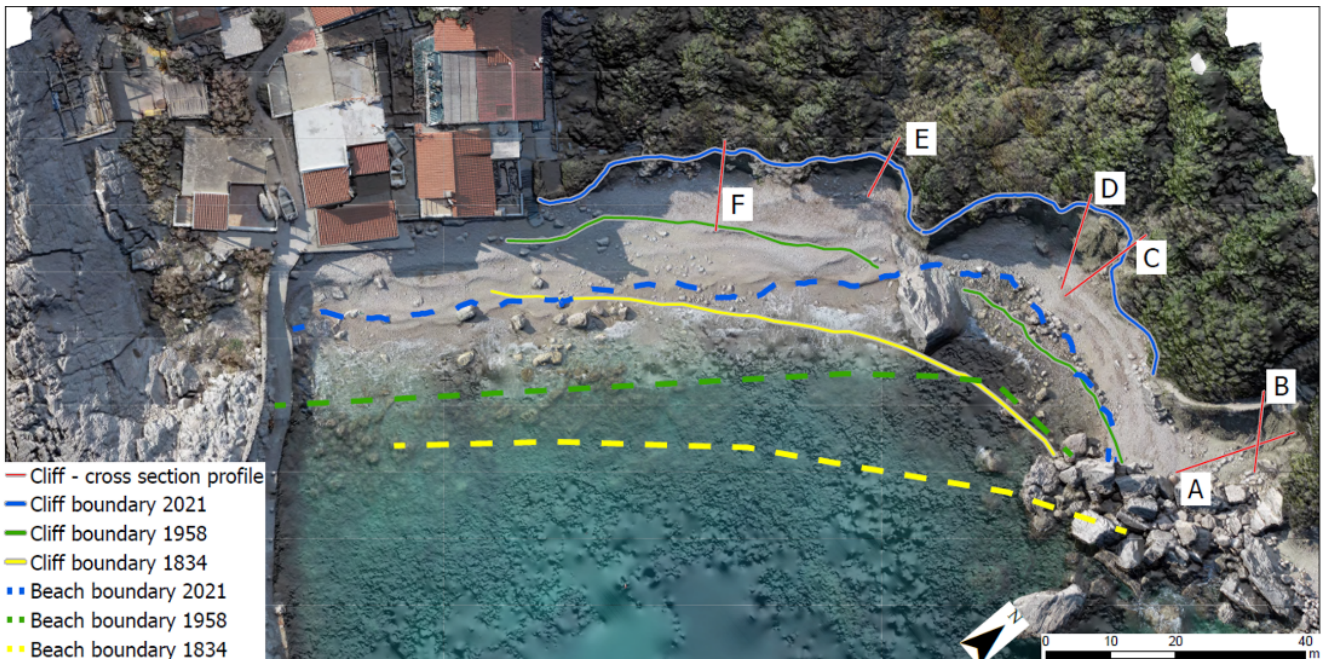
Figure 2. Beach and cliff boundary positions over ~200-year period (A-F profiles in Figure 3).
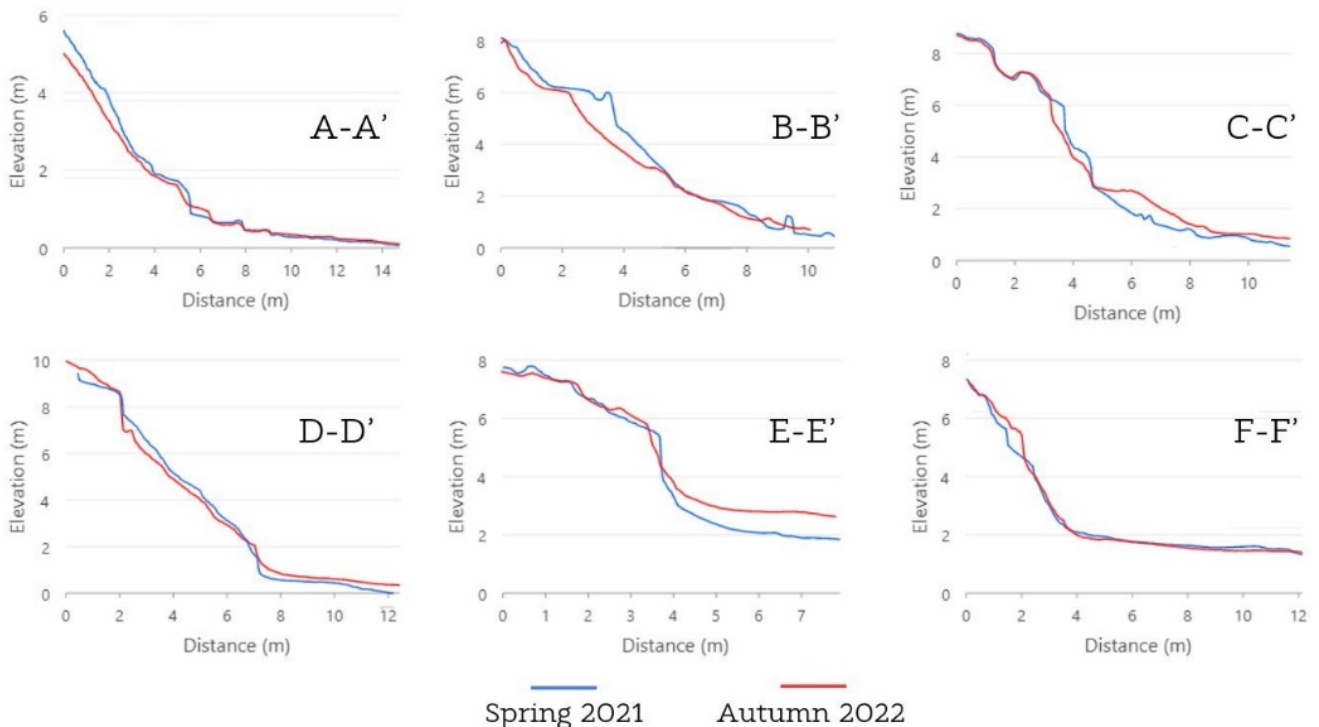
Figure 3. A-F cliff cross-section profile (marked in Figure 2).

caused cliff retreat of 16 meters on average over the past 200 years. However, there is some difference between the cliff segments. The cliffs (E-F) are partially covered by vegetation at their upper parts, which protects the sediment. On cliff segments with lower slope (profiles A-D) denudational processes have activated. Consequently, slope and denudational processes have contributed to the cliff retreat process in this area.

Similar studies conducted on the Slovenian coast suggest that slope processes, including landslides and collapses, act as accelerators of cliff retreats (Furlani et al. 2011, Šegina et al. 2012). Cliff retreat in flysch deposits was studied in the Split area. It was found to be of the order of 3–18 cm/year, with an average of 10 cm/year. Accordingly,

this corresponds to our findings at Zoraće Velo cliff. In addition to abrasion caused by sea level rise in the larger studied area slope processes played an important role in cliff retreat, leading to considerable erosion in places (Vlastelica et al. 2017).

5 Conclusions

This research has shown significant geomorphological changes in Zoraće Velo Bay, including beach erosion, beach shoreline retreat, and cliff retreat. The shoreline retreat of 17 m is driven by erosion of easily erodible flysch sediments influenced by denudational, gully erosion, slope processes and sea-level rise. These changes align with general erosion trends in coastal environments. Remote

sensing methods, such as the analysis of archival materials combined with fieldwork, have proven to be very useful for these analyses. The generated high-resolution models enabled a detailed analysis of short-term changes on the cliff with centimeter-level precision.

This study has highlighted the importance of understanding geomorphological processes and demonstrated how remote sensing methods and the application of UAVs in coastal geomorphology can be useful, and provide accurate results for various research objectives with the aim of sustainable coastal management.

6   References

Alexandrakis, G., Poulos, S.E., 2014. A holistic approach to beach erosion vulnerability assessment. Scientific Reports 4 (1), 1-8.

Bird, E.C., 2008. Coastal Geomorphology: An Introduction. John Wiley & Sons.

Brunel, C., Sabatier, F., 2007. Pocket beach vulnerability to sea-level rise. Journal of Coastal Research 604-609.

Casella, E., Drechsel, J., Winter, C., Benninghof, M., Rovere, A., 2020. Accuracy of sand beach topography surveying by drones and photogrammetry. Geo-Marine Letters 255-268.

Davison-Arnott, R., Bauer, B., Houser, C., 2019. Introduction to coastal processes and geomorphology. Cambridge University press. Cambridge. UK.

Faivre, S., Pahernik, M., Maradin, M., 2011. The gully of Potovošća on the Island of Krk–The effects of a short-term rainfall event. Geologia Croatica 64 (1), 67-80.

Furlani, S., Devoto, S., Biolchi, S., Cucchi, F., 2011. Factors triggering sea cliff instability along the slovenian coasts. Journal of Coastal Research 61, 387-393.

Luijendijk, A., Hagenaars, G., Ranasinghe, R., Baart, F., Donchyts, G., Aarninkhof, S., 2018. The state of the world's beaches. Scientific Reports 8 (1), 1-11.

Marco-Peretó, C., Durán, R., Toomey, T., Guillén, J., 2024. Controls on the morphological evolution of embayed beaches: Morphometry versus external forcing. Earth Surface Processes and Landforms 49 (4), 1289-1302.

Marinčić, S., Majcen, Ž., 1976. Osnovna geološka karta SFRJ 1:100,000, list Jelsa K33–34, Institut za geološka istraživanja Zagreb (1967–1968). Savezni geološki zavod, Beograd.

Miccadei, E., Mascioli, F., Ricci, F., Piacentini, T., 2019. Geomorphology of soft clastic rock coasts in the mid-western Adriatic Sea (Abruzzo, Italy). Geomorphology 324, 72-94.

Mićunović, M., Faivre, S., Gašparović, M., 2021. Assessment of remote sensing techniques applicability for beach morphology mapping: a case study of Hvar Island, Central Adriatic, Croatia. Journal of Marine Sciences and Engineering 9 (12), 1407.

Mićunović, M., Faivre, S., 2024. Evolution of Hvar island pocket beaches during the last 200 years (eastern Adriatic coast, Croatia). Geomorphology 447(109023).

Šegina, E., Komac, B., Zorn, M., 2012. Influencing factors the rockwall retreat of flysch cliffs on the Slovenian coast. Acta geographica Slovenica 52 (2), 303-334.

Vlastelica, G., Pikelj, K., Kordić, B., 2017. Erosional processes acting on coastal cliffs in the Split urban zone, Croatia. Revue Paralia, 4, 79-84.

Comparative Analysis of Unmanned Aerial Vehicle Land Cover Classification of Two Study Sites in Serbia

Ivana Miličić[1,], Nina Pajević[1], Bojana Ivošević[1]*

[1] BioSense Institute - Research and Development Institute for Information Technologies in Biosystems, University of Novi Sad, 21101 Novi Sad, Serbia, ivana.milicic@biosense.rs, nina.pajevic@biosense.rs, bojana.ivosevic@biosense.rs
* corresponding author

Abstract: In recent decades, using unmanned aerial vehicles (UAVs) for mapping and classifying the Earth's surface has surged. Ecological researchers increasingly rely on UAV imagery due to its centimeter-level resolution and rich information content compared to other remote sensing methods, such as satellite imagery. This study presents a comparative analysis of the land cover classification of orthomosaics in two distinct Serbian study sites using high-resolution imagery captured by different UAVs: the DJI Inspire 1 and DJI Phantom 4 Multispectral. In the study site Topli Do (Eastern Serbia), the DJI Inspire 1 equipped with RGB and NDVI modified cameras was utilized, generating the orthomosaic of six land cover classes. Random forest classification algorithms were employed achieving an overall accuracy of 92.46%. In the study site Glavica (Northern Serbia), aerial images were acquired using the DJI Phantom 4 Multispectral, featuring a multispectral sensor capturing data across blue, green, red, red-edge, NIR, and combined RGB ranges. Applying the random forest, five land cover classes were delineated with an accuracy of 95%. This finding underscores the transformative potential of multispectral cameras in enhancing land cover classification. Using spectral information captured in multiple bands has enabled determining plants up to the species level in heterogeneous vegetation types. Such classification represents a breakthrough in ecological monitoring, allowing scientists to gain insight into ecosystem dynamics, species distribution, and environmental change at the local scale.

Keywords: unmanned aerial vehicles; object-based image analysis; machine learning; land cover classification.

1 Introduction

Unmanned aerial vehicles (UAVs) have emerged as a prevalent method in remote sensing for land cover classification, owing to their capacity to capture very high-resolution (VHR) imagery. Beyond conventional RGB sensors, multispectral and hyperspectral sensors have expanded the potential for detailed land cover classification (Ahmed et al. 2017, Umut et al. 2022). VHR imagery, with its wealth of information, necessitates novel approaches to image analysis. Object-based image analysis (OBIA) has superseded traditional pixel-based classification methods, employing shape, texture, and spatial relationships to categorize pixels (Dronova 2015, Ivošević et al. 2021). Understanding the spatial distribution of land cover classes is imperative for effective land use planning and natural resource management (Verburg et al. 2009). These maps are instrumental in monitoring species distribution and implementing conservation strategies, particularly in ongoing biodiversity campaigns focusing on insects like hoverflies, bees, and butterflies. Integrated into analyses, these maps offer insights into ecological patterns, guiding targeted conservation efforts. Furthermore, beyond ecological studies, this data holds relevance for various machine learning methods, which have the potential to accelerate the classification process. Among these, ensemble learning methods like Random Forest (RF) are acclaimed for their superior accuracy and reliability (Ivošević et al. 2021, Umut et al. 2022).

2 Materials and methods

Materials used in this research are from two study sites in Serbia: Topli Do (Mt. Stara Planina, Eastern Serbia) and Glavica (Fruška Gora, Northern Serbia). Topli Do boasts diverse vegetation classes ranging from forest, shrubs, mowed meadows, roads, water, and rocks. Glavica is covered by forests (90% of the total area), followed by shrubs, mowed meadows, roads, and human-made objects. The UAV equipment used in the study sites is given in Figure 1. Image processing steps including rescaling, layer merging, segmentation, labeling, and classification were executed using QGIS 3.10 with the built-in Orfeo Toolbox, implemented in Python 5.3.

The schematic workflows of all the steps required for the methodology suggested by Ivosević et al. (2021) are shown in Figures 2 and 3 with some differences between the two study sites and UAV equipment used. Topli Do aerial data acquisition at the study site employed a DJI Inspire 1 quadcopter equipped with a Zenmuse X3 gimbal capable of camera interchangeability between RGB and NDVI modalities. Before the flight, placement, and measurement of five Ground Control Points (GCPs) ensured centimeter-level precision, facilitated by the NovAtel SMART6-L GNSS SMART Antenna. A double-grid flight mission yielded two sets of UAV images captured by RGB and NDVI cameras. Image stitching resulted in orthomosaic generation via Pix4Dmapper software. Red, green, blue, and Digital Surface Model (DSM) layers were derived from the RGB orthomosaic, while the NDVI orthomosaic enabled NDVI index map generation. Rescaling layers to a 0–255 bit range preceded the fusion into a five-band orthomosaic. Application of the Large-Scale Mean Shift (LSMS) algorithm enabled image segmentation, followed by manual labeling of training and validation polygons on the vectorized output. The image classification was applied using the RF classifier and land cover classes with percentage coverage were calculated.

DJI Inspire 1 RGB camera DUAL-FREQUENCY GNSS SMART6-L GNSS SMART Antenna Study site: Topli Do, Eastern Serbia

NDVI camera

DJI Phantom 4 Multispectral Multispectral camera DJI D-RTK 2 Study site: Glavica, Vojvodina

Red edge (RE) Near-infrared (NIR) Green (G)

Visible RGB Red (R) Blue (B)
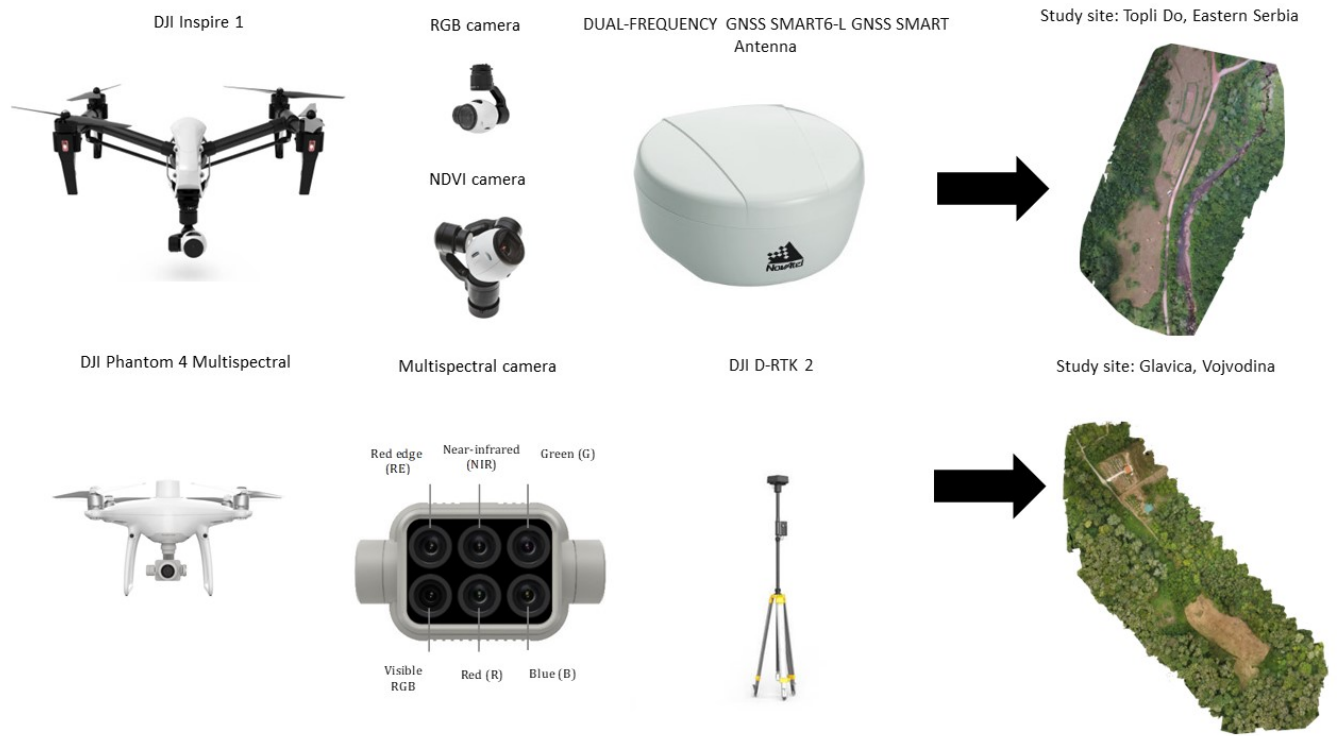
Fiqure 1. UAV equipment in the study sites.

1. Flight mission grid (2x) 2. Image stitching 3. Orthomosaics generation

Pix4D mapper
1. Initial Processing
2. Point Cloud and Mesh
3. DSM, Orthomosaic and Index

4. Image preprocessing 5. Image segmentation 6. Image classification

Rescaling and merging R, G, B, NDVI and DSM layers (Raster image) Merged layers (Raster image) Image after segmentation process (Vector image) Labeling training and validation sets (Vector image) Image after classification process (Vector image)

training set
validation set

Topli Do classified
forests
shrubs
mowed meadows
roads
water
rocks

Figure 2. Flowchart for Topli Do.

At the Glavica study site data acquisition employed a UAV DJI P4 Multispectral, equipped with a multispectral sensor capturing data across blue, green, red, red-edge, and NIR spectral ranges, in addition to combined RGB imaging. Utilizing a DJI DRTK-2 mobile station ensured real-time data acquisition with centimetre-level positioning accuracy. Notably, compared to the previous DJI Inspire 1 setup, this configuration featured an expanded flight channel count, enabling simultaneous capture across five channels in a single flight mission. The resulting multiband raster encompassed seven layers: red, green, blue, red-edge, NIR, DSM, and NDVI.

Following image segmentation, vector image labeling extracted polygons for training and validation datasets, essential for the subsequent RF classifier analysis. A common metric utilized to quantify the proportion of accurately classified class values is the overall accuracy (OA) (Equation 1). OA is calculated as the ratio of correctly predicted to total predictions.

1. Flight mission grid   2. Image stitching   3. Orthomosaic generation

Pix4D mapper
1. Initial Processing
2. Point Cloud and Mesh
3. DSM, Orthomosaic and Index

4. Image preprocessing   5. Image segmentation   6. Image classification

Glavica classified
forests
shrubs
mowed meadows
human-made objects
roads

training set
validation set

Rescaling and merging R, G, B, Red-Edge, NIR, NDVI and DSM layers (Raster image)

Merged layers (Raster image)

Image after segmentation process (Vector image)

Labeling training and validation sets (Vector image)

Image after classification (Vector image)

Figure 3. Flowchart for Glavica.

$$OA = \frac{\text{corrected prediction}}{\text{total prediction}} \qquad (1)$$

3   Results

The classification for study site Topli Do was performed using six land cover classes: forests, shrubs, mowed meadows, roads, water, and rocks. The achieved accuracy was 92.46%. Based on land cover maps, it is observed that Topli Do is mostly covered by shrubs and forests (34.53%, 34.05%), slightly less by mowed meadows (21.83%), and least by water (4.38%) and rocks (1.80%) (Figure 4).
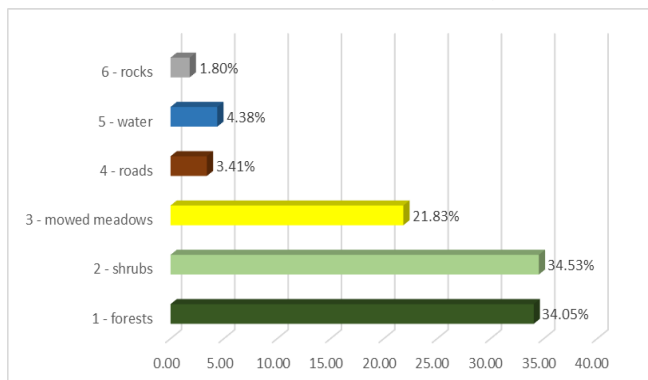
Figure 4. Percentage coverage of each class of study site Topli Do obtained by RF classification algorithm.

In the study site Glavica, the classification was performed using five land cover classes: forests, shrubs, mowed meadows, human-made objects, and roads. The RF classifier achieved an accuracy of 95%. The classification map showed that forests are the most dominant with a percentage coverage of 49.94%, followed by shrubs and mowed meadows (30.28% and 15.76% respectively), while human-made objects and roads are the least prevalent (0.97% and 3.04%) (Figure 5).
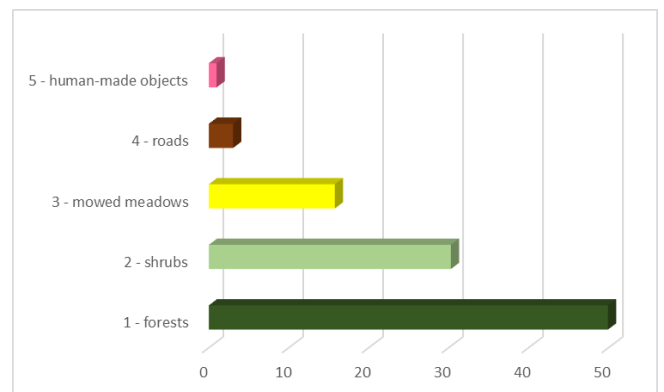
Figure 5. Percentage coverage of each class of study site Glavica obtained by RF classification algorithm.

4   Discussion

The results obtained from the RF analysis in the study sites offer valuable insights into the composition of land cover and the performance of the classification model. The used metrices serve as indicators of classification accuracy. However, initial object segmentation is a prerequisite for accurate classification. The overall accuracy of 92.46% in Topli Do and 95% in Glavica underscore the efficacy of the proposed classification algorithm in accurately categorizing land cover types. These findings align with previous research (Ivošević et al. 2021). In both study areas, forests and shrubs emerged as the dominant land cover types constituting a substantial portion of the landscape. The greatest challenge encountered by the RF classifier in the Topli Do was distinguishing between these two types due to their color, texture, and spatial similarity. This is evidenced by the lower precision values obtained for these classes compared to others: 88.24% for forests and 84.36% for shrubs. However, in the Glavica study site, increased precision values were observed for these two classes: forest – 99.63% and shrubs – 96.71%. This improvement

could be attributed to the increased number of features facilitated by multispectral UAV (Vali et al. 2020).

5   Conclusions

This study examines land cover classification using orthomosaics from two distinct study sites in Serbia. Using spectral information captured in multiple bands showcases revolutionary potential in enhancing the quality of land cover maps. Such classification represents a breakthrough in ecological monitoring, allowing scientists to gain insight into ecosystem dynamics, species distribution, and environmental change at the local scale. However, the RF classifier achieves good accuracy with the most errors when classifying between the forest and shrub classes, so the new model should be improved in terms of better precision. In future research, emphasis should be placed on the generalization and robustness of classification models by prioritizing the development of detailed methodologies for feature selection. Additionally, exploring new methods (deep learning, segment anything model) across different study sites can facilitate the evaluation of more generalized models for creating land use maps without manually labeling ground truth data.

6   References

Ahmed O.S., Shemrock A., Chabot D., Dillon C., Williams G., Wasson R., Franklin S.E., 2017. Hierarchical land cover and vegetation classification using multispectral data acquired from an unmanned aerial vehicle. International journal of remote sensing 38 (8-10), 2037-52.

Dronova I., 2015. Object-based image analysis in wetland research: A review. Remote Sensing, 7 (5), 6380-6413.

Ivošević B., Lugonja P., Brdar S., Radulović M., Vujić A., Valente J., 2021. UAV-Based Land Cover Classification for Hoverfly (Diptera: Syrphidae) Habitat Condition Assessment: A Case Study on Mt. Stara Planina (Serbia). Remote Sensing 13, 3272.

Umut G.S., Taskin K., Ismail C., Mertcan N., Muhammed Y. O., Samed A., Salih D., 2023. 3D positioning accuracy and land cover classification performance of multispectral RTK UAV. International Journal of Engineering and Geosciences 8 (2), 119-128.

Vali A., Comai S., Matteucci M., 2020. Deep learning for land use and land cover classification based on hyperspectral and multispectral earth observation data: A review. Remote Sensing 12 (15), 2495.

Verburg, P.H., Van De Steeg, J., Veldkamp, A., Willemen, L., 2009. From land cover change to land function dynamics: A major challenge to improve land characterization. Journal of Environmental Management 90 (3), 1327-1335.

Testing the Performance of Hand-held Personal Laser Scanning Systems for Precision Forest Inventory

Andro Kokeza[1,]*, Luka Jurjević[2], Fran Domazetović[3], Ivan Marić[3], Ante Šiljeg[3], Damir Medak[4], Krunoslav Indir[1], Danko Kuric[5], Ivan Balenović[1,]*

[1] Division for Forest Management and Forestry Economics, Croatian Forest Research Institute, Zagreb, Croatia, androk@sumins.hr, kindir@sumins.hr, ivanb@sumins.hr

[2] GeoUnit, Zadar, Croatia, jurjevic.geo@gmail.com

[3] Department of Geography, University of Zadar, Zadar, Croatia, fdomazeto@unizd.hr, imaric1@unizd.hr, asiljeg@unizd.hr

[4] Chair of Geoinformatics, Faculty of Geodesy, University of Zagreb, Zagreb, Croatia, dmedak@geof.hr

[5] Croatian Forests Ltd., Zagreb, Croatia, danko.kuric@hrsume.hr

* corresponding author

Abstract: This research tested the performance of hand-held personal laser scanning (PLS) technology for estimating the diameter at breast height (dbh) in a lowland pedunculate oak (*Quercus robur* L.) forest. More precisely, this study assessed: (i) the accuracy of two, high-end hand-held PLS systems (ZEB Horizon and Faro Orbis); and (ii) various scanning schemes with different complexities. Three scanning schemes of different complexity were used by both instruments, and Faro Orbis provided more accurate dbh estimates than ZEB Horizon for each scheme. The results revealed an increase in the PLS data estimation accuracy that corresponds to the increase in complexity of the scanning scheme Additionally, the new ability of Faro Orbis to perform 'flash' (static) scans that mimic TLS was also tested, and obtained results revealed that flash scans produce slightly less accurate dbh estimates compared to the most complex walking (mobile) scheme.

Keywords: LiDAR; hand-held personal laser scanning; scanning schemes; diameter at breast height; forest inventory.

1 Introduction

The potential of 'classical' remote sensing (e.g., satellite and aerial images, airborne laser scanning) in forest inventory has long been recognized by both forestry science and practice (White et al. 2016). During the last two decades, constant and rapid technological progress regarding sensor miniaturization and algorithm development led to the emergence of various close-range remote sensing technologies (Jurjević et al. 2020, Liang et al. 2022). Compared to classical remote sensing, close-range remote sensing provides the acquisition of highly detailed data, that enables it to be used in individual-tree-based forest inventory. Currently, the static terrestrial laser scanning (TLS) system has the highest geometric quality enabling accurate extraction and estimation of the main tree attributes (Liang et al. 2022). However, the main limitation of TLS that hinders its operational use in forest inventory is the speed of data acquisition (Gollob et al. 2020, Balenović et al. 2021). Namely, to obtain high-quality data and reduce the occlusion effect caused by surrounding trees, for each forestry plot a multi-scan approach has to be applied, which is labour-intensive and time-consuming. On the other hand, mobile laser scanning systems can reduce occlusion problems and acquisition time, and therefore present a time-efficient alternative to TLS (Balenović et al. 2021). This is especially true for lightweight and highly mobile hand-held personal laser scanning (PLS) systems.

The emergence and availability of progressively advanced PLS systems in recent years have resulted in increased research into the possibility of their application in forest inventory, primarily for the assessment of key tree attributes (e.g. tree position, dbh, tree height, tree volume, etc.) (Gollob et al. 2020, Jurjević et al. 2020, Sofia et al. 2021, Tupinambá-Simões et al. 2023). Since PLS systems are constantly and rapidly advancing in terms of technical characteristics, continuous research on their application in forest inventory is inevitable. The main goal of this research is to test the performance of hand-held personal laser scanning technology in forest measurement, more precisely for estimating the diameter at breast height (dbh) in a lowland pedunculate oak (*Quercus robur* L.) forest. Therefore, this study aims: (i) to assess the accuracy of two, high-end hand-held PLS systems; and (ii) to compare different acquisition scenarios, i.e., various scanning schemes with different complexities.

2 Materials and methods

The research was conducted in a 100-year-old, mixed, lowland, even-aged pedunculate oak forest stand located in the management unit "Bolčanski-Žabljački lug" in Central Croatia, 70 km east of Zagreb. For this preliminary research, one circular sample plot (Figure 1) with a radius of 12.62 m (45°51'43"N, 16°40'06"E; 117 m a.s.l.) was chosen from a larger set of permanent plots.

Both field and PLS data were collected during the leaf-off conditions in February 2024. The coordinates of the plot centre were measured using the GNSS receiver Trimble R12i (Trimble, Inc., Westminster, Colorado, USA) connected to the Croatian network of GNSS reference stations (CROPOS). The position of each tree in the plot with dbh ≥ 5 cm was recorded by measuring the distance and azimuth from the plot centre. For each tree with dbh ≥ 5 cm, tree species was determined and dbh was measured using the diameter tape with a 0.1 cm precision (Table 1).

Figure 1. Panoramic view of the sample plot.

Table 1. Descriptive statistics of the sample plot for field measurement.

Tree species	N of trees	Mean ± SD of dbh (cm)	dbh range (cm)
Quercus robur L.	6	42.8 ± 6.7	32.1 – 49.9
Carpinus betulus L.	6	22.3 ± 6.5	12.0 – 31.8
Pyrus pyraster (L.) Burgsd.	2	16.0 ± 1.3	15.1 – 16.9
Ulmus laevis Pall.	1	6.6 ± n.a.	n.a.
Total	15	28.6 ± 13.8	6.6 – 49.9

 PLS data were collected using the GeoSLAM ZEB Horizon (Geoslam Ltd., Nottinghamshire, UK) and Faro Orbis (FARO Technologies Inc., Lake Mary, Florida, USA). Faro Orbis is a successor to Zeb Horizon with improved technical characteristics (Table 2) and the addition of 'flash' (static) scans that mimic TLS. For sample plot scanning, three pre-planned scanning schemes of different complexity (Figure 2a-c) were used for both ZEB Horizon and Faro Orbis, while for Faro Orbis an additional two schemes were applied that incorporated flash scans (Figure 2d). One of these schemes included only flash scans (FS), while the second one included both flash scans and a scan obtained by walking between flash scans (FS*). To enable PLS point cloud georeferencing, four reference points were placed on the scan area and measured with a Trimble R12i receiver.

The pre-processing of the collected data was carried out in the Faro Connect (FARO Technologies Inc., Lake Mary, Florida, USA) software, which generated a point cloud. Georeferencing of the point cloud from the local to the HTRS96/TM coordinate system was carried out using the four reference points. Afterward, the point clouds were

exported in las (LASer) format and further processed in LiDAR360 v7 (GreenValley Intl, California, USA) throughout several steps (outliers removing, ground points classification, normalization, dbh estimation). Dbh of each tree in the plot was manually fitted by the circle method using the TLS Seed Point Editor option. In total, eight different point clouds were processed and from each point cloud dbh was estimated for all trees on the plot.

Table 2. Technical specifications of Zeb Horizon and Faro Orbis.

Feature	Zeb Horizon	Faro Orbis
Range (m)	100	120
Acquisition rate (points/sec)	300,000	640,000
Field of view; horizontal/vertical (°)	360/270	360x290
Precision (mm)	up to 6	5 (mobile) / 2 (static)
Raw data file size (MB/min)	25-50	350

The accuracy of dbh estimates from PLS was evaluated with field reference data, i.e., dbh measured using a diameter tape. The evaluation was performed using a mean error (ME), a relative mean error (ME%), a standard deviation (SD), a root mean square error (RMSE), and a relative root mean square error (RMSE%).

3 Results and Discussion

The evaluation results for both PLS instruments and each scanning scheme are presented in Table 3.

Observed by PLS instrument type, it can be noticed that Faro Orbis provides more accurate dbh estimates than ZEB
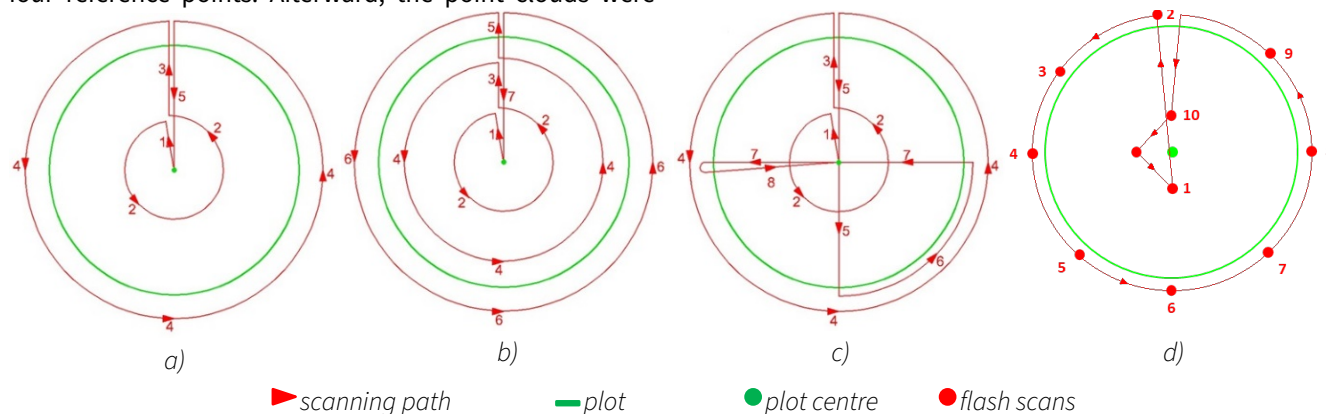
Figure 2. Pre-planned scanning schemes: a) scheme 1; b) scheme 2; c) scheme 3; d) scheme 4 with flash scans.

Table 3. Estimation accuracy of dbh for two PLS instruments (ZEB Horizon, Faro Orbis), and different scanning schemes in comparison to field reference data.

Scheme	ZEB Horizon			Faro Orbis				
	1	2	3	1	2	3	FS	FS*
ME (cm)	0.21	0.05	0.23	0.22	0.24	0.17	0.36	0.03
ME (%)	0.75	0.19	0.82	0.77	0.84	0.58	1.26	0.09
SD (cm)	0.95	0.81	0.76	0.49	0.52	0.37	0.32	0.42
RMSE (cm)	0.98	0.82	0.79	0.53	0.57	0.41	0.48	0.42
RMSE (%)	3.42	2.85	2.77	1.87	2.00	1.42	1.69	1.48

FS – individual flash scans, FS* - flash scans combined with walking scanning scheme.

Horizon. For Faro Orbis RMSE% values range from 1.42% to 2.00%, while for ZEB Horizon range from 2.77% to 3.42%. To the best of the authors' knowledge, this research is the first that tested the newest PLS instrument Faro Orbis in forest inventory. Comparison with other previous studies that utilized ZEB Horizon for dbh estimation (Gollob et al. 2020, Hyyppa et al. 2020, Sofia et al. 2021, Tupinambá-Simões et al. 2023), suggests that this study provides more accurate estimates. Namely, previous studies reported RMSE% values in the range from 3.50% to 12,01%. However, it should be considered that previous studies were conducted in different forest types with different forest structural and terrain characteristics. Also, they differ very much by plot size, scanning schemes, reference data (TLS or field reference data), software and algorithms for data processing and dbh estimation, etc.

Furthermore, the obtained results revealed an increase in the PLS data estimation accuracy that corresponds to the increase in complexity of the scanning scheme (from schemes 1 to 3) for ZEB Horizon. A similar situation is observed for Faro Orbis as well except for scanning scheme 2 which produced a slightly higher RMSE than scanning scheme 1. After detailed analysis, it can be confirmed that the main reason for slightly higher RMSE% values for scheme 2 is caused by a somewhat higher dbh estimation error (–1.0 cm) for one pedunculate oak tree (dbh = 49.0 cm). Similarly, ZEB Horizon scheme 2 also provides higher a dbh estimation error (–0.7 cm) for the same tree.

It is also revealed that Faro Orbis flash scans (FS) provide slightly less accurate dbh estimates (RMSE% = 1.69%)

compared to scheme 3 (RMSE% = 1.42%). Merging point clouds from flash scans and a scan obtained by walking between flash scans (FS*) improve the accuracy (RMSE% = 1.48%) very close to the accuracy obtained by scheme 3. Despite the better resolution of flash scans compared to classical mobile scanning, it is obvious that the spatial distribution of ten flash scans does not provide sufficient point cloud coverage of the sampling plot area. The addition of several flash scans within the plot area might improve accuracy but will also increase scanning and processing time.

s

Figure 3 shows RMSE% by tree species, i.e., for *Q. robur* and 'others' (*C. betulus*, *P. pyraster*, *U. laevis*). Results show that the dbh of *Q. robur* is estimated with considerably higher accuracy than the dbh of other tree species, which is somewhat expected. Namely, *Q. robur* trees in the plot have greater dbh and a more regular stem shape, unlike the other tree species (Table 1). This is in line with previous findings that reported greater errors in dbh estimation for smaller trees with dbh<10 cm (Ryding et al. 2015, Gollob et al. 2020). According to Gollob et al. (2020) due to the high noise of PLS, dbh of smaller trees is constantly overestimated regardless of various fitting methods applied. Dbh overestimations were also obtained within this research for all schemes and both PLS instruments. Furthermore, Figure 3 shows that both instruments and all scanning schemes estimate dbh of *Q. robur* with similar accuracy, i.e., with RMSE% ranging from 0.67% to 1.45%. On the other hand, it can be noticed that the accuracy of
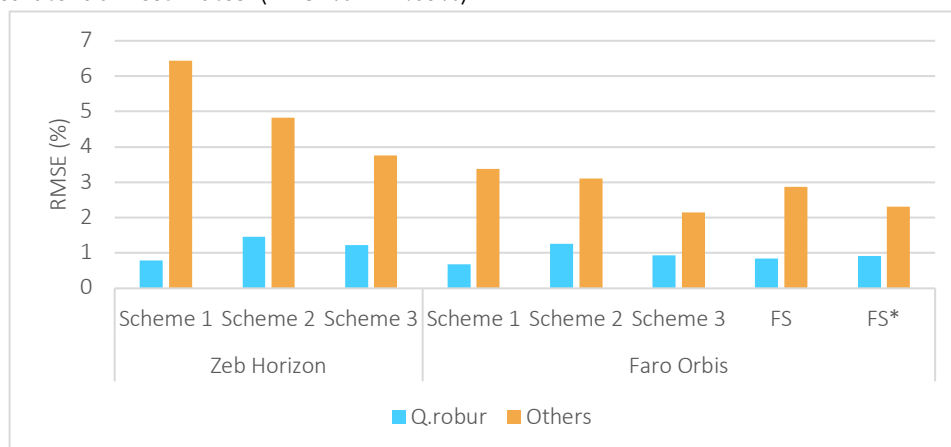
Figure 3. RMSE% values by Quercus robur and other tree species (Carpinus betulus, Pyrus pyraster, Ulmus laevis).

dbh estimates for other tree species is greatly dependable on the type of instrument used and the applied scanning scheme. The accuracy of dbh estimates significantly increases by increasing the complexity of scanning schemes. ZEB Horizon produces RMSE% of dbh estimates of 6.44%, 4.83%, and 3.76% for schemes 1, 2, and 3, respectively. Faro Orbis produces greater accuracy than ZEB Horizon, i.e., RMSE% of 3.38%, 3.10%, and 2.15% for schemes 1, 2, and 3, respectively.

4   Conclusions

For the first time, the performance of the newest commercial PLS instrument (Faro Orbis) was tested and compared with its predecessor (ZEB Horizon) and field reference data. Three scanning schemes of different complexity were used by both instruments, and Faro Orbis provided more accurate dbh estimates than ZEB Horizon for each scheme. Additionally, the new ability of Faro Orbis to perform 'flash' (static) scans that mimic TLS was also tested, and obtained results revealed that flash scans produce slightly less accurate dbh estimates compared to the most complex walking (mobile) scheme. Although flash scans generate point clouds of greater precision, the spatial distribution of ten flash scans did not provide sufficient point cloud coverage of the sampling plot area. However, this research confirmed the great potential of PLS technology in precision forest inventory, as well as provided preliminary results on the potential of the newest PLS instrument.

5   References

Balenović, I., Liang, X., Jurjević, L., Hyyppä, J., Seletković, A., Kukko, A., 2021. Hand-Held Personal Laser Scanning – Current Status and Perspectives for Forest Inventory Application. Croatian Journal of Forest Engineering 42 (1), 165-183.

Gollob, C., Ritter, T., Nothdurft, A., 2020. Forest Inventory with Long Range and High-Speed Personal Laser Scanning (PLS) and Simultaneous Localization and Mapping (SLAM) Technology. Remote Sensing 12 (9), 1509.

Hyyppä, E., Yu, X., Kaartinen, H., Hakala, T., Kukko, A., Vastaranta, M., Hyyppä, J., 2020. Comparison of Backpack, Handheld, Under-Canopy UAV, and Above-Canopy UAV Laser Scanning for Field Reference Data Collection in Boreal Forests. Remote Sensing 12 (20), 3327.

Jurjević, L., Liang, X., Gašparović, M., Balenović, I., 2020. Is field-measured tree height as reliable as believed – Part II, A comparison study of tree height estimates from conventional field measurement and low-cost close-range remote sensing in a deciduous forest. ISPRS Journal of Photogrammetry and Remote Sensing 169, 227-241.

Liang, X., Kukko, A., Balenović, I., Saarinen, N., Junttila, S., Kankare, V., Holopainen, M., Mokroš, M., … 2022. Close-Range Remote Sensing of Forests: The state of the art, challenges, and opportunities for systems and data acquisitions. IEEE Geoscience and Remote Sensing Magazine 10 (3), 32-71.

Ryding, J., Williams, E., Smith, M.J., Eichhorn, M.P., 2015. Assessing handheld mobile laser scanners for forest surveys. Remote Sensing 7 (1), 1095-1111.

Sofia, S., Sferlazza, S., Mariottini, A., Niccolini, M., Coppi, T., Miozzo, M., La Mantia, T., Maetzke, F., 2021. A Case Study of the Application of Hand-Held Mobile Laser Scanning in the Planning of an Italian Forest (Alpe di Catenaia, Tuscany). The International Archives of the Photogrammetry, Remote Sensing and Spatial Information Sciences XLIII-B2-2021, 763-770.

Tupinambá Simões, F., Pascual, A., Guerra Hernández, J., Ordóñez, C., de Conto, T., Bravo, F., 2023. Assessing the Performance of a Handheld Laser Scanning System for Individual Tree Mapping—A Mixed Forests Showcase in Spain, Remote Sensing 15 (5), 119.

White, J.C., Coops, N.C, Wulder, M.A., Vastaranta, M., Hilker, T., Tompalski, P., 2016. Remote Sensing Technologies for Enhancing Forest Inventories: A Review, Canadian Journal of Remote Sensing 42 (5), 619-641.

Utilization of Underwater ROVs for the Evaluation and Research of the Underwater Environment -Example of Marine Outfalls Surveillance in the Wider Aquatorium of the City of Split

Konrad Kiš[1],*, Katja Franc[1]

[1] DVOKUT-ECRO Ltd., Zagreb, Croatia, konrad.kis@dvokut-ecro.hr, katja.franc@dvokut-ecro.hr
* corresponding author

Abstract: In recent times, the usage of underwater robots (ROVs or submersibles) has become ever more frequent in the research and monitoring of the aquatic environment. The crucial difference between a submersible regarding unmanned aircraft vehicles (UAVs) is that wireless connection does not function underwater, which is why an ROV must relate to a controller (i.e. remote pilot) by a tether. Like UAVs, underwater robots are equipped with a camera that can take high-resolution photos and video footage, while some models accommodate the usage of exchangeable accessories such as a robotic arm, dead fish removal shovel, mud sampler, water sampler, and similar. When it comes to mid-priced underwater robots for wide use, these can go as deep as one hundred meters with a tether length of two hundred meters which suffices for the conduction of the most common tasks such as recording the aquatic habitats, collecting sediment samples under fish farms, or recording video footage of marine outfalls.

This paper describes the experience of recording video footage of marine outfalls in the wider aquatorium of the city of Split by using the underwater robots QySea Fifish V6 Expert and QySea Fifish V-EVO, and auxiliary equipment.

Keywords: underwater research; underwater robots (submersibles); underwater footage.

1   Introduction

When talking about close-range remote sensing, one usually refers to UAVs (unmanned aerial vehicles) or, to put it more precisely, UASs (unmanned aerial systems), because the whole equipment consists of a vehicle (drone), remote controller, and the remote pilot. UASs have been thoroughly described and researched and there are many articles regarding their utilization and application. However, underwater robots or ROVs are a much more recent phenomenon that yet must find its niche in the close-range remote sensing of the underwater environment. Nevertheless, there are articles on ROVs utilization for various underwater research purposes dating as far back as 2012 (Andaloro et al. 2012) which deal with assessing the suitability of ROVs to study fish communities associated with offshore gas platforms in the Ionian Sea, or more recent research by Sward, Monk and Barrett (2019) which gives more general research on the use of ROVs for visual assessment of fish assemblages, and broad research of McLean et al. (2020) on enhancing the scientific value of ROVs in the oceans.

Affordable and widely available ROVs can perform tasks like exploring hard-to-reach areas, data collection, sampling, inspection, maintenance, scientific research,

search and rescue, and environmental monitoring. Unlike UAVs, operating ROVs has minimal legal requirements - no piloting license is needed, only consent from the relevant ministry for recording marine habitats, underwater life, or anything beneath the sea surface, as per the Maritime Act (Official Gazette of the Republic of Croatia 2020).

This paper describes recording underwater footage of marine outfall pipes around Split. Using ROVs for this task is much cheaper and faster than traditional methods involving divers, sea scooters, and head cameras.

2   Materials and methods

The recording of Split's marine outfalls was conducted from September to November 2023 using a fast rubber boat, a QySea Fifish V6 Expert and V-Evo ROVs (Figure 1) with an Eco Flow portable power station, a high-luminosity tablet, and a cell phone for outdoor positioning (using the QField app).

Figure 1. The equipment comprised one QySea Fifish V6 Expert (top) and one QySea Fifish V-EVO ROV (bottom).

Before starting, we analyzed the number of outfalls, their length, and the depth of discharge points relative to the ROVs' capabilities (Figure 2). With the ROVs' maximum depth at 100 meters and the deepest discharge point at 60 meters, we determined the ROVs were suitable for the task. However, we did not initially account for challenges like sea currents, weather conditions, and significant turbidity caused by silty sediment in this part of the Adriatic.

Figure 2. Marine Outfalls in the wider aquatorium of Split. The first number is the length of the pipe, and the second is the depth of the discharge point (expressed in meters).

The equipment used comprised two ROVs which were used interchangeably (while one was operating, the other one was charging), an EcoFlow Delta 2 portable power station with 1 kWh capacity and an 1800 W output, a high-luminosity tablet required for monitoring of an ROV performance and a cellphone with QField application in which all outfalls and discharge points were added and which was used to navigate and find areas of interest on the sea. And, of course, a fast 8-meter rubber boat equipped with a powerful engine provided for fast movement between the outfalls.

The key difference between an ROV and a UAV is positioning: an ROV must be tethered due to the inability to use Wi-Fi underwater, and GPS signals don't work underwater. Underwater positioning systems exist but are costly and complex, so they weren't used here. Instead, an ROV is calibrated before deployment, and its sensor provides vertical position and bearing on-screen, which is sufficient for tracking its position and movement. Before recording, all equipment must be checked, bolts and screws tightened, batteries charged, and the SD card erased and inserted (Figure 3).

After deploying the ROV, the first step was to dive to the sea bottom and locate the pipe's starting point. This was done by positioning the boat near the pipe's estimated location and using the bearing information on the monitor. Once found, the ROV was positioned about half a meter above the pipe to begin video recording. Although the ROV

camera supports 4K, 1080HD footage was used to avoid glitches and excessive data.

Figure 3. The Company's marine biologist making final preparations for an ROV before the deployment.

Initially, visibility was good because larger sediment particles were closer to shore, but after recording one-third of the pipes, the water became too turbid to see clearly (Figure 4). Recording had to be paused and resumed from more favorable points. In extreme conditions, the ROV had to be positioned very close to the pipe, which stirred up sediment and obscured the view. The main challenge was finding the optimal position to see the pipe without disturbing sediment with the ROV's propellers.

The main challenge was determining the exact position of the ROV, as they lacked a self-sustained positioning system like UAVs. The approach used involved estimating the ROV's position through available data: the pipe's direction, the ROV's depth, and the length of the marked tether. This forms a right-angle triangle, and using the Pythagorean

Theorem, the horizontal distance from the boat can be calculated. Although the tether is rarely fully stretched due to sea currents, this method provides a sufficiently accurate estimate of the ROV's position.

Figure 4. An illustration of ultimate turbidity in the footage of the Podstrana outfall - the pipe (right side of the photograph) is barely visible.

Although extreme conditions were found at most of the outfalls, there is an exception of the shortest outfall, yet with the deepest discharge point - the Nečujam outfall located on the northern part of the isle of Šolta. The sediment on this part of the seabed consists of gravel and rocks, which therefore resulted in a much lesser turbidity than at any other outfall. On such depths, daily light gradually fades, and therefore ROV's powerful LED lights had to be deployed, resulting in crystal clear, colorful images of the seabed at 60 meters depth (Figure 5).

Figure 5. Discharge point of the Nečujam outfall at 60 meters depth, LED lights deployed.

3   Results

The purpose of this project was to record marine outfalls and discharge points to detect leaks, breaks, or other issues, and document their locations for future repairs by the utility. Despite several months of work in difficult conditions and some delays, the task was completed, and all necessary footage was finalized. Due to murky sea conditions caused by silty sediment and constant currents, recording had to be frequently paused and resumed from better positions. The footage was edited using Edius and compiled into unique videos for each outfall, accompanied by a written report and imagery mostly from video frames. The footage identified several pipe leaks and breaks, which were documented and included in the final report.

Split's aquatorium, with its silty seabed, posed significant challenges, contrasting with the clearer sea at the Nečujam

outfall near Šolta island. The project took roughly three months, hampered by difficult conditions and unsuitable weather. The final footage of the Čiovo outfall was completed using a more stable flounder boat, which improved the ROV's course stability.

The results included separate 1080HD video footage for all eight outfalls, a written report, and detailed photos of pipe irregularities. Although the project took longer than expected, it was completed. Future similar tasks require better preparation, though experience and ROV pilot skills remain crucial.

4   Discussion

As this was the Company's first ROV task, difficulties arose due to inexperience. Despite these challenges, the mission was completed. Coastal utilities must regularly obtain video footage of marine outfalls, a task previously done by divers, which was time-consuming, costly, and dangerous, especially at depths over 50 meters in murky conditions. ROVs are likely the future of underwater outfall recording due to their efficiency, cost-effectiveness, quality footage, and the elimination of risky diver involvement. Other researchers in this field also stress the importance of divers' safety, but also the advantages of ROVs due to the elimination of human error, precision, and time efficiency (EyeRov 2024).

5   Conclusions

The utilization of widespread, cost-effective ROVs is a rising industry in the field of underwater exploration and monitoring of widely affordable ROVs whose prices vary from approximately two to thirty thousand euros. This engagement proved that highly dangerous, time-consuming, and costly operations which were previously conducted solely by divers and pertaining equipment can be performed with an ROV, achieving the same or even better results.

Some of the widely spread tasks that ROVs can perform are as follows:

- Exploration: ROVs can explore depths that are difficult or dangerous for humans to reach, such as deep ocean trenches or beneath ice shelves.
- Data Collection: Equipped with various sensors and cameras, ROVs can collect high-resolution images, videos, and other data about underwater environments.
- Sampling: Some ROVs are equipped with manipulator arms capable of collecting samples of sediment, water, marine life, or geological formations.
- Maintenance: ROVs are used for underwater infrastructure inspection, maintenance, and repair, such as pipelines, cables, and offshore platforms.
- Scientific Research: ROVs are essential tools for studying marine biology, geology, oceanography, and archaeology, enabling researchers to observe and document underwater ecosystems and phenomena.
- Search and Rescue: ROVs equipped with sonar and cameras can assist in search and rescue operations,

locating lost vessels or aircraft, and providing real-time information to rescue teams.

- Environmental Monitoring: ROVs can be deployed to monitor environmental parameters such as temperature, salinity, pH, and pollution levels in marine environments.

In conclusion, there are numerous ways of utilization of commercially available ROVs which will transfer a great load of highly demanding tasks from divers and the evermore robust and expensive equipment that has been used so far. Successful completion of this task adds to this statement, while numerous other tasks lay ahead, waiting for ROVs of increased features and capabilities which are being produced as we speak.

6   References

EyeRov, 2024. Diving Deep: Unleashing the Power of ROVs for In-Depth Surveys of Marine Outfall Systems, https://www.eyerov.com/blog-details/diving-deep-unleashing-the-power-of-rovs-for-in-depth-surveys-of-marine-outfall-systems. (Accessed 7 June, 2024)

Global Market Insights, 2024. Remote Operated Vehicle Market Size, https://www.gminsights.com/industry-analysis/remote-operated-vehicle-market#:~:text=Remote%20Operated%20Vehicle%20(ROV)%20Market,technological%20advancements%20in%20ROV%20capabilities. (Accessed 7 June, 2024)

McLean, D.L., Parsons, M.J., Gates, A.R., Benfield, M.C., Bond, T., Booth, D.J., Bunce, M., Fowler, A.M., Harvey, E.S., Macreadie, P.I. and Pattiaratchi, C.B., 2020. Enhancing the Scientific Value of Industry Remotely Operated Vehicles (ROVs) in Our Oceans. Frontiers in Marine Science 7, 220.

Official Gazette of the Republic of Croatia (No. 181/04, 76/07, 146/08, 61/11, 56/13, 26/15, 17/19), Maritime Act, 2020., article 13.

ROV Innovations, 2024. Underwater Positioning, https://www.rovinnovations.com/positioning-systems.html. (Accessed 7 June, 2024)

Sward D., Monk, J., Barrett N., 2019. A Systematic Review of Remotely Operated Vehicle Surveys for Visually Assessing Fish Assemblages. Frontiers in Marine Science 6, 134.

Declining Sea Surface Height in the Caspian Sea Based on Sentinel-3A Data

Nilufar Makky[1,]*, Khalil Valizadeh Kamran[1]

[1] RSGIS Department, University of Tabriz, Tabriz, Iran, rsgis.nilufarmakki73@gmail.com, valizadeh@tabrizu.ac.ir
* corresponding author

Abstract: Our planet faces climate-related challenges, one significant concern revolves around the impact of global warming on oceans and lakes, especially the necessity of closely tracking changes in Sea Surface Height. In this study, we acquired data from the SRAL LEVEL2 sensor on Sentinel-3A to monitor the Caspian Sea throughout the year. With 276 passes overall and 23 observations per month, we monitored Sea Surface Height alongside meteorological data, including Precipitation, Sea Surface Temperature, and Water Vapor, obtained from the Google Earth Engine platform. We used the LSTM model and monitored the Sea Surface Height using Precipitation, Sea Surface Temperature, and Water Vapor as input variables. The model gave notable performance metrics with an R^2 value of 0.9765. Also, the trend of Sea Surface Height showed a significant reduction. This information is valuable for policymakers to management of the region's resources.

Keywords: Caspian Sea; passes; Sea Surface Height; Sentinel-3A; decreasing; climate change.

1   Introduction

Lakes and reservoirs, covering only about 2% of the Earth's land surface, are crucial for the national economy by regulating river runoff, supporting irrigation, providing industrial and drinking water, maintaining aquatic habitats, contributing to ecological balance, and facilitating transportation (Zhang 2023). However, these water bodies are highly vulnerable to human activities such as industrial operations, agriculture, aquaculture, and climate change, which can significantly alter their characteristics. Monitoring water levels in these bodies offers valuable insights into trends influenced by these factors, with accurate data collection and comprehensive spatiotemporal analyses essential for their conservation (Verpoorter et al. 2014). Wetlands, vital for biodiversity, face threats from reduced rainfall, higher temperatures, increased evaporation, and prolonged droughts. Climate change challenges highlight the importance of predicting sea surface height (SSH) changes for mitigation (Kamran et al. 2023, Makky et al. 2023). Satellite altimetry has revolutionized oceanography, improving SSH measurement precision and the study of coastal circulation (Fu et al. 2010, Raney 2011). SAR Delay-Doppler altimetry, particularly from the Sentinel-3A satellite, provides enhanced resolution and innovative coastal data processing (Feng et al. 2023). The SWOT mission further exemplifies advancements in capturing wide swath data (Srinivasan and Tsontos 2023). Sentinel-3, with SAR mode and 300-meter resolution, faces challenges in coastal areas, addressed by products like the Adaptive Leading Edge Sub waveform (ALES) tracker for precise sea level observations (Tomić et al. 2024). Previous studies by Makky et al. (2023) demonstrated that Jason2 radar altimetry data reliably monitors sea surface height based on precipitation and sea surface temperature. Furthermore, incorporating the effect of additional climatic features into predictions can enhance this type of research.

2   Materials and methods

As the world's largest isolated water reservoir, the Caspian Sea (Figure 1) with an area spanning 392,600 km² and mean and maximum depths of 208 m and 1025 meters (Mograne et al. 2019). Regarding the significant fluctuation in the level of the Caspian Sea in recent years, it is crucial to monitor it to protect it from potential destructive events in the future (Ardalan and Hashemifaraz 2024).
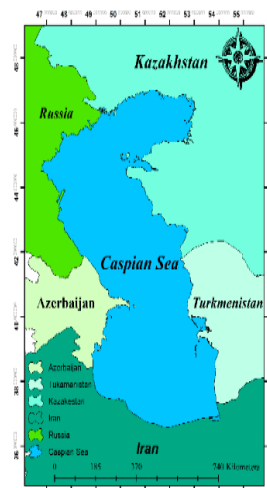
Figure 1. The geographical location of the Caspian Sea.

This study assesses Sea Surface Height (SSH) over the Caspian Sea using Sentinel-3A SAR mode datasets. A Long Short-Term Memory (LSTM) model predicts SSH based on meteorological features, including Water Vapor (WV), Precipitation, Sea Surface Temperature (SST), and SSH observations. The LSTM model is used to handle time series oceanic data by predicting oceanic data for the upcoming days (Braakmann-Folgmann et al. 2017), also LSTM model is trained on the training data, capturing temporal dependencies, and iterative optimization refines model parameters to enhance predictive performance.

Sentinel-3A and Sentinel-3B provide essential oceanic and atmospheric measurements for ocean forecasting, environmental monitoring, and climate studies. They operate in a high-inclination orbit (98.65°) to optimize coverage of high-latitude regions (EUMETSAT 2021).

This study uses Sentinel-3A satellite data from March 2023 to March 2024, focusing on Ku-band 20 Hz SSH data.

Processing involves extracting and organizing SSH measurements from NetCDF files and applying corrections to calculate SSH. These measurements are obtained from the SRAL (SAR Radar Altimeter) instrument and are provided with units and scaling factors for interpretation.

A comprehensive LSTM model predicts SSH using features like SST (Ren et al. 2024), precipitation (Wang et al. 2001), and surface water vapor (Gbetkom et al. 2023) from various datasets provided by Google Earth Engine.
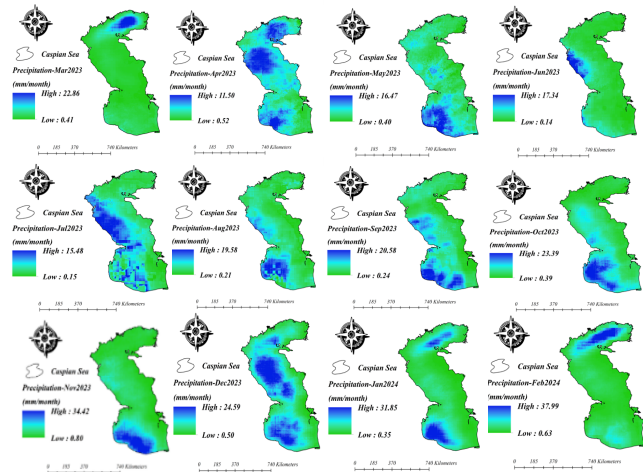
Figure 2. The precipitation data (mm/pentad) covering the period from March 2023 to March 2024 was acquired from the UCSB-CHG/CHIRPS/PENTAD mission.
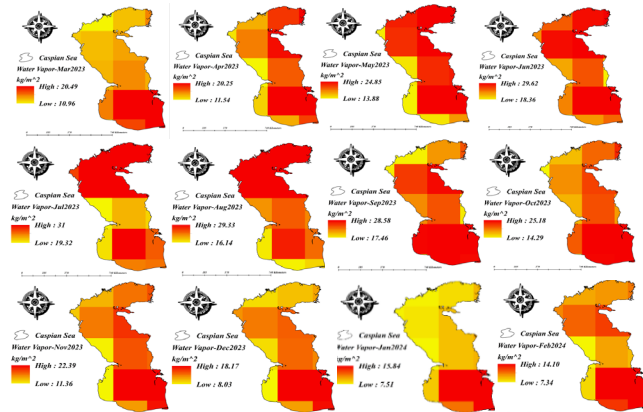
Figure 3. The WV data (kg/m^2) covering the period from March 2023 to March 2024 was acquired from the surface water vapor data from the NCEP_RE/surface_wv mission.
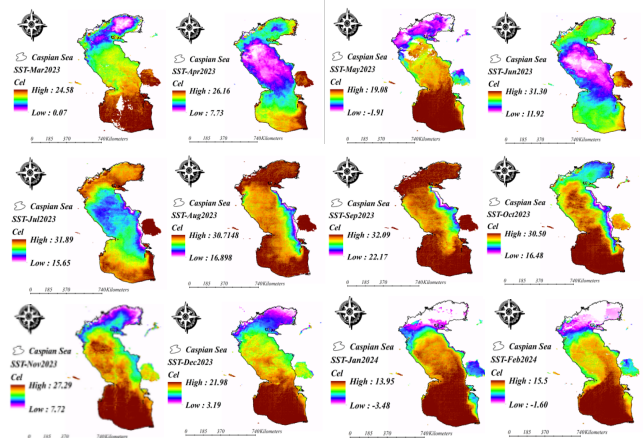
Figure 4. SST data (°C) covering the period from March 2023 to March 2024 was acquired from the JAXA/GCOM-C/L3/OCEAN/SST/V3 mission.

3 Results

The monthly meteorological data, including precipitation (Figure 2), water vapor (Figure 3), and sea surface temperature (Figure 4) from March 2023 to March 2024. Additionally, the compatibility between test and train data, and the trend of sea surface height (SSH) were shown in Figure 5 and Figure 6. The polar chart illustrating the correlation coefficient is presented in Figure 7 for additional detail.
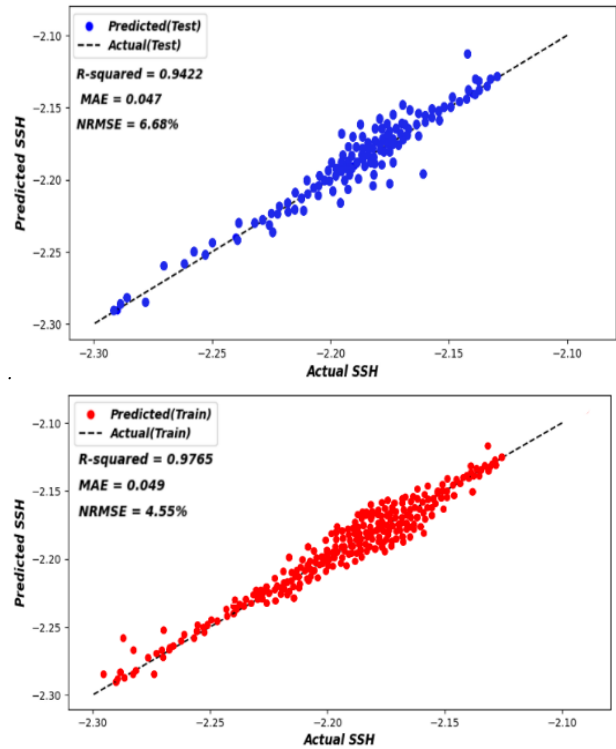
Figure 5. The compatibility between the actual data (top) and the predicted data (bottom) for both the training and testing sets of the LSTM model.
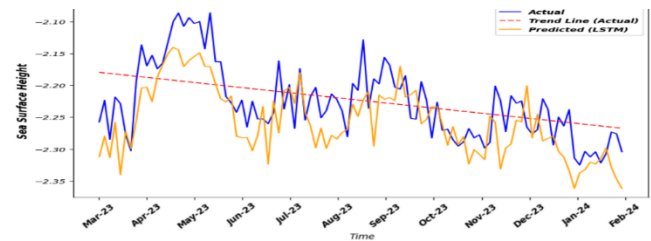
Figure 6. The LSTM model generated predicted time series data for Sea Surface Height for both the training and testing datasets.
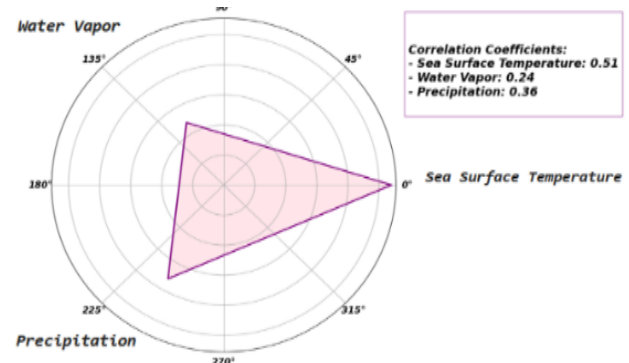
Figure 7. The polar chart depicts the correlation coefficients between meteorological factors.

4   Discussion

Examining precipitation patterns can provide valuable insights into how SSH dynamics in the Caspian Sea may evolve (Islam and Sato 2021). The correlation coefficient, as presented in the polar chart, indicates SST's dominant impact on SSH in the Caspian region. The predicted trend illustrates a decreasing SSH trend in the Caspian Sea, which could have adverse effects on the region. The objective is to develop a predictive model and identify which variable most significantly affects the SSH, with SST found to have the most substantial impact.

5   Conclusions

The data collected by the SRAL LEVEL2 sensor on Sentinel-3A indicated a decrease in the water height of the Caspian Sea. This study highlights the significant impact of key meteorological variables on the variability of Sea Surface Height. The model gave notable performance metrics with an R^2 value of 0.9765, NRMSE (Normalized Root Mean Squared Error) of 4.55%, and MAE (Mean Absolute Error) of 0.049 during training. Testing the model produced encouraging results, with an R^2 value of 0.9422, NRMSE of 6.68%, and MAE of 0.047. Additionally, correlation coefficients indicated significant associations, with SST exhibiting a correlation coefficient of approximately 0.51, precipitation at 0.36, and WV at 0.24 with sea surface height. The observed correlations between these variables and sea surface height provide valuable insights into the changes in the Caspian Sea. Temperature was found to have the most significant impact on decreasing SSH.

6   References

Ardalan, A.A., Hashemifaraz, A., 2024. How Satellite Altimetry Data Can Help Us Understand Sea Level Fluctuations and Classify Water Drainage Areas in the Caspian Sea. Preprints.

Braakmann-Folgmann, A., Roscher, R., Wenzel, S., Uebbing, B., Kusche, J., 2017. Sea level anomaly prediction using recurrent neural networks. arXiv preprint arXiv:1710.07099.

Eghrari, Z., Delavar, M.R., Zare, M., Beitollahi, A. and Nazari, B., 2023. Land subsidence susceptibility mapping using machine learning algorithms. ISPRS Annals of the Photogrammetry, Remote Sensing and Spatial Information Sciences. X-4/W1-2022. 129-136.

Eghrari, Z., Delavar, M.R., Zare, M., Mousavi, M., Nazari, B. and Ghaffarian, S., 2023. Groundwater level prediction using deep recurrent neural networks and uncertainty assessment. ISPRS Annals of the Photogrammetry, Remote Sensing and Spatial Information Sciences. X-1/W1-2023. 493-500.

Feng, H., Egido, A., Vandemark, D., Wilkin, J., 2023. Exploring the potential of Sentinel-3 delay Doppler altimetry for enhanced detection of coastal currents along the Northwest Atlantic shelf. Advances in Space Research, 71 (1), 997-1016.

Fu, L.L., Chelton, D.B., Le Traon, P.Y., Morrow, R., 2010. Eddy dynamics from satellite altimetry. Oceanography, 23 (4), 14-25.

Gbetkom, P.G., Crétaux, J.F., Tchilibou, M., Carret, A., Delhoume, M., Bergé-Nguyen, M., Sylvestre, F., 2023. Lake Chad vegetation cover and surface water variations in response to rainfall fluctuations under recent climate conditions (2000–2020). Science of The Total Environment, 857, 159302.

Handoko, E.Y., Fernandes, M.J., Lázaro, C., 2017. Assessment of Altimetric Range and Geophysical Corrections and Mean Sea Surface Models—Impacts on Sea Level Variability around the Indonesian Seas. Remote Sensing 9, 102.

Islam, M.A., Sato, T., 2021. Influence of Terrestrial Precipitation on the Variability of Extreme Sea Levels along the Coast of Bangladesh. Water, 13, 2915.

Kamran, K.V., Makky, N., Charandabi, N.K., 2023. Investigating the flooded area of Bangladesh by Sentinel_1 and CHIRPS images in the GEE system. Intercontinental Geoinformation Days (IGD), 6, 83-88, Baku, Azerbaijan.

Makky, N., Valizadeh Kamran, K., Karimzadeh, S., 2023. Impact of Global Warming on water height using machine learning algorithms, in Proceedings of the 5th International Electronic Conference on Remote Sensing, 7-21 November, Basel, Switzerland.

Mograne, M.A., Jamet, C., Loisel, H., Vantrepotte, V., Mériaux, X., Cauvin, A., 2019. Evaluation of five atmospheric correction algorithms over French optically-complex waters for the Sentinel-3A OLCI Ocean Color Sensor. Remote Sensing, 11 (6), 668.

Raney, R. K., 2011. CryoSat SAR-mode looks revisited. IEEE Geoscience and Remote Sensing Letters, 9 (3), 393-397.

Ren, J., Wang, C., Sun, L., Huang, B., Zhang, D., Mu, J., Wu, J., 2024. Prediction of Sea Surface Temperature Using U-Net Based Model. Remote Sensing, 16, 1205.

Srinivasan, M., Tsontos, V., 2023. Satellite Altimetry for Ocean and Coastal Applications: A Review. Remote Sensing, 15, 3939.

Tomić, M., Breili, K., Gerlach, C., Ophaug, V., 2024. Validation of retracked Sentinel-3 altimetry observations along the Norwegian coast. Advances in Space Research.

Verpoorter, C., Kutser, T., Seekell, D.A., Tranvik, L.J., 2014. A global inventory of lakes based on high-resolution satellite imagery. Geophysical Research Letters, 41, 6396-6402.

Wang, J., Cole, H., Carlson, D., 2001. Water Vapor Variability in the Tropical Western Pacific from 20-year Radiosonde Data. Advances in Atmospheric Sciences. 18. 752-766.

Yang, L., Jin, T., Gao, X., Wen, H., Schöne, T., Xiao, M., Huang, H., 2021. Sea Level Fusion of Satellite Altimetry and Tide Gauge Data by Deep Learning in the Mediterranean Sea. Remote Sensing, 13, 908.

Zhang, X., 2023. Impacts of Water Resources Management on Land Water Storage in the Lower Lancang River Basin: Insights from Multi-Mission Earth Observations. Remote Sensing, 15, 1747.

Zhang, Z., Yin, J., Wang, L., 2024. Multi-head attention ResUnet with sequential sliding windows for sea surface height anomaly field forecast: A regional study in North Atlantic Ocean. Applied Soft Computing, 111551.

Conservation and Biodiversity

TOWARDS DETAILED AND PUBLIC DATA ON CROATIAN SOIL AS A PREREQUISITE FOR SUSTAINABLE ENVIRONMENTAL MANAGEMENT AND NATURE CONSERVATION
Josip Križan, Luka Antonić, Tomislav Hengl, Oleg Antonić

SHRUB ENCROACHMENT AND SHRINKING OF PASTURES IN INNER AND WESTERN TIEN-SHAN, KYRGYZSTAN
Evgenii Shibkov

FOREST STORM DAMAGE DETECTION USING EO DATA AND MACHINE LEARNING
Damir Klobučar, Ivan Pilaš

PROTECTING BIODIVERSITY: EMPOWERING ENGAGEMENT THROUGH INTERACTIVE MAPS
Maja Maslać Mikulec, Karla Čmelar

POSSIBILITIES OF THE UTILIZATION OF UAS (UNMANNED AERIAL SYSTEMS) IN THE PREPARATION OF FOREST MANAGEMENT PLANS FOR PRIVATE FORESTS
Konrad Kiš, Ema Svirčević

A REVIEW OF GEOSPATIAL PREDICTION AND MODELLING APPROACHES IN BIOGAS PLANT SUITABILITY ASSESSMENT
Đurđica Kovačić, Dorijan Radočaj, Mladen Jurišić

LAND COVER CHANGES AND CONSERVATION EFFECTIVENESS OF PROTECTED AREAS: EVIDENCE FROM LANDLOCKED DEVELOPING COUNTRIES IN SUB-SAHARAN AFRICA
Jeffrey Chiwuikem Chiaka, Gengyuan Liu

AUTOMATED PLANT SPECIES IDENTIFICATION USING 3D LIDAR POINT CLOUDS: A CASE STUDY USING CABBAGE AND MAIZE PLANTS
Mukesh Kumar Verma, Manohar Yadav

Towards Detailed and Public Data on Croatian Soil as a Prerequisite for Sustainable Environmental Management and Nature Conservation

Josip Križan[1], Luka Antonić[1,], Tomislav Hengl[2], Oleg Antonić[3]*

[1] MultiOne j.d.o.o., Zagreb, Croatia, lantonic@multione.hr
[2] EnvirometriX Ltd, Wageningen, The Netherlands, tom.hengl@envirometrix.net
[3] Granum Salis Cooperative, Zagreb, Croatia, oantonic@zadrugagranumsalis.hr
* corresponding author

Abstract: Soil is an indispensable component of the terrestrial ecosystem. It is thus unimaginable to perform sustainable land management without information on the pedosphere, regularly collected by mapping pedocartographic units and/or sampling at typical locations for laboratory acquisition of physical and chemical parameters. Despite soil inventory having been done in Croatia for decades, complex interinstitutional relations with often poorly regulated jurisdiction, rights and obligations have led to the nonexistence of a public soil database to date, one that would assist in daily efforts of many stakeholders (farmers, foresters, conservationists, planners, consultants, authorities and various decision makers, among others), and would strongly improve environmental and natural resource management in our country. In a project implemented on behalf of the World Bank from 2020 to 2021, a 30 m resolution spatial dataset was produced with 16 standard pedological variables estimated by applying machine learning algorithms against satellite imagery alongside climatic, geological and geomorphometric indicators (for a total of 533 covariates), while unifying soil data from numerous sources, some of which are not publicly available, which limits the availability of the project results. However, subsequent analyses performed outside of the project and only on publicly available target data have yielded results of similar quality, providing new opportunity to many interested parties.

Keywords: soil mapping; machine learning; open data.

1 Introduction

Open access to high-resolution spatial data in general, and to soil data in particular, has the potential to be highly transformative to a wide palette of human activity, but perhaps most notably to environmental management (extending to agronomy and to most other forms of cultivation) and to nature conservation. Thus, effort is widely being made to provide open spatial data at a global (through Copernicus and similar initiatives) or at least continental scale (e.g. the HORIZON programmes of the European Commission). However, public funding (e.g. through various European Commission programmes) is also often spent on compiling datasets which end up having a singular purpose to meet the objectives of the project at hand, and shelved afterwards with no means of outside access, despite their potential usefulness for other purposes. Such cases are often lost opportunities to bring added value to work already completed, as well as to

prevent future duplication of work (and, by extension, funding). This is particularly observable at the national level, where public institutions often claim ownership of underlying data (despite the questionability of such claims upon any data which have invariably also been procured through public funding), and therefore prohibit any distribution of the derivatives thereof.

One such occurrence was during the STARS-RAS project, the basis for Agro-Ecological Zoning of Croatian territories. Through the course of the project, we were hired to produce a complete digital soil map of Croatia, consisting of 16 soil physical and chemical properties and soil classification as per the World Reference Base taxonomical standard, mapped across the entire country at 30 m resolution. Due to various government agencies claiming ownership on some of the underlying data used to produce these layers (both soil samples and covariates), any use of the products outside the project was prohibited. With the goal of bringing any potential value of these products to the wider Croatian public for further application, we have reproduced the described data products at our own cost, with fully analogous methodology, but this time only using publicly available covariates and soil samples, and have made the data products publicly available via Zenodo.

Physical and chemical soil properties and classification were modeled through ensemble machine learning (using gradient boosting trees, gradient boosting linear models and random forests). While the physical and chemical property models displayed mixed capability for generalization, many of the properties were modeled with sufficient quality to demonstrate usefulness (validation adjusted R^2 above 0.8). Classification modeling, however, displayed poor generalization capacity (validation weighted $f1 < 0.5$), indicating a need for methodology revision.

2 Materials and methods

The methodology for predictive soil mapping was adopted from Hengl and MacMillan, 2019. An ensemble machine learning approach was used against an exhaustive set of spatial covariates to model a total of 16 soil physical and chemical properties: organic carbon content (oc), total NCS nitrogen (n_tot_ncs), Mehlich3 extractable calcium (ca_mehlich3), potassium (k_mechlich3), magnesium (mg_mehlich3) and phosphorus (p_mehlich3), summary cation exchange capacity (cec_sum), saturation extract electrical conductivity (ec_satp), carbonate content

(caco3), 1:1 soil-water (ph_h2o) and soil-KCl suspension pH (ph_kcl), total clay (clay_tot_psa), silt (silt_tot_psa) and sand content (sand_tot_psa), coarse fragment content (wpg2), < 2 mm fraction ovendry bulk density (db_od) and depth to bedrock up to 400 cm (dbr), as well as soil type classification as per the World Reference Base taxonomical standard (wrb_rsg). Additionally, soil texture classification was derived from the modeled clay, silt and sand content, using the method described in Radočaj et al. (2020).

2.1 Target dataset

Target soil property data was compiled from the following sources: 1) data on Croatian soils collected by the former State Department for Environment and Nature Protection, consisting of 2199 pedological profiles sampled from 1963 to 1966 (Martinović and Vranković 1997), further referenced as martinovic_1997, 2) data from the project *Spatial variability of trace and toxic metals in agricultural soils of Croatia*, provided by the Faculty of Agriculture, Zagreb, consisting of 811 samples acquired on a 8x8 km grid (Romić 2013), further referenced as agricultural_2013, 3) data from the project *Change in soil carbon stocks and calculation of soil total nitrogen and organic carbon trends and C:N ratios*, consisting of 2519 samples collected from 1994 to 2004 (for the purpose of compiling the Geochemistry Atlas of Croatia) and 742 additional samples from locations revisited from 2015 to 2016 (URL-1), further referenced as azo_2013 and azo_2016. The depth to bedrock target dataset was further enhanced with national piezometric observations (Croatian Waters 2016), considering measurements of a minimum of 4 m, totaling in 812 additional observations. Data from all sources were harmonized through unit consolidation and extraction of measurements equivalent to the topsoil (0–30 cm) depth horizon. As the source measurements were performed at varying depth horizons (of below 30 cm width), topsoil equivalent was obtained as a weighted average of measurements from all horizons which overlap with topsoil, with overlap fraction used as the weight. The total number of topsoil observations obtained per soil parameter is listed in Table 1. The spatial distribution of observations is shown in Figure 1.

Figure 1. Target observation coverage per source dataset (top), total sample density (bottom).

Table 1. Number of observations obtained per soil parameter.

Parameter	Samples	Parameter	Samples
oc	3452	db_od	3148
n_tot_ncs	5074	p_mehlich3	2598
ca_mehlich3	726	ec_satp	685
k_mehlich3	3364	caco3	2624
mg_mehlich3	726	ph_h2o	2784
clay_tot_psa	3408	ph_kcl	2041
silt_tot_psa	3369	dbr	2576
sand_tot_psa	3407	wrb_rsg	5025
wpg2	2116		

2.2 Covariate set and preprocessing

The covariates used for modeling soil properties and taxonomy were as follows: 1) a total of 16 terrain property layers derived from the official Croatian elevation dataset (URL-2), produced using GRASS GIS (GRASS Development Team 2017) and WhiteboxTools (Lindsay 2016), 2) Sentinel-2 seasonal cloudless mosaics of 6 bands (blue, green, red, NIR, SWIR1, SWIR2) at 3 quantiles (P25, median and P75) from 2018 to 2020 for a total of 180 layers, 3) Sentinel-1 monthly mosaics for 2018 and 2019 of the VV and VH bands, mosaicked as monthly mean over pixel, totaling 48 layers, 4) Global surface water (GSW) dataset for 2019 (Pekel et al. 2016), 6 layers, 5) Surface soil moisture (SSM) dataset for 2018 and 2019 (URL-3), 6 layers, 6) CHELSA climate and bioclimatic data (URL-4), 50 layers, 7) 15-year global 1 km cloud cover (Wilson and Jetz 2016), 13 layers, 8) Long-term MODIS LST day-time and night-time temperatures (URL-5),

100 layers, 9) Long-term Aerosol thickness, monthly means and annual mean and standard deviation for period of 2000 to 2017 (URL-6), 14 layers, 10) Monthly precipitation at 1 km resolution based on SM2RAIN-ASCAT 2007–2018, IMERGE, CHELSA Climate and WorldClim (URL-7), 25 layers, 11) Monthly mean water vapor content for period of 2000 to 2017 (URL-8), 12 layers, 12) Geological map of Croatia (Croatian geological institute 2019), reclassified to 54 classes representing lithological composition, resulting in 54 layers representing pixel distance from nearest occurrence of each lithological class. All covariates were reprojected to ETRS89-extended / LAEA Europe and resampled in 30m resolution,

with the considered data mask consisting of the landmask dictated by the coverage of the terrain layers (corresponding to land on Croatian territory), with pixels classified as built-up areas and water bodies (Pflugmacher et al. 2019) left out of the mask. The total set of covariates resulted in over 400 individual layers, a very high number relative to the training sample size (as low as ~700 for some target variables). Furthermore, layers extracted from the same dataset were highly intercorrelated. To account for this, principal component analysis (PCA) was performed on the covariates to reduce the dimensionality of the input space. Predictors were divided into 10 groups and a separate PCA was performed on each group, such that the number of components accounted for 90% of cumulative variability of the group, resulting in under 70 total covariate layers across all groups. The PCAs were fitted on predictor values sampled at one million randomly chosen pixels within the data mask.

2.3 Model specification

Physical and chemical soil properties were modeled with two-level stacked regressor ensembles. The bottom level of the ensemble stack consisted of three groups of models: 1) gradient boosting trees, 2) gradient boosting linear models and 3) random forest models. For each target property, five models from each group were selected for the ensemble, through a random search over their respective hyperparameter space (consisting of learning rate, conservativity constraints and tree topology), spatially cross-validated with five folds consisting of samples grouped into discrete 10x10 km tiles over the spatial domain. At the top stack level, another gradient boosting tree model was fitted to predict the final output from the predictions of the fifteen bottom-level models, with output constrained to the value range of the training data. In order to normalize target distributions, all properties were modeled as the natural logarithms of the actual values, with the exceptions of sand_tot_psa, silt_tot_psa, clay_tot_psa, ph_h2o, ph_kcl and db_od, and were converted back during postprocessing.

Additionally, uncertainty of the predictions was estimated through two additional top-level models, fitted to predict the 5% and 95% quantiles of the output. Soil type classification was modeled with a voting classifier ensemble, with individual estimators trained in the same manner as with the regression models. The final class probability was obtained as a weighted soft vote between

the fifteen selected estimators, with the estimator weight equal to its mean *f1* score over the validation fold, multiplied by the ratio of test to train scoring in order to additionally penalize overfitting. In addition to pixel-wise probability of each class, uncertainty of the classification was estimated as pixel-wise relative entropy (ratio of prediction entropy to maximum possible entropy for the given number of classes). Modeling was performed in a Python environment with XGBoost (Chen and Hestrin 2016) and scikit-learn (Pedregosa et al. 2011), on a workstation equipped with a 12-core AMD Ryzen Threadripper 2920X CPU, a single NVIDIA RTX 2060 GPU and 64 GiB of memory.

Table 2. Regression metrics for physical and chemical soil properties, including R-squared, R-squared adjusted for number of predictors and observations, and concordance correlation coefficient (CCC), mean over training folds and validation folds.

Target	R^2 train	R^2 val	R^2_adj train	R^2_adj val	CCC train	CCC val
oc	0.98	0.92	0.98	0.91	0.99	0.96
ln(oc)	0.96	0.91	0.95	0.91	0.98	0.95
n_tot_ncs	0.86	0.75	0.86	0.74	0.92	0.85
ln(n_tot_ncs)	0.85	0.74	0.85	0.74	0.91	0.85
ph_h2o	0.94	0.85	0.94	0.85	0.97	0.92
ph_kcl	0.93	0.81	0.93	0.80	0.96	0.89
clay_tot_psa	0.93	0.86	0.93	0.86	0.96	0.93
silt_tot_psa	0.74	0.52	0.74	0.51	0.83	0.68
sand_tot_psa	0.87	0.74	0.86	0.74	0.92	0.85
db_od	0.79	0.70	0.78	0.70	0.88	0.82
dbr	0.99	0.94	0.99	0.94	0.99	0.97
ln(dbr)	0.98	0.93	0.98	0.93	0.99	0.96
caco3	0.95	0.74	0.95	0.73	0.97	0.85
ln(caco3)	0.93	0.81	0.93	0.80	0.96	0.90
wpg2	0.97	0.77	0.97	0.76	0.99	0.88
ln(wpg2)	0.98	0.87	0.98	0.87	0.99	0.93
p_mehlich3	0.96	0.70	0.96	0.69	0.98	0.84
ln(p_mehlich3)	0.90	0.78	0.90	0.77	0.94	0.87
k_mehlich3	0.94	0.82	0.94	0.81	0.97	0.90
ln(k_mehlich3)	0.92	0.83	0.92	0.83	0.95	0.91
ca_mehlich3	0.99	0.80	0.98	0.78	0.99	0.89
ln(ca_mehlich3)	0.99	0.88	0.99	0.86	0.99	0.93
mg_mehlich3	0.98	0.67	0.98	0.63	0.99	0.81
ln(mg_mehlich3)	0.97	0.76	0.97	0.73	0.99	0.86
ec_satp	0.99	0.73	0.99	0.69	1.00	0.83
ln(ec_satp)	0.99	0.78	0.98	0.75	0.99	0.87
cec_sum	0.88	0.73	0.88	0.72	0.93	0.84
ln(cec_sum)	0.89	0.74	0.88	0.73	0.94	0.85

3   Results and discussion

Soil property regression yielded mixed results overall, with the worst performing model achieving mean validation adjusted R^2 of 0.51 (soil silt content), while the top performer scored as high as 0.91 (organic carbon content), indicating that the methodology described, while capable of sufficient of even very good generalization for some soil properties, may not be uniformly applicable to the entire parameter space, at least with respect to the order of magnitude of the number of available target samples. Regression metrics for all targets are listed in Table 2.

Classification modeling yielded poor overall generalization, with a weighted *f1* score over the validation fold of 0.46, while the score over the entire sample space was 0.81, indicating high overfitting. Classification metrics are shown in Table 3, while the relative confusion matrix of the classifier, scatter plots for two of the regressors, as well as the soil texture map produced from the modeled silt, sand and clay contents are shown in Figure 2.

Table 3. Classification metrics over the validation fold and across the entire target dataset, including precision, recall, and f1 score, weighted with class sample size.

	precision	recall	f1
validation	0.47	0.50	0.46
All	0.85	0.81	0.81

A notable deficiency in the described methodology is the static nature of modeling soil properties without regard for the temporal dimension. Soil changes slowly relative to human perception, but it does indeed change, mainly through human activity and increasing change in climate. However, it is difficult to account for time variation when modeling soil at a local (national) level as described, due to low total number of available samples (which is why only a single, static layer was produced for each soil property, even though the target soil samples were collected over a span of 53 years). Consequently, efforts have been made (or are underway) at a continental or wider level (such as the soil layers listed at URL-9) in order to take advantage of
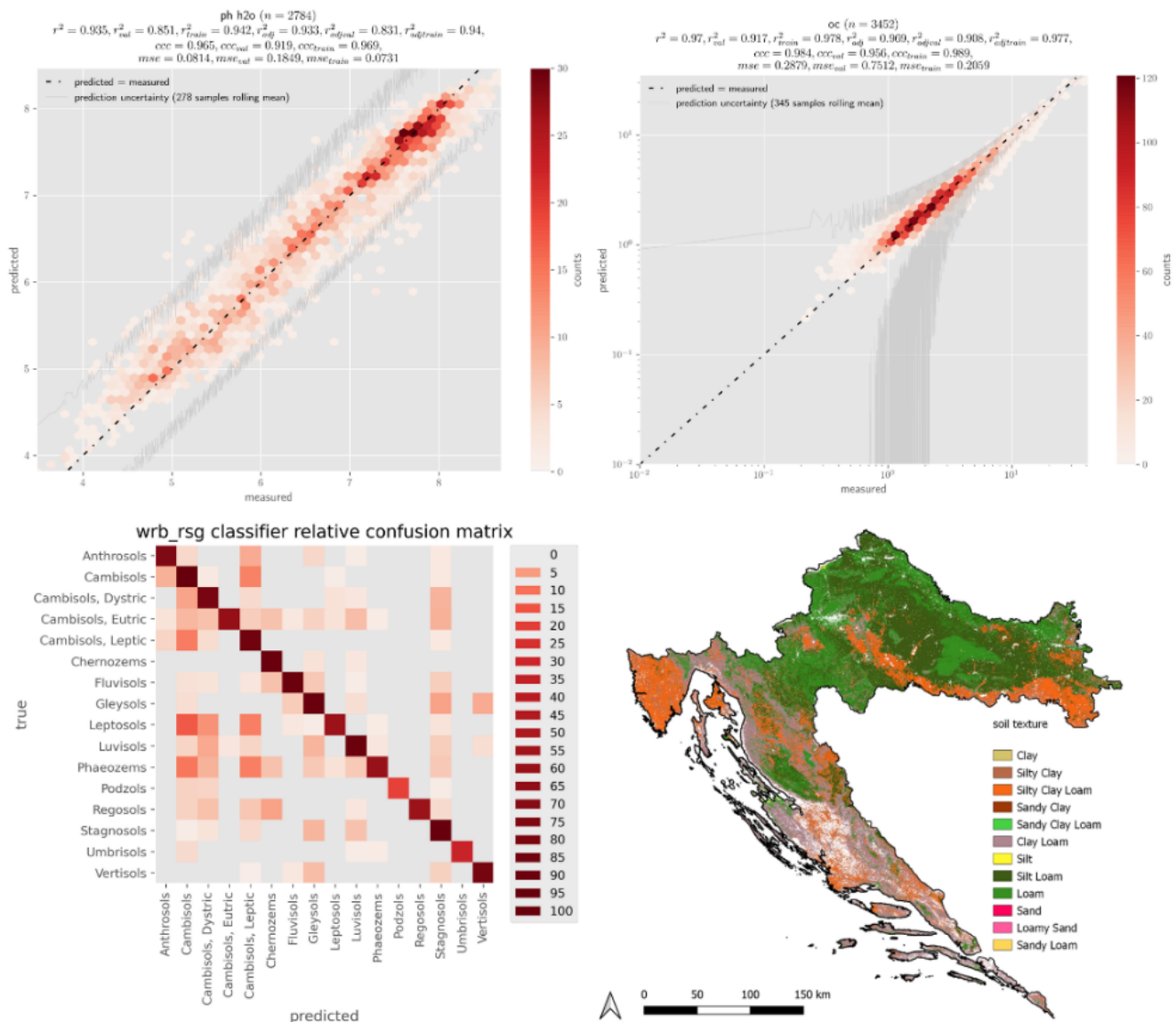

Figure 2. Soil pH prediction scatter and metrics (top left), organic carbon content prediction scatter and metrics - values unpacked from modeled logarithmic target (top right), soil taxonomy prediction relative confusion matrix (bottom left), soil texture classification map (bottom right).

the higher amount of available soil samples over such areas of interest. Additionally, there is notable temporal mismatch between the target data (collected from 1966 to 2016) and covariates (spanning 2000 onward) even in the context of producing a single, current-state dataset. While this was unavoidable due to availability of public soil sampling data in Croatia and the goal of the work to describe the current state of soils nationally, it is reasonable to assume that this affects the overall quality of the results. Further improvement, however, in contexts of both producing a current-state dataset and incorporating temporal dynamics, might come from utilising public soil samples collected in pedological and climatological conditions similar to those in Croatia. Nevertheless, we believe that this approach, which yielded the first public Croatian soil dataset in high spatial resolution, represents a step towards building national capacity for increasingly challenging environmental management.

4 Annex 1: Source code and data products

Source code used to produce the described layers is publicly available at: https://gitlab.com/jkrizan/dsmcroatia, all of the described data products are publicly available at: https://zenodo.org/records/10065971, and a small map portal was built for quick overview of the data products and made available at: http://hrsoil.multione.hr.

5 References

Chen, T., Guestrin, C., 2016. XGBoost: A Scalable Tree Boosting System, In Proceedings of the 22nd ACM SIGKDD International Conference on Knowledge Discovery and Data Mining, 785–794, New York, NY, USA: ACM.

Croatian Geological Institute, 2009. Geological map of the Republic of Croatia M 1:300 000, Croatian Geological Institute, Department of Geology, Zagreb.

Croatian Waters, 2016. Monitoring coordination programme, Zagreb, HR.

GRASS Development Team, 2017. Geographic Resources Analysis Support System (GRASS) Software, Version 7.2., Open Source Geospatial Foundation, https://grass.osgeo.org.

Hengl, T., MacMillan, R.A., 2019. Predictive Soil Mapping with R. OpenGeoHub foundation, Wageningen, NL, 370 pages, www.soilmapper.org.

Lindsay J.B., 2016. Whitebox GAT: A case study in geomorphometric analysis, Computers & Geosciences 95, 75-84.

Martinović, J., Vranković, A. (Editors), 1997. Database of Croatian soils, I. State Directorate for Environment and Nature protection, Zagreb, HR.

Pedregosa, F., Varoquaux, G., Gramfort, A., Michel, V., Thirion, B., Grisel, O., Blondel, M., Prettenhofer, P., Weiss, R., Dubourg, V., Vanderplas, J., Passos, A., Cournapeau, D., Brucher, M., Perrot, M., Duchesnay, E., 2011. Scikit-learn: Machine Learning in Python, JMLR, 12, 2825-2830.

Pekel, J. F., Cottam, A., Gorelick, N., Belward, A. S., 2016. High-resolution mapping of global surface water and its long-term changes, Nature 540 (7633), 418-422.

Pflugmacher D, Rabe A, Peters M, Hostert P., 2019. Mapping pan-European land cover using Landsat spectral-temporal metrics and the European LUCAS survey, Remote Sensing of Environment 221, 583-595.

Radočaj, D., Jurišić, M., Zebec, V., Plaščak, I., 2020. Delineation of Soil Texture Suitability Zones for Soybean Cultivation: A Case Study in Continental Croatia, Agronomy 10, 823.

Romić, M. (Project leader), 2013. Spatial variability of trace and toxic metals in agricultural soils of Croatia, Faculty of Agriculture, Zagreb, HR.

Wilson A.M., Jetz W., 2016. Remotely Sensed High-Resolution Global Cloud Dynamics for Predicting Ecosystem and Biodiversity Distributions, PLoS Biol 14 (3), e1002415.

URL-1: Change in soil carbon stocks and calculation of soil total nitrogen and organic carbon trends and C:N ratios, https://envi-metapodaci.azo.hr/geonetwork/srv/hrv/catalog.search#/metadata/c7980264-97af-41ec-8853-35c7de2f55e6, (Accessed 19 May, 2024).

URL-2: Digital terrain model - Republic of Croatia, National geodetic administration, https://dgu.gov.hr/proizvodi-i-usluge/podaci-topografske-izmjere/digitalni-model-reljefa/180, (Accessed 19 May, 2024).

URL-3: Surface Soil Moisture 2014-present (raster 1 km), Europe, daily - version 1, https://land.copernicus.eu/global/products/ssm, (Accessed 19 May, 2024).

URL-4: Climatologies at high resolution for the earth's land surface areas, https://chelsa-climate.org/, (Accessed 19 May, 2024).

URL-5: Long-term MODIS LST day-time and night-time temperatures, sd and differences at 1 km based on the 2000–2017 time series, https://zenodo.org/records/1435938#.X3Lxm2gzYUE, (Accessed 19 May, 2024).

URL-6: Aerosol Optical Depth - NASA Earth Observatory, https://earthobservatory.nasa.gov/global-maps/MODAL2_M_AER_OD, (Accessed 19 May, 2024).

URL-7: Monthly precipitation in mm at 1 km resolution based on SM2RAIN-ASCAT 2007-2018, IMERGE, CHELSA Climate and WorldClim, https://zenodo.org/records/3256275#.X3L1NmgzYUE, (Accessed 19 May, 2024).

URL-8: Water Vapor - NASA Earth Observatory, https://earthobservatory.nasa.gov/global-maps/MYDAL2_M_SKY_WV, (Accessed 19 May, 2024).

URL-9: Open Environmental Data Cube Europe, https://ecodatacube.eu, (Accessed 19 May, 2024).

Shrub Encroachment and Shrinking of Pastures in Inner and Western Tien-Shan, Kyrgyzstan

Evgenii Shibkov[1], *

[1] University of Central Asia, Graduate School of Development, Mountain Society Research Institute, 125/1 Toktogul Street, Bishkek, 720001, Kyrgyz Republic, evgenii.shibkov@ucentalasia.org
* corresponding author

Abstract: The pastoral tradition in Kyrgyzstan, shaped by the country's landscape, faces significant challenges due to various types of pasture degradation. According to official data from the pasture department, approximately 70% of Kyrgyz pastures are degraded. One type of degradation is the overgrowth of pastures by shrubs, such as caragana, juniper, and wild rose. This encroachment poses a threat to the sustainability of pastoralism, to reduce the pasture areas that are impacting rural livelihoods. Although, some pastures are transforming due to shrub reduction processes, leading to opposite socioeconomic and environmental consequences. At the same time, shrubs benefit pasture ecosystems by aiding biodiversity and soil stabilization. This problem has attracted attention in both government and local community discussions. However, local administrations responsible for pasture management since 2009 cannot effectively address the issue. One contributing factor is the lack of attention from the scientific community, which tends to prioritize more popular topics while neglecting this important issue. Another factor is that the scarcity of spatial data on pasture conditions hinders research efforts. The proposed research aims to enhance understanding by addressing three key questions: firstly, reviewing existing literature to comprehend government and local community awareness in managing shrub encroachment; secondly, exploring broader consequences beyond pasture use, such as ecological and environmental impacts; and finally, integrating spatial and remote sensing data into research methodologies. Achieving these objectives will facilitate the development of effective policies and strategies for managing shrub encroachment and ensuring the long-term sustainability of pastoralism in Kyrgyzstan.

Keywords: remote sensing; pastures; shrub encroachment.

1 Introduction

Mountain pastures are characterized by a complex topography with highly heterogeneous vegetation types, and plant communities play an important role in sustaining rural livelihoods in Kyrgyzstan. Pastoralism has a long history with different management regimes. However, pastoralism in Kyrgyzstan faces pasture degradation problems due to inappropriate grazing management and ongoing climatic changes.

 Mountain pastures are 9.147 million hectares and share 85% of the total agricultural land and 45.9% of the total territory of Kyrgyzstan. However, 70% of pastures are degraded (Pasture Department 2018). Over the past few decades, there has been a significant increase in areas covered by shrubs, leading to pasture degradation due to shrub encroachment. This has become a critical environmental issue in arid and semi-arid mountainous pastures. Shrub encroachment areas are expanded by Juniperus, Rosa, and Caragana shrub species (Figure 1). Expanding Caragana species creates more pasture use concerns, making those seasonal pastures unsuitable for grazing, threatening sustainable pastoralism, and affecting rural communities and the overall economic well-being of Kyrgyzstan.

Nevertheless, shrub encroachment may positively affect pasture ecosystems' multifunctionality and prevent slope soil erosions in mountain pastures.

On the other hand, the shrinkage of native pastures-shrubland-forest mosaics (further shrinkage) may lead to changes in primary vegetation cover and its spatiotemporal dynamics, as well as in environmental and socio-ecological systems. The understanding that strikes a balance between the positive environmental aspects of shrubs and the need to preserve productive grazing areas is essential for the long-term viability of pastoralism in Kyrgyzstan.

Pasture degradation issues in Kyrgyzstan have been widely reported and discussed (Dörre and Kasymov 2021, Tomaszewska and Henebry 2021). Few studies on shrub encroachment focused on the *Caragana* shrub species expansion in the Susamyr Valley of the Chu province from a pasture use perspective. Understanding shrub encroachment and shrinkage's environmental and socio-ecological aspects is critical for predicting vegetation communities that are essential in regulating pasture ecosystem functioning.

There are three main open questions concerning shrub encroachment and shrinkage in mountain pastures in Kyrgyzstan to fill a knowledge gap and show how the proposed research will address them. First, there is a need to understand and obtain information on the socioeconomic and socio-ecological impacts of shrub encroachment, shrinkage, reduced pasture areas, and perceptions of pasture users. Few studies have investigated the perceived impacts of shrub species expansion on pasture users and their livelihoods (Levine et al. 2019). Proposed research on those issues addresses the much-needed gap in understanding the impacts of shrub encroachment as perceived by pasture managers and users with different interests and priorities. Second, assessment and spatial data on shrub encroachment and shrinkage areas by various shrub species in seasonal pastures or vegetation types is crucial. The lack of effective measures and data for assessing and monitoring shrub encroachment at a large spatial scale limits research on the

modelling and simulation of shrub encroachment. Combining vast historical data on pastures with remote sensing data may provide vital data to the existing Kyrgyzstan's land resources database. Moreover, many studies worldwide utilize Geographic Information Systems (GIS) for this type of assessment (Anderson et al. 1996).

and Doboluu ayil aykmaks of Naryn districts of the Naryn region located in the central part of Kyrgyzstan (Inner Tien-Shan). The secondary study site is the pastures of the Chatkal region of the Jalal-Abad province, located in the western part of Kyrgyzstan (Western Tien-Shan) (Figure 2). Both study sites have high district status and hold equal

Figure 1. Shrub encroachment by Juniperus turkestanica (left), Caragana pleiophylla (center) and Rosa turkestanica (right) shrub species in Inner Tien-Shan mountain pastures.

Remote sensing techniques have certain limitations, relying primarily on medium-resolution satellite data (Landsat) and low-resolution (MODIS) (Ovakoglou et al. 2022). However, modern technologies, e.g., Unmanned Aerial Vehicles (UAVs), can overcome these limitations by harnessing cutting-edge data collection techniques for particular complex mountain terrains. Additionally, advanced machine learning algorithms will be employed to effectively classify and segment the remote sensing data, enabling accurate and efficient data interpretation.

Third, there is a lack of studies on the ecological characteristics of shrub species and the ecological implications of shrub encroachment and shrinkage on vegetation communities' structure and functioning, encroachment dynamics, spatial heterogeneity under grazing management, and environmental changes by vegetation types (ecological zones). Understanding the mechanism of shrub encroachment states and stages is crucial for managing and restoring semi-arid highland pastures.

The character of the study is interdisciplinary: to use tools and methods of GIS, remote sensing, and machine learning analyses, the identification, dynamics, mechanisms, and changes of shrub areas will be implemented. The social-economic, socio-ecological, and environmental cause-effect study - combines qualitative and quantitative data to analyse the interaction between the increase of shrubs on land use and their role in pasture management.

2 Materials and methods

2.1 Study Area

This research will be conducted on two study sites. The primary study site is the pastures of Naryn City, Jan-Bulak,

shrub encroachment concerns at different vegetation types. Each site possesses unique vegetation characteristics regarding shrub species diversity, ecological and environmental factors, and land use patterns. This study can comprehensively understand shrub encroachment and shrinkage by comparing diverse areas using standardized methodology and approaches.

2.2 Data Collection and Analysis

Data collection will involve several key parameters: pasture conditions and management, socioeconomic impacts of shrub encroachment. Following Ayil Aymaks (Local Government) selection from each study area, a baseline survey will be conducted in seasonal pastures at various distances from villages. Each pasture will be divided into three main groups depending on seasonal use. The chosen pastures will be randomly stratified based on the data collection results.

This study will apply primary qualitative and quantitative data collection methods and Rapid Rural Appraisal (RRA) tools (Gibbs 1985) at the different level. The theory of adaptive management (Holling 1980) will be used to investigate how farmers adapt to the issue of changing shrub areas. The theory of ecological coupling or resource conflict (Norton 2005) will be used to understand how ecological changes caused by shrub encroachment impact human activities. The results will be evaluated in the last stage by discussing them with local stakeholders, related government institutions, and non-governmental organizations.

Visual measurement of current shrub and pasture species coverage by vegetation types, historical data, GIS, remote sensing technologies, and modern computer science approaches will implement pasture conditions.
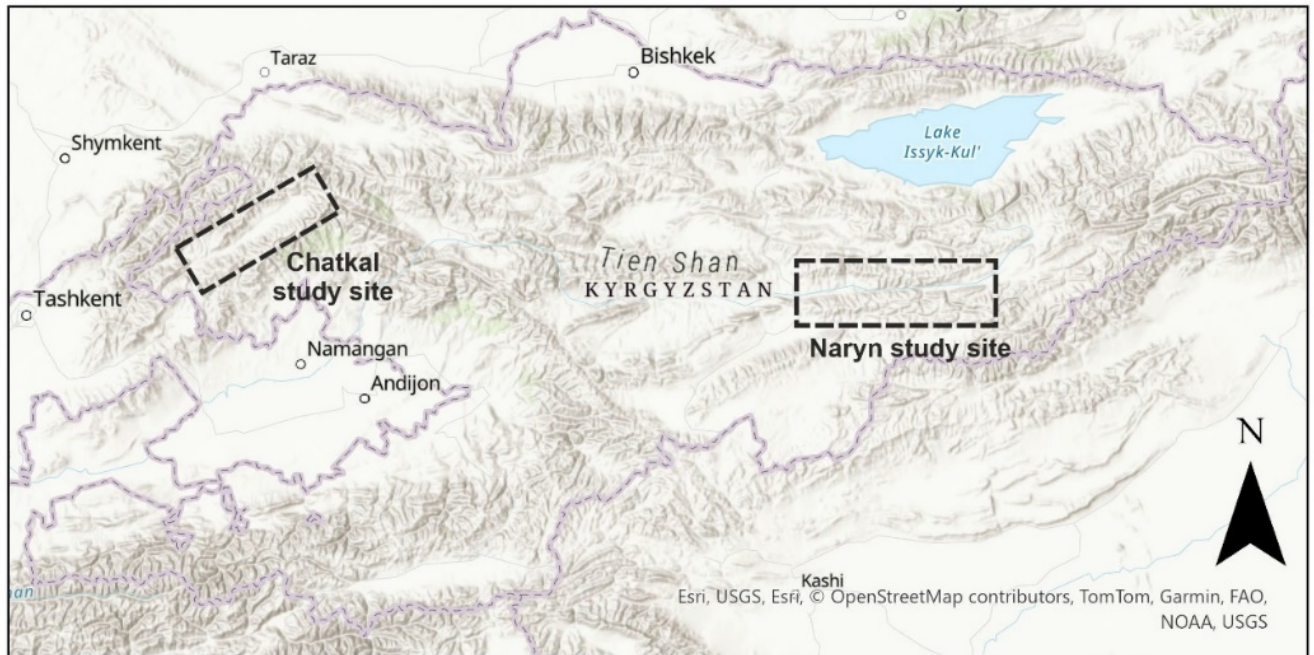
Figure 2. The map of study areas in Inner Tien-Shan and Western Tien-Shan mountain pastures.

Historical observations for the period from 1968 to 2020 will be carried out using available datasets such as Corona, Soviet Union aerial photographs, Landsat imagery, and Sentinel-2 for the same area. The aerial photographs will be obtained using a UAV. The locations of the photo flight will be randomly selected to achieve a representative sample of the shrub encroachment or degradation situation. All fieldwork sampling should cover 1 square kilometre of pastures (100 flights by 1 ha covering each flight). Sentinel-2 satellite images will also be used, with the corrections based on obtained UAV data for around 5000 square kilometres.

The Segment Anything Model (SAM) and U-Net neural networks will be used to acquire remote sensing data segmentation. Training U-Net requires annotations (Lovitt et al. 2022), which involve creating masks for each image that highlight areas occupied by shrubs equally as other objects. The SAM model will annotate historical and modern aerial photographs (Parulekar et al. 2024). The aerial photographs and their corresponding masks will then be converted to a compatible format for further training the U-Net neural network. Once trained, U-Net will be applicable for segmenting Sentinel-2 and historical satellite images.

The Quadrat and Line Point Intercept (LPI) methods will be used to collect ground-based measurements of shrub species (Root-Bernstein and Hoag 2022). A quadrat plot size of 25 m² will be used for shrubs to assess shrub species' ecological attributes and encroachment mechanism. Ground sampling will be performed using LPI techniques described by (Pellant et al. 2020). The collected data will serve as the basis for modelling ecological processes that determine the distribution of shrub species and their changes over time. We will use boosted regression trees (Elith and Leathwick 2017) to identify and quantify the potential factors influencing the likelihood of shrub encroachment and shrinkage. The influencing factors include climatic conditions (temperature and precipitation); terrain features (elevation, slope ratio, and aspect; percentages of natural or secondary shrubland and pastureland; and anthropogenic factors (distances to the nearest road, transitional pasture roads, and seasonal pasture shelters).

3   Expected results

This study is at the very beginning, so now we can talk about the first results where high resolution satellite images were compared of the same territories, but for a different period (Figure 3). The data obtained confirm that shrub area increasing leads to the degradation of pastures. Increasing shrubs density reduces the suitability of pastures for livestock grazing, negatively impacting the livelihoods of local people. Further research will provide important data for making pasture management decisions and understanding impacts on livelihoods.

Study findings can fulfil the shortage of spatial data and mapping material needed to assess and monitor shrub encroachment on a large regional and mountain systems scale by using advanced technologies such as UAVs and machine learning algorithms. This complex approach will contribute to a better understanding of shrub dynamics, facilitate the development of effective management strategies, and contribute to future research in this area. Third, an understanding of the ecological characteristics of shrub species and their influence on the structure and functioning of plant communities and biodiversity. Using a combination of different methods of environmental analysis, not only the predominant species of shrubs will be considered, but also spatiotemporal patterns, modelling the dynamics and mechanism of shrub encroachment and its further consequences and opportunities in sustainable pasture management.
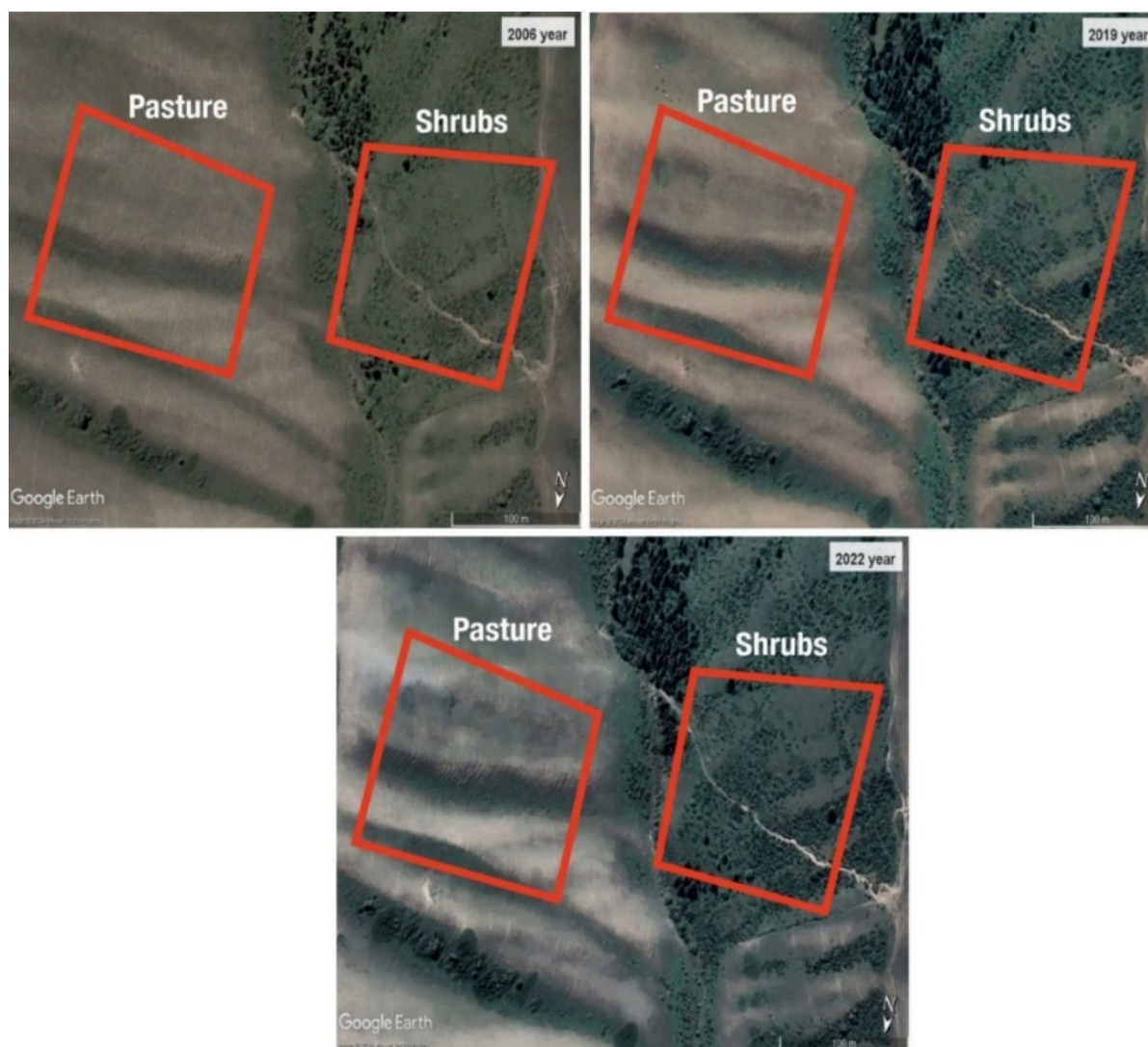
Figure 3. Shrub encroachment on the Naryn study site pastures in July 2006 (top left), July 2019 (top right), and July 2022 (bottom).

The study will analyse the interactions between human activities and ecological changes caused by shrub encroachment by applying theories such as adaptive management and ecological interactions. Furthermore, combined with the latest modern technical solutions, the research is intended to contribute to the diversity and versatility of scientific knowledge on this issue in Kyrgyzstan and the region.

4   Discussion

The expected results of this study should significantly enrich existing knowledge about the degradation of mountain pastures due to shrub growth. This knowledge is critical to understanding not only the socioeconomic impacts but also the socioecological effects caused by invasive shrub growth. Despite widespread discussions on the problem of shrub growth in pastures, many researchers only mention this phenomenon, leaving it badly studied (Andrade et al. 2015). The proposed research focuses on a multifaceted and complex analysis of this issue.

Research directly focused on shrubs is often limited to a superficial understanding based on previous research. A distinctive feature of this research is the use of ultra-high resolution aerial images (1–2 cm per pixel) collected from UAV. It is at variance with previous studies that used medium-resolution remote sensing data (MODIS, Landsat) (Bi et al. 2021). It will also apply advanced machine learning techniques, such as the combined use of neural networks, including SAM and U-Net, for high-precision segmentation of medium-resolution satellite imagery. The data collected during the field ecological survey will certainly provide a more comprehensive approach to understanding the problem of shrub growth.

Unlike other studies that have examined the problem of shrub degradation from the perspectives of land use and socioeconomic consequences, this study will address the potential positive environmental outcomes of this phenomenon, such as soil cover strengthening and increased biodiversity (Ridder et al. 2020). A separate aspect of the proposed research is the study of shrub drying in arid and semi-arid ecosystems, which can lead to changes in the primary vegetation cover and its spatiotemporal dynamics, equally in ecological and socioecological systems. Understanding the balance between the positive ecological aspects of shrub expansion and the need for conservation is essential for mountain pastures.

5 Conclusion

In conclusion, it is important to note that although the issue of pasture degradation to manage shrub growth is current and important, it has not received adequate attention among pasture observers in Kyrgyzstan. However, providing a comprehensive and detailed understanding using an integrated approach to the study of this phenomenon is important not only for understanding its general condition in society, but also for the socio-ecological situation. Using ultra-high-resolution aerial photography data and advanced machine learning techniques, the research objectives offer more detailed and mathematical analysis than the main studies, as well as historical dynamics of shrub growth. Considering the positive overall phenomenon under study brings additional versatility and complexity to this study.

The previous results of this study demonstrate that shrub encroachment directly affects the land use by the local community. However, as this research on the beginning stage, the future results are expected to significantly advance knowledge of the socio-ecological and socio-economic impacts of forest growth, providing valuable information for land management and conservation strategies. By addressing gaps in current research and providing a more holistic view, this research will contribute to the development of evidence-based policies and practices aimed at balancing environmental benefits with the need to consider rangeland management.

6 References

Anderson, G.L., Everitt, J.H., Escobar, D. E., Spencer, N.R., Andrascik, R. J., 1996. Mapping leafy spurge (euphorbia esula) infestations using aerial photography and geographic information systems. Geocarto International 11 (1), 81-89.

Andrade, B.O., Koch, C., Boldrini, I. I., Vélez-Martin, E., Hasenack, H., Hermann, J. M., Kollmann, J., Pillar, V. D., Overbeck, G. E., 2015. Grassland degradation and restoration: A conceptual framework of stages and thresholds illustrated by southern Brazilian grasslands. Natureza e Conservacao 13, 2, 95-104.

Bi, X., Chang, B., Hou, F., Yang, Z., Fu, Q., Li, B., 2021. Assessment of spatio-temporal variation and driving mechanism of ecological environment quality in the Arid regions of central asia, Xinjiang. International Journal of Environmental Research and Public Health 18 (13), 7111.

Dörre, A., Kasymov, U., 2021. User-Based Pasture Management in Kyrgyzstan: Achievements, Challenges, and Trends. XXIV International Grassland Congress / XI International Rangeland Congress (Sustainable Use of Grassland and Rangeland Resources for Improved Livelihoods) 6.

Elith, J., Leathwick, J., 2017. Boosted regression trees for ecological modelling and prediction. R Documentation, 1-22.

Gibbs, C.J.N., 1985. Rapid rural, apppaisal: an overview of concepts and application. International Conference on Rapid Rural Appraisal, 1-16.

Holling, C.S., 1980. Adaptive environmental assessment and management: an overview. Proc. Gulf of Mexico Coastal Ecosystem Workshop, September 1979, Port Aransas Texas.

Levine, J., Isaeva, A., Zerriffi, H., Eddy, I. M. S., Foggin, M., Gergel, S. E., Hagerman, S. M., 2019. Testing for consensus on kyrgyz rangelands: Local perceptions in naryn oblast. Ecology and Society, 24 (4).

Lovitt, J., Richardson, G., Rajaratnam, K., Chen, W., Leblanc, S. G., He, L., Nielsen, S. E., Hillman, A., Schmelzer, I., Arsenault, A., 2022. A New U-Net Based Convolutional Neural Network for Estimating Caribou Lichen Ground Cover from Field-Level RGB Images. Canadian Journal of Remote Sensing 48 (6), 849-872.

Norton, B. G., 2005. Sustainability: A Philosophy of Adaptive Ecosystem Management. University of Chicago Press, Chicago.

Ovakoglou, G., Alexandridis, T. K., Clevers, J. G. P. W., Gitas, I. Z., 2022. Downscaling of MODIS leaf area index using landsat vegetation index. Geocarto International 37(9), 2466-2489.

Parulekar, B., Singh, N., Ramiya, A. M., 2024. Evaluation Of Segment Anything Model (SAM) For Automated Labelling in Machine Learning Classication of UAV Geospatial Data.

Pasture Department., 2018. Information on pastures of KG.

Pellant, M., Shaver, P. L., Pyke, D. A., Herrick, J. E., Lepak, N., Riegel, G., Kachergis, E., Newingham, B. A., Toledo, D., Busby, F. E., 2020. Interpreting Indicators of Rangeland Health, Version 5. Tech Ref 1734-6, Issue 5.

Ridder, R., Azamat, I., Ulan, K. 2020., Transformation in pasture use in kyrgyzstan. What are the costs of pasture degradation? In Encyclopedia of Climate Change: Volume 11: (11 Volume Set).

Root-Bernstein, M., Hoag, C., 2022. Does shrub encroachment reduce foraging grass abundance through plant-plant competition in Lesotho mountain rangelands? PeerJ 10, e13597.

Tomaszewska, M. A., Henebry, G. M., 2021. Remote sensing of pasture degradation in the highlands of the kyrgyz republic: Finer-scale analysis reveals complicating factors. Remote Sensing 13 (17), 3449.

Tsatsenkin, I. A., 1974. Guidelines for geobotanical and cultural and technical inspection of natural pasture lands (In Russian). All-Union Institute of Fodders named by V.R. Williams.

Forest Storm Damage Detection Using EO Data and Machine Learning

Damir Klobučar[1],*, Ivan Pilaš[2]

[1] Croatian Forests Ltd., Ivana Meštrovića 28, 48000 Koprivnica, Croatia, damir.klobucar@hrsume.hr

[2] Croatian Forest Research Institute, Division of Ecology, Cvjetno Naselje 41, 10450 Jastrebarsko, Croatia, ivanp@sumins.hr

* corresponding author

Abstract: Forests are threatened by various harmful abiotic and biotic influences. Increased frequency of wind disturbances because of climate change represents the main source of damage in European forests. In a relatively short time, stormy winds can destroy large forest areas and thereby disrupt regular management. The main damage is fallen, broken, and permanently bent trees which usually occur together. These damages in the forest vary in intensity and scale, from complete damage on larger and smaller areas to group damage as well as damage to individual trees. Therefore, the effective detection and mapping of the described damages is extremely important for forest management. The thunderstorm which hit the continental Republic of Croatia in July 2023 caused enormous damage to forests in terms of area and intensity. Consequently, the aim was to use the example of this event to contribute methodologically to the assessment of the extent and intensity of damage using EO data and the appropriate machine learning algorithm. The manuscript investigates and presents the advantages and possibilities of detecting and mapping damage in the forest at three spatial scales (multi-scale assessments): state, regional and forest management unit, as well as at different degrees of damage. The presented methodology and obtained results provide useful information about the scale and intensity of damage for a wide range of users.

Keywords: forest damage; storm; earth observation; machine learning.

1 Introduction

Due to climate change, we are witnessing more and more frequent extreme weather events. In this sense, damage to forests from floods, ice, snow and wind is becoming more and more significant from a forest management perspective (Stanturf 2024). Of the abiotic factors, the most significant harmful effect is the wind (Gardiner et al. 2013, Kislov and Korznikov 2020). From the point of view of forest management, wind is significantly different from a storm. The basic characteristic of a storm or hurricane is a wind whose strength exceeds 8 Beaufort (> 17 m/s; > 60 km/h). Storm winds with movement faster than 8 Beaufort can cause great damage. In a short time, usually in a few minutes, they destroy large forest areas and cause major disruptions in management. Damages are threefold and usually occur together; these are windbreaks, fallen trees and permanently bent trees (Vajda 1974). To what extent the forest (structure) will be resistant to the force of the storm wind, depends on the condition of the habitat, vertical and horizontal structure, mixture, type of trees,

age, health and other environmental conditions (Ulanova 2000, Dalponte et al. 2020).

In continental Croatia, storms that cause material damage most often occur in weather situations with the appearance of clouds of strong vertical development with stormy winds, a large amount of precipitation of a short duration, and sometimes hail (Bajić 2008). Just such a thunderstorm hit the continental part of the Republic of Croatia (RC) on July 19, 2023, and on its way from the west to the east of the country caused enormous material damage (Figure 1). The most violent gusts of wind up to 180 km/h (11th and 12th Beaufort scale, severe storm and hurricane) accompanied by extremely heavy rain were recorded in the eastern part of the country, where catastrophic damage to forests occurred.
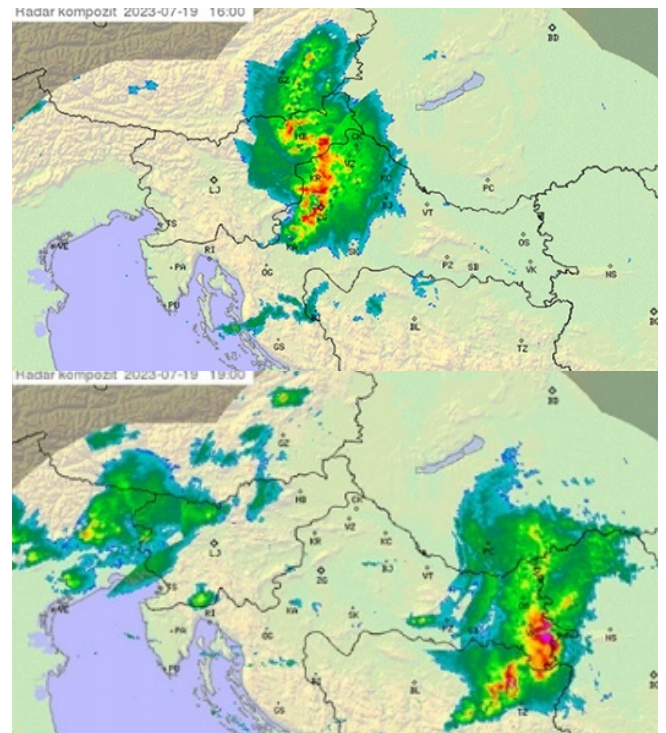
Figure 1. Radar composite: over part of northwestern RC on 07/19/2023. at 4 p.m. (top) and above over eastern RC at 7 p.m. (bottom). Source: https://meteo.hr/.

In the period of organized forest management, going back more than 250 years, no storm of this scale was recorded. In a relatively short time, the storm caused catastrophic damage to large forest areas and thus disrupted regular management. These damages in the forest are of different intensity and scale, from complete and partial damage on larger and smaller areas to damage on individual trees. From an economic point of view, the described damages

represent a significant economic loss and in this case are of primary importance. Damage detection and assessment are critical and fundamental procedures in the process of forest management after a natural disaster (Chirici et al. 2018, Hamdi et al. 2019, Dalponte et al. 2020). Namely, damages must be quickly identified and mapped in order to ensure the choice of adequate procedures and dynamics in wood harvesting and forest restoration. In this sense, Earth Observation (EO) data are more than suitable, and to date various data sources and methodological approaches have been used for this purpose (Einzmann et al. 2017, Rüetschi et al. 2019, Dalponte et al. 2020, Pilaš et al. 2020).

In the RC, this issue has not been sufficiently investigated, nor has an official operational methodology for the application of EO in damage assessment been developed (Šimić et al. 2015, Pilaš et al. 2020). Therefore, this manuscript investigates the operational methodology of assessing the scale (hectares) and intensity (degrees) of damage in the forest, using available EO data and machine learning.

2   Materials and methodology

2.1   Research area

The research area refers to the continental part of the Republic of Croatia and includes forest complexes that were hit by the described storm (Figure 1). The assessment of forest damage was carried out at several levels: country, regional and local spatial scale.

2.2   Country scale assessment

The first step in the detection of damaged forest areas was the comparison of satellite imagery immediately before and after the event according to the "Change detection" principle. The aim of the analysis was the preliminary determination of possible forest damage, which should then be verified by field observation. For this purpose, Sentinel-2 (S-2), surface reflectance images with a small percentage of clouds from the period immediately before (July 1– July 18, 2023) and after (July 20 – August 1, 2023) the natural disaster were used. For each of the mentioned periods, cloud masking was first performed, and then mosaic imagery was created based on the median values of pixels for each band. On the obtained mosaic imagery, the Green Leaf Index (GLI) was calculated according to the formula:

$$GLI = \frac{((GREEN - RED) + (GREEN - BLUE))}{((2 * GREEN) + RED + BLUE))} \quad (1)$$

The GLI index used was aimed at detecting differences in vegetation cover changes based primarily on the color change that occurs due to the disruption of the forest stands when the reflection from the bare surface under the disturbed forest canopy comes to the fore. The GEE platform was used for this purpose.

2.3   Regional scale assessment -Forest administration unit

Country scale assessment (2.2) was used to identify areas of interest and represented the initial step towards a more detailed regional analysis of damage. On the country spatial scale, the most significant areas with damages in the continental part of the RC were singled out (Figure 2, Frames: 1-4). For more precise analysis and damage mapping, the area of the Spačva basin, which belongs to the Vinkovci forest administration and includes forest areas of about 70,000 hectares, was selected (Figure 2, Frame 1). For this purpose, a standard machine learning framework was used in which S-2 composite imagery before and after the windstorm served as predictor variables. On the S-2 data, random sampling was carried out on areas where damage was visible and on a part of areas without visible signs of windstorm. In this way, 1242 samples were collected, of which 848 were set aside for training and 394 for testing. To create the model, the Random Forest (RF) algorithm was used, which proved to be one of the most effective and reliable in supervised learning of remote sensing data (Maxwell et al. 2018, Whyte et al. 2018). Standard validation methods on the test set were used to evaluate the implemented binary classification (damage/no damage): test accuracy, confusion matrix, Kappa, Consumers accuracy and Producers accuracy (Olofsson 2014). The developed RF algorithm was then used to predict forest damage in the entire area of the forest administration unit.

2.4   Local scale assessment - Forest management unit

Mapping of damage at the local level, or at the level of the forest management unit, was done with the aim of providing operative support for forest management in the regeneration of damage from storm. For this purpose, five damage classes were defined, depending on the proportion of damaged trees within the stand (Classes: A: 0–10%; B: 10–20%; C: 20–50%; D: 50–80%; E: 80–100%). The set for training and validation, as a necessary segment of the machine learning pipeline, was created based on a visual assessment of damage at several points, from an updated very high-resolution image in Google Earth Pro, which was updated immediately after the windstorm and on which it was possible to recognize visible signs of damage to stands. A total of 84 points were selected, of which 71 were used for training and 13 for validation. To build a multiclass RF model, the same methodology and evaluation metrics were used as described in section 2.3, except that due to the small number of samples, the confusion matrix and class-oriented evaluation were not considered.

3   Results and Discussion

By analyzing satellite S-2 imagery based on the differences between the GLI index before and after the storm, areas with potential damage from storm were detected (Figure 2). After the preliminary selection of areas with potential damage, contact was made with the forestry operation, and in most cases the occurrence of forest damage in the detected areas was confirmed.

A further, more detailed assessment of damage from storm was made for the area of the Spačva basin in the eastern part of the RC (Figure 2, Frame 1), where the forest economic complexes were singled out. The verification of the RF model at 394 test points confirmed the very high

reliability of the assessment, i.e. test accuracy of 0.96 (96%) and Kappa 0.93. The confusion matrix of binary classification confirmed that the RF model has a very small proportion of incorrectly estimated samples, i.e. only 3 false negatives and 11 false positives (Table 1).
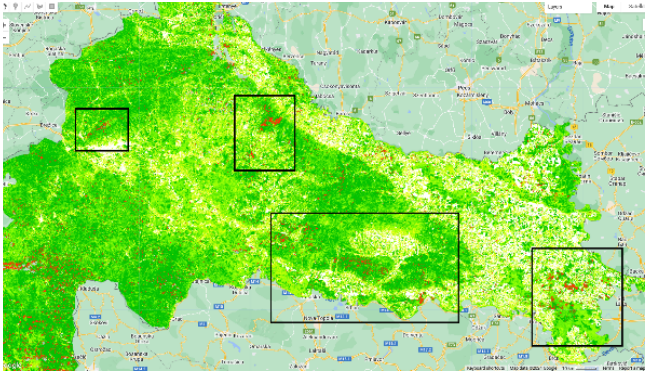
Figure 2. The continental part of RC with isolated potential locations with forest damage. Locations marked in red are highlighted on the recordings; (1) area of lowland forests - Spačva basin, (2) area of Slavonsko gorje (3) area of Bilogora and (4) Zagrebačka gora.

Producers' accuracy or a probability that a particular sample of the class is mapped as the same class in the classification map is 0.95 for positive category (Damage) and 0.98 for negative category (No damage). The consumer's accuracy, i.e. the accuracy of the map from the point of view of a map user is 0.98 for the positive category (Damage) and 0.94 for negative category (No damage). The achieved results are comparable to previous research (Einzmann et al. 2017, Hamdi 2019, Kislov and Korznikov 2020, Dalponte et al. 2020).

Table 1. Confusion matrix of binary classification with Random Forest algorithm.

		Actual values	
		Positive (Damage)	Negative (No damage)
Predicted values	Positive (Damage)	198	11
	Negative (No damage)	3	182

The developed RF was then used for the prediction and calculation of the forest areas affected by the storm for the entire Vinkovci forest administration (Figure 3 top). The total area of damaged forests was 11,929 hectares, which is about 15% of the total forest administration area of 77,199 hectares.

Validation of the created RF model for the multiclass classification of forest damages according to categories of forest cover damage (Classes: A: 0–10%; B: 10–20%; C: 20–50%; D: 50–80%; E: 80–100%) on the test data set confirmed the reliability of the assessment of 54% (total accuracy), in total for all classes and Kappa of 0.4. The above results are given preliminary. Although the achieved level of reliability of the assessment is significantly lower compared to binary classification, the results confirm the

effectiveness of the mentioned approach with the need for additional improvement, especially in terms of increasing the number of sample points. This is in accordance with the suggestions of Maxwell et al. (2018) on the meaning of sample size and quality in relation to the applied algorithm.

Subsequent checks in the field have established that the created model quite well observes changes in the state of the forest cover and degrees of damage, and as such is justified for operational use, which can significantly simplify and speed up work in the field related to damage analysis and planning of silvicultural operations. For this reason, a prediction of forest damage classes was made for the selected area (Figure 3 bottom) and put into operational use (Mergin maps).
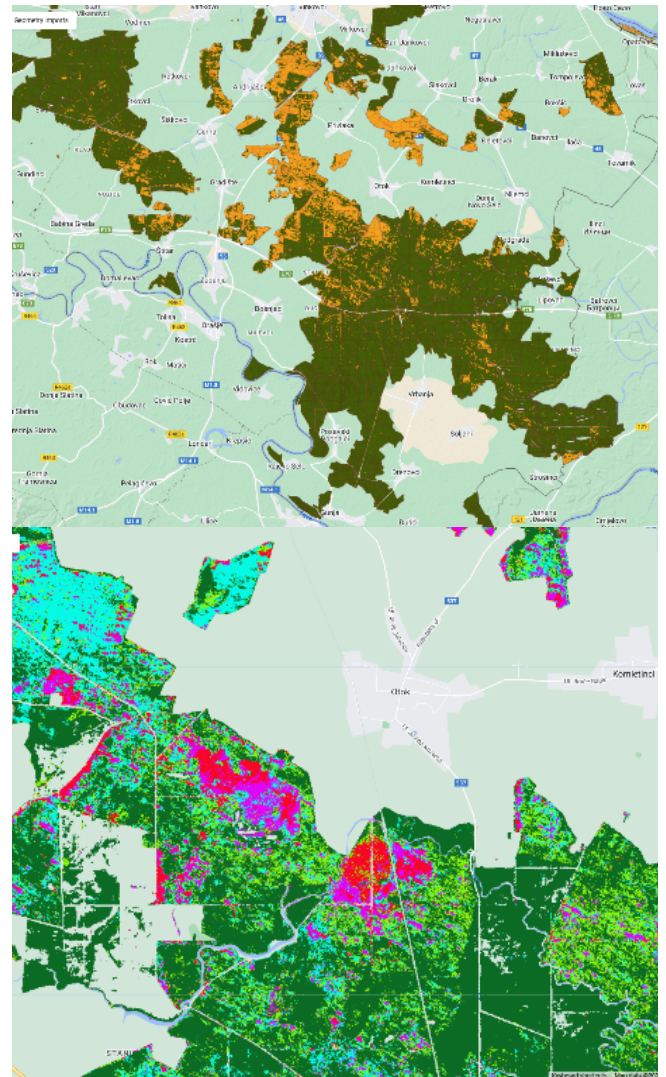
Figure 3. Prediction map of storm damage (brown color) in the Vinkovci forest administration area (top) and prediction of forest damage levels based on Sentinel-2 images and the RF model (bottom).

4   Conclusions

Forests are increasingly affected by adverse weather conditions. The storm from July 2023 is the last event with catastrophic consequences for the forests of continental of the RC. Therefore, the aim of this manuscript was to use the

example of the described event to provide a methodological contribution to the assessment and mapping of the extent and intensity of damage using EO data. For this purpose, three spatial scale assessments and mapping of damage in forests are presented. In the first country scale assessment, potential areas of application of S-2 data and change detection approach were detected. In the second, regional scale assessment, more detailed and accurate damage mapping was carried out. In the isolated area (eastern part of the RC), the analysis of forest damage using the RF algorithm and the multiband S-2 predictor before and after the windstorm, showed that using the mentioned approach it is possible to carry out very precise and reliable mapping of damaged forest areas. Damage mapping at the economic unit level (forest management unit) was carried out with the aim of providing support for operational works. Despite the slightly lower accuracy (primarily due to the small sample), the field check found that the created map gives a good and very realistic assessment of the five levels of damage. Therefore, this damage map was added as a layer to the information system (Mergin Maps) for the purpose of operational work in the forest.

5 References

Bajić, A., 2008. Olujni vjetar u Hrvatskoj. Zagreb.

Chirici, G., Bottalico, F., Giannetti, F., Del Perugia, B., Travaglini, D., Nocentini, S., ..., Gozzini, B., 2018. Assessing forest windthrow damage using single-date, post-event airborne laser scanning data. Forestry: An International Journal of Forest Research 91 (1), 27-37.

Dalponte, M., Marzini, S., Solano-Correa, Y.T., Tonon, G., Vescovo, L., Gianelle, D., 2020. Mapping forest windthrows using high spatial resolution multispectral satellite images. International Journal of Applied Earth Observations and Geoinformation 93, 102206.

Einzmann, K., Immitzer, M., Böck, S., Bauer, O., Schmitt, A., Atzberger, C., 2017. Windthrow Detection in European Forests with Very High-Resolution Optical Data. Forests 8 (1), 21.

Gardiner, B., 2013. Introduction. In: Gardiner B., Schuck, A., Schelhaas, M. J., Orazio C., Blennow, K., Nicoll, B. (Eds.), Living with storm damage to forests, European Forest Institute, Joensuu, Finland, pp. 11-14.

Hamdi Z.M., Brandmeier, M., Straub C., 2019. Forest Damage Assessment Using Deep Learning on HR Remote Sensing Data. Remote Sensing 11 (17), 1976.

Kislov, D.E., Korznikov, K.A., 2020. Automatic Windthrow Detection Using VH Resolution Satellite Imagery and Deep Learning. Remote Sensing 12 (7), 1145.

Maxwell, A. E., Warner, T. A., Fang, F., 2018. Implementation of machine-learning classification in remote sensing: An applied review. International Journal of Remote Sensing 39 (9), 2784-2817.

Olofsson, P., Foody, G. M., Herold, M., Stehman, S. V., Woodcock, C. E., Wulder, M. A., 2014. Good practices for estimating area and assessing accuracy of land change. Remote sensing of Environment 148, 42–57.

Pilaš, I., Gašparović, M., Novkinić, A., Klobučar, D., 2020. Mapping of the Canopy Openings in Mixed Beech–Fir Forest at Sentinel-2 Subpixel Level Using UAV and Machine Learning Approach. Remote Sensing 12 (23), 3925.

Rüetschi, M., Small, D., Waser, L.T., 2019. Rapid Detection of Windthrows Using Sentinel-1 C-Band SAR Data. Remote Sensing 11 (2), 115.

Stanturf, J.A., Conner, W., Coyle, D.R., Scott, G., 2024. Forest disturbances, McNulty, S. G. (Ed.), Future Forests, Elsevier, 2024, pp. 125-150.

Šimić Milas, A., Rupasinghe, P., Balenović, I., Grosevski P., 2015. Assessment of Forest Damage in Croatia using Landsat-8 OLI Images. South-east European forestry: SEEFOR 6 (2), 159-169.

Ulanova, N.G., 2000. The effects of windthrow on forests at different spatial scales: a review, Forest Ecology and Management 135 (1-3), 155-167.

Vajda, Z., 1974. Nauka o zaštiti šuma. Zagreb.

Whyte, A., Ferentinos, K.P., Petropoulos, G.P., 2018. A new synergistic approach for monitoring wetlands using Sentinels -1 and 2 data with object-based machine learning algorithms. Environmental Modeling & Software 104, 40-54.

Protecting Biodiversity: Empowering Engagement through Interactive Maps

Maja Maslać Mikulec[1],*, Karla Čmelar[1]

[1] Geonatura Ltd. Consultancy in Nature Protection, Zagreb, Croatia, mmmikulec@geonatura.hr, kcmelar@geonatura.hr
 * corresponding author

Abstract: Biodiversity conservation heavily relies on protected areas, with Natura 2000 serving as a network safeguarding Europe's most valuable and threatened species and habitats. Assessment of acceptability for ecological network is integral to Environmental Impact Assessments (EIAs), mandated by the 1998 Aarhus Convention, which advocates for inclusive, accessible, and transparent environmental decision-making. However, the complexity of EIA documents often poses challenges, rendering them inaccessible even to experts. To address this, digital initiatives are emerging to streamline EIAs, with interactive maps playing a key role in enhancing communication and stakeholder engagement. Utilizing the abundant spatial data generated by biological research, increasingly processed using Python or R, we present a dataset collected for an EIA alongside a potential interactive, user-friendly map using open-source options.

Keywords: nature protection; R markdown; environmental impact assessment; open-source tools; mapview.

1   Introduction

Biodiversity is essential for the processes sustaining life on Earth, including humans. To conserve biodiversity, the European Union has made extensive biodiversity conservation efforts establishing the extensive Natura 2000 ecological network of protected areas, one of the largest networks of conservation areas worldwide (Maiorano et al. 2015). When a new plan or project is likely to have a significant negative effect on a Natura 2000 site, to get it approved it must follow a specific procedure (EC 2017). This assessment of acceptability for ecological network is an integral part of Environmental Impact Assessments (EIAs), which ensures that environmental concerns are considered from the very beginning of a project. The procedure also allows the public to actively engage in the EIA procedure, which is mandated by the 1998 Aarhus Convention, advocating for inclusive, accessible, and transparent environmental decision-making. However, these documents are often criticised for being an administrative burden, ending with a bloated, inconsistent and inaccessible report replete with technical jargon that is difficult to navigate and understand (Digital EIA Project Partners 2020). An example is the UK's Environmental Statement for High Speed Two Phase 1 which stood at over 50,000 pages (Digital EIA Project Partners 2020).

With digital technology being promoted to create widely accessible and engaging information sources, it is no surprise that in recent years progressive digital reporting approaches have been adopted by environmental and engineering consultancies to digitalize EIA public-facing reports (Northmore et al. 2022). The main benefits of this approach include (RPS 2024, WSP 2024): (1) transforming a complex and lengthy document into a user-centric format that is easier to digest and navigate for local planning authorities, communities and stakeholders; (2) presenting information in a more clear and user-friendly way, igniting more effective public participation in the planning process; and (3) more clearly representing the key environmental effects of infrastructure and development, thus supporting quicker and more efficient decision making. Digital EIAs are the future, but like any new technology or product, they cannot be integrated into the planning system overnight. Therefore, best practice examples and lessons learned from prototypes should be widely shared to raise standards and promote innovation across the community (WSP 2024).

In addition to more accessible, user-friendly and comprehensible format, digital EIA provides a method to reduce environmental impacts of these projects. A recent wind farm development project in Croatia, which included a comprehensive fieldwork data collection, produced a massive EIA document totalling almost 1,000 pages. Ten copies of this document (in total 10,000 pages) were printed solely for the advisory expert committee, producing the emission of 6 kg of CO_2. This inspired us to make a prototype project using some of the data collected during this project to investigate communication of the main results in a digital environment and with the use of interactive maps.

In this project, we utilized open-source tools commonly used by biologists, to present how the shift towards digital EIA can be made as simple and with as little cost as possible. Our prototype focused on habitats, birds and large carnivores, each representing different data types, to evaluate different approaches for data presentation. With this prototype, we aim to demonstrate a quicker, simpler and more accessible way of assessing environmental effects.

2   Materials and methods

This prototype study entailed the conceptualization of a hypothetical wind farm comprising twelve turbines, devoid of association with any actual wind farm endeavour. Furthermore, for evaluation purposes, this hypothetical wind farm was situated proximate to four Nature 2000 sites, encompassing two Special Areas of Conservation (SAC) and Special Protection Areas (SPA), all of which were also hypothetical in nature. To facilitate comprehension and streamline analysis, only habitat data and data derived from field research on large carnivores and birds were utilized from a real wind farm baseline study (Geonatura's internal database). Utilizing the R programming language

(R Core Team 2024) a digital document in HTML format was generated using the "rmarkdown" package (Allaire et al. 2024) to enable interactive mapping and visualization. Processing of raster and vector data was accomplished by employing various packages including "sf" (Pebesma and Bivand 2023), "sp" (Bivand et al. 2013) and "raster" (Hijmans 2024). Vector data were displayed in the form of points, lines and polygons on which popup views were added. Interactive mapping functionalities were implemented using the "leaflet" (Graul 2016), "leafem" (Appelhans 2023), "mapview" (Appelhans et al. 2023) packages, with "leafpop" (Appelhans and Detsch 2021) utilized for the integration of graph, table, and image popups onto map layers. Graphical representations were generated using the "ggplot2" (Wickham 2016) package, complemented by "plotly" (Sievert 2020) package to integrate interactive features into the generated graphs.

3   Results

A digital document was created in HTML format providing a quicker, simpler and more accessible way of assessing environmental effects. To facilitate better navigation, interactive tabs were organized according to biodiversity groups (habitats, birds, and large carnivores), with the section about large carnivores further subdivided into tabs (Figure 1). Interactive maps featured multiple layers (wind turbine location, SCI and SPA areas, habitat, primary bird heatmap, overflights (Short-toed Snake-Eagle, Western Marsh-harrier and Golden Eagle) and camera traps locations), allowing users to toggle specific layers, zoom, and change base maps. The ability to switch base maps enabled map element inspection with different backgrounds without resetting the zoom or display position. Maps where spatial and non-spatial data were joined through popup windows were created. Table and plot popups allowed a combination of temporal and spatial data (Figure 2). Additionally, a map with raster and vector data on the same display was created, which was especially useful for bird data (Figure 3). However, presenting extensive data in a single interactive map increased computation time, prolonging HTML generation and making error correction and text modifications difficult.
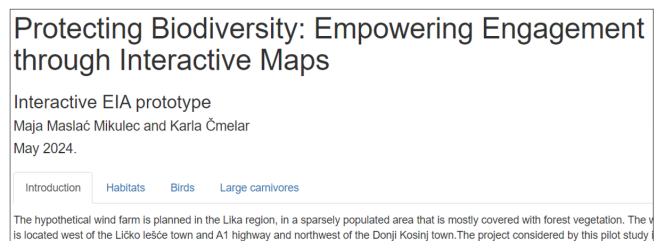

Figure 1. The appearance of main tabs of the pilot study.

4   Discussion

The interactive tab sections were beneficial as they segmented the text into smaller, more manageable sections, enhancing content acquisition and document navigation. Manipulating the basemap provided multiple views of the same data while maintaining zoom stability during basemap changes. Popup features further enhanced the interactive maps by consolidating data that would traditionally be spread across multiple pages into a single display. The mapview and leaflet packages are used for interactive, simple, and quick mapping so they have limitations, particularly regarding performance with large datasets, advanced customization, and in-depth spatial analysis. But this was not considered a significant disadvantage, since when comparing extensive with simpler interactive maps, Vincent et al. (2018) found that better spatial planning decisions were made using the simpler interactive maps. Also, interactive maps with fewer layers were faster to load and easier to compute, thus reducing the HTML production time compared to maps with more layers. To avoid this problem, one approach would be to first create the HTML document with text, ensuring there are no typographical errors, and then generate maps and all map features in a separate script. Once the document's text and maps are finalized, they can be combined into a single file. In this prototype study, the R programming language in the RStudio environment was used due to its simplicity and popularity among biologists, despite its decreased performance with large datasets. Depending on the study and data volume, Python is preferred for handling large datasets and computationally intensive tasks.

With all the benefits of digitalizing EIAs and interactive maps, available literature shows that digital EIA adoption is curtailed by four primary barriers (IEMA 2023): (1) EIA staff's lack of digital competency; (2) lack of standardization of digital EIA approaches, technology, and methods; (3) regulatory challenges; (4) and the increased cost to the proponent. Therefore, we have shown that there is a way of providing EIA information using available open-source tools, in a programming language most used by biologists, to try to tackle at least some of the curtailments.

Consequently, producing this type of digital document containing large amounts of data and maps with multiple layers could demand extended programming skills which could be challenging. However, programming skills are increasing among various disciplines and these challenges could be overcome using other programming languages and tools. On the other hand, at least in some transitional period to a digital EIA, interactive maps alone could be a separate digital document which could be used as a supplement to the main EIA study. Nevertheless, to lower the environmental impact of excess printing, we advocate for a change of regulations, so it is no longer necessary to submit printed copies of EIAs.

Other challenges should also be undertaken to ensure an effective implementation of digital EIAs, such as (IEMA 2020): setting and implementing new data standards (GIS); exploring ways to process the vast amounts of open data; collaborating with specialists in other fields to bring innovation; engaging with creative industries (marketing and communication professionals to explore new ways of presenting information); creating practical guidance on applying digital working throughout the EIA process. Moreover, we should consider ways of presenting important, but sensitive data (e.g. locations of eagle nests,

caves), which should not become completely public during an EIA process.
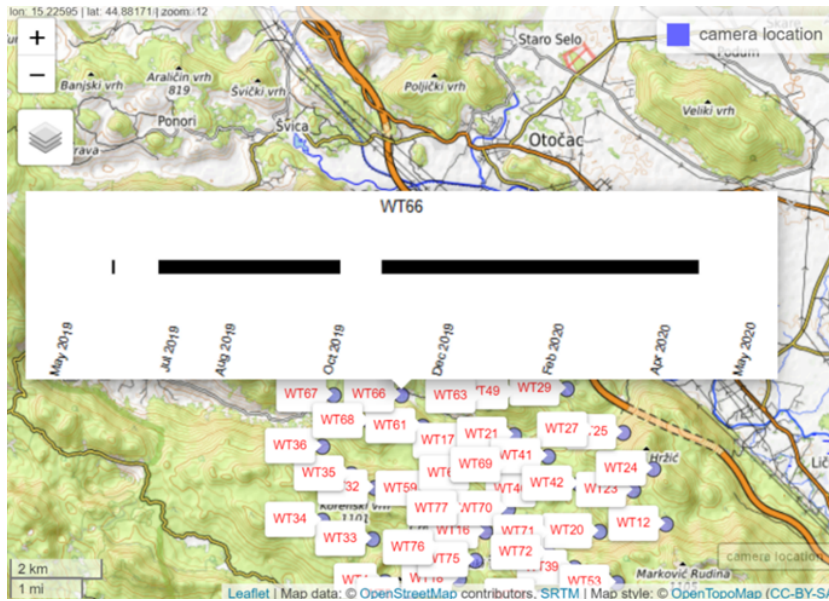
Figure 2. The interactive map of camera trap data with graph popup.
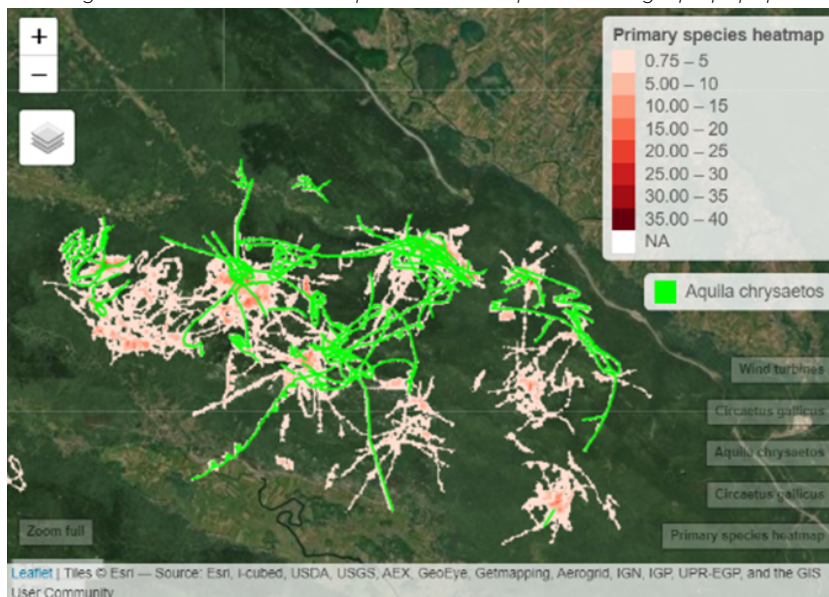
Figure 3. The interactive map with vector and raster data combined.

5   Conclusions

In the climate crisis, making sure the Environmental Impact Assessment process is efficient, effective and accessible is more important than ever (Digital EIA Project Partners 2020). With the growing amount of data, spatial complexity and size of assessment documents they are becoming challenging to truly comprehend, thus disabling the implementation of the 1998 Aarhus Convention. Also, due to regulatory standards, in many countries, like Croatia, it is still necessary to print these huge documents, adding on the environment impact. Here we presented a digital EIA prototype with interactive maps, made with widely used open-source tools, to show how easy (and not necessarily costly) it is to start transferring to the inevitable future of digital EIAs, with all its benefits.

6   References

Aarhus Convention, 1998. Convention on Access to Information, Public Participation in Decision-making and Access to Justice in Environmental Matters (6586). The Stationery Office.

Allaire, J. J., Xie, Y., McPherson, J., Luraschi, J., Ushey, K., Atkins, A., Wickham, H., Cheng, J., Chang, W., Iannone, R., 2020. rmarkdown: Dynamic Documents for R, https://github.com/rstudio/rmarkdown. (Accessed 13 June, 2024)

Appelhans, T., 2023. _leafem: 'leaflet' Extensions for 'mapview'_. R package version 0.2.3, https://CRAN.R-project.org/package=leafem. (Accessed 13 June, 2024)

Appelhans, T., Detsch, F., Reudenbach, C., Woellauer, S., 2023. mapview: Interactive Viewing of Spatial Data in R. R package version 2.11.2, https://git hub.com/r-spatial/mapview. (Accessed 13 June, 2024)

Appelhans, T., Detsch, F., 2021. _leafpop: Include Tables, Images and Graphs in Leaflet Pop-Ups_. R package version 0.1.0, https://CRAN.R-project.org/package=leafpop. (Accessed 13 June, 2024)

Bivand, R., Pebesma, E., Gomez-Rubio, V., 2013. Applied spatial data analysis with R, Second edition. Springer, NY. https://asdar-book.org/. (Accessed 13 June, 2024)

Digital EIA Project Partners, 2020. Digitising the Environmental Impact Assessment (EIA) Process: A user-centred approach to designing an EIA process for the future. United Kindom.

European Commission (EC), Directorate-General for Environment, 2017. Natura 2000 and spatial planning, Publications Office.

Graul, C., 2016. leafletR: Interactive Web-Maps Based on the Leaflet JavaScript Library. R package version 0.4-0, http://cran.r-project.org/package=leafletR. (Accessed 13 June, 2024)

Hijmans, R., 2024. raster: Geographic Data Analysis and Modeling. R package version 3.6-27, https://rspatial.org/raster. (Accessed 13 June, 2024)

IEMA, 2020. Digital Impact Assessment: A Primer for Embracing Innovation and Digital Working. UK.

IEMA, 2023. Digital EIA: When does the future become the present?, https://www.iema.net/articles/digital-eia-when-does-the-future-become-the-present. (Accessed 12 May, 2024)

Maiorano, L., Amori, G., Montemaggiori, A., Rondinini, C., Santini, L., Saura, S., Boitani, L., 2015. On how much biodiversity is covered in Europe by national protected areas and by the Natura 2000 network: insights from terrestrial vertebrates: Biodiversity Conservation in Europe. Conservation Biology 29, 986-995.

Northmore, L., Hudson, M., 2022. Digital environmental impact assessment: An exploration of emerging digital approaches for non-technical reports. Environmental Impact Assessment Review 92.

Pebesma, E., Bivand, R., 2023. Spatial Data Science: With applications in R. Chapman and Hall/CRC.

R Core Team, 2024. R: A Language and Environment for Statistical Computing_. R Foundation for Statistical Computing, Vienna, Austria. https://www.R-project.org/. (Accessed 13 June, 2024)

RPS, 2024. Moving EIAs into the digital world, https://www.rpsgroup .com/services/environment/environmental-impact-assessment/digital-environmental-impact-assessment/. (Accessed 12 May, 2024)

Sievert, C., 2020. Interactive Web-Based Data Visualization with R, plotly, and shiny. Chapman and Hall/CRC. ISBN 9781138331457, https://plotly-r.com. (Accessed 13 June, 2024)

Vincent, K., Roth, E.R., Moore, S.A., Huang, Q., Lally, N., Sack, C.M., Nost, E., Rosenfeld, H., 2018. Improving spatial decision making using interactive maps: An empirical study on interface complexity and decision complexity in the North American hazardous waste trade, Environment and Planning B: Urban Analytics and City Science 46, 1706-1723.

Wickham, H., 2016. ggplot2: Elegant Graphics for Data Analysis. Springer-Verlag New York. ISBN 978-3-319-24277-4. https://ggplot2.tidyverse.org. (Accessed 13 June, 2024)

WSP, 2024. Are digital environmental impact assessments a step towards "faster, better, greener" planning of transformative infrastructure?, https://www .wsp.com/en-gb/insights/digital-environmental-impact-assessments-better -planning-of-transformative-infrastructure. (Accessed 12 May, 2024)

Possibilities of the Utilization of UAS (Unmanned Aerial Systems) in the Preparation of Forest Management Plans for Private Forests

Konrad Kiš[1],*, Ema Svirčević[1]

[1] DVOKUT-ECRO Ltd., Zagreb, Croatia, konrad.kis@dvokut-ecro.hr, ema.svircevic@dvokut-ecro.hr
* corresponding author

Abstract: The management of private forests in Croatia differs from the management of state forests due to a variety of reasons. State forests have been managed for centuries and the current methodology for the preparation of management plans stipulated by the Ordinance on Forest Management mostly meets all the criteria for successful management. One of the crucial sources when drafting management plans is random samples, i.e. a certain percentage of forest surface which, regarding the forest type, varies between 2 and 7%, and based on which the parameters for forest stand are calculated. This methodology works fine in state forests of homogenous structure but is not applicable in private forests with a substantial number of owners with an average size of forest holding less than 1 hectare where a sampling intensity of 2% certainly does not reflect the true situation. Using advanced technologies like UAS with multispectral cameras and LiDAR, a new methodology for performing forest inventory in private forests could be developed, eliminating the sampling errors, and enabling insight into the factual situation, since such a survey would cover the entire forest area. Designing a reliable method for private forests using close-range remote sensing provides precise insight into real situations in private forests and enhances their management because, among other things, silvicultural measures could be prescribed for the specific area and not at the forest section level as is now the case. Also, the analysis of multispectral images provides an overview of the health state of forests.

Keywords: private forests; close-range remote sensing; forest inventory; multispectral images; LiDAR.

1   Introduction

This paper highlights the ongoing problem of regulating private forests and suggests that close-range remote sensing methods can help address it. While numerous studies exist on this topic (Goodbody et al. 2017, Dash et al. 2018, Liang et al. 2019, Ecke et al. 2022, Massey University 2022, Tomljanović et al. 2022), no universally accepted methodology has been established. Examples of successful utilization of Unmanned Aerial Systems (UAS) in forest inventory include disaster response and fire detection in Turkey (Abdurrahim and Eker 2019) and Finland (Forest.fi 2022). Another research by Gomes and Maillard (2016) shows that various hybrid algorithms using pattern recognition on very high-resolution images with an "ordinary" RGB camera can detect individual tree crowns in a forest. Despite ongoing research, no widely accepted method for conducting forest inventory using close-range remote sensing techniques has been developed.

Traditional field methods are effective for state-owned forests but provide limited insights for private forests.

2   Materials and methods

To illustrate the need for new methods in preparing forest management plans for private forests, a recent forest inventory for the "Zagreb – Medvednica" management unit will be used. The inventory highlights the discontinuity (Figure 1) and variability (Figure 2) of private forests, which are often composed of small estates. This variability emphasizes the need for more accurate methods, as traditional sampling intensities may not reflect the true situation. According to Božić et al. (2022), the majority, i.e. 85.15% of private forest owners' estates are less than 20 hectares in size, assuming of course that forest management "styles" greatly differ, which even more emphasizes the variability of private forests in Croatia. In such a situation, and this pertains to the most of private forests' management units due to the composition of private forest owners' estate size, the prescribed sampling intensity of 2% does not reflect the true situation.
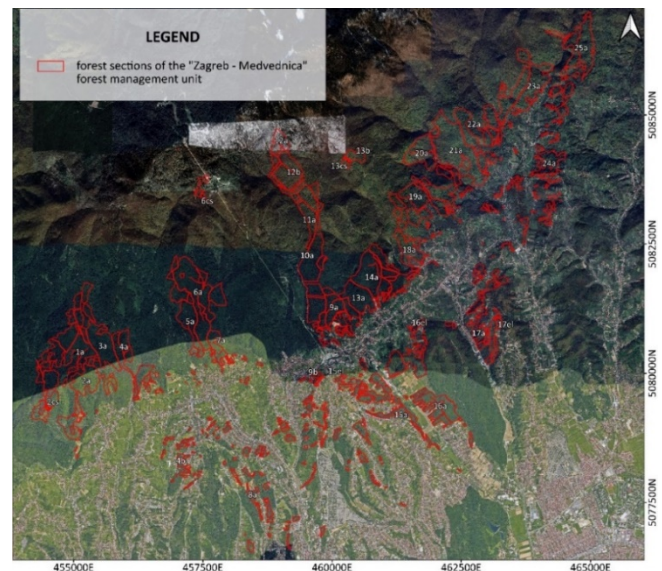
Figure 1. Private forests management unit "Zagreb – Medvednica" which depicts the discontinuity of forest sections in the observed area.

Furthermore, in situations like this where the area of interest (AOI) is utterly disjoined and scattered, it is almost impossible to apply the free-sampling method which should eliminate any researcher's bias. Often, sample points had to be offset from the original grid to fit into the AOI, which certainly increases the bias.

Figure 2. Part of forest section 17a depicts the colossal heterogeneity of private forests.

Having in mind all the facts, the conclusion is that current methods for performing the forest inventory in private forests are inadequate. The proposed methodology would comprise three major aspects:

- Scanning of the whole forest area with an airborne or terrestrial LiDAR, or both,
- Recording of the whole forest area with an RGB and a multispectral (if not even hyperspectral) camera,
- Complementary field research to determine the so-called "ground truth", i.e. confirmation of the close-range remote sensing findings.

3   Results

The major data that must be derived from the research are quantitative parameters such as tree diameter, tree height (from which volume can be determined), exact position of each tree in a stand (for future measurements, i.e. determining of increment), tree species, health status of forest and forest stand, digital elevation model (DEM) and the amount of deadwood within a stand.

When it comes to quantitative parameters, LiDAR tools are beyond doubting the best way to achieve them (Figure 3 and Figure 4). An airborne laser scanner (ALS) system is the most common type of LiDAR sensor and is the most suitable for application in forestry when compared to terrestrial and spaceborne scanners (Balenović et al. 2013). In combination with a terrestrial LiDAR which could be used for precise measurement of tree diameters, a model could be developed for the determination of a stand's quantitative parameters, although the same will require lots of machine learning and ground-truth determination.

A multispectral camera-equipped UAV can identify tree species and vegetation health within a stand. Developing a model for tree species identification via multispectral cameras requires extensive machine learning and ground-truth data across seasons. This involves significant field and desktop work but can ultimately produce an accurate model for determining stand biological features. The stand age for even-aged forests must be, though, acquired from

historical data, although recent research combines LiDAR and historical data in the preparation of the stand age model (Maltamo et al. 2020). A detailed description of the habitat and stand's health should be, however, complemented via field research.

This article aims to highlight the importance and necessity of using close-range remote sensing techniques for forest inventory, particularly in private forests. As it does not pertain to a specific project or field research, it does not generate results but rather raises awareness about the potential of these methods for private forests, even in their early stages. The use of UAV-generated images (RGB, multispectral, or hyperspectral) and LiDAR (terrestrial or airborne) for forest inventory has been addressed in recent research (Lin et al. 2022, Vivar-Vivar et al. 2022, Xiong et al. 2024, Ziegelmaier et al. 2024), emphasizing the significance of these techniques and technologies in this field.

4   Discussion

Although a comprehensive methodology for forest inventory in private forests using close-range remote sensing has not yet been developed, there are compelling reasons to do so. Private forests are becoming increasingly important in Croatia due to the restitution process (Ostoić et al. 2015), which has led to a significant increase in privately owned forests (Croatian Forests Ltd. 2017). This shift highlights the need for advanced technology to streamline forest inventory processes, reducing time consumption and costs. While field observations are still necessary, the use of close-range remote sensing can greatly reduce the time and effort required, increasing overall efficiency.

Close-range remote sensing methodologies offer several benefits in private forest management:

- Eliminate sampling errors by accurately assessing the entire forest area,
- Precisely prescribe silvicultural measures for specific areas,
- Reduce costs and time consumption compared to traditional methods,
- Increase competitiveness in the market through reduced costs and improved efficiency.

It is important, however, to state the disadvantages of this method at this point – the equipment for this methodology is rather costly, and it requires significant hardware resources to process a large amount of data. This can, however, be resolved by renting external hardware resources (cloud) where data can be easily and effectively processed, saving valuable time. Also, substantial time and financial resources will be required for the training of the staff.

5   Conclusions

Numerous studies and research have been and are still being conducted regarding the use of UASs equipped with LiDAR, multispectral, or hyperspectral cameras (Lin et al. 2022, Fassnacht et al. 2024, Xiong et al. 2024, Ziegelmaier et al. 2024), however there is still no holistic, comprehensive methodology for fully performing a forest

Figure 3. 3D model of an old oak stand taken by a DJI R300 drone equipped with an airborne LiDAR head, generated from point cloud (courtesy of "Croatian Forests" Ltd.).

Figure 4. 3D model of an old oak stand taken by a DJI R300 drone equipped with an airborne LiDAR head, generated from a point cloud with a graduated symbology of the height above sea level (courtesy of "Croatian Forests" Ltd.).

inventory. To develop one, future studies should be aimed at developing the methodology for deriving the wood volume of each tree from the LiDAR point cloud and determining tree species from multispectral and hyperspectral imagery, thus providing most relevant data for performing the forest inventory and preparation of the forest management plan.

Cutting-edge technology is particularly useful in private forest management units due to its ability to eliminate sampling errors, reduce costs, and increase efficiency. It allows for precise silvicultural measures and enhances competitiveness in the market. Although a comprehensive methodology for private forests does not yet exist, the benefits are too compelling to ignore, and it is only a matter of time before it is developed.

6   References

Abdurrahim, A., Eker, R., 2019. Using Unmanned Aerial Vehicles (UAV) in inventory, assessment, and monitoring of natural hazards in forested areas. Workshop Harmonious, Coimbra, 6 November 2019 (poster presentation).

Balenović, I., Alberti, G., Marjanović, H., 2013. Airborne Laser Scanning - the Status and Perspectives for the Application in the South-East European Forestry, SEEFOR 4 (2), 59-79.

Božić, M., Andabaka, M., Vedriš, M., Goršić, E., Teslak, K., 2022. Characteristics of Private Forest Owners in Relation to Their Activities in Enlargement of Forest Holdings, Journal of Forestry Society 1-2, 7.

Croatian Forests Ltd., 2017. Forest Management Plan for the Republic of Croatia for the Period 2016–2025, Zagreb 2017, pp. 465.

Dash, J.P., Pearse G.D., Watt, M.S., 2018. UAV Multispectral Imagery Can Complement Satellite Data for Monitoring Forest Health, Remote Sensing 10, 1216.

Ecke, S., Dempewolf, J., Frey, J., Schwaller, A., Endres, E., Klemmt, H. J., Tiede, D., Seifert, T., 2022. UAV-Based Forest Health Monitoring: A Systematic Review. Remote Sensing 14, 3205.

Fassnacht, F. E., White, J. C., Wulder, M. A., Næsset, E., 2024. Remote sensing in forestry: current challenges, considerations and directions, An International Journal of Forest Research 97, 11-37.

Forest.fi, 2022. Research promises revolutionary technology for preventing forest fires – a flock of drones can chase aerial patrolling off the map, https://forest.fi/article/research-promises-revolutionary-technology-for-preventing-forest-fires-a-flock-of-drones-can-chase-aerial-patrolling-off-the-map/#8a3c1d67. (Accessed 12 June, 2024)

Gomes, M.F., Maillard, P., 2016. Detection of Tree Crowns in Very High Spatial Resolution Images. IntechOpen, 2016.

Goodbody, T. R., Coops, N. C., Marshall, P. L., Tompalski, P., Crawford, P., 2017. Unmanned aerial systems for precision forest inventory purposes: A review and case study, The Forestry Chronicle 93, 71-81.

Krajter Ostoić, S., 2015. Forest Land Ownership Change in Croatia. COST Action FP1201 FACESMAP Country Report, European Forest Institute Central-East and South-East European Regional Office, Vienna.

Liang, X., Wang, Y., Pyörälä, J., Lehtomäki, M., Yu, X., Kaartinen, H., … Deng, S., 2019. Forest in situ observations using unmanned aerial vehicle as an alternative of terrestrial measurements. Forest ecosystems 6, 1-16.

Lin, Y.C., Shao, J., Shin, S.Y., Saka, Z., Joseph, M., Manish, R., Fei, S. Habib, A., 2022. Comparative Analysis of Multi-Platform, Multi-Resolution, Multi-Temporal LiDAR Data for Forest Inventory, Remote Sensing 14, 649.

Maltamo, M., Kinnunen, H., Kangas, A., Korhonen, L., 2020. Predicting stand age in managed forests using National Forest Inventory field data and airborne laser scanning. Forest Ecosystems 7, 1-11.

Massey University, New Zealand, 2022. Exploring the ways drones can be utilised in the forestry sector, https://www.massey.ac.nz/about/news/exploring-the-ways-drones-can-be-utilised-in-the-forestry-sector/. (Accessed 12 June, 2024)

Tomljanović, K., Kolar, A., Đuka, A., Franjević, M., Jurjević, L., Matak, I., … Balenović, I., 2022. Application of UAS for monitoring of forest ecosystems–a review of experience and knowledge. Croatian Journal of Forest Engineering: Journal for Theory and Application of Forestry Engineering 43 (2), 487-504.

Vivar-Vivar, E. D., Pompa-García, M., Martínez-Rivas, J. A., Mora-Tembre, L. A., 2022. UAV-Based characterization of tree-attributes and multispectral indices in an uneven-aged mixed conifer-broadleaf forest. Remote Sensing 14 (12), 2775.

Xiong, H., Pang, Y., Jia, W., Bai, Y., 2024. Forest stand delineation using airborne LiDAR and hyperspectral data, Silva Fennica 58 (2).

Ziegelmaier Neto, B.H., Schimalski, M.B., Liesenberg, V., Sothe, C., Martins-Neto, R.P., Floriani, M.M.P., 2024. Combining LiDAR and Spaceborne Multispectral Data for Mapping Successional Forest Stages in Subtropical Forests, Remote Sensing 16, 1523.

A Review of Geospatial Prediction and Modelling Approaches in Biogas Plant Suitability Assessment

Đurđica Kovačić[1,*], Dorijan Radočaj[2], Mladen Jurišić[2]

[1] Central Agrobiotechnical Analytical Unit, University of J.J. Strossmayer of Osijek, Faculty of Agrobiotechnical Sciences Osijek, Osijek, Croatia, djkovacic@fazos.hr

[2] Department of Agricultural Engineering and Renewable Energy Sources, University of J.J. Strossmayer of Osijek, Faculty of Agrobiotechnical Sciences Osijek, Osijek, Croatia, dradocaj@fazos.hr, mjurisic@fazos.hr

* corresponding author

Abstract: The European Union and Croatia's energy policy aims to ensure accessible, safe, affordable, and competitive energy through significant technical, technological, and social changes in all sectors of the economy. New production capacities, such as biogas plants, can alleviate capacity shortages, increase system flexibility, and significantly improve the security of supply. Therefore, this paper provides an overview of the factors that affect the selection of a location for biogas plants. Geospatial biogas potential assessment is the first step in determining the feasibility of biogas plants. Several factors can contribute to the economic viability and sustainable production of biogas plants, while sufficient availability of feedstock, as well as cost-effective logistics related to transportation and fulfilment of institutional requirements, are essential. There are two geospatial state-of-the-art methods for land suitability determination: Geographic Information System (GIS)-based multicriteria analysis and machine learning regression. These studies were dominantly based on the GIS-based multicriteria analysis using the analytic hierarchy process (AHP), using distance rasters to supply sources, roads, and settlements as primary criteria. They also strongly considered land use, slope, and elevation for the determination of biogas plant suitability. However, three key gaps were noted in the current state-of-the-art approach: 1) crude geospatial modelling of biomass supply, which is required for biogas production using co-digestion, except for single crop; 2) the lack of geospatial modeling of soil contamination as criteria; and 3) the lack of independent validation of predicted biogas plant suitability.

Keywords: biogas plant site selection; Web of Science; GIS-based multicriteria analysis; Sustainable Development Goals of the United Nations.

1 Introduction

European Union and Croatia's energy policy aims to ensure accessible, safe, affordable, and competitive energy through significant technical, technological, and social changes in all sectors of the economy (Republic of Croatia 2020). Europe possesses an abundance of renewable energy sources, and its countries have emerged as leaders in deploying renewable technologies in recent years. With targets for renewable energy set for each nation in Europe and the European Green Deal aiming to make Europe the first climate-neutral continent by 2050, efforts are being made to make Europe's energy systems more sustainable (IRENA 2022). Significant investments in energy efficiency, renewable energy, new low-carbon technologies, and transportation and storage infrastructure will be needed to achieve these goals. Integration of the infrastructure of the gas and electricity industries must also be done more intelligently and closely (Morino et al. 2023). Renewable energy projects and new production capacities should utilize the latest technological advances to increase conversion efficiency and energy density, reducing space requirements and environmental impact across the European Union. Renewable energy projects should consider the socio-economic characteristics of the surrounding area while respecting national environmental goals, to contribute to the development of local communities (Republic of Croatia 2020).

Croatia's energy transition also promotes renewable energy sources, potentially reducing the country's dependence on energy imports. According to the Energy Development Strategy of Croatia until 2030 with a view to 2050, it was concluded that the energy production capacities are insufficient to meet the energy needs of the Croatian electricity system. New production capacities, such as biogas plants, can alleviate capacity shortages, increase system flexibility, and significantly improve the security of heat and electricity supply, along with transportation fuels (Scarlat et al. 2018, Republic of Croatia 2019). In addition, the Croatian Ministry of Agriculture signed the Bioeast Vision 2030 declaration in 2018, focusing on sustainable biomass production, circular processing ("zero waste"), agro-food systems, and diversification of the rural economy. Croatia's energy transition goals can be significantly achieved by actively managing agricultural land and organic waste from livestock production for biogas production (Republic of Croatia 2019).

Continental Croatia, comprising 13 counties, has high agricultural and industrial potential. In 2022, there were 41 operational biogas plants in 10 counties with an installed capacity of 53 MW. However, it is estimated that Croatia has the potential to generate up to 300 MW of biogas according to the Report on biogas plants from the database of the Environmental Pollution Register of the Republic of Croatia for the period 2017 – 2021 (Republic of Croatia, 2023). Biogas potential assessment is the first step in determining the feasibility and plant suitability of biogas plants.

The goal of this review was to present the state of scientific studies available in scientific database Web of Science in the period from 2010 to 2023 that deal with accessing suitable locations for generally all biofuel and specifically

biogas plants by using geospatial prediction and modelling approaches, and their interlinking with the Sustainable Development Goals of the United Nations (SDGs). Also, the goal was to identify SDGs that most often appear in these studies and thus stress their importance and presence in the biogas industry.

2   Materials and methods

To investigate the available scientific work that dealt with possible locations for the construction of any biofuel and specifically biogas plant locations, a search for information is performed using the scientific database Web of Science with the following search topic: "land suitability" OR "site selection", AND "biofuel plant" OR "biogas plant" for biofuel studies, and "biogas plant" for biogas studies published between 2010 and 2023. The criteria for selecting the information were defined by the year in which the manuscript was published. Additionally, the Sustainable Development Goals of the United Nations (SDGs) for filtered studies were analyzed based on their indexing in the Web of Science.

3   Results

The data on the number of papers indexed in the Web of Science since 2010 on the topic of land suitability or site selection and a biofuel and biogas plant is presented in

Figure 1. Figure 2 represents the link between the biofuel and biogas plant suitability studies indexed in the Web of Science and SDGs.

The geographic distribution of biofuel and biogas plant suitability studies indexed in the Web of Science are presented in Figure 3, in which lighter colors indicate countries with a lesser number of biofuel and biogas plant suitability studies, whereas darker colors indicate countries with a larger number of biofuel and biogas plant suitability studies.

4   Discussion

The sustainable production of biogas plants and their economic viability can be attributed to various factors. Knowledge of the local availability of feedstock and its spatial distribution is important. Particularly, since different types of manures are usually the basic substrate for biogas production, the availability of manure is crucial. In a given area it depends on the population of livestock and poultry and the density of farms (Scarlat et al. 2018). Also, cost-effective logistics related to infrastructure, i.e. transportation and fulfillment of institutional requirements, are essential. Suitable infrastructure refers to road and rail networks, gas grids, and pipelines for transporting produced biogas from a biogas production facility to a distribution point or end-user (Feiz et al. 2022).
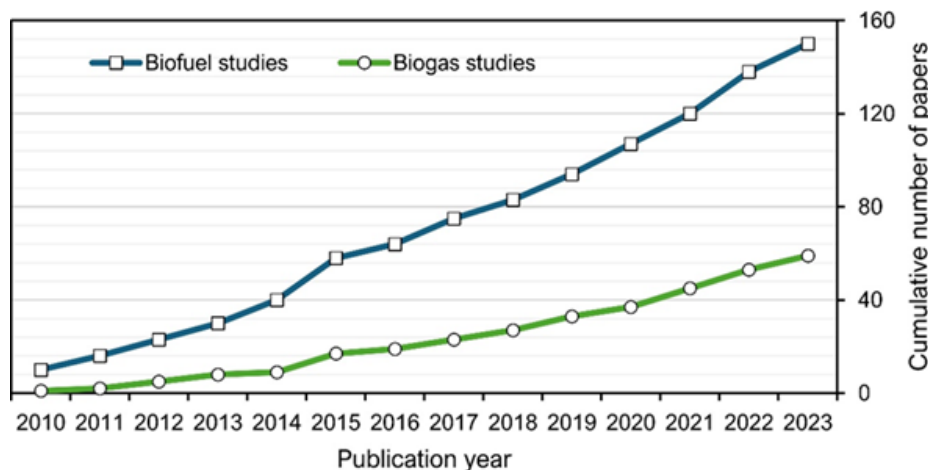

Figure 1. The cumulative number of papers indexed in the Web of Science since 2010 on the topic of ("land suitability" OR "site selection") AND: ("biofuel plant" OR "biogas plant") for biofuel studies; "biogas plant" for biogas studies.
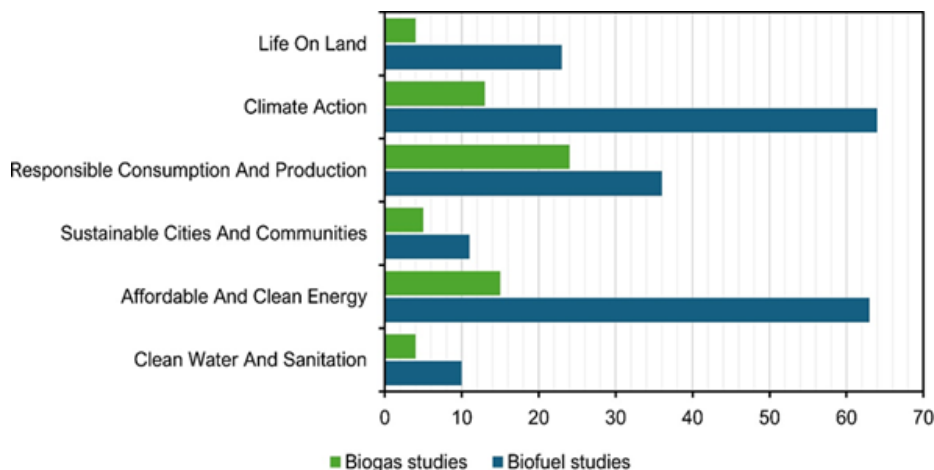

Figure 2. The SDGs of biofuel and biogas plant suitability studies indexed in the Web of Science.
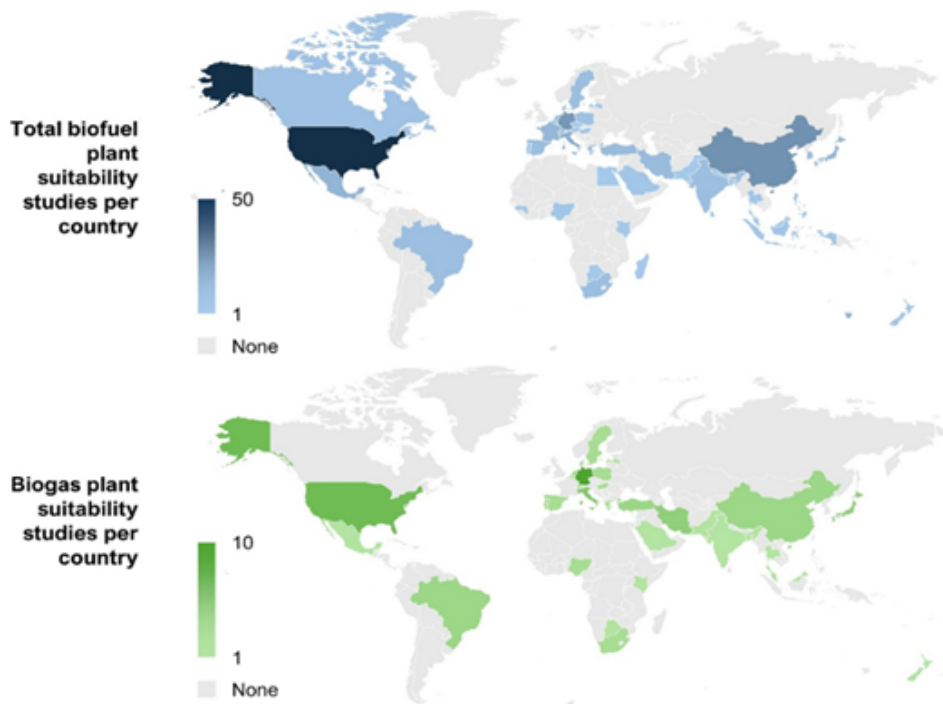
Figure 3. The geographic distribution of biofuel and biogas plant suitability studies indexed in the Web of Science.

Geographic Information System (GIS) has been used in several studies for biogas plant suitability determination across the world (Akther et al. 2018, Al-Ruzouq et al. 2021, Nantasaksiri et al. 2021, Soha and Hartmann 2022). These studies were dominantly based on the GIS-based multicriteria analysis using the Analytic Hierarchy Process (AHP), using distance rasters to supply sources, roads, and settlements as primary criteria. They also strongly considered land use, slope, and elevation to determine biogas plant suitability.

While GIS-based multicriteria analysis offers maximum flexibility in criteria selection and their weighting, thus being universally applicable in suitability studies, it is heavily relied on subjective expert knowledge and often lacks independent validation. To reduce the subjectivity effect, the Analytic Hierarchy Process (AHP) represents a state of the art for criteria weight calculation. This issue is completely resolved by the objective approach of machine learning regression for suitability prediction, which supports significantly more input covariates for prediction but requires reliable ground truth data (Radočaj and Jurišić 2022). The main reason for the prevalence of the GIS-based multicriteria analysis in comparison to machine learning regression for biogas plant suitability determination is the lack of straightforward ground truth data, which cannot be quantified to express the effectiveness of biogas production in a single indicator.

Regarding the scientific papers indexed in the database Web of Science, the year 2010 was chosen as the starting year, whereas the search ends with 2023. The results have shown that there have been only 150 biofuels and 59 biogas plant suitability studies published in that period (Figure 1), indicating that this is a niche scientific topic. However, their number steadily grew since 2010, with the record number of both biofuel and biogas plant suitability studies being indexed in 2022. A total of six SDGs were identified in the search of biofuel and biogas plant suitability studies indexed in the Web of Science (Figure 2), referring to life on land, climate action, responsible consumption and production, sustainable cities and communities, affordable and clean energy, and clean water and sanitation. The majority of the studies dealt with crucial global environmental issues related to climate action and affordable and clean energy. While a similar focus was present in more narrow biogas plant suitability studies, their dominant scope was on the responsible consumption and production goal, which is mandatory for reaching an independent energy policy.

The leading countries in the biofuel plant suitability research are the United States, China, and Germany (Figure 3). Moreover, it is notable that such research was dominantly focused on three global regions: North America, western Europe, and south-eastern Asia, with only a few studies indexed in the Web of Science outside these areas. The geographic distribution of specifically biogas plant suitability studies was further restricted, with Germany being the global leader in the number of research papers indexed in the Web of Science. This particular topic was even more prevalent in the European countries than more general biofuel plant suitability studies, with Italy being the third-ranked in this regard, slightly behind the United States.

5 Conclusions

To achieve sustainable development and energy and climate goals, policies that consider the synergies between various sectors, such as agriculture, rural development, and energy production, are necessary for fully utilizing the potential of biogas. GIS suitability assessment interconnects all these factors and enables the prediction of the spatial distribution of all resources important for selecting the biogas plant location. It is evident from the

literature that only a minor number of studies were published throughout the given period and the present state of scientific research on biofuel and biogas plant suitability is very restricted, even in regions that are global leaders in research, including North America, western Europe, and south-eastern Asia which brings the conclusion that GIS-based assessments are still insufficiently utilized in the scientific modelling related to the biofuel industry and the selection of locations for biofuel production plants. However, the number of published papers has an upward trend and because powerful GIS-based tools are becoming more available and influential, the authors strongly believe that in the future these tools will be increasingly applied for this purpose and that the number of published papers will continue this growing trend.

This observation strongly suggests the potential presence of major scientific gaps in this research topic, which should encourage scientists to address this issue in future studies and also in achieving energy independence and environmental sustainability, particularly for identified SDGs that most often appear in the database when searching for biofuel and biogas plant suitability studies.

6 References

Akther, A., Ahamed, T., Noguchi, R., Genkawa, T., Takigawa, T., 2019. Site suitability analysis of biogas digester plant for municipal waste using GIS and multi-criteria analysis. Asia-Pacific Journal of Regional Science, 3, 61-93.

Al-Ruzouq, R., Abdallah, M., Shanableh, A., Alani, S., Obaid, L., Gibril, M. B. A., 2022. Waste to energy spatial suitability analysis using hybrid multi-criteria machine learning approach. Environmental Science and Pollution Research, 29, 2613-2628.

Feiz, R., Metson, G.S., Wretman, J., Ammenberg, J., 2022. Key factors for site-selection of biogas plants in Sweden. Journal of Cleaner Production 354, 131671.

International Renewable Energy Agency (IRENA), 2022. https://www.irena.org/ How-we-work/Europe (Accessed 10 May, 2024).

Morino, E.M., Roth, A., Peterse, J., 2023. Market state and trends in renewable and low-carbon gases in Europe. A Gas for Climate report. Guidehouse Netherlands B.V.

Nantasaksiri, K., Charoen-amornkitt, P., Machimura, T., 2021. Integration of multicriteria decision analysis and geographic information system for site suitability assessment of Napier grass-based biogas power plant in southern Thailand. Renewable and Sustainable Energy Transition, 1, 100011.

Radočaj, D., Jurišić, M., 2022. GIS-based cropland suitability prediction using machine learning: A novel approach to sustainable agricultural production. Agronomy, 12, 2210.

Republic of Croatia, 2019. National Development Strategy Croatia 2030 Policy Note: Agriculture, Fisheries, and Food Processing in Croatia's Food & Bio-Economy. https://hrvatska2030.hr/wp-content/uploads/2020/10/Agricultu re-Fisheries-and-Food-Processing-in-Croatia_s-Food-_-Bio-Economy.pdf (Accessed 13 May 2024).

Republic of Croatia, 2020. Energy Development Strategy of the Republic of Croatia until 2030 with a look at 2050. https://www.zakon.hr/cms.htm ?id=43467 (Accessed 10 May, 2024).

Republic of Croatia, 2023. Report on biogas plants from the database of the Environmental Pollution Register of the Republic of Croatia for the period 2017 – 2021.

Scarlat, N., Fahl, F., Dallemand, J.-F., Monforti, F., Motola, V., 2018. A spatial analysis of biogas potential from manure in Europe. Renewable and Sustainable Energy Reviews 94, 915-930.

Soha, T., Hartmann, B., 2022. Complex power-to-gas plant site selection by multi-criteria decision-making and GIS. Energy Conversion and Management: X, 13, 100168.

Land Cover Changes and Conservation Effectiveness of Protected Areas: Evidence from Landlocked Developing Countries in Sub-Saharan Africa

Jeffrey Chiwuikem Chiaka[1,2,]*, Gengyuan Liu[1,3]

[1] State Key Joint Laboratory of Environmental Simulation and Pollution Control, School of Environment, Beijing Normal University, 100875 Beijing, China, jeffreychiaka@bnu.edu.cn

[2] Anambra-Imo River Basin Development Authority, Owerri, Nigeria

[3] Beijing Engineering Research Center for Watershed Environmental Restoration and Integrated Ecological Regulation, Beijing 100875, China, liugengyuan@bnu.edu.cn

* corresponding author

Abstract: It is evident that some existing protected areas (PAs) were established prior to the call for more effective management of PAs. This study looked at the conservation effectiveness of three selected PAs in landlocked developing countries (LLDCs) in sub-Saharan Africa prior and after the Strategic Plan for Biodiversity (2011-2020) using spatial analysis. The results indicated Zemongo Faunal Reserve (Central African Republic) and Central Kalahari Game Reserve (Botswana) had better conservation effectiveness compared to Harar-Wabi Shebelle (Ethiopia). Although there was also human activity in the form of cropland in the three protected areas, this was limited in 2020. The exception was Harar-Wabi Shebelle (Ethiopia). This study reiterates the need for continued effective management strategy and policy making for protected areas in sub-Saharan Africa.

Keywords: land use land cover; spatial analysis; protected area; landlocked developing countries; sub-Saharan Africa.

1   Introduction

The importance of protected areas (PAs) is gaining traction as seen from the numerous efforts from organizations developing various programmes to address the biodiversity decline and ecosystem service protection (CBD 2011). Hence, programmes like the Aichi Target 11, requires protecting 17 % of terrestrial and 10 % of marine areas by 2020. Additionally, the United Nations Sustainable Development Goals (UN-SDG) reiterate their commitment to see life below water (SDG 14) and life on land (SDG 15) safeguarded as to maintain nature's contribution to human well-being, as the ecosystem environment must be conducive for it to thrive (Krkoška lorencová et al. 2016). However, anthropogenic activities lead to biodiversity loss and impair ecosystem functions (Cardinale et al. 2012, Yang et al. 2022). Therefore, to ensure the protection of biodiversity and the environment, protected areas and other effective area-based conservation measures (OECMs) are being initiated in light of the threats that population growth, urbanization and climate change pose to ecosystem services (Hassan et al. 2016, Arowolo et al. 2018).

Interestingly, about 13% of Africa's land area is designated as protected areas and 8,000 of these protected areas are officially registered in the World Database of Protected Areas (WDPA) (Miranda et al. 2016, Parks 2023). The African continent is therefore not left out when it comes to achieving its goals, as the target is to protect 30% of terrestrial and coastal areas (Parks 2023). Conversely, there are reports of poor management and lack of monitoring of existing protected areas in both terrestrial and coastal areas in Africa (Parks 2023). As part of the Convention on Biological Diversity, a study examined the impact of the Strategic Plan for Biodiversity (2011–2020) on the protection of biodiversity in protected areas in nine selected countries. The study found that although the program had resulted in an expansion of protected areas, the countries studied were inadequately protected by 2020 (Jantke et al. 2024).

Nevertheless, in the context of location/ecoregion, this study assumes that the situation is different in coastal and terrestrial areas, especially in landlocked developing countries (LLDCs). For instance, an estimated one-third of the world's population lives in the coastal areas (Barbier et al. 2008), which contributes to more human pressure for food and livelihood, while LLDCs are considered geographically disadvantaged compared to other countries in terms of economic growth and sustainable development efforts, etc., and studies are yet to ask whether the geographical constraints common to LLDCs affect their environment and biodiversity. Hence, this study will specifically address the research gap on the site-specific status of protected areas in landlocked developing countries in sub-Saharan Africa before the start of the Strategic Plan for Biodiversity in 2011 and after its end in 2020. This will provide more precise evaluation of the protected areas considering the influence of its location on its conservation effectiveness. This is significant as researchers have questioned the call to expand protected areas to meet the mandate without considering the conservation effectiveness of existing areas (Watson et al. 2014), amidst intense human pressure (Jones et al. 2018). This is crucial to avoid efforts in futility considering the numerous benefits protected areas offer to human-wellbeing and environment (Watson et al. 2014, Tang 2020). Hence, monitoring PAs conservation effectiveness is the key to conservation efforts and biodiversity protection (Duncanson et al. 2023).

Various studies have analysed the conservation effectiveness of protected areas using human pressure data and discovered half of the world's protected areas are under severe human pressure, particularly in Africa,

Western Europe, and South Asia (Jones et al. 2018). Others used a metric score to assess protected area performance (Jantke et al. 2019), weighted least squares regressions (Heino et al. 2015), questionnaires (Laurance et al. 2012) and opportunity costs (Venter et al. 2014). Their observations ranged from higher forest loss within the boundaries of protected areas to the integrity of protected areas being compromised by surrounding areas. Also, based on location, biodiversity hotspot areas are not given much attention (Venter et al. 2014). However, there are paucity of studies looking into PAs conservation effectiveness among landlocked developing countries (LLDC) in sub–Saharan African. This raises the question if land cover drivers and PAs conservation effectiveness are location specific. Also, knowing the particularities surrounding LLDC, as 16 out of 44 in the world are in Africa, such as geographical constraints, access to coastal waters etc., does it affect the conservation effectiveness of their protected area. To fill this research gap, this study uses spatial analysis to assess land use change of existing PAs in landlocked developing countries (LLDC) in sub-Saharan African that were established prior the Strategic Plan for Biodiversity (2011–2020) to see their conservation effectiveness.

2   Materials and methods

This study utilized spatial analysis to assess the land cover changes of three selected PAs located in a landlocked developing country (LLDC) of sub–Saharan African, namely, Harar-Wabi Shebelle National controlled hunting area (Ethiopia), Zemongo Faunal Reserve (Central African Republic) and Central Kalahari Game Reserve (Botswana). This study examined their conservation effectiveness from 2001 to 2020, i.e. before and at the end of the Strategic Plan for Biodiversity (2011–2020). A major criterion for selecting the protected areas were based on their extent (size), designation as a national enterprise and most importantly, established prior to the Strategic Plan for Biodiversity (2011–2020).

The protected areas boundary was clipped from the land cover data in order to analyze the conservation effectiveness of the three selected PAs. Thereafter, the land cover inside the PA was determined after raster projection and image processing on ArcGIS 10.6, using MODIS International Geosphere-Biosphere Programme (IGBP) classification to delineate the land cover classes. The subsequent area changes were determined using Equation (1).

$$LULC_{change} = LC_{n2020} - LC_{n2001} \qquad (1)$$

where, end year and start year are land covers for 2020 and 2001, respectively, while n represents the individual land cover class.

The protected area extent and land cover images were collated from the United Nations Environment Programme World Conservation Monitoring Centre (UNEP-WCMC) and Moderate Resolution Imaging Spectroradiometer (MODIS) (Table 1).

Table 1. Summary of the data source information.

Data Source	Data	Year
UN Environment Programme World Conservation Monitoring Centre (UNEP-WCMC)	World Database on Protected Areas	2023
Moderate Resolution Imaging Spectroradiometer (MODIS)	500m Land Use Land Cover images	2001 and 2020

3   Results

The land use cover classification showed 7 land cover classes namely; forest, shrubland, savanna, grassland, cropland, built-up area and barren but varying among the three PAs (Figure 1). In Harar-Wabi Shebelle (Ethiopia), shrubland decreased significantly from 49% to 34% between 2001 and 2020, while grassland and cropland increased from 51% to 66% and from 0.02 to 0.12%, respectively. The Zemongo Faunal Reserve (Central African Republic) had a significant increase in forest cover from 10% in 2001 to 28% in 2020. However, other land covers in the protected area decreased. In the Central Kalahari Game Reserve (Botswana), on the other hand, there were only minimal changes in land cover. The land cover area changes in hectares are given in Table 2. Furthermore, n/a means the land cover class is not available (not detected).

Based on the land cover transition matrix, which indicates how the different land covers changed from one state to another, it is observed that apart from the built-up area, which was only present in Harar-Wabi Shebelle (Ethiopia), cropland was common among the three PAs, but was converted to other land cover classes in Zemongo Faunal Reserve (Central African Republic) and Central Kalahari Game Reserve (Botswana), while cropland increased in Harar-Wabi Shebelle (Ethiopia). This implies more effective management of protected areas in the Central African Republic and Botswana compared to Ethiopia.

To explain the presence of human activities that can have profound impact on biodiversity and climate, this study considered the individual land cover changes. The study observed that in Harar-Wabi Shebelle (Ethiopia), shrublands and grasslands were converted to croplands. While in Zemongo Faunal Reserve (Central African Republic) and Central Kalahari Game Reserve (Botswana), croplands were restricted in 2020 and later converted to shrublands, grasslands and savannas.
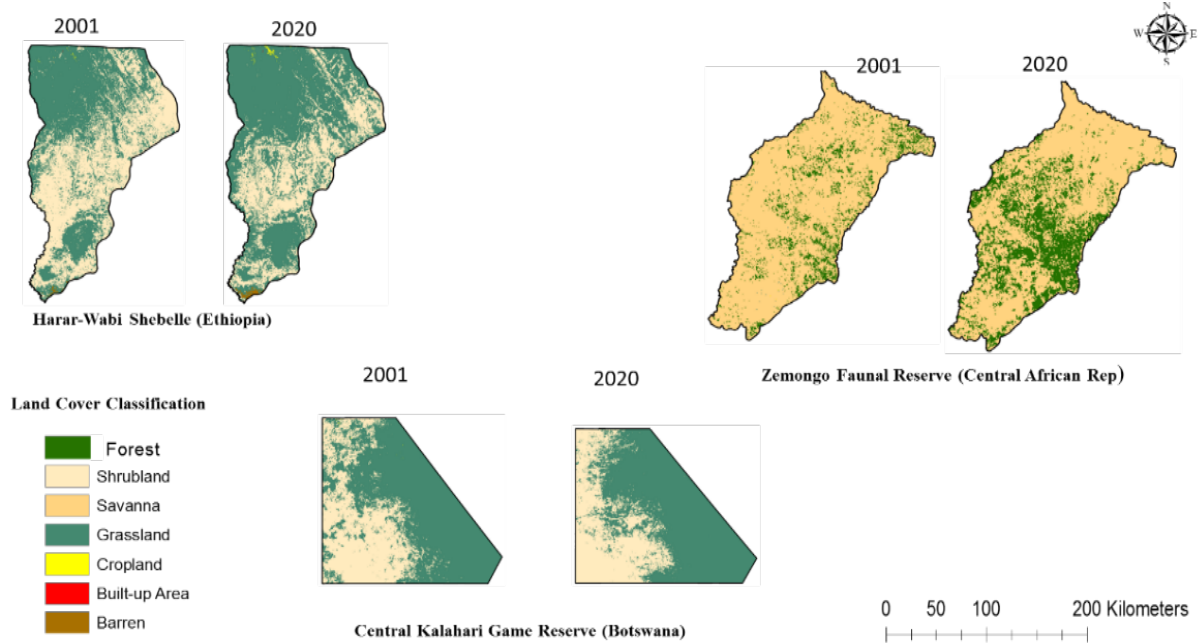
Figure 1. Land cover of the 3 Protected Areas located in Landlocked Developing Countries of Sub-Saharan Africa.

Table 2. Land use cover changes [Ha] across the PAs in Landlocked Developing Countries.

LULC	Harar-Wabi Shebelle			Zemongo			Central Kalahari		
	2001	2020	Change	2001	2020	Change	2001	2020	Change
Forest	n/a	n/a	n/a	143,729	379,618	235,889	n/a	n/a	n/a
Shrubland	1,632,322	1,116,421	-515,901	n/a	n/a	n/a	1,906,896	1,878,372	-28,524
Savanna	226	330	104	1,228,598	993,094	-235,504	3,321,957	3,351,337	29,380
Grassland	1,673,830	2,175,800	501,971	663	29	-604	0	29	29
Cropland	764	4761	3997	57	0	-57	1245	0	-1245
Built-up	65	65	No change	n/a	n/a	n/a	n/a	n/a	n/a
Barren	4126	13,184	9058	n/a	n/a	n/a	n/a	n/a	n/a

4 Discussion

The idea of nature conservation is to protect the natural ecosystem from degradation. Thus, considering the land use land cover changes in the three PAs analyzed, Zemongo Faunal Reserve (Central African Republic) and Central Kalahari Game Reserve, had a better conservation management effectiveness as they restricted cultivation by 2020, to stem degradation associated with agriculture. This shows conservation management efforts are effective as land use management plays a crucial role, even for ecosystem functions (Burkhard et al. 2012). In addition, their individual designation may have contributed to the rate of land cover changes. This is because appropriate management plans and strategies contribute to the sustainability and functions of protected areas (Yoo et al. 2024).

The goal of protected areas is the conservation of ecosystems. However, there were presence of human activities, like croplands in 2001 but was restricted in 2020 in some PAs. This further demonstrates PAs land use management system are different in countries. In addition, the difference in conservation approach has been known to be due to the management aims for the PAs and most importantly the authorities and stakeholders behind their establishments (Dudley 2008, Meli et al. 2019).

This study has highlighted the potential of spatial analysis in the assessment of the management of PAs in the three LLDCs and their outcome indicates their priority and management effectiveness as minimal ecological changes was observed specifically in Botswana and Central African Republic. However, crux of conservation effectiveness may seem to depend on the country's priority and subsequent conservation approach. Nevertheless, the establishment of protected areas remains crucial for the conservation of habitat quality and biodiversity (Geldmann et al. 2013).

5 Conclusions

In this study, the use of spatial analysis was utilized to assess the conservation effectiveness of PAs in some selected Landlocked Developing Countries (LLDCs) in sub-Saharan Africa prior the start of the Strategic Plan for Biodiversity in 2011 and after its end in 2020. As a result, the study observed the following: Zemongo Faunal Reserve (Central African Republic) and Central Kalahari Game Reserve (Botswana), had a better conservation management effectiveness as they restricted cultivation by 2020, to stem degradation associated with agriculture. Human activity was present in the three PAs in form of cropland activities but were restricted in 2020. The exception was Harar-Wabi Shebelle (Ethiopia), which was

meant to be a National controlled hunting area, implying a low conservation effectiveness and land use management. Management objectives of PAs may not solely lie on its designation, but from the land use management of the National or regional authority and stakeholders behind their establishments. In sum, the study contributes to advocacy for continued effective management strategy and policy-making related to management of protected areas in sub-Saharan African and the world at large.

6   References

Arowolo, A.O., Deng, X., Olatunji, O.A., Obayelu, A.E., 2018. Assessing changes in the value of ecosystem services in response to land-use/land-cover dynamics in Nigeria. Science of The Total Environment 636, 597-609.

Barbier, E.B., Koch, E.W., Silliman, B.R., Hacker, S.D., Wolanski, E., Primavera, J., ... Reed, D. J., 2008. Coastal ecosystem-based management with nonlinear ecological functions and values. Science 319 (5861), 321-323.

Burkhard, B., Kroll, F., Nedkov, S., Müller, F., 2012. Mapping ecosystem service supply, demand and budgets. Ecological Indicators 21, 17-29.

Cardinale, B.J., Duffy, J.E., Gonzalez, A., Hooper, D.U., Perrings, C., Venail, P., ... Naeem, S., 2012. Biodiversity loss and its impact on humanity. Nature 486 (7401), 59-67.

CBD, 2011. Decision adopted by the Conference of the Parties to the Convention on Biological Diversity at its tenth meeting. The Strategic Plan for Biodiversity 2011-2020 and the Aichi Biodiversity Targets. Convention on Biological Diversity.

Dudley, N., 2008. Guidelines for applying protected area management categories.

Duncanson, L., Liang, M., Leitold, V., Armston, J., Krishna Moorthy, S.M., Dubayah, R., ... Zvoleff, A., 2023. The effectiveness of global protected areas for climate change mitigation. Nature Communications 14 (1), 2908.

Geldmann, J., Barnes, M., Coad, L., Craigie, I.D., Hockings, M., Burgess, N.D., 2013. Effectiveness of terrestrial protected areas in reducing habitat loss and population declines. Biological Conservation, 161, 230-238.

Hassan, Z., Shabbir, R., Ahmad, S.S., Malik, A.H., Aziz, N., Butt, A., Erum, S., 2016. Dynamics of land use and land cover change (LULCC) using geospatial techniques: a case study of Islamabad Pakistan. SpringerPlus 5, 1-11.

Heino, M., Kummu, M., Makkonen, M., Mulligan, M., Verburg, P.H., Jalava, M., Räsänen, T.A., 2015. Forest loss in protected areas and intact forest landscapes: a global analysis. PloS one 10(10), e0138918.

Jantke, K., Kuempel, C.D., McGowan, J., Chauvenet, A.L.M., Possingham, H.P., 2019. Metrics for evaluating representation target achievement in protected area networks. Diversity and Distributions 25 (2), 170-175.

Jantke, K., Mohr, B., 2024. Little progress in ecoregion representation in the last decade of terrestrial and marine protected area expansion leaves substantial tasks ahead. Global Ecology and Conservation 52, e02972.

Jones, K.R., Venter, O., Fuller, R.A., Allan, J.R., Maxwell, S.L., Negret, P. J., Watson, J. E., 2018. One-third of global protected land is under intense human pressure. Science 360 (6390), 788-791.

Krkoška lorencová, E., Harmáčková, Z.V., Landová, L., Pártl, A., Vačkář, D., 2016. Assessing impact of land use and climate change on regulating ecosystem services in the Czech republic. Ecosystem Health and Sustainability 2(3), e01210.

Laurance, W.F., Carolina Useche, D., Rendeiro, J., Kalka, M., Bradshaw, C.J., Sloan, S. P., ... Scott McGraw, W., 2012. Averting biodiversity collapse in tropical forest protected areas. Nature 489 (7415), 290-294.

Meli, P., Rey-Benayas, J.M., Brancalion, P.H.S., 2019. Balancing land sharing and sparing approaches to promote forest and landscape restoration in agricultural landscapes: Land approaches for forest landscape restoration. Perspectives in Ecology and Conservation 17 (4), 201-205.

Miranda, J.J., Corral, L., Blackman, A., Asner, G., Lima, E., 2016. Effects of Protected Areas on Forest Cover Change and Local Communities: Evidence from the Peruvian Amazon. World Development 78, 288-307.

Parks, A., 2023. African Parks' 161 Strategy: Securing the Foundation of Africa's Protected Area Network.

Tang, X., 2020. The establishment of national park system: A new milestone for the field of nature conservation in China. International Journal of Geoheritage and Parks 8 (4), 195-202.

Venter, O., Fuller, R.A., Segan, D.B., Carwardine, J., Brooks, T., Butchart, S.H., ... Watson, J.E., 2014. Targeting global protected area expansion for imperiled biodiversity. PLoS biology 12 (6), e1001891.

Watson, J.E.M., Dudley, N., Segan, D.B., Hockings, M., 2014. The performance and potential of protected areas. Nature 515 (7525), 67-73.

Yang, Z., Zhan, J., Wang, C., Twumasi-Ankrah, M.J., 2022. Coupling coordination analysis and spatiotemporal heterogeneity between sustainable development and ecosystem services in Shanxi Province, China. Science of The Total Environment 836, 155625.

Yoo, Y., Hwang, J., Kim, Y., Lee, K.I., Lee, W.K., Biging, G.S., Jeon, S.W., 2024. Introducing a novel methodology for designation and management of protected areas in the context of climate change: A case study in the Republic of Korea. Ecological Indicators 158, 111536.

Automated Plant Species Identification Using 3D LiDAR Point Clouds: A Case Study Using Cabbage and Maize Plants

Mukesh Kumar Verma[1], *, Manohar Yadav[1]

[1] Geographic Information System (GIS) Cell, Motilal Nehru National Institute of Technology, Prayagraj, India, mukeshverma02feb@gmail.com, ssmyadav@mnnit.ac.in@gmail.com

* corresponding author

Abstract: Automated plant species identification plays a crucial role in various ecological, agricultural, and environmental monitoring applications. This paper proposes an effective approach utilizing 3D LiDAR point clouds for automated plant species identification. LiDAR technology provides detailed and accurate spatial information about the vegetation canopy, enabling precise characterization of plant structures in three dimensions. Our methodology involves several key steps. Initially, raw 3D LiDAR point cloud data is acquired from the two study areas (i.e., maize crop field and cabbage field). Next, preprocessing techniques are applied to filter noise and extract relevant features from the point cloud. Finally, plant volume, projected leaf area and plant heights of the two agricultural crops are estimated to differentiate the plant species on the basis of structural information. One of the significant advantages of our proposed approach is its ability to capture the intricate structural characteristics of different plant species with high accuracy and efficiency. By leveraging 3D LiDAR technology, our method transcends the limitations of traditional 2D imaging techniques, which often struggle to accurately differentiate between species with similar visual appearances. Experimental results demonstrate the effectiveness of our approach in accurately identifying plant species from 3D LiDAR point clouds. The proposed method shows promising performance across two types of vegetation and can further extended to other types of crops within the same field.

Keywords: 3D point cloud; plant phenotyping; terrestrial laser scanning; total station.

1 Introduction

Plant phenotyping is essential for plant species identification (Verma and Yadav 2024). Automated plant species identification using LiDAR technology is a promising approach for precise forest management and phenotyping. Various studies have demonstrated the effectiveness of LiDAR data in classifying tree species based on features like roughness parameters (Ana et al. 2022), scan angles (Brindusa et al. 2022), deep learning models (Bingjie et al. 2022) and intensity and texture features (Ao et al. 2022). These methods utilize advanced techniques such as K-means clustering, convolutional neural networks (CNNs), and random forest (RF) algorithms to accurately classify different plant species. LiDAR data enables the extraction of 3D structural information, individual tree point clouds, and phenotypic traits like leaf area and stem position, contributing to high-throughput phenotyping and precision agriculture applications (Lombard et al.

2020). By combining these diverse approaches, automated plant species identification using LiDAR proves to be a valuable tool for enhancing forest inventory, species discrimination, and plant phenotyping. We have developed methodology for the plant species identification using plant phenotyping parameters such as plant height, plant volume and projected leaf area using terrestrial laser scanner (TLS) and total station (TS) instruments.

2 Materials and methods

2.1 Study areas

The study area 1 chosen for the experiment and performance assessment of proposed methodology was located in Narayani Ashram (25° 29' 49.16273" N, 81° 52' 6.52379" E), a place in Govindpur area, Prayagraj, India.

(a)

(b)

Figure 1. Data collection from study areas (a) study area 1 (b) study area 2.

The selected study area 1 was a cabbage field with sandy loam soil that covered an area of 450 m2 (30 m × 15 m). Another study area 2 was chosen near Sam Higginbottom University of Agriculture, Technology and Sciences (25° 24' 29.9945" N, 81o 49' 56.6233"), Prayagraj, India. This study area 2 was an agricultural field having maize crop. Data collection was performed using TLS and TS. The maize crop in this study area was analyzed throughput its crop period and data collection were done at the tasseling stage of the maize crop. Figure 1 presents the study area 1 and 2.

2.2 Data acquisition

The data at two study areas were acquired using the experimental setup provided in the Figure 2. Five scan stations were setup to collect the complete 3D structure of the crops using FARO Focus[3D] Laser Scanner. The registration targets such as Spheres and Checkerboards are placed within the experimental setup to facilitates the registration process. The center of the checkerboards was also measured using the Trimble M3 Total Station. As center of checkerboards were measured using both the above instruments. Coordinate transformation is mandatory as we need the alignment of the z-axis towards the plumb line for the estimation of morphological parameters of the vegetable crops.
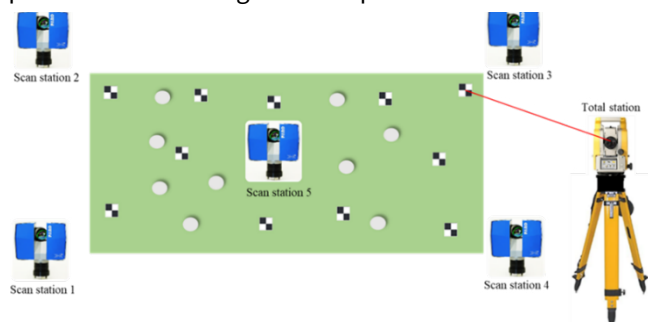

Figure 2. Experimental setup for data collection from study area 1 and 2.

The ground truth data was collected from the cabbage and maize crop field using measuring tape. The plant height, plant width and plant length were measured manually. And for maize crops the same parameters were measured. Projected leaf area and plant volume were calculated using the formulas given as equation (1) and (2) (Verma and Yadav 2024):

$$\text{Projected leaf area} = \pi * \frac{l}{2} * \frac{w}{2} \tag{1}$$

$$\text{Plant volume} = \frac{3}{4} * \pi * \frac{l}{2} * \frac{w}{2} * \frac{h}{2} \tag{2}$$

2.3 Proposed methodology

The data was collected from the study area 1 and 2 using instruments FARO Focus3D Laser Scanner and Trimble M3 Total Station. After the data collection based on the experimental setup in Figure 2, the raw point cloud data was merged and transformed using the FARO Scene software. Then, ground points were filtered using the methodology provided by Yadav et al. (2021). Then k-means algorithm was implemented to segment each individual from the non-ground points. Figure 3 presents the methodology workflow for plant species identification.
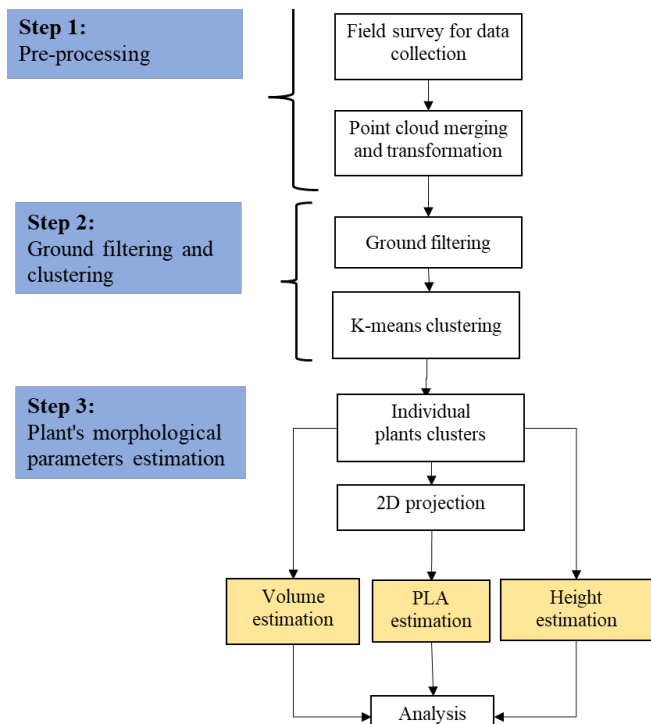

Figure 3. Methodology workflow.

2.3.1 Plant height estimation

The height of each plant was determined by averaging the distances between ten points located at both the top and bottom extremities of the plant. These averages were then subtracted to obtain the final height measurement, ensuring robustness against potential irregularities in plant morphology. Mathematically, the height (H) of each plant was calculated using the equation (3):

$$H = \frac{1}{10}\left(\sum_{i=1}^{10} P_i^{top}\right) - \frac{1}{10}\left(\sum_{i=1}^{10} P_i^{bottom}\right) \tag{3}$$

Where P_i^{top} and P_i^{bottom} represents the i-th point from the top and bottom of the plant, respectively. This meticulous approach ensured accurate and reliable height estimations for each individual plant, laying a solid foundation for subsequent analyses in our research.

2.3.2 Projected Leaf Area and Volume

The Quickhull algorithm offers an efficient method for computing the convex hull of a set of points in a plane. Initially, the algorithm identifies the leftmost (P_{left}) and rightmost (P_{right}) points as initial endpoints. These endpoints are then used to form a triangle encompassing all other points in the set. The process involves strategically partitioning the point set into subsets based on their position relative to the triangles formed by these initial endpoints and additional points. This partitioning is achieved by calculating the distance of each point (Pi) from the line segment connecting Pleft and Pright, represents the equation (4):

$$Hd_i = \frac{|(P_{right} - P_{left}) * (P_i - P_{left})|}{||P_{right} - P_{left}||} \tag{4}$$

Where × denotes the cross product and ||.|| denotes the Euclidean norm. Points with the maximum distance (dmax) are identified as the ones lying outside the current triangle. The process continues recursively until no points lie
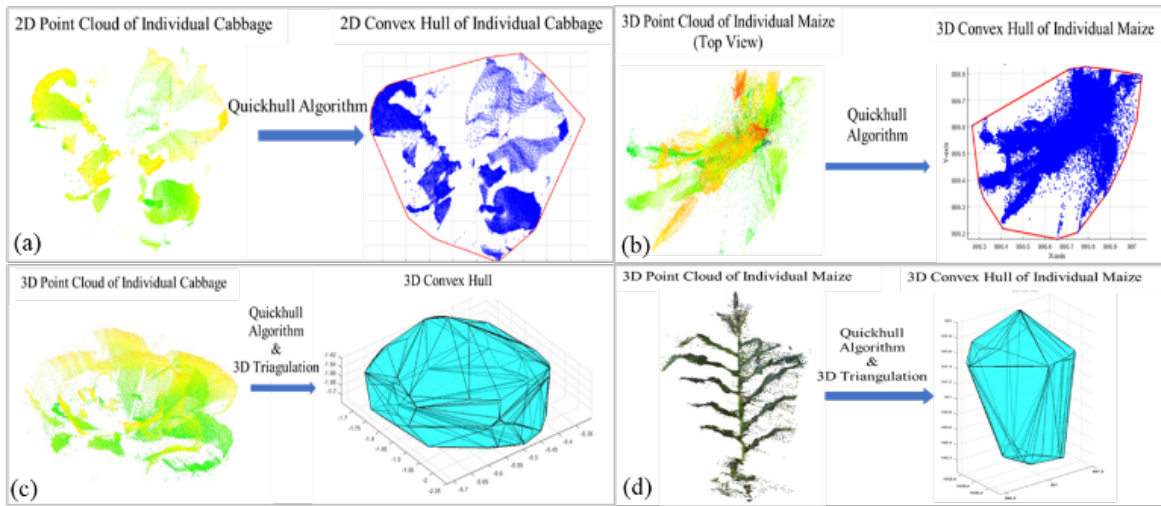
Figure 4. 2D convex hull of the plants after projection.

outside the current triangle. The process continues recursively until no points lie outside the triangles, at which point the convex hull is formed by merging the hulls of the subsets. This can be mathematically represented as equation (5):

$$\text{ConvexHull} = \text{Merge}(\text{QuickHull}(P_{left}, P_{right}, P_{outside})) \quad (5)$$

Where:

P_{left}: Points on the left side of a dividing line or plane.

P_{right}: Points on the right side of the same dividing line or plane.

$P_{outside}$: Points that lie outside the current convex hull being considered.

This iterative approach efficiently constructs the convex hull, making the Quickhull algorithm a valuable tool in computational geometry. Figure 4 presents the 2D convex hull of the crops.

3   Results

The plotted line graph (Figure 5) depicting cabbage plant height, projected leaf area, and volume, utilizing 3D point cloud data. At maturity, parameters were estimated to offer insights into plant development. These findings emphasize the complexity of cabbage plant growth and make evident the value of 3D point cloud analysis in understanding plant development dynamics. Figure 5 presents the variation in plant height, projected leaf area and volumes of the plants.

The stressed plants from the above plots (Figure 5) can be detected if the height of the plant is large and volume is less or large area is giving the less volume comparatively. A healthy plant should have optimized values of height, area and volumes. By comparing the respective height, area and volume parameters the plant species can be identified automatically. The variation in the plant height, volume and area can be easily differentiated among the cabbage and maize crops to differentiate between cabbage and maize crops. This study is a case study using cabbage and maize crops, further this methodology can be extended to differentiate between the greater number of crops automatically.
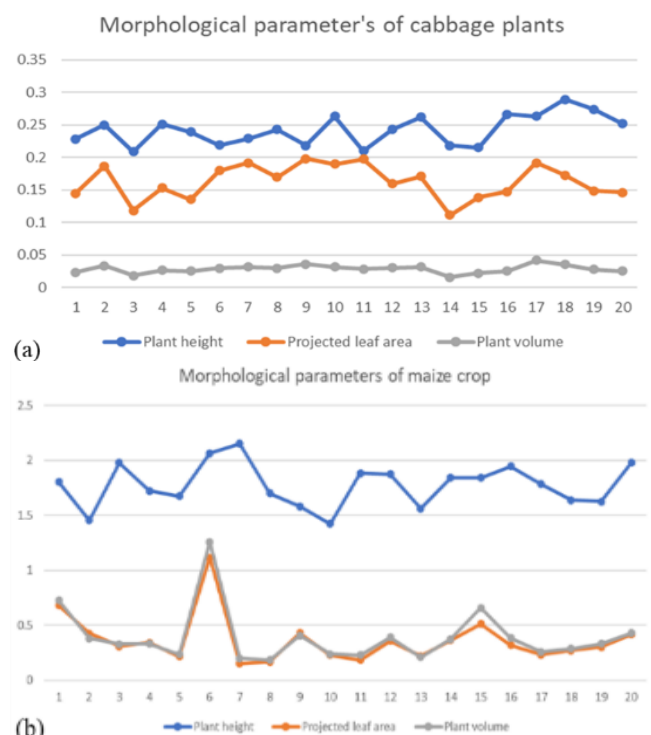
Figure 5. (a) Variation in the Plant Height, Projected Leaf Area and Volume of the individual cabbage plants (20 Sample Plants), (b) Variation in the Plant Height, Projected Leaf Area and Volume of the individual maize plants (20 Sample Plants).

4   Discussion

The study aimed to assess TLS data for mapping cabbage (low vegetation) and maize (high vegetation) by evaluating plant height, leaf area, and plant volume. TLS provided accurate estimations for cabbage but struggled with maize's complex foliage structure, impacting accuracy. Resolution influenced TLS's suitability, being advantageous for cabbage but insufficient for maize. Penetration depth into dense foliage, processing complexity, cost, and repeatability were significant considerations. Despite TLS's potential, challenges like resolution and processing complexity need addressing for effective monitoring. Future research should focus on

improving TLS resolution, processing efficiency, and integrating it with other remote sensing technologies for comprehensive agricultural vegetation monitoring.

5 Conclusions

This study explores the potential of TLS for mapping vegetation in agricultural landscapes, focusing on cabbage and maize. TLS accurately estimates vegetation parameters in low vegetation like cabbage but faces challenges with high vegetation like maize due to resolution limitations. Despite hurdles, TLS offers advantages like rapid, non-destructive data acquisition, enhancing vegetation monitoring in agriculture. Integrating TLS with other remote sensing tech like LiDAR and multispectral imaging shows promise for comprehensive vegetation mapping. Addressing TLS limitations requires ongoing research and technology improvements. Overall, TLS is a valuable tool for agricultural vegetation monitoring, with continued innovation vital for addressing agriculture challenges like crop monitoring and ecosystem management.

6 References

Ao, Z., Wu, F., Hu, S., Sun, Y., Su, Y., Guo, Q. Xin, Q., 2022. Automatic segmentation of stem and leaf components and individual maize plants in field terrestrial LiDAR data using convolutional neural networks. The Crop Journal 10 (5), 1239-1250.

Budei, B.C., St-Onge, B., Fournier, R.A. Kneeshaw, D., 2022. Effects of Viewing Geometry on Multispectral Lidar-Based Needle-Leaved Tree Species Identification. Remote Sensing 14 (24), 6217.

Liu, B., Huang, H., Su, Y., Chen, S., Li, Z., Chen, E. Tian, X., 2022. Tree species classification using ground-based LiDAR data by various point cloud deep learning methods. Remote Sensing 14 (22), 5733.

Lombard, L., Ismail, R. and Poona, N.K., 2020. Modelling forest species using Lidar-derived metrics of forest canopy gaps. South African Journal of Geomatics 9 (1), 31-43.

Novo, A., Gonzalez-Jorge, H., Comesana-Cebral, L.J., Lorenzo, H., Martinez-Sanchez, J., 2022. Semi-automated tree species classification based on roughness parameters using airborne lidar data. DYNA 97 (5), 528-534.

Verma, M.K. Yadav, M., 2024. Estimation of plant's morphological parameters using terrestrial laser scanning-based three-dimensional point cloud data. Remote Sensing Applications: Society and Environment 33, 101137.

Yadav, M., Khan, P., Singh, A.K. Lohani, B., 2021. An automatic hybrid method for ground filtering in mobile laser scanning data of various types of roadway environments. Automation in Construction 126, 103681.

Artificial Intelligence and Big Data

GLOBAL LAND COVER MAPPING – NEED FOR DISCRETE GLOBAL GRID SYSTEM
Frane Gilić, Martina Baučić, Samah Termos

QUANTIFYING TOTAL IMPERVIOUSNESS FROM BUILDING FOOTPRINT AREA AND VERY HIGH RESOLUTION AIR PHOTOGRAPHS
Dennis M. Fox, Mostafa Banitalebi, Richard Fournie, Yacine Bouroubi

A COMPARATIVE ANALYSIS OF PIXEL-BASED AND OBJECT-BASED APPROACHES USING MULTITEMPORAL PLANETSCOPE IMAGERY FOR LAND COVER CLASSIFICATION
Dino Dobrinić, Mario Miler, Damir Medak

THE ROLE AND USE OF BIG DATA IN SPATIAL ANALYSIS OF TOURISTIFICATION – EXAMPLE OF THE HISTORIC CORE OF DUBROVNIK
Dino Bečić

MAPPING LONG-TERM TRENDS IN ACTUAL EVAPOTRANSPIRATION IN DATA-SCARCE CONDITIONS IN AFGHANISTAN
Fazlullah Akhtar, Christian Borgemeiste, Bernhard Tischbein

DATA AUGMENTATION WITH GENERATIVE ADVERSARIAL NETWORK FOR SOLAR PANEL SEGMENTATION FROM REMOTE SENSING IMAGERY
Justinas Lekavičius, Valentas Gružauskas

Global Land Cover Mapping – Need for Discrete Global Grid System

Frane Gilić[1,], Martina Baučić[1], Samah Termos[2]*

[1] Faculty of Civil Engineering, Architecture and Geodesy, University of Split, Split, Croatia, fgilic@gradst.hr, mbaucic@gradst.hr

[2] Remote Sensing Center, Lebanese National Council for Scientific Research, Beirut, Lebanon, samahtermos@gmail.com

* corresponding author

Abstract: The quality of land cover maps is gradually advancing in terms of increased spatial and temporal resolution, and classification accuracy. However, the aspect of spatial referencing and techniques for representing land cover data has not been advancing. Representing land cover data in the form of a planar raster geospatial data model is still common, despite the various issues especially evident when working with global land cover data. This paper first analyses current approaches in georeferencing global LCLU datasets. Then it examines differences in areal calculations from raster data georeferenced in projected and geographic coordinate reference systems (CRSs). This analysis is performed for the case study of calculating built-up land cover change for the Lebanese 10-km coastal zone. Finally, this paper introduces the topic of discrete global grid systems (DGGSs) as a relatively new approach to handling global geospatial data. DGGSs manage spatial data on the surface of the ellipsoid, rather than in the flattened raster model and thus represent a step forward in managing global geospatial data.

Keywords: land cover; land use; raster; map projection; DGGS.

1   Introduction

Satellite images and the development of methods for their automatic analysis made possible producing land cover / land use (LCLU) data covering large areas, even the whole surface of the Earth. These kinds of satellite-images-derived LCLU products are almost exclusively delivered in a raster data format (Table 1) which is the reason why the analysis in this paper is limited only to the raster datasets. Well known problem that is related to handling geospatial data that cover large areas is the problem of distance, shape and area distortions associated with the traditional approach of flattening data from the Earth's surface. In the case of LCLU data, this flattening is usually performed by equal-area map projections.

The study elaborated by Steinwand et al. (1995) has identified the equal-area projections with the smallest distortions for raster data. In addition to distortions due to map projection, the authors analysed pixel distortion caused by reprojection. The study identified the interrupted Goode Homolosine, the interrupted Mollweide, the Wagner IV and Wagner VII as the best for global maps, the Lambert Azimuthal Equal-Area for hemispheric maps, and the oblated Equal-Area and the Lambert Azimuthal Equal-Area for continental maps. The interrupted map projections introduce computational issues and are not fully supported by today's software (Moreira de Sousa et al. 2019). However, by examining recent global LCLU products, the trend is to georeference global LCLU datasets in geographic coordinate reference systems (CRSs), rather than in projected ones. This can be observed from the data in Table 1 which lists some technical characteristics of five notable recent global LCLU products: ESA WorldCover (Zanaga et al. 2021), Esri's Sentinel-2 LCLU (Karra et al. 2021), GLC_FCS30D (Zhang et al. 2024), Dynamic World (Brown et al. 2022), and GLAD (Global Land Analysis and Discovery laboratory) LCLU dataset (Potapov et al. 2022). Visualisations of these LCLU datasets over the Lebanese capital Beirut are shown in Figure 1.

Georeferencing raster LCLU datasets in geographic CRS imposes various issues, including data replication due to meridian convergence (Figure 2a). This issue can be solved by keeping angular pixel size constant in a north-south direction and defining latitudinal zones with varying pixel sizes in an east-west direction (e.g., Defence Gridded Elevation Data standard (DGED, DGIWG 2020)). Another issue is related to performing areal calculations, which, although possible in modern GIS applications, is more complex in geographic CRSs than in projected ones. From the LCLU point of view, a particularly interesting class of DGGSs are equal-area ones that have cells with the same area on the same refinement level (i.e., hierarchical level).
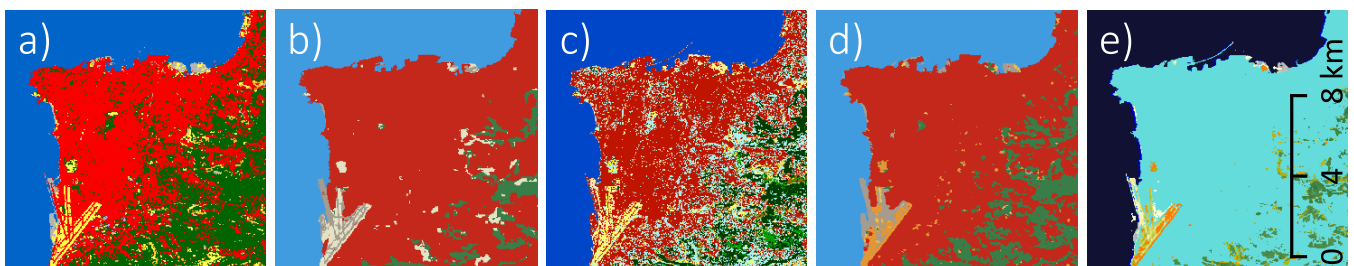

Figure 1. Visualizations of recent global LCLU products over Beirut, capital of Lebanon: (a) ESA WorldCover, (b) Esri's Sentinel-2 LCLU, (c) GLC_FCS30D, (d) Dynamic World, and (e) GLAD LCLU.
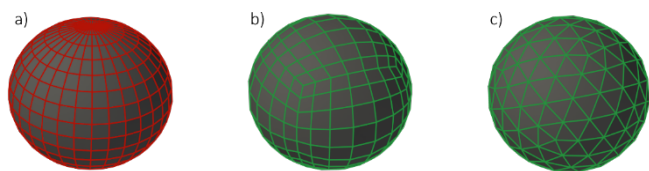
Figure 2. Discretisation of the surface of the ellipsoid by (a) grid of meridians and parallels and discrete global grid with (b) quadrangle cells and (c) triangle cells.

Table 1. Data format, CRS, and pixel size of recent global LCLU products.

LCLU product	Data format	CRS	Pixel size
ESA WorldCover	Raster, GeoTIFF (unsigned 8-bit integer, DEFLATE compression)	Geographic, WGS 84 (EPSG:4326)	0.30" (≈ 9.3 m at the equato)
Esri's Sentinel-2 LCLU	Raster, GeoTIFF (unsigned 8-bit integer, LZW compression)	Projected, WGS 84 / UTM	10.0 m
GLC_FCS30D	Raster, GeoTIFF (unsigned 8-bit integer, LZW compression)	Geographic, WGS 84 (EPSG:4326)	0.97" (≈ 30.0 m at the equator)
Dynamic World*	Raster, GeoTIFF (unsigned 8-bit integer, LZW compression)	Geographic, WGS 84 (EPSG:4326)	0.32" (≈ 10.0 m at the equator)
GLAD LCLU	Raster, GeoTIFF (unsigned 8-bit integer, LZW compression)	Geographic, WGS 84 (EPSG:4326)	0.90" (≈ 27.8 m at the equator)

*listed data correspond to the default download options on the Google Earth Engine.

Therefore, DGGSs solve the problem of distortions imposed by map projections by directly discretizing the surface of the ellipsoid (Figure 2b and 2c) and equal-area ones simplify the problem of areal calculations on the surface of the ellipsoid. DGGS can be viewed as a way of georeferencing spatial data, instead of using coordinates, and as a geospatial data format, along with vector and raster models (Kmoch et al. 2022). Differences between

DGGS and traditional (i.e., flattened) GIS approaches are provided by Li and Stefanakis (2020).

In this paper we examine differences in calculation procedures and obtained results from calculating change in an area of built-up land cover class from LCLU data georeferenced in projected and in geographic CRS. We also discuss what would be the benefits of referencing LCLU data with DGGSs.

2   Materials and methods

To illustrate the difference in processing procedure and obtained results when working with data georeferenced in the geographic and in projected CRSs, we decided to calculate the change in built-up area from 2015 to 2020 for the Lebanese 10-km coastal zone (i.e., zone that is 10 km inland from the coastline, hereafter 10-km CZ). We have chosen the GLC_FCS30D LCLU product for this calculation, which, as can be seen from Table 1, is delivered as a raster dataset georeferenced in the WGS 84 geographic CRS. Pixels are 0.97" wide in latitude and longitude direction. For the Lebanese 10-km CZ, which approximately spans from a latitude of 33°05' N to 34°39' N (WGS 84), GLC_FCS30D pixel sizes in east-west direction range from 25.2 to 24.7 m. In the north-south direction, pixel sizes are more stable, ranging from 29.8 m at the equator to 30.1 m at the poles. Along with GLC_FCS30D, we used the coastline and administrative border of Lebanon to construct a 10-km CZ which we afterwards spatially intersected with the Lebanese governorates. Those data were exported from the OpenStreetMap vector data and are also georeferenced in WGS 84 geographic CRS. All calculations were performed in the QGIS (version 3.28.6) free and open-source GIS application (with GDAL library version 3.6.4 and GRASS GIS provider plugin version 2.12.99).

2.1   Calculating area in projected CRS

When there is a task to compute areal statistics from data georeferenced in geographic CRS, the traditional approach would be to first convert data from geographic CRS to projected CRS that is based on the equal-area map projection or projection that introduces a tolerable level of areal distortions. After this conversion, the area is calculated by simply counting the number of desired pixels and then multiplying it with the constant area of each pixel. However, the problem with this approach is that it requires reprojecting the LCLU raster dataset, which inevitably introduces data loss (Lu et al. 2018). In this research, we decided to reproject the GLC_FCS30D LCLU raster to the projected Universal Transverse Mercator (UTM) zone 36N CRS (EPSG: 32636) with target pixel sizes of 25x30 m. UTM is not an equal-area projection but for most applications level of deformations it introduces is negligible. Calculating area, in this case, is straightforward: with the *Zonal statistics* tool in QGIS, it is possible to count the number of pixels corresponding to the built-up class in each governorate within a 10-km CZ and then multiply it with 750 m^2 (25x30 m^2) for 2015 and 2020.

2.2 Calculating area in geographic CRS

Another approach is to keep GLC_FCS30D data in geographic CRS. Pixels in this case are quadrangles bounded by meridians and parallels and it is possible to determine their area with a direct formula (Lapaine and Lapaine 1991). GRASS GIS provider, which is a QGIS plugin, enables using tools from the GRASS GIS application. One such tool is a *r.mapcalc.simple* tool that implements an *area()* expression. This expression enables generating a new raster in which pixel values correspond to the area of each GLC_FCS30D pixel on the surface of the ellipsoid. Then, with a common *Raster calculator* tool in QGIS, it is needed to generate a new raster with extracted pixels that correspond to the built-up class for each year. Finally, to calculate the final built-up areas, a *Zonal statistics* tool is required to summarize pixel values (i.e., their areas) within each Lebanese governorate.

3 Results

Table 2 lists areas of built-up land cover class calculated from GLC_FCS30D raster data georeferenced in WGS 84 geographic CRS (section 2.2) and from GLC_FCS30D data that were reprojected to the UTM projected CRS (section 2.1). These areas in Table 2 are given for 2015 and 2020, along with changes in built-up area and corresponding percentages. Percentages express built-up area change relative to the built-up area in 2015.

When comparing percentages of built-up area changes calculated from data georeferenced in geographic CRS, and in projected one, the largest difference is 0.03% for the Nabatieh governorate. For all other governorates, there is either no difference or the difference is 0.01%, which can partly be attributed to the rounding-related issues. When comparing built-up areas for each year calculated from data in different CRSs, differences go up to 0.05 km^2 (Akkar and Mount Lebanon Governorates).

4 Discussion

From the results listed in Table 2, it can be concluded that when a change in the built-up area has to be calculated, reprojecting data georeferenced in WGS 84 CRS to UTM CRS does not introduce significant differences from changes directly calculated from the data in WGS 84. Although this difference is not significant, traditionally common reprojection step is, as we have shown, obsolete, since modern GIS applications provide a way to make calculations from data georeferenced in geographic CRS. All geospatial raster data have some level of uncertainty associated with them and reprojecting them further increases those uncertainties. Therefore, reprojecting should, if possible, be avoided.

On the other hand, when comparing areas (not changes) in Table 2 that are calculated from data in WGS 84 and in UTM CRS, larger differences can be observed. It is interesting to notice that for both years differences in areas calculated

Table 2. Areas of built-up land cover class calculated from data in different CRSs for 2015 and 2020 and their change for the 10-km coastal zone of Lebanon.

Governorate (area in 10–km CZ)	Built–up area (km²)			
	CRS	2015	2020	Change*
Akkar (207.04 km2)	WGS 84	32.22	36.49	4.27 (13.25%)
	UTM	32.27	36.54	4.28 (13.25%)
	Difference (abs.)	0.05	0.05	0.01 (0.00%)
North (450.65 km2)	WGS 84	70.10	71.74	1.64 (2.33%)
	UTM	70.10	71.74	1.64 (2.34%)
	Difference (abs.)	0.00	0.00	0.00 (0.01%)
Keserwan–Jbeil (305.99 km2)	WGS 84	46.94	46.47	−0.47 (−0.99%)
	UTM	46.98	46.52	−0.47 (−1.00%)
	Difference (abs.)	0.04	0.05	0.00 (0.01%)
Beirut (21.47 km2)	WGS 84	17.11	17.03	−0.08 (−0.47%)
	UTM	17.10	17.02	−0.08 (−0.46%)
	Difference (abs.)	0.01	0.01	0.00 (0.01%)
Mount Lebanon (492.97 km2)	WGS 84	115.24	114.91	−0.33 (−0.29%)
	UTM	115.28	114.94	−0.34 (−0.28%)
	Difference (abs.)	0.04	0.03	0.01 (0.01%)
South (582.70 km2)	WGS 84	83.58	85.73	2.15 (2.56%)
	UTM	83.62	85.76	2.14 (2.57%)
	Difference (abs.)	0.04	0.03	0.01 (0.01%)
Nabatieh (35.21 km2)	WGS 84	3.33	3.53	0.20 (6.02%)
	UTM	3.34	3.54	0.20 (6.05%)
	Difference (abs.)	0.01	0.01	0.00 (0.03%)

* change is calculated as: (area in 2020) – (area in 2015); percentages as: [(area in 2020) – (area in 2015)] / (area in 2015)

from data in UTM and in WGS 84 are larger than corresponding differences built-up area change. This means that approximately the same level of difference was introduced in areal calculations for each year, but differences were almost nullified when calculating the change. Although we do not find observed differences to be significant, it must be emphasized that the presented analysis was limited to a relatively small geographical area. If the analysis was performed globally, the calculation procedure would either be notably more complex, or differences would be much larger. Previously stated issues related to georeferencing LCLU data in geographic or projected CRS can be mitigated by georeferencing them with DGGS. By referencing global LCLU products in equal-area DGGS, the process of calculating the area of each LCLU class would be as simple as calculating it from raster data in equal-area projection, while keeping data georeferenced directly on the surface of the ellipsoid. LCLU data production workflow can also benefit from DGGS since it is particularly suitable for 'vertically' integrating data that are linked to a specific location (Li and Stefanakis 2020). This means that all input data that are used for generating LCLU data can first be converted to DGGS and then classification can be performed. However, it should be noted that there are still various issues related to the implementation and acceptance of DGGSs by the GIS community. As Goodchild (2019) states, DGGS is computationally more demanding than current flattened data models and it is conceptually more complex than rasters. From the LCLU data perspective, one issue is the fact that cell size in DGGSs is predetermined by a specific DGGS implementation. This means that DGGS cell size might not match the pixel size of satellite images from which land cover data were extracted.

5 Conclusions

In this paper, we compared two methods of calculating the area of built-up land cover change from LCLU data delivered in raster format. The same raster datasource was used in both methods, but in one method raster was georeferenced in geographic CRS, and in another it was transformed to the projected CRS before calculations. Because of the relatively small geographical scope of the analysis (Lebanese 10-km CZ), no significant differences were observed. However, we showed that it is quite easy to make calculations directly from data in geographic CRS, which is a traditionally avoided approach. We also discussed the benefits of using DGGS in relation to representing LCLU data, especially global ones. One of the main reasons for the potential of the DGGS becoming more widely used is the fact that it represents geographic reality in a way that is more adapted to the actual shape of the Earth, as compared to the current flattened approaches.

6 References

Brown, C.F., Brumby, S.P., Guzder-Williams, B., … Tait, A.M., 2022. Dynamic World, Near real-time global 10 m land use land cover mapping. Scientific Data 9, 251.

[DGIWG] Defence Geospatial Information Working Group, 2020. DGIWG 250 Defence Gridded Elevation Data Product Implementation Profile.

Goodchild, M.F., 2019. Preface. Cartographica 54, 1-3.

Karra, K., Kontgis, C., Statman-Weil, Z., … Brumby, S.P., 2021. Global land use / land cover with Sentinel 2 and deep learning, in: 2021 IEEE International Geoscience and Remote Sensing Symposium IGARSS. 4704-4707.

Kmoch, A., Matsibora, O., Vasilyev, I., Uuemaa, E., 2022. Applied open-source Discrete Global Grid Systems. AGILE: GIScience Series 3, 1-6.

Lapaine, Miljenko, Lapaine, Miroslava, 1991. Površina elipsoidnog trapeza. Geodetski list 45 (68), 367-373.

Li, M., Stefanakis, E., 2020. Geospatial Operations of Discrete Global Grid Systems—a Comparison with Traditional GIS. Journal of Geovisualization and Spatial Analysis 4, 26.

Lu, M., Appel, M., Pebesma, E., 2018. Multidimensional arrays for analysing geoscientific data. ISPRS International Journal of Geo-Information 7.

Moreira de Sousa, L., Poggio, L., Kempen, B., 2019. Comparison of FOSS4G Supported Equal-Area Projections Using Discrete Distortion Indicatrices. ISPRS International Journal of Geo-Information 8, 351.

Potapov, P., Hansen, M.C., Pickens, A., … Kommareddy, A., 2022. The Global 2000-2020 Land Cover and Land Use Change Dataset Derived From the Landsat Archive: First Results. Front. Remote Sensing 3, 856903.

Steinwand, D.R., Hutchinson, J.A., Snyder, J.P., 1995. Map projections for global and continental data sets and an analysis of pixel distortion caused by reprojection. Photogramm. Engineering and Remote Sensing 61, 1487-1497.

Zanaga, D., Van De Kerchove, R., De Keersmaecker, W., … Arino, O., 2021. ESA WorldCover 10 m 2020 v100.

Zhang, X., Zhao, T., Xu, H., Liu, W., … Liu, L., 2024. GLC_FCS30D: the first global 30 m land-cover dynamics monitoring product with a fine classification system for the period from 1985 to 2022 generated using dense-time-series Landsat imagery and the continuous change-detection method. Earth System Science Data 16, 1353-1381.

Quantifying Total Imperviousness from Building Footprint Area and Very High Resolution Air Photographs

Dennis M. Fox[1],*, Mostafa Banitalebi[1], Richard Fournie[2], Yacine Bouroubi[2]

[1] Université Côte d'Azur, UMR ESPACE CNRS, Nice, France, dennis.fox@univ-cotedazur.fr, mostafa.banitalebi@univ-cotedazur.fr

[2] Department of Applied Geomatics, CARTEL, Université de Sherbrooke, Sherbrooke Canada, Richard.Fournier@USherbrooke.ca, Yacine.Bouroubi@USherbrooke.ca

* corresponding author

Abstract: Imperviousness is the sealing of the soil surface by artificial materials that inhibit water transfer between the surface and soil. It has become a major environmental indicator of land cover change due to its impacts on hydrological and energy fluxes in the environment. Quantifying imperviousness has improved in the past decades with remote sensing technologies, but several challenges remain due to classification errors. We developed an innovative method based on vector building and road layers to quantify total imperviousness with greater accuracy when compared to current methods. Imperviousness was predicted with an accuracy approaching or surpassing 90% depending on the method (random forest, regression): with building footprint alone, R^2 value is about 0.88 when comparing simulated to observed values, and this increases to 0.94 when a road layer is added.

Keywords: imperviousness; building footprint area; machine learning.

1   Introduction

The conversion of agricultural or natural land covers to urban/suburban uses represents one of the fastest land cover transitions occurring globally. As cities expand onto agricultural and natural soils, the surface is overlain with impervious materials that inhibit water flow into the soil. Imperviousness therefore lowers groundwater recharge and increases flood risk by increasing peak discharge and total storm runoff (Arnold and Gibbons 1996, Jacobson 2011). In addition, imperviousness aggravates urban heat island effects (Hua et al. 2020, Shi et al. 2023) among other impacts. Imperviousness is therefore a key environmental indicator that is evolving rapidly both spatially and temporally throughout the world. The objective of this study is to improve imperviousness estimates by using vector building footprint and road layers in combination with very high resolution (20 cm) ortho-rectified aerial photographs.

2   Materials and methods

Quantifying imperviousness was carried out in 2 steps. Firstly, imperviousness was quantified for a selection of cities in France; secondly, statistical methods were used to relate imperviousness to building footprint and road vector layers.

2.1   Quantifying imperviousness

For 37 main cities located throughout France, 100 x 100 m polygons were created over a range of apparent building density conditions. Cities from all 13 regions were included. The number of polygons per city ranged from 4 to 20 with a total of 230 polygons in all. For each polygon, 100 random points were generated. The points were overlain on high resolution (20 cm) aerial photographs, and the surface of each point was visually classed as impervious (building, road, parking lot or other) or pervious (vegetation, agricultural field). In all, 23,000 points were visually identified and manually inputted into an attribute table. These observations provided the reference or "Observed" imperviousness values.

2.2   Creating the imperviousness model

Observed imperviousness was related to 3 potential predictors: 1 – building area alone, 2 – building area and cumulative road length, 3 – building area and road area. Hence, for each of the 230 polygons, the building area, road length, and road area were extracted automatically from the National Geographic Information (IGN) BD-TOPO database; road area was calculated as the product of road length * road width. To predict imperviousness, several techniques were initially tested to relate imperviousness to the predictors described above. These were progressively reduced to the following methods: random forest, non-linear regression, and linear regression on transformed (square root) variables. For each method, the total sample of 230 observations was divided into 160 calibration polygons (70%) and 70 validation polygons (30%). Metrics used to evaluate model performance were the following: R^2, Mean Absolute Error (MAE), Root Mean Square Error (RMSE). For a selection of 68 polygons located in the central region of France, imperviousness values were categorized as Urban continuous or Urban discontinuous (Suburban).

3   Results

Results are presented in two sub-sections: the first provides basic descriptive statistics of the variables used in the analysis and the second deals with the prediction results.

3.1   Polygon data characteristics

In theory, the random point method should provide representative distributions of building area in the polygons. However, the distributions shown in Figure 1 (left and middle) are not identical. Both distributions show a

first mode in the 0-5% range, but the random numbers method shifts the second mode to greater values than the BD-TOPO footprint area data. Mean and median random number building footprint areas are 31.2% and 30.5%, respectively; corresponding values for the BD-TOPO data are 25.7% and 20.8%, respectively. The random numbers method therefore has slightly greater building area values than the BD-TOPO method. Figure 1 (right) plots random numbers percentage building area versus BD-TOPO percentage building area, and the curve shows that the initial imperviousness values, in the range of about 0-10% fall on the 1:1 line, but that most of the remaining values are slightly greater with the greatest spread in the 10–50% range. Visual examination shows that the building footprint in the BD-TOPO layer is based on ground level contours whereas the air photo random number method includes overhanging rooftops, so values are greater. The Pearson-r correlation coefficient for this plot is 0.94.
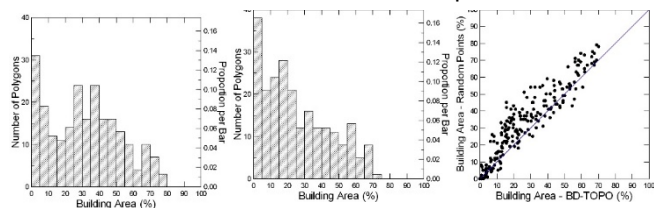

Figure 1. Frequency histogram of building area from random point data (left), Frequency distribution of building area from BD-TOPO (middle), Building area from random points versus building area from polygon layer (right).

Road length unit (m) (Figure 2 left) is different from the other values, so comparing distributions has limited meaning. The frequency histogram is provided nonetheless for other modelers; mean and median road length values are 212.8 m and 202.6 m per 10,000 m^2 polygon, respectively. Road area (middle) values are presented in the same % unit as building area values, and percentage road area rarely surpasses 20% of the total polygon area. Mean and median values are 8.4% and 8.1%, respectively. This corresponds roughly to about 25% to 30% of the percentage building area within a polygon.
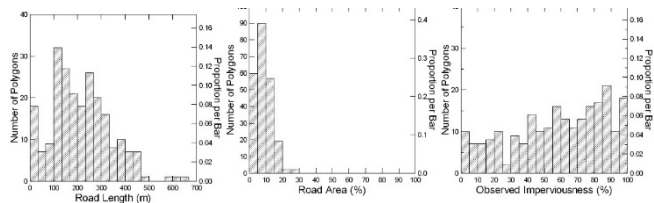

Figure 2. Frequency histogram of cumulative road length (left), Frequency histogram of road area (middle), Frequency Distribution of observed imperviousness values (right).

The distribution of observed imperviousness (right) reflects the cumulative impervious surfaces within a polygon. Where building area never surpassed 80%, imperviousness can reach 100%. For a selection of 68 polygons, mean and median impervious values for Urban were 88.6% and 89.5%, respectively. As expected, corresponding values for the Suburban category were lower at 70.3% and 73.0%, respectively. The range in imperviousness values was greater for Suburban (from 20.0% to 99.0%, std. dev 19.1%) compared to Urban, which ranged from 47.0% to 100.0% (std. dev. 10.3%), so in terms

of imperviousness, the Urban category represents a less heterogenous environment than Suburban where imperviousness can be quite low to very high.

3.2 Predicting imperviousness from building and road layers

Prediction results will be presented according to the explanatory variables used, from the simplest (building area alone) to the most elaborate (building area and road area). Accuracy metrics for all the prediction methods are summarized in Table 1.

Figure 3 shows results for building area alone. Although the results are globally less good than when road length is included, the accuracy metrics shown in Table 1 remain high. Non-linear regression gives the best results, ahead of random forest, and linear regression has the lowest accuracy. This order is maintained throughout the results regardless of the explanatory variables used. In addition, residuals are clearly not randomly distributed in the linear regression model used.

Table 1. Accuracy metrics for the different predictive models from validation data (bold numbers represent best results).

Method	R^2	MAE	RMSE
RF Bldg. Area	0.83	8.37	11.69
Non-Lin., Bldg. Area1	0.90	6.25	8.97
Linear, Bldg. Area2	0.84	9.40	12.06
RF Bldg. Area & Road length	0.90	7.25	10.47
Non-Lin., Bldg. Area & Road length3	0.93	5.63	7.59
Linear, Bldg. Area & Road length4	0.87	9.22	11.52
RF Bldg. Area & Road area	0.90	6.32	8.81
Non-Lin., Bldg. Area & Road area5	0.93	5.41	7.39
Linear, Bldg. Area & Road area6	0.88	8.91	11.08

[1] imperv.$=(8.661+3.982*x)/(1+0.025*x)$;
x=percentage building area;
[2] sqrt. imperv.$=2.760+0.954*x$;
x=sqrt. percentage building area;
[3] imperv.$=(-1.431+4.033*x_1+2.322*x_2)/(1+0.030*x_1+0.009*x_2)$;
x_1=percentage building area,
x_2=road length;
[4] sqrt. Imperv.$=1.595+0.820*x_1+0.651*x_2$;
[5] imperv.$=(-1.148+4.224*x_1+0.082*x_2)/(1+0.033*x_1)$; x_1=percentage building area, x_2=percentage road area;
[6] sqrt.Imperv.$=1.752 + 0.825 *x_1 +0.115*x_2$;
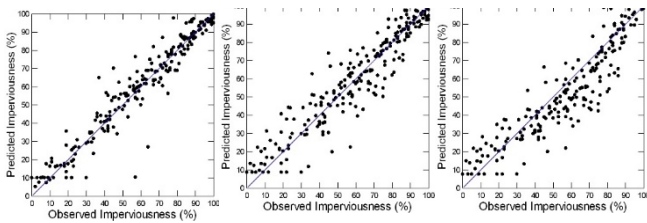x_1=sqrt. building area,
x_2=sqrt. road area

Figure 3. Imperviousness predicted from Random Forest on building area alone (left), non-linear regression on building area alone (middle), linear regression on building area alone (right).

Metrics improve as road length is added to percentage building area as an explanatory variable (Figure 4). The improvement is greatest for random forest which increases by 0.07 units in the R^2 value and the MAE decreases by about 1.1%. Corresponding values for non-linear regression are 0.03 and 0.62%.
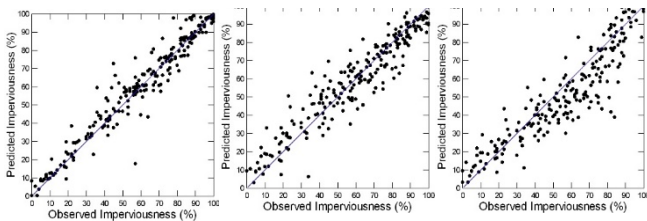

Figure 4. Imperviousness predicted from Random Forest on building area and road length (left), non-linear regression (middle), linear regression (right).

Using road area (Figure 5) instead of road length to predict imperviousness did not change the R^2 values for random forest or non-linear regression, but it improved both the MAE and the RMSE substantially (Table 1). When all three accuracy metrics are taken into account, the best performance is the non-linear regression using percentage building and road areas, non-linear regression using percentage building area and road length, and finally, random forest using percentage building and road areas.

Figure 6. Example of high imperviousness and low building/road areas.

4 Discussion

The methods described above provide a quick and efficient means of estimating imperviousness accurately from building and road vector layers. The most frequent cases of outliers (e.g. the 2 points in the lower right corner of Figure 3) arise in the presence of large parking lots where there are few buildings and roads but a high impervious surface (Figure 6).

When the observed values are compared to the values in the 100-m Copernicus Imperviousness Density 2018, the Pearson R-value is high (0.90), but Figure 7 shows that Copernicus tends to underpredict imperviousness below an imperviousness threshold of about 40% compared to our observed results. Similar results were also observed in Norway (Strand 2022).

5 Conclusions

Imperviousness was estimated accurately from building and road vector layers. Explained variance for the best models

was greater than 90% and MAE values were less than 6%. Where national building layers are available, quantifying the entire national coverage can take only a few hours versus several weeks or months of extensive image classification. Most countries are currently elaborating their own building footprint layers, so we can expect data
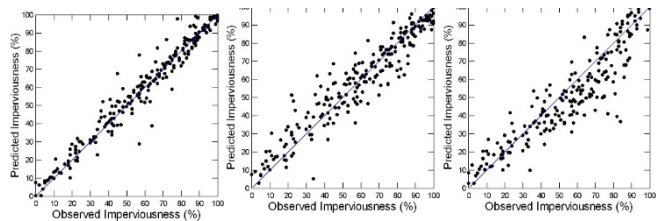

Figure 5. Imperviousness predicted from Random Forest on building area and road area (left), non-linear regression on building area and road area (middle), linear regression on building area and road area (right).
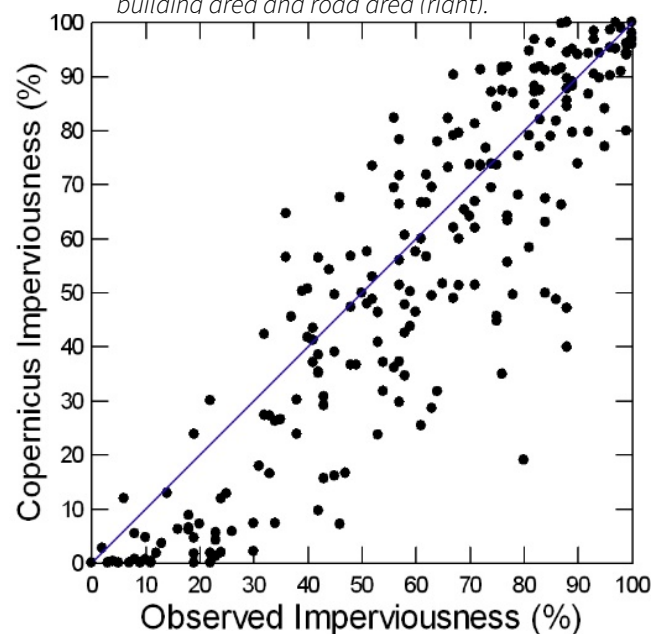
Figure 7. Copernicus imperviousness versus Observed imperviousness.

availability to grow exponentially. We are currently starting to explore the potential of extrapolating our results to other countries with freely available building polygon data.

6   References

Arnold, C.L., Gibbons, C.J., 1996. Impervious surface coverarge: the emergence of a key environmental indicator. Journal of the American Planning Association 62, 243-258.

Copernicus, n.d. High Resolution Layer Imperviousness, https://land.copernicus.eu/en/products/high-resolution-layer-imperviousness. (Accessed 11 June 2024).

Hua, L., Zhang, X., Nie, Q., Sun, F., Tang, L., 2020. The Impacts of the Expansion of Urban Impervious Surfaces on Urban Heat Islands in a Coastal City in China.

Jacobson, C.R., 2011. Identification and quantification of the hydrological impacts of imperviousness in urban catchments: A review. Journal of Environmental Management 92, 1438-1448.

Shi, Z., Li, X., Hu, T., Yuan, B., Yin, P., Jiang, D., 2023. Modelling the intensity of surface urban heat island based on the impervious surface area. Urban Climate 49, 101529.

Strand, G.H., 2022. Accuracy of the Copernicus High-Resolution Layer Imperviousness Density (HRL IMD) Assessed by Point Sampling within Pixels. Remote Sensing 14 (15), 3589.

A Comparative Analysis of Pixel-Based and Object-Based Approaches Using Multitemporal PlanetScope Imagery for Land Cover Classification

Dino Dobrinić[1],*, Mario Miler[1], Damir Medak[1]

[1] University of Zagreb Faculty of Geodesy, Chair of Geoinformatics, Zagreb, Croatia, dino.dobrinic@geof.unizg.hr; mario.miler@geof.unizg.hr; damir.medak@geof.unizg.hr

* corresponding author

Abstract: Remote sensing plays a crucial role in monitoring and managing land cover change and provides valuable insights for various applications, including environmental monitoring, urban planning, and natural resource management. In recent years, advances in sensor technology have led to the availability of high-resolution satellite imagery, enabling fine analysis of land cover dynamics. The study uses a multitemporal approach, where PlanetScope imagery are acquired at different points in time to capture temporal variations in land cover characteristics. The eight spectral bands provide improved ways to distinguish between different land cover types, including vegetation, water bodies, urban areas, and agricultural fields. Two classification approaches are evaluated: pixel-based (PB) classification, which assigns a land cover class to each individual pixel based on its spectral characteristics, and object-based (OB) classification, which groups neighbouring pixels into objects or segments and assigns a class label to each object based on its spectral, spatial, and contextual attributes. The OB approach performed better than the PB approach with an overall accuracy of 85.43%, compared to 81.90%, respectively. Also, 'salt-and-pepper effect' was significantly reduced using the OB approach. The study also investigates the potential advantages and limitations of each approach in capturing subtle land cover changes, spatial heterogeneity, and spectral variability.

Keywords: land cover classification; OBIA; pixel-based; Random Forest; segmentation.

1   Introduction

In recent decades, the increasing availability of remote sensing (RS) data, characterized by improved spectral, spatial, and temporal resolution, has been increasingly exploited for the detection and classification of different land use/land cover (LULC) types (Georganos et al. 2018). However, accurate mapping of land cover classes remains a challenge due to the high spectral variation within a class and spectral similarities between different classes (Dobrinić et al. 2021). These challenges cannot be effectively addressed with conventional approaches that rely solely on spectral information for image classification. Spectral heterogeneity within certain land cover types often leads to misclassification of pixels, resulting in a 'salt-and-pepper effect' (Hirayama et al. 2018).

In recent years, Object-Based Image Analysis (OBIA) has established itself as an efficient method for classifying high-resolution satellite imagery (Blaschke 2010). Object-

Based Image Analysis (OBIA) methods have been developed to effectively classify satellite imagery with medium to high spatial resolution. These methods present a compelling alternative to traditional pixel-based (PB) approaches. Rather than examining individual pixels, OBIA aggregates pixels into objects or segments using homogeneity criteria, such as spectral or spatial attributes. This approach provides additional geographic and geometric features associated with the objects, including shape, length, neighbourhood, and topology. Therefore, much of the research has focused on comparing pixel- and object-based classifications in heterogeneous landscapes using different machine learning algorithms (Tassi et al. 2021, Qu et al. 2021). Both papers compared PB and OBIA approaches for LULC classification and proved that classification results were improved when applying object-based classification models. Furthermore, additional features were used in these studies to improve classification accuracy, such as spectral indices, topographic features and/or texture variables.

Previous research improved classification accuracy using low-resolution satellite imagery (e.g. Landsat-8 with a spatial resolution of 30 meters). Therefore, the aim of this research is (1) to use the multi-temporal, high-resolution PlanetScope product with a spatial resolution of 3 meters and eight spectral bands for land cover (LC) classification and (2) to compare the accuracies of pixel-based (PB) and object-based (OB) classification methods in delineating land cover types.

2   Materials and methodology

2.1   Research area

The city of Varaždin as an urban settlement and its surrounding areas (e.g. forest, urban green areas, arable land) were selected for land cover classification. Varaždin has a warm-summer, humid continental climate (Dfb) bordering on a maritime climate (Cfb), with an average annual temperature of 10°C and an average annual precipitation of 843.1 mm. For this study, an area of approx. 600 km2 was divided into the following land cover classes: Arable land, forest, water, cultivated soil, bare soil, grassland and orchard (Dobrinić et al. 2021).

2.2   Data

This study used commercial PlanetScope (PS) data for multitemporal (MT) land cover classification. Since 2016, Planet Inc. has provided four-band multispectral imagery (i.e., blue, green, red, and near–infrared - NIR), and since

2019, the SuperDove (PSB.SD) satellite constellation has provided 3-meter multispectral image resolution with eight spectral bands (Table 1). Therefore, three PSB.SD images were selected for LC classification, with 0% cloud cover and as a Level 3A product (Gašparović et al. 2023).

Table 1. Overview of the PSB.SD images used in this research.

Parameter	Value			
Bands	Coastal Blue (B1)	Blue (B2)	Green I (B3)	Green (B4)
	Yellow (B5)	Red (B6)	Red-Edge (B7)	Near-Infrared (B8)
Resolution	3 m			
Date	20/06/2023	20/07/2023	21/08/2023	

2.2.1 Vegetation Indices

As mentioned in section 2.2, PSB.SD offers four additional spectral bands compared to the original PS data, which leads to a better differentiation of the different LC classes. Furthermore, a wider range of spectral indices (e.g. vegetation, soil, urban) can be derived from the PSB.SD images, providing a deeper insight into the environmental dynamics. Therefore, NDVI (normalized difference vegetation index), NDWI (normalized difference water index), EVI (enhanced vegetation index), SAVI (soil adjusted vegetation index), and GRVI (green-red vegetation index) were considered in this study. For EVI and SAVI, the L-factor was set to 0.5.

2.3 Land Cover Classification

2.3.1 Pixel-based

Pixel-based classification is often used in remote sensing, e.g. in the LC classification of satellite images, where each pixel of the image is assigned a class label. Each pixel is classified independently without considering its spatial context, which can be problematic in complex landscapes. Compared to object-based classification, it is easier to implement and less computationally expensive. In addition, it often relies on spectral indices or statistical methods for classification.

2.3.2 Object-based

In object-based image analysis (OBIA), classification is based on pixel groups that take into account both the spectral and spatial properties of the image objects. Therefore, OBIA is well suited for LC classification in heterogeneous landscapes with spatially coherent features. In this study, the image was segmented before classification using the multi-resolution segmentation (MRS) algorithm, which is known as a bottom-up method for merging regions (Liu et al. 2018). The selection of optimal segmentation parameters, i.e., scale, shape, and compactness, is often based on trial and error (Hay and Castilla 2008), and the parameters were set to 45, 0.3, and 0.5, respectively.

2.4 Accuracy Assessment

The results of the pixel- and object-based classifications were evaluated using a standard confusion matrix to calculate the overall accuracy (OA) and the kappa coefficient (Olofsson et al. 2014). In addition, producer and user accuracy was determined to assess omission and commission errors for each class (Olofsson et al. 2014). Furthermore, stratified random sampling was performed for LC classification (Table 2). A total of 662 samples were randomly divided into a training set (70%) and a test set (30%).

Table 2. The number of used pixels for PB and number of image objects for OB classification.

Class	Pixel-based	Object-based
Cropland	61205	100
Forest	67204	39
Water	207246	40
Built-up	6233	248
Bare soil	68736	40
Grassland	55957	195

3 Results and discussion

The results of LC classification using pixel-based and object-based approaches and multitemporal PS images are shown here. Although the focus of this study was on the comparison between the PB and OB, it should be noted that Random Forest (Breiman 2001) was used as the machine learning method. The OB approach performed better than the PB approach with an OA of 85.43%, compared to 81.90% (Table 3). Similar performance was achieved in the study by Qu et al. (2021), where the OB approach outperformed the PB approach by 1.81% and showed better performance in identifying smaller objects, resulting in a reduction of the salt-and-pepper effect. Similar performance (i.e. OB outperformed the PB approach) was also shown in the study by Cui et al. (2022), where PS images were used with the RF algorithm and an OA of 93.87% was achieved.

In addition, Table 3 shows a detailed insight into the ability to discriminate between land cover classes by the accuracy of the user (UA) and producer (PA). The highest accuracy was obtained for the water class (large homogeneous area) for both approaches, while the OB approach proved its superiority for small objects assigned to the built-up class. Lower accuracy values were obtained for the vegetation LC classes (i.e. cropland, grassland) in heterogeneous landscapes. There are two possible reasons for this: (1) lower quality of vegetation patterns used from the national ARKOD Land Parcel Identification System (LPIS), and (2) for the OB approach, the segmentation parameters, i.e. scale, shape and compactness, need to be fine-tuned for the delineation of agricultural fields. Aguilar et al. (2016) tested different combinations of shape and compactness values for extracting greenhouses from WorldView-2 images to determine the optimal setting of segmentation parameters for multi-resolution parameters.

As mentioned in the Introduction, the traditional PB classification method can lead to a "salt and pepper" effect, while the OB approach reduces this problem by considering the neighborhood information of a given pixel (Luo et al. 2021).

Table 3. Overall and per-class accuracy (%) for PB and OB approach.

Class / accuracy	Pixel-based		Object-based	
	PA	UA	PA	UA
Cropland	66.67	72.73	63.33	70.37
Forest	100.00	71.43	100.00	85.71
Water	100.00	100.00	100.00	100.00
Built-up	90.00	87.10	95.95	91.03
Bare soil	78.95	76.92	75.00	90.00
Grassland	78.95	84.37	79.66	81.03
OA	81.90		85.43	
Kappa	0.76		0.80	

Figure 1 shows a comparison of LC classification with the PB approach (left side) and the OB approach (right side). Due to the limited scope of the paper, only a subset of the study area is shown, but the improvements in LC classification with the OB approach can be seen in the central part of Figure 1 for the "Built-up" class and for the vegetation classes (i.e. forest and grassland) in the northern part of Figure 1. The delineation of the arable land class is also better recognizable with the OB approach.
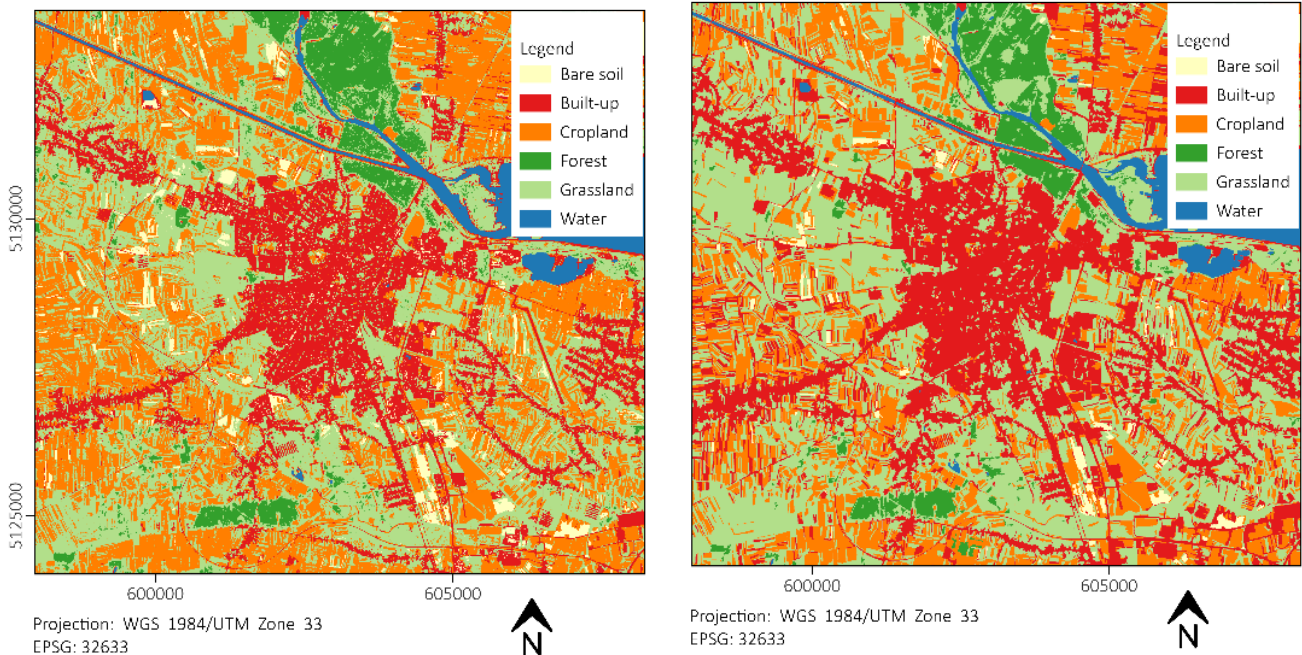
classification task and their determination can directly influence the subsequent classification (Ma et al. 2017).

4 Conclusions

The aim of this study was to use multi-temporal, high-resolution PlanetScope imagery and compare the performance of pixel-based (PB) and object-based (OB) approaches to land cover classification. The OB method performed better than PB with an overall accuracy (OA) of 85.43% compared to 81.90%. Possible factors contributing to lower accuracy per class include the quality of vegetation samples from the national Land Parcel Identification System (LPIS) and the need for finer adjustment of segmentation parameters for agricultural field delineation in the OB approach.

Overall, this comparative analysis highlights the potential of the OB approach using multitemporal PlanetScope imagery for land cover classification while highlighting areas for further refinement and optimization, especially in the context of vegetation classification in heterogeneous landscapes. Further research should focus on more advanced deep learning techniques (e.g., convolutional neural networks), which can exploit relations between

Figure 1. LC classification with the PB (left) and the OB (right) approach using the RF algorithm.

Although the OB approach outperformed the PB approach in LC classification using MT Planetscope images, some limitations of the study need to be mentioned. First, the samples were collected via the national ARKOD LPIS database and manually. Since the overall accuracy of LC classification depends on the quality and semantic distribution of the reference dataset, its refinement needs to be ensured e.g. by the CORINE or LUCAS LC database (Dobrinić et al. 2021). In addition, further research should focus on a specific task (e.g. classification of urban areas, vegetation mapping, wetland monitoring, etc.), as the segmentation parameters are highly dependent on the

pixels and objects on the satellite imagery.

5 References

Aguilar, M. A., Aguilar, F. J., García Lorca, A., Guirado, E., Betlej, M., Cichón, P., …, Parente, C., 2016. Assessment of multiresolution segmentation for extracting greenhouses from WorldView-2 imagery. The International Archives of

the Photogrammetry, Remote Sensing and Spatial Information Sciences 41, 145-152.

Blaschke, T., 2010. Object based image analysis for remote sensing. ISPRS journal of photogrammetry and remote sensing 65 (1), 2-16.

Breiman, L., 2001. Random forests. Machine learning 45, 5-32.

Cui, B., Huang, W., Ye, H., Chen, Q., 2022. The suitability of PlanetScope imagery for mapping rubber plantations. Remote Sensing 14 (5), 1061.

Dobrinić, D., Gašparović, M., Medak, D., 2021. Sentinel-1 and 2 time-series for vegetation mapping using random forest classification: A case study of Northern Croatia. Remote Sensing 13 (12), 2321.

Gašparović, M., Dobrinić, D., Pilaš, I., 2023. Mapping of Allergenic Tree Species in Highly Urbanized Area Using PlanetScope Imagery—A Case Study of Zagreb, Croatia. Forests 14 (6), 1193.

Georganos, S., Grippa, T., Vanhuysse, S., Lennert, M., Shimoni, M., Kalogirou, S., Wolff, E., 2018. Less is more: Optimizing classification performance through feature selection in a very-high-resolution remote sensing object-based urban application. GIScience & Remote Sensing 55 (2), 221-242.

Hay, G., Castilla, G., 2008. Geographic object-based image analysis (GEOBIA): a new name for a new discipline. In: Blaschke, T., Lang, S., Hay, G.J. (Eds.), Object-Based Image Analysis: Spatial Concepts for Knowledge-Driven Remote Sensing Applications, Springer, pp. 75–89.

Hirayama, H., Sharma, R. C., Tomita, M., Hara, K., 2019. Evaluating multiple classifier system for the reduction of salt-and-pepper noise in the classification of very-high-resolution satellite images. International journal of remote sensing 40 (7), 2542-2557.

Luo, C., Qi, B., Liu, H., Guo, D., Lu, L., Fu, Q., Shao, Y., 2021. Using time series sentinel-1 images for object-oriented crop classification in google earth engine. Remote Sensing 13(4), 561.

Ma, L., Li, M., Ma, X., Cheng, L., Du, P., Liu, Y., 2017. A review of supervised object-based land-cover image classification. ISPRS Journal of Photogrammetry and Remote Sensing 130, 277-293.

Olofsson, P., Foody, G. M., Herold, M., Stehman, S. V., Woodcock, C. E., Wulder, M. A., 2014. Good practices for estimating area and assessing accuracy of land change. Remote sensing of Environment 148, 42-57.

Qu, L. A., Chen, Z., Li, M., Zhi, J., Wang, H., 2021. Accuracy improvements to pixel-based and object-based lulc classification with auxiliary datasets from Google Earth engine. Remote Sensing 13 (3), 453.

Tassi, A., Gigante, D., Modica, G., Di Martino, L., Vizzari, M., 2021. Pixel-vs. Object-based landsat 8 data classification in google earth engine using random forest: The case study of Maiella national park. Remote sensing 13 (12), 2299.

The Role and Use of Big Data in Spatial Analysis of Touristification – Example of the Historic Core of Dubrovnik

*Dino Bečić[1,]**

[1] Faculty of Science, University of Zagreb, Zagreb, Croatia, dbecic.geog@pmf.hr
* corresponding author

Abstract: Big data is a term used to define large volumes of data which are generated, collected, and analysed. It can be structured, unstructured, or semi-structured. Also, the come from various sources such as sensors, mobile devices, satellite imagery, and internet, including social networks that generate big amounts of data daily. Big data represent a significant potential data source that can be utilized in various analyses, both qualitative and quantitative. The process analysed in this study is touristification, the process by which destinations become increasingly oriented towards tourism. Since touristification is a highly complex process, this study will not cover all its elements but will focus solely on analysing specific social media data. In the context of researching the touristification of the Historic Core of Dubrovnik, social media data analytics can provide additional insights into the characteristics of the process. Big data were collected from the Booking.com platform, one of the most visited tourism platforms. This platform allows users to search, view, and book touristic accommodation. These accommodations, along with their descriptive data and location information, can be observed and analysed as elements of touristification. The research involved data collection, analysis, and visualization, through the R programming language.

Keywords: touristification; R; spatial analysis.

1   Introduction

In the era of big data, many scientific disciplines are leveraging extensive datasets for complex analyses and data-driven decisions. The interdisciplinary field of "data science" encompasses principles, algorithms, and processes to extract useful patterns from large datasets (Kelleher and Brendan 2018). Big data represents a paradigm shift in data management, characterized by the "3Vs": volume, velocity, and variety. The fusion of data science and Geographic Information Systems (GIS) has revolutionized spatial analysis, enabling access to vast amounts of geospatial information (Oliviera et al. 2024). Spatial data management in GIS involves data science techniques like spatial indexing, geocoding, and spatial queries for efficient geographic data processing. This area is often seen as a subset of data science, termed spatial (geographic) data science (Brunsdon and Comber 2019, Rey et al. 2023). Traditional GIS applications and software, initially designed for smaller datasets, now incorporate big data technologies to handle large spatial datasets from sources like satellite imagery and social media. Programming languages and open-source tools such as R and Python have become popular in both data science and GIS for their flexibility, scalability, and cost-effectiveness,

facilitating advanced spatial analysis (Brunsdon and Comber 2019, Oliviera et al. 2024). A notable application of these technologies is analysing touristification, a process transforming a destination to focus primarily on tourism, impacting socio-cultural, ecological, and economic dimensions. Touristification often leads to the commercialization of residential spaces and displacement of residents, driven by platforms like AirBnB and Booking.com. This growth in tourist accommodation affects central urban areas, impacting housing prices and residents' quality of life. Cities like Lisbon, Malaga, Barcelona, and Madrid have seen rapid increases in short-term rentals, leading to significant social, economic, and urban transformations (García Bujalance et al. 2019, Antunes et al. 2021, Ardura et al. 2021, Porfido et al. 2023). This paper demonstrates the integration of geographic data analytics methods in collecting and processing spatial data to manage the touristification process, highlighting the importance of geographic data analytics as an enhancement of traditional GIS techniques.

2   Materials and methods

Considering social media and internet platforms in general, which contain vast amounts of data, including spatial data, they offer opportunities for spatial analysis. As mentioned, one aspect of touristification is tourist accommodation. This study will demonstrate data collection from the Booking.com online platform, followed by processing, analysis, and visualization. The selected online platform is Booking.com. By retrieving data from this platform and analyzing it, certain spatial patterns can be observed. The chosen area, or tourist destination for this research, is Dubrovnik, specifically the Historic Core of Dubrovnik. Booking.com is one of the most visited online platforms for browsing, booking, and reviewing accommodation units. According to another internet portal, Statista.com, the number of monthly visits to the Booking.com website amounts to 556.1 million. The portal contains numerous data about accommodation units, including nightly rates, location, ratings, reviews, number of accommodation units, number of beds, and many others. Such information can serve various analyses, including spatial ones, given that platforms naturally possess addresses of accommodation units. For research purposes, the following data about accommodation units have been selected: name, address, unit rating, number of reviews, indication of whether the property is managed by a private individual or a company, and number of accommodation units. Such data are not structured for spatial analyses, and they need to be collected and processed to be suitable for spatial analyses. Getting such type of data, available on internet portals, can be achieved

using a method called web scraping. Web scraping is the process of extracting data from websites. This technique involves using software tools to access web pages, extract desired data, and store it in a structured format for further analysis or use. This technique is crucial for obtaining geographic information and other attributes from web content. The steps include identifying the target website, reviewing the structure of the page, writing a scraper that involves setting up the environment, accessing the website, parsing HTML, handling dynamic content, extracting data, cleaning, and storing the data (Brenning and Henn 2023).

Key concepts of web scraping include automation tools such as Selenium, BeautifulSoup, Scrapy, rvest, which are used through programming languages like R or Python, as well as standalone programs and platforms like Octoparse, etc. They are all designed to automate the process of accessing web pages and extracting data. Websites are primarily composed of HTML. Data extraction involves parsing HTML to identify and retrieve relevant information. Selectors, such as CSS selectors and XPath, allow for precise determination of parts of the website from which data is extracted. After extraction, the data is stored in a structured format to facilitate easier access and analysis (Brenning and Henn 2023). For this research, a code was written in the R programming language, which includes accessing the Booking.com page for the location "Historic Core of Dubrovnik," where all accommodation units in that area are listed, using web scraping packages. Then it includes saving all links for each accommodation unit separately followed by accessing each accommodation unit by opening the link and retrieving desired data and storing it for each unit. Then workflow includes - Processing attributes and structuring. After that we do spatial analysis and geovisualization.
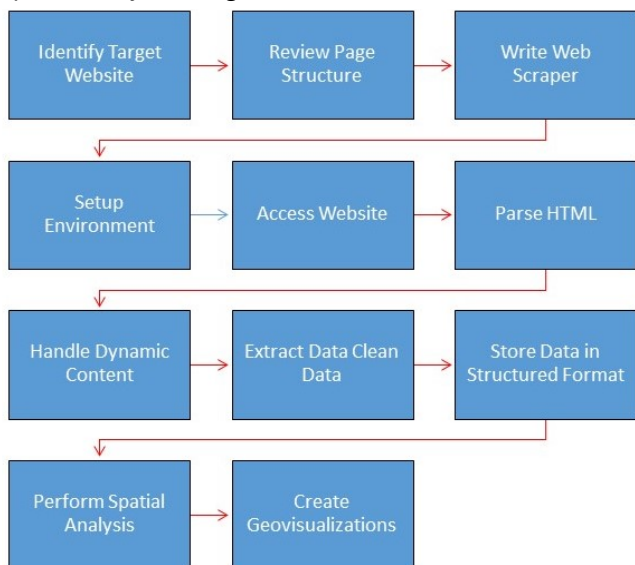

Figure 1. Flowchart.

This generated workflow used packages, or libraries, or extensions, which enabled such an approach to research, from data retrieval, storage, processing, and finally visualization, including RSelenium, rvest, sf, ggplot2, dplyr. Through the written code, each accommodation unit was accessed separately, automatically, and the necessary data

was retrieved from it, which was later structured into a new format suitable for analysis (Figure 1).

3   Results

Data from the Booking.com platform about accommodation units in the Historic Core of Dubrovnik were collected on March 31, 2024. On that day, there were 550 advertised tourist accommodations on the platform. Using web scraping tools within the R language, data for all 550 advertised accommodations were gathered. After data processing, the processed table contained information about the name of the property, property rating, number of reviews, coordinates, number of accommodation units, and whether the property is managed by a physical or private individual. The processed data, in this format, within the RStudio application, can be analysed qualitatively, quantitatively, and spatially.

As mentioned, web scraping collected data for a total of 550 advertised listings. The average rating for all properties is a high 8.91, with the highest rating being 10, while one property has an average rating of 4.2. Regarding the management of properties, 299 are managed by individuals, while 251 are managed by companies. The average rating for properties managed by individuals is 9, while the rating for properties managed by companies is 8.79. The maximum number of accommodation units at one location is 16, while the minimum is 1. The average number of accommodation units per property is 1.78. As mentioned, there is one property with a rating in the category up to 5, while in the rating range from 9 to 10, there are as many as 245 properties, which makes up almost half of the total number of advertised properties (Figure 2).
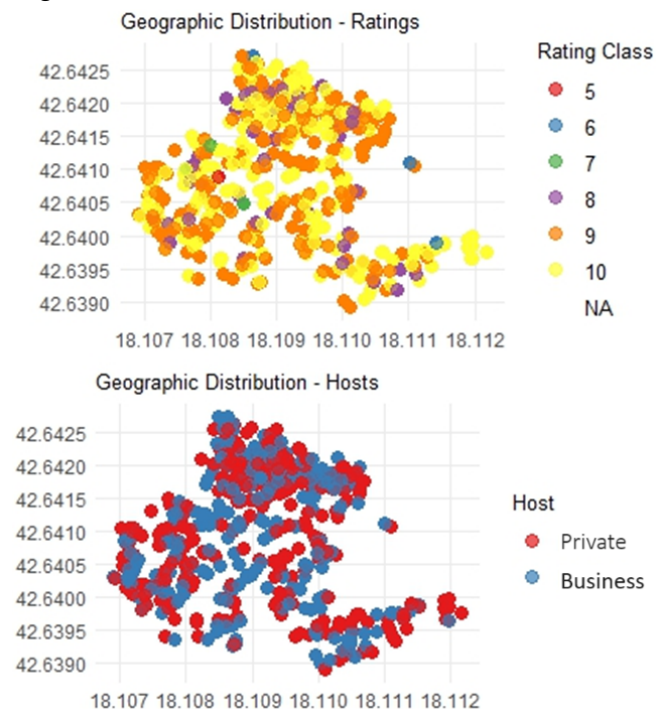

Figure 2. Geovisualalization of geographic distributions.

In a geographic context, since the data includes coordinates, it is possible to create spatial clusters using the k-means method. K-means is a data clustering

algorithm used to identify similar groups of data, or clusters. The algorithm starts by randomly selecting initial cluster centers, or centroids. Then, each data point is assigned to the cluster whose centroid is closest to it. After that, new cluster centers are calculated by computing the mean of all points in each cluster. These steps are repeated iteratively until the centroids stabilize. The result is the grouping of data into a certain number of clusters, where points within the same cluster are as similar as possible, while points from different clusters are as different as possible. In this specific analysis, the variable used for data clustering is location. The number of clusters was defined using the elbow method, which resulted in three clusters. The elbow method in clustering is a technique used to determine the optimal number of clusters in a dataset. It involves plotting the explained variation as a function of the number of clusters and picking the elbow of the curve as the number of clusters to use. The elbow point represents the number of clusters where adding another cluster does not significantly improve the model's performance. The variable used for data clustering is location. Specifically, the clustering algorithm utilized the latitude and longitude coordinates of the data points to form clusters. No other variables, such as rating, were used in the clustering process. Overall, the k-means clustering with three clusters based on geographic coordinates provides a meaningful way to segment the data into distinct geographic regions. Adjustments to the number of clusters can be made depending on the desired granularity of the analysis (Figure 3).
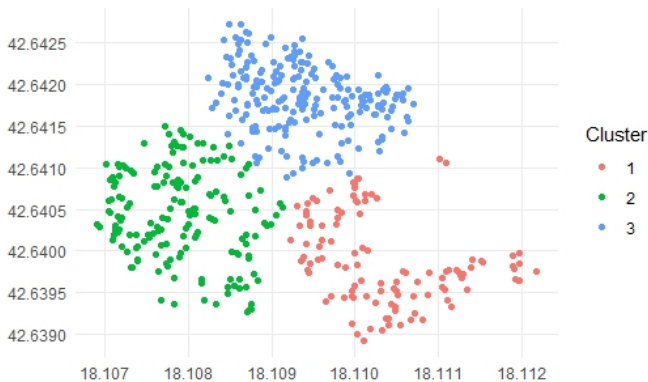

Figure 3. K-means clusters.

4   Discussion

In the context of analyzing touristification in the Historic Core of Dubrovnik, the analysis of collected data suggests that the destination is facing a pronounced phenomenon of touristification that may have negative implications. The high number of 550 advertised accommodation units indicates an intense pressure of tourism on this area. The increase in the number of accommodation units, especially owned by individuals, can lead to issues such as excessive resource consumption, infrastructure overload, and loss of authenticity of the local community. This aligns with findings from other historic cities experiencing similar trends (Curto et al. 2022, Chamizo-Nieto et al. 2023). The spatial clusters identified areas particularly affected by tourism Spatial analysis through the k-means method can

identify areas that are particularly under pressure from tourism, serving as a basis for planning measures to protect and preserve natural and cultural resources. The study demonstrates data collection from Booking.com, using web scraping to retrieve information about tourist accommodations in Dubrovnik. Data on property names, addresses, ratings, reviews, and management types were collected and processed using R packages such as RSelenium, rvest, sf, ggplot2, and dplyr. Spatial clustering was performed using the k-means method to identify geographic patterns.

5   Conclusions

Web scraping serves as a method for collecting data that can contribute to big data analysis, including in a geographic context. Web scraping can gather large amounts of data from multiple web pages or entire websites, significantly contributing to the volume of big data. Automated tools can collect data at high speed, providing a continuous flow of information, which aligns with the characteristic of velocity in big data. Although web scraping itself is not synonymous with big data, it is a critical component for gathering diverse and large datasets needed for big data analysis. In a geographic context, web scraping provides additional opportunities for data collection. Programming languages like R, used in this research, enable the structuring and management of data, as well as their analysis and visualization. Considering touristification as the observed process, the collected data on the locations of accommodation units provided additional insight into their spatial distribution within the Historic Core of Dubrovnik. Additionally, although this study involved spatial analysis of accommodation unit locations, they were not presented and analyzed through GIS applications like ESRI ArcGIS PRO, or QGIS; instead, geographic data science methods were used with R programming language. This approach showcases the potential for enhancement, as spatial analysis in GIS integrates principles of big data analysis and advanced statistics into a geographic context. Integrating these interdisciplinary disciplines allows for a deeper understanding of spatial phenomena through complex models and analytical techniques. The usage of geographic data science provides a comprehensive approach to spatial data analysis, which is crucial for addressing complex spatial problems, such as the component of touristification analyzed in this study, namely the location of accommodation units.

6   References

Antunes, G., Ferreira, J., 2021. Short-term rentals: how much is too much – spatial patterns in Portugal and Lisbon. Tourism and hospitality management 27 (3), 581-603.

Ardura Urquiaga, A., Lorente-Riverola, I., Ruiz Sanchez, J., 2020. Platform-mediated short-term rentals and gentrification in Madrid. Urban Studies 57 (15), 3095-3115.

Brenning, A., Henn, S., 2023. Web scraping: a promising tool for geographic data acquisition. arXiv Preprint 2305.19893v1.

Brunsdon, C., Comber, L., 2019. An Introduction to R for Spatial Analysis and Mapping, second ed. SAGE Publications Ltd., London.

Chamizo-Nieto, F.J., Nebot-Gómez de Salazar, N., Rosa-Jiménez, C., Reyes-Corredera, S., 2023. Touristification and conflicts of interest in cruise destinations: the case of main cultural tourism cities on the Spanish mediterranean coast. Sustainability 15 (8), 6403.

Curto, R.A., Rubino, I., Verderosa, A., 2022. Investigating Airbnb evolution in an urban tourism context: the application of mathematical modelling and spatial analysis. Current Issues in Tourism 25 (10), 1666-1681.

García Bujalance, S., Barrera-Fernández, D., Scalici, M., 2019. Touristification in historic cities. Reflections on Malaga. Revista de Turismo Contemporâneo 7 (1), 93-115.

Goodchild, M.F., 2016. GIS in the Era of Big Data. Cybergeo: European Journal of Geography. n. pag.

Kelleher, J.D., Brendan, T., 2018. Data Science. The MIT Press, Cambridge.

Lestegás, I., Seixas, J. and Lois-González, R.-C., 2019. Commodifying Lisbon: A Study on the Spatial Concentration of Short-Term Rentals. Social Sciences 8 (2), 33.

Oliveira, A., Fachada, N., Carvalho, J., 2024. Data Science for Geographic Information Systems. arXiv Preprint 2404.03754.

Ojeda, A.B., Kieffer, M., 2020. Touristification. Empty concept or element of analysis in tourism geography? Geoforum 115, 143-145.

Porfido, E., Tomàs, M., Marull, J., 2023. A new urban diagnostics approach for measuring touristification: The case of the Metropolitan Area of Barcelona. Journal of Urban Management 12 (3), 195-207.

Rey, S., Arribas-Bel, D., John Wolf, L., 2023. Geographic Data Science With Python, first ed. Chapman and Hall/CRC, New York.

Simas, T.B., Oliveira, S.A.L.C.D., Cano-Hila, A.B., 2021. Tourismophobia or touristification? An analysis of the impacts of tourism in Poblenou, Barcelona. Ambiente Construído 21 (3), 117-131.

Mapping Long-Term Trends in Actual Evapotranspiration in Data-Scarce conditions in Afghanistan

Fazlullah Akhtar[1,]*, Christian Borgemeiste[1], Bernhard Tischbein[1]

[1] Center for Development Research (ZEF), University of Bonn, Bonn, Germany,
fakhtar@uni-bonn.de, cb@uni-bonn.de, Tischbein@uni-bonn.de

* corresponding author

Abstract: The agricultural sector in Afghanistan, the highest consumer of water resources, is crucial for food production and employment for over 50% of the population. As one of the top four most vulnerable countries to climate change, monitoring actual evapotranspiration (ETa) is imperative. However, conducting detailed investigations in countries facing data scarcity, like Afghanistan, remains challenging. Therefore, this study uses the TerraClimate dataset (4.6 km spatial resolution) to explore long-term ETa variation and trends in the Kabul River Basin (KRB). Integrating remote sensing data with advanced analytics, we examine the spatial and temporal dynamics of ETa in the Alingar watershed, a KRB subbasin. The results show that from 1980 to 2023, the mean annual ETa was 364±38mm. The Mann-Kendall test showed a significant trend (p-value < 0.05). This comprehensive investigation provides critical information for sustainable water management in Afghanistan.

Keywords: data-scarcity; TerraClimate; evapotranspiration; Kabul River Basin; Afghanistan.

1   Introduction

The agricultural sector in Afghanistan is the largest consumer of the country's water resources, playing a crucial role in ensuring food security and providing livelihoods for over half of the population. The country owns only 12% arable land (World Bank 2024) of which only 1.5–2.5 million ha are irrigated (Pervez et al. 2014). Despite the highest consumption (~98%) of the country's water resources (FAO 2019), the existing production does not meet the country's food demand. According to Akhtar et al. (2018), the supply-based irrigation system in Afghanistan is suffering from inefficiency in both conveyance and application. The conventional irrigation system has a water use efficiency (WUE) of 0.58 to 0.66 kg/m³. In the downstream of the Kabul River Basin (KRB), where laser land levelling has been implemented and the water supply is reliable, the highest application efficiency is 46% (Jalil et al. 2020). However, these interventions cover only a small fraction of the total irrigated area and are not representative of the entire country.

Given Afghanistan's ranking as one of the top four countries most vulnerable to climate change (DRMKC 2024), efficient water management is critical. Climate change may further affect water availability, potentially decreasing the current productivity of irrigated land. Therefore, regular monitoring of water resources is essential for understanding the water cycle, consumption patterns, and for developing sustainable agricultural practices and plans. However, Afghanistan faces the challenge physical

data scarcity, which hampers detailed hydrological studies and effective water management strategies. Conventional ground-based data collection methods are often unrealistic in such regions due to logistical limitations and the infrastructure shortage. In this context, remote sensing and global datasets offer a valuable alternative, enabling researchers to monitor and analyse hydrological variables over large and inaccessible areas (Sagintayev et al. 2012). By integrating remote sensing data with advanced analytical methods, this study utilizes the TerraClimate dataset (Abatzoglou et al. 2018), which provides high-spatial resolution (4.6 km), to map long-term changes and trends in ETa within the Kabul River Basin (KRB), a region characterized by its heterogeneous landscape and different agro ecological conditions.

2   Materials and methods

2.1   Study Area

This study was conducted in the Alingar watershed (Figure 1), a subbasin of the Kabul River Basin (KRB) within the larger Indus Basin. The total area of this watershed is around 6,239 km². Its elevation varies between 601–5399 m above mean sea level. The mean annual precipitation received at this watershed during 2000–2019 was 634 mm. The forest coverage of this watershed is 31%, while rangeland including settlements and barren land covers around 64% of the total area; the water bodies are spread over 1% of the total area while 3% is the irrigated area in this watershed. The major rivers of this watershed are Alingar and Alishing.
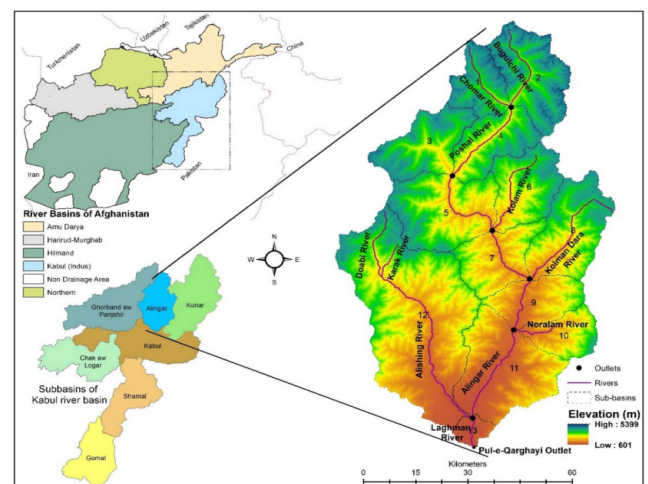

Figure 1. Geographic location and map of the Alingar watershed (Akhtar et al. 2022).

2.2 Data

In this study, we used the TerraClimate dataset, prepared by the University of Idaho, which provides monthly temporal resolution and climatic water balance information for terrestrial surfaces worldwide. It is based upon climatically aided interpolation and combines climatological normals derived from the WorldClim dataset. This product has a higher spatial resolution of 4.6 km, making it suitable for smaller scales studies in data-scarce regions. The TerraClimate data is available from 1. 1. 1958 to 31. 12. 2023, it contains fourteen bands, which are listed in Table 1.

Table 1. TerraClimate bands, University of Idaho (Abatzoglou et al. 2018).

Description	Min	Max	Units	Scale
Actual evapotranspiration (ET$_a$)	0	3140	mm	0.1
Climate water deficit (Def)	0	4548	mm	0.1
Palmer Drought Severity Index (PDSI)	−4317	3418		0.01
Reference evapotranspiration (PET)	0	4548	mm	0.1
Precipitation (Pr)	0	7245	mm	0
Runoff (Ro)	0	12560	mm	0
Soil moisture (SM)	0	8882	mm	0.1
Downward surface shortwave radiation (Srad)	0	5477	W/m^2	0.1
Snow water equivalent (SWE)	0	32767	mm	0
Minimum temperature (T$_{min}$)	−770	387	^{0}C	0.1
Maximum temperature (T$_{max}$)	−670	576	^{0}C	0.1
Vapor pressure (Vap)	0	14749	kPa	0.001
Vapor pressure deficit (Vpd)	0	1113	kPa	0.01
Wind-speed at 10m (WS)	0	2923	m/s	0.01

2.3 Estimation of actual evapotranspiration (ET$_a$)

As mentioned earlier, the TerraClimate has 14 bands, containing normal climate parameters to water balance components. We used Google Earth Engine to derive the ET$_a$ covering a period of 1980–2023 by masking the study area.

2.4 Using Mann-Kendall Statistics test for Monotonic Trend in ET$_a$

For trend detection in the long-term ET$_a$ estimations, we used Mann-Kendall (MK) test that provides the best alternative when the data is either positively or negatively skewed. The following equation (1) was used for MK statistics on monthly ET$_a$:

$$S_i = \sum_{i=1}^{n-1} \sum_{j=i+1}^{n} sgn(x_j - x_i) \ \forall_i = 1 \dots 12 , \qquad (1)$$

where n is the number of data points in the time series, x_i and x_j are data values at time i and time j respectively. The variance of S is given by equation (2):

$$VAR(S) = \frac{n(n-1)(2n+5) - \sum_{p=1}^{g} t_p(t_p-1)(2t_p+5)}{18} , \qquad (2)$$

where g is the number of tied groups in the data, t_p is the number of tied data values in the pth group. Once S and its variance are calculated, the following equation (3) test was performed to compute the standardized Z statistics:

$$Z = \begin{cases} \dfrac{S-1}{\sqrt{VAR(S)}} & \text{if } S>0 \\ 0 & \text{if } S=0 \\ \dfrac{S+1}{\sqrt{VAR(S)}} & \text{if } S<0 \end{cases} \qquad (3)$$

3 Results

3.1 Annual variation in mean actual evapotranspiration

The mean annual ET$_a$ in the Alingar watershed during 1980–2023 was 364±38mm. The highest mean annual ET$_a$ ever estimated during this period was 451 mm while the minimum ET$_a$ was 287 mm. Figure 2 shows that the mean annual ET$_a$ declined from 1996 until 2000. During this period, the country faced its most severe droughts on record, coinciding with internal conflicts among various warlords and their factions, resulting in substantial damage to irrigation infrastructure. With the establishment of a democratic government in 2001, initiatives targeting agriculture and irrigation were initiated. Consequently, a visible increase in ET$_a$ is observed, reflecting the impacts of these interventions. From 2008, the mean annual ET$_a$ consistently exceeds historical averages, indicating an increase in crop water consumption. This trend likely reflects a relatively stable water availability within the watershed during this period.
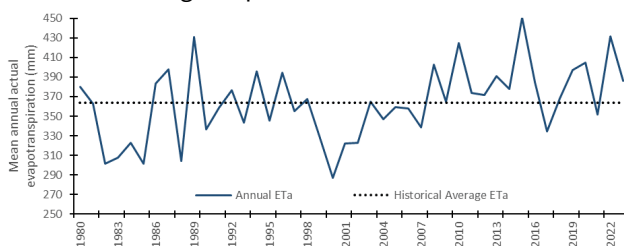
Figure 2. Variation in mean annual actual evapotranspiration (mm).

3.2 Inter-annual Variability in Monthly Mean Actual Evapotranspiration

Figure 3 given below shows that there is larger variation in the months of May-July, these are the months with highest crop water demand. These months overlap with higher temperatures and increase solar radiation that triggers the evapotranspiration rates. Specifically, in the month of May, the mean monthly ET$_a$ was 80±13 mm, indicating a considerable amount of water required for crop growth during this time. The higher variation observed in May to

July can also be attributed to fluctuations in water availability, particularly in the form of excessive rainfall exceeding normal conditions in Spring and Monsoon seasons where precipitation amounts may vary adding more moisture to the crop root zone.
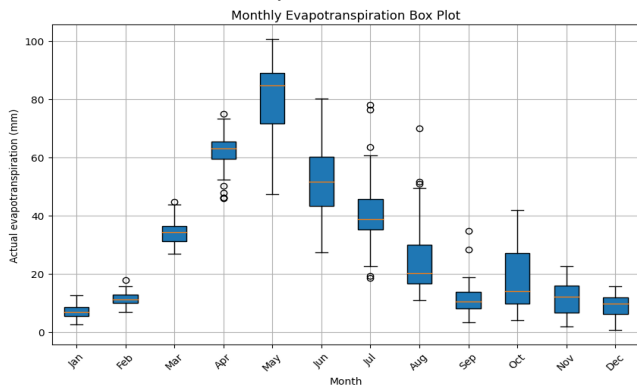

Figure 3. Inter-annual Variability in Monthly Mean Actual Evapotranspiration.

3.3   Trend Analysis

We used the Mann-Kendall non-parametric test (Mann 1945, Kendall 1975) to identify if the ET_a analysed for the study area follow any upward or downward trend. The summary of the results of the two-tailed MK test is given below in Figure 4.

The test results show a p-value of 0.002, which is less than the significance level (alpha) of 0.05 (Table 2). This indicates a statistically significant trend in the mean annual ET_a. The positive value of Kendall's tau (0.324) indicates the strength and direction of the trend, with positive values signifying an increasing trend. The slope value is 1.493, which is also positive and provides an estimate of the magnitude of the trend. A positive slope value confirms that the trend is increasing.

Table 2. Summary statistics of the two-tailed Mann-Kendall test.

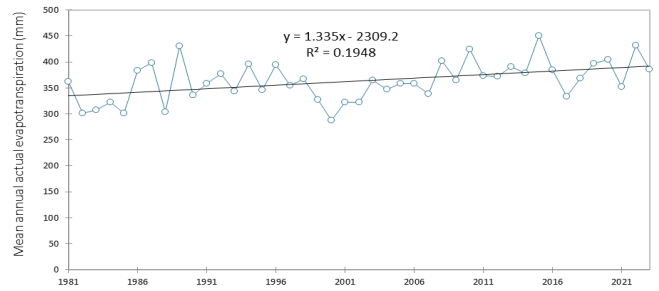| Mann-Kendall trend test / Two-tailed test		Sen's slope			
Kendall's tau	0.324		Value	Lower bound (95%)	Upper bound (95%)
S	292	Slope	1.5	0.62	2.341
Var(S)	9129.3	Intercept	−2632.5	−4330.3	−877.06
p-value (Two-tailed)	0.002				
alpha	0.05				

Figure 4. Trend analysis in the mean annual actual evapotranspiration.

4   Conclusions

The study of the Alingar watershed revealed that the mean annual ET_a from 1980 to 2023 was 364±38mm, with a range of 287mm to 451mm. A decline in mean annual ET_a from 1996 to 2000 corresponded with severe droughts and internal conflicts damaging irrigation infrastructure. Post-2001, agricultural and irrigation interventions led to an increase in ET_a, surpassing historical averages from 2008 onwards, indicating stable water availability and higher crop water consumption. The highest inter-annual variability in monthly ET_a occurred from May to July, reflecting variations in water availability. The Mann-Kendall trend test showed a significant positive trend in ET_a, with a p-value of 0.002, Kendall's tau of 0.324, and a Sen's slope of 1.49. The long-term analyses carried out by using the global datasets can help understand the hydrological and meteorological processes in the absence of physical datasets. Hence, it contributes to the planning and investment initiatives in the field of water resources management. However, the key limitation of using the global datasets for ET_a estimation is their spatial and temporal resolution, atmospheric interference and the need for validation against the ground-based measurements, which is difficult in data scarce situations.

5   References

Abatzoglou, J. T., Dobrowski, S. Z., Parks, S. A., Hegewisch, K. C., 2018. TerraClimate, a high-resolution global dataset of monthly climate and climatic water balance from 1958–2015. Scientific Data 5 (1), 170191.

Akhtar, F., Awan, U. K., Tischbein, B., Liaqat, U. W., 2018. Assessment of irrigation performance in large river basins under data scarce environment - A case of Kabul river basin, Afghanistan. Remote Sensing 10 (6), 972.

DRMKC, 2024. Country risk profile: Afghanistan. https://drmkc.jrc.ec.europa.eu/ inform-index/INFORM-Risk/Country-Risk-Profile. (Accessed 6 May, 2024)

FAO, 2019. Country Fact Sheet: Afghanistan. https://storage.googleapis.com/fao-aquastat.appspot.com/countries_regions/factsheets/summary_statistics/en/AFG-CF.pdf. (Accessed 22 May, 2024)

Jalil, A., Akhtar, F., Awan, U. K., 2020. Evaluation of the AquaCrop model for winter wheat under different irrigation optimization strategies at the downstream Kabul River Basin of Afghanistan. Agricultural Water Management 240, 106321.

Kendall, M. G., 1975. Rank correlation methods. Griffin, London. J. Econom 13, 245-259.

Mann, H. B., 1945. Nonparametric tests against trend. Econometrica: Journal of the econometric society, 245-259.

Pervez, M. S., Budde, M., Rowland, J., 2014. Mapping irrigated areas in Afghanistan over the past decade using MODIS NDVI. Remote Sensing of Environment 149, 155-165.

Sagintayev, Z., Sultan, M., Khan, S. D., Khan, S. A., Mahmood, K., Yan, E., Marsala, P., 2012. A remote sensing contribution to hydrologic modelling in arid and inaccessible watersheds, Pishin Lora basin, Pakistan. Hydrological Processes 26 (1), 85-99.

World Bank, 2024. Arable land (% of land area) - Afghanistan. https://data.world bank.org/indicator/AG.LND.ARBL.ZS?locations=AF. (Accessed 6 May, 2024)

Data Augmentation with Generative Adversarial Network for Solar Panel Segmentation from Remote Sensing Imagery

Justinas Lekavičius[1],*, Valentas Gružauskas[1]

[1] Institute of Computer Science, Vilnius University, Lithuania, me@justinaslekavicius.com, valentas.gruzauskas@mif.vu.lt

* corresponding author

Abstract: With the increasing popularity of solar energy in the electricity market, demand arises for data such as precise locations of solar panels for efficient energy planning and management. However, this data is not easily accessible; information such as precise locations sometimes does not exist. Furthermore, existing data sets for training semantic segmentation models of photovoltaic installations are limited, and the manual annotation of remote sensing imagery is time-consuming and labour-intensive. Therefore, the pix2pix generative adversarial network (GAN) is used to create additional remote sensing data, enriching the original resampled training data of varying ground sampling distances without compromising its integrity. Experiments with the DeepLabV3 model, ResNet-50 backbone, and pix2pix generative adversarial network architecture were conducted to discover the advantage of using GAN-based data augmentations for a more accurate remote sensing imagery segmentation model. The result is a fine-tuned solar panel semantic segmentation model, trained using transfer learning and an optimal amount – 60% of GAN-generated RS imagery for additional training data. The findings demonstrate the benefits of using GAN-generated images as additional training data, addressing the issue of limited data sets, and increasing IoU and F1 metrics by 2% and 1.46%, respectively, compared to classic augmentations. The improved semantic segmentation model allows for better solar panel detection in remote sensing images and the potential development of a regional photovoltaic installation map for better electricity network planning and risk management.

Keywords: solar panels; semantic segmentation; data augmentation; generative adversarial network; remote sensing.

1   Introduction

The usage of renewable energy is becoming more widespread every year due to its increasing availability for homeowners and energy production possibilities for electricity providers. The growing expansion of solar panel usage also increases the need for data such as precise panel locations, types, and specifications for effective energy grid planning and management (Guangul and Chala 2019). Nevertheless, such data is limited due to various factors such as privacy concerns, relaxed requirements, and the time-consuming and resource-intensive nature of collecting this data. The combination of machine learning and remote sensing emerges as a solution for this problem, specifically using satellite imagery for solar panel detection and analysis. Semantic segmentation using convolutional neural networks such as

U-Net (Ronneberger et al. 2015) and FCN (Long et al. 2015) allows for accurate solar panel identification in remote sensing images. Furthermore, the solar panel segmentation task can be achieved with better results with the introduction of even more advanced networks such as RU-Net (Li and Lau 2022) and EfficientNet-B5 (Ge et al. 2022). Despite these advances, the issue of the need for annotated and diverse datasets for effective model training remains (Sun et al. 2021). To solve this problem, data augmentation techniques are helpful, including classic augmentations such as rotations and scaling adjustments, and generative adversarial networks for domain translations and brand-new data creation. One of these networks for image-to-image translation is pix2pix (Isola et al. 2018), introducing the possibility of creating new realistic images from already existing limited data. This additional data can be used as supplementary imagery for semantic segmentation model training, increasing its performance. The goal of this study is to improve the solar panel detection accuracy of the DeepLabV3 semantic segmentation model, using the pix2pix generative adversarial network for additional training data creation. Transfer learning and fine-tuning are also applied for the DeepLabV3 model, and the issue of a limited dataset and manual labelling is addressed by creating new training data as an alternative to classic augmentations, which do not create entirely new images.

2   Materials and methods

A collection of various remote sensing images and solar panel segmentation mask pairs was used for the training of both the semantic segmentation model and the generative adversarial network. These images are of various spatial resolutions (0.8m, 0.3m, 0.2m, 0.1m) and sizes (1024x1024, 400x400, 256x256). For each spatial resolution, 640 image-mask pairs were selected, and the total amount of data was 2560 pairs, with an 80/10/10 split for training, validation, and testing subsets. To solve the issue of imagery resolution differences and to avoid scale discrepancies, the images were resampled to 512x512 target size and 0.1m target spatial resolution for consistency during model training. The width and height of the image and its segmentation mask are resampled as shown in equation (1).

Then the newly resampled images and masks are either padded or cropped depending on whether the size is smaller or larger than the target size. If they are smaller, padding is applied, as shown in equation (2). If they are larger, cropping in the region of interest (center of largest solar panel object in segmentation mask) is applied. This is done to prevent as much information loss as possible.

The pix2pix generative adversarial network is trained using the same training data as for the DeepLabV3 semantic segmentation model, for the task of translating semantic segmentation masks (input data) to real remote sensing images (target data). In the process, the generator attempts to generate realistic images that are faithful to the target data, while the discriminator tries to tell apart real images from fake ones. The D_real and D_fake losses are back-propagated to the discriminator, indicating how well the discriminator can identify real and fake generated images. The G_L1 and G_GAN losses are back-propagated to the generator and signal the difference between the original and synthetic image, and how well the generator can fool the discriminator. The training process is displayed in Figure 1.

Because the new remote sensing images are generated from existing training data (2048 image-mask pairs), the result is an additional 2048 pairs of new data that provide more variety compared to regular augmentation applications. An example of generated images compared to original data can be seen in Figure 2.
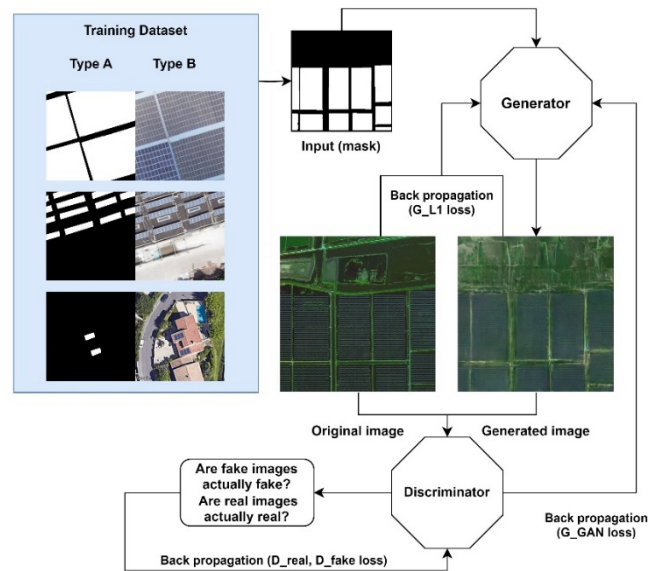

Figure 1. Diagram of Pix2pix generative adversarial network training process for creating new remote sensing images from segmentation masks.

$$\text{new dimension} = \text{original dimension} * \left(\frac{\text{spatial resolution}}{\text{target spatial resolution}}\right) \quad (1)$$

$$\text{padding dimension} = \left(\frac{\text{target dimension} - \text{new dimension}}{2}\right) \quad (2)$$

Figure 2. Original remote sensing images (top) and newly GAN-generated data (bottom).

Six different models were trained to test the benefits of using GAN-generated data as additional data for semantic segmentation model training versus using regular augmentations. The regular data augmentations performed for the training data were random horizontal flip with a 50% chance of it being applied, random rotation of 5 degrees,

random perspective change with 0.05 distortion scale, and 50% chance of it being applied, and random application of

Gaussian blur (5x5 kernel size and standard deviation of 0.1 min and 2.0 max) with 50% chance of it being used. The trained models are:

- No_a – trained with the original training subset.
- Basic_a – trained with additional applied classic augmentations.
- Gan25 – trained with 25% GAN-generated images as extra training data.

- Gan25a – trained with additional applied classic augmentations.
- GanO – trained with the optimal amount of GAN-generated images as extra training data.
- GanO_a – trained with additional applied classic augmentations.

3 Results and discussion

To determine the optimal GAN-generated data amount for training the semantic segmentation model, sensitivity analysis was performed, training the DeepLabV3 model using transfer learning and incremental amounts of additional GAN-generated data. This method finds the

displayed improvements across all metrics, with pixel accuracy increasing by 0.78%, precision – 3.41%, sensitivity – 2.49%, F1 – 2.71%, IoU – 3.19%, and the loss decreasing by 0.0282. Based on the IoU metric, which is important in determining the percentage of correctly segmented solar panels, the 256 images in the testing subset were categorized by good segmentation (At least 50% of the solar panel found), poor segmentation (less than 50% of the solar panel found), and by no solar panels found. The model GanO, trained with an additional optimal amount (60%) of GAN-generated data, also correctly segmented more solar panels in remote sensing images compared to the baseline No_a model.
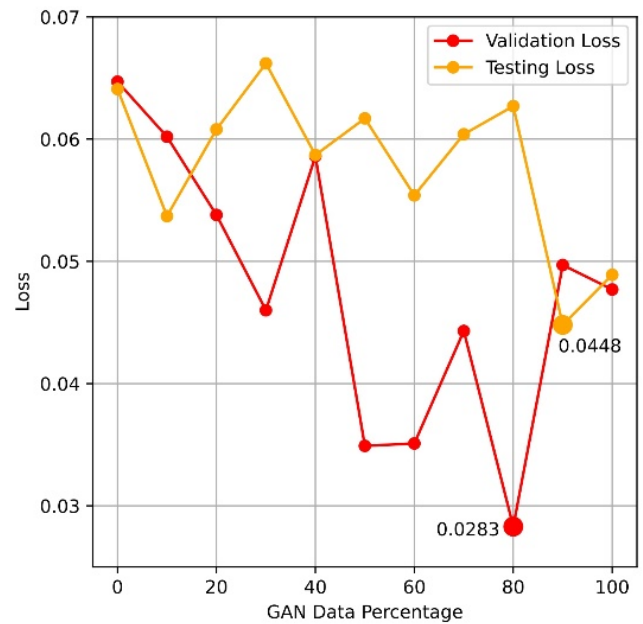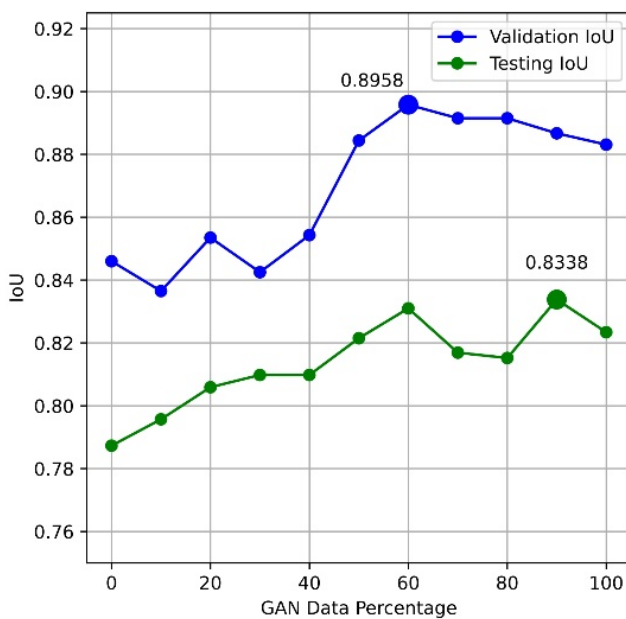

Figure 3. Sensitivity analysis of DeepLabV3 model training using transfer learning and various percentages of additional GAN-generated training data.

Table 1. Testing results of various models trained during the experiments.

Model	Avg Acc (%)	Avg Prec (%)	Avg Rec (%)	Avg F1 (%)	Avg IoU (%)	Avg Loss	Segmented Solar Panels (IoU)		
							Good ≥ 0.5	Poor < 0.5	None = 0
No_a	97.89	86.72	85.62	85.25	80.13	.0650	229	12	15
Basic_a	97.88	89.63	86.51	86.50	81.32	.0547	235	13	8
Gan25	98.09	89.11	85.94	85.71	80.42	.0586	229	16	11
Gan25a	97.91	88.84	87.25	87.08	81.41	.0550	238	8	10
GanO	98.67	90.13	88.81	87.96	83.32	.0368	237	11	8
GanO_a	98.04	89.82	87.69	87.77	82.90	.0611	238	9	9

optimal amount of generated synthetic data before the model is impacted negatively. Validation and testing subset IoU and loss metrics were compared, and the changes with additional GAN data usage are detailed in Figure 3. Because the criteria used for determining the best-performing variation of the model was validation IoU, 60% was selected as the best number of GAN-generated images to use for appending the original training data.

The testing results of all six models are compared in Table 1. Compared to the baseline model No_a, the model GanO

4 Conclusions

In summary, using the generative adversarial network is beneficial for training dataset augmentation with brand new remote sensing images from existing limited data, especially when the optimal amount of GAN-generated data is determined with a sensitivity analysis. Expanding a limited data set with newly generated pictures helps train the solar panel segmentation model for better accuracy and segmentation quality compared to using classic data augmentations. Furthermore, having new images

produced using the generative adversarial network eliminates the need for time-consuming manual annotations for training data creation With even more improvements to not only the segmentation model hyperparameters but also the generative adversarial network parameters, fine-tuned semantic segmentation model may be used for even more precise solar panel detection in remote sensing images and development of a regional solar panel map, allowing for more accessible solar panel market analysis and risk management.

5   References

Ge, F., Wang, G., He, G., Zhou, D., Yin, R., Tong, L., 2022. A Hierarchical Information Extraction Method for Large-Scale Centralized Photovoltaic Power Plants Based on Multi-Source Remote Sensing Images. Remote Sensing 14, 4211.

Guangul, F.M., Chala, G.T., 2019. Solar Energy as Renewable Energy Source: SWOT Analysis, in: 2019 4th MEC International Conference on Big Data and Smart City (ICBDSC). Presented at the 2019 4th MEC International Conference on Big Data and Smart City (ICBDSC), pp. 1-5.

Isola, P., Zhu, J.-Y., Zhou, T., Efros, A. A., Image-to-Image Translation with Conditional Adversarial Networks. arXiv, Nov. 26, 2018. http://arxiv.org/abs/1611.07004 (Accessed 11 June, 2024).

Li, L., Lau, E., 2022. RU-Net: Solar Panel Detection From Remote Sensing Image, in: 2022 IEEE Green Energy and Smart System Systems (IGESSC). Presented at the 2022 IEEE Green Energy and Smart Systems Conference (IGESSC), IEEE, Long Beach, CA, USA, pp. 1-6.

Long, J., Shelhamer, E., Darrell, T., 2015. Fully Convolutional Networks for Semantic Segmentation.

Ronneberger, O., Fischer, P., Brox, T., 2015. U-Net: Convolutional Networks for Biomedical Image Segmentation.

Sun, X., Wang, B., Wang, Z., Li, Hao, Li, Hengchao, Fu, K., 2021. Research Progress on Few-Shot Learning for Remote Sensing Image Interpretation. IEEE J. Sel. Top. Appl. Earth Observations Remote Sensing 14, 2387-2402.

Climate Change Mitigation Politics

ADAPTATION OF CROATIAN WINE-GROWING ZONES TO CLIMATE CHANGES
Branimir Omazić, Maja Telišman Prtenjak,
Jasminka Karoglan Kontić, Marko Karoglan, Darko Preiner, Ivan Prša

USER-FRIENDLY METHODOLOGY AND PROTOTYPE FOR OPERATIONAL DEPLOYMENT OF A SATELLITE-BASED MONITORING SYSTEM FOR EU – FOR MORE RESILIENT TERRITORIAL MANAGEMENT WITH LESS IMPACT ON ENVIRONMENT AND CLIMATE
Kristian Milenov, Viktor Milenov

REQUIREMENTS FOR GEOREFERENCING AND DIGITALIZATION OF SPATIAL DATA IN THE NEW EU LEGISLATION ON CLIMATE, ENVIRONMENT, AND BIODIVERSITY
Višnja Grgasović, Branimir Pavlinec, Domagoj Stjepan Krnjak, Vlatka Palčić,
Tatjana Antolić, Hana Mesić, Vida Posavec Vukelić, Martina Pekčec

CMIP6 AND CLIMATE CHANGE: A GLOBAL ANALYSIS OF RESEARCH AND COLLABORATIONS ON THE WATER BUDGET
Sayed Ishaq Deliry, Uğur Avdan

GEOMATICS APPLICATIONS FOR FARM'S SUSTAINABILITY
Amanzholova Raushan, Amanzholov K., Murat Daulet,
Dani Sarsekova, Syed Imran Moazzam Shah, Rebecca King,
Baktybek Duisebek, Janay Sagin

Adaptation of Croatian Wine-growing Zones to Climate Changes

Branimir Omazić[1,], Maja Telišman Prtenjak[1], Jasminka Karoglan Kontić[2], Marko Karoglan[2], Darko Preiner[2], Ivan Prša[3]*

[1] Department of Geophysics, Faculty of Science, University of Zagreb, Zagreb, Croatia, branimir.omazic@gfz.hr

[2] Department of Viticulture and Enology, Faculty of Agriculture, University of Zagreb, Zagreb, Croatia

[3] Croatian Agency for Agriculture and Food, Osijek, Croatia

* corresponding author

Abstract: Most parts of Croatia are suitable for viticulture, but the choice of grape variety depends heavily on the temperature conditions of the areas and thus on the wine-growing regions and zones in which the areas are located. Since the last revision of the wine-growing zones, the temperature characteristics in Croatia have changed, making it necessary to revise the existing zones and regions. In this study, the changes of five biometeorological indices (Growing Degree-Days (GDD), Temperature Growing Season (TGS), Huglin Index (HI), Cool night Index (CI) and Dryness Index (DI)) were calculated at 80 stations of the Croatian Hydrometeorological Institute in the period 1961–2020 and in three CORDEX Regional Climate Models (RCMs) simulations for period 2041–2070. The observed and modelled data were spatially interpolated using regression kriging, assuming a linear relationship between the meteorological parameters and four predictors: Latitude, Longitude, Elevation and Distance from the Sea. The results show significant changes in the bioclimatic indices over the observed period, which were not always accompanied by administrative changes in the wine-growing regions and zones. As a result of climate change, there are also new areas suitable for viticulture, and climate model simulations indicate further changes and shifts in the regions and zones.

Keywords: viticulture; climate change; wine-growing zones; bioclimatic indices; regional climate models.

1   Introduction

Global climate data shows that air temperatures have risen in the last decades of the 20th century and are likely to continue to rise in the 21st century. Climate change is affecting the entire biosphere, including viticulture (Lalić et al. 2018). Recent changes in temperature and precipitation have led to changes in the growth and development of grapevines (Van Leeuwen et al. 2019), in the quantity and quality of the harvest (Bock et al. 2013) and in the concentration of sugars and acids in the must (Omazić et al. 2020). In addition, the areas suitable for viticulture in Europe have been moved further north of the continent or to higher elevations (Malherio et al. 2010). Wine-growing areas are divided into different zones. The wine-growing zone division differ according to climate and soil, but also according to other conditions that are important for the cultivation of vines. This division is directly related to the regulations defining protected designations of origin and application of certain viticultural and oenological techniques (Prša 2022). The division of Croatia into wine-growing zones was first made in the 1970s. The basis for division was the study by Winkler (Fazinić and Fazinić 1983). The aim of this study is to re-examine whether the administrative wine-growing zones correspond to the current climatic conditions and how fast the bioclimatic indices are changing in the current and future climate to determine the optimal time frame in which the zones should be revised again.

2   Materials and methods

The starting points for determining the suitability of a grapevine growing are bioclimatic indices. Four temperature indices have been calculated and are described in Table 1: the Temperature Growing Season (TGS), the Growing Degree-Days (GDD), the Huglin Index (HI) and the Cool night Index (CI), complemented by the Dryness Index (DI). Administratively, Croatia is divided into four wine-growing regions (Prša 2022) and had more than 18,000 ha of vineyards in 2020. To obtain indications of changes in the bioclimatic indices in Croatia, this study used data on the daily values of minimum, maximum and mean (Tmin, Tmax, T, °C) air temperature as well as daily precipitation (P, mm) and wind speed (v, m/s) from 80 meteorological stations throughout Croatia from 1961 to 2020. The spatial and temporal interpolation proposed by Perčec Tadić (2010) was performed due to missing measurements (instrument malfunction or missing

Table 1. Bioclimatic indices used in the study.

Index/ Reference	
Temperature Growing Season (TGS) (Jones 2006)	$\text{TGS (°C)} = \sum_{1.4.}^{31.10.} \left(\frac{T_{max} + T_{min}}{2} \right)$
Growing degree-days (GDD) (Winkler et al. 1974, Jones et al. 2012)	$\text{GDD} = \sum_{1.4.}^{31.10.} \left(\frac{T_{max} + T_{min}}{2} - 10 \right)$
Huglin Heliothermal Index (HI) (Huglin 1978)	$\text{HI} = \sum_{1.4.}^{30.9.} \left(\frac{T + T_{max}}{2} - 10 \right) \cdot k$ k- parameter dependent on the latitude of the location
Cool night Index (CI) (Tonietto 1999)	$\text{CI (°C)} = \frac{1}{30} \sum_{j = 1.9.}^{30.9.} T_{min,j}$
Dryness Index (DI) (Riou et al. 1994, Tonietto and Carbonneau 2004)	$\text{DI (mm)} = W_0 + P - T_v + E_s$ W_0 – estimated initial water reserve P – mean monthly precipitation amount T_v – potential transpiration E_s – evaporation

observation). In addition, simulations of three regional climate models (CLMcom-CCLM4-8-17, SMHI-RCA4, CNRM-ALADIN5.3) from the EURO-CORDEX database with a grid spacing of 0.11° are used. The selected models proved to be good for predicting bioclimatic indices in the present climate (Omazić et al. 2020). The observed and modeled data were spatially interpolated using regression kriging, assuming a linear relationship between the meteorological parameters and four predictors: Latitude, Longitude, Elevation and Distance from the Sea. The predictors were derived from the digital 1-km elevation model.

3   Results

In the 30-year period from 1961 to 1990, the TGS in most of the Croatian mainland was between 15 and 17 °C (Figure 1a). This temperature favours the cultivation of vines, especially white varieties. In the coastal areas, the TGS was mostly between 17 and 24 °C over the same 30-year period. This air temperature favours the cultivation of almost all grape varieties. However, the sharp increase in air temperature in the period 1991-2020 compared to the period 1961-1990 is worrying (Figure 2a). The GDD indicates the suitability of most areas for viticulture and as expected, follows the characteristics of the spatial

distribution of the TGS for the same periods. Most of continental Croatia has index values of 1389-1667 °C units for the period 1991-2020 (Figure 2b). These index values indicate good conditions for the cultivation of white grape varieties such as Graševina and Chardonnay, for which these areas are famous. In the coastal areas, the GDD values during the growing season are so high that the climate is suitable for the cultivation of almost all grape varieties and the high quality of the wine produced. However, as with temperature, the sharp increase in GDD compared to the period 1961–1990 is also worrying (Figure 1b, 2b). Similar to the previous two indices, the distribution of HI also shows further warming and changes in the categories by area (Figure 1c, 2c). The CI and divides the lowlands into two categories: "very cool nights" and "cool nights", while the coastal area is warmer and is mainly

represented by the two warmest categories (Figure 1d, 2d). Certain differences can be seen in the spatial distribution of the DI (Figure 1e, 2e). These characteristics show a deviation in the southern part of Croatia, which is "moderately dry" (negative DI values) compared to the rest of the country, which is characterized by "humid" conditions. These relatively dry conditions contribute to the production of high-quality, mostly red wines in
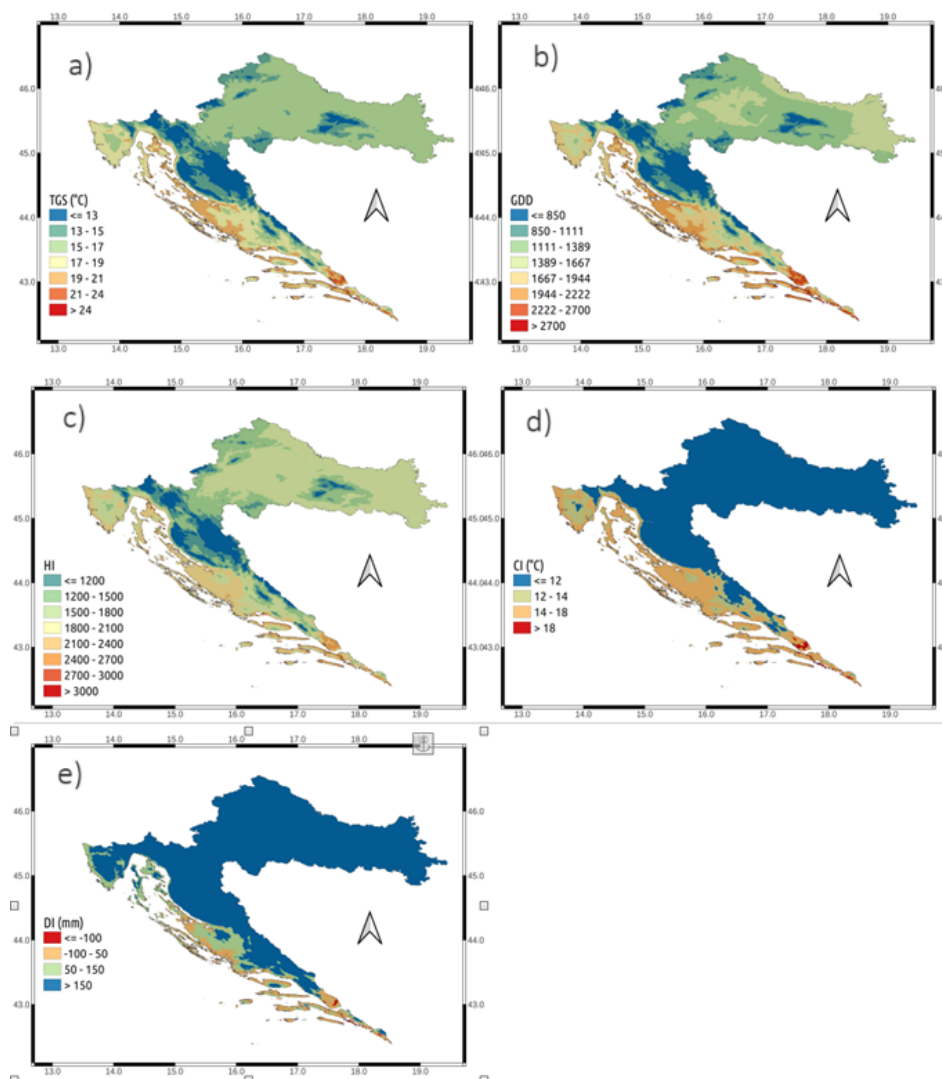

Figure 1. Spatial distribution of bioclimatic indices: a) TGS, b) GDD, c) HI, d) CI and e) DI in 1961–1990 period.
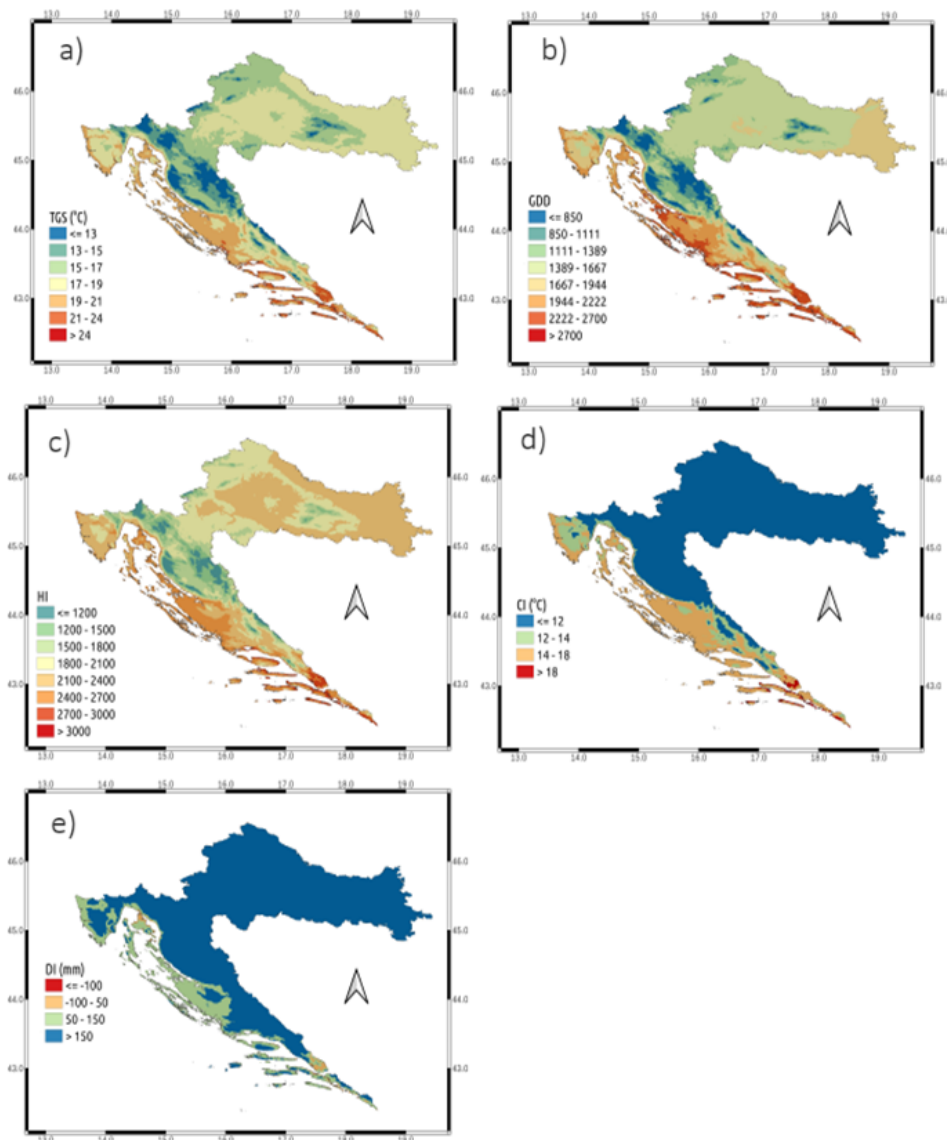
Figure 2. Spatial distribution of bioclimatic indices: a) TGS, b) GDD, c) HI, d) CI and e) DI in 1991–2020 period.

southern Croatia. The distribution of DI also shows the differences between the two climatic norms, which indicates a further drying out of the southern part of the Croatian territory. Climate models indicate a further increase in air temperature over the course of the year,

particularly during the growing season (Omazić et al. 2020). In the period 2041–2070, a further increase in air temperature of 2.25 °C to 2.75 °C is expected for the whole of Croatia compared to the period 1971–2000. In addition to the increase in air temperature, a further change in the precipitation regime is also expected, with increasingly frequent dry periods. The wine-growing area with reduced DI is increasing under climate change, which indicates a further water deficit on Croatian territory. and their ratio is to be expected in Croatia under future climatic conditions.

4   Discussion

The value of all indices clearly shows that almost all of Croatia is suitable for viticulture, but it can be seen that the temperature has risen by 2–3 °C throughout Croatia. A look at the GDD values shows that eastern Croatia itself has slightly higher values than the rest of continental Croatia,

and this area offers the opportunity for the successful cultivation of more resistant black varieties such as Merlot. Similarly, the vines in certain mountainous areas can accumulate enough heat (more than 1111 °C units) and are thus suitable for growing vines in areas with lower elevation, because although we have enough heat during the growing season, the risk of frost is still much higher here than in continental areas. The production map is changing or will change very soon in the future, and they would have to be ready to adapt to new administrative and technological changes. All current evidence on climate change indicates that the atmosphere will continue to warm, increasing the likelihood of far-reaching and irreversible consequences for people and the ecosystem. Good and timely adaptation is key to maintaining tradition and quality in this agricultural and economic sector. The increase in TGS is particularly pronounced in the far south of Croatia, where we already have extremely high air temperatures, and such a further increase will only make production more difficult. Since the results shown here indicate a further warming of the climate, which could be accompanied by more frequent longer periods with air temperatures above 30 °C (especially an increase in TGS,

followed by GDD and HI) and more frequent droughts (a decrease in DI), a significant change in the characteristics of grapes (sugar, acidity and their ratio) is to be expected in Croatia under future climatic conditions. In addition to droughts, a further increase in the number and intensity of extreme events in the future climate (such as hail) is expected, which would further threaten the vineyards.

5   Conclusions

In this study, the bioclimatic indices for the wine-growing regions of Croatia were analyzed in detail. Data from measurements in the period from 1961 to 2020 and climate models with climate projections up to 2070 were used. On this basis, we can conclude that the current boundaries of climate zones can still be considered largely relevant based on average data for the period 1991–2020. However, if we look at the detailed data within this period, it becomes clear that there is significant warming and an increase in the value of temperature indices in the second and especially the third decade of this series. The largest and most rapid changes are observed in zone B, i.e. in the region of Central Hilly Croatia where it is already justified to recommend the correction of the boundaries of climate zones B and C I. This correction is supported by climate models for the period 2041–2070, which indicate further warming of the atmosphere. In the far east of Croatia, the bioclimatic indices tend to increase, and it is expected that these areas will, over time, have climatic conditions corresponding to zone C II. It is, therefore, crucial to establish a high-quality system for monitoring climate change and its impact on viticulture. In view of the observed trend of changes, it is necessary to carry out a regular review of the climatic zones every ten years.

6   References

Bock, A., Sparks, T.H., Estrella, N., Menzel, A., 2013. Climate-induced changes in grapevine yield and must sugar content in Franconia (Germany) between 1805 and 2010, PLoS One 8, e69015.

Fazinić, N., Fazinić, M., 1983. Klimatske zone vinove loze SR Hrvatske. Jugoslovensko vinogradarstvo i vinarstvo, 10-11, 19-22.

Huglin, M.P., 1978. Nouveau mode d'évaluation des possibilités héliothermiques d'un milieu viticole.

Comptes Rendus de l'Académie d'Agriculture de France 64, 1117-1126.

Jones, G.V., 2006. Climate and terroir: Impacts of climate variability and change on wine, Geoscience Canada Reprint Series 9, 203-217.

Jones, G.V., Reid, R., Vilks, A., 2012. Climate, grapes, and wine: structure and suitability in a variable and changing climate. In: Dougherty P. (Eds), The geography of wine: regions, terroir, and techniques. Springer Press, 255.

Lalić, B., Eitzinger, J., Dalla Marta, A., Orlandini, S., Firanj Sremac, A., Pacher, B., 2018. Agricultural Meteorology and Climatology, Manuali – Scienze Tecnologiche, 8, Firenze University Press.

Malheiro, A.C., Santos, J.A., Fraga, H., Pinto, J.G., 2010. Climate change scenarios applied to viticultural zoning in Europe. Climate Research 43, 163-177.

Omazić, B., Telišman Prtenjak, M., Prša, I., Belušić Vozila, A., Vučetić, V., Karoglan, M., Karoglan Kontić, J., Prša, Ž., Anić, M., Šimon, S., Güttler, I., 2020. Climate change impacts on viticulture in Croatia: viticultural zoning and future potential. International Journal of Climatology 40, 5634-5655.

Perčec Tadić, M., 2010. Gridded Croatian climatology for 1961-1990. Theoretical and Applied Climatology 102, 87-103.

Prša, I., 2022. Utjecaj vremenskih i klimatskih uvjeta na vinogradarsku proizvodnju u Hrvatskoj, University of Zagreb, 285.

Riou, C., Carbonneau, A., Becker, N., Caló, A., Costacurta, A., Castro, R., Pinto, P.A., Carneiro, L.C., Lopes, C., Clímaco, P., Panagiotou, M.M., Sotez, V., Beaumond, H.C., Burril, A.,Maes, J., Vossen, P., 1994. Le déterminisme climatique de la maturation du raisin: application au zonage de la teneur emsucre dans la communauté européenne. Luxembourg: Office des Publications Officielles des Communautés Européennes.

Tonietto, J., 1999. Les macroclimats viticoles mondiaux et l'influence du mésoclimat sur la typicité de la Syrah et du Muscat de Hambourg dans le sur de la France: méthodologie de caráctérisation. Ecole Nationale Supéricure Agronomique, Montpellier.

Tonietto, J., Carbonneau, A., 2004. A multicriteria climatic classification system for grape-growing regions worldwide, Agricultural and Forest Meteorology 124, 81-97.

Van Leeuwen, C., Destrac-Irvine, A., Dubernet, M., Duchêne, E., Gowdy, M., Marguerit, E., Pieri, P., Parker, A., de Rességuier, L., Ollat, N., 2019. An update on the impact of climate change in viticulture and potential adaptations. Agronomy 9, 514.

Winkler, A.J., 1974. General Viticulture. University of California Press, 710.

User-friendly Methodology and Prototype for Operational Deployment of a Satellite-based Monitoring System for EU – for More Resilient Territorial Management with Less Impact on Environment and Climate

Kristian Milenov[1, *], Viktor Milenov[1]

[1] ASDE-ECOREGIONS/Stalker-KM LTD, Sofia, Bulgaria, k.milenov@stalkerkm.com, vikplaysmc@gmail.com
* corresponding author

Abstract: The integration of Satellite Data in local Spatial Data Infrastructures (SDIs) and AI-driven analytical solutions is of strategic importance, supporting territorial management and decision making on national, regional, and municipal level. EO Copernicus can be a disruptive source of knowledge to improve territorial and environmental management and delivery of effective public policies and risk prevention services. However, due to the lack of resources and competences at organizational and individual level, as well as low awareness among political decision makers, the uptake of existing satellite data and services is challenging. Their integration in added-value services for local and regional administrations is far from optimal. Complex scientific studies and services exist, but they require high expertise also do not effectively help the widespread use of innovative solutions combating CC and risk prevention. There are gaps to bridge to achieve the vision.

The aim is to develop a user-friendly municipal expert system on risk prevention and strengthening resilience. We propose an in-house developed operational solution, combining so-called Exposure and Loss databases and the SmartCover Databases. It combines three main tools – the description of land cover through Land Cover Meta Language – LCML (ISO 19144-2); local master plans legal nomenclature and associated spatial data (functional zones) – "urban/functional bricks" concept; and satellite-based algorithms for automatic data interpretation, developed by Stalker-KM LTD (upgraded ASDE-ECOREGIONS).

Keywords: risk prevention; AI; EO; in situ; CbM; land cover; land use.

1   Introduction

Our study and solution are based on long user-oriented experience on sustainable and resilient territorial management. Thus, we are trying to integrate the combined EO remote and in-situ monitoring mechanisms, with efficient, objective, legally justified, mandatory, and easy to understand services results. One of the main targets is the application of automatic assessment of data from various sources and risk prevention analysis, using a simplified "traffic light" approach.

The proposed solution may be applied on urban, agricultural and nature territories, covering all main types on Earth environmental coverage. The use of the new world standard ISO 1944-2 allows the application of the monitoring package not only in the EU, but also worldwide.

The paper is a follow-up action of the research work of experts of Stalker-KM LTD, during a period of ten years, extracting best experience from real-life projects, assigned by different municipalities in Bulgaria. The succession work of ASDE-ECOREGIONS has upgraded the developed tools, with exchange of knowledge and high expertise with EC-mainly DG JRC Food Security unit and collaborative territorial monitoring projects, financed by UN-FAO and state administration. One of our major aims is to harmonize and orient towards user needs, the land cover/land use monitoring methods among the countries from the South-East European region.

2   Materials and methods

Because of the conference requirements, our study is limited to the Sofia Municipal urban area. Integrated EO remote data from Sentinel 2 satellite images and in-situ various data from the Sofia Master plan sources are used. On other side our solution is much oriented towards supporting the EU policies, such as the LULUCF" (Milenov et al. 2022). To obtain much better efficiency, accuracy and land cover/land use description, the following main tools are used:

- Land cover/Land use semantic model, using hierarchical manner, using the LCML, based on the principles laid down in the LCCS classification system by UN-FAO (ISO 19144-2:2023).
- Combined remote and in-situ data interpretation, applying COPERNICUS (Sentinel 2) data and services, including the monitoring framework of DG JRC – Change by Monitoring (CbM, Loudjani et al. 2023).
- Risk prevention resilience concept - Combined semi-automatic and (in future) AI-supported algorithm, assessing urban, agricultural or nature units, which are mandatory defined by local state or municipal legal system ("tegon" Devos et al. 2014, "urban bricks" Ordinance No. 7, 2003).

When using Sentinel 2 images for assessing urban areas, a problem is the relatively low spatial resolution – 20 and 10 at the most. Results are not usable at local administrative and business end-user's level. This means that we had to apply another mechanism of efficient data use, different than the traditional one, based on area mapping. Here comes the proposed application of the urban-brick as basic reference element for analysis (Figure 1). The "urban

bricks" are 3-dimensional land cover units, which spatial extent matches with the functional zones, which are units of land with stable and monitorable boundaries, with homogeneous type of land use, as prescribed by the City Master Plan (Figure 2). The main advantage is that with the "urban brick" concept we are not trying to depict the detailed areas occupied of the individual physical objects, but we are assessing the land cover status by derived statistical metrics from the satellite signal at the level of the functional zone, as our reference unit. Another argument in favour of such approach is that the functional zones are legally defined and approved by the local administration and adhere to specific facility and construction rules and regulations, including risk management and change monitoring, established by law in Bulgaria – The Territory Development/Management Law/Act–(ZUT).
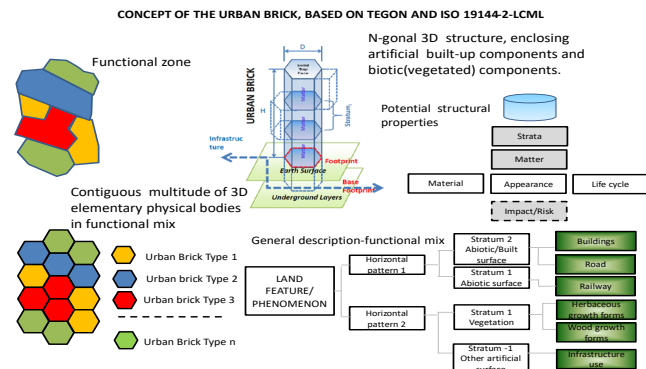

Figure 1. Illustration of the "urban-brick" concept.

Figure 2. Illustration of the "urban-brick" (in blue contour), representing a contiguous piece of land with specific biophysical characteristics and functional purpose (ex. residential). The spatial extent of the "urban bricks" matches with the outlines of the functional zones. The background image is from Google Earth.

As example, for the urban-brick UB1 Residential Functional zone, the end-user (local administration, auditors, public organizations, etc) may monitor the following indicators, territorial device parameters, which are mandatory for sustainable territorial management and risk resilience (Figure 3):

- maximum building density – %;
- maximum intensity factor – ratio between the unfolded built-up area and the area of the landed property;
- minimum green area;
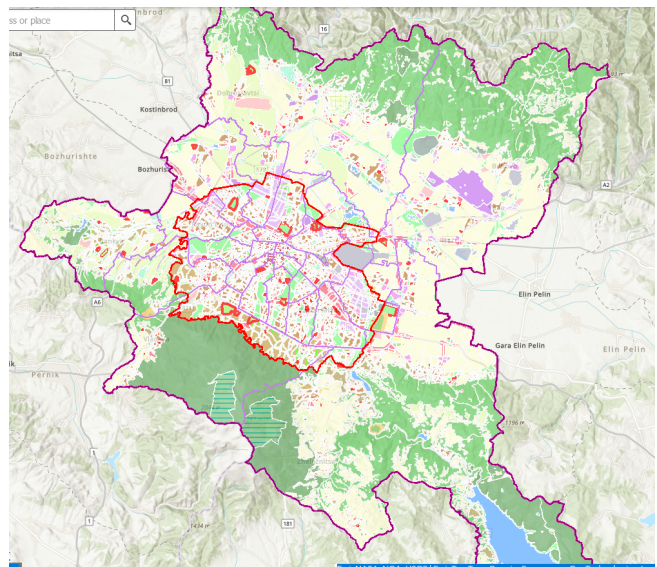- maximum elevation/high of buildings.

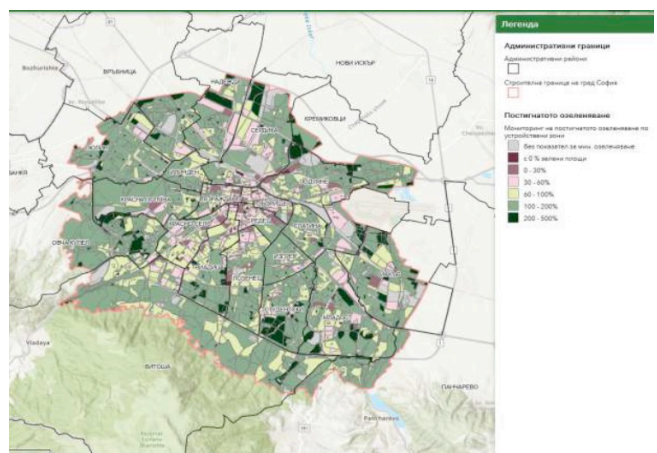Figure 3. Sofia Municipality Master Plan.

Figure 4. Sofia Thematic map of Grassing achieved.

It must be underlined that sometimes, monitoring green indicator is confused with monitoring green mass increase (Figure 4). A mandatory free from sealing area for the urban units, to be used for vegetation, must be maintained without being replaced by another parameter.

The satellite-based method uses the HR-VPP product developed by the European Environment Agency (EEA) as part of the Copernicus Land Monitoring Service (CLMS), to assess the percentage of potential green spaces within the functional zones, on yearly basis. The obtained values are compared with the prescribed minimum percentages for

green spaces for each functional zone. Linear regression analysis is performed to detect negative trends with respect to the share of green spaces (Figure 5).

For the EO objective for monitoring of open and green space trends for Sofia Municipality, the HR_VPP – total productivity (TPROD) for Sofia Municipality, using based on Sentinel 2 data (2017-2023) is used. Data is incorporated into a new semi-automatic tool for monitoring changes (CbM) – Risk prevention algorithm – RiskMON. It starts with precise application on selected pilot area and after finalising this preliminary stage it will be applied on the whole territory in future. Further enhancement with AI-based methods is foreseen at later stage. Further development of the expert system to assess the
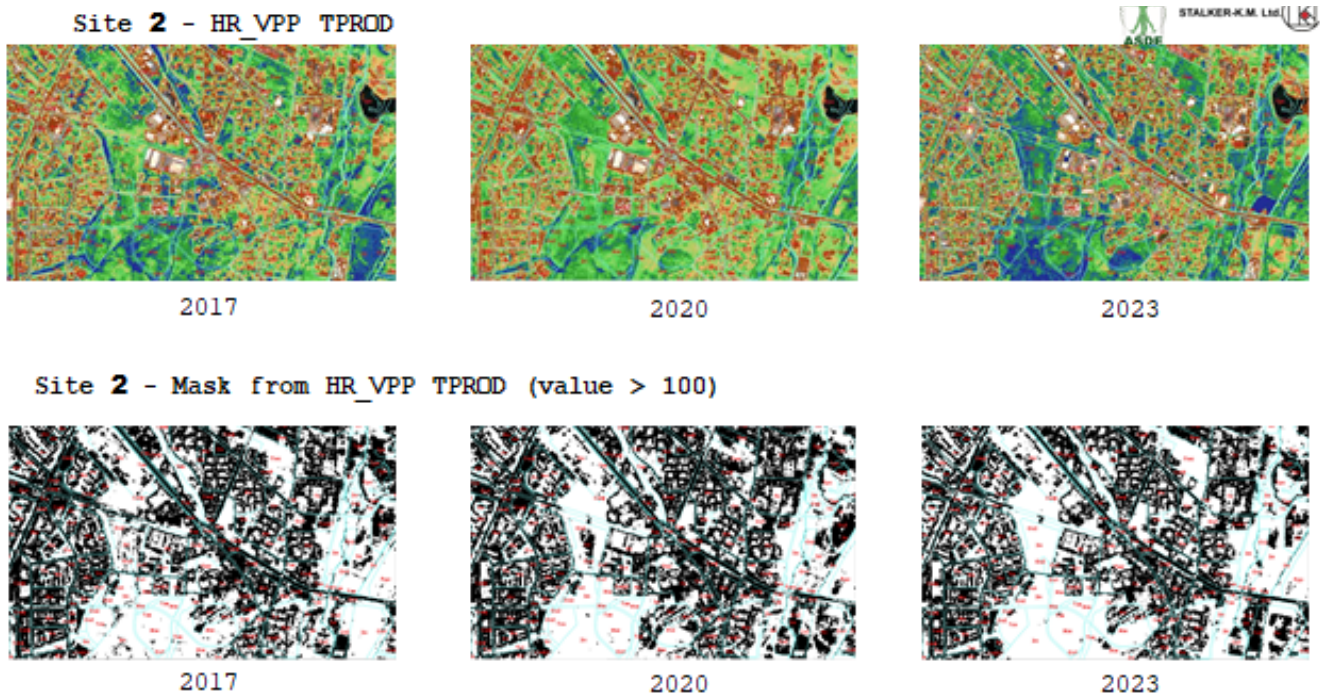
Figure 5. EO objective Monitoring of Grassing tendencies - HR_VPP – total productivity (TPROD), Sentinel 2 – 2017-2023.

vulnerability (flooding) of the so-called "urban bricks" – "functional units" (FM) will be done in the context of a Proposal of Algorithm on flood risk prevention.

Scope: The assignment deals with the annual update of the information on the percentage of the area potentially covered with green vegetation, within the functional units of the city master plan. The collected data allows for the update of the values of attributes "Min Green Area (Mg)", Max Allowed residential /public area (Ra) and Min area of recreational space (Mr) of the Asset score of the table on "Risk Assessment".

Method: Overlay the geometries of the functional units with a gridded (raster) dataset reflecting vegetation phenology, as derived from satellite data. Extract the zonal statistics (count, sum and mean) of the pixels value distributions within each polygon of the functional unit.

Expected output: A new vector (polygon-based) file with the geometries of the functional units, with additional set of attributes reflecting the distribution of the green vegetation and artificial surfaces within each functional unit. The update is produced once per year with data for the precedent year (Figure 6). It covers all the years from 2017 until 2022/23. The assignment is developed using data from the Master Plan of the Sofia Municipality.

3   Results and discussion

Providing Basic solution SEE countries resilience**.** The aim of ASDE-ECOREGIONS is together with colleagues from EU countries (priority South-East Europe), to develop a user-friendly locally objective/effective/efficient/economic monitoring system on assessing the resilience and vulnerability/natural hazards, air pollution, flooding, landslides, earthquake, using EO COPERNICUS services and mandatory territorial units – the so-called "tegon" and "urban bricks".

Proposal for Trans-border collaboration on common solution for Development of methodology and prototype for operational deployment of a satellite-based system for EU wide agri-ecological zoning for the purpose of more effective agricultural management with less impact on environment and climate.
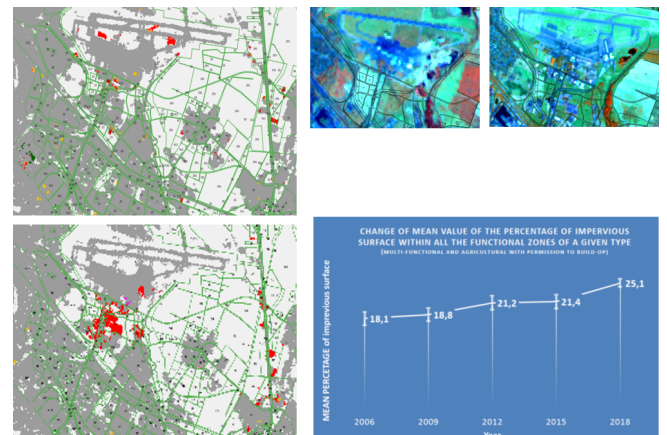

Figure 6. Assessing trends in urbanised territories using Copernicus HRLs.

Proposal for Trans-border collaboration on common solution for Development of methodology and prototype for operational deployment of a satellite-based system for EU wide urban-resilient zoning for the purpose of more effective territorial, natural resources, and critical infrastructure management with less impact on environment, climate, and economy (Figure 7).

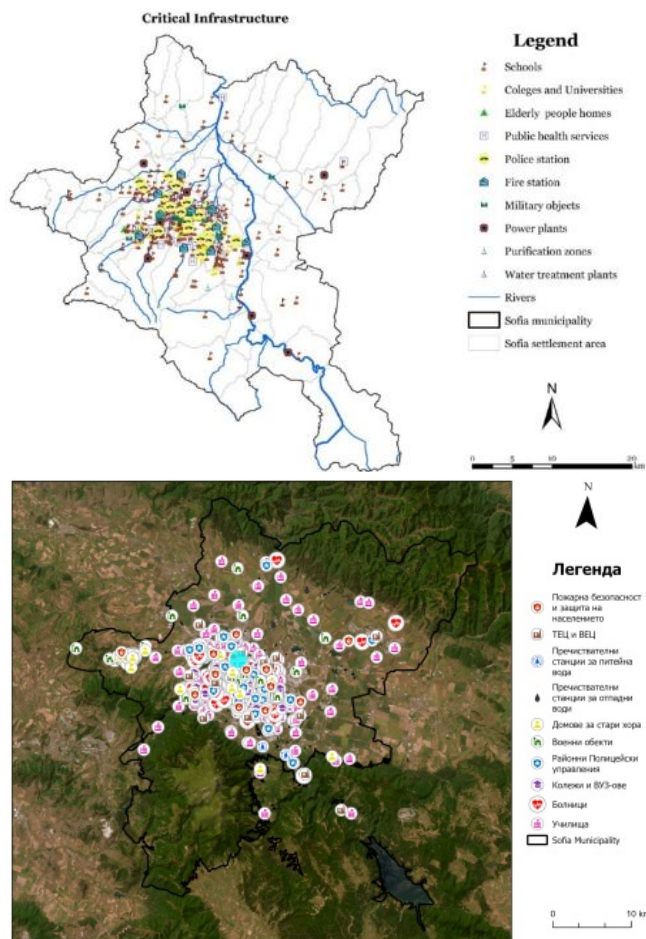It should also support the Carbon Border Adjustment Mechanism (*CBAM*) – Reg. (EU) 2023/956 and „EU Fit for 55").

Figure 7. Sofia Assets and Critical infrastructure – Exposure (top) and Loss data (bottom) sets.

4   Conclusions

Our efficient solution: A Trans-national/Trans-border Bottom-up APPROACH from EU guidelines, R&D projects, EU (RRF) (RRPs) towards local operational capacity from post-event recovery towards risk prevention/resilience policy. Considering climate impact, but also negative human impact – lack of efficient management, neglecting surveillance measures, etc. Operational solution, combining the so-called Exposure and Loss databases/SmartCover Databases with three main tools – the ISO 19144-2/3; local mandatory nomenclature; the AI/ML algorithm on satellite data interpretation.

We propose collaborative projects under the HORIZON 2020, INTERREG, Danube Program, ESA-PECS program for South-East Europe**.**

1. Network of Risk Prevention Regional centers network (an up-grading of the EC supported concept from 2010–2011)
2. Methodology and prototype for operational deployment of a satellite-based system for EU wide agri-ecological zoning for more effective urban/agri-management with less impact on environment and climate.
3. Prototype for satellite-based detection and mapping of photovoltaic installation in agricultural areas. Assessment of their typology in relation to their impact on soil health.

5   References

Devos, W. and Milenov, P., 2012. Introducing the TEGON as the elementary physical land cover feature. In Conference Proceedings: Proceedings of the 1st International Conference on Agro-Geoinformatics 2012. Amsterdam, Netherlands, Elsevier B.V., JRC72112.

ISO 19144-2:2023(en). Geographic information—Classification systems—Part 2: Land Cover Meta Language (LCML)-https://www.iso.org/obp/ui/en/#iso:std:iso:19144:-2:ed-2:v1:en (Accessed 11 June, 2024)

Loudjani, P., Sima, A., and Devos, W., 2023. Use of geotagged photographs to evidence Land Cover and Land Use across EU policies, Ispra, JRC135007.

Milenov P., Sima A., Puerta-Pinero C., Angileri V., Devos W., Lugato E., 2022. Deliverable 1: Methodology for identification and mapping of candidate peatlands and wetlands areas for LULUCF, EC-JRC, Ispra.

Ordinance No. 7 of December 22, 2003 on rules and standards for the structure of different types of territories and development zones https://www.lex.bg/laws/ldoc/2135476546 (Accessed 11 June, 2024)

Requirements for Georeferencing and Digitalization of Spatial Data in the New EU Legislation on Climate, Environment, and Biodiversity

Višnja Grgasović[1], Branimir Pavlinec[2], Domagoj Stjepan Krnjak[1,], Vlatka Palčić[1], Tatjana Antolić[1], Hana Mesić[2], Vida Posavec Vukelić[2], Martina Pekčec[2]*

[1] Department for Climate Activities, Ministry of Environmental Protection and Green Transition, Zagreb, Croatia, visnja.grgasovic@mzozt.hr, vlatka.palcic@mzozt.hr, domagojstjepan.krnjak@mzozt.hr, tatjana.antolic@mzozt.hr

[2] Institute for Environment and Nature, Ministry of Environmental Protection and Green Transition, Zagreb, Croatia, branimir.pavlinec@mzozt.hr, hana.mesic@mzozt.hr, vida.posavecvukelic@mzozt.hr, martina.pekcec@mzozt.hr

* corresponding author

Abstract: Since 2019 a significant number of EU legislative acts related to climate and energy policies, as well as policies on environmental protection and biodiversity restoration, have been adopted, amended, or are still in the process of being revised and enacted. These legal initiatives require georeferencing and digitalization of spatial data collected through remote environmental monitoring. The aim of these legislative efforts is to leverage technical and technological capabilities to obtain more precise monitoring data on policy performance in these sectors and to ensure the credibility of law enforcement through certification of fulfilled obligations and achieved goals. Additionally, the more accurate data collected over time will contribute to the development of new models and the improvement of EU policies aimed at achieving UN Millennium Goals and the EU climate neutrality targets by 2050, as well as long-term goals for biodiversity restoration and the protection of the environment. For monitoring and implementing these policies, Member States need to advance their capabilities for tracking emissions and collection environmental data according to the new legislation requirements. Therefore, Republic of Croatia is conducting a demonstration project to develop a multi-scale and multi-purpose system – CROatian Land Information System (CROLIS). The LIFE CROLIS project is co-financed by the EU LIFE Programme. This paper provides an overview of the new EU legislation and the requirements for georeferencing spatial data within the National Emission Inventory System and requirements for monitoring climate, environmental and biodiversity components that could be integrated into a such unified monitoring system.

Keywords: LULUCF; georeferencing; climate; biodiversity; environment.

1 Introduction

Development and establishment of the Croatian Land Information System through the LIFE CROLIS project is a response to the package of European Union laws that require more precise reporting on greenhouse gas (GHG) emissions and carbon sinks in Member States, with the aim of achieving GHG emission reduction goals. The new EU legislation aligns with two out of the six priorities set by the European Commission (Leyen 2019) for the period from 2019 to 2024: The European Green Deal, A Europe fit for the digital age based on strategic documents (COM(2019) 640,

COM(2020) 380, COM(2020) 66, C(2022) 4388) and within legislative initiatives (Decision (EU) 2022/2481, COM(2021) 550). This set up further strengthen the goals of preserving and restoring the natural environment and reducing greenhouse gas emissions by at least 55% by 2030, with the aim of achieving climate neutrality by 2050. To this end, a significant number of legal acts have been prepared, some of which have already been adopted and enforced, while others are still in the process of negotiations between EU institutions and Member States. All these acts significantly impact or will impact the lives of EU citizens in the coming years.

This paper encompasses an overview of the EU laws falling under the jurisdiction of the Directorate for Climate Policy and the Institute for Institute for Environment and Nature of the Ministry of Environmental Protection and Green Transition. In this paper, we provide an overview of the obligations and requirements of the new EU legislation related to climate, environment, and nature protection in terms of digitization, data management, remote monitoring, and georeferencing various data for reporting purposes, verification of EU law enforcement, and assessment of visible effects of these laws implementation that could be aggregated and tracked through a comprehensive, multi-level, and multipurpose land monitoring system. For each new regulation we specify arising obligations, as well as geospatial data that need to be collected, digitized, and reported.

2 Requirements for georeferencing and digitalization of spatial data in the new EU legislation

At EU level, the general rules for establishing infrastructure for spatial information required for reporting and data exchange have been defined by the INSPIRE Directive since 2007 (Directive 2007/2/EC). New regulation (Regulation (EU) 2019/1010) amended a group of European laws to enhance environment information management, simplify reporting, and reduce administrative burden. This regulation lays the groundwork for improving databases for future assessments and increases transparency of data of public interest. Additionally, changes to the legislative package determine the format and method of digital data sharing.

2.1 Climate and Energy

The new EU legislative package "Fit for 55" has introduced amendments to laws governing climate and energy with the aim of achieving at least a 55% reduction in greenhouse gas emissions by 2030 and creating conditions for climate neutrality by 2050.

In pursuit of EU climate goals, the sector of Land Use, Land-Use Change, and Forestry (LULUFC) plays a crucial role. To achieve climate neutrality (where emissions equal removals), it is essential to balance remaining emissions—after appropriate reduction measures have been taken in both EU ETS (EU Emissions Trading System) and non-EU ETS sectors — by permanently storing carbon in natural sinks (such as vegetation, soil, deadwood, and wood products) or by technological storage methods (such as carbon capture and storage or carbon capture and utilization).

The potential and accounting of carbon storage in natural reservoirs in the calculation of emission balance presents a unique problem for each country. The methodology for accounting for these emissions is prescribed by the IPCC guidelines for national greenhouse gas inventories (IPCC 2006).

When reporting in all sectors including the LULUCF sector, we distinguish three levels of methodological complexity: Tier 1 (basic method that uses international emission factors and has a high degree of calculation uncertainty), Tier 2 (medium complexity, with lower calculation uncertainty and use national emission factors) and Tier 3 (most demanding in terms of complexity and data requirements, with low calculation uncertainty and use emission factors specific to individual categories/facilities/processes.

The Regulation (EU) 2023/839, defines an obligation of Member States to use at least Tier 2 methodology in the LULUCF sector from 2028 while from 2030, Member States shall use Tier 3 methodology. The Tier 3 methodology r requires a significant effort from Member States to properly identify, monitor, and precisely determine/georeference land cover, land use, and land use changes to ensure that calculations are credible.

According to the specified obligations Croatia, along with other Member States, should establish a system for monitoring land use changes with geographically explicit data on land conversion by 2030. This monitoring should be done on regular basis across the entire surface of Croatia, using specific carbon sink factors based on climate-vegetation zones and types of land cover/crops/products. Additionally, it should consider background emission levels caused by natural disasters (such as fires, floods, landslides, desertification...) in accordance with the IPCC guidelines.

2.2 Nature Restoration

Despite the European Union's longstanding active environmental and habitat protection policies, a Final evaluation report (Trinomics B.V. 2022) conducted as part of the evaluation of the EU Biodiversity Strategy up to 2020 (COM(2011) 244) reveals that the EU has not halted biodiversity loss between 2011 and 2020, nor has achieved the voluntary goal of restoring at least 15% of degraded ecosystems by 2020 (SWD(2022) 284).

Due to these negative indicators, as well as numerous other negative signs of pressures on natural habitats and biodiversity, the European Commission introduced the Proposal for a Regulation on Nature Restoration (COM(2022) 304) in 2022, in line with the new EU Biodiversity Strategy for 2030, titled "Bringing Nature Back into Our Lives" (COM(2020) 380).

Among the proposed measures to improve the state of nature, there are plans to develop national restoration plans for the period up to 2050. These plans will need to establish georeferenced maps of areas included in nature restoration efforts, along with prescribed actions.

The proposed regulation requires periodic delivery of data on the location and extent of areas covered by measures for the restoration of terrestrial, coastal, and freshwater ecosystems, as well as marine ecosystems, including georeferenced maps of these areas. Monitoring results will need to be submitted annually through Monitoring Reports, while data on the location and extent of areas covered by restoration measures will need to be provided every three years, including georeferenced maps of those areas.

2.3 Resilience of forests

Due to increasing stress caused by climate change, unsustainable direct or indirect human use and activities, as well as related land use changes, a proposal for a new Regulation (COM(2023) 728) was introduced in 2023. The proposed regulation envisions the establishment of a forest monitoring system. The forest monitoring system should consist of:

- a geographically explicit identification system for mapping and locating forest units,
- a framework for collecting forest data on annual basis,
- a framework for exchanging forest data.

The forest monitoring system should include electronic databases and geographic information systems, allowing for data exchange and integration with other electronic databases and geographic information systems, including those developed for monitoring emissions and sinks in the LULUCF sector as previously mentioned. The collected data should be standardized, and the framework for data collection and responsibilities for collecting specific data will be distributed between Member States and the European Commission.

2.4 Deforestation

Under EU law (Regulation (EU) 2023/1115) certification is required for certain goods and certain products associated with deforestation and forest degradation when made available on the Union market and for export from the Union. The aim of the regulation is to prevent deforestation, and products such as soy, beef products, and timber products will need to have a certificate of origin that must not be associated with deforestation. To this end, an information system is being established that, among

other things, should georeference land parcels larger than four hectares that are used to produce relevant goods.

2.5 Soil Monitoring

All Member States are faced with problems of soil degradation, erosion, pollution and sealing. Research conducted by the European Commission (Veerman et al. 2020) shows that between 60 to 70% of soils in the European Union are not healthy. Therefore, in 2023, the European Commission presented a Proposal for a Soil Monitoring Act (COM(2023) 416) which establishes measures for monitoring and assessing soil health, sustainable soil management, and contaminated sites.

For this purpose, Member States will need to establish a framework for monitoring soil health, contaminated sites and their remediation, and permanent coverage (so-called sealing), and conduct regular measurements on soil samples taken "in situ." Member States will need to report results and trends every five years.

The proposal for the new Directive envisages the establishment of a digital portal for soil health data that should be compatible with the EU's data strategy and EU data spaces and serve as a hub for accessing soil data from various sources.

2.6 Protection of carbon-rich soil

EU law (Regulation (EU) 2021/2115) establishes rules for supporting strategic plans developed by Member States within the framework of the Common Agricultural Policy (CAP). It mandates the implementation of GAEC 2 standards (Standard for good agricultural and environmental condition of land) to protect carbon-rich soil through the preservation of wetlands and peatlands. Member States are required to comply with this obligation starting in either 2024 or 2025. The regulation further demands the identification (including geolocation) of such areas, as well as agricultural land (within the LPIS system), where agricultural activities supported by CAP annual payments are assessed (cross-compliance checks) against the GAEC 2 standard.

2.7 Certification framework for carbon removals

Carbon certification is an additional mechanism that could contribute to achieving high-quality carbon removals, thereby contributing to the Union's goal of achieving climate neutrality by 2050. The new legislative proposal (COM(2022) 672) on the certification of carbon removals (in the adoption phase) establishes a voluntary framework for the entire EU, sets criteria for high-quality carbon removals, and a procedure for monitoring, reporting, and verifying the authenticity of these removals. According to the EU framework, there are several ways to remove and store carbon, which can be certified:

- natural solutions such as forest restoration, soil, and innovative agricultural practices,
- technological solutions such as bioenergy with carbon capture and storage or direct air capture and storage of carbon,
- long-lasting products and materials, such as wood-based construction.

Also, a series of certification methodologies tailored to the main types of carbon removal activities will be developed to ensure the correct, harmonized, and cost-effective implementation of the EU's quality criteria for carbon removals.

Farmers and forest owners will be able to certify carbon storage using a credible system such as the existing LPIS or a similar credible system. Operators who permanently store carbon through technological carbon storage in geological structures must also have georeferenced storage locations. The explicit geolocation of the storage must be stated in the appropriate certificate with which the operator participates within the certification scheme.

3 Discussion

The presented package of EU legislation promotes the digitalization of information and data, their georeferencing (i.e., precise spatial positioning), and their sharing. The requirements of the new legislation are focused on:

- determining the actual state of the environment based on remote monitoring and georeferencing of collected data,
- exchange of digital information among Member States and other stakeholders,
- standardization of data collected from different sources and exchange of these data,
- establishing a timeline for collecting data and information to monitor changes and trends in the environment and climate.

This aims to obtain detailed and credible information, which will be important for evaluation of implementation of existing policies and for designs of new policies, as well for certification or participation in certification schemes, which can be or are a source of income for individuals, entrepreneurs, and Member States.

The quality of collected information and spatial data is always a challenge, which is addressed by specifying data requirements for established reporting systems or by data evaluation during audits for developing reporting systems.

4 Conclusions

The development of a comprehensive monitoring system for different indicators on climate, nature and environment changes and their impacts to society, as well as information on the effects of policies implementation in these areas against the time is becoming increasingly important. Pairing and interpretation of data based on objective indicators and models is necessary for making informed decisions.

In the area of climate and energy, environment, and nature policies EU not only set high requirements for the collection, standardization, and processing of data but also enable, encourage, promote, and assist Member States in establishing monitoring systems.

5   References

Commission staff working document, Evaluation of the EU Biodiversity Strategy to 2020, 6.9.2022, SWD(2022) 284 final.

Communication from the Commission (...), Our life insurance, our natural capital: an EU biodiversity strategy to 2020, 3.5.2011. COM(2011) 244 final.

Communication from the Commission (...), The European Green Deal, 11.12.2019. COM(2019) 640 final.

Communication from the Commission (...), A European strategy for data, 19.2.2020. COM(2020) 66 final.

Communication from the Commission (...), EU Biodiversity Strategy for 2030 Bringing nature back into our lives, 20.5.2020. COM(2020) 380 final.

Communication from the Commission (...), 'Fit for 55': delivering the EU's 2030 Climate Target on the way to climate neutrality, 14.7.2021. COM(2021) 550 final.

Communication to the Commission European, Commission digital strategy Next generation digital Commission, 30.6.2022. C(2022) 4388 final.

Decision (EU) 2022/2481 of (...) 14 December 2022 establishing the Digital Decade Policy Programme 2030, OJ, L 323, 19.12.2022, pp. 4-26.

Directive 2007/2/EC (...) of 14 March 2007 establishing an Infrastructure for Spatial Information in the European Community (INSPIRE), OJ, L 108, 25.4.2007, pp. 1-14.

IPCC Guidelines for National Greenhouse Gas Inventories, 2006, Volume 4, Agriculture, Forestryand Other Land Use.

Leyen, U., 2019, A Union that strives for more, European Commission, Directorate General for Communication, Brussels.

Proposal for a Directive (...) on Soil Monitoring and Resilience (Soil Monitoring Law), 5.7.2023. COM(2023) 416 final.

Proposal for a Regulation (...) on nature restoration, 22.6.2022. COM(2022) 304 final.

Proposal for a Regulation (...) establishing a Union certification framework for carbon removals, 30.11.2022. COM(2022) 672 final.

Proposal for a Regulation (...) on a monitoring framework for resilient European forests, 22.11.2023. COM(2023) 728 final.

Regulation (EU) 2019/1010 (...) of 5 June 2019 on the alignment of reporting obligations in the field of legislation related to the environment (...), OJ, L 170, 25.6.2019, pp. 115-127.

Regulation (EU) 2021/2115 (...) of 2 December 2021 establishing rules on support for strategic plans to be drawn up by Member States under the common agricultural policy (CAP Strategic Plans) (...), OJ, L 435, 6.12.2021, pp. 1-186.

Regulation (EU) 2023/839 (...) of 19 April 2023 amending Regulation (EU) 2018/841 as regards the scope, simplifying the reporting and compliance rules, and setting out the targets of the Member States for 2030, (...), OJ, L 107, 21.4.2023, pp. 1-28.

Regulation (EU) 2023/1115 (...) of 31 May 2023 on the making available on the Union market and the export from the Union of certain commodities and products associated with deforestation and forest degradation (...), OJ, L 150, 9.6.2023, pp. 206-247.

Trinomics B. V., 2021. Support to the evaluation of the EU Biodiversity Strategy to 2020, and follow-up: Final study report, Roterdam.   https://www.cde.ual.es/wp-content/uploads/2022/04/KH0122166ENN.en_.pdf

Veerman, C., Pinto Correia, T., Bastioli, C. ... 2020. Caring for soil is caring for life – Ensure 75% of soils are healthy by 2030 for food, people, nature and climate – Report of the Mission board for Soil health and food, European Commission, Directorate-General for Research and Innovation, Publications Office.

CMIP6 and Climate Change: A Global Analysis of Research and Collaborations on the Water Budget

Sayed Ishaq Deliry[1],*, Uğur Avdan[2]

[1] Department of Remote Sensing and Geographical Information Systems, Eskisehir Technical University, Eskisehir, Türkiye, deliry.ishaq@gmail.com

[2] Institute of Earth and Space Sciences, Eskisehir Technical University, Eskisehir, Türkiye, uavdan@eskisehir.edu.tr

* corresponding author

Abstract: Global water resources are significantly impacted by climate change, necessitating advanced tools and methodologies for accurate analysis. Although numerous studies have employed the use of Coupled Model Intercomparison Project Phase 6 (CMIP6) models, only a limited number have specifically concentrated on their use in assessing the impacts of climate change on water budgets. This bibliometric analysis utilizes data from the Web of Science Core Collection, covering the period from 2014 to 2024. The analysis was conducted using VOSviewer mapping and visualization software and aims to identify the publication trends and collaborative efforts in CMIP6 research. The analysis reveals a significant growth in CMIP6-related research, with 3,184 publications highlighting the model's extensive adoption in climate science. However, it also reveals a notable gap, with only 64 studies specifically addressing water budget evaluations. Key journals, such as the Journal of Climate and Geophysical findings Letters, played a crucial role in spreading this research. The results also demonstrate significant international collaboration, primarily among developed countries, and emphasize the need for more geographically diverse research partnerships. Moreover, the correlation between research findings and Sustainable Development Goals pertaining to water and climate action illustrates the practical implications of CMIP6 models. The findings of this study offer pathways for future research and collaboration.

Keywords: bibliometric analysis; climate change; CMIP6; sustainable development goals; water budget.

1 Introduction

The Coupled Model Intercomparison Project Phase 6 (CMIP6) is an essential framework for simulating climate scenarios of the past, present, and future, enabling a more profound comprehension of climate changes and their impact on various environmental subsystems (Eyring et al. 2016, O'Neill et al. 2016, Chen et al. 2021). The complex correlation between climate change and water resources requires thorough examination, as changes in the water cycle have a direct impact on hydrological extremes, agriculture, and worldwide water management methods.

CMIP6 data is crucial for understanding the water cycle of the Earth (Jie et al. 2020, Guo et al. 2021). This comprehensive compilation of climate models enables scientists to examine various aspects such as precipitation, evaporation, and runoff (Wang et al. 2022, Balu et al. 2023, Risley and Ammit 2023). Moreover, CMIP6 allows researchers to forecast forthcoming alterations in the water cycle under various emission scenarios, offering vital insights for the management of water resources and the development of adaptation measures (Shafeeque and Luo 2021). Although CMIP6 is a widely accepted tool, current research aims to enhance the precision of the models and minimize uncertainty in future estimates (Sengupta et al. 2022).

Given the escalating impact of climate change on global water resources, this study aims to provide a bibliometric analysis of global research patterns and collaborations related to CMIP6 with a specific focus on its utilization for water budget evaluations. The significance of this research is emphasized by the growing susceptibility of water resources to climate change, a crucial matter that intersects with various United Nations Sustainable Development Goals (SDGs), particularly those aimed at ensuring clean water and sanitation and taking immediate action to combat climate change and its consequences (Carlsen and Bruggemann 2022).

2 Materials and methods

The methodology used in this study includes a systematic search for articles in the Web of Science Core Collection, including publications from January 2014 to January 2024. The bibliometric analysis of the data obtained from the Web of Science database was performed using VOSviewer mapping and visualization software. This software enables the generation of several network visualizations, including co-authorship, citation, co-citation, and bibliographic coupling networks (Arruda et al. 2022, Badola and Agrawal 2023). These visualizations offer a comprehensive perspective of the scientific landscape. These methods enable the measurement of time trends, identification of articles with high citation rates, detection of authors, journals, institutions, and countries with high productivity, as well as the computation and ranking of scientific output and collaboration (Arruda et al. 2022). The descriptive bibliometric analysis focused on the metrics of journals, authors, and documents to provide a detailed overview of the major data.

Two distinct search queries were utilized: one particularly focusing on "CMIP6" and the other combining "CMIP6 AND Water Budget". The exact two queries were TS=(CMIP6) and (TS=(CMIP6)) AND TS=(water budget), respectively. This approach enables a two-tiered analysis, examining both broad patterns in CMIP6 research and detailed observations of its specific use in water budgets.

3 Results

For the bibliometric analysis of CMIP6-related papers, two separate queries were used to assess the quantity of research and the specific areas of focus. The initial search, specifically focusing on "CMIP6", resulted in a substantial total of 3,184 publications from the Web of Science Core Collection between 2014 and 2024. The second query, which involved the combination of "CMIP6" and "water budget", yielded 64 results.

3.1 Publication Trends

Figure 1 shows a significant growth in the number of publications on CMIP6, indicating a progressive surge in interest and funding toward climate modeling.
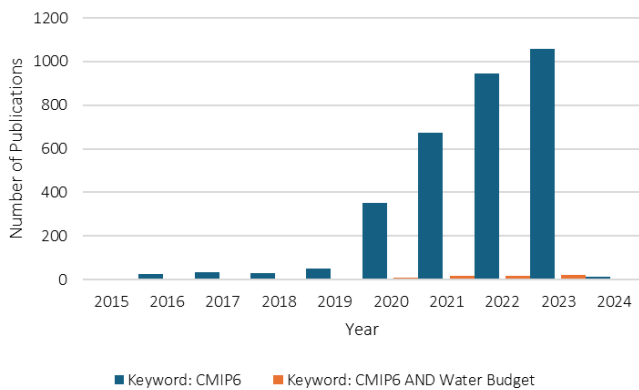

Figure 1. Publication trends over the years 2014–2024.

3.2 Core Journals and Articles

Table 1 lists the journals most active in publishing CMIP6-related research, highlighting their respective impact factors and the volume of contributions.

3.3 Global Collaboration Networks

Figure 3 illustrates the bibliographic coupling between countries, demonstrating a strong network of international collaborations, mainly among developed nations. The colors represent different clusters of research communities based on their geographic and collaborative connections.
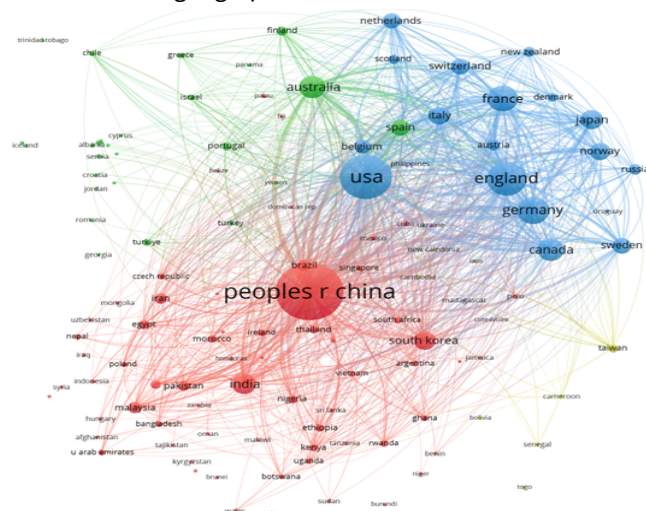

Figure 2. Bibliographic coupling of corresponding author's country.

3.4 Contribution to Sustainable Development Goals

Figure 3 directly correlates the research outputs with specific Sustainable Development Goals, particularly those related to water and climate.
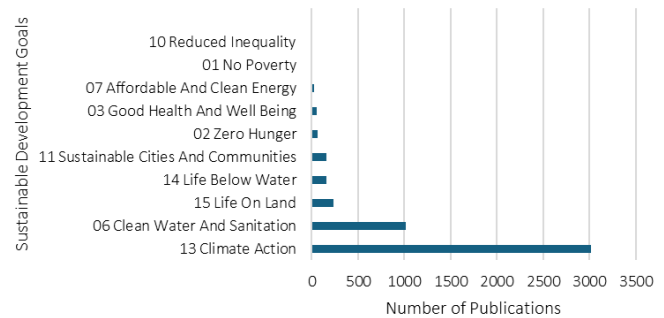

Figure 3. Sustainable Development Goals for the timespan 2014–2024.

4 Discussion

This bibliometric analysis summarized the trends of CMIP6 publications, which offers crucial insights into the utilization of this modeling tool in the context of climate change and its influence on water budgets.

The prominence of journals such as the 'Journal of Climate' and 'Geophysical Research Letters' in publishing CMIP6-related articles highlights their significant role in spreading advanced research in the field of climate science (Table 1). The high impact factors of these journals indicate their significant influence and their ability to attract and publish high-quality research. Other journals such as the 'Science of the Total Environment' and 'Sustainability' also play an important role not only for their focus on environmental studies but also for their interdisciplinary approach, integrating diverse aspects of environmental science, including the implications of climate models such as CMIP6.

The bibliographic coupling data shown in Figure 2 demonstrates a strong network of collaborations mostly concentrated in China, North America, and Europe. These regions are the focal point of climate modeling research, characterized by established infrastructures and substantial funding for climate science. Nonetheless, the limited amount of cooperation with academics in Africa, Central Asia, and South America indicates a geographical imbalance in climate research. This disparity could hinder the worldwide applicability of research findings, as areas that are most susceptible to climate impacts may not be well represented in scientific outputs. Previous research has emphasized the significance of inclusive global research collaborations to ensure the effectiveness of climate adaptation methods in various geographical contexts (Eyring et al. 2016, Wang et al. 2022).

Figure 3 demonstrates the connection between CMIP6 research outputs and UN SDGs, highlighting the significant contribution of scientific research in tackling worldwide issues. The focus on ensuring access to clean water and proper sanitation, as well as taking measures to address climate change, emphasizes the capacity of academic

Table 1. Most relevant journals (CMIP6).

Journals	Number of Articles	Impact Factor
Journal of Climate	208	5.38
Geophysical Research Letters	190	5.58
Geoscientific Model Development	133	5.1
Science of the Total Environment	61	10.75
Journal of Advances in Modeling Earth Systems	58	6.80
Atmospheric Chemistry and Physics	54	6.13
Water	54	3.4
Sustainability	42	3.9
Atmospheric and Oceanic Sciences	38	2.3

research to provide valuable insights for policy-making and practical implementation. This relationship is crucial because it highlights the practical consequences of theoretical models and simulations. By matching research objectives with these global goals, the scientific community can focus its efforts on areas of crucial importance, thereby increasing the societal influence of their work. This strategy is substantiated by literature indicating that conducting research in line with Sustainable Development Goals tends to receive wider societal approval and has a greater probability of impacting policy modifications (Sianes et al. 2022).

The results of this bibliometric analysis demonstrate a constantly changing and developing field of climate change research, which has been made possible by CMIP6. The rise in publications during the study period suggests a strong interest and continuous requirement for advanced climate modeling tools to forecast and mitigate climatic impacts. Furthermore, the integration of CMIP6 data into water budget analyses emphasizes the crucial overlap between hydrological and climatological investigations, which are vital for formulating adaptive approaches considering global warming.

5 Conclusions

This bibliometric analysis has revealed the widespread use and influence of CMIP6 in climate change research, revealing both broad adoption and specific applications. Between 2014 and 2024, a substantial amount of literature, consisting of 3,184 publications, has been found, illustrating the extensive application of the model in different areas of climate science. However, when particularly considering the incorporation of CMIP6 into water budget investigations, only 64 papers were found, highlighting a significant gap in the research field. The significant contrast in publication volumes highlights a crucial area for future research—the application of CMIP6 in understanding the hydrological impacts of climate change. The Journal of Climate and Geophysical Research Letters, among other journals, has been recognized as actively promoting the dissemination of CMIP6 research. Furthermore, the analysis of international collaboration networks emphasizes the requirement for broader and more geographically varied research partnerships, which are essential for creating comprehensive and universally relevant climate solutions. In conclusion, although the CMIP6 has made substantial progress in climate modeling, its specific applications in water budget analysis are underrepresented. This highlights the need for more research and practical investigation in this important field. By broadening our attention to this matter, we may significantly improve our comprehension and control of the impacts of climate change on global water resources. This approach closely aligns with the Sustainable Development Goals that pertain to clean water and climate action. This study establishes a fundamental basis for future efforts, emphasizing the need for a wider range and more extensive incorporation of climate models in hydrological research.

6 References

Arruda, H., Silva, E.R., Lessa, M., Proença, D. Jr, Bartholo, R., 2022. VOSviewer and Bibliometrix. Journal of the Medical Library Association 110 (3), 392-395.

Badola, A., Agrawal., R.K., 2023. Forty-Five Years of International Journal of Intercultural Relations: A Bibliometric Analysis. International Journal of Intercultural Relations 94, 101785.

Balu, A., Ramasamy, S., Sankar, G., 2023. Assessment of Climate Change Impact on Hydrological Components of Ponnaiyar River Basin, Tamil Nadu Using CMIP6 Models. Journal of Water and Climate 14 (3), 730-747.

Carlsen, L., Bruggemann, R., 2022. The 17 United Nations' Sustainable Development Goals: A Status by 2020. International Journal of Sustainable Development and World Ecology 29 (3), 219-229.

Chen, C.A., Hsu, H.H., Liang, and H.C., 2021. Evaluation and Comparison of CMIP6 and CMIP5 Model Performance in Simulating the Seasonal Extreme Precipitation in the Western North Pacific and East Asia. Weather and Climate Extremes 31, 100303.

Eyring, V., Bony, S., Meehl, G.A., Senior, C.A., Stevens, B., Stouffer, R.J., Taylor, K.E., 2016. Overview of the Coupled Model Intercomparison Project Phase 6 (CMIP6) Experimental Design and Organization. Geoscientific Model Development 9 (5), 1937-1958.

Guo, H., Bao, A., Chen, T., Zheng, G., Wang, Y., Jiang, L., De Maeyer, P., 2021. Assessment of CMIP6 in Simulating Precipitation over Arid Central Asia. Atmospheric Research 252, 105451.

Jiang, J., Tianjun, Z., Xiaolong, C., Lixia, Z., 2020. Future Changes in Precipitation over Central Asia Based on CMIP6 Projections. Environmental Research Letters 15 (5), 054009.

O'Neill, B.C., Tebaldi, C., van Vuuren, D.P., Eyring, V., Friedlingstein, P., Hurtt, G., Knutti, R., … Sanderson, B.M., 2016. The Scenario Model Intercomparison Project (ScenarioMIP) for CMIP6. Geoscientific Model Development 9 (9), 3461-3482.

Risley, J. C., Ammit, C., 2023. Simulating the Hydrologic Response to Climate Change in Three New Zealand Headwater Basins Using CMIP6 Datasets. Earth Interactions 27 (1), e220018.

Sengupta, A., Waliser, D.E., Massoud, E.C., Guan, B., Raymond, C., Lee, H., 2022. Representation of atmospheric water budget and uncertainty quantification of future changes in CMIP6 for the Seven US National Climate Assessment Regions. Journal of Climate 35 (22), 7235-7258.

Shafeeque, M., Luo, Y., 2021. A Multi-Perspective Approach for Selecting CMIP6 Scenarios to Project Climate Change Impacts on Glacio-Hydrology with a Case Study in Upper Indus River Basin. Journal of Hydrology 599, 126466.

Sianes, A., Vega-Muñoz, A., Tirado-Valencia, P., Ariza-Montes, A., 2022. Impact of the Sustainable Development Goals on the Academic Research Agenda. A Scientometric Analysis. Plos One 17 (3), e0265409.

Wang, A., Miao, Y., Kong, X., Wu, H., 2022. Future Changes in Global Runoff and Runoff Coefficient from CMIP6 Multi-Model Simulation Under SSP1-2.6 and SSP5-8.5 Scenarios. Earth's Future 10 (12), e2022EF002910.

Geomatics Applications for Farm's Sustainability

Amanzholova Raushan[1,], Amanzholov K.[1], Murat Daulet[2], Dani Sarsekova[2], Syed Imran Moazzam Shah[1], Rebecca King[1], Baktybek Duisebek[1,2], Janay Sagin[1]*

[1] School of Information Technology and Engineering, Kazakh-British Technical University, Almaty, Kazakhstan, r_amanzholova@kbtu.kz; k_amanzholov@kbtu.kz; s.shah@kbtu.kt; r.king@kbtu.kz; b.duisebek@kbtu.kz; j.sagin@kbtu.kz

[2] Faculty of Water, Land and Forest Resources, Kazakh National Agrarian University, Almaty, Kazakhstan, sarsekova.dani@kazatu.kz; dauletmurat8080@gmail.com

* corresponding author

Abstract: Kazakhstan, like many countries in the world, experienced big floods this Spring 2024. Big droughts could occur during the summer of 2024, even worse than it was in 2023. These devastating droughts occurred during the last several years from 2020, causing big losses for Kazakhstan's farmers. Floods-droughts disasters, connected to climate change and anthropogenic disruptions, require the proper mitigation strategies, programs, and technologies. Engineering efforts, such as intervention in the natural water movement should be chosen carefully. Intervention in nature must be prudent and rational, the mitigation output should lead to increased processes of adaptation, not destruction. It is critical to predict and to reliably model in advance how nature will react to man's intervention in the existing equilibrium. Unfortunately, most of the flood mitigation activities in Kazakhstan are still based mostly on fighting with nature– settlements in flood zones and dam constructions. This also includes intensive exploitation of once fertile lands and the very geometric locations of settlements, shape of farm plots: rectangular, without considering the terrain, increased erosion, and diminish the natural water movement. A more rational, sustainable approach is to consider the local topography when dividing land combined with planting forest belts. The contour-strip organisation of the territory for the division of the catchment into several contour strips along horizontal lines combined with the Flood-MAR (Managed Aquifer Recharge) technologies are a more sustainable approach to mitigate floods-droughts issues. Geomatics tools, technologies application are under investigation by the group of researchers for farmlands sustainability improvement.

Keywords: Flood-MAR; geomatics; contour-strip; sustainability; farming.

1   Introduction

Flood and droughts are becoming complicated issues worldwide with accelerated climate change (Adenova et al. 2023). The proper flood-drought mitigation strategies with the proper technologies, including Geomatics, will be promising to expand in the practical applications in Kazakhstan, CA regions. Some countries started to apply more Flood-MAR programs. Historically California constructed many structures to control water movement with big dams, reservoirs for intensive surface and groundwater use. These days, California is moving toward a more sustainable approach by restoring the natural water movement system by replenishing its underground water resources. California expands the community farmer-based user-friendly Flood-MAR Hub (Flood-MAR 2023). Along with California, the Canada - US transboundary River Basin committee group of farmers also use the Flood-MAR strategy for flood-drought mitigation activities (RRBC 2023). Keller's group of researchers (Keller et al. 2000) analysed different strategies for water storage: water in soil profiles, subterranean aquifers, small reservoirs (ponds), and big reservoirs with dams. Storing water in underground aquifers is recommended as the sustainable approach: water can be stored for years, with little or no evaporation loss; can be used in drought years; can be near or directly under the point of use; can be immediately available through pumping. Conjunctive use of groundwater and connected chains of ponds with groundwater recharge are generally the best systems for flood-drought mitigation and water sustainability programs (Keller et al. 2000). Another great advantage of groundwater is that as water slowly percolates down into the aquifer, it is usually purified of biological pollutants. Thus, groundwater is usually the best source of drinking water, especially in rural areas of developing countries where water treatment facilities are not available. The critical issue facing many groundwater aquifers today is that the volume of water withdrawal exceeds long-term recharge, resulting in rapidly declining groundwater levels in many areas.

2   Materials and methods

Currently we are working on the German-Kazakh "Urbane water management: German experience for Kazakh cities" project (TERESA), supported by the German Federal Ministry of Education and Research (BMBF) under the CLIENT II Programme "International Partnerships for Sustainable Innovations" (TERESA 2024). The aim of the project is to learn the German experience with flood issues and mitigation programs and adapt the sustainable concepts for water management programs. This Includes analysing sustainable urban drainage systems (SUDS 2024) to reduce and to manage flooding using advanced simulation tools and applications of MAR and to increase the cross-seasonal water availability using web-based simulation tools (INOWAS 2004). The research group is targeted to expand this TERESA project adaptation for rural regions, for Kazakh's farmers with Geomatics applications for farm's sustainability.

Research questions within this Flood-MAR Geomatics applications effort: 1) Will it be possible to adapt the Flood-MAR approach to Kazakh farmers?; 2) How the contour-strip division of the farmer land catchment combined with the Flood-MAR would mitigate floods-droughts issues?; 3) What strategy, tools, technologies, should be used for these activities?

Effectiveness of various infiltration scenarios on the different soil types are under investigation based on local and regional water balance evaluations for SUDS and modified MAR efforts (Figure 1).
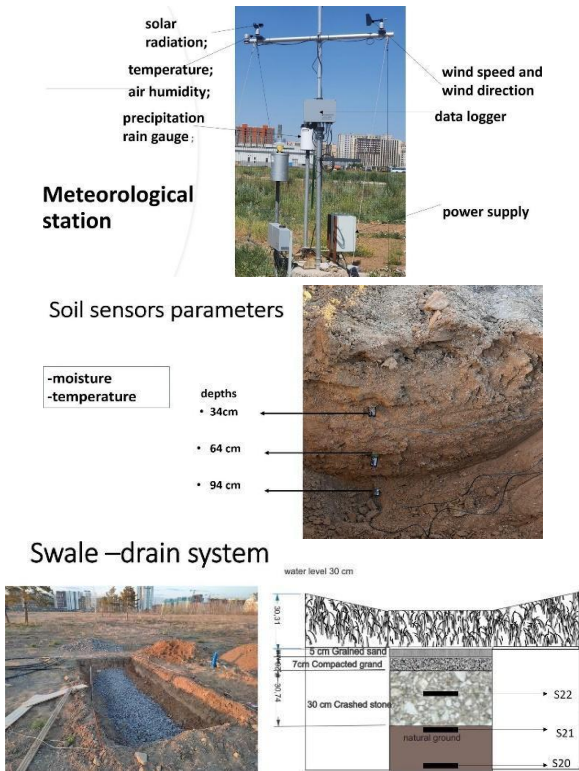

Figure 1. TERESA project INOWAS MAR research training polygon test site.

Within the TERESA project INOWAS MAR research training polygon test site facility is used for the research and training activities. With the promotion of the big international banks, big corporations, many developing countries focus mostly on modern capitalism in growth, in terms of the monetary value of aggregate goods and services, causes widespread ecological damage and is not necessary for the further increase of human living standards (D'Alisa et al. 2015). Degrowth theory with connections to the more natural friendly approach in development, is not popular and not supported by some of the developing countries (Hickel 2022). More aggressive natural resources extractions and agricultural land use are supported and subsidised in many countries (Horowitz 2023). Degrowth is an academic and social movement critical of the hegemony of economic growth perpetuated by capitalism. Degrowth initiates an equitable and democratically-led downscaling of production and consumption to achieve environmental sustainability, social justice and well-being (Bokat-Lindell 2021). The natural eco-friendly technologies are missing the proper support in Kazakhstan. Kazakh Government provides the financial subsidising support mostly to the big mining companies, big agrarian groups, which quite often extract resources, by destroying the natural wetlands, lakes, swamps. Kazakh people's efforts to preserve the natural system, swamps, and lakes are often ignored (Vigano 2022).

3 Results

We are working on promoting the Flood-MAR approach to Kazakh farmers', convincing the local farmers to adapt and apply more MAR combined with forest shelterbelts for snow water retention activities. A key element in this strategy is the optimal utilisation of the MAR method to address the persistent issue of drought on farmlands. By applying MAR, farmers can be more sustainable in drought seasons, and be more efficient in water resource management, by having more reliable solutions to alleviate irrigation water scarcity. KazGer farm, located in the North part of Kazakhstan, Akmola region, had shown interest in working with us on adaptation of the TERESA INOWAS MAR approach. Currently we are investigating and preparing KazGer farmlands for potential MAR applications combined with shelterbelts for snow water retention (Figure 2). On KazGer farmlands we are working on Geomatics applications, providing the geodesy topographic surveys to identify potential locations to set up the snow water retention lowest areas combined with MAR and shelterbelts. We need to provide the proper contour-strip division of the farmer land catchment combined with the flood-MAR; it should eventually work for the floods-droughts mitigation issues.
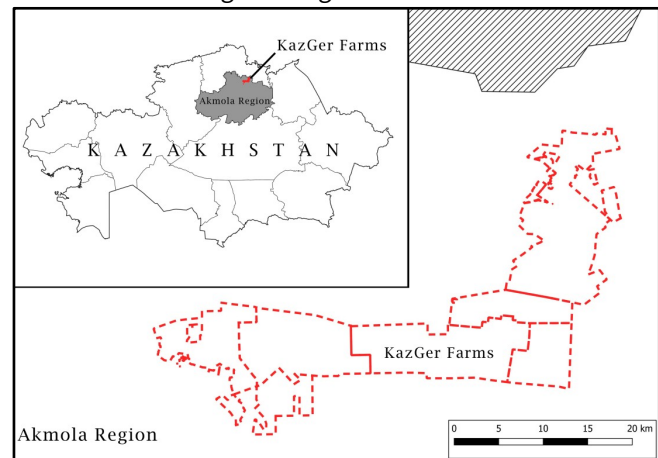

Figure 2. KazGER farmlands, located in the North Kazakhstan, Akmola region, shown in red to adapt the TERESA INOWAS Flood-MAR approach

4 Discussion

With Geomatics applications, we are working on the geodesy topographic surveys to delineate the proper contour-strip organisation of the farmland territory on the division of the catchment into several contour strips along horizontal lines. The main water-regulating structures are shafts combined with water-absorbing ditches filled with organic materials. We need to identify potential small pond locations with MAR to set up the snow water retention lowest areas combined with shelterbelts (Figure 3).
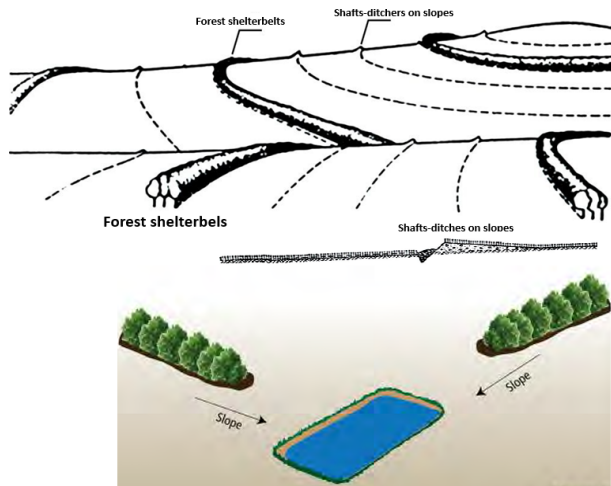
Figure 3. The contour-strip organisation of the farmland with shafts-ditches and small pond locations for MAR, adapted-modified from (Shelterbelts 2010).

5   Conclusions

Kazakhstan has many problems with disaster events, including floods and droughts. The most strategies that Kazakhstan has used are based mostly on the direct intervention in the natural water movement by building big dams, engineering constructions with settlements and development in the flood zones. The farmlands are also under intensive exploitation with mostly geometric shapes of farm plots: rectangular, without considering natural topography, terrain, to follow the water movement. The contour-strip organisation of the territory for the division of the catchment into several contour strips along horizontal lines combined with the Flood-MAR technologies should be a more sustainable approach to mitigate floods-droughts issues with reasonable financial expenses. Geomatics technologies and expertise are required to improve these types of programs for farm's sustainability.
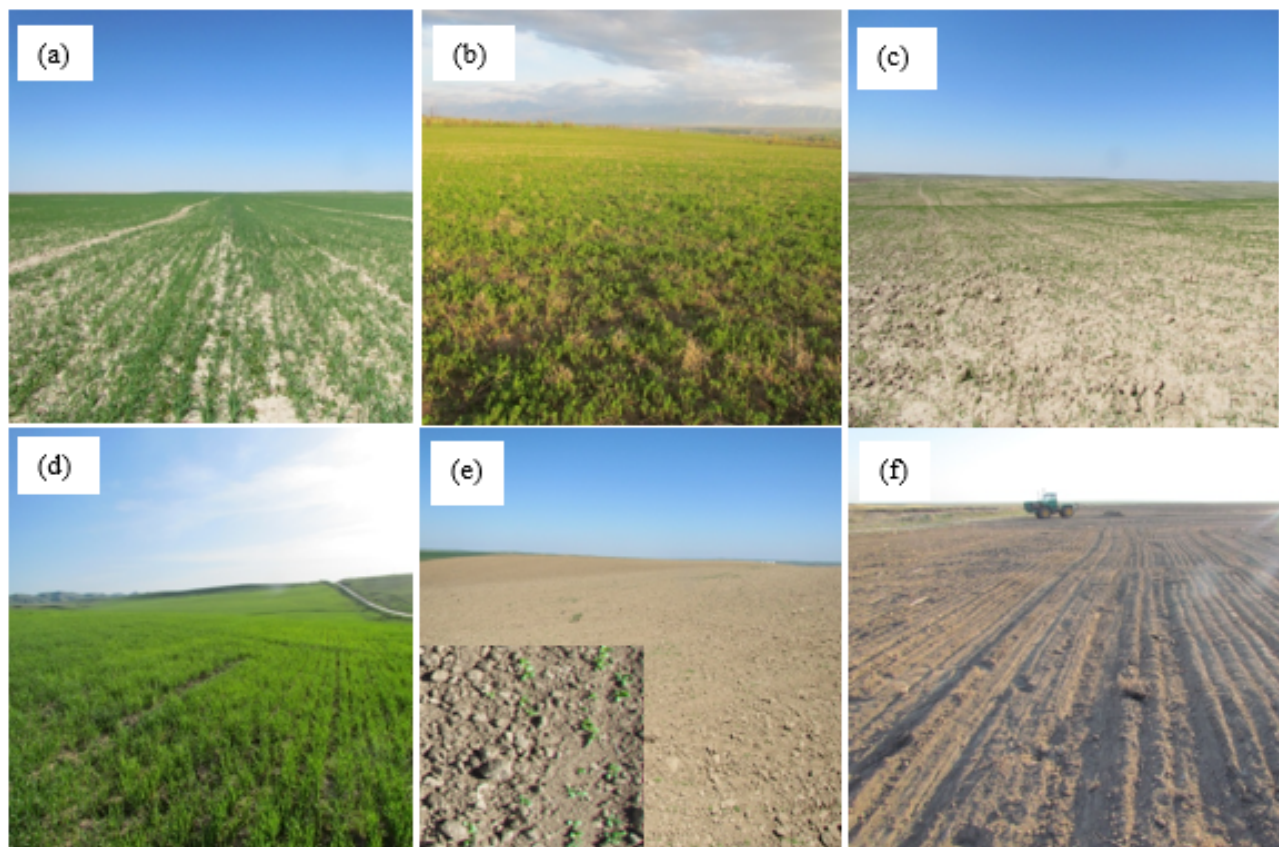

Figure 4. The preliminary survey of the farmland in the foothill zone: (a) winter wheat; (b) perennial alfalfa; (c) spring barley; (d) winter wheat (beginning of tillering); (e) safflower seedlings; (f) safflower cultivation and sowing, which requires the proper contour-strip organisation with shafts-ditches and potential pond locations that may work for water collection with MAR approach, combined with shelterbelts.

Our preliminary farmland investigations had shown that farmers do not have the proper contour-strip organisation of the farmland with shafts-ditches and potential pond locations which may work water collection with MAR approach, combined with shelterbelts (Figure 4). Farmers complained that it is necessary to improve the water collection system and set up the irrigation system properly.

6   References

Adenova, D., Tazhiyev, S., Sagin, J., Absametov, M., Murtazin, Y., Trushel, L., Miroshnichenko, O., Zaryab, A., 2023. Groundwater Quality and Potential Health Risk in Zhambyl Region, Kazakhstan. Water 15 (3), 482.

Bokat-Lindell, Spencer, 2021. Opinion : Do We Need to Shrink the Economy to Stop Climate Change?. The New York Times. ISSN 0362-4331. (Assessed 3 May, 2024).

D'Alisa, Giacomo, … eds. 2015. Degrowth: A Vocabulary for a New Era (Book info page containing download samples). London: Routledge. ISBN 9781138000766.

Flood-MAR, 2023. California's Flood-MAR Hub. What is Flood-MAR? https://floodmar.org/. (Accessed 25 April, 2024)

Hickel, J., Kallis, G., Jackson, T., O'Neill, D.W., Schor, J.B., Steinberger, J.K., Victor, P.A., Ürge-Vorsatz, D., 2022. Degrowth can work – here's how science can help. Nature 612 (7940), 400-403.

Horowitz, J., 2023. Degrowth: A dangerous idea or the answer to the world's biggest crisis? CNN Business. CNN. (Accessed 4 May, 2024)

INOWAS, 2024. Innovative Groundwater Solutions, https://www.inowas.com/. (Accessed 2 May, 2024)

Keller, A., Sakthivadivel, R., Seckler, D., 2000. Water scarcity and the role of storage in development. IWMI Research Rep. 39, IWMI, Colombo, Sri Lanka.

RRBC, 2023. RED RIVER BASIN COMMISSION, Three States, One Province, Two Countries, ONE Red River Basin. https://www.redriverbasincommission.org/. (Accessed 28 April, 2024)

SUDS, 2024. Sustainable drainage. https://www.susdrain.org/. (Accessed 20 April, 2024)

Shelterbelts, 2010. Design Guidelines for Farmyard, Field, Roadside, Livestock, Wildlife, and Riparian Buffer Plantings on the Prairies, Agriculture and Agri-Food Canada, https://www1.agric.gov.ab.ca/$Department/deptdocs.nsf/all/ epw10940/$FILE/Shelterbelts_Design_and_Guidelines.pdf. (Accessed 3 May, 2024)

TERESA, 2023. Urban water management: German expertise for Kazakh cities. https://www.teresa.inowas.com/. (Accessed 23 April, 2024)

Vigano M., 2022. Kazakh people are fighting to preserve the natural lakes. https://www.birdlife.org/news/2022/01/17/kazakh-people-are-fighting-to-preserve-the-natural-lakes-of-nur-sultan/. (Assessed 5 May, 2024)

Sponsors

The conference is organized as part of the project Assessment of the Long-term Climatic and Anthropogenic Effects on the Spatio-temporal Vegetated Land Surface Dynamics in Croatia using Earth Observation Data (ALCAR, IP-2022-10-5711) funded by the Croatian Science Foundation.

HRZZ
Croatian Science Foundation

ALCAR

Gold sponsors:

Geomatika SMOLČAK d.o.o.

OIKON®
WITH US DEVELOPMENT IS NATURAL

GeO WILD

HBOR
HRVATSKA BANKA ZA OBNOVU I RAZVITAK

Bronze sponsors:

GEO CENTAR

MultiOne

ERSTE Bank

listlabs
location intelligence space technologies

U. O. I. G. VIDMAR

Zagreb CROATIA

Supported by:

REPUBLIC OF CROATIA
Ministry of Science, Education and Youth

Copernicus
Europe's eyes on Earth

isprs
information from imagery

eCognition®
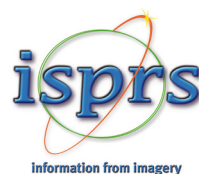
Image to
Information

OIKON®
WITH US DEVELOPMENT IS NATURAL

OIKON Ltd. – Institute of Applied Ecology

OIKON is a leading licensed and accredited consulting company and research institute in the field of applied ecology in Croatia and the region.

With over **26 years** of experience, we offer services in the fields of **nature and environmental protection**, industrial ecology, renewable energy, sustainable development, natural resources management, ecological modelling, landscape analysis and design, **geographic information systems (GIS), remote sensing** and ICT, environmental law, policy and economics, feasibility studies, as well as program and project management.

- **Extensive EO Experience and Achievements**: Over 20 years of EO expertise and numerous projects in forestry, agriculture, and ecosystem monitoring.

- **Leading the way in Habitat Mapping and Preservation**: creating detailed spatial datasets crucial for mapping and preserving both marine and terrestrial habitats, utilizing EO data and other advanced methods to enhance conservation efforts across diverse environments.

- **Commitment to European Green Initiatives and Sustainability Goals**: supporting the EU Biodiversity Strategy for 2030 and other EU Green Deal initiatives, and contributing to the UN SDGs.

Follow us on:

Visit our web:

OIKON.HR

Ge🌐 WILD

Savska cesta 144a, 1000 Zagreb
tel: 01 309 47 90, e-mail: geowild@geowild.hr
www.geowild.hr

Leica Geosystems

PART OF HEXAGON

POVOLJNI KREDITI ZA ULAGANJA

subjekata privatnog i javnog sektora iz okvira Nacionalnog plana oporavka i otpornosti (NPOO)

◆ **Kamatne stope već od 0,4 % za ulaganja posebnih segmenata malih i srednjih poduzetnika, izravno kreditiranje**

(početnici, žene poduzetnice, mladi poduzetnici, poduzetnici koji ulažu u posebna područja RH ili komercijalizaciju RDI projekata)

◆ **Subvencija kamatne stope do 75 % za male, srednje i velike poduzetnike i subjekte javnog sektora, kreditiranje izravno i putem 15 poslovnih banaka**

Sredstva su namijenjena:
- ulaganjima u projekte zelene i digitalne tranzicije
- ulaganjima na posebna područja RH
- ulaganjima u RDI projekte
- ulaganjima subjekata javnog sektora za obnovu od potresa
- ostalim ulaganjima za povećanje konkurentnosti i otpornosti.

Saznajte više putem mrežnih stranica HBOR-a na
www.hbor.hr

JAMSTVA ZA INVESTICIJSKE KREDITE

subjekata srednje tržišne kapitalizacije i velikih poslovnih subjekata iz okvira Nacionalnog plana oporavka i otpornosti (NPOO)

◆ **Pokriće jamstvom do 80 % glavnice kredita**

ovisno o vrsti ulaganja

◆ **Subvencija naknade za jamstvo do 100 % i subvencija kamate po kreditu do 75 %**

ovisno o pravilima o državnim potporama

◆ **Krajnji korisnici (korisnici kredita) su subjekti srednje tržišne kapitalizacije i veliki poslovni subjekti**

◆ **Korisnici jamstva su poslovne banke, leasing društva i HBOR**

◆ **Sredstva su namijenjena:**
- ulaganjima u projekte zelene i digitalne tranzicije
- ulaganjima na posebna područja RH
- ulaganjima u RDI projekte
- ostalim ulaganjima za povećanje konkurentnosti i otpornosti.

HBOR

Financira Europska unija
NextGenerationEU